1196

TRANSPORTATION RESEARCH RECORD

Pavement Evaluation and Rehabilitation

TRANSPORTATION RESEARCH BOARD
NATIONAL RESEARCH COUNCIL
WASHINGTON, D.C. 1988

Transportation Research Record 1196
Price: $41.50

mode
1 highway transportation

subject areas
24 pavement design and performance
40 maintenance

Transportation Research Board publications are available by ordering directly from TRB. They may also be obtained on a regular basis through organizational or individual affiliation with TRB; affiliates or library subscribers are eligible for substantial discounts. For further information, write to the Transportation Research Board, National Research Council, 2101 Constitution Avenue, N.W., Washington, D.C. 20418.

Printed in the United States of America

Library of Congress Cataloging-in-Publication Data
National Research Council. Transportation Research Board.

Pavement evaluation and rehabilitation.
p. cm.—(Transportation research record, ISSN 3061-1981; 1196)
Papers from the 67th annual meeting of the Transportation Research Board held in Washington, D.C., 1988.
ISBN 0-309-04771-4
1. Pavements—Maintenance and repair. I. National Research Council (U.S.). Transportation Research Board. II. National Research Council (U.S.). Transportation Research Board. Meeting (67th: 1988: Washington, D.C.) II. Series.
TE7.H5 no. 1196
[TE250]
388 s—dc20
[625.8] 89-13057
CIP

Sponsorship of Transportation Research Record 1196

GROUP 2—DESIGN AND CONSTRUCTION OF TRANSPORTATION FACILITIES
Chairman: David S. Gedney, Harland Bartholomew & Associates

Pavement Management Section
Chairman: R. G. Hicks, Oregon State University

Committee on Pavement Rehabilitation
Chairman: James F. Shook, ARE Inc.
Secretary: Richard W. May, Asphalt Institute
Paul Autret, Michael C. Belangie, James L. Brown, Martin L. Cawley, John A. D'Angelo, Warren G. Davison, Paul J. Diethelm, Denis E. Donnelly, Wade L. Gramling, Jerry J. Hajek, John P. Hallin, Joseph B. Hannon, James W. Hill, Walter P. Kilareski, Joe P. Mahoney, William G. Miley, David E. Newcomb, Louis G. O'Brien, John C. Potter, R. N. Stubstad, Shiraz D. Tayabji, Robert L. White, Loren M. Womack

Committee on Strength and Deformation Characteristics of Pavement Sections
Chairman: J. Brent Rauhut, Brent Rauhut Engineering Inc.
Joseph H. Amend III, Gilbert Y. Baladi, Richard D. Barksdale, Stephen F. Brown, Albert J. Bush III, George R. Cochran, Billy G. Connor, Amir N. Hanna, R. G. Hicks, Ignat V. Kalcheff, William J. Kenis, Thomas W. Kennedy, Erland Lukanen, Robert L. Lytton, Michael S. Mamlouk, Edwin C. Novak, Jr., Lutfi Raad, Byron E. Ruth, Gary Wayne Sharpe, James F. Shook, Roger E. Smith, R. N. Stubstad, Marshall R. Thompson, Ulian I. Tufektchiev, Thomas D. White

Committee on Pavement Monitoring, Evaluation and Data Storage
Chairman: William A. Phang, Ontario Ministry of Transportation and Communications
Secretary: Don H. Kobi, Paris, Ontario, Canada
A. T. Bergan, Frank V. Botelho, Billy G. Connor, Brian E. Cox, Michael I. Darter, Karl H. Dunn, Wouter Gulden, William H. Highter, James W. Hill, Andris A. Jumikis, Scott A. Kutz, Kenneth J. Law, W. N. Lofroos, K. H. McGhee, Edwin C. Novak, Jr., Freddy L. Roberts, Ivan F. Scazziga, S. C. Shah, Roger E. Smith, Herbert F. Southgate, Elson B. Spangler, Richard L. Stewart, Loren M. Womack, John P. Zaniewski

Committee on Surface Properties—Vehicle Interaction
Chairman: A. Scott Parrish, Maryland Department of Transportation
Louis E. Barota, Robert R. Blackburn, James L. Burchett, Gaylord Cumberledge, Thomas D. Gillespie, Wouter Gulden Lawrence E. Hart, Carlton M. Hayden, Rudolph R. Hegmon, John Jewett Henry, Walter B. Horne, Don L. Ivey, Michael S. Janoff, Kenneth J. Law, Jean Lucas, David C. Mahone, William G. Miley, Robert L. Novak, Bobby G. Page, Richard N. Pierce, John J. Quinn, Jean Reichert, Elson B. Spangler, William H. Temple, James C. Wambold

George W. Ring III, Transportation Research Board staff

Sponsorship is indicated by a footnote at the end of each paper. The organizational units, officers, and members are as of December 31, 1987.

NOTICE: The Transportation Research Board does not endorse products or manufacturers. Trade and manufacturers' names appear in this Record because they are considered essential to its object.

Transportation Research Record 1196

Contents

Asphalt Pavement Evaluation Using Fuzzy Sets

D. J. ELTON AND C. H. JUANG

A new method of asphalt pavement evaluation using fuzzy sets is proposed. The purpose is to provide a simple, consistent, cost-effective procedure for pavement evaluation. Consistent pavement evaluation is needed for adequate pavement maintenance. The large turnover pending in the pavement engineering field over the next five years will leave many pavement agencies without adequate expertise to evaluate their pavement systems. A computer program, Fuzzy Evaluation of Asphalt Pavement Systems (FEAPS), is presented to facilitate the method. The program uses the fuzzy weighted average operation to combine distress ratings for five different types of pavement distress (roughness, alligator cracks, transverse cracks, longitudinal cracks, rutting). A fuzzy set representing the pavement condition is produced. This final fuzzy set can be translated to a natural language descriptor. A new function for comparing the final fuzzy sets is described, allowing ranking of the pavements. With FEAPS, the user can change the pavement weights reflecting the local expert opinions to allow for differences of interpretation of local pavement distress types.

Asphalt pavement maintenance is a very important issue facing the state and local highway engineer today (*1, 2*). Proper maintenance requires proper pavement evaluation. Unfortunately, the wide variety of pavement types, loading conditions, and soil types makes pavement evaluation a complex task. Current effective pavement evaluation methods require the services of a highly trained and experienced expert, which entails significant costs in time and money. The methods proposed by Shahin and Kohn (*3*) and the U.S. Department of Transportation (*4*) are examples which, while effective, are also time-consuming, expensive, and often unsuitable for many agencies responsible for pavement maintenance and repair. This paper proposes a new evaluation procedure that reduces the need for an expert to perform the pavement evaluation. The procedure uses the experience of past experts and fuzzy arithmetic. Fuzzy sets, introduced by Zadeh (*5*), fuzzy arithmetic, and fuzzy logic have been applied to many areas of engineering problems where the inputs are vague or ill-defined (*6–9*). A recent National Science Foundation workshop at Purdue University examined areas in civil engineering where fuzzy sets could be applied and included pavement evaluation as one of those areas (*6*).

Many large highway structures in the U.S. are reaching the end of their design lives and thus are requiring more maintenance. The problem is exacerbated by the anticipated retirement in the near future of large numbers of experienced pavement engineers and experts (*10–12*). Many of these engineers were hired by highway departments at the start of the National System of Interstate and Defense Highways, which was created by the Federal-Aid Highway Act of 1956. Because the interstate system has grown slowly, hiring and turnover rates have been low. Consequently, few new pavement engineers have been available to become expert at pavement evaluation. The low turnover in these positions has led to low job demand, and many universities have removed pavement engineering from their curricula. Finally, the dropping enrollments in civil engineering curricula at universities have reduced the supply of potential pavement engineers (*13*). These factors accentuate the need for a consistent and simple pavement evaluation procedure that reduces the need for an expert. The procedure proposed here does not require an expert.

Pavement evaluation schemes are very local in character and can vary even from county to county. Only local knowledge of the relative importance of such factors as soil type, weather, asphalt types, significance of distress types, and seasonal variations and magnitudes of pavement loadings is useful at a given location. Therefore, pavement evaluation procedures must be tailored to every locale.

The combination of these factors has created an impending crisis in pavement engineering. In order to avert the crisis, a method of preserving the knowledge of pavement evaluation experts must be found and implemented.

A procedure employing fuzzy logic can be a great aid in solving this problem. The procedure presented herein can capture local knowledge about the importance of various forms of pavement distress in the form of weights for distress types. This knowledge is stored in a computer program and can be recalled. Each type of pavement distress is rated for severity, which is represented as a fuzzy set and then combined with the severity of other distress types, using fuzzy arithmetic to produce the pavement rating. The procedure for capturing knowledge and manipulating it is explained below.

METHODOLOGY

Use of Fuzzy Sets

Fuzzy set theory can account for the uncertainty associated with the evaluation of engineering parameters. There is considerable uncertainty in pavement evaluation, as is evidenced by the unclear terms used to describe pavement condition. For example, such general terms as "real bad," "poor," "good," and "excellent" are often used, and a range of pavement conditions is associated with each descriptor. Fuzzy sets describe that range well.

D. J. Elton, Civil Engineering Department Auburn University, Ala. 36849. C. H. Juang, Civil Engineering Department, Clemson University, Clemson, S.C.

In conventional mathematics, a single numerical rating might be assigned to each descriptive term. This number might represent the mean value, for example, when in reality some range of values might all be classified with that same number. Fuzzy sets can be used to describe this uncertainty. Rather than assigning a single number to represent the pavement rating, a fuzzy set is used. This is a set of numbers that describe the "degree of belonging" or "support" (*14*) to each level of rating to which the particular pavement belongs. In this study, a computer program performs fuzzy operations on the linguistic assessments of the pavement condition to produce the pavement rating.

Pavement Evaluation

Five forms of visual distress of asphalt pavements were selected for this study: rutting, longitudinal cracks, transverse cracks, alligator cracks, and roughness. All are indicators of structural distress. Although safety conditions are also important in evaluating pavements and could be included in the procedure proposed herein, they were not included, for the sake of brevity and clarity. A more complete list of pavement distress is given by the Asphalt Institute (*15*) and Turner et al. (*16*).

The various forms of distress were weighted to reflect their relative importance, and the weights were determined through the collection of expert knowledge. Several experienced experts in asphalt pavement analysis were interviewed for this study, in order to ascertain the importance of particular distress types. The experts used natural language terms, such as "not important" or "very important," which reflected the fuzziness associated with pavement evaluation. Each distress type was given a weight, shown in table 1, that reflects the experience of the local experts and was incorporated in the Fuzzy Evaluation of Asphalt Pavement Systems (FEAPS) program. However, the user can easily change the weights to accommodate his or her own experience. The weights reflect the differing importance of the same distress in different locales. For example, where the soils are very susceptible to pumping, small cracks in the pavement assume more significance. Similarly, where the soils are very susceptible to the formation of ice lenses, cracks allowing infiltration might have more significance than in soils where ice lenses do not form. This feature of the procedure allows for important local variations in soil types, weather, asphalt types, significance of distress types, and seasonal variations and magnitudes of pavement loadings to be incorporated in the methodology. Such flexibility makes FEAPS very versatile.

It is important to note that the results obtained are a direct function of the experts chosen to assign weights. While agreement in the selection of experts is not likely to be unanimous, some measure of expertise can be applied to aid in the selection of experts. Unfortunately, the profession still awaits a perfect method to select and evaluate experts.

The pavement rating is assigned based on visual criteria established by the agency conducting the survey. A trained individual is required to identify the kind and degree of distress. The training for this task can be done in a short period of time, whereas the training to understand the significance of distress may take years and is expert knowledge. The computer program described herein provides the pavement evaluation, a much more difficult task than distress evaluation.

Once the linguistic ratings are obtained, they are entered into the computer program. The ratings are represented internally by fuzzy sets. The overall rating of the pavement is determined from the fuzzy weighted average described below and defined in equation 1 by Schmucker (*17*) as

$$R = \frac{\Sigma R_i * W_i}{\Sigma W_i} \tag{1}$$

where

R = the fuzzy set that represents the overall rating of the pavement,
R_i = the fuzzy set that represents the linguistic rating of a particular distress i, and
W_i = the fuzzy set that represents the weight (or relative importance) of a particular distress i, as compared to other distress.

The five major distress types have varying importance. The weight of each type is shown in table 1. The fuzzy sets representing each weight are given in table 2. Note that the weight indicates the relative importance of one distress type compared to the others. The weight is not an absolute scale. Thus, the table does not, for example, imply that transverse cracks are absolutely "not important."

The shape of the membership functions shown in figure 1 (as indicated by the fuzzy set) has been shown to have little effect on the fuzzy weighted average operation used in this study (*18*). Figure 1 shows that the relative importance of each distress ranges from 1 to 9, with 9 representing the domain element of greatest importance. "Support" values, which express membership, range from 0.0 to 1.0. Thus, for example, in table 2 the weight "not important" is fully supported (1.0) at domain element 1 and also partially supported (0.5) at domain element 2. No support (0.0) is indicated at domain elements 3 and above, indicating that there is no high level importance associated with the rating "not important."

TABLE 1 WEIGHT SCALE FOR PAVEMENT DISTRESS

Distress	Weight
Rutting	important
Longitudinal cracks	moderately important
Transverse cracks	not important
Alligator cracks	extremely important
Roughness	very important

TABLE 2 WEIGHTS USED TO EVALUATE PAVEMENT DISTRESS

Weight	Symbol	Fuzzy Set Representation
not important	A	{1.0/1, 0.5/2, 0/3}
moderately important	B	{0/1, 0.5/2, 1.0/3, 0.5/4, 0/5}
important	C	{0/3, 0.5/4, 1.0/5, 0.5/6, 0/7}
very important	D	{0/5, 0.5/6, 1.0/7, 0.5/8, 0/9}
extremely important	E	{0/7, 0.5/8, 1.0/9}

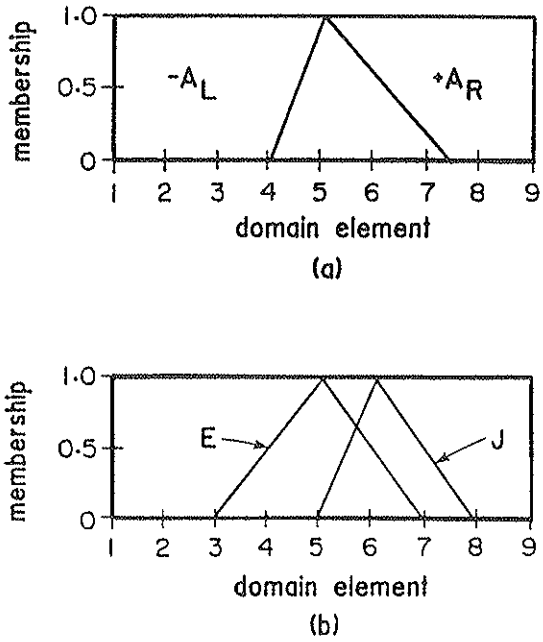

FIGURE 1 (a) Model of the distress index. (b) Comparison of fuzzy sets for the distress index calculation.

As mentioned above, the rating of the evaluated pavement was expressed in linguistic terms. Because rating of the pavement by individuals is very subjective, use of linguistic terms appears to be more natural and appropriate than use of single numeric values. Consequently, fuzzy set representations of these linguistic ratings have been used in the proposed evaluation procedure. Table 3 gives the fuzzy sets corresponding to the linguistic rating grades used in this study. The domain elements for these rating grades range from 1 to 9, with 9 representing the domain element of greatest severity. As before, "support" values, which express membership, range from 0.0 to 1.0. Thus, for example, in table 3, the rating "slight" is unsupported (0.0) at domain element 1, partially supported (0.5) at domain element 2, fully supported (1.0) at domain element 3, partially supported (0.5) at domain element 4, and unsupported (0.0) at domain element 5. No support (0.0) is indicated at domain elements 5 and above, indicating that there is no high level severity associated with the rating "slight."

Tables 1, 2, and 3 represent the opinion of the experts used in this study. Other fuzzy sets could be used in the computer program to describe the pavement rating and weights, as desired. Once these opinions are in place, and the pavements ratings have been obtained, equation 1 can be used to calculate the final fuzzy set which represents the overall pavement rating.

Several pavements can be rated with this method, and their final results compared, resulting in a ranking of pavements for use in maintenance strategies. This comparison is a rational way to establish the repair priority of each pavement, based on structural evaluation of the pavement. The comparison is facilitated by the establishment of a distress index, explained below.

TABLE 3 RATING SCALE: QUALITATIVE RATING OF THE DISTRESS

Rating Grade	Symbol	Fuzzy Set Representation
none	A	{1.0/1, 0.5/2, 0/3}
slight	B	{0/1, 0.5/2, 1.0/3, 0.5/4, 0/5}
significant	C	{0/3, 0.5/4, 1.0/5, 0.5/6, 0/7}
severe	D	{0/5, 0.5/6, 1.0/7, 0.5/8, 0/9}
extremely severe	E	{0/7, 0.5/8, 1.0/9}

DISTRESS INDEX FOR COMPARISON OF PAVEMENTS

Pavements can be compared using a ranking index based on the fuzzy sets representing the pavement condition. This index is a quantitative measure of pavement distress. The ranking index, here called the distress index (*DI*), can also be used as an absolute measure of the pavement condition, based on local criteria.

The proposed distress index is based on a model proposed by Juang and Kalidindi (*19*). Referring to Figure 1a, the distress index is

$$DI = \frac{A_L - A_R + C}{2C} \tag{2}$$

where

DI = distress index,
A_R = area to the right of the membership function which characterized the final fuzzy set,
A_L = area to the left of the membership function which characterized the final fuzzy set, and
C = a constant, equal to the area enclosed by the universe.

The distress index value ranges from 0.0 to 1.0. A low index indicates better pavement condition, while a high index indicates worse condition. For example, pavements with overall ratings represented by fuzzy sets E and J, given in figure 1b, are readily compared as follows:

E = {0/3, 0.5/4, 1.0/5, 0.5/6, 0/7}

For E,

$$DI = \frac{3 - 3 + 8}{2(8)} = 0.50$$

J = {0/5, 1.0/6, 0.5/7, 0/8}

For J,

$$DI = \frac{4.5 - 2 + 8}{2(8)} = 0.66$$

Thus, the pavement represented by fuzzy set J is in worse condition than the pavement represented by fuzzy set E.

The distress index can be translated back into the natural language rating, if desired, by assigning natural language descriptions to "standard" fuzzy sets representing different pavement conditions. The DI for each of these fuzzy sets is calculated, and the DI of the pavement under consideration is compared to the DI of the standard. Table 4 gives standard fuzzy sets that might be assigned the natural language descriptions shown there.

TABLE 4 NATURAL LANGUAGE TRANSLATION OF THE DISTRESS INDEX (*DI*)

Final Evaluation Descriptor	Fuzzy set	DI
no distress	= {1.0/1, 0.5/2, 0/3}	0.06
moderate distress	= {0/1, 0.5/2, 1.0/3, 0.5/4, 0/5}	0.25
distress	= {0/3, 0.5/4, 1.0/5, 0.5/6, 0/7}	0.50
severe distress	= {0/5, 0.5/6, 1.0/7, 0.5/8, 0/9}	0.75
total distress	= {0/7, 0.5/8, 1.0/9}	0.94

FUZZY WEIGHTED AVERAGE

The fuzzy weighted average (FWA) operation is defined in equation 1. The summation, multiplication, and division in equation 1 are fuzzy arithmetic operations and are defined by Schmucker (*17*) as follows:

First, let

$$X = \{x(i) \quad | \quad i\ ;\ 1 \le i \le n\}$$

$$Y = \{y(j) \quad | \quad j\ ;\ 1 \le j \le n\}$$

where i, j and n are integers, and $x(i)$ and $y(i)$ are membership functions that characterize fuzzy sets X and Y respectively. Then, fuzzy addition is defined as

$$X + Y = \{\min [x(i), y(j)] \quad | \quad (i + j)\ ; \quad 1 \le i, j \le n\} \qquad (3)$$

The fuzzy summation is simply fuzzy addition repeated. Fuzzy multiplication is defined as

$$X * Y = \{\min [x(i), y(j)] \quad | \quad (i * j)\ ; \quad 1 \le i, j \le n\} \qquad (4)$$

Lastly, fuzzy division is defined as

$$X/Y = \{\min [x(i), y(j)] \quad | \quad (i/j)\ ;\ 1 \le i, j \le n\} \qquad (5)$$

The implementation of fuzzy addition and multiplication is straightforward; fuzzy division, however, is less so. For many applications, the Clements algorithm may be sufficient to solve this problem. Mullarkey and Fenves (*20*) consider this algorithm to be the best for fuzzy division.

The Clements algorithm involves two assumptions: (1) any division (i/j) not resulting in an integer is deleted, and (2) any division resulting in a quotient greater than n is discarded.

Another concern in the implementation of equation 1 is whether the fuzzy "normalization" should be conducted after each fuzzy operation (addition, multiplication, or division). Earlier studies (*17, 20*) have indicated that more reasonable results can be obtained with normalization than without normalization. Fuzzy normalization is defined by Schmucker (*17*) as follows. Let

$$Z = \text{NOR}\ [X]$$

then

$$Z = \{z(i)/i\ ;\ 1 \le i \le n\} \qquad (6)$$

where

$$z(i) = x(i)/\max\ [x(i),\ 1 \le i \le n] \qquad (7)$$

Fuzzy normalization was used in this study.

COMPUTER PROGRAM

Created to perform the pavement evaluation, the FEAPS program was written in FORTRAN 77 and, using the WATFOR77 compiler (*21*), runs on IBM PC and IBM-compatible microcomputers.

The simplified flowchart for the program is shown in figure 2. The first part of the program accepts information from the user. The program then allows the user to tailor the evaluation by assigning linguistic weights to the five different distress types, based on his or her experience. The user can also

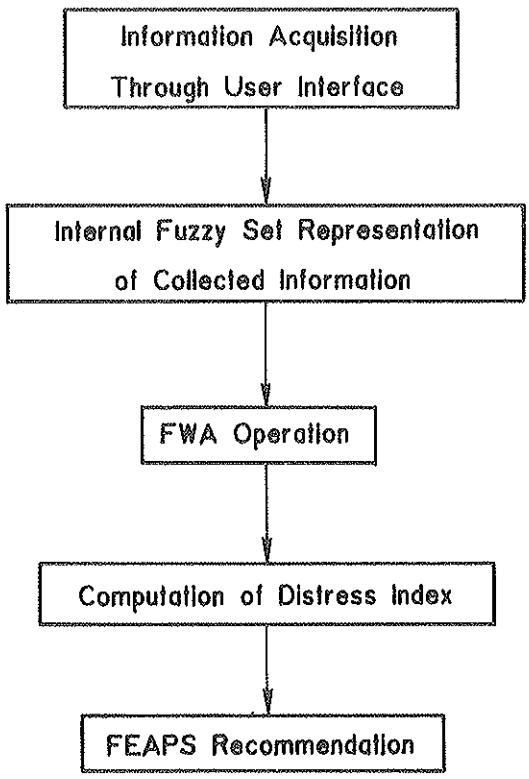

FIGURE 2 General flowchart for FEAPS.

TABLE 5 CASE STUDY 1: FOUR PAVEMENT RATINGS

Distress	Pavement			
	1	2	3	4
Rutting	B	C	C	D
Longitudinal cracks	C	B	C	C
Transverse cracks	D	E	B	C
Alligator cracks	B	C	E	E
Roughness	B	B	C	D
Distress Index	0.32	0.43	0.60	0.74

[a] NOTE: pavement ratings made according to the following scale -
A - none
B - slight
C - significant
D - severe
E - extremely severe

select default weights embodied in the program, which are expressed in linguistic terms (or phrases) for ease of use. Similarly, the rating of any pavement evaluated according to each of the distress criteria is expressed in linguistic terms.

The second part of the program translates the input linguistic expressions into fuzzy sets. Once the required data are input and translated into fuzzy sets, the FWA operation is performed. The result is a final fuzzy set that represents the pavement rating.

Finally, the distress index of the final fuzzy set is calculated, and this process is repeated for each pavement evaluated. The pavement with the lowest *DI* is in the best condition.

CASE STUDIES

The procedure explained above was evaluated by selecting and rating four pavements. The default weights shown in table 1 and the rating scale shown in table 3 were used.

Case 1

Four pavements are shown in table 5: each exhibited a different combination of distress. Pavements with different degrees of distress were chosen to show how the proposed procedure could be used to differentiate among them. Pavement 1 ratings intuitively indicate good condition. In particular, the small amount of alligator cracks indicates good condition. Visual inspection of the ratings for pavements 2, 3, and 4 indicates that the condition of these pavements decreases with increasing pavement number.

Evaluation using FEAPS was performed. The *DI* for each is shown in table 5. As expected, pavement 1 is in the best condition (lowest *DI*), while pavement 4 is in the worst condition (highest *DI*). Pavements 2 and 3 are arranged in order of decreasing condition.

Case 2

Four more pavements are shown in table 6, each again exhibiting a different combination of distress. Intuitively, pavement 8 is in better condition than pavement 5, the only difference between the two being the lower rating given for alligator cracks for pavement 5. Pavement 6 is in worse condition than pavement 5, since all the ratings for pavement 6 are less than or equal to the rating for pavement 5, except for the alligator cracks. Although pavement 6 has a better rating for alligator cracks than pavement 5, the overall rating is less, because of the lower ratings for several other distresses (particularly roughness, which is heavily weighted). The FEAPS evaluation ranks the pavements 8, 7, 5, and 6 from best to worst, as indicated by their respective distress indices.

Pavements 2 and 7 had very similar distress indices. However, they had different amounts of distress. Although pavement 2 had a much better rating for longitudinal cracks (which were weighted as "moderately important"), it had a slightly lower rating for alligator cracks (which were weighted as "very important"). This heavy weight resulted in the lower overall rating. The similarity in *DI* with pavement 7 indicates that FEAPS was able to weight longitudinal and alligator cracks properly. Pavements 1 and 8 have different amounts of transverse cracks and roughness distress, but similar distress indices. This indicates that FEAPS was able to weight these types of distress properly.

CONCLUSION

A computer program for the structural evaluation of asphalt pavements has been presented that captures the knowledge of experts and puts it in a fuzzy framework. The pavement ratings, also represented by fuzzy sets, are used as program input. The knowledge and the ratings are combined using the fuzzy weighted averaging technique in the computer program FEAPS to produce a fuzzy set that represents the pavement condition. The program provides a consistent, reliable, and facile method of evaluating pavements. As such, it provides a tool that many pavement agencies—especially those with limited resources—can use to reduce the impact of the loss of expertise during the next few years.

TABLE 6 CASE STUDY 2: FOUR PAVEMENT RATINGS

Distress	Pavement			
	5	6	7	8
Rutting	B	D	C	B
Longitudinal cracks	C	D	E	C
Transverse cracks	A	A	E	A
Alligator cracks	E	D	B	B
Roughness	C	D	B	C
Distress Index	0.55	0.70	0.41	0.35

[a] NOTE: pavement ratings made according to the following scale -
A - none
B - slight
C - significant
D - severe
E - extremely severe

ACKNOWLEDGMENTS

The authors are indebted to the asphalt pavement experts who shared their knowledge with us: E. R. Brown, R. Griffin, F. Parker, and F. Roberts.

REFERENCES

1. A. F. DiMillio. *Highway Infrastructure: Opportunities for Innovation*. ASCE, New York, 1986.
2. K. A. Godfrey. Truck Weight Enforcement on a WIM. *Civil Engineering*, Vol. 56, No. 11, 1986, pp. 60–63.
3. M. Y. Shahin and S. D. Kohn. Pavement Maintenance Management for Roads and Parking Lots. U.S. Army Engineer Construction Engineering Research Laboratory Technical Report M-294, 1981.
4. *Pavement Maintenance Management for Roads and Parking Lots*. FHWA, U.S. Department of Transportation, 1979.
5. L. A. Zadeh. Fuzzy Sets. *Information and Control*, Vol. 8, 1965, pp. 338–353.
6. C. B. Brown, J. L. Chameau, R. N. Palmer, and J. T. P. Yao, eds. *Proc., NSF Workshop on Civil Engineering Applications of Fuzzy Sets*, Purdue University, W. Lafayette, Ind., 1985.
7. A. C. Boissonnade, W. Dong, N. C. Shah, and F. S. Wong. Identification of Fuzzy Systems in Civil Engineering. *Proc., International Symposium on Fuzzy Mathematics in Earthquake Engineering*, China, 1985.
8. C. B. Brown and J. T. P. Yao. Fuzzy Sets and Structural Engineering. *Journal of Structural Engineering*, Vol. 109, No. 5, 1983, pp. 1211–1255.
9. M. Gunaratne, J. L. Chameau, and A. G. Altschaeffl. Fuzzy Multiattributes Decision Making in Pavement Management. *Journal of Civil Engineering Systems*, Vol. 2, Sept. 1985, pp. 166–170.
10. *Special Report 207: Transportation Professionals. Future Needs and Opportunities*. TRB, National Research Council, Washington, D.C., 1985.
11. R. S. Page. Transportation Education—Meeting the Challenge. *TR News*, No. 116, 1985, pp. 11–16.
12. Survey of Transit Agencies for the Transportation Professional Needs Study. American Public Transit Association. *Special Report 207: Transportation Professionals. Future Needs and Opportunities*. TRB, National Research Council, Washington, D.C., 1985.
13. Scientific Manpower Commission. *Supply and Demand for Scientists and Engineers*. Washington, D.C., 1982.
14. L. A. Zadeh. The Concept of a Linguistic Variable and its Application to Approximate Reasoning. *Information Sciences*, vol. 8, 1975, pp. 199–249.
15. *A Pavement Rating System for Low-Volume Roads*. Asphalt Institute, College Park, Md., 1977.
16. D. S. Turner, J. V. Walters, T. C. Glover, and R. R. Mansfield. *A Pavement Rating Procedure*. Report No. 112-85. Transportation Management Systems Association, University, Ala., 1985.
17. K. J. Schmucker. *Fuzzy Sets, Natural Language Computations, and Risk Analysis*. Computer Science Press, Rockville, Md., 1984.
18. C. H. Juang and D. J. Elton. Some Fuzzy Logics for Estimation of Earthquake Intensity Based on Building Damage Records. *Journal of Civil Engineering Systems*, Vol. 3, Dec. 1986, pp. 187–191.
19. C. H. Juang and S. N. Kalidindi. *Development and Implementation of a Fuzzy System for Bid Tender Evaluation on Microcomputers*. In Proc. (J. L. Chameau and J. T. P. Yao, eds.), NAFIPS, May 1987, pp. 353–373.
20. P. W. Mullarkey and S. J. Fenves. Fuzzy Logic in a Geotechnical Knowledge-based System: CONE. *Proc., NSF Workshop on Civil Engineering Applications of Fuzzy Sets*, Purdue University, W. Lafayette, Ind., 1985.
21. G. Goschi and B. Schueler. *WATFOR77 User Guide*. WATCOM Publications, Ltd., Waterloo, Ontario, Canada, 1986.

Publication of this paper sponsored by Committee on Pavement Monitoring, Evaluation, and Data Storage.

Measuring Pavement Deflections Near a Super-Heavy Overload

W. A. NOKES

Effects on in-service pavements from super-heavy overloads weighing over 2,000,000 pounds are investigated. A field study was performed in which a crack survey was conducted, pavement deflections were measured using a Dynaflect before and after overload transport, and several instruments were deployed to measure surface deflection when the overload traversed the pavement. The field study also characterized materials, determined dimensions of structural layers, and measured wheel loads applied to the pavement. Measured deflections are compared to predictions that are based on models used for flexible pavement design. Results of crack surveys show no change in the visible condition of the pavement after transporting the overloads. Dynaflect measurements after transport were approximately equal to pavement deflections measured before hauling the overloads. In-transit deflection measurements show that a "big basin" results from widely distributed trailer axle/tire loads. Deflections from tractor tires were not substantially different from those caused by trailer tires. Measured in-transit deflections agree reasonably well with maximum displacement predicted using elastic layer models.

Historical data from California's Department of Transportation (CALTRANS), which is responsible for evaluating permit and variance requests, indicate that variances are being requested for heavier loads each year. Since 1982, permits and variances for overweight loads jumped 57%, from approximately thirty-seven thousand to sixty-one thousand. A conspicuous increase is the number of permits approved for super-heavy overloads, which typically exceed 300,000 pounds gross vehicle weight (GVW). Only one permit was approved in 1983; nearly twenty were granted in 1987.

California's continuing industrial and population growth promises an increasing number of heavier loads. One reason for this trend is a lower cost associated with foreign manufacture of large components, such as chemical reactor vessels, power generators and electrical transformers. However, when large components are not fabricated on site, costs and logistics of transporting these parts become very important. When public roads are used, a crucial constraint in transporting these loads is the physical limitation of highway structures, such as inadequate bridge strength (*1*).

Effects of super-heavy overloads on pavement deserve investigation. In California, as in other states, typical overloads are limited to no more than structural load limits established for bridges and overcrossings on a route. These limits, which generally use GVW, number of axles, and axle spacing as criteria, are based on structural analysis and load equivalencies. When loads slightly exceed the criteria, engineering judgment is generally invoked to set a safe load limit. However, when no structures are traversed and GVW greatly exceeds previously permitted loads, an accurate procedure for routine evaluation is not available, and engineering experience is limited.

A field study and computer modeling analysis were conducted to investigate effects of super-heavy overloads on pavements. The goals of the investigation were to determine if any observable damage was caused by overloads; to check for invisible pavement damage; to measure pavement deflections near the loads in transit; and to compare in-transit deflections to predictions from mechanistic models.

BACKGROUND

In the spring of 1987, variances were requested to haul the two heaviest loads ever moved on a California state highway. Transporting these overloads on a state highway provided an opportunity to study in-place pavement response and short-term damage. They were to be transported on State Route 213, from the Port of Los Angeles to a refinery in Torrance, California (see figure 1). Route 213 is a four-lane, urban, principal arterial with peak hour traffic volume from 1,150 to 1,850 vehicles, and an annual average daily traffic (ADT) ranging from 19,400 to 31,000 vehicles (*2*).

The GVW of each load was estimated at 2,100,000 pounds, composed of 1,600,000 pounds from a chemical reactor vessel and approximately 500,000 pounds trailer tare. The reactors could not be transported by rail because they exceeded weight and width limits. Figure 2 shows dimensions and typical configuration of each reactor, trailers, and tractors. Table 1 shows trailer and tractor tire specifications. A total of 384 tires supported each reactor, using 24 axle lines and 16 tires per axle line. Each trailer shown in figure 2 was composed of four German-made Goldhofer trailers interconnected. These trailers have steerable axles and hydraulic suspensions that can be adjusted to maintain a balanced load during transport. Tractor GVW was approximately 110,000 pounds, composed of 62,000 pounds unladen weight and approximately 49,000 pounds from added counterweights.

Before granting variances, a reliable procedure was sought to predict pavement damage from these overloads. A literature search revealed that a Highway Research Board task force developed guidelines and recommended evaluation procedures in the early 1970s (*3*). It was recognized at that time that methods were not available for engineers to predict accurately the destructive effects of overloads on pavement. Con-

State of California Department of Transportation, Division of Construction, Office of Transportation Laboratory, 5900 Folsom Boulevard, Sacramento, Calif. 95819.

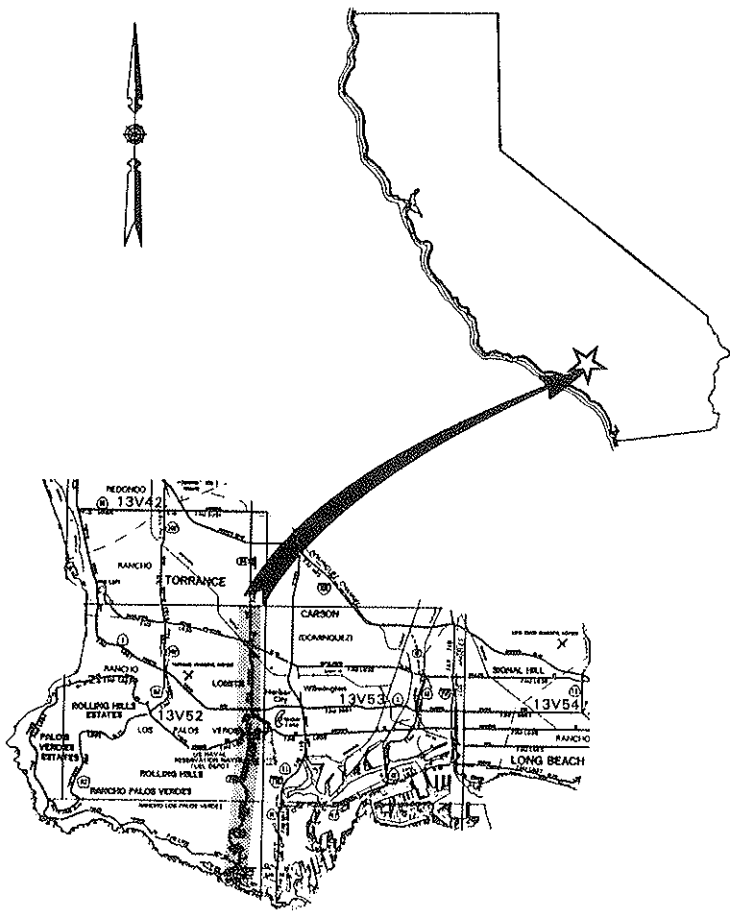

FIGURE 1 Location map for transport of overloads.

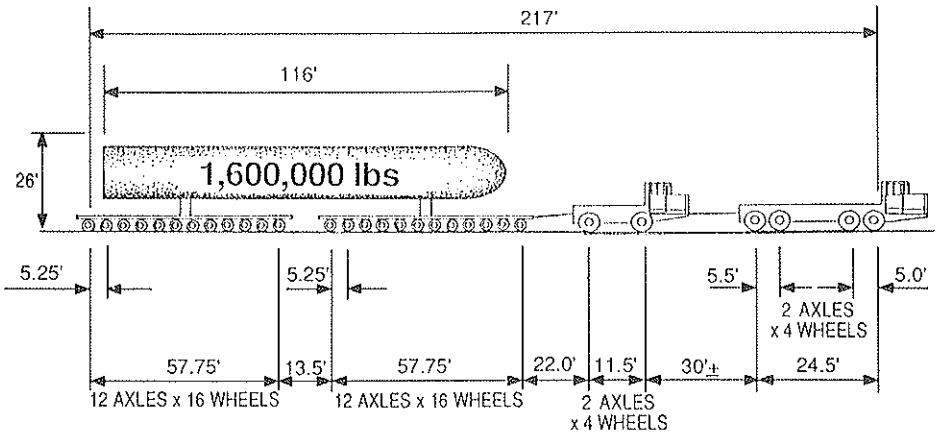

FIGURE 2 Overload configuration and dimensions.

cerns about the accuracy of predictive techniques remain to the present day.

The task force recommended a mechanistic procedure that was used subsequently in several studies (*4–6*). The mechanistic approach uses computer models and elastic layer theory to predict the allowable number of 18 kip equivalent axle load (EAL) applications on a structural section. The task force presented stress/strain limits to estimate the number of EALs that would cause failure by cracking and rutting. However, the task force warned that "it is . . . difficult to specify allowable values for stress or strain since these data are not as yet readily available from experience" (*3*). The task force's uncertainty remains justified because stress/strain response and failure of pavements under super-heavy overloads are still not known completely.

FIELD STUDY

Methodology

Concern about the uncertainties of the mechanistic approach led to a field study in which pavement response was investi-

TABLE 1 TRAILER AND TRACTOR TIRE SPECIFICATIONS

	Average Load[1] Per Tire, lbs.	Tire Size	Contact[2] Area, sq.in.	Contact Pressure, psi	Tire Pressure, psi
Trailer	5,500	8.25 x 15	60	92	70
Tractor	15,000	18.00 x 25	306	49	70

[1] Average trailer tire loads from second reactor were approximately 12% higher.

[2] Area shown has tread area of 15% (assumed) already deducted. Total area is estimated using field measurements of static contact perimeter.

gated. Observable damage was recorded by conducting a visual crack survey before and after passage of the reactors on Route 213. Comparing crack records would show visible distress caused by each reactor. Invisible damage was investigated by measuring pavement deflections using a Dynaflect before and after each reactor was transported along the route. Reduced structural strength of the highway would be inferred if Dynaflect deflections increased significantly after transporting the reactors.

To define existing structural sections along the route, district staff extracted cores a few days before the reactors were moved. Cores and a visual survey of the route were used to select roadway sections for before-and-after evaluation of pavement condition, as well to choose level test sites for in-transit measurements.

The most innovative aspect of the field study was measurement of pavement deflection near the outer trailer tires as each reactor passed sensors located on the surface. To measure in-transit deflections, a seismometer, accelerometer, and displacement tracker were deployed at test sites on Route 213. Deflections from trailers and tractors were also measured at the Port of Los Angeles. A seismometer was used in all field tests. The accelerometer and optron recorded deflections from reactor 2 only. No routine, mobile, and nondestructive procedures are available for measuring pavement displacement under these circumstances. Instrumenting a pavement section with linear variable differential transducers was considered, but time and funding constraints precluded their use. In fact, deflection was chosen as the measure of pavement response because instrumenting pavement sections with strain gauges was not feasible. Pavement deflections from an overload were measured by Mahoney (*5*) using Benkelman beams in a tandem configuration. The outside beam measured deflections at the fulcrum of the inside beam, which measured deflections near the trailer tires. This was done to compensate for the extraordinarily large deflection basin expected under all the closely spaced, heavily loaded trailer tires. Alternative methods were sought that could detect the trailer's "big basin" and that would provide a permanent record of deflections as the pavement was loaded and unloaded.

Only one instrument was used successfully when the first reactor was moved. A seismometer, that is, a velocity transducer, was evaluated at TransLab, and it showed that it could sense pavement displacement at frequencies expected from each trailer axle. A seismometer offered the distinct advantage of using the center of the earth as a reference point instead of measuring differential displacement from some fixed point nearby. Considering all constraints, it was the only readily available instrument to measure deflections from the first reactor. Several other methods were suggested, such as displacement transducers, optical precision levels, and laser transits, but none satisfied all constraints.

The seismometer used in the field study is a Kinemetrics model SS-1. Its practical minimum frequency response is 0.25 Hz. Its resonant frequency is 0.5 Hz, overshoot ratio is 0.05, and the damping factor is 0.70. Its use requires calibration factors that were determined at TransLab. Correction factors for near-resonant vibrations were provided by the manufacturer. The seismometer was linked to a Kinemetrics SC-1 signal conditioner, then to a Clevite brush 16-2300-00 oscillograph. Damping calibrations were performed prior to field measurements and seismometer calibration factors were verified at TransLab after the first reactor was moved. This system has a long history of stability and sensitivity in vibration studies conducted previously by CALTRANS personnel.

Figure 3 shows a plan view of the seismometer, event marker, and tire, as well as other instruments that were used when the second reactor was transported. A tire-triggered event marker was placed next to the seismometer to correlate loading with displacement and to check speed (i.e., frequency) of load.

The seismometer's trace of velocity with respect to time provides a record of zero-to-peak vertical particle velocity as the surface of the pavement near the tires is displaced. Displacement and velocity are related as shown below based on sinusoidal loading:

$$D = \frac{V}{\pi f} \tag{1}$$

where

D = peak-to-peak particle displacement,
V = zero-to-peak particle velocity, and
f = the frequency of sensor excitation.

Some limitations are inherent in this approach. Axles may excite the seismometer below threshold so that the sensor does not detect some displacement. This appeared to be pos-

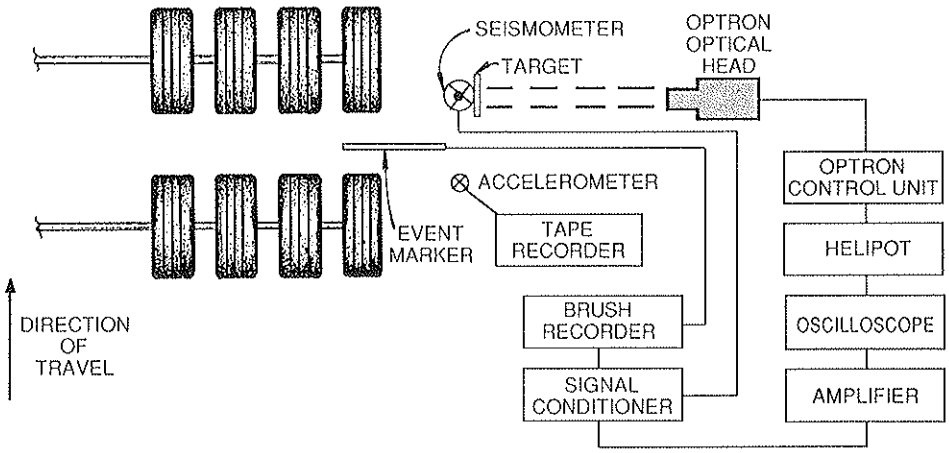

FIGURE 3 Plan schematic of instrumentation used in field studies.

sible but could not be determined without knowing the frequency of loading and the extent of deflections near the trailer tires. For example, the idealized pavement response shown in figure 4 compares one long duration, low frequency load/unload cycle under an overload to typically higher frequency axle loads from a legal-sized truck (*5*). A deflection trace for an overload is composed of repetitious displacements, which are caused by individual axle loads. These displacements are superimposed on a lower frequency cycle, which induces larger deflections than those from individual axles. These larger deflections form a "big basin" under the trailer. A seismometer was expected to detect deflections from individual axles; however, its ability to measure a "big basin" was uncertain. Another limitation is that deflections determined from the seismometer are relative displacements that are not necessarily additive. In addition, only one sensor detected data in the deflection basin. More seismometers would have been deployed had they been available.

After the first reactor was moved, there was considerable concern that substantial deflections due to the "big basin" were not detected by the seismometer. This concern was reinforced by the substantially higher model predictions (described below). These factors made it important to find instruments that were more sensitive or that could measure deflections directly.

When the second reactor was moved, two more instrument were used: a piezoelectric accelerometer and an electro-optical displacement tracker. Figure 3 shows how these instruments were deployed at the test site.

The accelerometer is a model 8318 piezoelectric sensor manufactured by Brüel and Kjaer (B&K) Instruments, Inc. Frequency response for the accelerometer is 0.1 Hz to 1 kHz. Deflections from the accelerometer were recorded on a B&K 7005 tape recorder. Frequency response on the tape recorder is 0 to 12.5 kHz. Recorded data were subsequently evaluated on a B&K dual channel signal analyzer, type 2034. Frequency range of the analyzer is 0 to 25.6 kHz.

A trace of pavement surface acceleration with respect to time provides a record of zero-to-peak vertical particle acceleration as the surface is displaced. Displacement and accel-

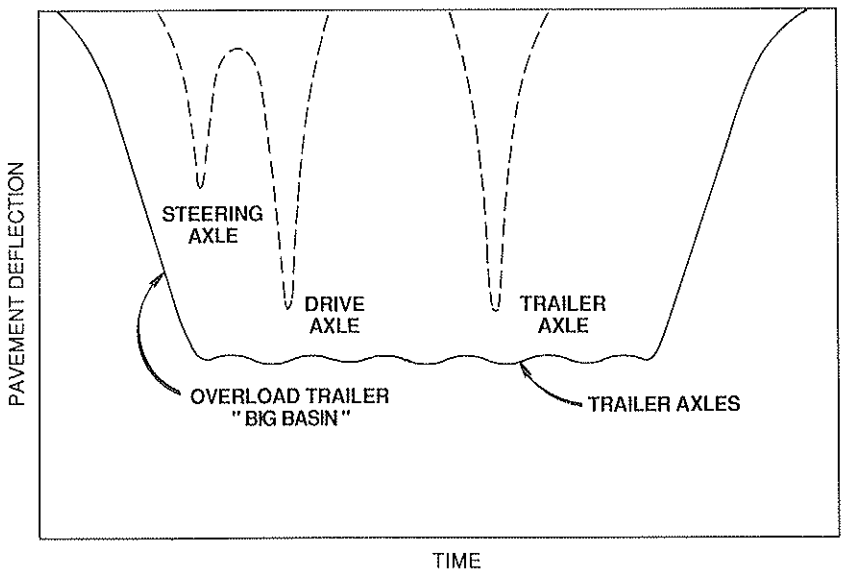

FIGURE 4 Idealized pavement response for super-heavy trailer and a typical truck.

eration are related as shown below based on sinusoidal loading:

$$D = \frac{A}{2\pi^2 f^2} \tag{2}$$

where

D = peak-to-peak particle displacement,
A = zero-to-peak particle acceleration, and
f = the frequency of sensor excitation.

The electro-optical displacement tracker, or optron, consists of a model 805M optical head and model 501 control unit, manufactured by Optron Corporation, Woodbridge, Connnecticut. The optron is used for production and testing by companies such as IBM, Xerox, Ford, and General Motors. It has been used for research at the National Aeronautic and Space Administration, Rutgers University, the University of Southern California, and by the U.S. armed forces.

Frequency response of the optron is from DC to 25 kHz. Changeable lenses allow measuring displacements with the optical head as close as 2.6 inches or as remote as 704 feet from the target. Resolution of displacement is 0.0008 inch (0.8 mils) at 11 feet, which was the distance used during this field study. The optron was linked, via other instruments shown in figure 3, to a Kinemetrics SC-1 signal conditioner, then to a Clevite brush 16-2300-00 oscillograph.

Optron displacement trackers follow the motion of a discontinuity in the image of a moving object, which in this study was a black-over-white rectangular target attached to the seismometer. The image of the target is focused on the photocathode of an image dissector tube in the optical head (see figure 5). Electrons are emitted from each point of the photocathode in proportion to the image's light intensity. The resulting electron image is refocused on a plate with a small aperture. Electrons traversing the aperture form a signal current proportional to the intensity at the corresponding point of the target. The signal is amplified and is used by a patented servo loop to keep the electron image of the target centered on the dissector aperture. As the optical target image moves, the servo control changes the current in deflecting coils so that the electron image returns to its initial position. The deflection current required to recenter the electron image corresponds to displacement of the target.

The optron offers several advantages, including direct measurement of displacement and capability of measuring DC, eliminating concerns about frequency response. It therefore has the best chance of recording displacements due to a "big basin." The optron can document pavement response during loading and unloading, providing evidence of plastic deformation if it did not rebound to its preloaded level. The target, which is expendable, can be placed closer to a tire than an expensive accelerometer or seismometer. Using the optron does have disadvantages: it is sensitive to light intensity, and the displacement record ceases if the light beam from the target is broken. Calibration of the sensitive optron can be difficult and should be performed at the test site.

In addition to measuring deflections on the highway as the reactors passed, pavement deflections were measured using the seismometer at the Port of Los Angeles before the second reactor was moved. Measurements were recorded near the trailer as it was hauled past the seismometer. Later, the trailer was detached and only the tractor passed close to the seismometer.

The purpose of measurements at the port was to compare deflections near the trailer with those near the tractor. Terrel and Mahoney (*4*) used mechanistic procedures to conclude that high tractor tire loads could be more damaging than tire loads from a trailer. It was hoped that measurements at the port would provide a rough comparison of pavement deflections under tractor and trailer tires.

Data Analysis

For reactor 1, a site to measure pavement response during the move was chosen at post mile (PM) 2.28. The structural section at this site is 0.4 foot asphalt concrete (AC) pavement, 1.3 feet untreated aggregate base, over damp silty clay. Peak hour traffic volume is 1,150 and annual ADT is 19,400 vehicles (*2*). California's Pavement Management System (PMS) contains condition survey data that were collected in 1985 along this section of Route 213. The PMS indicates that a maximum of 15% of one wheel path and 8% of both wheel paths exhibited alligator cracks. The 1985 survey also showed minor bleeding and no ruts greater than ¾ inch.

The condition survey showed no discernible difference in the pavement surface after the first reactor passed. The survey was done the afternoon before and the morning after the reactor was moved. Dynaflect measurements show substantially the same deflections before and after the reactor was

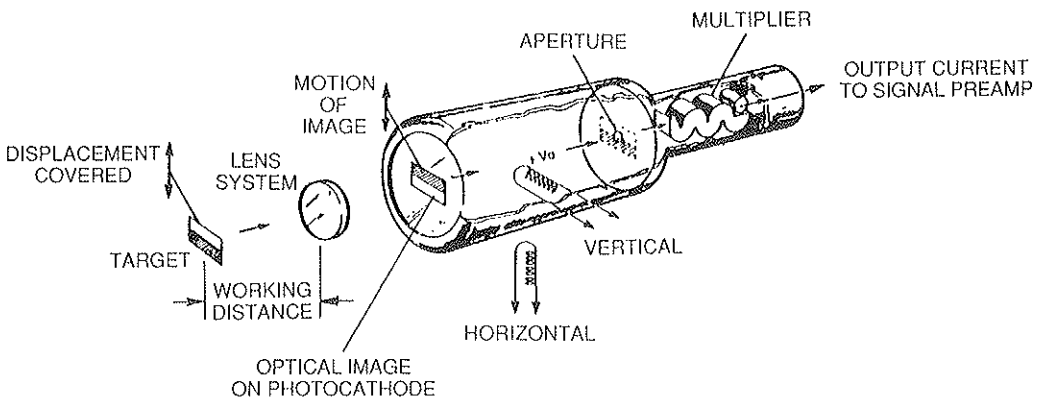

FIGURE 5 Components of optron optical head.

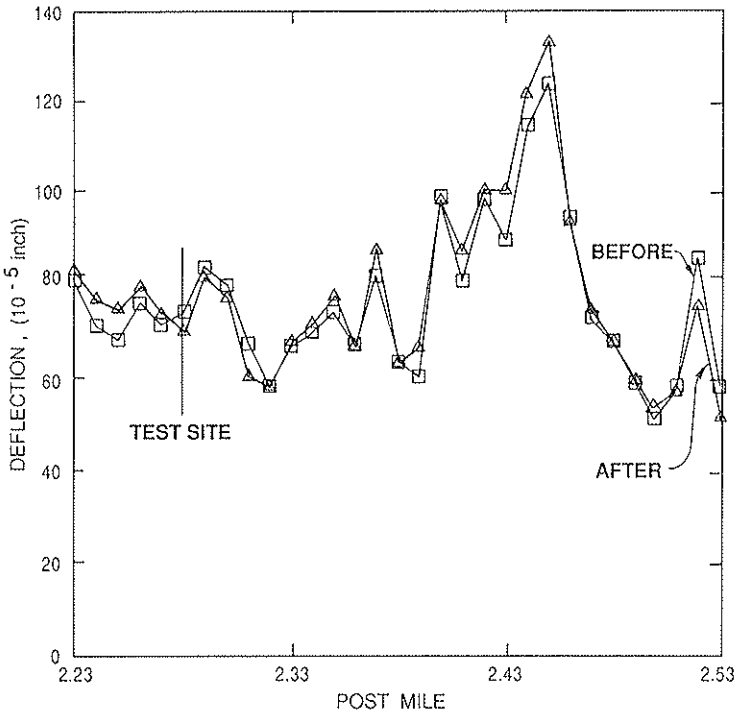

FIGURE 6 Sensor 1 Dynaflect deflections before and after moving reactor 1.

moved. Figure 6 shows sensor 1 deflections measured at PM 2.23–2.53. Before moving the reactor, deflections were measured when air temperature was 65°F and pavement temperature was estimated at 65°F under clear skies. These conditions are typical at the site during the spring (*7*). Deflections were later measured when air temperature was 70°F and pavement temperature was estimated at 90°F under sunny skies. Deflections were corrected for differences in temperature using the American Association of State Highway and Transportation Officials design guide for 1986 (*8*). Mean daily temperatures for the preceding five days were obtained from the Long Beach airport.

Deflections were measured at PM 2.23–2.53, 2.80–3.10, and 5.88–6.18 in the early morning before the reactor was transported. Deflections were measured again at the same sites in the late morning after the reactor was moved. Dynaflect measurements were recorded by a driver as another technician walked alongside to paint spots on the pavement where sensor 1 deflection was measured. After the reactor was moved, the walking technician spotted the Dynaflect to assure sensor 1 measurements were recorded on the same spots.

Results of the condition survey and Dynaflect measurements indicate that either no short-term damage occurred or else damage was not detectable using these methods. In addition, pavement response during loading is unknown. The third component of the field study, measuring in-transit deflections, provides this useful information.

The seismometer successfully measured deflections as the first reactor passed the test site. Table 2 summarizes pertinent data from in-transit measurements. The first trailer passed at a constant distance from the seismometer. The second trailer veered substantially more than the first, which seemed unfortunate initially. However, deflections closer to the tires were measured as a result. The frequency at which the individual trailer axles/tires passed was well above the minimum detectable by the seismometer. Air temperature was approximately 65°F and pavement temperature was estimated to be 75°F. The event was recorded on videotape for later verification of distances and speeds during the trailer's passage.

Pavement deflection data were studied to examine how displacement varied with distance and to estimate displacement under the outer trailer tires. Deflection data and a least-squares regression line are shown in figure 7. Pavement deflection under the outer trailer wheel is estimated to be 29 mils, although adjustments of the regression line within the confidence limits would alter this value. Figure 7 shows 95% confidence limits as dotted lines above and below the regression line. The correlation coefficient is significant at a 99% confidence interval using a two-tail test (*9*).

The seismometer velocity trace is depicted in figure 8. The abscissa shows the number of seconds since the recorder was turned on. Figure 8 shows a scale for peak vertical velocity also. Axle 9 on the second trailer caused a deflection that was unreadable. Axle 11 grazed the seismometer, which is why the trace jumped off scale. A subsequent check of the seismometer's calibration indicated no significant change.

The seismometer trace generally agrees with the pattern of deflections expected from individual axles shown for an overload trailer in figure 4. The repetitious velocity shifts in figure 8 correspond to deflections induced by individual axles. The seismometer data do not indicate additional deflection expected from a "big basin," however. Assuming that such a basin did in fact exist, the rate of pavement displacement probably occurred below the detection level of the seismometer.

For reactor 2, a site was chosen at PM 5.90 to measure

TABLE 2 SUMMARY OF IN-TRANSIT SEISMOMETER MEASUREMENTS

	Distance, feet		Deflection, mils		Average Vehicle	Frequency of Loading, Hz	
	Range	Mean	Range	Mean	Speed, mph	Range	Mean
REACTOR #1							
(PM 2.28)							
1st Trailer	2.0	2.0	1.6 - 2.3	1.9	3.8	0.98 - 1.12	1.06
2nd Trailer	0.2 - 1.0	0.6	6.5 - 24.5	12.7	3.8	0.82 - 1.19	1.07
REACTOR #2							
(PM 5.90)							
1st Trailer	2.5 - 3.0	2.8	0.5 - 1.1	0.6	3.0	0.80 - 0.90	0.84
2nd Trailer	2.3 - 3.2	2.8	0.4 - 1.3	0.6	3.4	0.90 - 1.00	0.96
REACTOR #2							
(Port)							
Run 1 -							
1st Trailer *	2.0	2.0	1.3 - 2.3	1.9	1.8	0.50	0.50
2nd Trailer	2.0	2.0	1.0 - 3.7	2.7	2.1	0.50	0.50
Run 2 -							
1st Trailer	3.2 - 3.9	3.5	0.5 - 1.3	0.8	4.4	2.50	2.50
2nd Trailer	0.8 - 3.0	1.3	1.4 - 9.3	6.4	4.6	1.14 - 1.39	1.28
Tractor **							
Front Axle	2.7 - 5.2	3.6	0.20 - 2.0	1.2	3.7	0.89 - 2.50	1.50
Rear Axle	2.7 - 5.2	3.6	0.3 - 3.8	1.8	3.7	0.72 - 1.39	0.99

* Average wheel load on trailer was approximately 6,200 lbs/tire.

** Average wheel load on axle 1 was approximately 12,800 lbs/tire. For axle 2, average load was 16,000 lbs/tire.

pavement response during passage of the reactor. The structural section at this site is 0.2 feet AC, 0.65 feet portland cement concrete pavement (PCCP), over fine, brown silty sand. Traffic at the site is typical for this route, peak hour traffic volume is approximately 1,200, and annual ADT is estimated at 20,400 vehicles (*2*). The PMS contains condition survey data that were collected in 1985 along this section of Route 213 and indicates that 16% of one wheel path and 6% of both wheel paths showed alligator cracks. The 1985 survey also showed localized bleeding and no ruts greater than ¾ inch.

As before, the pavement condition survey showed no discernible difference in the pavement surface from transporting the second reactor. The survey was done the morning before and the morning after reactor 2 was moved. Dynaflect measurements again show similar deflections before and after reactor 2 passed. Figure 9 shows sensor 1 deflections measured at PM 5.92–6.22. Dynaflect deflections measured before hauling the reactor were recorded when the air temperature was 80°F and pavement temperature was 85°F under clear skies. Deflections measured after the reactor passed were taken when the air temperature was 65°F and pavement temperature was 69°F under hazy skies. Again, these are typical spring conditions at the site (*7*). Deflections again were adjusted for differences in temperature (*8*). A wider difference between before and after deflections is partially attributable to a more complex response of overlaid PCCP to temperature changes. In addition, joints and cracks that were not visible in the underlying PCCP may have affected deflections.

Deflections were measured midday before reactor 2 was

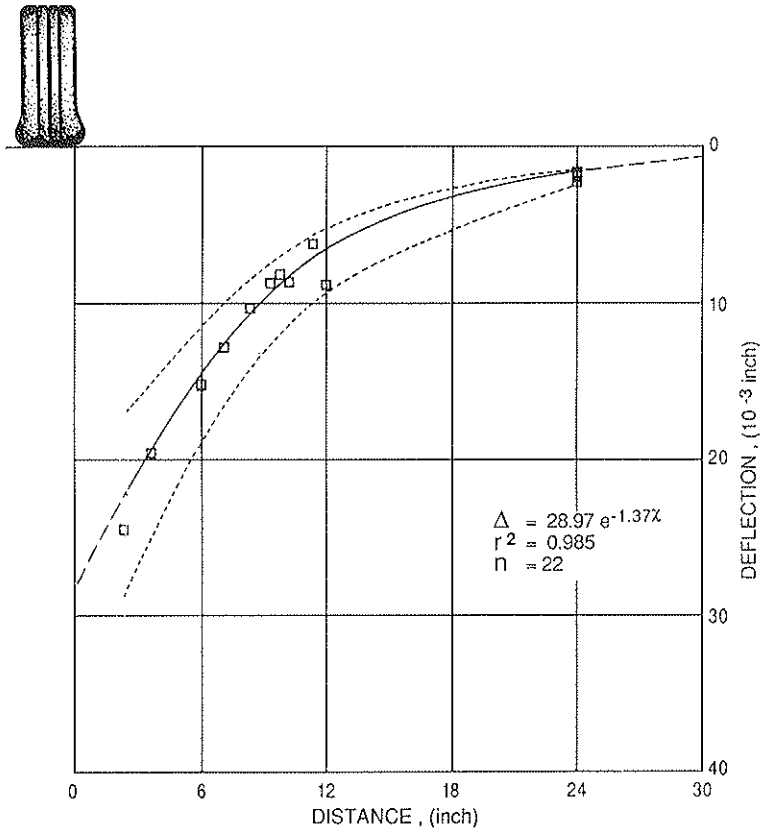

FIGURE 7 Pavement surface deflections near outer trailer tires for reactor 1.

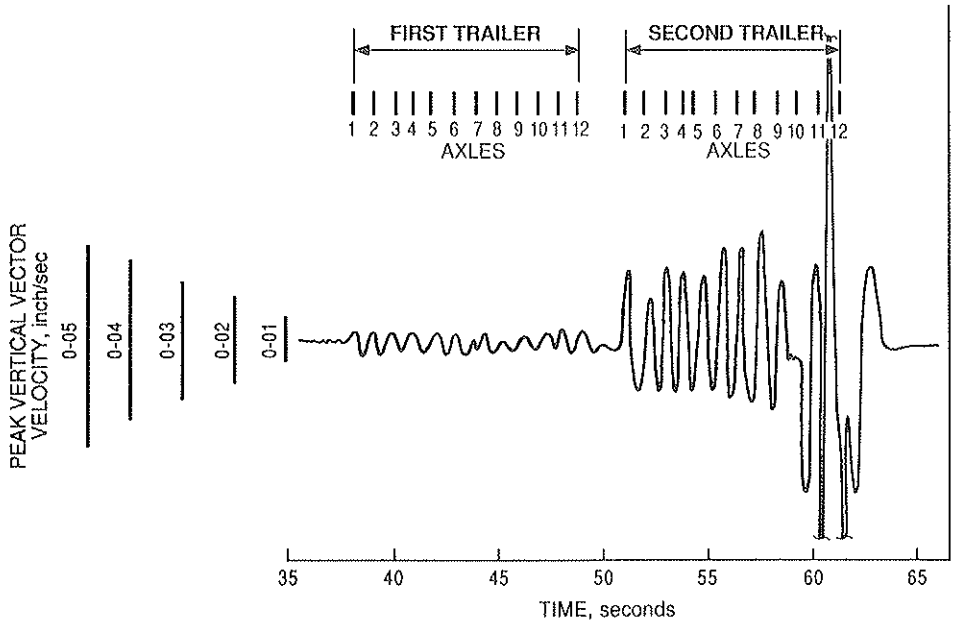

FIGURE 8 Seismometer velocity trace.

moved and the morning after. Deflections were measured at PM 5.40–5.70, 5.92–6.22, and 7.00–7.30. Unlike the first study, Dynaflect measurements were taken by only one technician. He judged from the driver's seat how close sensor 1 was to its previous locations. This probably caused some of the difference between before-and-after measurements mentioned above.

As was the case with the condition survey and Dynaflect results for the first reactor, either no short-term damage occurred or damage was not detectable by these means.

All instruments successfully measured deflections from the second reactor. Table 2 shows pertinent in-transit data for reactor 2. Frequency of tire load application varied from 0.80 to 0.90 Hz, which is above the minimum frequency detectable

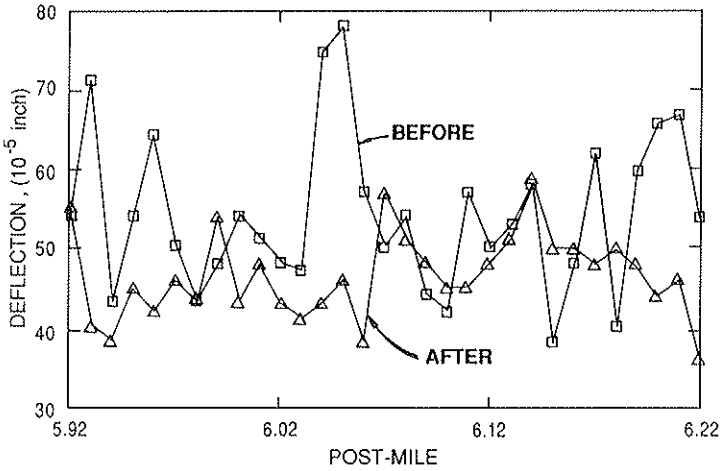

FIGURE 9 Sensor 1 Dynaflect deflection before and after moving reactor 2.

by the seismometer and accelerometer. Air temperature was approximately 65°F and pavement temperature was measured at 70°F when the reactor passed.

The optron deflection trace shown in figure 10 provides evidence of a "big basin." Displacements inferred from seismometer velocities are depicted superimposed on the optron trace, assuming that it represents mean deflection. Optron deflections were typically three to four times the displacement detected by the seismometer. The ratio of optron/seismometer measurements is important to discussions presented later in this paper. The optron trace clearly shows a slow displacement occurring during three to four seconds as the first trailer axle approached the target; no deflection is evident based on the seismometer trace during this time. After the last axle passed, the seismometer almost immediately returned to zero, although the optron shows that rebounding continued for nearly eight seconds. The optron trace shows that the target returned to its initial position.

Preliminary analysis of accelerometer data showed general agreement with the optron in detecting the "big basin." These data are being studied further. The accelerometer data also show some higher frequency vibrations. It was concluded that the accelerometer bounced slightly on the pavement as the tractor and trailers passed, probably because of its light weight (470 grams). Displacements due to these vibrations were filtered in computing deflections.

Pavement deflections again were studied as a function of distance from tires. Least-squares regression did not show the good correlation that was seen for the first reactor. Poor correlation is likely caused by the consistent remoteness of the trailer wheels from the sensors and by dissimilar response of the AC overlay and PCCP layers. Unobserved joints and cracks probably also contributed to this response. Peak deflection was not estimated for this test site.

To compare effects from tractor tires to those from trailer tires, deflections were recorded near berth 131 at the Port of Los Angeles. The structural section where deflections were measured is 9 inches AC over 8 inches untreated aggregate base on compacted silty sandy clay (*10*). No surface cracking or rutting was evident in the test area. Air temperature during the test was approximately 75°F, and pavement temperature was estimated to be 100°F.

The seismometer successfully measured deflections from trailer and tractors at the port. Deflection data from the trailers and tractors are shown in table 2. Deflections and distances were well-distributed during run 2 and are the basis of the

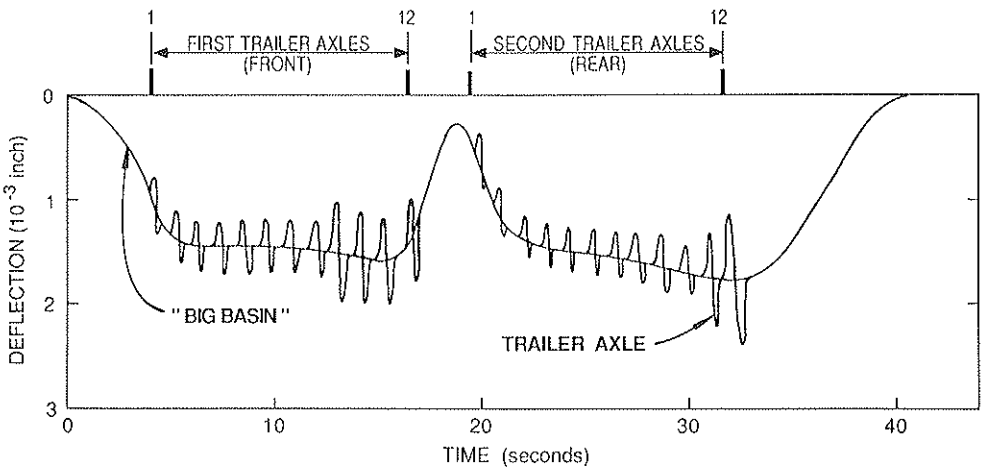

FIGURE 10 Optron displacement showing superimposed deflections from seismometer trace.

regression line shown in figure 11. For run 1, consistent deflection levels resulted from the minor change in distance from the tires to the sensor. In addition, frequency of axle loadings was near the seismometer's resonant frequency. Therefore, these data were not included in the least-squares regression analysis and are not shown in figure 11. The tractor made several passes at roughly equal speeds. Figure 11 shows deflections and distances from the tractor tires. Unfortunately, tractor tires came no closer than 2.7 feet to the sensor because of concerns about hitting the seismometer.

Figure 11 provides a rough comparison of deflections that resulted from trailer and tractor tires. It also shows a regression line and 95% confidence limits for deflections from trailer tires. Most of the tractor-induced deflections fall close to the regression line for displacements from the trailers. A least-squares regression line is not shown for the tractor data because of the few number of deflections measured at a limited range of distances.

The trend in deflection shown in figure 11 is similar to that in figure 7. Deflections are close to those from reactor 1. Pavement deflection under the outer trailer wheel is estimated to be 18 mils. Once again, adjustments of the regression line within the confidence limits would alter this value substantially. The correlation coefficient is significant at a 99% confidence interval using a two-tail test (*9*).

Deflections from tractor tires are not substantially higher than displacements from trailer tires at the distances measured. Figure 11 shows that deflections from the tractor's rear axle were higher than for the front. The rear axle was about 25% heavier because the counterweight was carried toward the back of the tractor. Figure 11 also shows that most of the deflections from the tractor's rear axle are significantly higher than displacements from trailer wheels. Based on seismometer data, deflections close to the tractor tires could be inferred to be several times higher than those measured close to trailer wheels. However, it is believed that deflections from tractor wheels were not significantly higher. In fact, peak deflections may be very close, if seismometer deflections from the trailer are increased by a factor of three to four. This increase is based on the ratio of optron/seismometer measurements discussed previously and assumes that seismometer measurements of tractor-induced deflections do not need adjustment. Similar deflections for tractors and trailers are likely due to the fact that, even though tractor wheel loads were two to three times as heavy as trailer tires, lower contact pressures (from larger contact area—see table 1) occur under the tractor tires. Levels of stress, strain, and shear induced by trailer and tractor tires remain unknown but should be investigated.

MECHANISTIC MODELING

Model predictions that were used initially to evaluate the variance request were subsequently compared to measured deflections. In this way, measurements served as a verification database. Field verification of model predictions could eventually yield a sufficiently accurate mechanistically-based procedure for routine evaluation of variance requests.

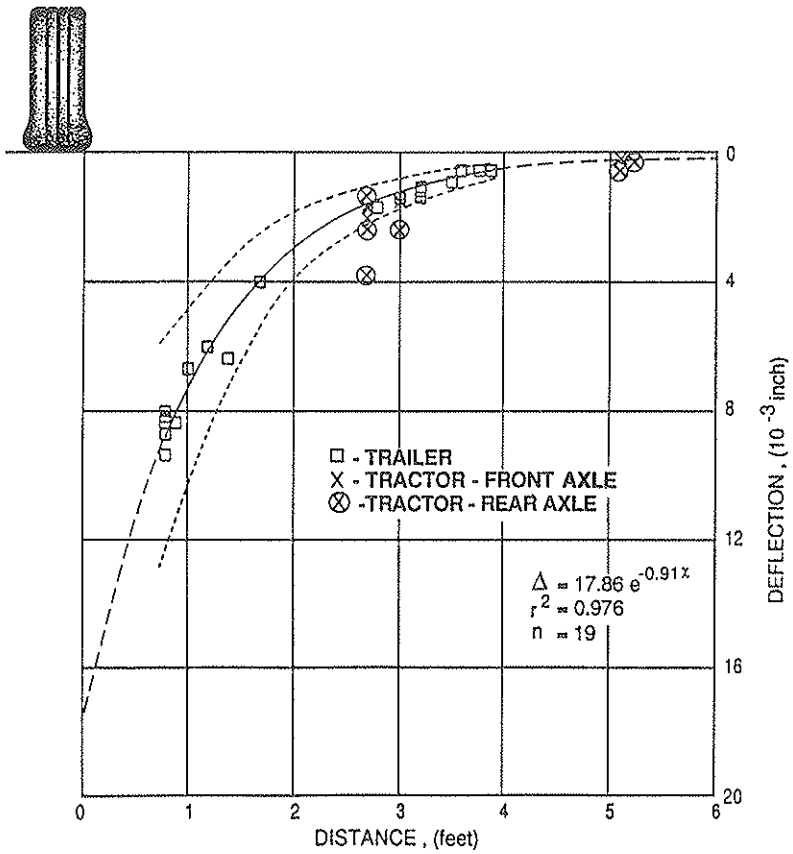

FIGURE 11 Pavement surface deflections near outer tires of trailer and tractor.

TABLE 3 INPUTS USED FOR COMPUTER MODELS

Layer	Thickness	Poissons Ratio	Resilient Modulus, ksi	
			Best Case	Worst Case
1-ACP	5"	0.40	1,000	500
2-Base	5"	0.35	35	25
3-Base	5"	0.35	30	20
4-Base	5"	0.35	25	15
5-Subgrade	∞	0.35	10	4

Wheel Load

Load:	5,500 lbs/tire
Contact Area:	55 in^2
Contact Pressure:	100 psi

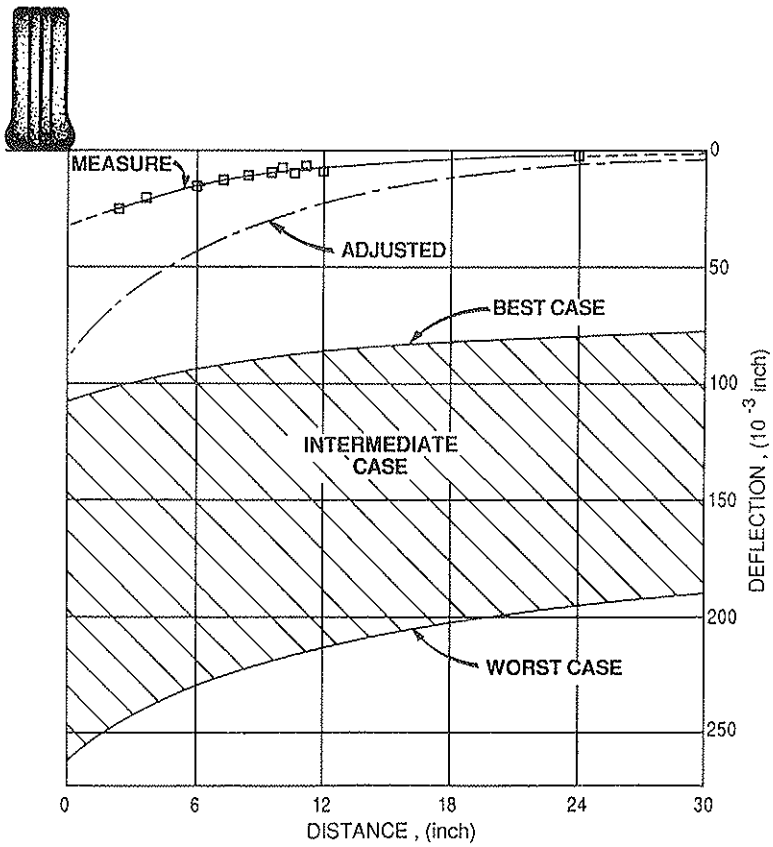

FIGURE 12 Predicted, measured, and adjusted pavement surface deflections near outer trailer tires for reactor 1.

Measurements recorded when the first reactor was moved were compared to predictions from elastic layer computer models. Computer modeling was not done for the second reactor, because a computer model for rigid pavement was not available. Deflections measured at the Port of Los Angeles were not modeled due to substantial uncertainty about material properties used in the test area (*10*). Model predictions were used to set seismometer signal attenuation prior to the field study and are presented here for a comparison to subsequent seismometer and optron measurements.

Predictions were obtained using ELSYM5 and BISAR computer models, which rely on elastic layer theory and simplifying assumptions to calculate primary response (*11, 12*). Structural section geometry was characterized using data from

cores. Load inputs were based on information from the transporter. Best- and worst-case scenarios were developed using estimated materials properties (*6, 13*). Table 3 shows inputs used for model predictions. Figure 12 shows measured data and predicted deflections under best- and worst-case scenarios.

Generally poor correlation in magnitude of predicted-to-measured deflections is shown in figure 12, although the gradient of deflections is similar for measurements and predictions. A likely reason for systematic overprediction is incorrect characterization of materials properties and conditions (such as resilient modulus, moisture content, and density, among others).

Another reason for poor correlation is that the seismometer detected only localized deflections caused by each passing axle and missed the "big basin" deflection. For example, when the second reactor was moved, the optron recorded deflections that typically were three to four times higher than those detected by the seismometer. The optron's sensitivity to direct displacement allowed it to record slow loading and rebounding that the seismometer could not detect. The "adjusted" deflection line shown in figure 12 results if a factor of three is multiplied times the seismometer regression line. This "adjusted" line represents an estimate of deflections that the optron likely would have measured. It nearly intersects the best case line at the ordinate axis, where the maximum deflection occurs.

A more accurate determination of the ratio of optron displacement to seismometer deflection is not possible with these data, but three appears to be a reasonable minimum. Detection of displacement by the seismometer should have been very similar for both reactors since load frequency for both reactors was approximately 1 Hz, which is well above the minimum frequency detectable by the seismometer. In addition, air and pavement surface temperatures were nearly identical when each reactor passed by. It is unclear, however, how the PCCP at the second site influences this ratio.

CONCLUSIONS

1. Results from the condition surveys do not show any discernible short-term damage to the pavement after the reactors were moved. Damage may have occurred that is simply not detectable by these means.
2. Measurements from the Dynaflect reveal that pavement deflections are not perceptibly different from those recorded before the reactors traversed Route 213.
3. Deflections measured near the tires must be evaluated in light of the instruments used to detect them. Seismometer deflections provide a good estimate of localized deflections due to individual axles. However, optron data show a "big basin" under the trailers that the seismometer did not detect. The accelerometer appears to have detected this basin also. Optron deflections were a minimum of three times the displacements detected by the seismometer.
4. Deflections from the tractor tires were not substantially different from those caused by trailer tires. However, the optron was not available to verify or augment these measurements.
5. Mechanistic models yielded conservative estimates of seismometer deflections. Predicted maximum deflection is close to measured deflection when seismometer data are adjusted by a factor of three, which is the ratio of optron/seismometer measurements.

RECOMMENDATIONS

1. Condition surveys should be used to evaluate visible effects from overloads but should not be the sole basis of investigating damage.
2. A Dynaflect or other nondestructive instrument should be used to detect invisible damage. Backcalculation of layer moduli should be further studied for evaluating changes in material conditions after passage of super-heavy overloads. Laboratory and field analyses (such as resilient modulus, moisture content, and density, among others) should be a part of future investigations.
3. Further research will be conducted to compare instruments used for in-transit measurements. A seismometer should not be used for loads that move as slowly as those described herein. Use of an accelerometer and optron should be further investigated for measuring deflections induced by slow moving loads. The optron will be correlated to seismometer response and used for further pavement research.
4. Accelerated pavement failure due to excessive stresses and strains from super-heavy overloads should be investigated. Better understanding of failure mechanisms from such overloads ultimately will improve the accuracy of mechanistic-based predictions.

ACKNOWLEDGMENTS

This study was conducted in cooperation with the FHWA. The author wishes to express special appreciation to Rudy Hendriks for assistance and guidance in this project and to Dick Wood, Eugene Lombardi, and other CALTRANS staff for their help conducting field studies. Additional appreciation is extended to Carl Monismith for lending his expertise and to Jorge Sousa for encouraging preparation of this paper. Special thanks go to Marti Garcia-Corralejo for typing and editing.

REFERENCES

1. D. O. Wells. *Super Heavy Transportation*. C&H Transportation Co., 1984.
2. *1986 Traffic Volumes on the California State Highway System*, California Dept. of Transportation, 1986.
3. *Highway Research Circular Number 156: Transporting Abnormally Heavy Loads on Pavements*. HRB, National Research Council, Washington, D.C., May 1974.
4. R. L. Terrel and J. P. Mahoney. Pavement Analysis for Heavy Hauls in Washington State. *Transportation Research Record 949*, TRB, National Research Council, Washington, D.C., 1983, pp. 20–31.
5. J. P. Mahoney. *A Study of Heavy-Haul Trailer Effects on a Pavement Structure*. Department of Civil Engineering, University of Washington, 1986.
6. C. L. Monismith. *Analysis of Proposed Overload Haul on California State Highway*. Department of Civil Engineering, University of California, 1984.

7. *Climatological Data, California (1984–86)*. National Oceanic and Atmospheric Administration, National Weather Service, Vols. 88–90.
8. *AASHTO Guide for Design of Pavement Structures, 1986*. American Association of State Highway and Transportation Officials, 1986.
9. J. B. Kennedy and A. M. Neville. *Basic Statistical Methods for Engineers and Scientists*. Harper & Row, 1976.
10. Richard Davidson. Personal communication with author. Mechanical Section, Port of Los Angeles, 17 July 1987.
11. ELSYM5 Code and Documentation, University of California, Berkeley.
12. D. J. DeJong, M. G. F. Peutz, and A. R. Kornswagen. *Computer Program BISAR, Layered Systems Under Normal and Tangential Surface Loads*. Report AMSR 0006.73. Koninklijke/Shell Laboratorium, Amsterdam, The Netherlands, 1973.
13. R. D. Barksdale and R. G. Hicks. *Special Report 140: Material Characterization and Layered Theory for Use in Fatigue Analyses*. HRB, National Research Council, Washington, D.C., 1973.

The State of California does not endorse products or manufacturers discussed in this paper. Trade or manufacturers' names appear herein only because those identifications are considered essential to this paper.

Publication of this paper sponsored by Committee on Pavement Monitoring, Evaluation, and Data Storage.

Some Approaches in Treating Automatically Collected Data on Rutting

C. A. LENNGREN

New methods of collecting data on pavement rutting have enabled a more extensive use of this distress for pavement maintenance. However, rut depth is merely an indicator of road rideability and does not itself provide enough information on the cause of pavement rutting. A statistical analysis of longitudinal variation of rut depth may indicate whether a certain layer is deformed, compacted or abraded. Traffic and environmental data seem to be needed for feasible analyses. Measurements repeated three times a year or more will certainly indicate if rutting can be attributed to studded tire wear, and one may also infer from these measurements when deformation during hot days occurs. Deep-lying deformations may be related to wet seasons or freeze-thaw cycles. Finally, by comparing certain properties of transversal profiles, such as how wide and how far apart the wheel tracks are, one may have a good basis for taking the right maintenance actions as the distress itself reflects the cause of it. In order to do so, it is imperative that the resolution be adequate both transversally and longitudinally. If this is the case, the profile evaluation method seems to be most appropriate when climate, subgrade, pavement and traffic data are scarce.

An appropriately designed, constructed, and maintained road will eventually wear down due to climate and traffic. This ageing can be recognized in flexible roads as fatigue cracking and pavement rutting. In a very generic way, one may consider the former distress typical for asphalt concretes with hard binders and, consequently, one associates rutting with soft binders.

Pavement rutting usually refers either to deformation or compaction by heavy wheel loads in one or more layers. Abrasion by studded tires is often included in this definition, largely because the adverse effect on traffic seems similar, that is, one may quantify the maximum rut depth as a term in the serviceability index (PSI). In this context, rutting will refer to the phenomenon of longitudinal depression of the road surface, whatever its cause.

However, the cause of rutting is not unimportant. Different causes will most certainly engender different maintenance actions. Furthermore, assuming that the maximum depths are the same, ruts caused by compaction of a deep-lying layer are not as severe for traffic as are deformation ruts near the surface. Ruts from studded tire wear may be very difficult to master, because they are often narrow and have steep edges. The extra wear and tear on pavements and tires inherent in such ruts make repair actions feasible when they are shallower than the other causes of rutting.

Over the years, rut depth has been considered in assessing the quality of road sections and whether to take maintenance actions. Typically, a rut ½ inch deep would yield routine maintenance, and a rut ¾ to 1 inch deep would render an overlay. Some confusion prevails regarding the definition of the depth. In the AASHO road test, for instance, a rather short (4 foot) straightedge was used. By increasing the base (length of the straightedge), up to 30% greater depths may be recorded (*1*). The accuracy and frequency of measurements may also affect the result. It is evident, however, that manual measurements are extremely tedious and that rut depth is of little significance in the PSI formula as long as it is fairly moderate. Therefore, a visual estimate is often considered sufficient for rating purposes, especially where relatively hard binders are used and rutting is of little or no significance.

In regions where softer binders are used, typically where great temperature differences occur, rutting may be the dominating distress, as well as a good indicator of the state of the road. In sections with much studded tire traffic, ruts develop which are directly related to the number of passing studded tires. Low-volume roads with thin asphalt-bound layers are also susceptible to rutting. Carefully estimating the extent, severity, and type of rutting for these road categories is essential to sound pavement management.

In the wake of tedious manual measurements, various types of equipment have been developed, many of which are electromechanical. Ultrasonics, interferometers, and lasers have recently been used either to obtain a reliable profile (standing still) or to acquire data at high speeds on entire roadnets. Much of the data can be stored and treated in ways that make it possible to judge road distress more delicately than as a mere value of maximum depth within a profile.

It is important to determine the initial cause of a rut. In some cases, this may be simple, especially if construction, maintenance, climate, and traffic data are known. However, in most cases, different factors combine to cause ruts, making a mathematical model desirable that contains all possible combinations.

This modeling provides several options that use the parameter depth. Depth, as such, is often considered the third dimension, with length and width the first and second dimensions. Time is generally denoted as the fourth dimension. Relating these dimensions to depth may indicate the type of distress. Using all four dimensions might provide feasible guidelines for further maintenance strategies.

Royal Institute of Technology, Department of Highway Engineering, S-100 44 Stockholm, Sweden.

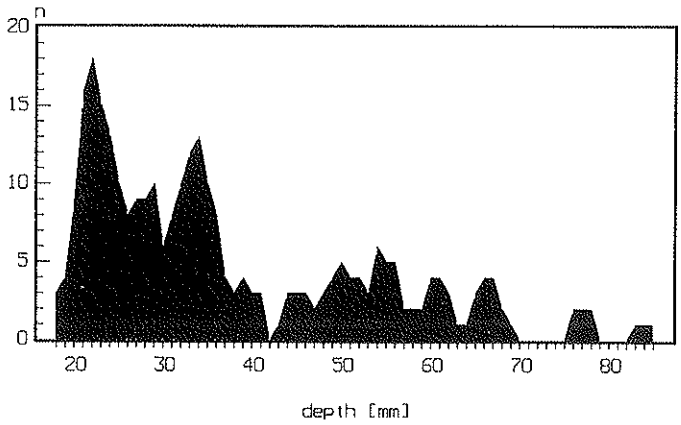

FIGURE 1 Frequency diagram of rut depth: low volume road.

VARIATION OF MAXIMUM RUT DEPTH ALONG A SECTION

The variation of rut depth along the road (i.e., along the third and first dimensions) can be utilized in an analysis because studded tire wear is lengthwise more uniform than are deformations, at least when no excessive traction, side, or braking forces are applied. Pavement deformation is a much more temperature-dependant variable, and therefore variation is likely to occur due to shadows and different materials in the road structure.

Because materials also vary lengthwise, a good record is required of what is in the road. If rutting results from deformations lying deep in the structure, a thin asphalt pavement might sustain a certain degree of deformation and then crack, giving way to even more deformation. A frequency graph of rut depths may show two maxima, one for the uncracked portion and one for the parts with thoroughly propagated cracks. If the process is allowed to continue, the asphalt layer will crack in all directions, a typical fatigue crack pattern will occur, and the bound layer will no longer be able to provide load distribution support to the underlying layers. In such cases, a third group of ruts may be agglomerated around a still deeper value, which is illustrated in figure 1. In this particular case, maximum depths were measured every meter over a 100 m section of road with no apparent variation of subgrade and pavement properties. A millimeter precision of classes and a moving average of three measurements is presented in the figure. Thus, the influence of macrostructure is suppressed.

A different example from a high-volume road is shown in figure 2. In this case the bound layers were roughly a foot (300 mm) thick together, and no cracking was evident. Consequently, the rut depth does not vary greatly, even though the average is as high as an inch (25 mm).

The differences in thickness in the examples above may be detected statistically by calculating the second, third and fourth moments of distribution. A low-volume road having a thin pavement yields high variance and skewness values but a low kurtosis. A high-volume road having a more symmetrical distribution is less skewed. It is understood that these quantities may also be useful in determining a criterion for overlay and routine maintenance, especially for thin pavements.

In the above examples, measurements were carried out manually along every meter of the sections. With automatically collected data, the sampling rate could be more frequent. It is not known if a higher sampling rate would improve the statistical data or if a lower resolution could be permitted without deteriorating it. An appropriate rate can be determined by autocorrelating various sample rates.

TIME-RELATED RELATIONSHIPS

A growth history can be obtained by relating rut depth to time. Classically, a new road will be aftercompacted by traffic,

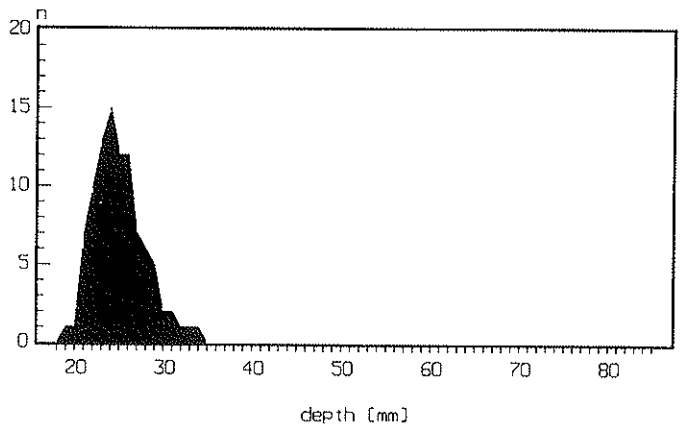

FIGURE 2 Frequency diagram of rut depth: studded tire wear.

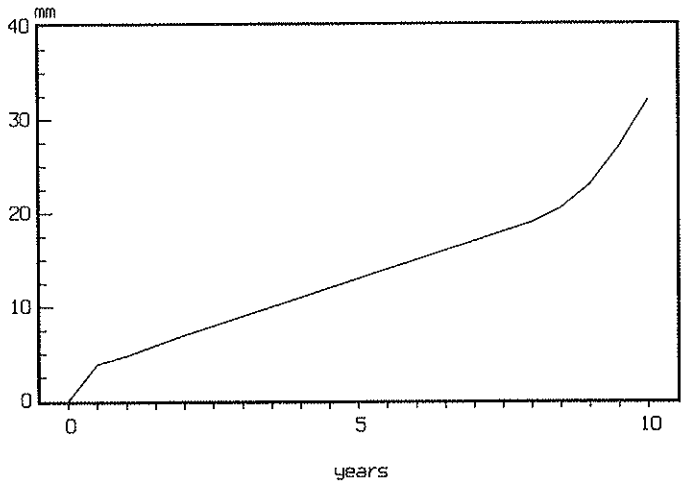

FIGURE 3 Classical rut growth.

that is, both granular and bound layers will be densified. Therefore, depths of ⅛ to ¼ inch develop relatively quickly, then the process slows. As ageing occurs, the asphalt layer becomes more brittle and susceptible to cracking. The cracked asphalt-bound layer cannot provide an adequte load distribution on the granular courses, and growth accelerates (see figure 3). Ruts caused by studded tire wear, however, are directly related to the number of studded tires passing the section, as illustrated in figure 4. This type of wear is even more apparent if measurements are made at least twice a year, before and after each stud season, which is the concept illustrated in figure 5. Figure 6, on the other hand, illustrates deformation caused by heavy loads and high temperatures. In a similar way, compaction and/or deformation of deeper-lying layers may be detected if rutting is recorded before and after a wet season. Figures 3 through 6 illustrate well-known concepts in rut growth. In reality, however, a combination of causes often makes it difficult to appraise the growth satisfactorily. Therefore, determining the causes by evaluating rut growth will require repeated measurements and a good backlog of previously-known relationships.

MEASURING THE RUTS TRANSVERSALLY

The profile transversal to the direction of travel represents the second and third dimensions. It contains information on the width of the ruts and on how far separated they are. Deformation is usually caused by heavy loads in vehicles whose tire configuration differs from passenger cars with studs. By carefully evaluating the profile, one may draw conclusions from this fact and act accordingly. This is probably the best way to trace the cause of ruts when earlier information on the state of the road is poor and when the pavement and underground materials are scarcely known.

Commercial vehicles are wider than passenger cars, therefore the outer distance from tire wall to tire wall is much greater. However, as implied by load, most trucks have dual tires on each side. The inner distance from tire to tire is therefore about the same as for passenger cars. To determine which vehicle category caused the ruts, the mean distance between tires can be measured. It can be assumed that a rut will be deepest in the center if it was due to the same type of vehicle. The vehicles passing the section, however, are

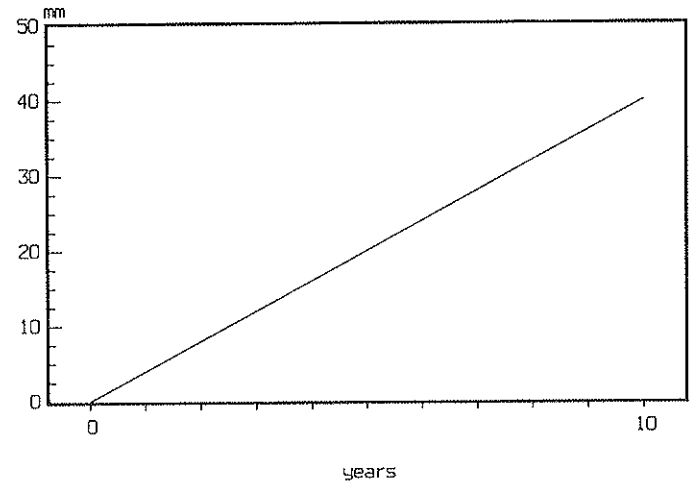

FIGURE 4 Studded tire wear growth.

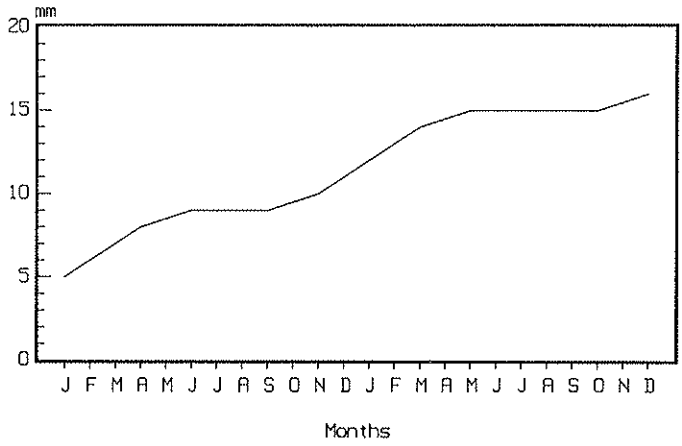

FIGURE 5 Studded tire wear growth: monthly measurements.

randomly distributed transversally over the lane. Thus, provided the section is passed by the same type of vehicle, one may determine the gauge by measuring the distance between the bottom points of the ruts. However, if the section is trafficked by various types of vehicles (as it is in most cases), using this distance would not suffice. For example, the wearing course may be deformed primarily by heavy traffic. In those ruts, studded tires wear down a few millimeters of the surface. Then, by taking the maximum-to-maximum depth distance between the ruts, studded tire wear will be indicated, albeit the deformation dominates.

A measurement based on worn or depressed areas may provide a better indication of the cause. This is done by determining the distance transversal to the direction of travel between the points where each rut profile area is divided in two equal halves. Thus, the distance between ruts can be determined based on the deformed or worn profile area of each rut, as shown in figure 7.

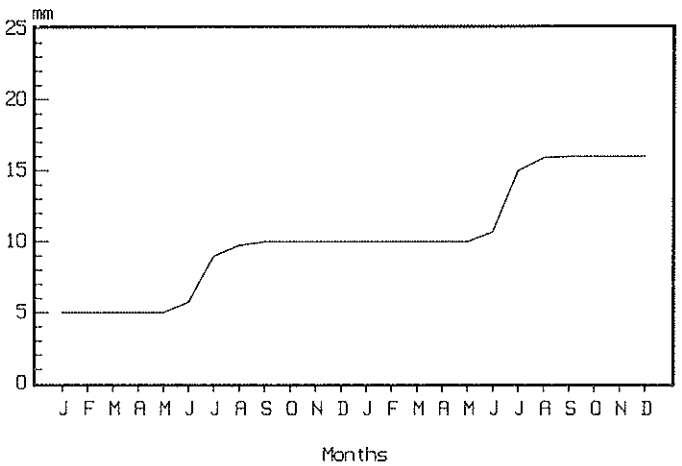

FIGURE 6 Deformation growth: monthly measurements.

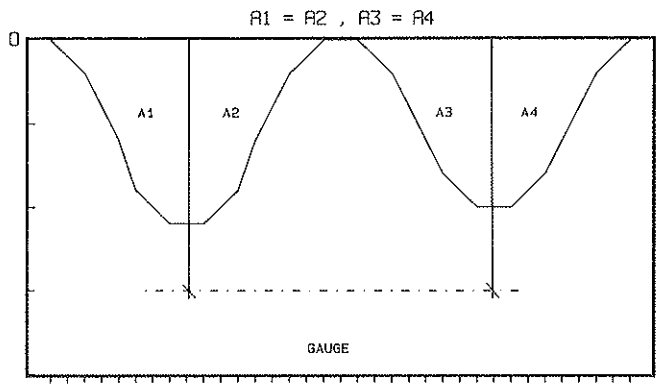

FIGURE 7 Definition of rut gauge.

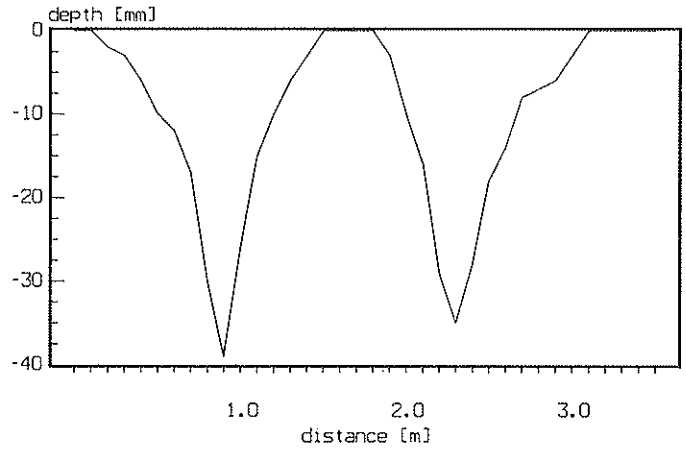

FIGURE 8 Profile of studded tire wear.

Another indicator of vehicle category is the width of the ruts. Naturally, ruts from heavy vehicles are wider because of their wheel configuration. Examples are shown in figure 8, which is taken from a lane dominated by passenger cars, and figure 9, which is a profile from a lane with slow and heavy traffic. The difference between these extremes is obvious. For most cases, however, it may be more difficult to discern the dominating cause. Often the road is repaired with materials whose properties differ from the original materials, often three lanes are made into four, and so forth. In such cases, the width of the ruts may complement the gauge mark determinations. The rut width can be determined as the gauge distance. A certain portion of the rutted (abraded) area around the middle of the rut can be considered (see figure 10). A studded tire rut is much narrower than a deformation rut of the same profile area; deep-lying deformations are even wider.

Widespread use of super single tires also affects these measurements. The ruts resulting from this category of vehicles

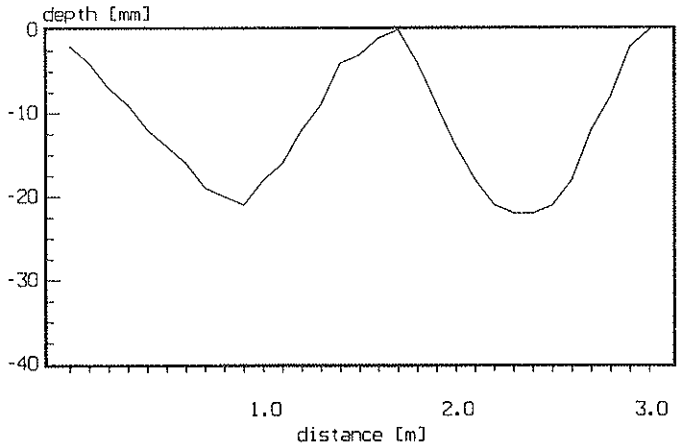

FIGURE 9 Profile of deformation.

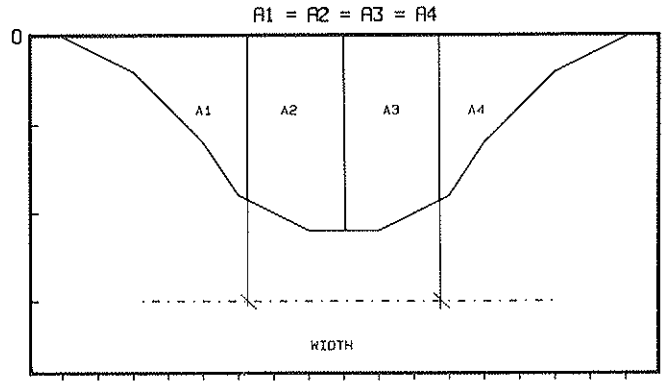

FIGURE 10 Definition of rut width.

are probably narrower than the standard dual-wheel load configuration and even wider than those from studded passenger cars. The distance between ruts, however, is greater than for any other vehicle category.

Quantifying these measures presents a method of determining rut cause without necessarily having data on traffic, road, and climate. Width and gauge can easily be determined by measuring systems currently in use, since the algorithms are very simple. However, readings must be taken sufficiently close transversally in order to obtain a profile detailed enough to trace the narrow studded tire rut. Examples of measurements are shown in tables 1 and 2. The first example is a section from a fast, leftmost lane dominated by passenger cars. The second is from a section where traffic often is congested, and thus the influence from heavy vehicles is larger. (Corresponding graphs are shown in figures 8 and 9, respectively.) The examples are excerpted from an unpublished study on wheel track rutting on various pavement types in the city of Stockholm. Roughly one hundred profiles were analyzed in the study, most of them from high volume roads. In order to validate these concepts, further research is needed under controlled conditions, employing a wide range of traffic compositions, as well as construction types and climate conditions.

CONCLUSION

New methods of collecting data on pavement rutting have enabled a more extensive use of this important distress category in pavement management. Rutting, as such, may be caused by several factors and combinations thereof. A simple maximum value of a transverse profile, known as rut depth, is merely an indicator of road rideability and will not provide information on the cause of rutting.

Rutting data must be treated statistically to see if the variation of depths follows a known rule for a certain reason. The reasons, as well as traffic data, must be known, or it will be difficult to differentiate studded tire wear from shallow

TABLE 1 CHARACTERISTICS OF A PROFILE FROM A SECTION WITH MUCH STUDDED TIRE WEAR

Measured profile at E4N, Left lane at Ulriksdal February 1984

Distance, [mm]:	100	200	300	400	500	600	700	800	900	1000
Depth, [mm]:	0	0	0	2	3	6	10	12	17	30
Distance, [mm]:	1100	1200	1300	1400	1500	1600	1700	1800	1900	2000
Depth, [mm]:	39	26	15	10	6	3	0	0	0	0
Distance, [mm]:	2100	2200	2300	2400	2500	2600	2700	2800	2900	3000
Depth, [mm]:	3	10	16	29	35	28	18	14	8	7
Distance, [mm]:	3100	3200	3300	3400	3500					
Depth, [mm]:	6	3	0	0	0					

Worn/Depressed Area, Left Rut:	179 cm^2
Worn/Depressed Area, Right Rut:	177 cm^2
Worn/Depressed Area, Total:	356 cm^2
Width of Left Rut:	29 cm
Width of Right Rut:	31 cm
Distance between ruts:	146 cm

TABLE 2 CHARACTERISTICS OF A PROFILE FROM A SECTION WITH SLOW TRAFFIC

Measured profile at 275W, Right lane at Brommaplan, July 1984

Distance, [mm]:	100	200	300	400	500	600	700	800	900	1000
Depth, [mm]:	2	4	7	9	12	14	16	19	20	21
Distance, [mm]:	1100	1200	1300	1400	1500	1600	1700	1800	1900	2000
Depth, [mm]:	18	16	12	9	4	3	1	0	4	9
Distance, [mm]:	2100	2200	2300	2400	2500	2600	2700	2800	2900	3000
Depth, [mm]:	14	18	21	22	21	18	12	8	2	0

Worn/Depressed Area, Left Rut:	187 cm^2
Worn/Depressed Area, Right Rut:	149 cm^2
Worn/Depressed Area, Total:	336 cm^2
Width of Left Rut:	50 cm
Width of Right Rut:	36 cm
Distance between ruts:	149 cm

asphalt layer deformation, since both causes have small longitudinal variations.

Measurements repeated preferably three times a year or more will indicate with certainty if the rutting can be attributed to studded tire wear. If pavement temperatures are known, one may also conclude when deformation in hot weather occurs and thus obtain criteria for restraining loads for certain pavement temperatures. Deep-lying deformations may be related to wet seasons or freeze-thaw cycles.

Finally, comparing certain properties of transversal profiles, such as how wide and how far apart wheel tracks are, one may have a firm basis for taking the right actions as the distress itself reflects the cause of it. In order to do so, both transversal and longitudinal resolution must be adequate. Provided that these criteria are fulfilled, this evaluation method seems to be most appropriate when climate, subgrade, pavement, and traffic data are scarce.

REFERENCE

1. G. Kunz. Spurrinnen- und Befahrbarkeitsmessungen auf der N1 und der N6 im Kanton Bern. *Strasse und Verkehr*, No. 8, 1975.

Publication of this paper sponsored by Committee on Pavement Monitoring, Evaluation, and Data Storage.

Field Survey Equipment and Data Analysis for Highway Rehabilitation Planning

H. TAURA, W. P. KILARESKI, AND M. OHAMA

Highway systems are deteriorating at a rapid rate due to increased traffic loads and severe climatic conditions. In order to keep these highways in good condition, maintenance and repair strategies must be based on the precise understanding of pavement conditions. Visual observations of pavement distress by trained engineers is the most common practice for monitoring and evaluating pavement surface conditions. Since pavement management needs are great, alternative methods of data collection and evaluation are needed to manage the data rapidly and accurately. In response to this need, the Japanese were among the first to develop high-speed photographic methods that successfully measure cracking and rutting. The Japanese were also successful in the development of field equipment for longitudinal profile surveys made with a three-laser sensor system. In a parallel effort, the development of an overall Road Surface (Pavement) Condition Evaluation System for Japan was begun in 1975. The application system was combined with the field hardware to form an integrated system of pavement performance modeling. In this paper, a typical application of the road surface condition survey and data reduction in Japan is discussed. An example of actual use of the high-speed photographic recorders for surface distress and the longitudinal profile measuring device with three laser sensors is presented.

Many pavement systems are deteriorating at a rapid rate due to increased traffic loads and severe climatic conditions. Highway agencies are now facing reduced budgets and a shortage of experienced engineering staff. The combination of these trends can create difficult operating requirements for the highway agency. Within the past few years, many of these agencies have begun to implement pavement management systems (PMS) to help organize and manage their highway infrastructure.

Most PMS require that a centralized database be established as a repository for all information pertaining to the highway system. This database is then used to provide information which is used to improve management of the highway network. Data such as geometric design information, accident statistics, construction costs, and maintenance records can be found in the database. All of this information is important to the agency; however, some specialized data are more specific for PMS, including pavement condition surveys, rut depth measurements, longitudinal roughness, skid measurements, deflections, and drainage.

H. Taura, Department of Engineering, Tokai University, Kanagawa Pref., Japan. W. P. Kilareski, The Pennsylvania Transportation Institute, The Pennsylvania State University, University Park, Pa. M. Ohama, PASCO USA Inc., 1-J Frasetto Way, Lincoln Park, N.J. 07035.

Considering the size and geographic distribution of highway networks, it can be seen that data collection and management can become an enormous task for a typical highway agency. This paper discusses equipment which is available to collect PMS data at normal highway speeds. The paper also discusses a decision-analysis process which can be used to assess network- and project-level PMS needs. At this time, only rutting, longitudinal roughness, and surface conditions lend themselves to high-speed data collection techniques. Skid resistance, drainage, and other parameters such as deflections do not lend themselves to continuous data collection methods. Consequently, they will not be addressed in this paper.

The equipment and data analysis techniques that are described in this paper were developed in Japan. Feasibility studies and the design of the equipment began in the early 1970s. The system description in this paper is a summary of the state of the art of the Japanese pavement management system. Concepts, equipment, and algorithms are applicable, however, to any PMS.

PAVEMENT SURFACE CONDITION SURVEY EQUIPMENT AND DATA REDUCTION

Field Survey Equipment

The field survey equipment is mounted on a single-survey vehicle chassis. A major component of the data collection system is an automatic, photographic recording system which is used for surface distress measurements. Distress types such as cracking, patching, joint deterioration, and potholes can be measured with continuous photo equipment. Other photo instrumentation (pulse) is used to measure rut depths. Noncontact sensors are used to measure longitudinal roughness. The complete field survey system is shown, in schematic form, in figure 1. Since all of the measurement equipment is mounted on a single vehicle chassis, the data collection can be done at normal highway speeds. This is an advantage since the data collection does not interfere with traffic flow. The data collection is also much safer than manual data collection, which often requires that a rater walk along the pavement or drive at slow speeds.

Surface Distress with Photographic Recorder

The surface distress of the pavement is measured with a high-speed photographic system. The recording system utilizes a 35-mm slit camera that continuously photographs the pave-

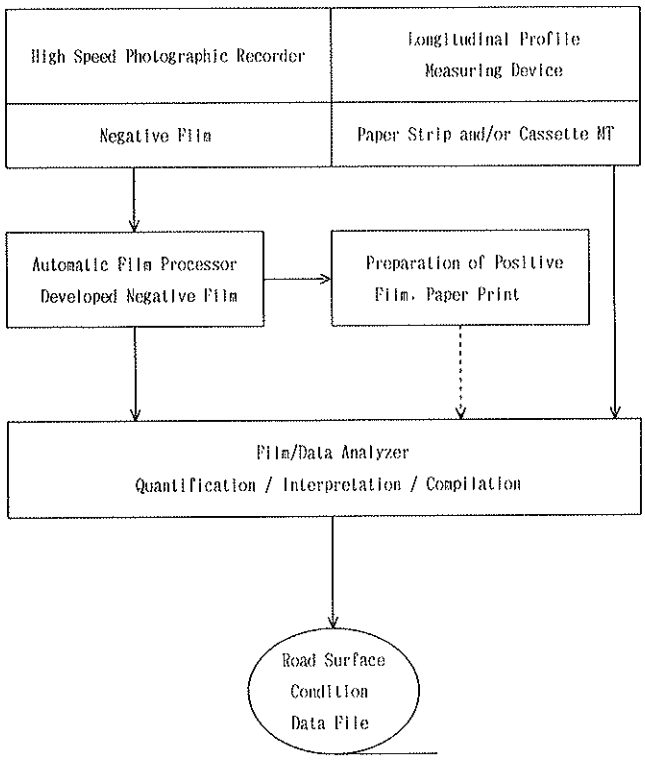

FIGURE 1 Outline of field survey and data reduction procedure.

ment surface. Pavement widths of up to 16 feet can be photographed in a single pass. This enables a travel lane and a shoulder to be filmed at the same time. A single roll of film can capture approximately 37 miles of pavement for analysis. The operating principle and configuration of the system are shown in figures 2 and 3.

As can be seen in figure 2, an image, which is the size of the slit, is formed on the film as the object is projected on the film by the lens. The film speed is synchronized with the vehicle speed so that a continuous photograph can be recorded. The photo becomes an actual record of the condition of the pavement surface. This type of record is very useful to the highway engineer and administrator, because it can be used to create digital information pertaining to the distress. The photo also becomes a historical record of the pavement condition. Pavement deterioration over time can be seen with a series of plots.

The surface distress measurements are made at night, because the pavement surface must be illuminated to maintain a high degree of photographic detail. Because the lighting is constant (no shadows, for example), the various distress types can be easily determined from the photos. A typical photograph of a highway section is shown in figure 4.

Surface Distress Data Processing

The exposed film is processed by an automatic film processor which develops, fixes, washes, and dries the film in one unit.

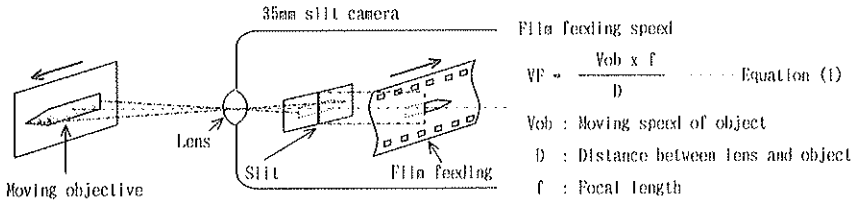

FIGURE 2 Operating principle of photographic recorder for surface distress.

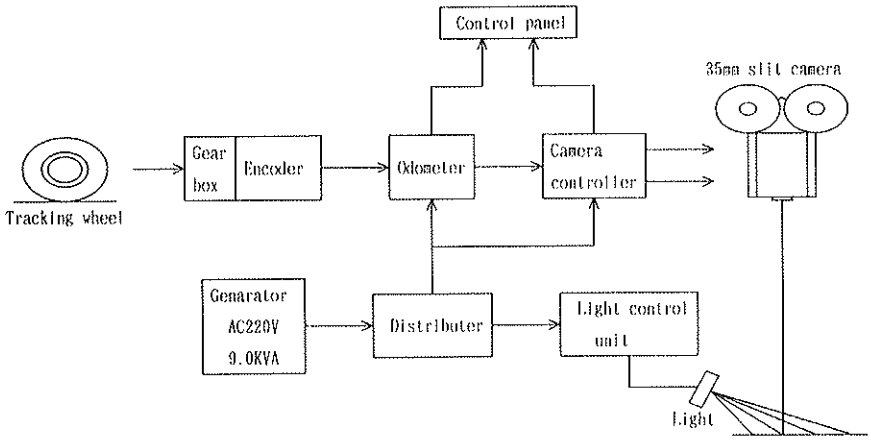

FIGURE 3 Configuration of high-speed photographic recorder for surface distress.

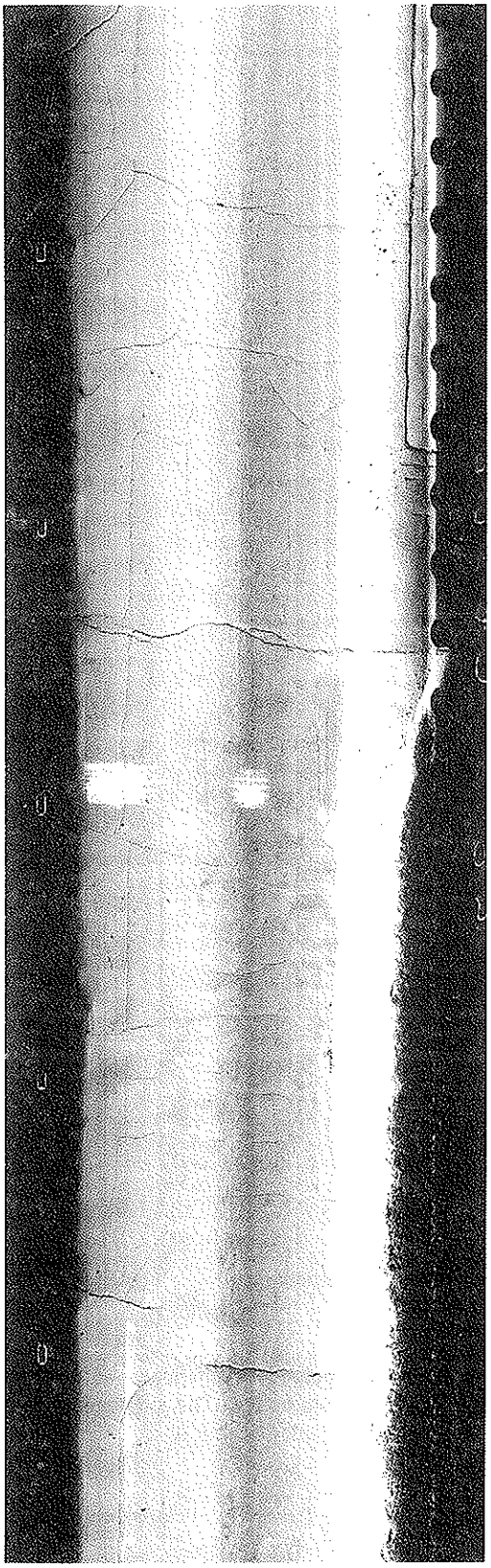

FIGURE 4 Part of continuous photo taken by high-speed photographic recorder for surface distress.

The 35-mm film is then in negative form, but it can be easily developed on positive paper if needed. After the film is in negative form, pavement cracking can be digitized.

Quantification of the cracking is performed by a grid-cell method based on the images of ten magnification. The grids can be imposed on the negative film as shown in figure 5. Digitized data can then be used to develop a cracking ratio. The cracking ratio (percent) and cracking index (in^2) are quantified by the following formulas:

Asphalt Pavement

$$\text{Cracking Ratio} = \text{Crack Ratio (percent)} + \text{Patching Ratio (percent)}$$

$$\text{Crack Ratio (percent)} = \frac{\text{Crack Area } (yd^2)}{\text{Observed Area } (yd^2)}$$

$$\text{Patching Ratio (percent)} = \frac{\text{Area of Patching } (yd^2)}{\text{Observed Area } (yd^2)}$$

Cement Concrete Pavement

$$\text{Cracking Index } (in./yd^2) = (\text{Total Length of Linear Crack} + \text{Area of Patching} \times 100/1.0 \text{ ft}) \div \text{Observed Area } (yd^2)$$

Rut Depth with Photographic Record

Rut depth surveys can also be carried out at normal highway speeds with photographic techniques. The system is designed to identify photographically the sectional profile of the pavement with a 35-mm pulse camera. The pulse camera is mounted on the front of the vehicle and operates as shown in figure 6. The camera photographs hairline optical bars which are projected onto the pavement surface. The camera shutter and hairline projector are synchronized according to the distance covered by the vehicle.

In this projection transformation method, a straight dark line is projected at an angle of 26°33′. Since the pulse camera is mounted vertically, the distortions of the photograph line are the rutting in the pavement. The operating principle of the rut depth measurements is presented in figure 7.

Rut Depth Data Processing

The film taken with the pulse camera is developed by an automatic film processor. A typical rut depth photo is shown in figure 8. The rutting can have several definitions, depending on the agency preference, as shown in figure 9. The rut depth photos are enlarged to ten times the negative size and then digitized. The complete sequence for the digitizing of the rut depth information is presented in figure 10.

Longitudinal Roughness Using Laser Sensors

Pavement longitudinal roughness is measured with three non-contact laser sensors. This enables a continuous record of the

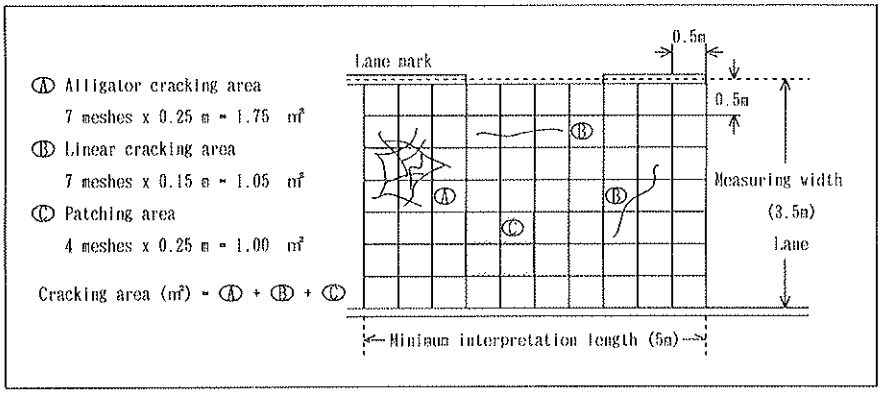

FIGURE 5 Measurement of cracking area by mesh method.

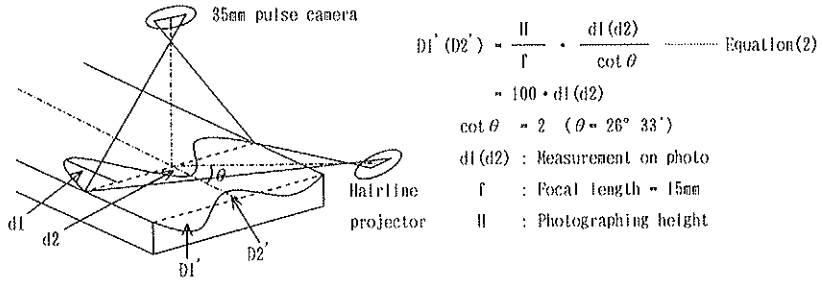

FIGURE 6 Operating principle of high-speed photographic recorder for rutting.

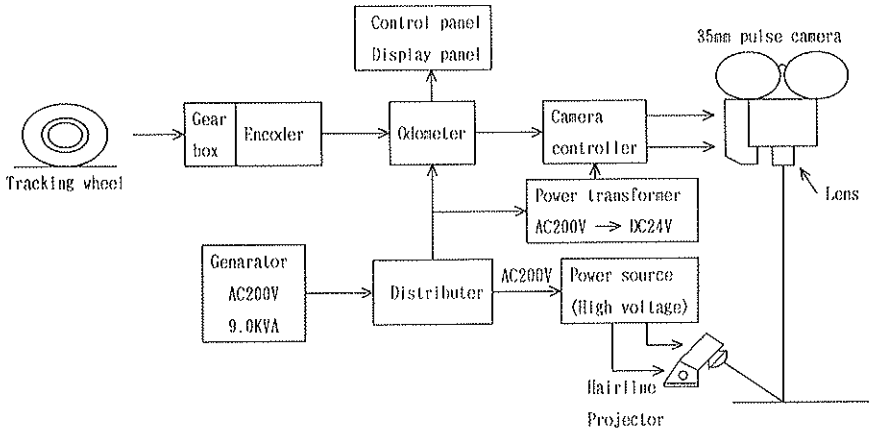

FIGURE 7 Configuration of high-speed photographic recorder for rutting.

longitudinal profile. The roughness measurement is also made at normal highway speeds.

The operating principle of the roughness measuring system is shown in figure 11. The three laser sensors are installed on the vehicle 4.9 feet apart in the longitudinal direction. The operation configuration is presented in figure 12. As can be seen, the encoder detects the distance traveled and conveys a signal to the input/output (I/O) controller to generate basic signals for equal interval data acquisition. Each time a certain interval is covered, the I/O controller and the system controller are activated to permit differential measurement from the noncontact laser sensor. The differential measurements are then processed. An example of the roughness data is shown in figure 13. Longitudinal data are recorded on magnetic tape, which is then edited. The longitudinal roughness is represented by the standard deviations for the unit pavement sections.

Application System for Pavement Surface Condition Data

The application system is designed to provide necessary information for the effective implementation of pavement maintenance and rehabilitation programs. The analysis system efficiently and effectively applies the road surface condition data to the schedule of repair and rehabilitation treatments. It

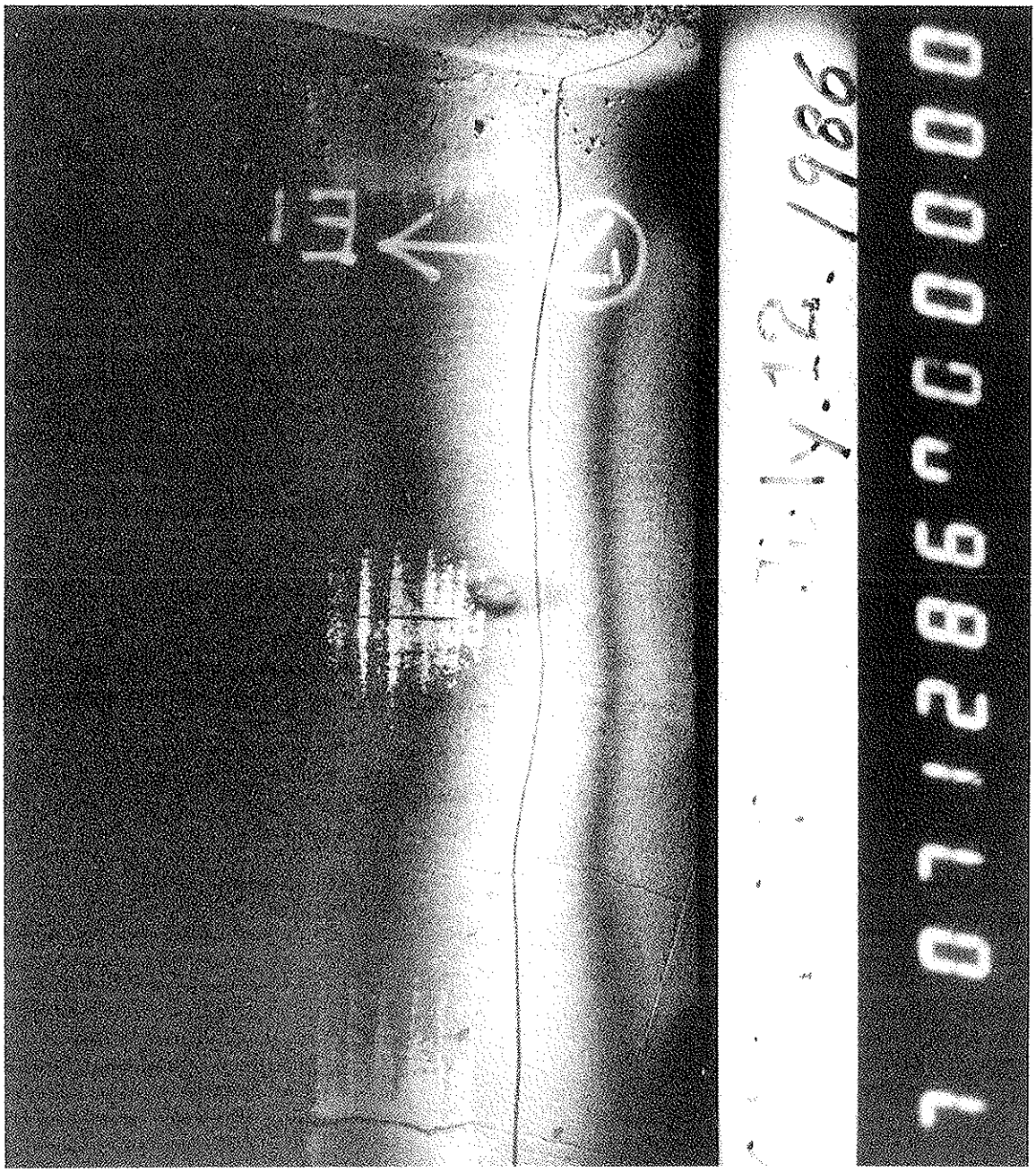

FIGURE 8 Example of photo taken by high-speed photographic recorder for rutting.

consists of the three parts which are explained further in the following sections in terms of concept, methodology, and present status of application.

Pavement Condition Evaluation System

In the past, many evaluation formulas were often based on regression analysis. AASHO road test design equations and the Japanese construction ministry evaluation formula are all based upon field experiments and statistical analysis. The regression type of analysis requires a large number of sample highway sections that are selected and evaluated for pavement conditions. Ultimately, the engineer expects to use the evaluation formulas to predict performance of the pavement system. Consequently, a relationship must be established to relate the subjective rater evaluations to the mechanical measurements of rutting, cracking, and roughness.

A long-term study was conducted in Japan to determine the relationship between the rater and the data collected with the equipment described above. Pavement evaluations were visually made to rate overall pavement conditions in five categories (A, B, C, D, and E) with five numerical values (5, 4, 3, 2, and 1). In general, these methods attempt to establish relationships between the evaluation values and the data obtained with the survey vehicle.

The first question concerning the relationship was whether human judgment is discriminative enough to distinguish among

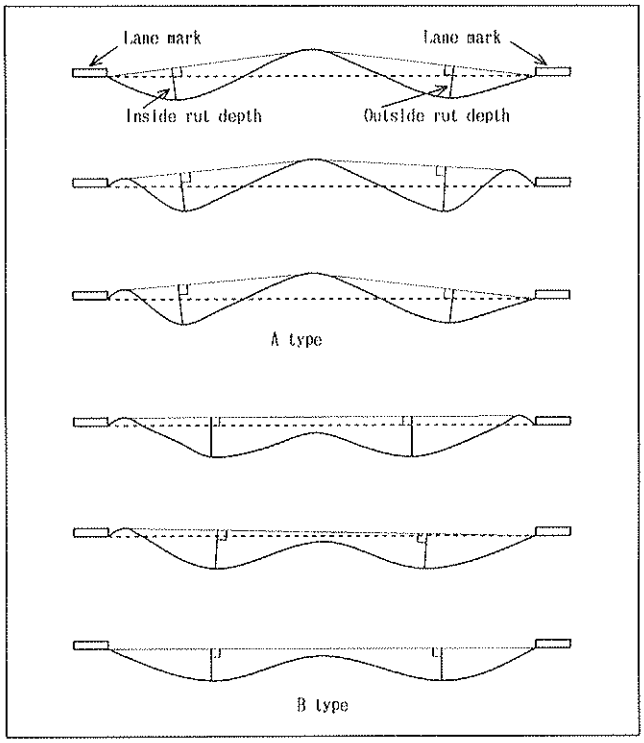

FIGURE 9 Definition of rutting volume (rut depth).

as many as five levels of condition. The study involved the one-pair comparison method, the Hayashi method, and the multidiscriminant analysis. It was concluded that the multidiscriminant analysis approach was the most rational method. It was determined that it is beyond human capability to discriminate rationally among five categories. Therefore, it was decided to use three levels for condition surveys.

This final selection of three levels was based upon a Japanese study involving fifty asphaltic, concrete pavement sections, which was used to form the basis for the development of evaluation formulas and predictive models in Japan. A panel of twenty-one expert highway engineers visually rated the pavements and ranked them into five categories. The same pavements were then evaluated with the equipment for rutting, cracking, and roughness. The data were studied with the multidiscriminant method. As is shown in figure 14, groups C, D, and E overlapped and were indistinguishable from each other. Therefore, in this study, it appeared more reasonable to combine C, D, and E into one group, F. This resulted in the formation of the three groups: A, B, and F.

Development of Performance Prediction Evaluation Formula

In the development of accurate, overall evaluation formulas, the reliability of visual observation by pavement ratios is a

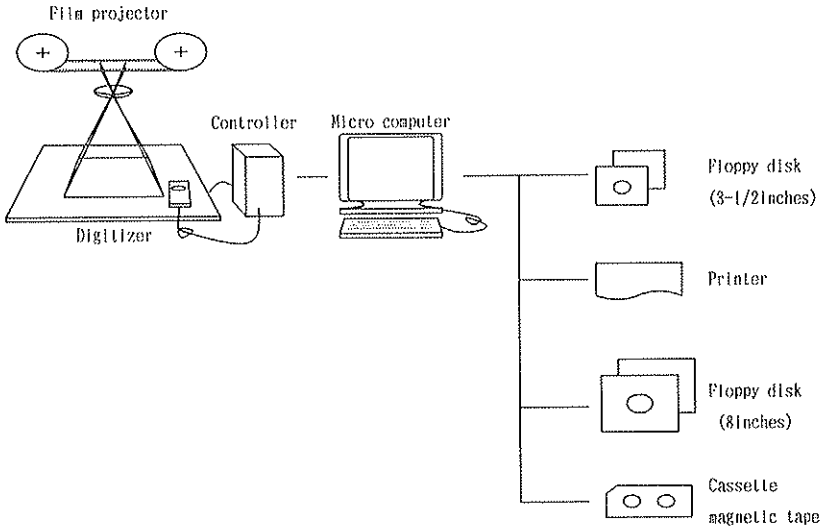

FIGURE 10 Film and data analyzer.

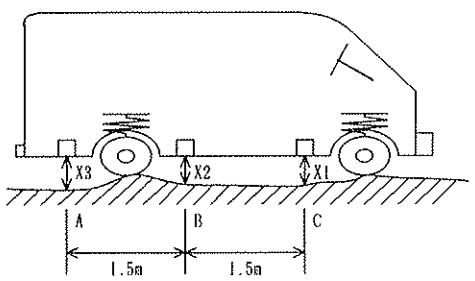

$$Xn = \frac{X1n + X3n}{2} - X2n \quad \text{Equation(3)}$$

X1n : Distance at 1st Sensor
X2n : Distance at 2nd Sensor
X3n : Distance at 3rd Sensor
n = Sampling No.
(n=1,2,3,4,...)

$$= \frac{L}{l} + 1$$

L :Evaluation Unit Length

FIGURE 11 Operating principle of measurement.

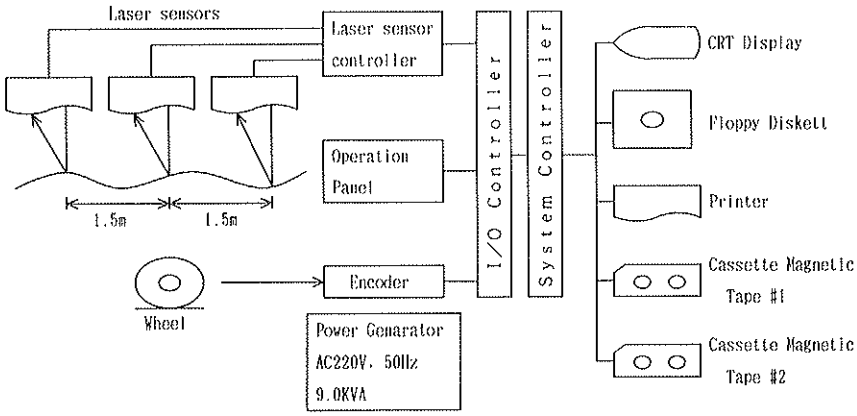

FIGURE 12 Configuration of longitudinal profile measuring device.

critical factor. Consequently, there was a need to examine the reliability of individual evaluation data. Individual visual evaluation ratings were compared in terms of correlation ratios. The ratings of inspectors with an exceptionally small ratio were deleted since they were considered unreliable.

In the next step, these visual ratings were related to the survey data on cracking, rutting, and longitudinal roughness by discriminant analysis (as discussed earlier). The relationship was then expressed as a polynomial. The formula, thus developed by discriminant analysis, was then compared with the one based on regression analysis. It was found that the multidiscriminant method performed better in matching visual ratings with manual data.

Example of Overall Evaluation Formula Development

Thirty-nine asphalt concrete pavement sections were studied in Switzerland during an investigation of the Japanese system. Eleven raters visually surveyed the pavement for overall condition rating. Subsequently, the pavement was surveyed with the equipment for cracking, rutting, and longitudinal roughness. The following formulas were developed from the discriminant analysis:

Asphalt Concrete Pavement

$$EVA = 5 - 0.0489X1 - 0.0279X2 - 0.1257X3 - 0.0532X4$$

PCC Concrete Pavement

$$EVA = 5 - 0.1306X1 - 0.0378X2 - 0.2915X3 - 0.2229X4$$

where

EVA = General evaluation rating,
$X1$ = Cracking (percent),
$X2$ = Rutting (mm),
$X3$ = Longitudinal roughness (mm), and
$X4$ = Pothole (percent).

Visual ratings by individual inspectors were compared by correlation ratios, as shown in table 1. It can be seen that inspectors 5 and 9 had exceptionally low ratio values. These ratings were determined to be biased and were, therefore, deleted.

In the next step, the data from the remaining eight inspectors were used for a discriminant analysis. A discriminative distribution of the data is seen in figure 15. The data were found to be distributed distinctly among A, B, and C.

The rates of matching (rates of samples whose categorization of visual evaluation ratings matches those of the evaluation formula) were sought and compared with the rates of matching obtained from the same data using an evaluation formula based on regression analysis. The results show that the rates of matching are higher for the evaluation formula based on discriminant analysis (66.7%) than for the formula based on regression analysis (60.2%).

Road Surface Condition Forecast System Model

To develop a forecast formula, road surface condition data values as they relate to the factors that are accountable to them were theoretically classified. The relationships, however, are actually extremely complex and almost impossible to explain (as discussed above). Therefore, an attempt was made to approximate a relationship by building a mathematical model that was simple but accurate enough to be applicable in a practical manner.

The model was constructed in the following manner. Assuming an arbitrarily chosen road section, i, with a potential for deterioration, D_i, and that the load it receives for the first year, α_2, results in cracking, C_{i1}, their relationships are expressed as

$$C_{i1} = \alpha_1 D_i$$

and similarly,

$C_{i2} = \alpha_2\alpha_1 D_i$ for the second year

$C_{ij} = \alpha_j \ldots \alpha_2\alpha_1 D_i$ for the j year

and further,

$$C_{ij+1} = \alpha_{j+1}\alpha_j \ldots \alpha_2\alpha_1 D_i$$

therefore,

$$C_{ij+1} = \alpha_{j+1} C_{ij}$$

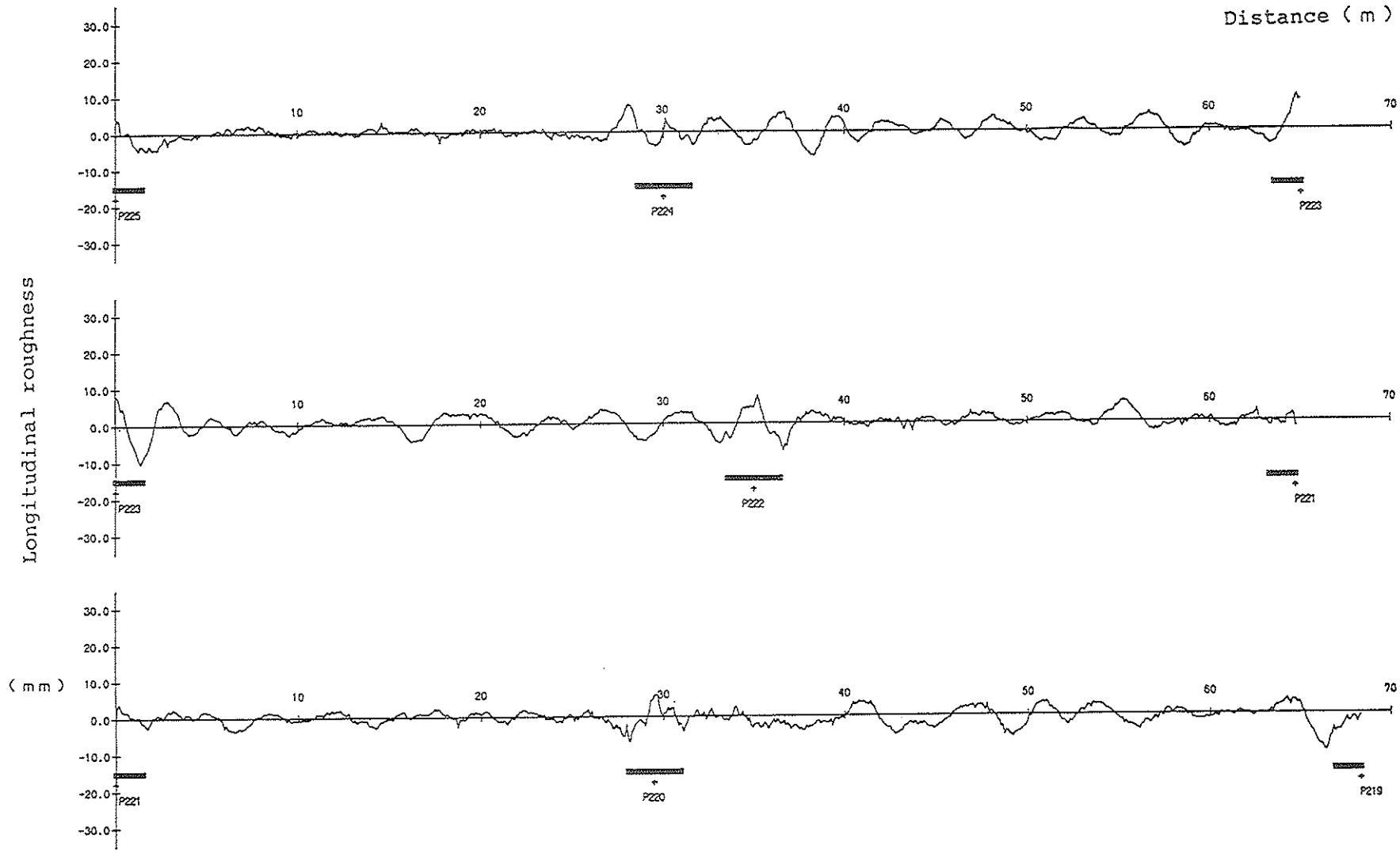

FIGURE 13 Longitudinal profile surveyed by three laser sensors.

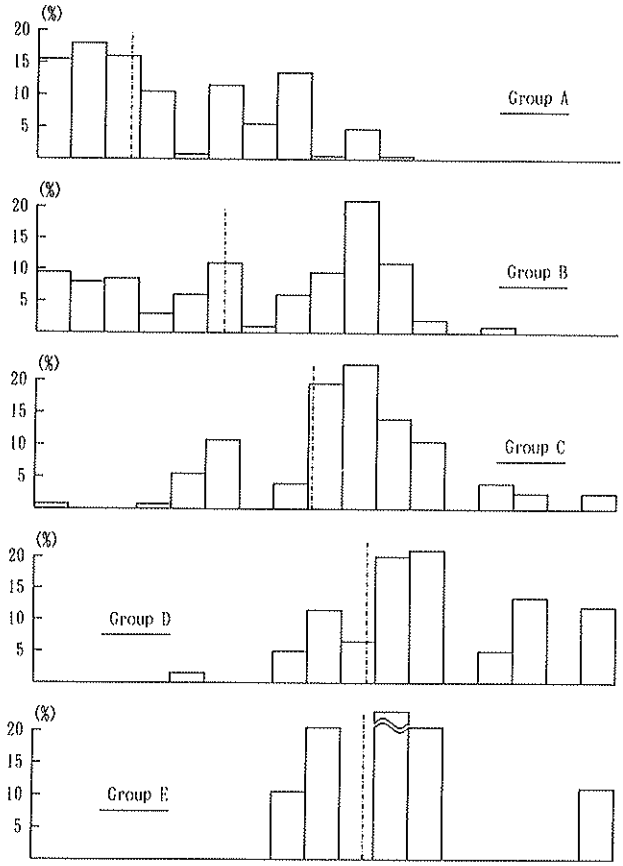

FIGURE 14 Frequency distribution of engineering judgment.

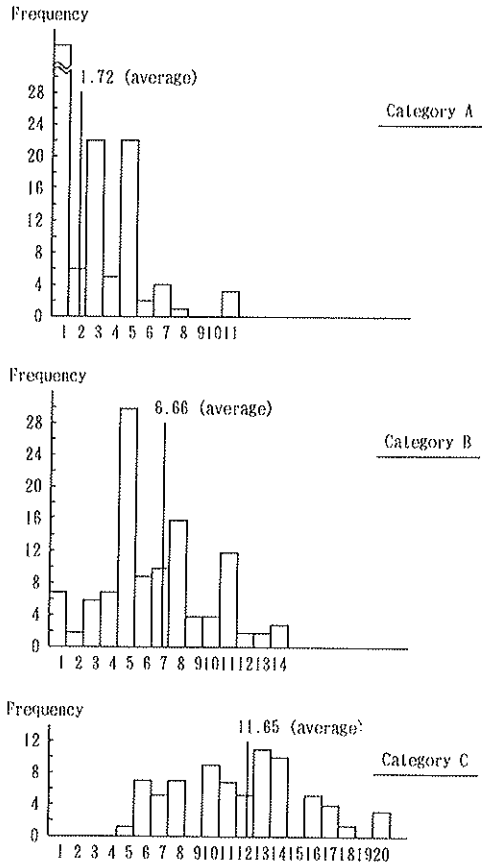

FIGURE 15 Frequency distribution.

TABLE 1 VISUAL EVALUATION DATA CORRELATION RATIO MATRIX

NO	1	2	3	4	5	6	7	8	9	10
1	1.000	0.880	0.779	0.863	0.529	0.898	0.908	0.797	0.543	0.690
2	0.870	1.000	0.743	0.891	0.651	0.817	0.870	0.847	0.553	0.833
3	0.749	0.733	1.000	0.767	0.435	0.569	0.834	0.852	0.507	0.646
4	0.872	0.920	0.842	1.000	0.575	0.870	0.910	0.847	0.495	0.720
5	0.542	0.671	0.450	0.576	1.000	0.468	0.542	0.586	0.557	0.449
6	0.889	0.818	0.683	0.871	0.434	1.000	0.857	0.705	0.480	0.714
7	0.908	0.880	0.855	0.917	0.529	0.829	1.000	0.887	0.461	0.690
8	0.790	0.857	0.858	0.882	0.579	0.712	0.884	1.000	0.501	0.638
9	0.497	0.518	0.461	0.556	0.556	0.446	0.442	0.457	1.000	0.391
10	0.694	0.870	0.659	0.703	0.442	0.807	0.694	0.634	0.414	1.000

TABLE 2 COEFFICIENT α: ASPHALT PAVEMENT

Year \ Crack (%)	0.0-0.9	1.0-9.9	10.0-19.9	20.0-29.9	30.0-
1	4.37	1.94	1.38	1.31	1.27
2	4.12	1.92	1.36	1.29	1.25
3	4.06	1.89	1.35	1.28	1.23
4	4.01	1.86	1.33	1.26	1.21
5	3.95	1.84	1.31	1.24	1.20
6	3.89	1.81	1.29	1.22	1.18
7	3.84	1.78	1.27	1.21	1.16
8	3.78	1.76	1.25	1.19	1.14
9	3.72	1.73	1.23	1.17	1.13
10	3.67	1.70	1.21	1.15	1.11
11	3.61	1.67	1.20	1.13	1.09
12	3.55	1.65	1.18	1.12	1.08
13	3.49	1.63	1.16	1.10	1.06
14	3.44	1.60	1.14	1.08	1.04
15	3.38	1.58	1.12	1.06	1.02
16	3.32	1.55	1.10	1.05	1.01
17	3.26	1.52	1.07	1.03	
18	3.20	1.49	1.05	1.02	
19	3.15	1.47	1.04		
20	3.09	1.44	1.03		

Coefficient α represents such factors as pavement structure, traffic volume, years in service, and surface deterioration. Of these factors, it can be assumed that traffic volume is, in general terms, proportional to the number of years the road has been in service and the deterioration as represented by cracking.

The coefficient α was expressed by a two-dimensional matrix of pavement structure, years in service, and cracking rate. Forecast values obtained from this table were examined, and results showed that forecast values projected three years into the future were good enough for practical application. Similarly, forecast formulas were developed for rutting and longitudinal roughness.

In 1977, 423 pavement sections were surveyed in Japan, and a matrix was developed for coefficient α with respect to cracking (tables 2 and 3). The values illustrated in tables 2 and 3 were used to forecast cracking rates for 1979. In 1979, the same road sections were surveyed, and the survey results were compared with the forecast values, as shown in table 4. The results show a close relationship, which is acceptable for practical application. The accuracy of the forecast formula was tested several more times with similar results.

Application of Forecast Formula

When the field survey of road surface conditions involves extensive lengths of pavements, in many cases, the entire roadway cannot be analyzed at one time due to budgetary constraints. In such cases, the entire road length can be equally

TABLE 3 COEFFICIENT α: CEMENT PAVEMENT

Year \ Crack (%)	0.0-0.9	1.0-9.9	10.0-19.9	20.0-29.9	30.0-
1	3.70	1.63	1.25	1.18	1.14
2	3.68	1.63	1.24	1.18	1.14
3	3.67	1.62	1.23	1.17	1.13
4	3.66	1.62	1.23	1.17	1.13
5	3.65	1.61	1.23	1.16	1.12
6	3.63	1.60	1.22	1.16	1.12
7	3.62	1.60	1.22	1.16	1.11
8	3.69	1.59	1.21	1.15	1.11
9	3.59	1.58	1.21	1.15	1.11
10	3.57	1.57	1.20	1.14	1.10
11	3.56	1.57	1.20	1.14	1.10
12	3.54	1.56	1.19	1.13	1.09
13	3.53	1.56	1.19	1.13	1.09
14	3.51	1.55	1.16	1.12	1.08
15	3.50	1.55	1.18	1.12	1.08
16	3.48	1.54	1.17	1.11	1.07
17	3.47	1.53	1.17	1.11	1.07
18	3.45	1.52	1.16	1.10	1.06
19	3.44	1.52	1.16	1.10	1.06
20	3.42	1.51	1.15	1.09	1.06

TABLE 4 ACCURACY ANALYSIS OF CRACKING FORECAST

(Asphalt Pavement)

Item \ Cracking rate	5.0-14.9	15.0-24.9	25.0-34.9	35.0-
Average ($\bar{x}$)	8.05	18.64	29.15	40.39
Standard deviation of error (σ)	2.84	2.87	4.87	3.45
$\sigma/\bar{x}$	0.35	0.15	0.17	0.09
Sampling size	179	30	12	14

(Concrete Pavement)

Item \ Rutting	5.0-14.9	15.0-24.9	25.0-34.9	35.0-
Average ($\bar{x}$)	8.55	17.04	30.65	38.83
Standard deviation of error (σ)	2.59	1.84	1.32	3.68
$\sigma/\bar{x}$	0.30	0.11	0.04	0.09
Sampling size	66	36	24	18

TABLE 5 LIST OF SECTIONS TO BE REPAIRED

NO 1 ROUTE NAME
ROUTE 16 (GUIDE LINE >= 1 L = 300m / 500m)

NO	CP NAME	DIS. KP	L.	CR	PH	RD	SO	SR	DEF	EVA		
10	KP151	100	500	7.2	0.02	16	3.71	0.39	1.54	3.75	100	6
10	KP151	600	594	1.6	0.00	23	2.85	0.67	0.82	3.86	100	6
1	KP146	0	500	0.5	0.00	24	3.35	0.29	0.73	3.68	100	6
1	KP146	2000	502	0.6	0.10	16	3.14	0.32	0.77	4.17	100	6
6	KP149	500	583	0.1	0.00	16	1.20	0.65	1.61	4.38	100	6
7	KP149	1100	500	0.1	0.08	22	3.02	0.48	1.19	4.00	100	5
7	KP149	1600	508	0.8	0.14	19	3.38	0.08	1.41	4.00	100	5
13	KP152	200	500	1.1	0.02	21	2.29	0.81	0.46	4.08	100	5
1	kP146	500	500	0.4	0.03	17	2.83	0.31	0.31	4.14	100	5
7	KP149	600	500	0.2	0.00	18	2.69	0.82	2.05	4.14	100	5
7	KP149	100	500	0.5	0.02	19	2.38	0.24	0.60	4.14	100	5
1	KP146	1500	500	0.0	0.00	13	1.64	0.50	0.50	4.43	100	5
1	KP146	1000	500	0.1	0.02	9	2.34	0.87	0.87	4.45	60	3

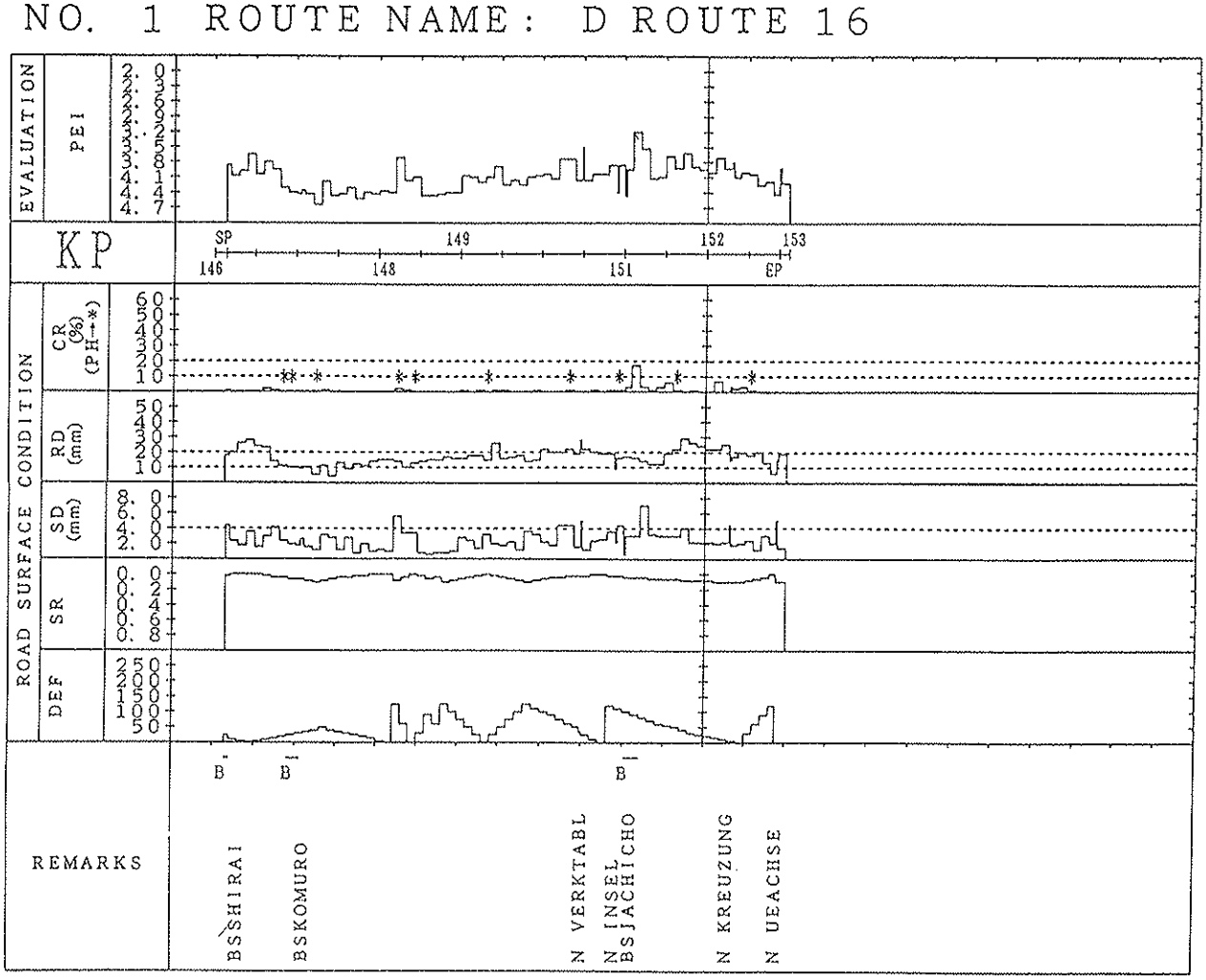

FIGURE 16 Pavement performance chart.

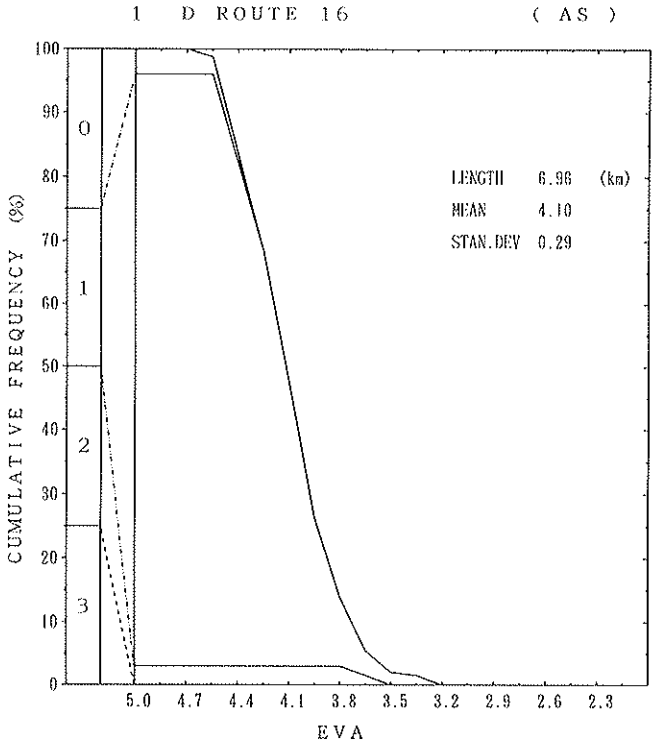

FIGURE 17 Cumulative frequency diagram.

divided into three parts, so that surveying can be conducted on one part while forecasting is done on the remaining two-thirds. Thus, the entire length of the road is constantly and conveniently monitored in one way or another.

In order for the highway agency to make the best use of the limited funds available each year for pavement maintenance and repairing, it is important for it to determine efficiently and effectively the locations of highway sections which require maintenance. The methodology used to identify such locations consists of (1) identifying from the pavement surface condition data those sections of the road that require maintenance and repair; (2) establishing priority for each of the road sections on the basis of overall evaluation data; and (3) combining both of these techniques, which results in the selection of the road sections for which maintenance and repair will be conducted.

In order to facilitate this procedure, pavement performance charts (figure 16) can be developed. Cumulative frequency diagrams from overall evaluation data (figure 17), a list of sections to be repaired, and a tabulation of overall evaluation data (table 5) can also be developed.

CONCLUSION

Based upon this study, the following conclusions can be made:

1. It is possible to photograph a continuous section of pavement using a 35-mm slit camera. The photographs can be digitized and a surface condition survey can be obtained from the photos.
2. A pulse camera can be used to measure rut depths in a pavement. The data can be digitized from the photos.
3. The surface condition slit camera and the pulse camera can be mounted on a single vehicle with laser sensors so that rutting, surface condition, and roughness can be measured at highway speeds with one vehicle.
4. Visual conditions survey data can be related to field measurements with a multidiscriminant analysis method. The data can then be used to develop prediction formulas for pavement rehabilitation and repair scheduling.

Publication of this paper sponsored by Committee on Pavement Monitoring, Evaluation, and Data Storage.

Comparison of Methods and Equipment To Conduct Pavement Distress Surveys

K. R. BENSON, G. E. ELKINS, W. UDDIN, AND W. R. HUDSON

Selected distress survey methods and equipment, representing a range in automation, were tested and evaluated. The following methods and devices were included in the testing: manual mapping; detailed visual surveys using manual recording and automatic data logging; and the PASCO ROADRECON, Groupe Examen Routier Photographic (GERPHO), Automatic Road Analyzer (ARAN), and Laser Road Surface Tester (RST) high-speed survey vehicles. Field tests were conducted on flexible, rigid, and composite pavements exhibiting a range of pavement distresses. The distress survey methods and equipment were evaluated based on their performance and capabilities in the field. The study concludes that, at present, the GERPHO and PASCO ROADRECON can be used for both network level and project level distress surveys and are well suited for pavement research studies. The ARAN and Laser RST are recommended for consideration in network-level surveys. It is also recommended that automatic data loggers be used when manual distress surveys are conducted.

The Strategic Highway Research Program (SHRP) will produce results in the areas of pavement design, construction, and rehabilitation. One phase of this program is entitled "Long-Term Pavement Performance" (LTPP) and will involve the collection of uniform evaluation and performance data on numerous pavement sections throughout the United States. The Federal Highway Administration initiated the study Pavement Condition Monitoring Methods and Equipment to assist in this effort by providing a better understanding of the procedures and devices that are used to evaluate pavements. Although the study was initiated to aid in the SHRP-LTPP program, the results that were produced are of great value to state highway agencies and other agencies in their project- and network-level pavement management. This paper documents information pertaining to the study in which selected distress survey methods and devices were tested and evaluated (*1*).

INTRODUCTION

Pavement distress surveys, or condition surveys, are an important part of any pavement performance study or management system. They are used to quantify the condition of a pavement by classifying the amount and extent of distress present at a given time. The information collected from distress surveys can be used to document the performance of a pavement and can help determine appropriate rehabilitation alternatives.

Distress surveys have been traditionally performed by raters who walk or drive along the road and classify the distresses based on their visual observations. The distresses are recorded on data forms and the information is later reduced in the office. This type of manual procedure is slow, labor-intensive, and subject to transcription errors. Consistency between classification and quantification of the distresses can also be a problem.

Methods have been devised by various agencies to standardize distress classifications and to speed up the process by automating the recording, reduction, processing, and storage of the data. Condition survey manuals which define distress classifications using pictures and detailed descriptions have been developed to minimize interpretation differences among raters. Some procedures employ detailed measurements of the distress to minimize quantification errors. Small, hand-held computers and data loggers have been used to improve efficiency in recording and transferring the data from field to office. Vehicles which take photographs or other visual images of the pavement to be later interpreted in the office were developed to speed the field data collection time and provide a permanent visual record of the actual pavement condition. Other survey vehicles carry on-board microcomputers for manual entry, recording, and storage of the data directly in the field. In addition, a new class of condition survey vehicles is emerging which uses objective measures of the pavement surface to classify and quantify different types of distress.

The type and extent of condition survey performed depend upon its intended use. Condition surveys for network-level screening of sections may need only a windshield survey of the pavement in which only a few distresses are rated. At the other end of the spectrum are the detailed condition surveys needed for research studies such as SHRP-LTPP. This type of survey attempts to classify and quantify precisely all distresses and other features of a pavement which may influence its performance. The required level of effort and cost to conduct these different types of condition surveys varies with the intensity of the data collection effort.

EQUIPMENT SELECTED FOR FIELD TESTING

To study improved methods of conducting distress surveys, a variety of distress survey procedures employing different levels of automation were selected for field testing. The base level of distress survey methods was manual mapping of the

K. R. Benson and G. E. Elkins, ARE Inc. Engineering Consultants, 2600 Dellana Lane, Austin, Tex. 78746. W. Uddin, Center for Transportation Research, The University of Texas at Austin, 3208 Red River Street, Suite 200, Austin, Tex. 78705. W. R. Hudson, Department of Civil Engineering, The University of Texas at Austin, ECJ 6-100, Austin, Tex., 78712.

distress on the pavement section. The next level was using a detailed visual survey in which the distresses were recorded on data sheets. A detailed visual survey was also conducted using an automated data logger. The next level of automation was using photographic survey vehicles in which the film was interpreted in the office. Two other survey vehicles, which combined the use of on-board computers to record data and objective measures to detect and quantify certain types of distresses, were also investigated in this study. The distress survey methods and devices selected for the field testing were as follows:

- Manual mapping
- Detailed visual survey, manual recording
- Detailed visual survey, automated data logging
- PASCO ROADRECON survey vehicle, featuring photographic equipment and laser height sensors
- GERPHO survey vehicle, featuring photographic equipment
- Automatic Road Analyzer (ARAN) survey vehicle, featuring video equipment, ultrasonic height sensors, and on-board computer
- Laser Road Surface Tester (RST) survey vehicle, featuring laser height sensors and on-board computer

DESCRIPTION OF SELECTED METHODS AND EQUIPMENT

A description of each of the distress survey procedures and devices selected for field testing is presented below.

Manual Mapping

The manual mapping method used for field testing consisted of a rater walking the pavement section and manually drawing a map showing the type and exact location of all distresses present on the section. This procedure is similar to the one used at the AASHO road test (*2*). The severity level of each distress was identified and recorded on the map. The mapping form shown in figure 1 was used to record the distresses. All distresses were identified and measured according to the standards found in the Highway Pavement Distress Identification Manual (*3*).

Detailed Visual Survey

The PAVER and Concrete Pavement Evaluation System (COPES) methods of conducting condition surveys were

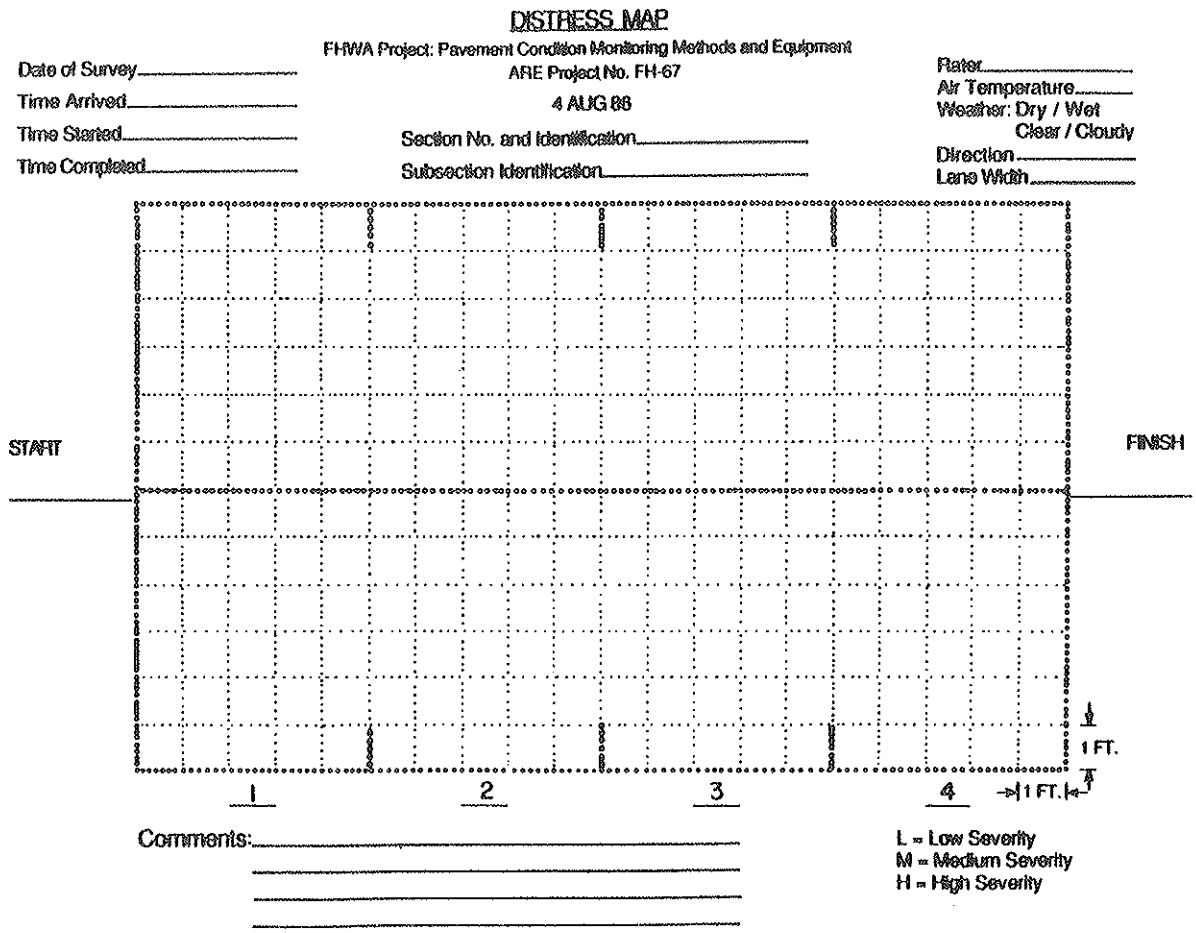

FIGURE 1 Manual mapping form used in the field.

selected as representative detailed visual distress survey methods. PAVER is a pavement evaluation system developed by the U.S. Army Construction Engineering Research Laboratory (*4*). The detailed condition survey procedure employed by the PAVER system was used for the flexible, composite, and jointed reinforced concrete pavement sections in the field study. The COPES distress survey method was used to rate the continuously reinforced concrete pavement (CRCP) sections, since PAVER was not developed for CRCP. COPES was developed in an NCHRP study (*5*) for evaluation of plain jointed, jointed reinforced, and continuously reinforced concrete pavement.

Automated Data Logger

The detailed distress survey using a field data logger was performed using a battery-operated Epson HX-20 portable computer programmed by ARE Inc. to record distress and section information. The interactive program prompts the rater for input of the severity and extent of each previously defined distress category. The information is stored on a computer-encoded microcassette. This allows the information to be downloaded in the office, using hardwired connections between computers and a communications program. Paper tapes that are produced in the field as the information is recorded serve as a backup. The automatic data logging keyboard is shown in figure 2.

Flexible pavement sections were rated using a procedure developed for the Rhode Island Department of Transportation by ARE Inc. (*6*), since the Epson was already programmed for this procedure. The distress categories were similar to those used in the PAVER system. The distress categories from the COPES method were used for the rigid pavement sections.

PASCO ROADRECON Systems

PASCO Corporation of Japan developed the continuous pavement surface photographing device (ROADRECON-70) in the late 1960s (*7*). The first operational survey vehicle was produced in 1970. Cracking, patching, and other distresses are recorded using the ROADRECON-70. The vehicle travels at speeds between 3 and 53 mph (5 and 85 kmph). A continuous photographic record of the pavement surface is made using a 35-mm slit camera. The system synchronizes film feed speed and camera aperture with the speed of the vehicle in order to equalize image density and photographic reduction. Road width of up to 16 feet (5 m) can be filmed.

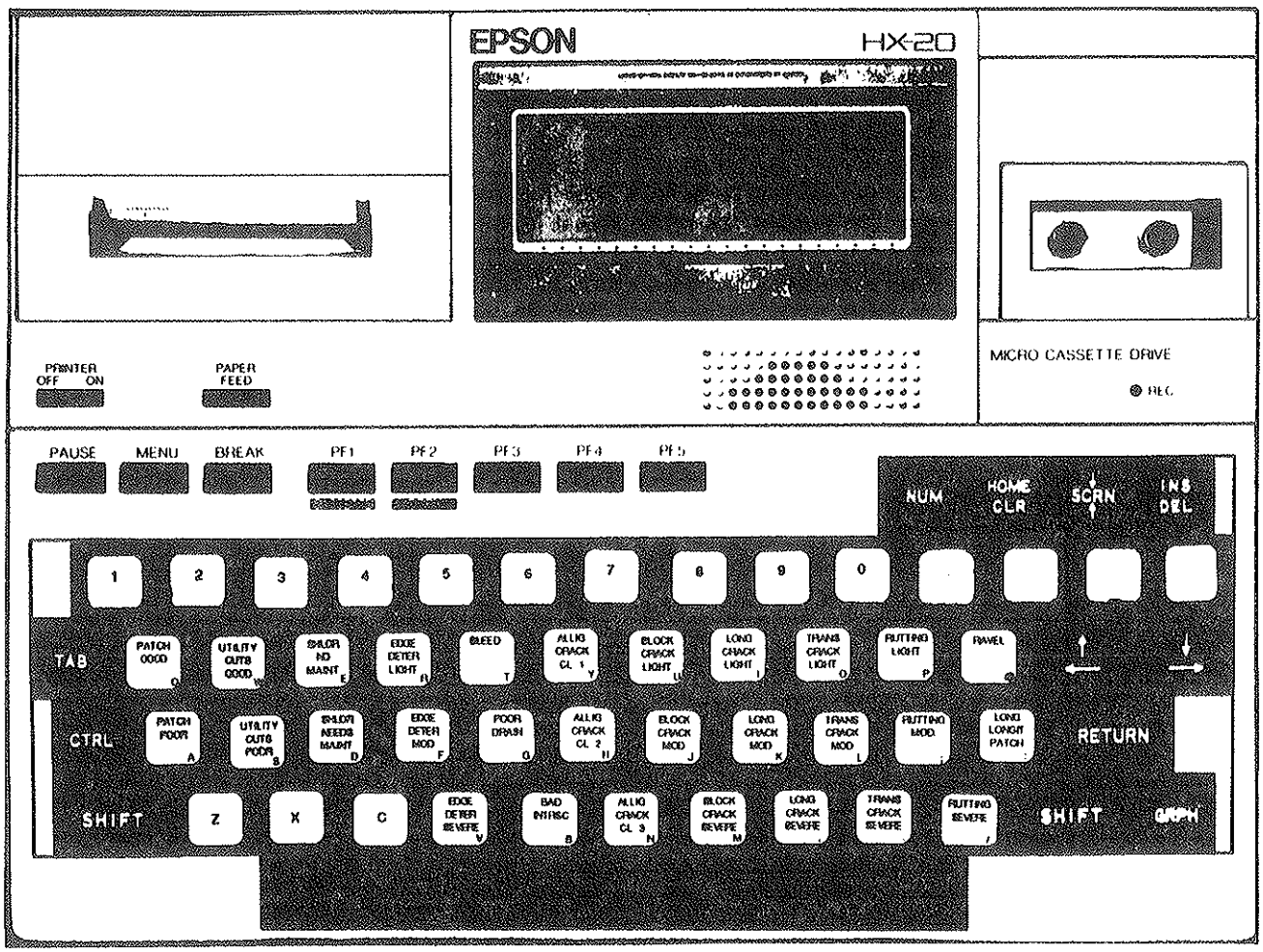

FIGURE 2 Epson HX-20 keyboard used for automatic distress data logging.

Photographing is performed at night using on-board lights. The lights are set at an angle to the road surface so that shadows are produced at cracks and other defects in the surface, making interpretation easier. Interpretations of the distresses are made by a technician viewing the developed 35-mm film enlarged ten times on the ROADRECON film digitizer. A grid pattern is overlaid on the film to aid in quantification of the distress for input into a computer database. The ROADRECON-70 survey vehicle and other systems used for the field testing are illustrated in figure 3.

Rut depth surveys can be carried out at speeds up to 50 mph (80 kmph) using the ROADRECON-75 system (*7*). A pulse camera mounted on the vehicle photographs hairline optical bars projected onto the road. The camera shutter and hairline projector are synchronized according to the distance covered by the projection vehicle, so the system is able to create a photographic record of rutting at variable distance intervals. The film is projected onto a digitizing table and traced with a computer "mouse," enabling the wave patterns to be processed into a transverse profile of the pavement surface.

Longitudinal roughness can be measured with the ROADRECON-77 by means of a tracking wheel, differential transformer, and an accelerometer. Longitudinal profile measurements can be made with this device at speeds up to 38 mph (60 kmph) (*7*). The data are stored on magnetic cassette tapes and plotted on a strip chart. Roughness is expressed as the standard deviation of the pavement profile measurements.

A high-speed automatic longitudinal profile and rutting survey device (ROADRECON-85B) was developed to measure longitudinal profile and estimate rutting at speeds up to 50 mph (80 kmph) (*7*). Three laser sensors, mounted on the rear bumper, are used to measure the longitudinal profile in the center of the vehicle and in both wheel paths. The data are recorded on magnetic tape and/or a paper chart.

GERPHO System

The Groupe Examen Routier Photographic (GERPHO) system, developed in France by the Ministere des Transports, employs a survey vehicle to take continuous 35-mm photographs of the pavement surface (*8*). The GERPHO has been used extensively in France since 1972. It has also been used to a limited extent in several other countries, including Spain, Portugal, and Tunisia (*9*). This system is similar to the PASCO ROADRECON-70.

The GERPHO system consists of a 35-mm continuously running (strip film) camera, mounted on a van, with a light source that illuminates the pavement, as illustrated in figure 4. The pavement surveys are conducted at night to allow for uniform lighting conditions. The camera is fitted with a 14.5-mm lens with an aperture of F-3.5. The picture covers a width of pavement of 15 feet (4.6 m). The film and light source are controlled as a function of vehicle speed. The

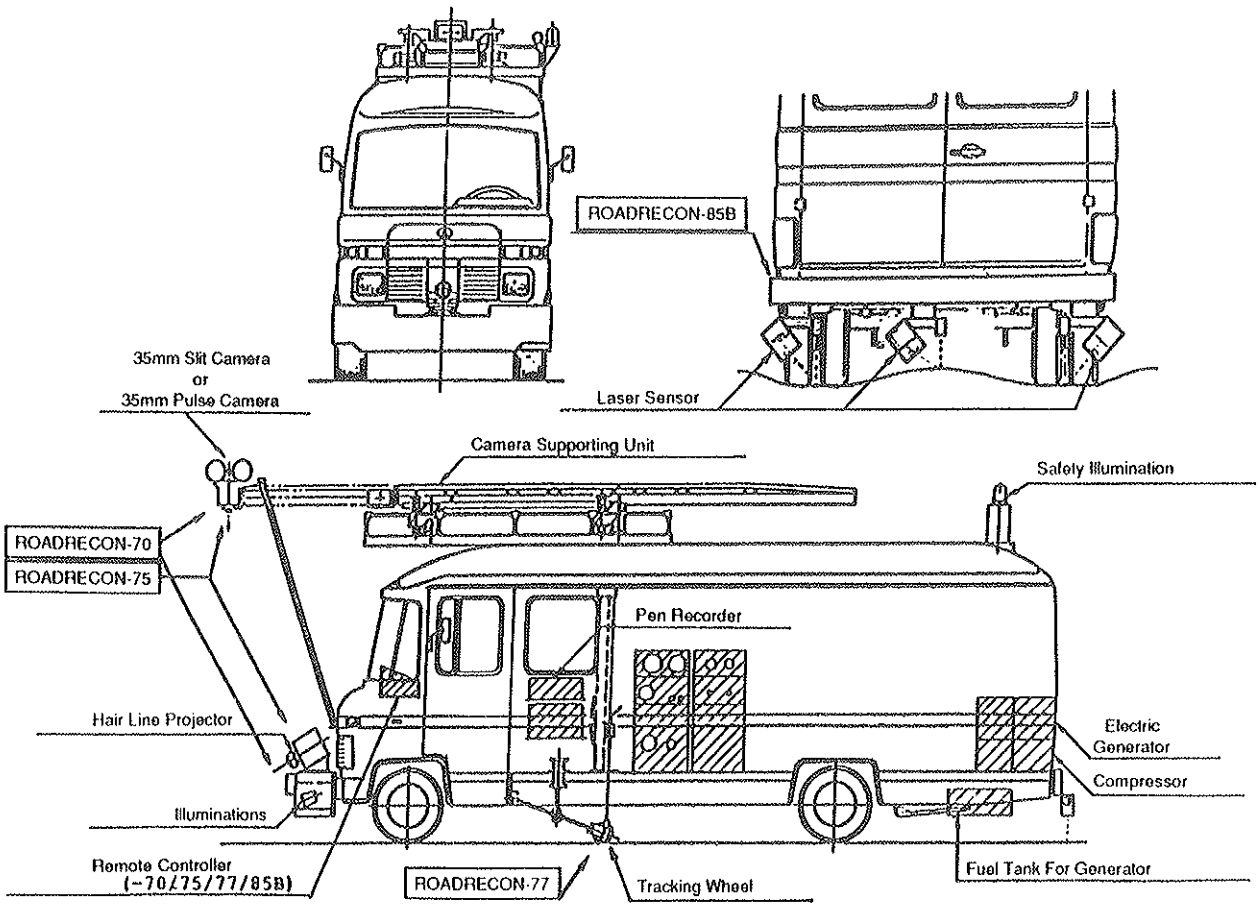

FIGURE 3 Schematic illustrating components of PASCO ROADRECON systems (*7*).

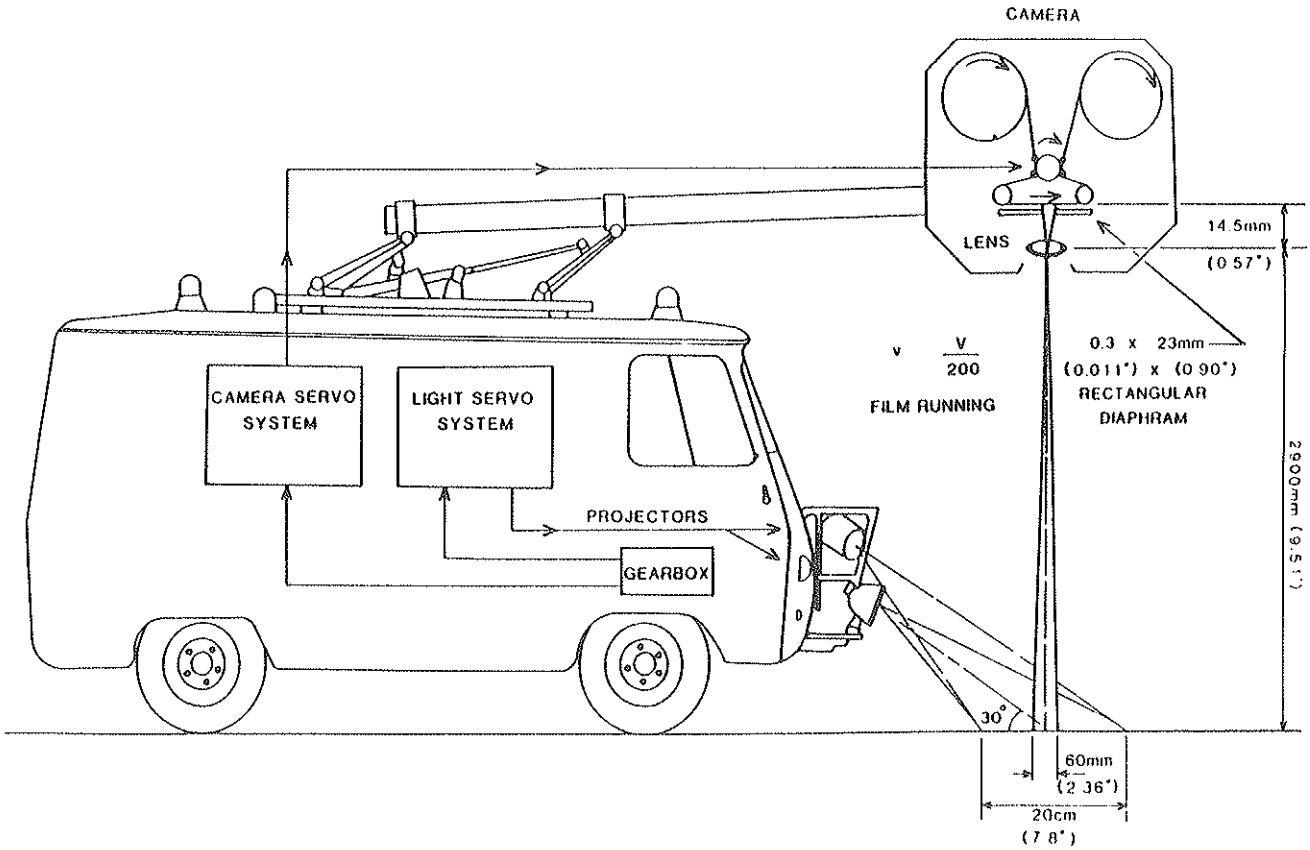

FIGURE 4 Schematic illustrating principles of GERPHO's automated photographic system (*8*).

GERPHO system takes a continuous image of the pavement surface at speeds up to 40 mph (60 kmph).

The interpretation of distresses from the negative films is done using a viewing table and data storage operating station. The distress data is directly entered into a microcomputer, using a keyboard equipped with a special template of distress codes. The microcomputer, special keyboard, CRT, and printer form the operating station.

Automatic Road Analyzer

The Automatic Road Analyzer (ARAN) vehicle is produced by Highway Products International, Inc. of Paris, Ontario, Canada. An ARAN Model III unit was used in the field testing (figure 5). The ARAN measures rut depth and transverse profile with ultrasonic sensors and ride/roughness quality with an accelerometer on the rear axle. The ARAN also takes a video picture of the road right-of-way through the windshield and the pavement surface with a shuttered video camera (in which the shutter takes thirty stills per second) behind the vehicle, and uses an on-board microprocessor to record distress data (*10*). Seven ultrasonic sensors on 12-inch (305-mm) centers, mounted in a front bumper rut bar, are reported by the manufacturer to measure the distance to the pavement surface with one millimeter precision at operating speeds up to 55 mph (90 kmph). Additional sensors and bar extensions can be used to extend the rut bar to a width of 10, 11, or 12 feet (3.1, 3.4, or 3.7 m). A calibration sensor is used to compensate for changes in air density due to temperature variation. Microprocessor-controlled, plug-in keyboards, with built-in liquid crystal displays, automate the collection and recording process. Dual keyboards have the capacity to handle up to twenty distresses with three severity categories.

Laser Road Surface Tester

The Laser Road Surface Tester (RST) was developed by the Swedish road and traffic research institute and has been used in Sweden for about three years (*11*). The Laser RST can reportedly measure crack depths and widths, rut depths, longitudinal profile from which roughness is computed, macrotexture, cross profile, and distance. A "windshield" condition survey can also be performed by one of the operators to identify types of cracking and other distresses. The device used in the field tests has eleven bumper-mounted laser range finders and an accelerometer to measure the transverse road profile and detect cracks while traveling at speeds of 18 to 55 mph (30 to 80 kmph) (personal communication, W. Uddin, Sept. 1986). A pulse transducer, mounted on the wheel hub, measures the distance traveled by the unit. Seven of the lasers pulse at 16 kHz and are used for the rut depth measurements. Four of the lasers pulse at 32 kHz and are used for measurement of rut depth and cracking. Two of these lasers are used for macrotexture and longitudinal profile measurements. These lasers have a reported accuracy of 0.01 inches (0.26 mm). An on-board microcomputer integrates the sensor signals with the accelerometer and distance transducer, averages the data into manageable sections, and provides the processed data in

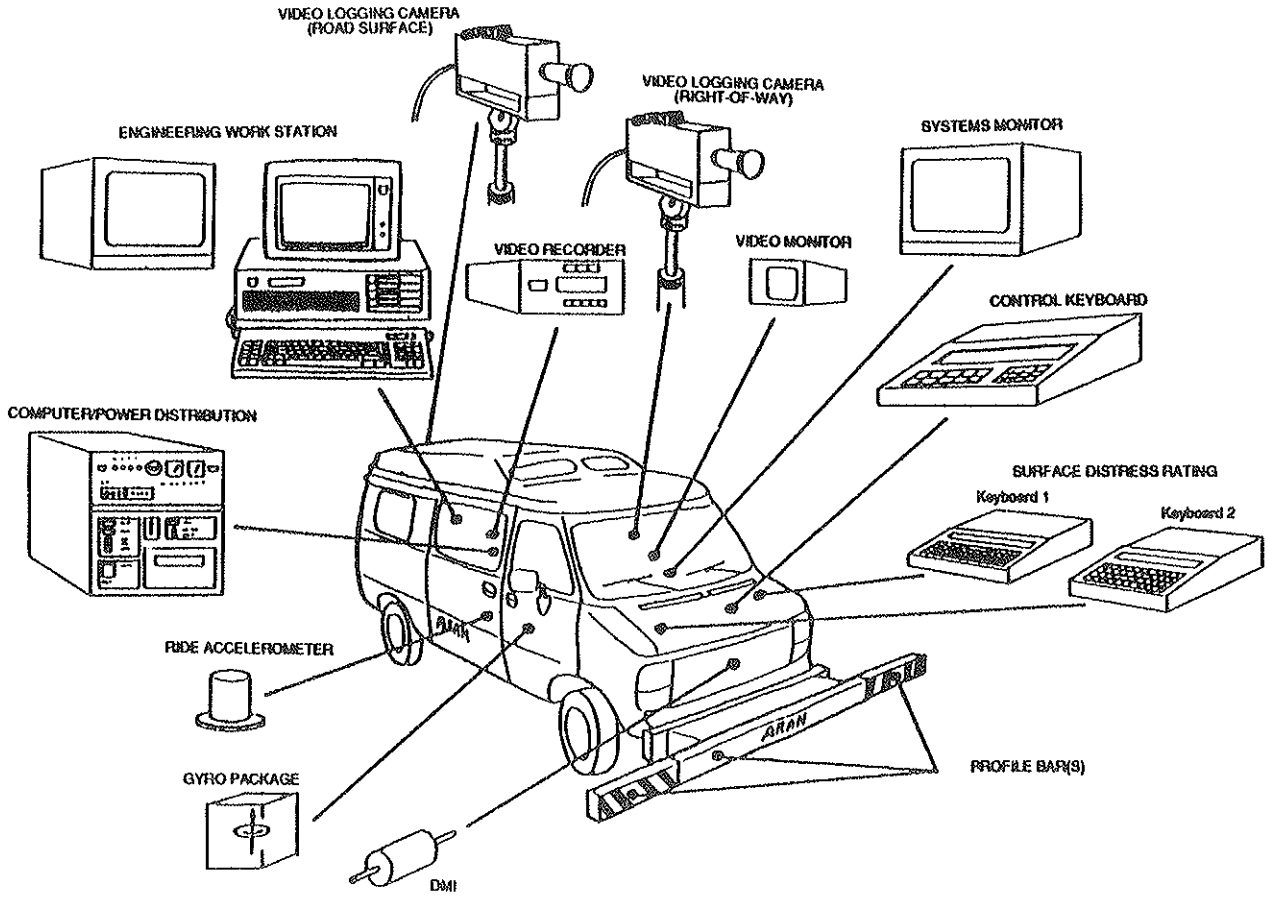

FIGURE 5 Schematic illustrating components of the ARAN (*10*).

real time. Eight three-position toggle switches are used to rate types of cracking and other distresses. An illustration of the Laser RST is provided in figure 6.

DESCRIPTION OF FIELD TEST SECTIONS

Test sections were selected to represent rigid, flexible, and composite (flexible overlay on a portland cement concrete pavement) types of pavement structure exhibiting good, moderate, and poor levels of distress. Potential locations were surveyed by members of the study staff and classified, based on subjective opinion, into the three distress-level categories. Twenty-five pavement sections, located in the central Texas area to minimize travel time, were selected.

Each test section was 1,000 feet (305 m) long. The sections were divided and marked at 100-foot (30.5-m) intervals. All of the sections were located on in-service trafficked roads. Two of the sections were located on the inside lane; the rest of the test sections on multilane highways were located in the outside lane.

In order to obtain meaningful results from the surveys, experienced raters and trained equipment operators were used for each procedure. The manual mapping, detailed condition surveys (PAVER and COPES), and detailed condition surveys using the data logger were performed by ARE Inc. personnel who had experience in performing the type of survey conducted. The surveys performed with the instrumented survey vehicles used the operating configuration, standard test procedure, and equipment operators which the manufacturer or technical representative considered to be most appropriate.

"Repeat" and "replicate" measurements were performed on a subset of the test sections. Repeat measurements were taken immediately after the initial survey was completed. Replicate measurements were taken three to four days after the initial survey, and the section numbers were changed in an effort to reduce bias from the previous measurements made on the sections.

It was initially planned to conduct side-by-side tests of all the devices. Due to scheduling difficulties and time constraints, the field surveys were instead performed at different times over a three-month period. The test sections were monitored on a regular basis by the study staff to detect any significant changes in the distresses present on the sections or any maintenance to the section which would change its characteristics. No significant changes were observed during the testing period.

EVALUATION OF THE SELECTED DEVICES

Comparative evaluation of the manual methods and the instrumented survey vehicles was made from several perspectives: (1) availability of a permanent record of the pavement surface, (2) evaluation and comparison based on the analysis of the surface distress and rutting data collected dur-

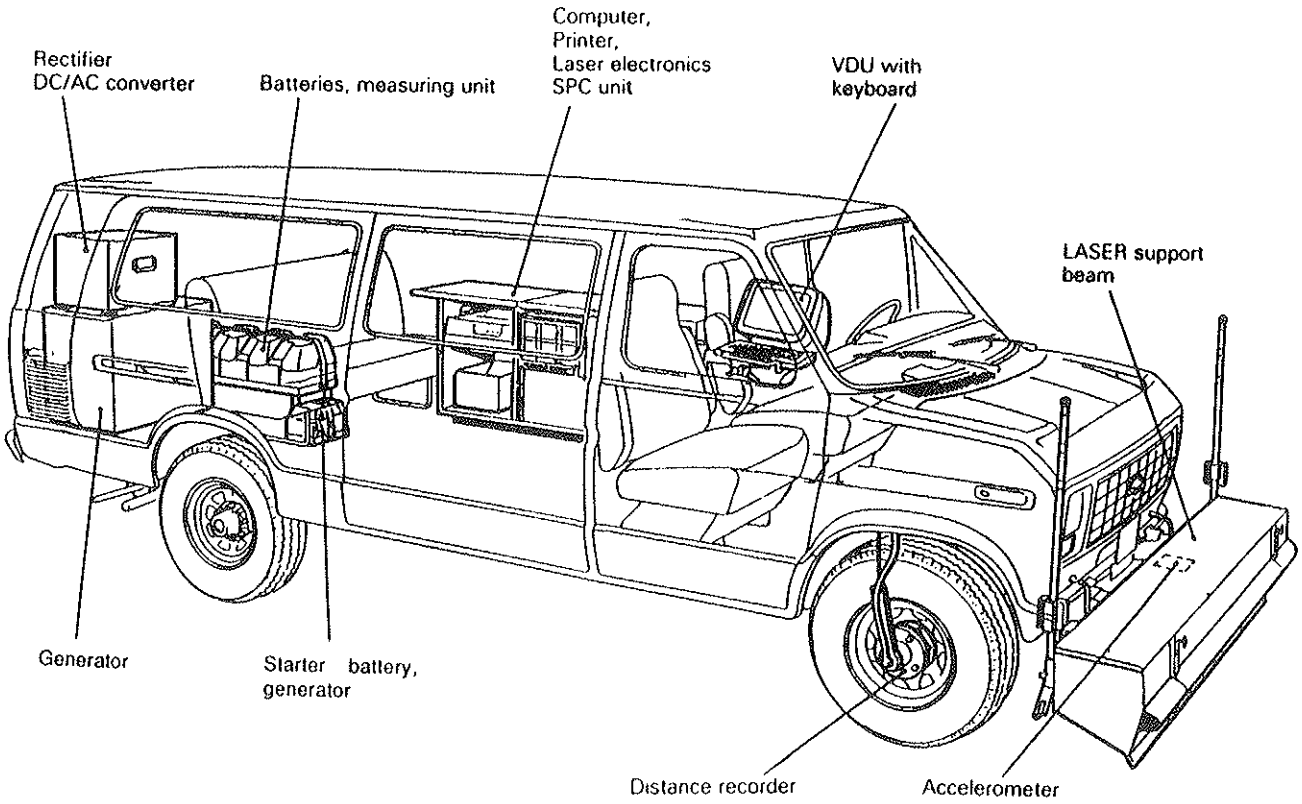

FIGURE 6 Schematic illustrating components of the Laser RST.

ing the field tests, (3) instrumentation evaluation and comparison of the performance based on hands-on experience and field tests, and (4) cost-effectiveness. Table 1 presents the criteria used for comparison and ranking of the selected methods.

Permanent Record of Pavement Surface

An image of pavement surface serves as a useful permanent record of pavement surface features. It facilitates fast and easy checking of the data without having to make a return visit to the field. Side-by-side comparisons of the images of a pavement surface, obtained during distress surveys performed at different times, allow investigation of the development of distresses. This is especially useful for long-term pavement performance research studies.

The detailed visual surveys and Laser RST do not create images of the pavement surface. Their output consists of numbers indicating the severity and extent of the observed distresses and characteristics of the pavement surface. Future investigations of the historical development of distress on a pavement section have no recourse but to rely on these ratings and measurements. Thus, these methods were rated "Very Poor" in terms of a permanent record of the pavement surface.

Reliability

The manual mapping method produces detailed maps prepared in the field. For reliability, this method was rated "Fair" because of the subjective nature of identifying distress types and severity, as well as inherent variation due to human factors. The GERPHO and PASCO ROADRECON-70 develop images from 35-mm film. Because this film, in the undeveloped state, is subject to loss due to improper handling and exposure, these devices were rated "Good" (rather than "Very Good") in terms of reliability. The ARAN video image can be viewed while it is being made and any problems can be detected immediately. Due to this feature, its reliability was rated "Very Good."

Field Productivity

Manual mapping is the most time-consuming and laborious method and was ranked "Very Poor" in field productivity. PASCO, GERPHO, and ARAN all use objective procedures at relatively high speeds to produce an image of the pavement surface and were rated "Very Good."

Usefulness

PASCO's and GERPHO's films are very sharp and were judged adequate for interpretation of distresses. The photographs from the PASCO device were slightly clearer than those from the GERPHO, although both were very acceptable. The usefulness of both of these devices' photographs of the pavement surface were rated "Very Good." The video images produced by the ARAN were judged "Poor" and not adequate for interpretation of all types of pavement distress. Its usefulness was ranked "Poor."

TABLE 1 A SUMMARY OF COMPARISON AND RANKING OF THE SELECTED METHODS

CRITERIA	Manual Mapping	GERPHO	PASCO, ROAD RECON	ARAN	Laser RST	DETAILED VISUAL SURVEY	
						Manual Recording	Automated Data Logger
1. Permanent Record of Pavement Surface							
Reliability	3	2	2	1	5	5	5
Field Productivity	5	1	1	1	5	5	5
Usefulness	3	1	1	4	5	5	5
2. Field Data Collection, Processing, Interpretation, and Summary							
Level of Automation	5	2	2	2	1	4	3
Accuracy	2	2	2	4	4	3	3
Quality of Rut Depth Data	1	5	1	2	2	3	3
Repeatability	2	1	1	3	3	3	3
Ease of processing	2	3	4	2	2	2	3
Ease of interpretation of outputs	1	1	2	3	3	1	1
3. Operating Restrictions							
Environmental Effects	2	2	2	3	2	2	2
Traffic Interference	5	1	1	1	1	5	5
Operating Speed	5	1	1	1	1	5	4
4. Equipment Durability and Robustness	1	1	1	2	2	1	1
5. Cost Effectiveness	5	1	2	2	1	4	3

Rankings: 1 = Very Good 2 = Good 3 = Fair 4 = Poor 5 = Very Poor

The usefulness of the manually prepared maps was judged "Fair," because of the subjective nature of the distress interpretations and the possibility that pavement features are not recorded which appear insignificant, but which may become important at a later date.

Field Data Collection, Processing, Interpretation, and Summary

Criteria in this category include level of automation, accuracy of surface distress data, quality of rut depth data, repeatability, ease of processing, and ease of interpretation of outputs.

Level of Automation

Automation is a primary consideration for cost-effective distress survey procedures. Mapping is not an automated method and was rated "Very Poor." In detailed manual visual survey methods, field data collection, processing, and interpretation are done manually, although the data can be input into the computer and used to generate reports. Therefore, they were ranked "Poor." The automated data logger was given a "Fair" rating, due to the reduction in time and cost to transfer the field data to an office computer for processing. The GERPHO, PASCO, and ARAN instrumented vehicles were rated "Good" because data collection is automated, but further processing of the field data is required in the office. The automation of the Laser RST was rated "Very Good" because all of the information collected with this device is processed in the field with the on-board computer.

Accuracy of Surface Distress Data

Accuracy of the distress survey data was defined as how close the reported distress data corresponded to the distresses actually on the test sections. The "truth" was taken as the ratings from the three manual methods when they were all in agreement. Where conflicts in the data from the manual methods existed, return trips to those sites were made by the members of the study team to resolve the conflicts.

No single method was found to be totally correct for all sections. The manual mapping method yielded results that approximated what the truth was judged to be and was given a "Good" rating. The information from the GERPHO was also in close agreement with the observed distresses and given a "Good" rating. The form of distresses reported from the

PASCO ROADRECON-70 were somewhat difficult to directly compare, but was judged to be of "Good" accuracy. The accuracy of the detailed visual surveys was judged "Fair," even though the surveys were used, in part, to help define the actual conditions. As might be expected, the accuracy of the surface distress information collected through the windshield of the ARAN and Laser RST were not as accurate as the other methods and was judged "Poor."

Quality of Rut Depth Data

Quality of the rut depth measurements was based on the accuracy of the measurement and the amount of detail provided for the transverse profile. Accuracy of the rut depth measurements was determined by comparison against transverse rut profiles manually measured with a 10-foot (3-m) straightedge. The amount of detail was judged "Good" if both a transverse profile and maximum rut depth were produced.

Since the GERPHO does not measure rut depth, it was rated "Very Poor" in this category. The manual mapping method was rated "Very Good" because the 10-foot (3-m) straightedge was considered as a part of this technique.

Since the PASCO ROADRECON-75 rut depth measurements corresponded very well with the straightedge measurements, and detailed transverse profiles were produced, it was rated "Very Good."

The maximum rut depth measurements made with the ARAN and Laser RST were less than those measured with the straightedge. However, due to differences in measurement intervals, the accuracy of these rut depths could not be directly evaluated against the straightedge measurements. Although the ARAN measured a transverse profile using sensors spaced at 1-foot (0.3-m) intervals, only the maximum rut depth was reported. The Laser RST gave the average and standard deviation of the depth measurements made with each laser, which gives some information on the transverse profile shape, but did not give profiles for each measurement made. Since the Laser RST made approximately 3,000 measurements on each section, if transverse profiles were produced the amount of information would be overwhelming. Based on these considerations, the ARAN and Laser RST quality of rut depth measurements were rated "Good."

The accuracy and detail provided with the detailed visual surveys were rated "Fair." Some discrepancies were found in both the extent and severity of rutting reported by these methods. These survey techniques are not designed to produce information on the transverse profile of the pavement.

Repeatability

This criterion is related to the differences between the reported distresses from initial surveys and from surveys performed immediately following or several days later. The PASCO measurements showed excellent agreement between initial and repeat measurements and was therefore ranked "Very Good." The distresses from the GERPHO photographs were not interpreted for the repeat measurements. Since the repeat photographs of the test sections made with the GERPHO were judged by the study staff to be equal in quality to the initial photographs, the repeatability of this device was also rated "Very Good." The rut depth measurements made with the ARAN and Laser RST had "Good" repeatability. However, significant differences were found in the ratings of the othersurface distresses. Since rut depth is only one distress category, these two devices were rated "Fair" in overall repeatability.

Detailed survey methods showed discrepancies between raters, but repeat measurements with the same rating team yielded "Fair" repeatability. The repeatability of the manual mapping technique was rated "Good."

Ease of Processing

The ease of processing the raw data is rated based on the required background and training for the technician(s) and the complexity involved in the processing. The lower the requirements for operator training and the less complex the process, the higher the rating. These ratings are relative to each other and should not be considered as an absolute measure, that is, a method rated as "Poor" was judged to require more operator training and be more complex than one with a "Fair" rating. Mapping was rated "Good" even though it is laborious and time-consuming. It is a straightforward process requiring technicians to summarize, from the prepared maps, the distresses which have been interpreted in the field. The ease of processing the GERPHO photographs was rated "Fair" because a technician trained to interpret the photographs with keyboard skills is required.

The PASCO techniques were rated "Poor" overall in the ease of processing because of the complexity of the procedures and the following requirements for technicians: that they operate a digitizing computer for rut depth measurements, that they be trained for interpretation of the distresses from the photographs, and that they have keyboard skills for entry of the interpreted data into a computer. Because the technicians who process the raw data from the ARAN and Laser RST are not required to interpret the distresses, the ease of processing was rated "Good." The ease of processing the data from the detailed condition survey was also rated "Good." Although keyboard entry skills are required to enter the data into the computer, the technicians processing the data are not required to interpret distresses. The automated data logger was rated as "Fair" because it was slightly more complex due to the need to have the technician transfer the field data to the office computer prior to final processing.

Ease of Interpretation of Outputs

The case of interpreting the reports or final output from each method was rated according to how easy it was to understand the outputs. All of the manual methods and GERPHO were ranked "Very Good" because the reports were given in terms of severity and extent of distresses in clearly distinguishable categories. The reports from the PASCO ROADRECON device were only rated as "Good," primarily because they were produced on an output format printed in Japanese and because cracking, patching, and potholes were grouped into one category. It should be noted that a user agency should be able to reformat reports into its desired format, using the ROADRECON equipment. The ARAN and Laser RST

devices were ranked "Fair" because interpretation of their output was complex and not straightforward. The manuals and written procedures which accompanied their reports were also found to be complex and required more effort to understand than the other methods.

Operating Restrictions

The three criteria in this category are summarized in table 1 and discussed below.

Environmental Effects

No method can be used during all weather conditions, or at all times of the day and night. All methods are rated "Good" except ARAN, which was rated "Fair" due to the problems caused by the rain with the ultrasonic sensors during field tests.

Traffic Interference

Traffic interference during distress surveys affects the quality and quantity of distress data. None of the four instrumented survey vehicles interrupts traffic, poses hazards, or requires lane closure or other traffic controls for routine use. These were ranked "Very Good." All manual methods are subject to potential conflicts with traffic because of the presence of the rating team taking measurements on the side of the road or in the traffic lane. Therefore, the manual mapping and visual condition survey methods were ranked "Very Poor."

Operating Speed

The operating speed is related to productivity and cost-effectiveness of the complete system. Labor-intensive methods (mapping and manually-recorded detail survey) were ranked "Very Poor," followed by the automated data loggers, which was somewhat faster but rated "Poor" in comparison to the instrumented survey vehicles. The instrumented survey vehicles were all rated "Very Good."

Equipment Durability and Robustness

Equipment durability and robustness are important considerations for the long-term performance of a device. The manual mapping and detailed visual distress survey methods use equipment that is not subject to breakdowns or that requires little maintenance and were, therefore, rated as having "Very Good" equipment durability and robustness. The GERPHO and PASCO ROADRECON devices, which also rated "Very Good," have a long history of use in their respective countries and performed without problems during the field tests. The ARAN device tested in this study had two malfunctions during the testing period that were corrected without great delay. Although it was a new machine which had not had all of the "bugs" worked out, it was assigned a "Good" reliability rating in comparison to the other methods. The Laser RST was also given a "Good" rating is equipment reliability and robustness, because the instrumentation involved with the use of lasers and interfaces with the on-board computers could be subject to more potential problems than the equipment rated as "Very Good."

Cost-Effectiveness

Cost-effectiveness involves costs associated with several parameters: field productivity, operating crew size, office data processing time, manpower requirements, and usefulness of data. Cost analyses based on these criteria (*1*) resulted in the GERPHO and Laser RST ranked "Very Good," followed by the other two instrumented survey vehicles. The automated data logger was rated "Fair." The manual recording of visual survey method and manual mapping were ranked "Poor" and "Very Poor," respectively.

CONCLUSIONS

Distress surveys for pavement management purposes are conducted at two levels, network- and project-level evaluations. Network-level evaluations are conducted over a road or highway network to determine its condition and establish priorities for improvements to the sections competing for limited funding. Project-level evaluations are conducted to provide information with which to design specific improvements or "4R" measures (resurfacing, rehabilitation, restoration, and reconstruction). There is a wide variation in the type and application of distress surveys for network- and project-level evaluations. A great deal depends on the magnitude of the network, the type of pavement structures, the type of agency, and the available funding.

The PASCO and GERPHO photographic survey vehicles can be used for both network-level and project-level distress surveys. The GERPHO and PASCO devices are also well suited as high-speed distress survey devices for research studies. They are capable of covering extensive networks in a relatively short time. Either summary or detailed distress information can be interpreted from the photographs as desired. Photographs taken over time can yield useful information on the development of distress to update distress prediction models. The additional rut depth and roughness measurement equipment contained on the PASCO vehicle gives it additional utility for both network- and project-level surveys. While these vehicles provide the basis for good quality distress information, the costs associated with film development, office interpretation, and film storage may offset their advantages for some agencies. Although a permanent visual record of a pavement surface has many advantages, these records may not be necessary for a network-level pavement management system.

The other two distress survey vehicles investigated in this study, the ARAN and Laser RST, lend themselves to network-level distress surveys. They both supplement windshield-type distress ratings with measurements of rutting and roughness. They are capable of covering networks in a relatively short time. Since the distress information and pavement surface measurements are recorded on on-board microcomputers, the turnaround time on completion and assembly of the processed information is relatively short.

The video cameras on the ARAN provide additional information that may be useful to an agency. The through-the-windshield view of the road environment provides information useful for inventory purposes. Although the image of the pavement surface from the shuttered video camera was not adequate for interpretation of all distresses, it does provide a record of major distresses, such as potholes, that can be useful to the engineer in the office as a check on questionable ratings, or to investigate a section of road that is of interest, prior to making a field trip.

Manual surveys are the traditional approach to distress surveys. Automated data loggers are more cost-effective than manual recording, and thus it is recommended that an agency performing manual surveys use an automated data logger to record the distress survey information in the field and for transfer to an office computer. Because manual mapping is laborious and time-consuming in the field, as well as during office data reduction, it is not recommended for network- or project-level distress surveys for pavement management purposes.

ACKNOWLEDGMENT

The work reported in this paper was sponsored by the U.S. Department of Transportation, Federal Highway Administration. The authors would like to acknowledge the support of Douglas Brown of the Federal Highway Administration, the cooperation of the Texas State Department of Highways and Public Transportation, and the participation of the various distress survey equipment representatives.

REFERENCES

1. W. R. Hudson, G. E. Elkins, W. Uddin, and K. T. Reilley. *Improved Methods and Equipment to Conduct Pavement Distress Surveys*. Report FHWA-TS-87-213. FHWA, U.S. Department of Transportation, 1987.
2. *Special Report 61E: The AASHO Road Test Report 5 Pavement Research*. HSB, National Research Council, Washington, D.C., 1962.
3. R. E. Smith, M. I. Darter, and S. M. Herrin. *Highway Pavement Distress Identification Manual*. FHWA Contract DOT-FH-11-9175 and NCHRP Project 1–19. University of Illinois at Urbana-Champaign, March 1979.
4. *APWA PAVER Implementation Manual* (Draft). American Public Works Association Research Foundation, April 1983.
5. M. I. Darter, J. M. Becker, M. B. Snyder, and R. E. Smith. *NCHRP Report 277: Portland Cement Concrete Pavement Evaluation System, COPES*. TRB, National Research Council, Washington, D.C., Sept. 1985.
6. R. F. Carmichael, III, D. S. Halbach, and L. O. Moser. *Pavement Condition Survey Manual for Rhode Island Pavement Evaluation and Management System*. Final Report No. RI-2/2. ARE Inc., Jan. 1985.
7. *Report on Pavement Condition Monitoring Methods and Equipment*. PASCO USA Inc., Lincoln Park, N.J., Sept. 1985.
8. MAP Inc., Washington, D.C. *Pavement Condition Monitoring Methods and Equipment*. Final Report on GERPHO Survey for ARE Inc. Austin, Federal Highway Administration Strategic Highway Research Program, August 1986.
9. M. DeWilder. GERPHO and the APL. *Proc., Roadway Evaluation Equipment Workshop*. Report FHWA-TS-85-210. FHWA, U.S. Department of Transportation, May 1985.
10. *Automatic Road Analyzer Mobile Data Acquisition Vehicle*. Product Bulletin. Highway Products International, Inc., 1985.
11. R. L. Novak. Swedish Laser Road Surface Tester. *Proc., Roadway Evaluation Equipment Workshop*. Report FHWA-TS-85-210. FHWA, U.S. Department of Transportation, May 1985.

Publication of this paper sponsored by the Committee on Pavement Monitoring, Evaluation, and Data Storage.

Effect of Reflected Waves in SASW Testing of Pavements

J. C. SHEU, K. H. STOKOE II, AND J. M. ROESSET

The Spectral-Analysis-of-Surface-Waves (SASW) method is a rapidly developing in situ seismic method for nondestructively determining Young's modulus profiles of pavement sites. The method is based on the generation and measurement of surface waves (Rayleigh waves). Due to the complex theoretical solution of surface wave propagation in pavements, a multilayered half space with infinite lateral extent has been assumed in the analytical solutions of SASW testing. In addition, only plane surface waves were considered. The existence of direct and reflected body waves and any reflected surface waves, although known to occur in pavements, was neglected in the analytical solutions. To understand the impact of reflected surface waves and direct and reflected body waves in SASW testing, a simplified analytical model was developed. Reflecting boundaries such as edges or joints of a pavement system or the horizontal interfaces between pavement layers were considered. To examine the validity of the model, field tests on a jointed concrete pavement were performed. The results show that reflected surface waves cause fluctuations to occur in the field data (dispersion curves) which would otherwise be a smooth function if only direct surface waves were present. Direct and reflected body waves also create a similar result but to a much lesser extent. Reflected SV-waves (shear waves with vertical particle motion) exhibit the most influence of all direct and reflected body waves, with the effect more important at wavelengths longer than the pavement surface layer. The adverse effect of reflections can be minimized by properly orienting the test array (line passing between the source and receivers) in the field with respect to joints, edges, and cracks in the pavement. For instance, when a vertical reflecting boundary such as a joint is oriented perpendicularly to the SASW array, the adverse effect of reflections can be minimized and nearly eliminated by placing the source between the reflecting boundary and the receivers. When a vertical reflecting boundary such as the pavement edge is near the zone of testing, the effect of reflections can be greatly minimized by orienting the array parallel to and near (about 0.1 times the receiver spacing) the edge.

Nearly all nondestructive testing of pavements involves stress wave propagation. Due to the complex nature of stress wave propagation in pavements, most analytical models are based on the assumption that the seismic waves propagate in a layered half space with no additional boundaries or interfaces. As a result, reflected surface and body waves created by boundaries in the real finite system are not included in these solutions. In fact, whenever a pavement system is tested using a stress wave propagation method, such as the Spectral-Analysis-of-Surface-Waves (SASW) method, reflected waves from discontinuities such as edges, joints, or cracks are inevitably generated. The key reflecting boundaries are nearly always those in the top layer, such as the concrete layer in a rigid pavement.

The existence of reflected surface waves is not considered in the analytical model used to analyze (invert) SASW dispersion curves (*1–3*). Therefore, it is important to investigate how and to what extent reflected waves influence field results (dispersion curves) so that possible errors created by neglecting their existence are not accidentally overlooked. It may then be possible either to avoid or reduce the influence of reflected waves by adjusting the field test procedure and/or in-house data reduction process.

In addition, only plane surface waves are assumed to exist in the inversion process used in the SASW method (*1–3*). However, when the test is carried out in the field, surface waves are generated by applying a point load (impact) on the surface. As a result, body waves (compression and shear) are generated simultaneously with the surface waves. These body waves may propagate directly from the source to the receivers (direct body waves), or they may be reflected, just like surface waves, by discontinuities in the system and then reach the receivers (reflected body waves). The effect of direct and reflected body waves on the dispersion curve is not known and needs to be studied. Sanchez-Salinero et al. (*4*) initiated a formulation which incorporates all waves in the system. However, more work is necessary before this formulation can be easily used and parametric studies can be performed.

A mathematical model which is capable of simulating the effect of direct and reflected body waves and reflected surface waves on dispersion curves in presented herein. Use of this model is first explained with a simple example involving surface waves reflected from the edge of a concrete pavement. To evaluate further the validity of this approach, modeled dispersion curves are compared to actual dispersion curves measured in the field for various locations of pavement joints and edges relative to the general location and orientation of the source and receivers used in SASW testing. Confidence in this model is established with these comparisons, and the model is further used to predict the behavior of dispersion curves for other conditions of interest, such as for the influence of direct and reflected body waves and for multiple reflections of body and surface waves.

BACKGROUND OF SASW METHOD

The SASW method is an in situ seismic method which is used for near-surface profiling of pavement sites. The general

J. C. Sheu, Dames & Moore, 221 Main Street, San Francisco, Calif. 94105. K. H. Stokoe II and J. M. Roesset, Geotechnical Engineering, The University of Texas at Austin, Austin, Tex. 78712.

arrangement of the source, receivers (vertical sensors), and recording equipment is shown schematically in figure 1. The source is a transient vertical impact, often delivered by a hand-held hammer, which generates a group of surface waves with various frequencies. The surface waves travel along the surface in all directions from the source. Two vertical receivers, either geophones or accelerometers, are placed on the surface in a linear array and are used to monitor the propagation of surface wave energy. By analyzing the phase of the cross power spectrum determined between the two receivers, surface wave velocities are determined over the range of frequencies generated. The shear wave velocity profile is then obtained from the surface wave velocities, and finally the Young's modulus profile is determined (*1–4*).

Since the stiffness of a pavement site varies with depth, the velocity of the surface wave becomes a function of wavelength (or frequency). The variation of surface wave velocity with respect to wavelength (frequency) is called a dispersion curve. This dispersive characteristic of Rayleigh (surface) waves is the basis upon which the SASW method is founded. This dispersion curve can be considered the "raw data" collected in the field. The purpose of this paper is to show how joints, edges, and other discontinuities in the pavement system affect the field dispersion curve.

The dispersion curve only represents the relation between surface wave velocity and wavelength. When the medium consists of layers with different stiffnesses (in terms of shear wave velocities or elastic moduli), the relationship between the elastic modulus profile and the field dispersion curve becomes quite complex (*4, 5*). As a result, development of the modulus profile from a measured dispersion curve is one of the key steps in the SASW method. This process, by which the modulus profile is back-calculated from the corresponding field dispersion curve, is called inversion of the dispersion curve (or in short, inversion). However, this aspect of the SASW method (inverting) is not addressed herein because the effects of reflections are more directly seen in the raw data, the measured dispersion curve.

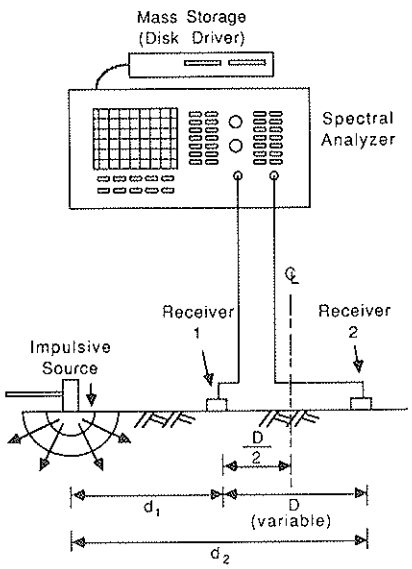

FIGURE 1 Field arrangement of source, receivers, and recording equipment for typical SASW testing.

SIMPLIFIED MATHEMATICAL MODEL

No theoretically complete solution yet exists for wave propagation with vertical, horizontal, and oblique boundaries in a layered system such as a pavement which involves all seismic waves (*6, 7*). In an attempt to simulate wave propagation problems associated with such kinds of systems, a simplified mathematical model was developed. This simplified modeling technique assumes that a true dispersion curve derived solely from direct surface waves is known. The dispersion curve which includes the effects of reflected and/or other direct waves is calculated based on the true dispersion curve by simply adding the influence of any reflected and/or additional direct waves to the true dispersion curve as outlined below.

Imagine that a vertical forcing function is applied at a point on the surface of a layered system, and a pure sine wave with a frequency, f_0, is generated. Two receivers are attached to the surface of the layered system and aligned with the point source to form a linear array (straight line connects source and all receivers) as in SASW testing. The receivers are used to track vertical surface motion. Direct surface waves propagate along the surface in all directions from the source. In addition, reflected waves are created due to the existence of discontinuities in the layered system. As a result, surface (vertical) motion detected by the two receivers is a combination of direct (surface and/or body) waves and reflected (surface and/or body) waves.

Schematic representations of the time records of each receiver are shown in figure 2. Suppose time signals detected by the two receivers after the surface is excited by this point-forcing function are represented by $g(t)$ and $h(t)$, respectively. Then $g(t)$ and $h(t)$ can be expressed by

$$g(t) = \sum_p a_{1p} \sin 2\pi f_0(t - t_{1p}) \tag{1}$$

$$h(t) = \sum_q a_{2q} \sin 2\pi f_0(t - t_{2q}) \tag{2}$$

in which a_{1p} and a_{2q} are amplitudes of various wave arrivals measured by the first and second receivers, respectively, and t_{1p} and t_{2q} are the times of the various wave arrivals at the first and second receivers, respectively. The definitions of a's and t's are shown schematically in figure 3. In the above and following equations, the subscripts are used to denote a specific wave arrival at a particular receiver. The first subscript is used to demote the receiver number, and the second subscript is used to denote the number of the wave arrival. For example, a_{23} represents the amplitude recorded by the second receiver of the third wave arrival (which could be a direct or reflected wave).

Let $G(f)$ and $H(f)$ be the Fourier transforms of $g(t)$ and $h(t)$, respectively. The transforms can then be expressed as

$$G(f) = \sum_p a_{1p} \exp(-i\,2\,\pi\,f_0\,t_{1p}) \quad \text{for } f = f_0 \tag{3a}$$

$$G(f) = 0 \quad \text{for } f \neq f_0 \tag{3b}$$

and

$$H(f) = \sum_q a_{2q} \exp(-i\,2\,\pi\,f_0\,t_{2q}) \quad \text{for } f = f_0 \tag{4a}$$

$$H(f) = 0 \quad \text{for } f \neq f_0 \tag{4b}$$

The cross power spectrum, G_{yx}, for this pair of time signals

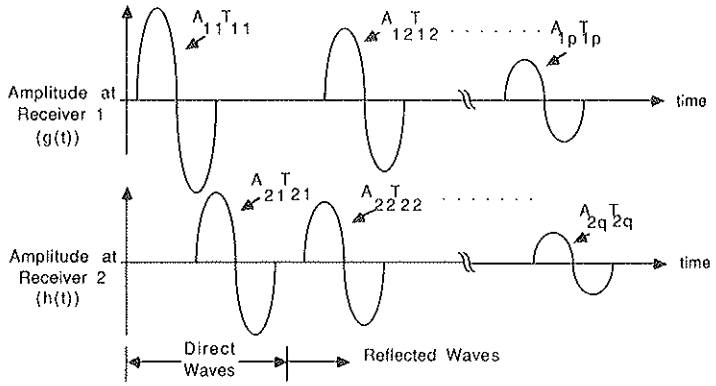

FIGURE 2 Representation of time domain records received by each receiver in SASW testing illustrating combined direct and reflected (packets of energy) waves.

is defined as

$$G_{yx} = G^* \times H \tag{5}$$

in which G^* denotes the complex conjugate of G. The phase of the cross power spectrum at frequency f_0, $\phi(f_0)$, is

$$\phi(f_0) = \text{Tan}^{-1}\left[\frac{\sum_p \sum_q a_{1p}a_{2q} \sin 2\pi f_0(t_{1p} - t_{2q})}{\sum_p \sum_q a_{1p}a_{2q} \cos 2\pi f_0(t_{1p} - t_{2q})}\right] \tag{6}$$

This phase is the key variable used to calculate wave velocity.

In a real SASW test, a wide range of frequencies is generated simultaneously by applying a vertical impact on the surface of the system. As a result, each arrival is no longer a single-frequency arrival but contains a certain range of frequencies. Since equations 1 through 6 were derived with the consideration of only a single frequency, the following modifications are made so that they can be applied to the multiple-frequency condition. Assume while f_0 varies over a range of frequencies generated by the vertical impact, values of a_{1p}, a_{2q}, t_{1p}, t_{2q} vary accordingly. Let A_{1p}, A_{2q}, T_{1p}, and T_{2q} be the amplitude and time functions of frequency at receivers 1 and 2, respectively. Therefore, the functions can be written as

$$A_{1p}(f) = a_{1p}(f_1) + a_{1p}(f_2) + a_{1p}(f_3) + \ldots \tag{7}$$

$$A_{2q}(f) = a_{2q}(f_1) + a_{2q}(f_2) + a_{2q}(f_3) + \ldots \tag{8}$$

$$T_{1p}(f) = t_{1p}(f_1) + t_{1p}(f_2) + t_{1p}(f_3) + \ldots \tag{9}$$

$$T_{2q}(f) = t_{2q}(f_1) + t_{2q}(f_2) + t_{2q}(f_3) + \ldots \tag{10}$$

in which the notations for each subscript of T's and A's, as well as t's and a's, are the same as previously defined and frequencies f_1, f_2, f_3, and so forth are the desired modeling frequencies. Hence, equation 6 can be rewritten as

$$\phi(f) = \text{Tan}^{-1}\left\{\frac{\sum_p \sum_q A_{1p}(f)A_{2q}(f) \sin 2\pi f[T_{1p}(f) - T_{2q}(f)]}{\sum_p \sum_q A_{1p}(f)A_{2q}(f) \cos 2\pi f[T_{1p}(f) - T_{2q}(f)]}\right\} \tag{11}$$

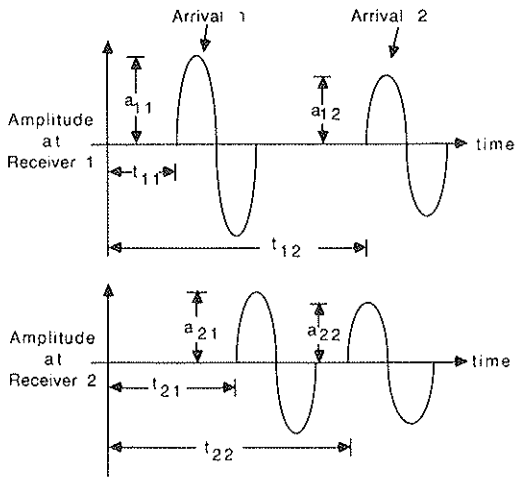

FIGURE 3 Representation of amplitudes (a's) and arrival times (t's) for two single-wave arrivals at each receiver.

Each A, with two subscripts, is a series of amplitudes which are a function of frequency and correspond to the particular arrival denoted by the subscripts. The absolute value of A actually represents the amplitude of the linear spectrum for this particular arrival. Each T, with two subscripts, is a series of travel times which are a function of frequency and correspond to the particular arrival denoted by the subscripts. It is necessary to note that the connotation of "arrival" used in equation 6 is somewhat different than that used in equation 11. In equation 6, each "arrival" has energy at only one frequency. On the other hand, in equation 11, each "arrival" represents a packet of energy containing a range of frequencies. Since equation 6 is a special case of equation 11 and the latter was used for all studies, the second connotation of "arrival," namely a packet of energy over a range of frequencies, is used herein.

It is important to notice that both T's and A's are functions of frequency, and each arrival has its own T and A. Since T is directly related to the arrival times of different frequencies forming the arrival of a particular packet of energy, dispersive characteristics (that is, waves corresponding to different frequencies traveling at different velocities) of this particular

arrival can be accurately modeled by using the proper travel time in "T" for each frequency. In addition, since the arrival of each packet of energy has its own T, waves with different dispersive characteristics can be analyzed together; that is to say, each arrival could have its own dispersion curve. A typical need of modeling waves with more than one type of dispersive characteristic is in the case when combined surface wave and body wave effects are considered. Examples of this type of modeling are illustrated in the following sections.

The amplitude of the linear spectrum, A, for the arrival of each impulse (packet of energy) is simply a measure of the amplitudes of the different frequencies transmitted by this packet of energy. Therefore, the value of A is directly related to the damping characteristics and reflection coefficients of the system being tested. Due to the fact that the arrival of each impulse has its own A, amplitudes of different frequencies which attenuate at different rates can be modeled by using different ratios of amplitudes between different arrivals of the impulse at different frequencies.

In the present inversion process in SASW testing, it is assumed that only plane surface waves exist (*4–6*). As a result, it is implicitly assumed that only one surface wave arrival is detected by the receivers. Let T_{11} and T_{21} be the arrival times of this direct surface wave at each receiver. The corresponding phase of the cross power spectrum, $\phi(f)$, can be expressed as

$$\phi(f) = 2\pi f[T_{11}(f) - T_{21}(f)] \tag{12}$$

Equation 12 is just a special case of equation 11 with p and q both equal to 1. Also notice that in equation 11, it is not necessary to have T_{11}, T_{21}, A_{11}, and A_{21} associated with the arrival of the direct surface wave. In fact, arrivals in equation 11 can be considered in any random order. However, to avoid any possible confusion, T_{11}, T_{21}, A_{11}, and A_{21} are used to represent only direct surface wave arrivals for all discussions presented hereafter.

The problem faced in typical SASW testing in terms of reflections is now clear. In the field, measured phases of cross power spectra are in the fashion of equation 11, but during the in-house inversion stage, the phases of cross power spectra are assumed to be in the fashion of equation 12. The difference between these two equations is the error introduced by waves other than the direct surface wave. As such, it is possible to study the influence of reflected and direct waves on field dispersion curves by using equations 11 and 12, as shown in the following sections.

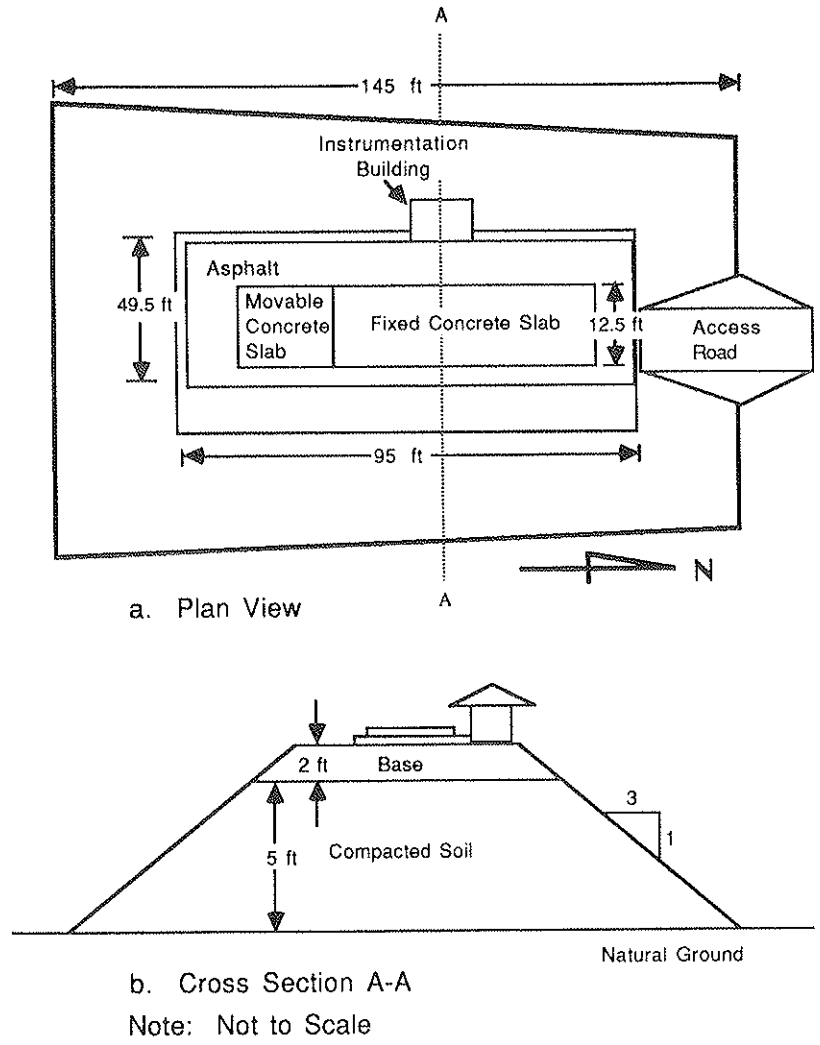

FIGURE 4 Plan and cross-sectional views of BRC pavement facility.

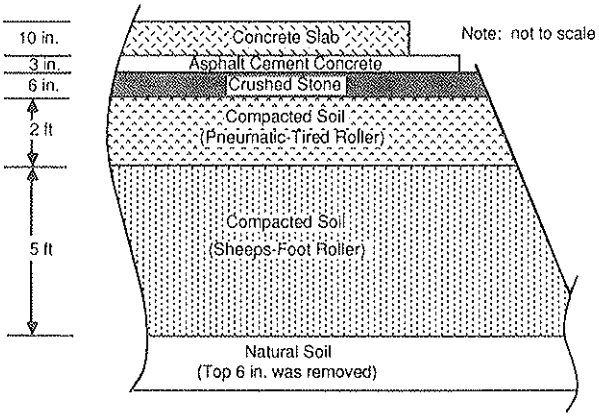

FIGURE 5 Material profile at BRC pavement facility.

FIELD TESTING

To investigate the validity of the simplified mathematical model, field tests were performed. All field data referred to in this work are from tests performed on the jointed concrete pavement at the research facility at Balcones Research Center (BRC), The University of Texas at Austin. This research facility was designed for the study of nondestructive pavement evaluation devices such as the SASW, Dynaflect, and falling weight deflectometer devices (*8*). A schematic of the BRC facility is shown in figure 4, and the material profile at the facility is presented in figure 5.

A Hewlett Packard model 3562A dynamic signal analyzer was used in the field for data collection, mainly phases of the cross power spectrum and coherence functions (*3, 9, 10*). Different types of accelerometers and geophones were used to monitor motions on the pavement surface. Most field data, however, were collected using PCB model 308B02 accelerometers as motion monitoring devices. Field data (phases of cross power spectra) were transferred to a MASSCOMP model MC5500 minicomputer through a general-purpose interface bus for further processing. With the MASSCOMP computer, the user is able to filter out low quality and questionable phase information acquired in the field, calculate the dispersion curves from the filtered phase information, average the dispersion curves from different receiver spacings to find the final (averaged) dispersion curves, and perform other miscellaneous plotting and numerical manipulations.

SIMPLE EXAMPLE

A simple example is given here to illustrate the use of the equations and procedures outlined above. This example models a field test performed at the BRC facility on January 3, 1986. The test was performed on the north end of the fixed concrete slab. A detailed layout of this test is shown in figure 6. Three nearby reflecting boundaries are denoted as A, B, and C, as shown in figure 6. Receivers were placed with a 40-foot (122 cm) spacing between them, and each one was 4 feet (122 cm) away from the nearest reflecting boundary. The source was placed at the edge of reflecting boundary A. The existence of reflecting boundary C was neglected in this example.

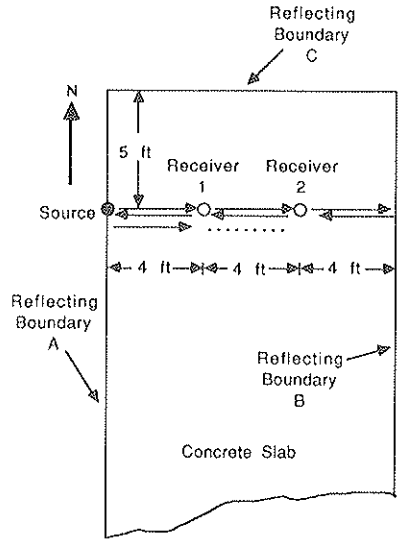

FIGURE 6 Detailed layout of SASW testing used in modeling example.

As soon as a pulse is generated with the source, this pulse starts to travel from the source to receiver 1 and then receiver 2 and finally reaches reflecting boundary B. Before this pulse reaches reflecting boundary B, it is considered as a direct surface wave. After the pulse reaches reflecting boundary B, it will reflect back and ne considered a reflected surface wave from now on. The reflected pulse will travel past receiver 2 and then receiver 1 and finally reach reflecting boundary A. It will then be reflected by boundary A and head towards reflecting boundary B. The pulse will eventually be bounced back and forth by reflecting boundaries A and B until all energy is dissipated. Typical field time records for this site are shown in figure 7. The reflected surface waves detected by each receiver can easily be identified and are indicated by

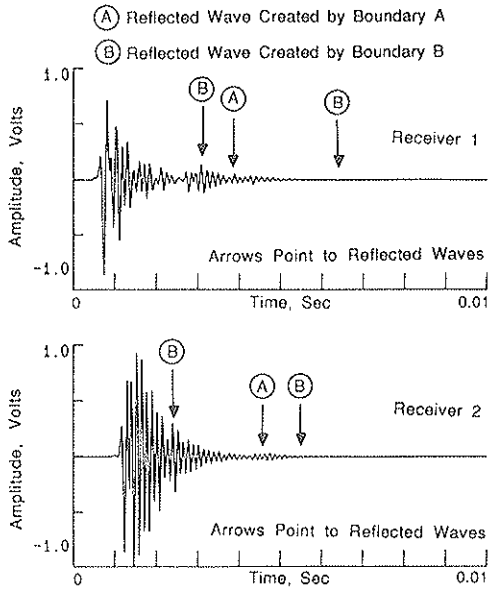

FIGURE 7 Typical time record illustrating the influence of reflected surface waves for test arrangement shown in figure 6.

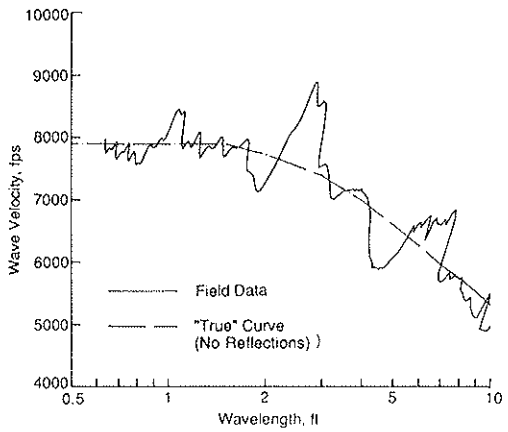

FIGURE 8 Comparison of field (measured) dispersion curve with the dispersion curve ("true") for no reflections for the test arrangement in figure 6.

the arrows shown in the figure. (Of course, there are more reflections than those indicated, but those indicated are the key reflections.)

To simplify this example, the effect of reflecting boundary C is neglected, and only the first reflected surface wave from boundary B is considered. THe measured (field) dispersion curve is shown by the solid line in figure 8. The "true" dispersion curve for this case should look like the smooth, dashed line drawn through the dispersion curve in figure 8. (The "true" dispersion curve is the dispersion curve for only direct surface waves in a layered system with infinite horizontal extent.) From figure 6, the distances that a direct pulse travels from the source to receivers 1 and 2 are 4 and 8 feet (122 and 244 cm), respectively. Since the "true" dispersion curve is known (figure 8), $T_{11}(f)$, $T_{21}(f)$ and "true" phase corresponding to each frequency can be calculated. The "true" phase derived from this "true" dispersion curve is shown in figure 9a, and the corresponding "true" dispersion curve (which has been shown in figure 8) is shown in figure 9b.

Notice that although there is a significant wave velocity change in the dispersion curve shown in figure 9b at a wavelength of about 1.5 feet (46 cm), the change is barely observable in the phase of the cross power spectrum (corresponding to figure 9a when the frequency is smaller than about 4000 Hz).

From figure 6, the first reflected pulse detected by receiver 1 is the one which travels from the source to reflecting boundary B and then back to receiver 1. The distance of travel for this pulse is 20 feet (6.1 m). By the same token, the first reflected pulse detected by receiver 2 is the one which travels from the source to reflecting boundary B and then back to receiver 2. The distance of travel for this pulse is 16 feet (4.9 m). Based on this information and by assuming that reflected surface waves have the same dispersive characteristics (same dispersion curve shown in figure 9b) as direct surface waves, it is possible to calculate $T_{12}(f)$ and $T_{22}(f)$ at all frequencies for both reflected waves.

Reflecting boundary B represents a free boundary at the edge of the concrete pavement. Therefore, reflected waves should have displacements in phase with direct waves. (All A's should have the same sign.) The amplitudes for each pulse detected by receiver 1, $A_{11}(f)$ and $A_{12}(f)$, are assumed to be

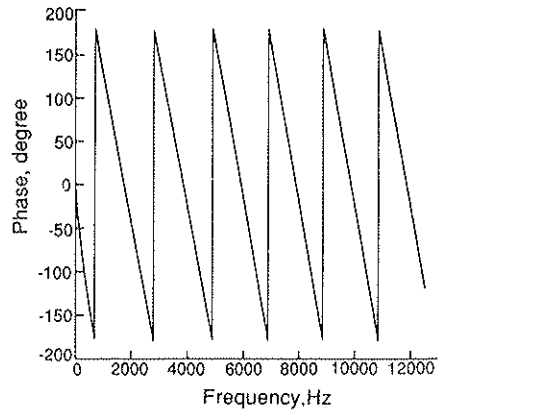

a. Phase of Cross Power Spectrum for 4-ft Receiver Spacing

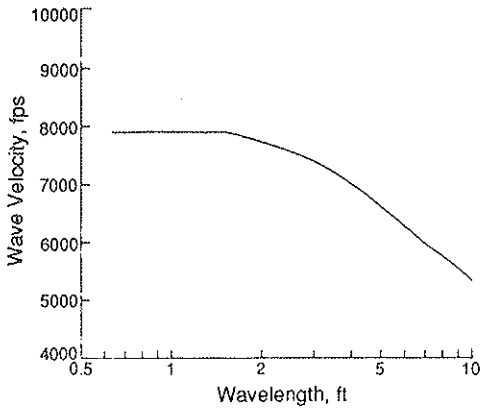

b. Dispersion Curve Associated with Phase Shown Above

FIGURE 9 (a) "True" phase of the cross power spectrum and (b) corresponding "true" dispersion curve for test arrangement shown in figure 6 (only direct surface wave).

1.0 and 0.36, respectively. The amplitudes detected by receiver 2, $A_{21}(f)$ and $A_{22}(f)$, are assumed to be 0.9 and 0.4, respectively. The relative magnitudes of the amplitudes used for the direct and reflected surface waves are more or less in the same order as shown in figure 7. However, it is not correct to use the exact amplitudes measured from the time records shown in figure 7, because reflected waves tend to overlap with the direct waves and with other reflected waves. As a result, their real amplitudes are distorted. All needed information is complete at this point, and the modeled dispersion can be calculated by using equation 11.

Comparison of the modeled and measured phases of the cross power spectrum is shown in figure 10. Comparison of the modeled and field dispersion curves in shown in figure 11. These two comparisons indicated that equation 11 is quite capable of modeling the fluctuations (ripples) that appear in the field data. The amplitudes and locations of the modeled ripples are somewhat different, but are close to the field data. The similarity of modeled and field data give strong support to the modeling process discussed earlier. It also seems that even though the lack of knowledge about amplitudes of all arrivals led to crude estimates of A's in equation 11, the model still generated a dispersion curve which is similar to the field data.

It is also interesting to note that all ripples in the modeled phase (figure 10) have very similar amplitudes, but the ampli-

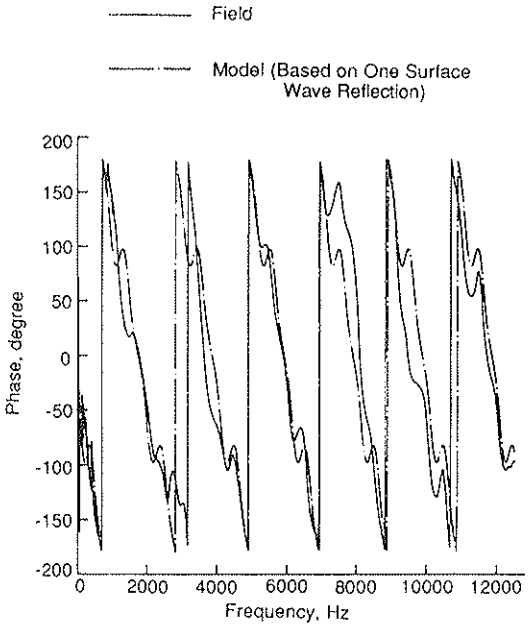

FIGURE 10 Comparison of field and modeled phases of cross power spectra for test arrangement in figure 6.

tudes of the ripples in the dispersion curve (figure 11) have an increasing trend as wavelength increases. This same phenomenon is found in the field data. In fact, experience indicates that this phenomenon commonly exists in most field data. This is due to the fact that when the phase of the cross power spectrum is translated to the dispersion curve, any disturbance in the high frequency range, which corresponds to the short wavelength range, is deamplified. Any disturbance in the low frequency range, on the other hand, corresponds to the long wavelength range and is amplified. As a result, disturbances in the low frequency range cause more problems than disturbances in the high frequency range. In terms of sampling depth, short wavelengths sample shallow depths. Therefore, material properties sampled at shallow depths are less sensitive to disturbances caused by reflected surface or body waves. This material sampling characteristic of the SASW method results in the method being very accurate for measurement of near-surface material properties, such as in the pavement surface layer (*11*).

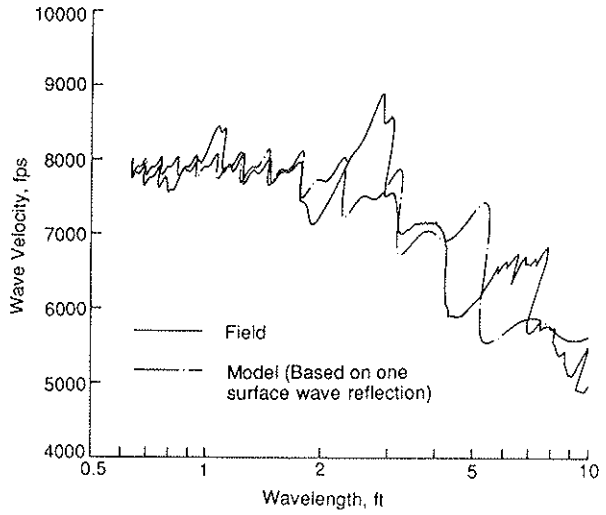

FIGURE 11 Comparison of field and modeled dispersion curves for test arrangement in figure 6.

REFLECTED SURFACE WAVES

The study of reflected surface waves was divided into three major subjects: (1) the effect of reflected surface waves from a vertical reflecting boundary oriented perpendicularly to the source/receiver array, (2) the effect of reflected surface wave from a vertical reflecting boundary oriented parallel to the source/receiver array, and (3) the effect of the distance between a vertical reflecting boundary and the source/receiver array. Model and experimental studies were performed on all subjects, with the exception that a model study was not performed on the effect of distance between the source/receiver array and a vertical reflecting boundary oriented perpendicularly to this array. This latter problem is directly related to damping (not geometry) in the system and is outside the scope of the simplified mathematical model.

Typical results for the effects of cases 1 and 2 cited above are shown in figures 12 and 13. First, consider the field dispersion curves shown in figures 12 and 13. These curves consist of a basic smooth curve upon which ripples or fluctuations are imposed. In the range of wavelengths shorter than about 0.5 foot (15 cm), this basic curve can be approximated by a horizontal line with an average wave velocity of about 7800 fps (2377 m/s). This average surface wave velocity correctly represents the stiffness of the concrete layer (modulus equal to 5.4×10^6 psi) and shows that the field data should be "smoothed" to eliminate the effect of surface wave reflections.

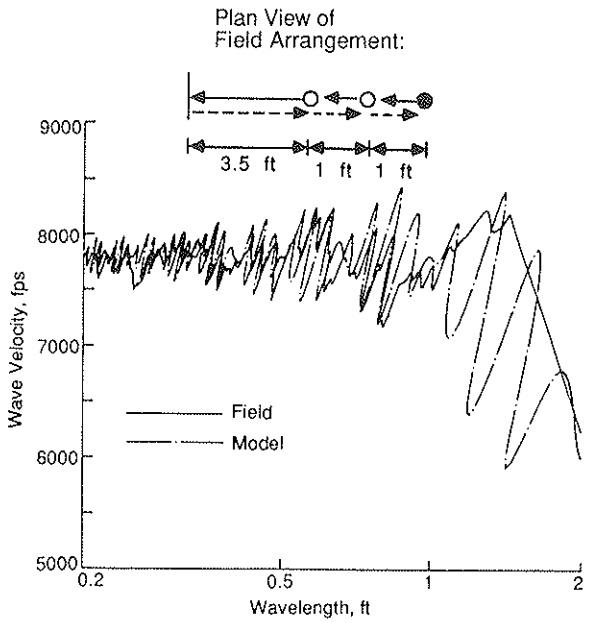

FIGURE 12 Comparison of field and modeled dispersion curves for surface waves reflected from a vertical boundary; receivers placed between source and reflecting boundary.

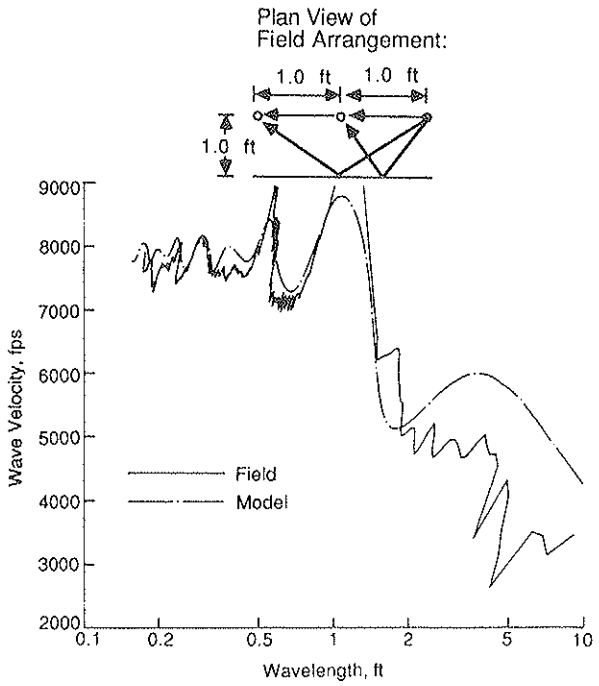

FIGURE 13 Comparison of field and modeled dispersion curves for surface waves reflected from a vertical boundary; test array oriented parallel to reflecting boundary.

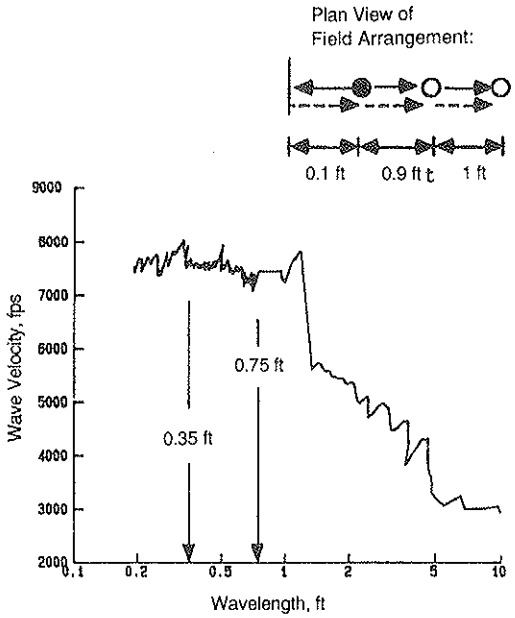

FIGURE 14 Field dispersion curve for surface wave reflected from a vertical boundary; source placed between receivers and reflecting boundary.

Modeled dispersion curves, shown in figures 12 and 13, closely describe the main ripples (fluctuations) present in the field data. It is clear that reflections impose ripples or fluctuations onto the dispersion curves. Although not all peaks and troughs overlap for both curves, the modeled dispersion curve shows the significant characteristics of the fluctuations. Since only one kind of reflected wave with only one reflection is considered in this model, minor discrepancies between the modeled and field data are possibly due to other reflected waves which are not considered in this first approximation model. In addition, uncertainties in estimating amplitudes and times (A's and T's) also introduce some errors into the modeled dispersion curves. However, it is clear that the model is reproducing the general trend and major fluctuations in the field curve. More importantly, the model shows that fluctuations in the field data should be smoothed to represent the theoretical assumption of a multilayered half space with infinite lateral extent.

The model shows that the effects of reflected surface waves from a reflection boundary oriented perpendicularly to the source/receiver array are minimized by placing the source between the boundary and the receivers. When this configuration is used, reflected surface waves travel in the same direction as the direct surface waves, and both the direct and reflected waves can be combined and treated as one direct wave of longer duration. This combination is not possible when the direct and reflected surface waves travel in opposite directions, as occurred in the testing illustrated in figure 12.

Field verification of the beneficial effect of orienting the testing array so that reflected and direct surface waves propagate in the same direction is shown in figure 14. Upon comparison of the field dispersion curves shown in figures 12 and 14, especially in the range of wavelengths from about 0.35 to 0.75 foot (11 to 23 cm), one can see that the amplitudes of the ripples in figure 14 are much smaller than in the case illustrated in figure 12. This result occurs because, for the case shown in figure 12, the reflected surface waves are propagating in the opposite direction to the direct surface waves. Hence, there is an adverse effect on the dispersion curve in figure 12. In the case shown in figure 14, the reflected surface waves are propagating in the same direction as the direct surface waves, and essentially no interference occurs.

The model and experimental studies involving the effect of reflected surface waves from vertical boundaries oriented parallel to the test array also showed that the adverse impact of reflected waves could be minimized by proper placement of the array. As the center line of the SASW array is moved away from the pavement edge, reflected surface waves are increasingly out of phase with respect to direct waves and, hence, have a more adverse effect on the dispersion curves. However, at the same time, the amplitudes of reflected waves decrease with increasing distance from the boundary which reduces the adverse effect on the dispersion curves. The combination of these two effects makes the choice of the best center line location of the array relative to the pavement edge not completely straightforward. Suppose that the source/receiver spacing is defined as D, as shown in figure 15, and the distance between the array and the parallel boundary is $k \times D$. The field and modeled data lead to the conclusion that there are two possible ranges for k which result in minimizing the effect of reflected surface waves. These ranges for k can be expressed as

$$k \geq 3.0 \tag{13}$$

or

$$k \leq 0.2 \tag{14}$$

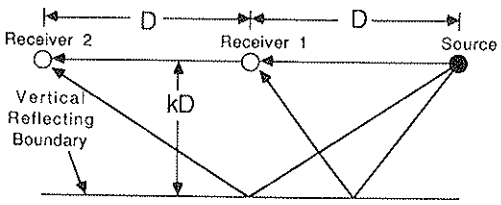

FIGURE 15 Normalized scale illustrating array/boundary configuration for the test array oriented parallel to the reflecting boundary.

Either of these criteria will result in making the influence of reflected surface waves relatively small and can be used as a guide for locating the test array.

DIRECT AND REFLECTED BODY WAVES

Surface impacts, generally from hammers or drop weights, are used to generate surface waves in SASW testing. In addition to generating surface waves, surface impacts also generate unwanted body waves. These body waves reach the receivers either directly or through reflections. Problems arise from the fact that body waves propagate with different velocities and have different dispersive characteristics than surface waves. As a result, body waves can alter the measured dispersion curve adversely.

The adverse impact of body waves on the dispersion curve is expected to be less than the effect of reflected surface waves just shown. This expectation is based on the fact that the energy generated by a vertically oscillating source on the surface of a homogeneous half space is distributed as follows (*12*): 67% in Rayleigh (surface) waves, 26% in shear waves (S-waves), and 7% in compression waves (P-waves). It is clear, therefore, that body waves carry only a small portion of the total energy generated by a surface impact. Furthermore, geometrical damping for body waves in much higher than for surface waves, which means that the negative impact from body waves is further diminished.

There are instances when the boundary which reflects body waves (such as the bottom of the pavement surface layer) is much closer to the test array than the boundary which reflects surface waves. Under these conditions, reflected body waves may become important, and their influence on dispersion curves needs investigation. The effects of body waves on dispersion curves have not been evaluated in the past. Therefore, studies were conducted with the simplified mathematical model in an attempt to identify their influence, to evaluate the severity of their influence, and to provide guidelines for reducing their adverse effects on dispersion curves.

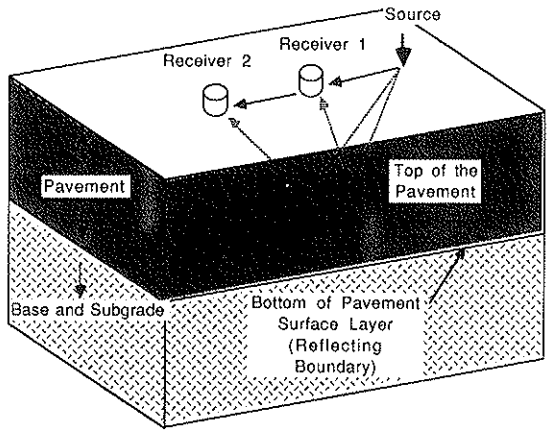

FIGURE 16 Generation of reflected body waves from bottom of concrete slab.

The generation of reflected body waves from the bottom of the pavement surface layer is shown schematically in figure 16. Three kinds of body waves commonly exist in a pavement system: P-waves, SH-waves, and SV-waves. Since both the direction of the impacts and the direction of the receivers are oriented vertically in SASW testing, particle motions in the vertical direction are usually dominant and are best measured. As a result, the influences of direct SV-waves, reflected SV-waves, and reflected P-waves are of the greatest concern. However, in this study, reflected SV-waves were found to be the most important, so only these results are presented herein.

Ray paths of shear waves used in the model simulation are shown in figure 17. Only one reflecting boundary is considered in this study, which is the bottom of the top concrete pavement layer. Because this interface represents a location of significant stiffness change, a fair amount of energy will be reflected by this interface. (An interface with a large stiffness change reflects more energy than an interface with a small stiffness change.) In addition, this interface usually is much closer to the source and receivers than other reflecting boundaries. Therefore, this reflecting boundary was selected for study.

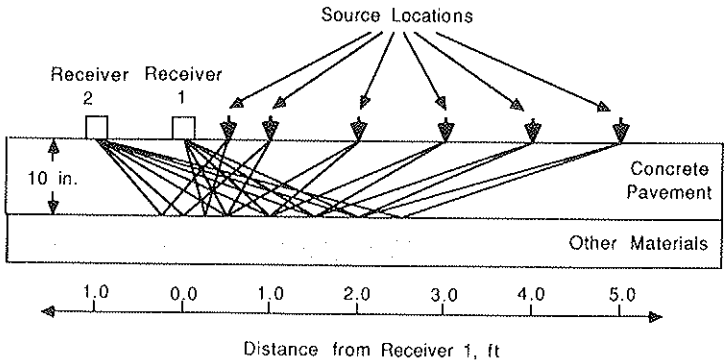

FIGURE 17 Ray paths assumed for body waves reflected from bottom of concrete pavement.

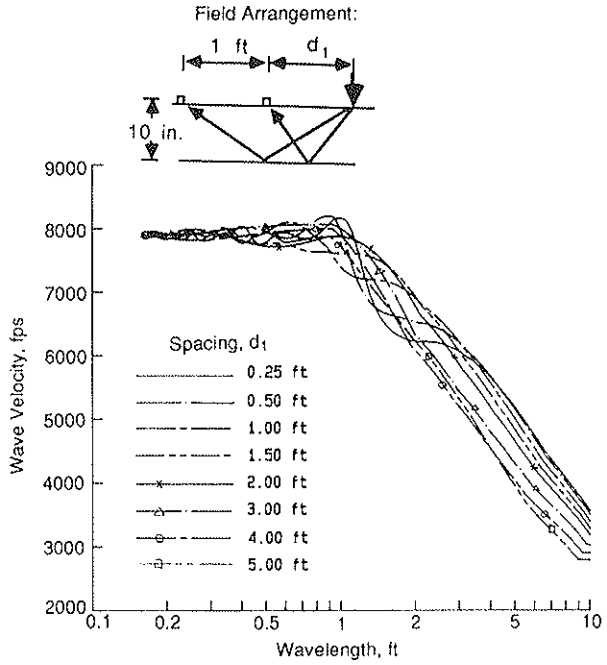

FIGURE 18 Modeled dispersion curves for shear waves reflected from bottom of concrete pavement; fixed receivers spacing of 1 foot and various source-to-receiver distances.

The modeled dispersion curves are shown in figure 18. The amplitudes, A, used for direct surface waves at receivers 1 and 2 are 1.0 and 0.9, respectively, and for reflected shear waves are 0.15 and 0.12, respectively. These amplitudes are used without any change for all cases, so that the effect of source/receiver distance can be more easily identified. Since shear (body) waves attenuate at a much faster rate than surface waves, their effect on the dispersion curves will decrease as the source/receiver distance increases. Therefore, the effect of reflected waves is somewhat overestimated for larger source/receiver spacings in the model.

The modeled dispersion curves shown in figure 18 demonstrate that, as the source/receiver spacing increases, fluctuations in the dispersion curve decrease. In addition, the shear wave has more influence in the long wavelength range (greater than about 0.7 foot, or 21 cm) than in the short wavelength range. For wavelengths of less than about 0.5 foot (15 cm), the effect is negligible. Since surface waves with wavelengths less than 0.5 foot (15 cm) sample basically the top concrete layer, reflected shear waves barely affect the measurement of material stiffness in the concrete layer, an important observation.

The effects of the direct compression and shear waves, as well as reflected compression waves, were much less than that shown in figure 18, and, therefore, are not shown here. A relative comparison of the effect on dispersion curves of reflected body waves versus reflected surface waves is illustrated in figure 19. The effect of body waves reflections, shown in figure 19a, is not nearly as important as the effect of a single surface wave reflection (for the case of a reflected surface wave propagating in the opposite direction to the direct surface wave) which is imposed on the body wave reflections in figure 19b. As such, one can see that reflected surface waves can cause the bulk of the fluctuations in the measured dispersion curves in these tests. Body waves only contribute more at wavelengths greater than the concrete slab thickness.

SUMMARY AND CONCLUSIONS

Seismic wave propagation methods, such as the SASW method, have proven through the years to be powerful methods for assessing moduli profiles. The nondestructive and easy-to-apply nature of the SASW method has made this technique attractive to engineers. Significant theoretical and practical advances in the SASW method have occurred in the past few years, and this method is rapidly becoming an important method for nondestructive testing of pavement systems.

An investigation of the adverse effects of reflected surface waves and direct and reflected body waves on field dispersion curves, the "raw data" of the SASW method, is presented. A simplified mathematical model to account for these effects is given. Field measurements were performed at the rigid pavement facility at Balcones Research Center to compare with the model. The usefulness of the model is confirmed by the good agreement between modeled and field dispersion curves. In the past, it was a puzzle to determine if the fluctuations in dispersion curves were really caused by fluctuations in the material properties or whether there were some other explanations. In this study, it is found that the reflected waves can impose ripples (fluctuations) onto the "true" dispersion curves. If the effect of reflected waves on the dispersion curves is removed, the dispersion curve is basically a smooth curve. At most pavement sites, the dispersion curve corresponding to short wavelengths (about equal to the thickness of the top layer and less) is very flat and close to a straight line, which indicates that the material property in the top pavement layer is usually very uniform.

Based on both model and field studies, it is concluded that the adverse effects from reflected surface waves upon dispersion curves can be reduced by proper arrangement of the source and receiver relative to the boundary. In the case when the vertical reflecting boundary is oriented perpendicularly to the test array, the adverse effect of reflected waves can be reduced to a minimum by placing the source between the reflecting boundary and the receivers. In the case when the reflecting boundary is oriented parallel to the test array, it is better to have the test array located either very close to the reflecting boundary, so that reflected surface waves are very much in phase with the direct surface waves, or as far as possible from the reflecting boundary, so that the amplitudes or reflected surface waves are relatively low compared to the direct surface waves.

Direct and reflected body waves were also studied with the analytical model. Reflected body waves are more important than direct body waves in the top pavement layer and result from reflections at the interfaces at the top and bottom of this layer. As shown in this study, body waves also cause fluctuations in the field dispersion curve, but to a much lesser extent than reflected surface waves.

ACKNOWLEDGMENTS

The project was sponsored by the Texas State Department of Highways and Public Transportation, whose support is

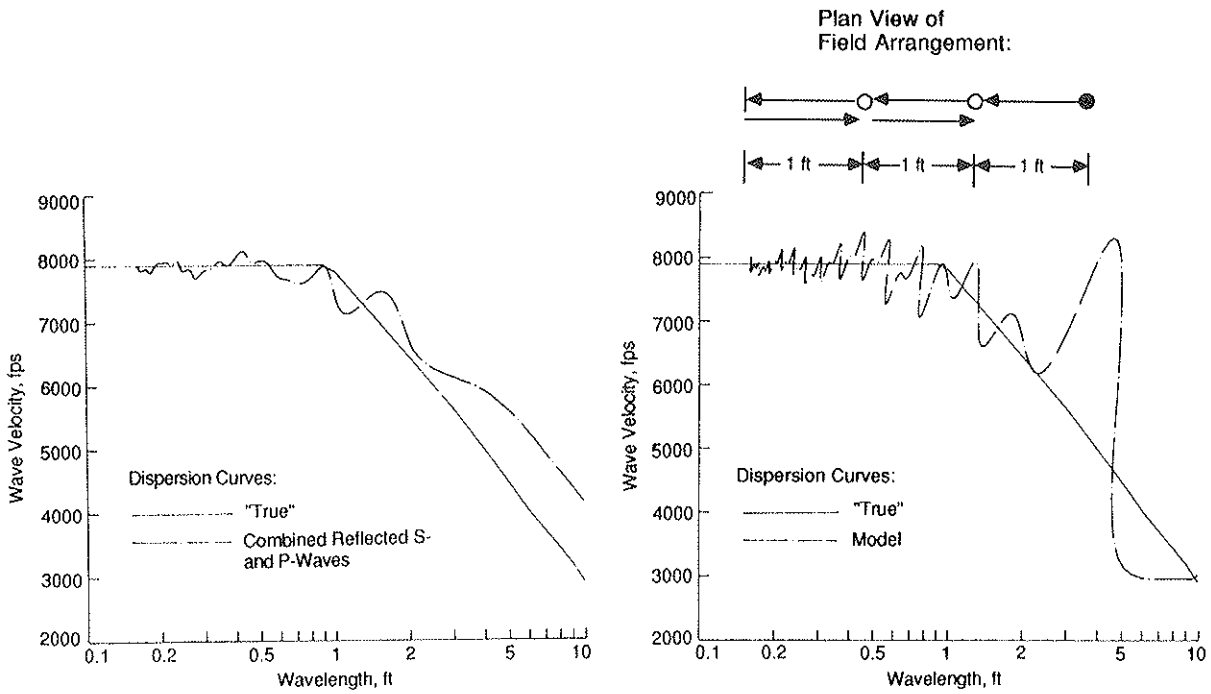

a.) Modeled Dispersion Curve with Combined Reflected S-Waves and Reflected P-Waves.

b.) Modeled Dispersion Curve with Combined Effect from Body Wave Reflections and Reflected Surface Wave.

FIGURE 19 Comparison of the relative effect of reflected body waves versus reflected surface waves on dispersion curves.

gratefully acknowledged. The encouragement and helpful suggestions of R. Briggs and R. Rogers of that department and the constructive discussions and guidance of S. Nazarian, I. Sanchez-Salinero and G. Rix of The University of Texas are sincerely appreciated.

REFERENCES

1. S. Nazarian and K. H. Stokoe, II. In Situ Determination of Elastic Moduli of Pavement Systems by Spectral-Analysis-of-Surface-Waves Method (Practical Aspects). *Research Report 368-1F*. Center for Transportation Research, The University of Texas at Austin, May 1986, 187 pp.
2. S. Nazarian and K. H. Stokoe, II. In Situ Determination of Elastic Moduli of Pavements Systems by Spectral-Analysis-of-Surface-Waves Method (Theoretical Aspects). *Research Report 437-2*. Center for Transportation Research, The University of Texas at Austin, Aug. 1986, 78 pp.
3. S. Nazarian and K. H. Stokoe, II. Use of Surface Waves in Pavement Evaluation. In *Transportation Research Record 1070*, TRB, National Research Council. Washington, D.C., 1986, 39 pp.
4. I. Sanchez-Salinero, E. W. Chang, J. M. Roesset, and K. H. Stokoe, II. Complete Analytical Solution for Wave Propagation in a Layered System, *Research Report 1123-1*. Center for Transportation Research, The University of Texas at Austin (in press).
5. S. Nazarian. *In Situ Determination of Elastic Moduli of Soil deposits and Pavement Systems by Spectral-Analysis-of-Surface-Waves Method*. Ph.D. dissertation. The University of Texas at Austin, Dec. 1984.
6. I. Sanchez-Salinero. *Analytical Investigation of Seismic Methods Used for Engineering Applications*. Ph.D. dissertation. The University of Texas at Austin, Dec. 1986.
7. J. C. Sheu, K. H. Stokoe, II, J. M. Roesset, and W. B. Hudson. Applications and Limitations of the Spectral-Analysis-of-Surface-Waves Method. *Research Report 437-3F*. Center for Transportation Research, The University of Texas at Austin, 206 pp.
8. R. White, W. R. Hudson, A. H. Meyer, and K. H. Stokoe, II. Design and Construction of a Rigid Pavement Research Facility. *Research Report 355-1*. Center for Transportation Research, The University of Texas at Austin, 121 pp.
9. S. Nazarian, K. H. Stokoe, II and R. C. Briggs. Nondestructively Delineating Changes in Modulus Profiles of Secondary Roads. In *Transportation Research Record 1136*, TRB, National Research Council, Washington, D.C., 1987.
10. S. Nazarian, K. H. Stokoe, II, R. C. Briggs, and R. Rogers. Determination of Pavement Layer Thicknesses and Moduli by SASW Method. In *Transportation Research Record 1196*, TRB, 1988.
11. J. C. Sheu, G. J. Rix and K. H. Stokoe, II. Rapid Determination of Modulus and Thickness of Pavement Surface Layer. Presented at the Transportation Research Board Annual Meeting, 1988.
12. F. E. Richart, Jr., J. R. Hall, Jr., and R. D. Woods. *Vibrations of Soils and Foundations*. Prentice-Hall, Inc., Englewood Cliffs, N.J., 1970.

Publication of this paper sponsored by the Committee on Pavement Monitoring, Evaluation, and Data Storage.

Pavement Condition Diagnosis Based on Multisensor Data

K. MASER, B. BRADEMEYER, AND R. LITTLEFIELD

High-speed sensors have developed rapidly in recent years, and numerous such sensors can be operated from highway speed vehicles. This sensing technology can now provide pavement condition and performance information far beyond what is currently exploited in pavement management. Data from these sensors, coupled with established knowledge of pavement behavior, can be used to infer causes of pavement conditions and to predict performance. Knowledge of cause can also be used to select appropriate maintenance strategies. This paper demonstrates how the mechanisms of flexible pavement deterioration can be inferred from the data obtained from a "suite" of pavement sensors. Included are data on subsurface moduli, asphalt thickness, and subgrade moisture, none of which are currently measured with high-speed sensors. The paper goes on to show how the subsurface moduli can be computed from continuous data describing rut depth and fatigue cracks, both of which are measurable with current technology. Finally, the computation of asphalt thickness and subgrade moisture content from continuous radar profiles is described. Thus, a complete data set for explaining pavement condition and predicting future performance can now be provided by high-speed sensors. What remains is to integrate these sensor data into current pavement management systems.

During the past fifteen to twenty years, several pavement management systems have been developed and implemented in the United States, Canada, Europe, and Australia. These systems are quite diverse in the concepts and analytic approaches which they use to address equally diverse sets of pavement management decisions. In all of these systems, however, maintenance and rehabilitation management decisions are based on measures of the condition and performance of the pavement.

Pavement conditions are routinely surveyed for four distinct aspects: surface distress, longitudinal profile, structural response, and skid resistance. A variety of instruments is utilized to obtain measures of these four features, and the readings from these instruments are converted into various performance indices. These aggregate indices, such as the pavement condition index (PCI) are then used as a basis for maintenance management decisions. These condition and performance indices, although simple and widely used, aggregate away much of the information available from condition sensors and, more importantly, fail to explain the basic behavior of the pavement.

K. Maser, INFRASENSE, Inc., 19-R Brookline Street, Cambridge, Mass. 02139. B. Brademeyer and R. Littlefield, Massachusetts Institute of Technology, 77 Massachusetts Avenue, Cambridge, Mass. 02139.

Concurrent with the emergence of pavement management systems has been an explosion in technologies of high-speed sensing. While these technologies have originated in areas such as geophysics, remote sensing, nondestructive testing, and factory automation, they are now expanding into the domains of civil engineering. Many such technologies have been and are being developed for high-speed surveying of pavement condition. Examples of such developments are acoustic, laser, and optical strobe techniques for continuous measurement of transverse profile (*1*); automated detection and quantification of cracking and surface distress using optical techniques and image processing (*2*); and sensing of pavement layer thickness, subsurface moisture, and voids using ground penetrating radar (*3*). All of these technologies can be implemented from highway speed vehicles, thus permitting frequent and comprehensive surveys of pavement condition.

With this rapid development of high-speed sensors, it is now clear that the current generation of pavement management systems is based on outdated measurement technology. Thus, these systems are incapable of fully utilizing the information that is available from these new and emerging sensor systems. Now that the full potential of these sensors is beginning to emerge, it is time to reconsider their impact on pavement management. The current reliance on indices noted above is an example of a practice which limits the full potential of the management system. Since these indices (for example, PSI and PCI) do not explain patterns and causes, they cannot serve to project future performance, nor can they suggest the appropriate maintenance.

The approach developed in this paper is to pursue a more diagnostic description of the pavement, which goes beyond the simple index. As discussed in the next section, such a description is now possible with the great deal of information provided by high-speed sensors.

BACKGROUND

The pavement conditions measured by sensors are all manifestations of some behavior of the pavement. For example, rutting comes from accumulated plastic deformation; roughness from spatial variations in rutting, frost heaves, and surface distress; cracking from accumulated strain producing fatigue; and so on. Pavement behavior has been studied for many years, and many of these cause-effect relationships are well established. Therefore, if enough manifestations can be picked up by sensors, it should be possible to infer the basic mechanisms which are consistent with the manifestations that are sensed.

Knowledge of pavement behavior is extensive. For example, it is known that excessive deformation of the pavement surface is a common manifestation of distress in flexible (asphalt) pavement systems. Permanent deformation, in the form of wheel path ruts, results either from shear failure, usually in the asphalt layer, or from consolidation in one or more of the granular pavement layers. The presence of water in either the granular layers or the subgrade acts to reduce internal friction and, hence, to lower resistance to consolidation, particularly during periods of spring thaw. Cracking is another major manifestation of distress in flexible pavements. Extensive cracking contributes to loss of subgrade support and swelling by permitting moisture to directly infiltrate the pavement structure. Fatigue cracking involves fracture of the asphalt material under repetitive loads at stress levels considerably below the ultimate tensile strength of the mix. Asphalt modulus is strongly temperature-dependent, leading to a material which exhibits high levels of strain and plastic behavior in the summer, and which behaves in a more elastic and brittle manner in the winter. As such, susceptibility to fatigue cracking is greatest during the spring and fall, when the material is less brittle but the strains are considerably greater than in the winter months.

Much of the qualitative knowledge described above has been formalized in a quantitative manner. For example, empirical models have been developed to predict the performance of pavement over time based on certain pavement parameters (*4*). More complex models have been developed to represent the changes in pavement structural properties by season or as a function of pavement age or condition. These models can include the preventive and restorative impacts of a hierarchy of potential maintenance and rehabilitation activities (*5*). Mechanistic models employing either continuum mechanics or finite element methods have been developed to incorporate elaborate materials/traffic/environment interactions on the stresses, strains, and deformations within the pavement structure. These are utilized in conjunction with empirical relations to predict the damage manifestations resulting from these stress/strain/deformation histories (*6*).

Most of the knowledge described above has been applied to new design rather than to condition assessment, diagnosis, and maintenance management. The aim of this paper is to show how it can be employed to interpret the data from sensors, and thus to serve as a basis for pavement management. The following section describes how the data from a suite of sensors can be used to infer pavement properties and causes of observed conditions.

DIAGNOSIS FROM SENSORS

Figure 1 shows data obtained from a suite of sensors on a hypothetical stretch of flexible pavement. In this data set, the definitions and sources of data are as follows:

SV represents slope variance and is obtained from a sliding window of profile data (200 feet long, for example), using a commercially available pavement profilometer (*1*).

RD represents rut depth and is derived from transverse profile as obtained by one of the devices mentioned earlier.

CR is density of fatigue (alligator) cracking and is derived from crack sensing devices mentioned earlier as a running average of the percentage of length cracked.

E_a is asphalt modulus, which currently cannot be continuously measured from a high-speed sensing device. Spatial variations in E_a can be inferred from *RD* and *CR*, as described later in this paper.

E_s is the combined base and subgrade modulus, which also cannot be continuously measured, but whose spatial variations can also be inferred from *SV* and *CR*.

h_a is asphalt thickness, which can be continuously measured using ground penetrating radar. h_a is an important variable in explaining *RD* and *CR*, and in predicting E_a.

MC is moisture content in the subgrade, whose variations can be continuously monitored using ground penetrating radar. *MC* is useful in explaining variations in E_s.

Figure 1 thus represents a suite of direct and indirect sensor data which can be used to explain flexible pavement conditions. For example, locations where *SV* correlates with rapid fluctuations in *RD* suggest that the mechanisms causing rutting are dominating the pavement profile (and performance). Where high values of *SV* do not correlate with fluctuations in *RD*, the profile is dominated by other mechanisms, such as differential settlement and frost heaves. This latter conclusion can be reinforced by correlating fluctuations in E_s and *MC*. Where high *RD* is correlated with low h_a, one can infer that the rutting is due to deformation in the asphalt. Where this correlation does not exist, the source of rutting is in the deformation of the base and subgrade. This latter conclusion can be reinforced by correlating reductions in E_s. Where high *CR* is correlated with low E_s and high E_a, one can infer that the cracking of the asphalt is due to excessive asphalt strains due to a weak base and subgrade. Where high *CR* is correlated with high E_s, one can infer that the cracking in the asphalt is due to its brittleness, related to inadequacy of the mix.

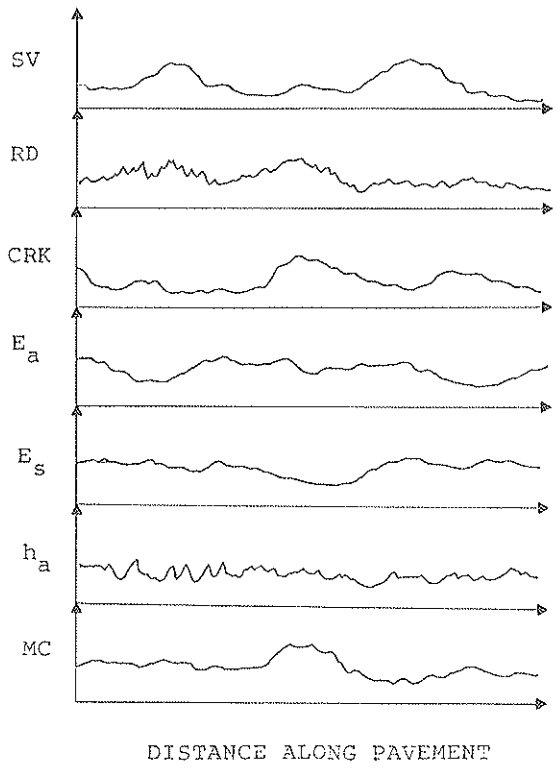

FIGURE 1 Pavement sensor data.

The inferences discussed above provide valuable information for maintenance management. The understanding of the mechanisms producing the observed behavior can lead to the choice of the appropriate model for predicting performance. The explanation of cause can lead to the proper selection of maintenance techniques. For example, if the source of fatigue cracking is known to be weakness in the subgrade, then it would make no sense simply to resurface the road, since the new surface will soon crack as well.

The simultaneous use of multiple sensor data, as discussed above, can be implemented for pavement management in the foreseeable future. Before this can happen, however, certain tasks, like those described below, must be completed.

Completion of the Sensor Picture

Some of the data in figure 1 are not currently available. Based on their current research and development status, automated crack sensing devices should be available within the next two years. Existing radar equipment now exists for continuous monitoring of asphalt thickness, and finalizing this capability for routine field application remains to be accomplished. Monitoring of changes in subsurface moisture content is an inherent radar capability which has already been demonstrated for asphalt-overlaid bridge decks (*21, 22*). Some further demonstration of this capability will be required for asphalt pavements, as discussed later in this paper. Finally, a capability for continuous monitoring of asphalt and subgrade modulus has been explored, but this capability does not appear realizable in the foreseeable future. As noted earlier, these properties can be inferred from rut depth and cracking.

Incorporation of Sensor Information into Pavement Management

Once the sensor picture of figure 1 is complete and available, mechanisms for utilizing the information must be incorporated into pavement management systems. These mechanisms will include adaptation of performance predictions to knowledge of current conditions and their causes, as well as specifying maintenance appropriate to the existing and projected conditions.

The work described in the remainder of this paper focuses on the completion of the sensor picture for flexible pavements. The computation of E_a and E_s from rut depth and cracking will first be discussed, and an algorithm along with numerical results will be presented. This will be followed by a discussion of ground penetrating radar, including its capability for sensing asphalt thickness and base and subgrade moisture content.

MODULI DETERMINATION FROM RUTTING AND CRACKING DATA

It was assumed in this study that sensor data would be available describing rut depth and fatigue cracking of asphalt pavements. Rut depth (inches or mm) is reported at regular distance intervals (e.g., every foot or 10 feet). Fatigue cracking, which assumes a characteristic alligator pattern in its advanced stages, is (assumed to be) reported as "Yes" or "No" values at similar distance intervals. No measure of the severity of the cracking is being considered at this time. The cracking sensor reports the percentage of cracked area over a pavement length of interest.

The method for moduli determination utilizing these two sensor inputs can be summarized as follows: (a) formulate quantitative relationships which can predict rutting and cracking based on design, loading, and environmental parameters; and (b) using the measured rutting and cracking values, invert the quantitative relationships formulated above to determine the underlying pavement moduli.

The quantitative relationships for predicting rutting and cracking are described below.

Rutting

Rutting of asphalt pavements can be attributed primarily to plastic deformation, if the rutting occurs in the shear/consolidation mode (*7*). In this formulation, the cumulative permanent deformation Δ of a material specimen subjected to a series of N repeated, identical load pulses is logarithmically proportional to the peak elastic deformation δ produced by any given load pulse, which is assumed to remain constant.

$$\Delta = \mu\delta N^{\alpha} \tag{1}$$

where

Δ = the permanent deformation of the material after N load cycles,
δ = the peak elastic deformation of the material in a load cycle, assumed independent of N,
N = the number of applied load cycles, and
μ, α = materials properties related to compactibility.

The materials parameters μ and α are known to depend on the stress state, load duration, temperature, and moisture content (*8–10*). Subsequent research (*11, 12*) indicates that the permanent deformation properties of asphalt concrete are primarily a function of modulus; those of granular layers are dependent on stress state, while those of subgrade soils depend on moisture content.

The permanent deformation parameters for the pavement structure as a whole have been determined in previous research by regression analysis of the permanent deformations as a function of the number of loads applied to the pavement structure. Analyses of numerous sections from the AASHTO road test results have shown that system μ values range between 0.25 and 0.50 for a spectrum of seasonal conditions and axle loads, while system α values are typically between 0.25 and 0.30 (*13, 14*).

The peak elastic deformation of the pavement structure can be computed mechanistically from the load footprint parameters, layer thicknesses, and layer moduli and Poisson's ratios using elastic layer theory. A simplified relation (*15*) is

$$\delta = \frac{3pa^2}{2KE(a^2 + Z^2)^{1/2}} \tag{2}$$

where

δ = the peak elastic deformation of the pavement surface,
p = the average footprint contact pressure,
a = the radius of the footprint (assumed circular),
K = the fraction of total elastic deformation contributed by the subgrade (typically 0.7 to 0.8 in the AASHTO sections analyzed in the research cited above),
E = the subgrade modulus of elasticity, and
Z = "equivalent" subgrade depth based on Odemark's method (*15*) for equivalencing the deflection of a multilayer elastic half space to that of a homogeneous half space, and is a function of all the layer thicknesses and moduli.

Since the amount of rutting occurring in a given season will depend on the amount of consolidation present at the start of the season, the seasonal traffic, and the seasonal pavement properties, an iterated prediction methodology can be applied to account for the discontinuities across seasonal boundaries. This methodology results in the end-of-season rutting for each season, and, hence, provides the total rutting at any given time by combining the contributions of all previous seasons.

Fatigue Cracking

Fatigue cracking is phenomenologically understood through the empirical validation of Miner's hypothesis. This relation is represented as (*16*)

$$\%C = 20\text{Log } D \qquad (D > 1) \tag{3}$$

where $\%C$ is the percentage of wheelpath area cracked and D is Miner's fatigue index.

By Miner's criterion, the fatigue index is defined as

$$D_j = \sum_{i=1}^{j} \frac{n_i}{N_i} \tag{4}$$

where

D_j = the fatigue index at the end of season j,
n_i = the number of load applications in season i, and
N_i = the number of loads to failure in season i.

The number of loads to failure at a given strain level and environment is empirically known from laboratory tests (*7*) to be

$$N = K_1 \varepsilon^{-K_2} \tag{5}$$

where

N = the number of loads to failure in the laboratory,
ε = the applied tensile strain, and
K_1, K_2 = brittleness materials properties.

The maximum tensile strain in the pavement structure is assumed to occur at the bottom of the asphalt layer. This strain can be mechanistically computed from the load footprint parameters, layer thicknesses, and layer moduli, using elastic layer theory. A simplified relation, based on the work of Odemark (*15*), is

$$\varepsilon = \frac{3pa^2H}{4E(a^2 + H^2)^{3/2}} \tag{6}$$

where

ε = the maximum tensile strain,
p = the average footprint contact pressure,
a = the radius of the footprint (assumed circular),
E = the subgrade modulus of elasticity, and
H = an "equivalent" depth based on equivalencing the maximum tensile strain in a multilayer, elastic half space to the strain in a homogenous half space, and is a function of all the layer thicknesses and moduli.

The prediction of fatigue cracking also incorporates the seasonal variation in pavement properties. These are particularly significant, since asphalt modulus can increase by an order of magnitude from summer to winter, while subgrade properties are also changing.

From a measurement perspective, observation of fatigue cracking is related to the fact that the pavement at that location has exceeded its fatigue life. The cracking model reported herein computes peak seasonal strain at the bottom of the asphalt layer for each sampled point in the surveyed section. Average seasonal asphalt moduli are determined from an empirical modulus-temperature relation. Local values of subgrade modulus are determined from the average modulus and the statistics of the rutting sensor. The local values of the granular layer moduli (base and subbase) are determined from an empirical relation between granular modulus, and granular thickness and subgrade modulus.

A seasonal value of the "brittleness" coefficient K_1 can be determined as a function of asphalt modulus. The relationship used in this work was regressed from laboratory test data, as shown in figure 2. The coefficient K_2 was found to be related to K_1 as follows:

$$K_2 = 1.859 - 0.241 \text{ Log} K_1 \tag{7}$$

where K_1 and K_2 are as given in equation 5.

The probability of cracking at any location is determined from the following bounded approximation to equation 3, valid for all $D \geq 0$:

$$\text{Prob (Crack)} = \text{Sin}^2\left(\frac{\pi}{2} \cdot \frac{aD^b}{1 + aD^b}\right) \tag{8}$$

where

D = Miner's damage index (see equation 4),
a = 0.217, and
b = 0.266.

Finally, the estimated percent of cracked pavement area is determined by summing the probability of cracking over all locations, and dividing by the total number of sampled points.

Inversion Algorithm

The relationships presented above can be used to predict pavement rutting and cracking, given pavement material properties and loading and environmental parameters. Since the objective here is to predict pavement moduli from measurements of rutting and cracking, an iterative algorithm has been developed to invert these relationships. The function of this algorithm is to compute local average values (at reference

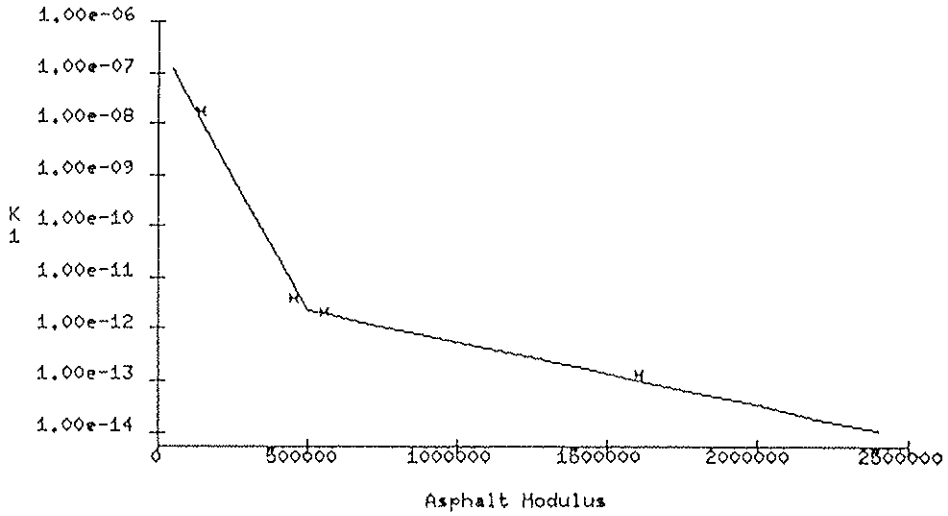

FIGURE 2 Fatigue coefficient K_1 as a function of asphalt modulus.

environmental conditions) of the asphalt and subgrade moduli which reproduce the observed behavior.

A flow chart of the inversion algorithm is shown in Figure 3. The iterative process is initiated by having the user assume values for the reference subgrade modulus, E_s, and the reference asphalt modulus, E_a. The rut depths and percent cracking are then computed and compared with the sensor data. The reference moduli values are then adjusted to force the computed and measured rutting and cracking into greater coincidence. This process continues until the computed and measured values are within some small tolerance (2%, for example), at which point the algorithm is assumed to have converged. The following section describes numerical experiments carried out using this algorithm.

Computational Experiments

The algorithmic approach described above was tested on synthesized pavement data. The algorithm, when applied to synthetic data, should yield the properties which were assumed in the synthesis. If it does not, then there is a problem with the algorithm.

The synthesis generates random values of asphalt thickness and modulus, base course thickness, and subgrade modulus, at 1-foot intervals. The values are determined from a second-order, autoregressive process, which requires a mean value, standard deviation σ_x, and two correlation coefficients ρ_1, ρ_2 for each parameter. Figure 4 shows typical results from this synthesis, together with the sensitivity of these results to changes in standard deviation and correlation coefficients. The synthesized pavement data were then utilized to generate rutting and cracking "measurements" using the quantitative models described earlier. The synthesized rutting and cracking values were used as simulated sensor data, to serve as input to the inversion algorithm.

The testing of the inversion algorithm on these data began by using pavement properties known to be incorrect (i.e., different from those used in the synthesis), computing pavement properties using the algorithm, and comparing the resultant properties with those assumed in the pavement synthesis. Figure 5 shows a typical result of such an analysis. The entries in the body of the figure are the subgrade modulus (the upper value in each cell) and asphalt modulus (the lower value) computed by the inversion of the algorithm. These computations were made for various combinations of initial subgrade and asphalt moduli, and cumulative traffic loads (N). The values used in the synthesis were 5,000 psi, 500,000 psi, and 1,000,000 axle loads, respectively. The results show convergence to within $\pm 20\%$ of the correct moduli values for a fairly wide spread of input assumptions.

As can be seen in the figure, the results are considerably improved if the traffic estimate is correct (N = 1 million). However, even in such cases, both moduli tend to be slightly underestimated. This is partly due to the fact that the variance of the observed rutting is not being used in the calculation of the subgrade modulus, which results in an underestimate of the mean modulus in order to account for modulus variation. Inclusion of this effect (a slight modification of equation 1) would raise the computed moduli values.

The moduli also tend to be underestimated because all variation in the rutting observations is assumed to be represented by local variation in the subgrade modulus. Thus, any variation in asphalt modulus or thickness or base thickness will be reflected in a reduced estimation of the subgrade modulus. However, given the current quantitative understanding of pavement damage, information from additional sensors is required in order to resolve the causes of variation in the observed distress patterns.

Discussion of Results

The above results show that local average values of E_a and E_s can be computed from measured rut depth and cracking. This is exactly the information identified in figure 1. It is clear that the accuracy of this prediction is sensitive to a number of assumptions, such as the number of axle loads, climatic changes, and various numerical constants and parameters. Most of these assumed values (e.g., traffic) are constant over a given stretch of pavement. Since our objective is to correlate spatial changes in E_a and E_s with such changes in other sensor

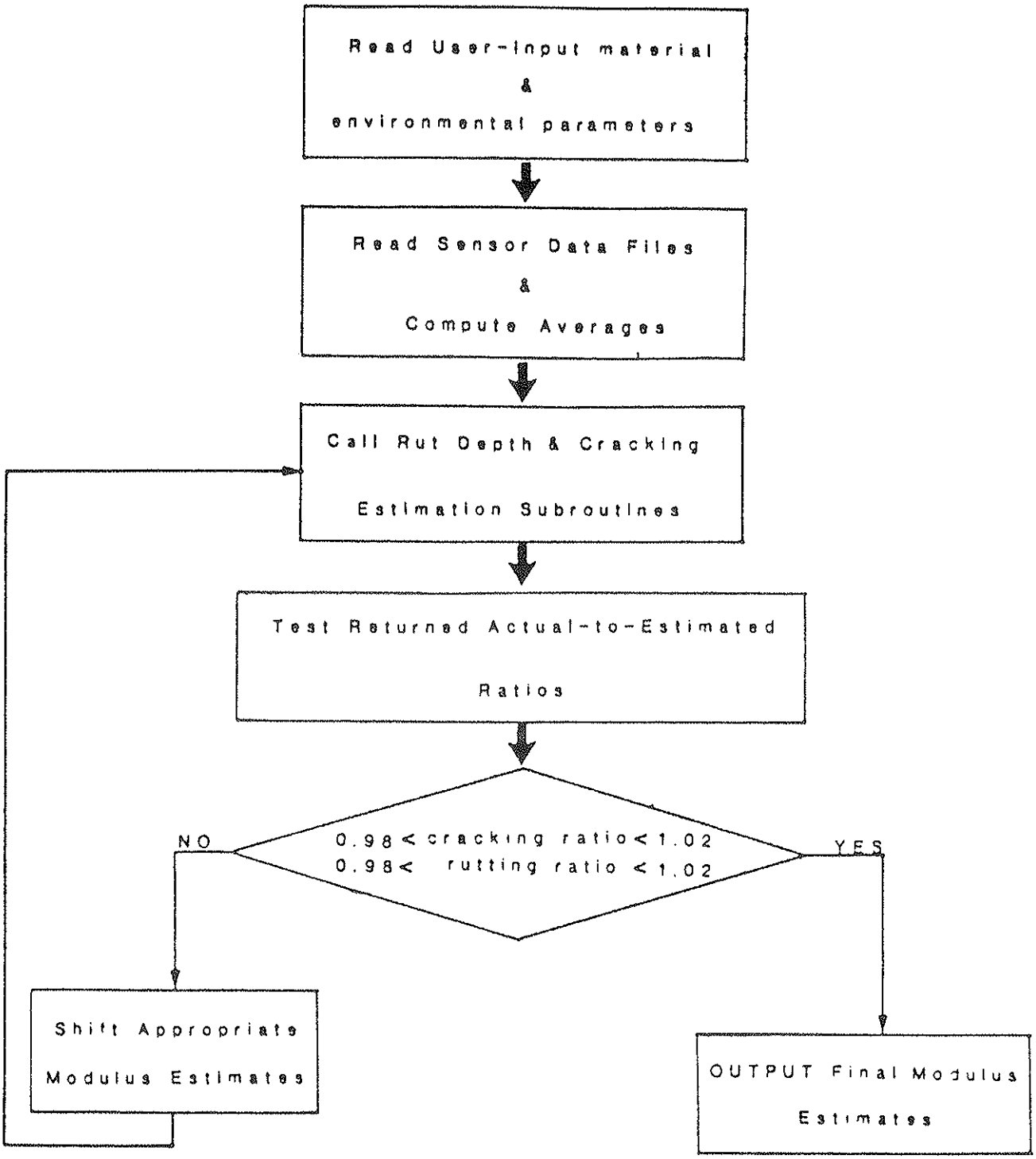

FIGURE 3 Inversion algorithm.

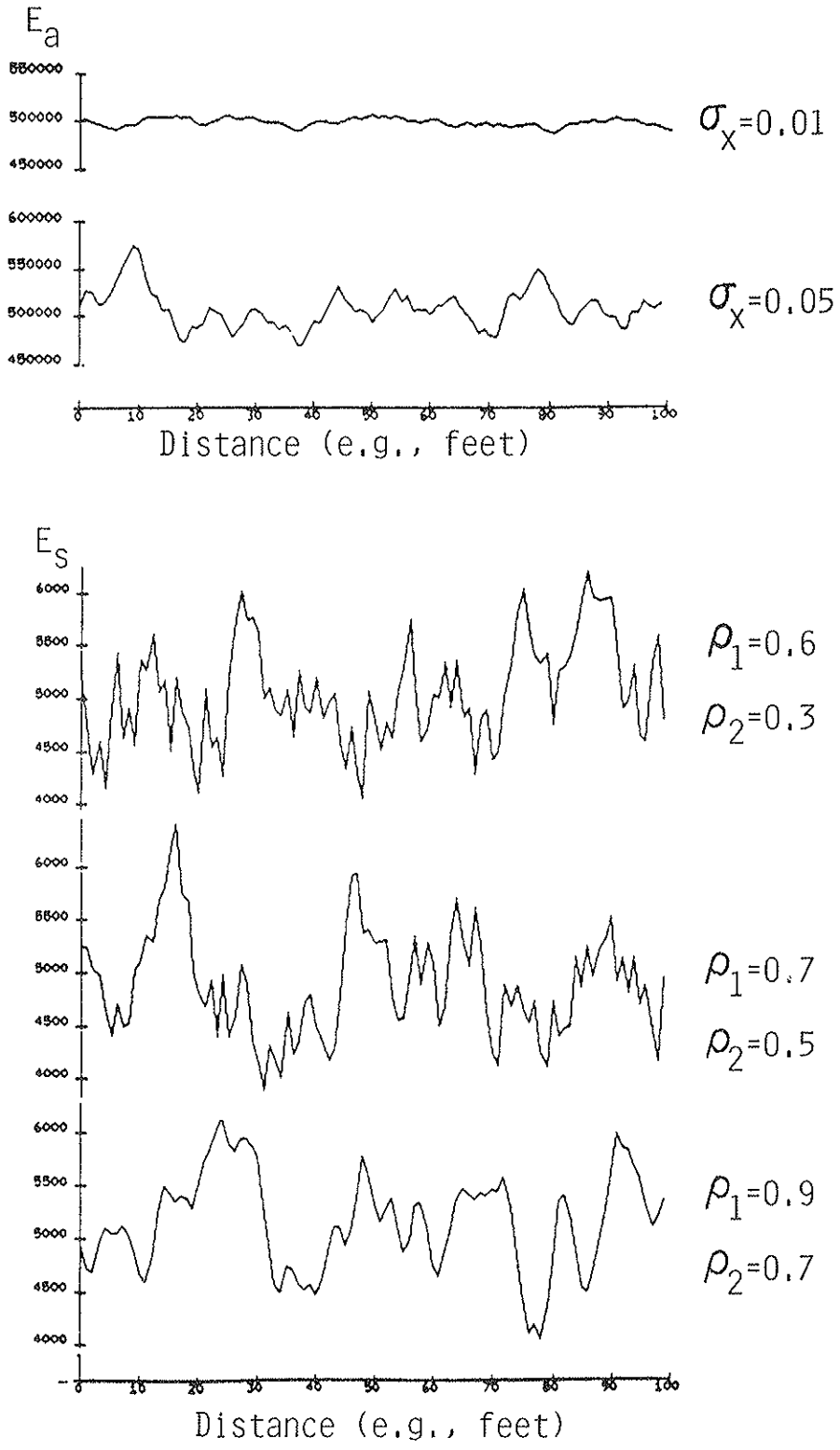

FIGURE 4 Synthesized pavement data.

EXAMPLE DATA

$h_a = 6"$ $h_{base} = 20"$

$E_a = 500$ ksi $E_s = 5$ ksi

$N = 10^6$ $RD_{avg} = 0.55"$ % cracking = 22%

RESULTS

INPUT E_a \ E_s (ksi)	250	500	1000
2.5	487 4.79	488 4.79	487 4.79
5.0	488 4.78	490 4.76	487 4.80
10.0	487 4.80	488 4.77	487 5.61

FIGURE 5 Results of moduli prediction using inversion algorithm.

data, absolute accuracy is not important. An incorrect assumption will displace the entire curve of figure 1 up or down, but it will not affect the variations.

GROUND-PENETRATING RADAR FOR DETERMINATION OF ASPHALT THICKNESS AND SUBGRADE MOISTURE

Ground-penetrating radar is the electromagnetic analog to ultrasound. In radar, short pulses of electromagnetic energy are emitted from an antenna. These pulses penetrate materials which act as dielectrics (e.g., rock, soil, concrete, and asphalt). Dielectric discontinuities in these materials, such as material interfaces and metal inclusions, produce echoes which are received at the antenna. The pattern of echoes, referred to as the waveform, is produced by successive arrivals of echoes from different interfaces. Thus, the waveform contains information regarding the location of interfaces, the nature of the material contrast at the interface, and the properties of the material layers. Radar has been applied to the determination of thicknesses and subsurface properties in concrete pavements (*3*) and bridge decks (*17, 18*). The basic principle underlying its application to asphalt pavements is illustrated in figure 6. Here it is seen that the principal components of the waveform are the reflection from the top of the asphalt, the reflection from the asphalt/base boundary, and the reflection from the base/subgrade boundary. The intensity of these reflections will be proportional to the strength of the contrast in dielectric properties between layers.

Asphalt Thickness

Asphalt thickness can be computed from the time difference between points A and $C(t_{AC})$ shown in Figure 6, and from the velocity of the electromagnetic wave in asphalt, V_a. The

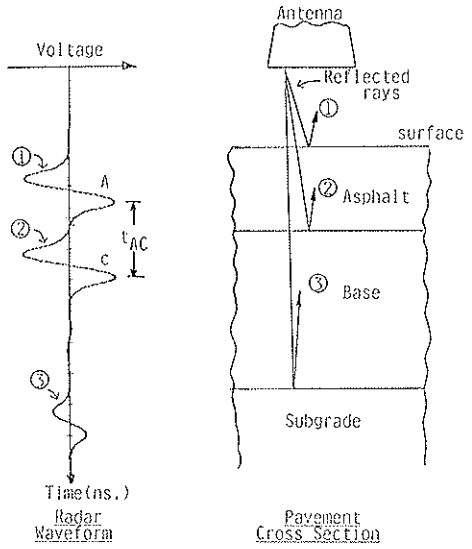

FIGURE 6 Radar model for pavement.

velocity, V_a, can be computed as

$$V_a = 11.8/\sqrt{\varepsilon_a}(\text{inches/nanosecond})$$

where ε_a is the dielectric permittivity of asphalt. The dielectric permittivity can be estimated using the flat plate reflection test (*19*) on the asphalt of interest. Measurements by one of the authors yield values of ε_a ranging from 5.0 to 6.0, with associate V_a ranging from 4.8 to 5.3 in./ns. Since t_{AC} is the round-trip travel time of the pulse in the asphalt layer, the thickness can be computed as

$$h_a = V_a t_{AC}/2$$

Figure 7 shows typical field data collected on a newly constructed 9-inch thick asphalt pavement. In the data set illustrated, fifty waveforms were generated for each second of vehicle travel, which, at 30 mph, yields approximately one waveform per foot of pavement. The waveforms shown in figure 7 represent a subsample of these data at 5-foot intervals. Note the sensitivity of t_{AC} to gradual changes in h_a at this sampling scale.

Subgrade Moisture

The response of radar to a layered medium can be predicted analytically if one knows the thickness, dielectric permittivity (ε) and conductivity (σ) of each layer. Such a model has been developed for bridge decks (*18*) and applied to pavements (*20*). Littlefield has computed the dielectric properties of the subgrade ε_s and σ_s as a function of moisture content, and has studied the radar response versus subgrade moisture content. Figure 8 shows a typical result of this work. The amplitude of the reflection from the top of the subgrade is plotted versus moisture content of the subgrade. Note that the relationship is strong, suggesting that this portion of the radar waveform can be used to infer spatial variations in moisture content.

The relationship described above has been successfully used to detect moisture under the asphalt overlay of reinforced-concrete bridge decks (*21*). Its adaptation to asphalt pavements is straightforward, but will require consideration of the normal variation in subgrade material properties.

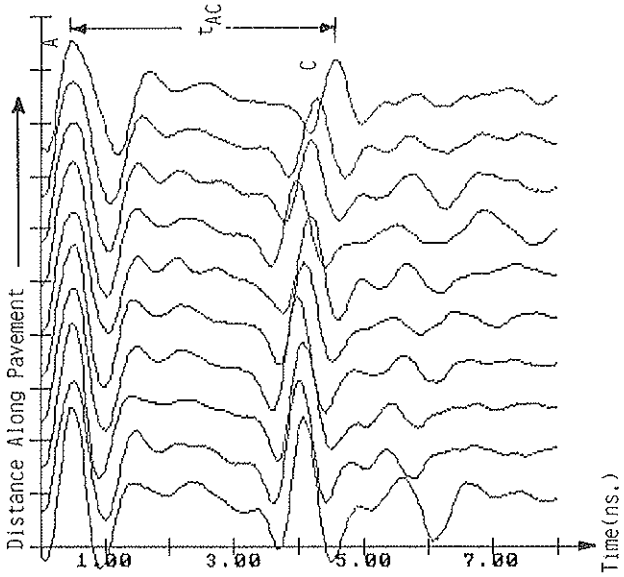

FIGURE 7 Radar field data.

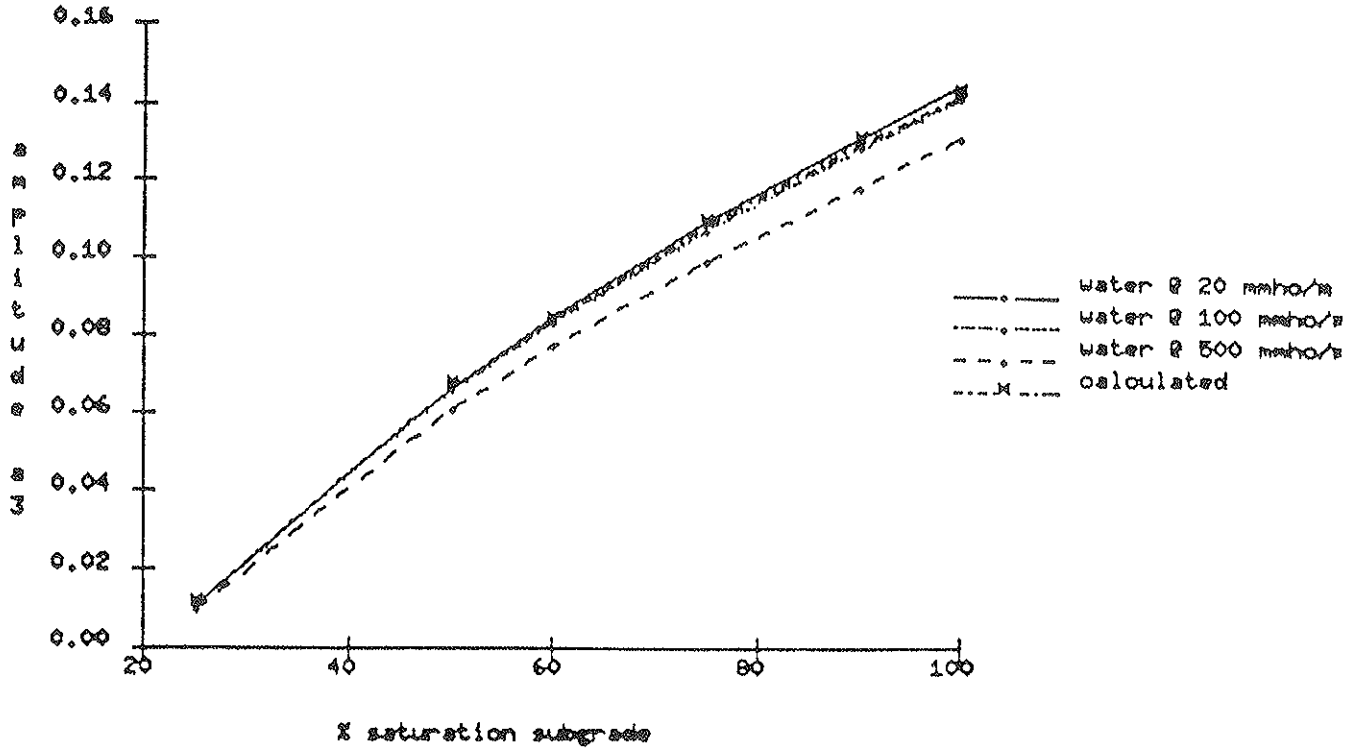

FIGURE 8 Subgrade return (a_3) versus saturation of subgrade (base course 25%).

CONCLUSIONS

This paper has described the level of information that state-of-the-art sensors can provide to pavement management. This level of information is far greater than that being considered by the current generation of pavement management systems. In addition, the nature of the sensor data is different from that which is currently utilized by pavement management systems. A suite of high-speed sensor data representing slope variance, rut depth, cracking, asphalt and subgrade moduli, asphalt thickness, and subgrade moisture content has been described as a basis for explaining the condition and predicting the performance of asphalt pavement. It has been shown that the two moduli, while not continuously measurable directly, can be inferred from rut depth, cracking, and asphalt thickness. Also, it has been shown that spatial variations in asphalt thickness and subgrade moisture content can be determined using ground-penetrating radar. Thus, the sensor suite described above can be completed using highway speed survey vehicles. What remains now is to complete the development of the

cracking and moisture sensors and to develop means for incorporating all these data into the pavement management process.

ACKNOWLEDGMENT

The authors would like to acknowledge the National Science Foundation for its support, and Peter Kopac of the Federal Highway Administration's Turner-Fairbanks Research Center for making a radar van available for this work.

REFERENCES

1. J. A. Epps and C. L. Monismith. *NCHRP Synthesis 126: Equipment for Obtaining Pavement Condition and Traffic Loading Data*. TRB, National Research Council, Washington, D.C., Sept. 1986.
2. D. H. Mendelsohn. Automated Pavement Crack Detection: An Assessment of Leading Technologies. *Proc., Second North American Conference on the Management of Pavements*, Toronto, Ontario, Canada, 1987.
3. W. J. Steinway, J. D. Echard, and C. M. Luke. *NCHRP Report 237: Locating Voids Beneath Pavement Using Pulsed Electromagnetic Waves*. TRB, National Research Council, Washington, D.C., Nov. 1981.
4. P. Ulldítz and B. K. Larsen. Mathematical Modeling for Predicting Pavement Performance. In *Transportation Research Record 949*, TRB, National Research Council, Washington, D.C., 1984, pp. 45–55.
5. M. Shahin and S. Kohn. *Pavement Maintenance Management for Roads and Parking Lots*. Technical Report, M-294. U.S. Army Corps of Engineers Construction Engineering Research Laboratory, Oct. 1981.
6. J. Sharma, L. L. Smith, and B. E. Ruth. Implementation and Verification of Flexible Pavement Design Methodology. *Proc., Fourth International Conference Structural Design of Asphalt Pavement*, Ann Arbor, Mich., 1977, pp. 175–187.
7. W. M. Kenis. Predictive Design Procedure—A Design Method for Flexible Pavements Using the VESYS Structural Subsystem. *Proc., Fourth International Conference on the Structural Design of Asphalt Pavements*, 1977.
8. D. R. McLean and C. L. Monismith. Estimation of Permanent Deformation in Asphalt Concrete Layers Due to Repeated Traffic Loading. In *Transportation Research Record 510*, TRB, National Research Council, Washington, D.C., 1974, pp. 14–30.
9. R. D. Barksdale. Laboratory Evaluation of Rutting in Base Course Materials. *Proc., Third International Conference on the Structural Design of Asphalt Pavements*, 1972.
10. C. L. Monismith, N. Ogawa, and C. R. Freeme. Permanent Deformation Characterization of Subgrade Soils Due to Repeated Loading. In *Transportation Research Record 537*, TRB, National Research Council, Washington, D.C., 1975, pp. 1–17.
11. J. B. Rauhut and P. R. Jordahl. *Effects of Flexible Highways of Increased Legal Vehicle Weights Using VESYS-IIM*. Report 77-116. FHWA, U.S. Department of Transportation, Washington, D.C., 1977.
12. W. J. Kenis and J. A. Sherwood. *Sulphex Pavement Performance Evaluations from Laboratory Tests*. TRB, National Research Council, Washington, D.C., 1982.
13. B. D. Brademeyer, N. J. Delatte, and M. J. Markow. Analysis of Moving Dynamic Loads on Highway Pavements—Part II: Pavement Response. Presented at the International Symposium on Heavy Vehicle Weights and Dimensions, Kelowna, British Columbia, Canada, June 1986.
14. W. J. Kenis, J. A. Sherwood, and T. F. McMahon. Verification and Application of the VESYS Structural Subsystem. *Proc., Fifth International Conference on the Structural Design of Asphalt Pavements*, 1982.
15. N. Odemark. *Design of Pavements According to the Theory of Elasticity*. Stockholm, Sweden, 1949.
16. M. J. Markow and B. D. Brademeyer. *EAROMAR Version 2, Final Technical Report*. Report 82-086. FHWA, U.S. Department of Transportation, Washington, D.C., 1982.
17. C. R. Carter, T. Chung, F. B. Holt, and D. G. Manning. An Automated Signal Processing System for the Signature Analysis of Radar Waveforms from Bridge Decks. *Canadian Electrical Engineering Journal*, Vol. 11, No. 3, 1986.
18. K. R. Maser. Detection of Progressive Deterioration in Bridge Decks Using Ground Penetrating Radar. *Proc., Experimental Assessment of the Performance of Bridges*. EM Division, ASCE convention, Oct. 1986
19. R. P. Joyce. *Rapid Non-Destructive Delamination Detection*. Final report. Contract DTFH-81-C-00072. FHWA, U.S. Department of Transportation, April 1985.
20. R. G. Littlefield. *Use and Interpretation of High Speed Sensors in the Diagnosis of Flexible Pavement Conditions*. M.S. Thesis. Massachusetts Institute of Technology, Jan. 1987.
21. K. R. Maser. *New Technology for Bridge Deck Assessment*. Final Report. New England Transportation Consortium, Center for Transportation Studies, Massachusetts Institute of Technology, Cambridge, Oct. 1989.
22. K. R. Maser. From Guesswork to Guarantee. *Civil Engineering Magazine*, Vol. 59, No. 9, Sept. 1989, pp. 78–79.

Publication of this paper sponsored by the Committee on Pavement Monitoring, Evaluation, and Data Storage.

Three-Dimensional Analysis of Slab on Stress-Dependent Foundation

A. M. IOANNIDES AND J. P. DONNELLY

Research described in this paper constitutes the final stage of a multicomponent project, which examined current computerized analysis techniques for slabs on grade. For a more realistic representation of a pavement system, an existing three-dimensional finite element program (GEOSYS) was modified. This can be used to analyze flexible or rigid pavements, thereby validating conclusions reached on the basis of conventional two-dimensional analysis. In the first part of this study, many runs were conducted to develop user guidelines for the fruitful utilization of the GEOSYS model. Effects considered included, among others, mesh fineness, vertical and lateral subgrade extent, boundary conditions, and stress extrapolation from computer results. Practical applications of the three-dimensional approach are presented in the second part of the paper. The three fundamental loading conditions, namely, the interior, edge, and corner of a slab resting on a stress-dependent, elastic, solid foundation are examined. Two typical single-wheel and multiwheel U.S. Air Force aircraft (F-15 and C-141) are considered. An iterative scheme is introduced to account for subgrade stress dependence, and the effect of stress softening, typical of cohesive soils, is evaluated and discussed. Results from this program are compared to those from conventional two-dimensional analyses, employing finite element, finite difference, and numerical integration techniques.

In a recent report for the U.S. Air Force Office of Scientific Research (*1*), an exhaustive examination was presented of existing tools that may be applied to the analysis of slab-on-grade pavement systems, within the context of two-dimensional plate theory. Findings from this research clearly indicated that no current procedure can model fully the behavior of a slab of finite size, supported by a stress-dependent cohesive subgrade extending beyond the slab edges. In a follow-up study (*2*), an existing three-dimensional finite element model (GEOSYS) was adapted to provide a more realistic representation of a pavement system. The model can be used to establish baseline structural response data for flexible or rigid pavements, representative of complex boundary and foundation support conditions, thereby validating and reinforcing conclusions drawn on the basis of two-dimensional analysis.

Results from more than one hundred three-dimensional, finite element runs from that study examining a slab on grade are interpreted and discussed in this paper. In the first part, guidelines for the fruitful utilization of the GEOSYS model are developed, to account for such effects as the sensitivity of the model to mesh fineness, vertical and lateral subgrade extent, boundary conditions, and so forth. Investigations for both interior and edge loading conditions have been conducted (*2*). Only the former are discussed in this part, however, because they have been found to be adequately representative.

In the remainder of the paper, an examination is presented of a slab on grade (rigid pavement) subjected to the three fundamental loading conditions, that is, interior, edge, and corner, using typical single-wheel and multiwheel U.S. Air Force aircraft. An iterative scheme is introduced to account for subgrade stress dependence. The effect of stress softening, typical of cohesive soils, is evaluated and discussed.

GEOSYS PACKAGE

GEOSYS was originally developed in the early 1970s by a group of engineers, members of the technical staff of Agbabian Associates, in El Segundo, California (*3*). For the purpose of this study, the linear, isoparametric, three-dimensional hexahedral brick element was employed. This has eight nodes with three degrees of freedom per node (the displacements in each of the x, y, and z directions). The subgrade is modeled as an elastic solid foundation. A typical input file for GEOSYS consists of several hundred lines, each formatted according to a strict pattern. Since data for different slab-on-grade analysis runs are generally similar in structure, a preprocessor, called "GEZIN" (GEOSYS Easy INput), was coded early in this study. This automatically prepares the data in the required format. Input for GEZIN includes fewer than ten data cards, the format of which is similar to the one used for ILLI-SLAB (*1*). Thus, data preparation is reduced to an almost trivial task, and the probability of errors during this stage is practically eliminated. Several post-processing programs were also coded during this investigation to assist interpretation of computer results. These postprocessors are used in conjunction with an iterative scheme introduced to account for the stress-dependent behavior of fine-grained soils.

SELECTION OF STRESS EXTRAPOLATION METHOD

The problem of a slab on grade may be investigated in three dimensions using a finite element mesh similar that shown in Figure 1. The slab rests on a cube of soil, carved out of the Boussinesq half space and maintained intact by the assumption of boundary conditions on the four vertical sides and on the base. Taking advantage of symmetry, where it exists, allows only a portion of the system to be modeled.

A. M. Ioannides, Department of Civil Engineering, University of Illinois, 208 N. Romine St., Urbana, Ill. 61801. J. P. Donnelly, Wiss, Janney and Elstner Associates, 330 Pfingsten Road, Northbrook, Ill. 60062.

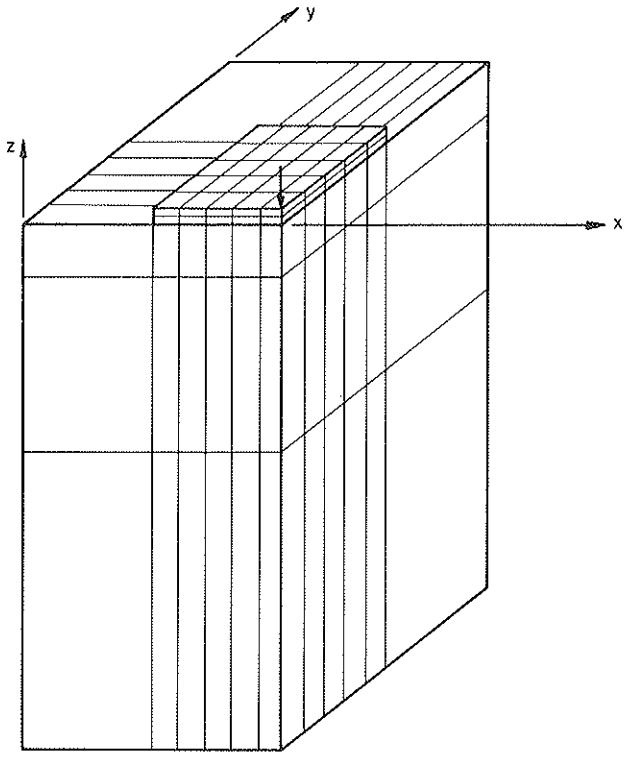

FIGURE 1 Typical three-dimensional finite element mesh.

For the linear solid (brick) element employed, displacements are calculated at each of the eight nodal points, but stresses (and strains) are determined only at the centroid of the element. It is, therefore, often necessary to extrapolate from calculated values to obtain the required stresses at the critical locations. Results from several runs suggested that orthogonal linear extrapolation (employing four known stresses in each determination) should be used in analyzing bending stress results (*2*). This method may also be used with subgrade stress data. When the stress state is known to be axisymmetric, for example, subgrade stress due to an interior load, diagonal linear extrapolation (employing three known stresses in each determination) is also appropriate.

VERTICAL AND LATERAL SUBGRADE EXTENT

Several runs were performed to determine the depth to which the subgrade should be modeled, as well as the size of the soil cube in the horizontal direction, so that boundary effects are eliminated, and computer storage required remains within the available limits. A typical plot of maximum responses obtained is shown in Figure 2. It is observed that both maximum bending and subgrade stresses (σ_i and q_i) converge to a constant value fairly quickly. Increasing the subgrade depth, Z, beyond 20 to 25 feet (or five to seven times the radius of relative stiffness, l_e) will have no effect on these stresses.

The behavior of deflection, however, requires more attention. Maximum deflection, δ_i, increases with subgrade depth as expected, but does not converge to a constant value, even for a depth of 35 ft (9 l_e). This is due to the presence of lateral boundaries at a finite distance, X, from the slab edges. As a result, vertical strains in the subgrade reach a level where they remain constant, rather than decrease as in a truly semi-infinite elastic solid, since they are not allowed to be distributed beyond the model boundaries. Further investigations revealed that the depth at which vertical strain decreases to a constant value, as well as this value itself, are both influenced by the lateral extent of the subgrade (*2*). Therefore, for a given lateral subgrade extent, the finite element model will overestimate vertical deformation, if the subgrade extends vertically beyond the constant vertical strain depth, z_{cvs}. Although

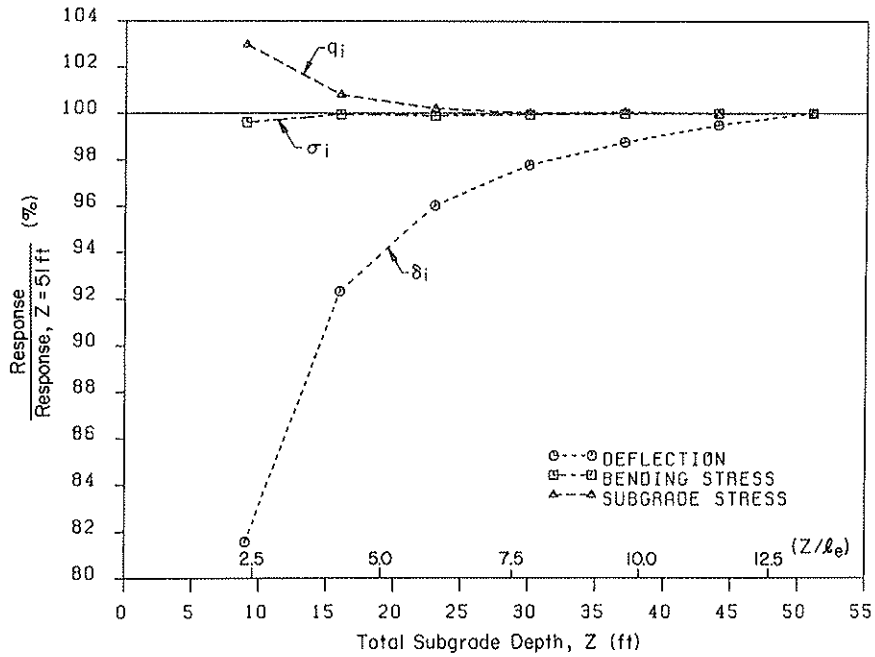

FIGURE 2 Effect of subgrade vertical extent.

this is influenced by the lateral extent of the subgrade, a subgrade depth of about 40 ft (10 l_e) may be used as a typical value. A lateral extent between 25 and 35 ft (or 7–9 l_e) is recommended.

BOUNDARY CONDITIONS

In order to examine the behavior of the two main types of lateral boundaries (i.e., free or on rollers), deflection basins from four runs are compared in Figure 3. These confirm that the system response is more sensitive to the boundary conditions used when the lateral boundaries are closer to the load. Furthermore, maximum deflection, δ_i, was once again affected much more significantly than the other two maximum responses, σ_i and q_i (*2*). Based on these results, neither boundary condition appears to have an advantage over the other. Consideration of radial strains in the surface subgrade layer, however, led to the adoption of roller-type lateral boundaries. The bottom boundary is also assumed to be on rollers, so that elements can move laterally and distribute their load by deforming.

VERTICAL DIVISION OF SLAB AND SUBGRADE

Results indicated that although there is a slight improvement in accuracy as the number of layers used in modeling the pavement slab increases, adequately reliable maximum responses can be determined even using only two slab layers (*2*).

Additional analyses led to the following conclusions with respect to the subgrade. The soil cube may be divided into three portions in the vertical direction. The upper portion should extend from 0 to 4 feet (0 to 1 l_e) and should consist of layers not more than 1 to 2 feet thick (0.25 to 0.5 l_e). The middle portion should extend from 4 to 15 feet (1 to 4 l_e) or half the constant vertical strain depth, z_{evs}, if known, and should be divided into at least two layers. Finally, the lower portion should cover the remainder of the soil cube and may be divided into one or more layers.

HORIZONTAL SLAB AND SUBGRADE MESH FINENESS AND ELEMENT ASPECT RATIO

Three series of GEOSYS runs were conducted to examine the influence of horizontal slab mesh fineness on the response of the three-dimensional slab on grade. The trends observed in Figure 4 are similar to those noted in earlier two-dimensional finite element studies (*1, 4*), inasmuch as all three maximum responses converge from below. Deflection and subgrade stress appear to be less sensitive to horizontal mesh fineness, and adequate accuracy may be expected as the mesh fineness ratio ($2a/h$) of the (short) side length of the finite element (plan view) to the slab thickness approaches the value of 0.8. This is similar to the value determined from the two-dimensional studies. Bending stress appears to be more sensitive to this effect, requiring values of ($2a/h$) less than 0.8 for convergence.

It was also found that the solution generally deteriorates as the maximum slab element aspect ratio, α_{max}, increases. This is defined as the ratio of the element's long side, $2b$, to its short side, $2a$ (in plan view). The impact of this factor is limited if α_{max} is kept below 4.

The overriding importance of mesh fineness was first identified and quantified in previous University of Illinois studies, using two-dimensional models (*1, 4*). A major conclusion reached was that a more stringent mesh fineness criterion is required under the loaded area than elsewhere in the finite element mesh (*5*). This counterbalances the approximation involved in discretizing applied distributed loads. A corollary

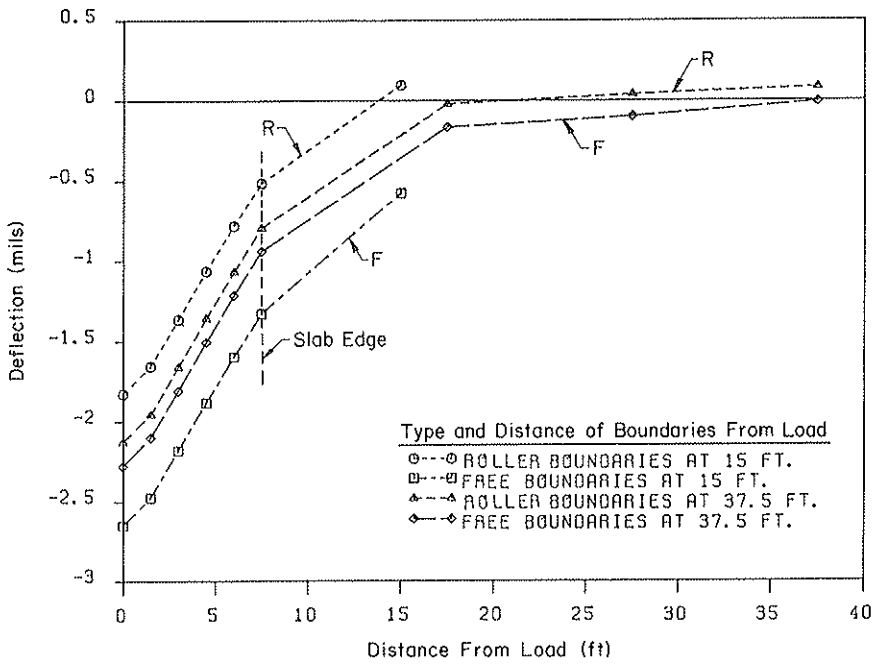

FIGURE 3 Effect of boundary conditions on subgrade surface deflection profile.

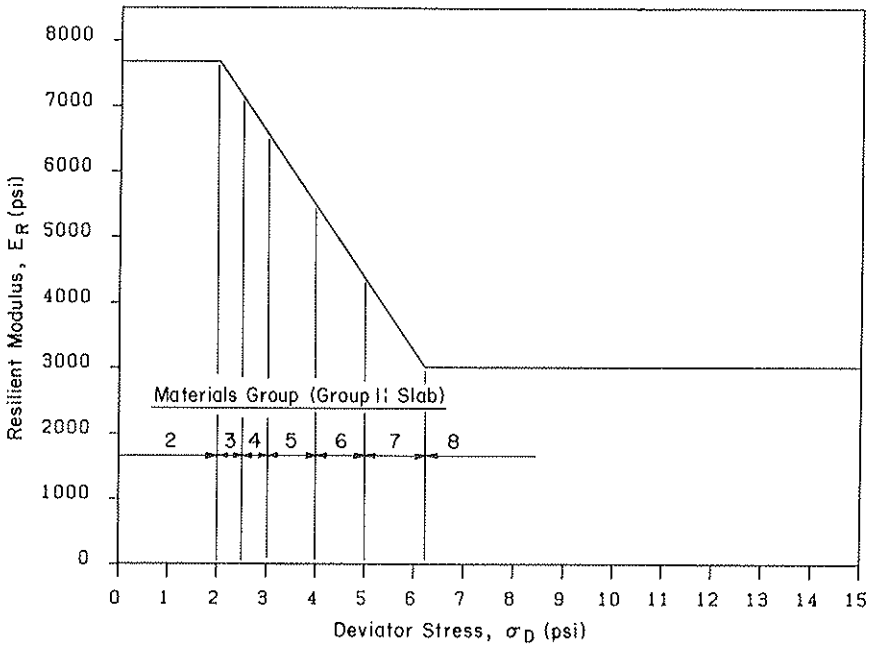

FIGURE 4 Effect of horizontal slab mesh fineness (interior loading).

TABLE 1 INVESTIGATION OF INTERIOR LOADING: F-15 SWL

SOLUTION	δ_i		q_i		σ_i	
	mils	%	psi	%	psi	%
GEOSYS-3D (Cycle 1)	32.15	90	5.031	104	609.55	96
ILLI-SLAB-2D	37.26	104	5.099	106	697.18	110
CLOSED-FORM	35.92	100	4.832	100	636.63	100

Notes:

$E = 4 \times 10^6$ psi $\quad \mu = 0.15 \quad h = 8$ in.
$E_s = 7682$ psi ('SOFT') $\quad \mu_s = 0.45 \quad \ell_e = 33.10$ in.
Slab: 15 ft x 15 ft ($L/\ell_e = 5.44$)
Load: 30 kips @ 355 psi, converted to 4 work equivalent loads (c = 9.193 in.)

-GEOSYS Mesh (Double symmetry - slab extends between underlined coordinates):
x-coordinates: 0; 30; 35; 36.5; 38; 39; 40; 41; 41.75; 42.5 ft
y-coordinates: 42.5; 12.5; 7.5; 6; 4.5; 3.5; 2.5; 1.5; 0.75; 0 ft
z-coordinates: 0.6; 0.3; 0; -0.5; -1.0; -2.5; -6.5; -17.5; -40 ft
In slab: $(2a/h)_{min}$=1.125; χ=2.0; α_{max}=2.0; (c/2a)=0.511.

-All responses are at interior of slab, under load:
δ_i : at top of slab;
q_i : at surface of subgrade, by diagonal extrapolation;
σ_i : at bottom of slab, by orthogonal extrapolation of σ_x values.

-ILLI-SLAB-2D: (2a/h) = 0.75; square elements.
CLOSED-FORM: Equations by Losberg (13), for infinite slab.

of this, which has serious implications with respect to recent efforts to model non-uniform pressure distributions (*6, 7*), may be stated as follows: in view of the conversion of external distributed loads into nodal components (which inevitably leads to at least some approximation, especially in the case of partially loaded elements), refinement of the applied pressure distribution, for the purpose of simulating observed deviations from simplistic uniformity, without due consideration and reciprocal improvement of mesh fineness, will be self-defeating, leading only to an illusion of improved accuracy.

Based on additional results obtained (*2*), it is recommended that the lateral extent of the subgrade beyond the slab edges, X, be divided into two elements, one 4 feet in size near the slab (1 l_e) and another 26 feet for the remainder (7 l_e).

PRACTICAL APPLICATIONS

In the analyses presented in the remainder of this paper, the following two fundamental questions are addressed:

1. How do three-dimensional analysis results compare with those from two-dimensional programs, such as ILLI-SLAB (*1, 4*), FIDIES (*8*), H51ES (*9, 1*), CFES (*5*), and others? A corollary to this is whether three-dimensional finite element analysis is necessary, and what the implications of its results are on the routine application of two-dimensional models.
2. How important is the effect of introducing stress-dependent resilient subgrade behavior? This effect was found earlier to depend on the placement and severity of the applied loads, using the two-dimensional resilient subgrade in ILLI-SLAB (*10*).

Simplified versions of the curves of subgrade resilient modulus, E_R, versus repeated deviator stress, σ_D, developed by Thompson and Robnett (*11*), are incorporated into the three-dimensional GEOSYS analysis to account for subgrade stress dependence. This is achieved through an iterative procedure implemented by a postprocessor, a program that receives as input results from GEOSYS. This iterative procedure is similar to that used for two-dimensional ILLI-SLAB analysis (*12, 10*). The modified E_R versus σ_D relation for the "soft" subgrade as employed in this study is shown in Figure 5. The deviator stress was defined in this case as the maximum difference between the three principal stresses determined by GEOSYS. Based on the σ_D level, the subgrade elements are classified into seven groups, and an average E_R is assigned to each.

FINITE ELEMENT MODEL FOR SINGLE-WHEEL INTERIOR LOADING

In a previous study, it was shown that subgrade stress dependence is not important when slab-on-grade pavements are loaded by a single tire print at the interior (*10*). To magnify any subgrade stress dependence effects, this study considered a relatively high load on a thin slab (8 inches thick), resting on the "soft" subgrade. The load applied at the interior is an F-15 single-wheel load (SWL) of 30 kips at 355 psi. Other pertinent information for this case is given in Table 1. This table also presents the maximum responses from GEOSYS, ILLI-SLAB, and the closed-form solutions (*13*). In view of symmetry, only one-quarter of the system needs to be modeled.

Effect of Subgrade Stress Dependence

A good indicator of the effect of subgrade stress dependence is the number of elements exceeding the 2 psi limit in σ_D, below which constant modulus behavior is assumed. For this GEOSYS run, only 5 out of 54 subgrade elements (or 9 per-

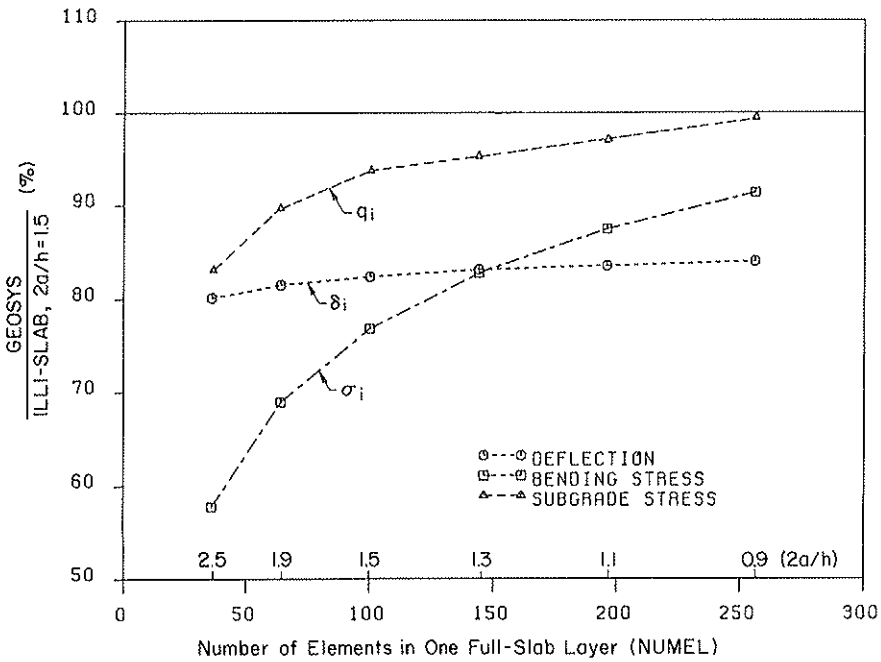

FIGURE 5 Simplified E_R vs. σ_D relation for "soft" subgrade as used in GEOSYS.

cent) had a σ_D above 2 psi. The range of σ_D values in these elements was 2.059 to 2.270 psi, with an average of 2.135 psi. The five overstressed elements (which in a subsequent iteration would change subgrade group) were located in the upper 2.5 feet of the subgrade, underneath the applied load. The updated E_R value for these would be 7,533 psi, a decrease of less than 2 percent from the initial 7,682 psi assumed for the constant, low-stress foundation modulus. It is evident that additional runs would not be very useful, since such a small change cannot be expected to affect the system significantly.

Comparison with Two-Dimensional Results

In Table 1, maximum interior deflection, subgrade and bending stress (δ_i, q_i, σ_i) from the three-dimensional GEOSYS run are compared to those from a similar two-dimensional ILLI-SLAB run. Values predicted by the closed-form solutions (*13*) are also tabulated. The ILLI-SLAB run employed a rather fine mesh. One-quarter of the slab was divided into 225 square elements, compared to only 49 elements used in the GEOSYS model. According to the results of extensive investigations using ILLI-SLAB (*1, 4*), such a fine mesh is necessary for results of adequate accuracy. The coarseness of the GEOSYS mesh is considered to be the prime source of the discrepancy between the finite element results and the closed-form solutions. The investigations conducted in the first part of this study indicate that only about 5 percent of this discrepancy may be attributed to an overall mesh fineness effect. The remainder is probably due to the fact that the mesh near the load needs to be even finer than elsewhere. In the mesh used, the load only partially covered the central element; this leads to some loss of accuracy when the applied load is converted to four work equivalent nodal loads.

The necessity for an even finer mesh under the load than elsewhere was confirmed in a previous study (*5*). This additional mesh fineness requirement over the area of applied load can also explain the high ILLI-SLAB results. All three responses may be expected to converge from above as the tire-print is subdivided into more elements. This assertion is reinforced by preliminary results obtained using the CRAY X-MP/24 supercomputer (*14*). Both GEOSYS and ILLI-SLAB results are also affected by the finite size of the slab in these analyses (compared to the infinite slab assumed in the closed-form solutions). This factor may partially explain why ILLI-SLAB δ_i and q_i are higher than the corresponding closed-form solutions, since these responses converge from above as slab size increases (*4, 5, 8*). Bending stress, however, converges from below, so the relatively high σ_i obtained by ILLI-SLAB cannot be attributed to the slab size factor. The primary source of this discrepancy, therefore, is the mesh fineness effect related to the size of the loaded area.

EDGE LOAD CASE

In this investigation, an F-15 SWL is applied to a relatively thin slab on a weak subgrade. The same slab-and-subgrade system used for interior loading is retained here for comparison. The pertinent characteristics of this system have been presented in Table 1. The finite element mesh was modified appropriately, according to the recommendations formulated in the first part of this investigation. Bending stresses developing in such a slab would be excessive in practice and are only considered here so that the effect of subgrade stress dependence is magnified.

Convergence Criteria

The iterative scheme introduced above may be used to account for the stress-dependent behavior of the subgrade. Figure 6 shows maximum responses for each of five cycles performed for the single-wheel edge loading case, normalized with respect to the corresponding average values from the second and third iterations. A uniform E_s of 7,682 psi is assumed in the first iteration, and its results correspond to those from a conventional linear elastic analysis. It is observed that the maximum responses oscillate about a value to which, presumably, they would eventually converge, if enough cycles were conducted. The amplitude of oscillation becomes progressively smaller as more cycles are performed.

The oscillation between maximum responses from the fourth and fifth iterations is only of the order ± 2 percent. This indicates that for most practical purposes, five cycles are more than adequate to achieve convergence. Furthermore, the average of the values of maximum responses obtained from the second and third iterations consistently give an estimate within ± 2 percent of the projected converged values. It is, therefore, recommended that three iterations be performed and that the average of the responses from the second and third cycles be adopted.

Effect of Subgrade Stress Dependence

A direct way to evaluate the effect of subgrade stress dependence for the F-15 SWL at the slab edge is to compare the maximum responses from the first iteration (which correspond to those from a conventional linear elastic analysis using a uniform, low σ_D soil modulus) to the average of those from

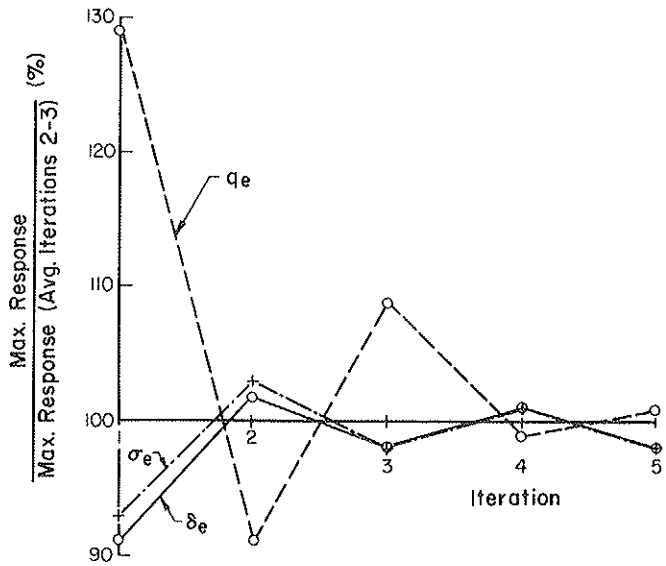

FIGURE 6 Maximum responses normalized with respect to average of second and third iterations.

the second and third iterations. Such a comparison shows in this case that maximum deflection and bending stress increase by 10 percent and 8 percent, respectively. This change is comparable to that observed with the two-dimensional K_R model in ILLI-SLAB (*10, 12*). On the other hand, maximum subgrade stress appears to be much more sensitive to stress dependence, decreasing by about 23 percent. It will be shown below that this is largely due to the development of high subgrade stress concentrations near the loaded edge. Subsequent iterations redistribute these stresses, thereby modeling local yielding, which would occur in a real soil subjected to these high stresses.

Results from this study indicate that the overall behavior of the slab is quite similar for the constant modulus and the stress-dependent subgrades. Furthermore, the differences in behavior that do exist, occur in and around the location of the subgrade elements with decreased resilient moduli. Only about 8 percent of all the subgrade elements experience a decrease in E_R. These elements are located in the upper 6.5 feet of the subgrade. Additional bending stress and deflection accumulate in elements in and under the slab as more iterations are performed, due to the decrease in subgrade support. The surface deflection basin observed after five iterations is, therefore, deeper than the one obtained after the first iteration.

A different phenomenon is observed beyond the slab, in the subgrade adjacent to the loaded edge. There, the cycle 5 profile is generally shallower than the cycle 1 profile. In addition, deflection of the stress-dependent subgrade (cycle 5) is reduced to 50 percent of the maximum value within only 6 inches from the loaded slab edge. The structural contribution of the subgrade beyond the slab is less significant for the stress-dependent model than for the constant modulus subgrade. Therefore, it can be seen that stress dependence tends to move the elastic solid model toward the direction of the dense liquid idealization, in which the contribution of the subgrade adjacent to the slab edges is altogether neglected.

Comparison with Two-Dimensional Results

Results obtained using GEOSYS may be compared to those from a number of two-dimensional models available, in order to establish the relative adequacy of the two approaches. In this section, results from programs FIDIES (*8*), H51ES (*1, 9*), and ILLI-SLAB (*4*) will be considered. FIDIES is a two-dimensional finite difference solution, employing square elements throughout the slab. The external loads are converted to point loads, applied at the center of each element. Responses are calculated at these points alone. Thus, an extrapolation, similar to that used with GEOSYS results, is necessary to obtain the edge responses. H51ES may only be used to calculate maximum bending stress at the edge, but its results are akin to a closed-form solution. Thus, they are not a function of user-specified parameters, such as mesh fineness, and element aspect ratio. These considerations can be crucial in the case of programs such as FIDIES and ILLI-SLAB. On the other hand, the latter two programs can account for the finite size of the slab and can determine the spatial distribution of all three responses, rather than just the maximum value of one of them.

Table 2 presents results obtained using these programs. The grid employed in the FIDIES run consisted of 441 square elements (no symmetry capability exists in FIDIES at this time). Previous studies (*1, 8, 15*) suggest that this grid may be slightly coarse, but it is dictated by computer memory limitations. In any case, the approximation involved in representing the applied load as a point load, located a few inches from the edge, is the overriding consideration here. Unfortunately, this approximation cannot be avoided. The ILLI-SLAB run was conducted using a mesh found to produce results of adequate accuracy (*15*). The other results are normalized in Table 2 with respect to the ILLI-SLAB responses.

The value of σ_e from ILLI-SLAB is about 11 percent higher than the closed-form solution from H51ES. This discrepancy cannot be explained by reference either to an inadequate mesh fineness or to the small slab size, since increasing these parameters would tend to increase the ILLI-SLAB value of σ_e. A similar discrepancy was observed with the dense liquid foundation as well, and was related to the size of the loaded area. For the (c/l_e) value of 0.28 used, the discrepancy was 10 percent (*1*), which is close to that observed here. Preliminary results using the CRAY X-MP/24 (*14*) indicate that this discrepancy disappears when the mesh under the loaded area is refined further.

On the other hand, FIDIES values of δ_e and σ_e are higher than the corresponding ILLI-SLAB ones, while q_e is lower. Again, overall grid fineness and slab size considerations cannot explain the discrepancy observed. It is considered that the major sources of this are the conversion of the external load to a point load acting at the center of an edge element, and the extrapolation involved in obtaining the values in Table 2 from the FIDIES output.

In Table 2, GEOSYS results from the first cycle are also presented. Comparison with those from ILLI-SLAB suggests that three-dimensional analysis gives q_e and σ_e values that are lower than those from ILLI-SLAB by about 60 percent and 30 percent, respectively. Maximum edge deflections are in relatively better agreement, the ILLI-SLAB value being only 9 percent higher than the corresponding one from GEOSYS. Part of these discrepancies (5 to 10 percent) may be attributed to the coarse mesh used with GEOSYS. The remainder of the discrepancy is probably due to the fact that both GEOSYS σ_e and q_e are extrapolated from calculated values at the centroid of each brick element. This is particularly important in the case of subgrade stresses. The contour plot of subgrade stresses in Figure 7 indicates that high subgrade stresses occur in a narrow zone along the loaded edge. Such a drastic increase in subgrade stress right at the edge of the slab has also been observed under interior loading (*5*), and is similar in nature to the infinite reactions predicted by Boussinesq's theory at the edge of a rigid punch. The linear extrapolation used to determine q_e from GEOSYS results is unable to reproduce the high stress gradients in this area.

In the narrow region immediately adjacent to the loaded edge, local yielding of the soil will occur. Thus, the theoretical value of the subgrade stress at the physical edge of the slab may not be of practical significance. A more meaningful value may be the subgrade stress developed a few inches inside from the edge, for example, at a distance of $0.2\,l_e$. A previous study showed that this value is relatively insensitive to mesh fineness (*5*). Additional iterations have the effect of redistributing the stress away from highly stressed elements. Thus, introducing subgrade stress dependence enables the user to model local

TABLE 2 COMPARISON OF TWO- AND THREE-DIMENSIONAL SOLUTIONS: F-15 EDGE SWL

SOLUTION	δ_e		q_e		σ_e	
	mils	%	psi	%	psi	%
GEOSYS-3D (Cycle 1)	60.32	91	24.63	42	826.0	70
FIDIES-2D (Linear extrap.)	73.21	111	30.93	53	1518.1	129
FIDIES-2D (Quadr. extrap.)	73.61	111	35.36	60	1605.8	136
H51ES	-	-	-	-	1055.9	89
ILLI-SLAB-2D (23x13 Mesh)	66.09	100	58.84	100	1180.8	100

Notes:

-For slab and subgrade characteristics, see Table 1.

-GEOSYS Mesh (Symmetry about x-axis employed - slab extends between underlined coordinates):
x-coordinates: 0; 18.5; 37; 41; 45; 47; 48; 49; 49.5; 50; 50.9375; 51.875; 53.750; 55.625; 57.5; 60; 62.5; 65; 95 ft
y-coordinates: 42.5; 12.5; 7.5; 5.625; 3.75; 1.875; 0 ft
z-coordinates: 0.6; 0.3; 0; -0.5; -1.0; -2.5; -6.7; -19.27; -40 ft
In slab: $(2a/h)_{min}$=2.81; χ=2.0; α_{max}=2.0; (c/2a)=0.20.

FIDIES mesh: (Δ/h) = 1.07; 21x21 square elements;
ILLI-SLAB mesh (symmetry about x-axis employed):
(23x13): $(2a/h)_{min}$=0.575; χ=3.0; α_{max}=2.18;
H51ES: 50 points used to define outline of applied load.

-All responses at intersection of loaded edge and centerline of load:
δ_e : at top of slab;
q_e : at surface of subgrade, by orthogonal extrapolation;
σ_e : at bottom of slab, by orthogonal extrapolation of σ_y values.
FIDIES results extrapolated using 2 (linear) or 3 (quadratic) elements along the slab centerline;
No extrapolation is involved in ILLI-SLAB and H51ES results.

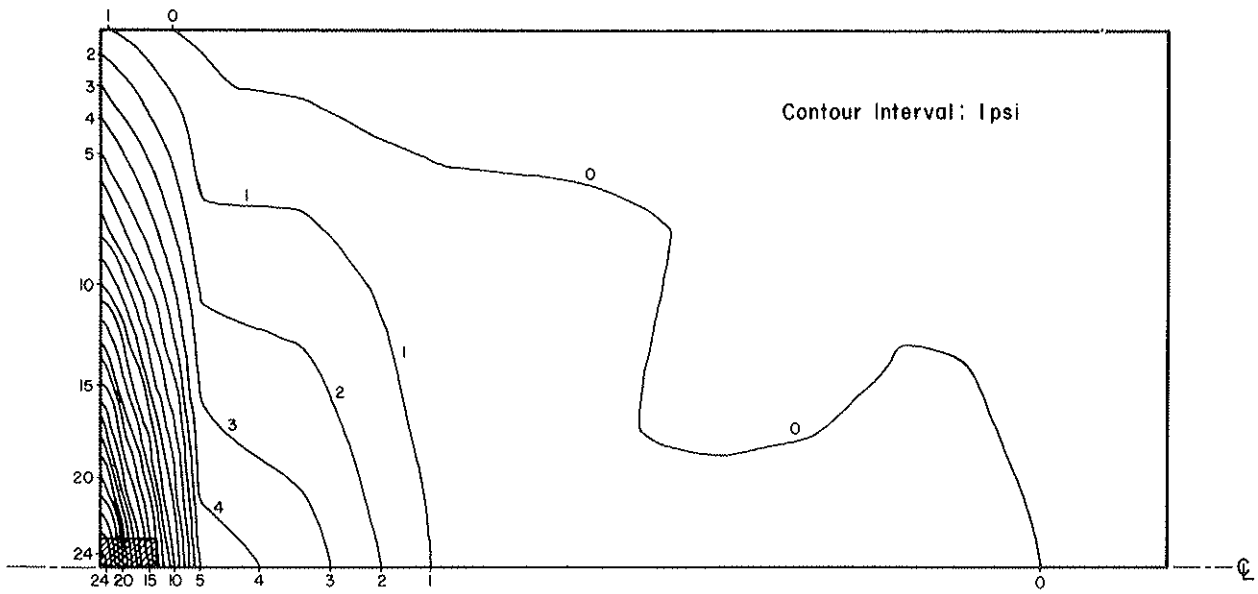

FIGURE 7 Surface subgrade stress contours from GEOSYS under slab: constant modulus subgrade (cycle 1).

yielding that would occur in a real subgrade. Notwithstanding the differences in their maximum responses, ILLI-SLAB and GEOSYS produce similar response distributions outside the critical edge region. The plots in Figure 8 reinforce the validity of the comments made above.

Similar conclusions were also reached from an investigation of multiwheel edge loading (MWL), using one landing gear from a C-141 aircraft. The effect of accounting for subgrade stress dependence is quite significant in this case. Maximum deflection increases by about 30 percent, and maximum bending stress by more than 20 percent. On the other hand, maximum subgrade stress decreases by more than 30 percent. Furthermore, the extent of the region of reduced resilient moduli obtained with the C-141 load is much larger compared to the F-15 case. The subgrade stress distributions in Figure 9 indicate that comparing only the maximum q_c values from the two- and three-dimensional models may be misleading. The overall system responses are much closer to each other than the individual maximum values would suggest. This is especially true when fine meshes are used.

CORNER LOAD CASE

To complete the series of three-dimensional investigations using GEOSYS, the corner loading condition is examined in this section, with an F-15 single-wheel load. Unfortunately, the lack of symmetry along either of the two major coordinate axes of the slab dictates the use of a full mesh in the finite element idealization. This results in prolonged execution times (in excess of 12 CPU hours on the HARRIS 800-2 virtual memory computer), even using a rather coarse mesh, which gives rise to less accurate results. General trends, however, may still be observed and these can be useful despite any limitations in the accuracy of individual response values.

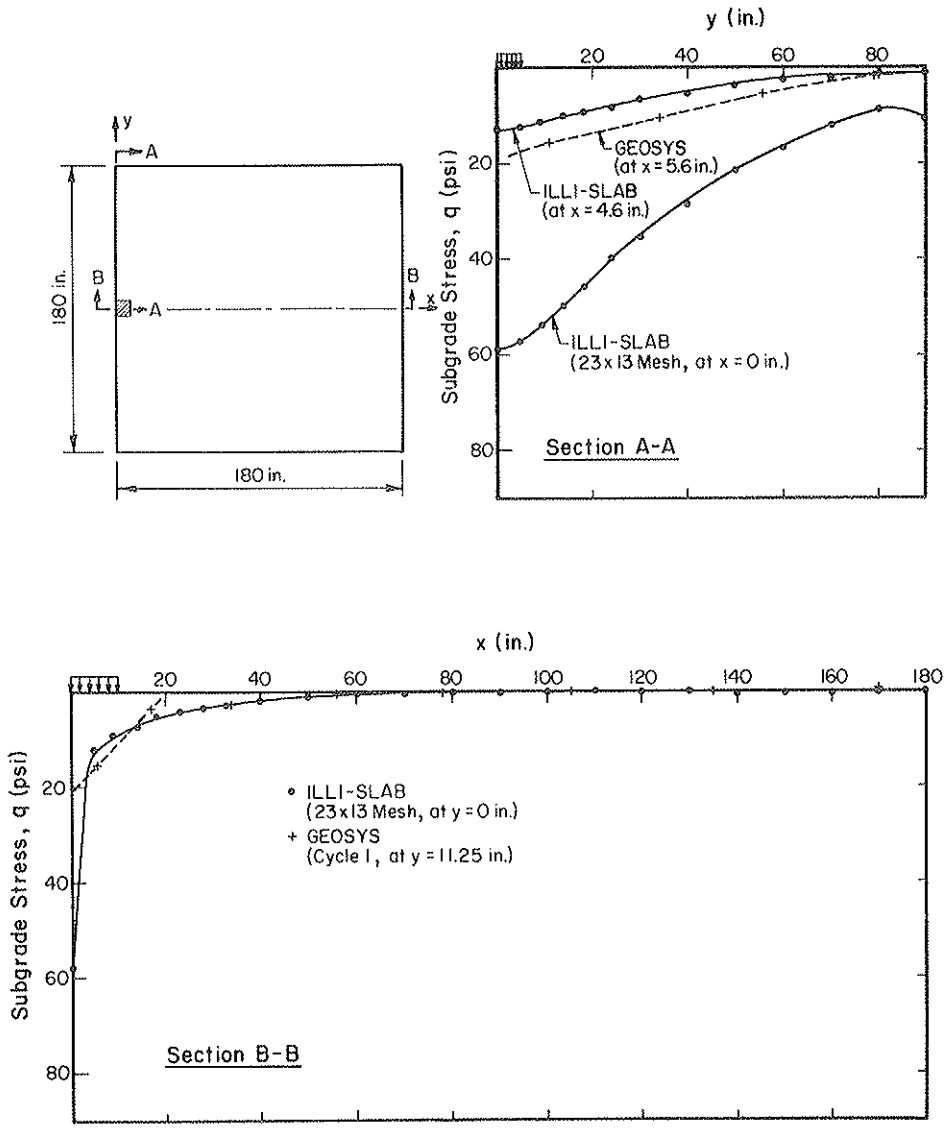

FIGURE 8 Comparison of GEOSYS and ILLI-SLAB surface subgrade stress distributions for F-15 edge SWL, under slab.

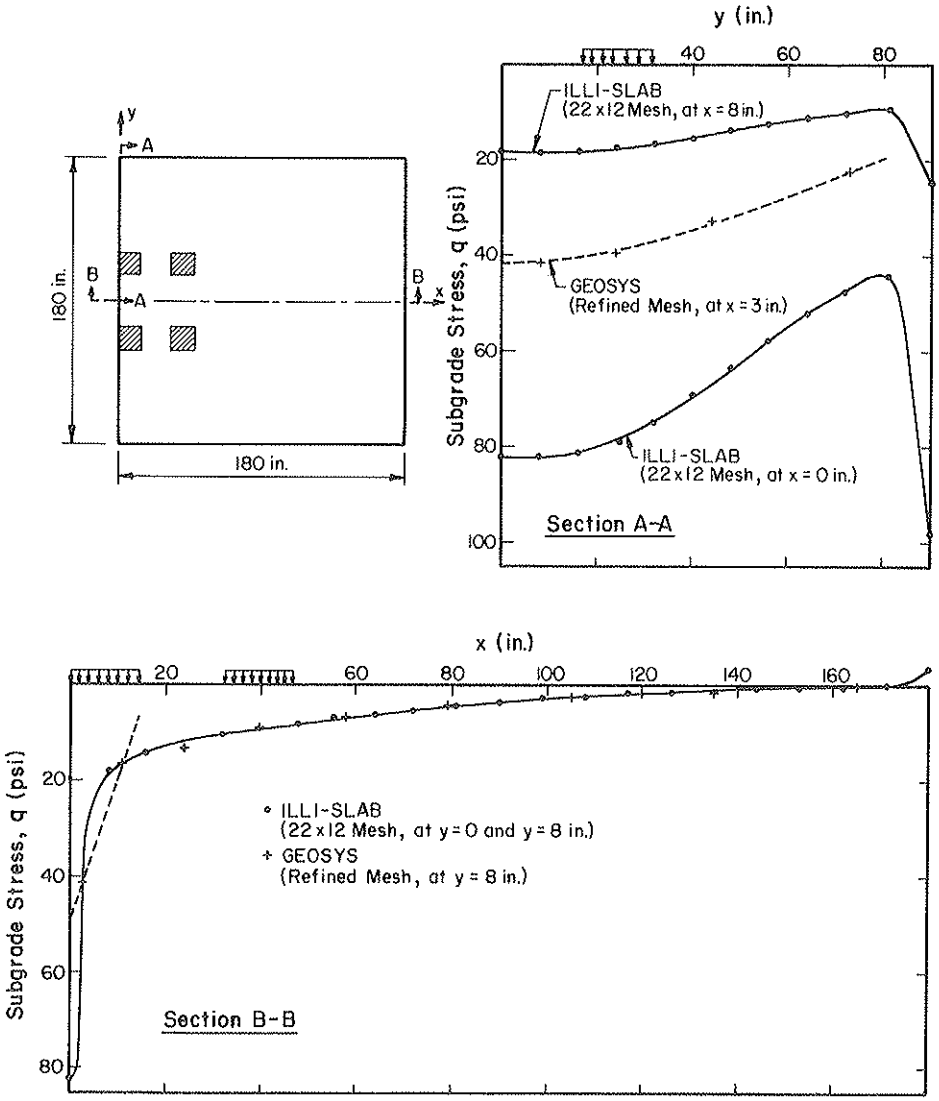

FIGURE 9 Comparison of GEOSYS and ILLI-SLAB surface subgrade stress distributions for C-141 edge MWL, under slab.

Effect of Subgrade Stress Dependence

Table 3 presents a summary of maximum responses obtained form three iterations performed for this case. Maximum deflection, δ_c, and subgrade stress, q_c, occur at the corner of the slab. On the other hand, maximum (tensile) bending stress, σ_c, occurs at the top of the slab, some distance from the corner. Preliminary results using ILLI-SLAB (*15*) suggest that a slab resting on an elastic solid also develops a high tensile bending stress at the bottom fiber under the load. This cannot be confirmed at this time using GEOSYS, however, since a much finer mesh would be required.

Subsequent iterations in Table 3 lead to a maximum deflection that is almost 20 percent higher than the value obtained from cycle 1. Similarly, an increase of more than 10 percent is observed in the maximum bending stress developing in the slab. On the other hand, a dramatic decrease in the value of the maximum subgrade stress predicted by the first iteration is obtained as subgrade stress dependence is considered. This reflects the redistribution of high subgrade stresses concentrated at the slab edges, observed earlier. Local yielding of soil in the corner region prevents these high stresses from developing, and this is accounted for by the iterative procedure used with GEOSYS. The maximum subgrade stress occurring at the slab corner itself, therefore, may not be a meaningful response. The subgrade stress developing under the center of the load, q_c^*, for example, may be a more realistic indication of subgrade response. This will be substantially lower than the value at the corner and, therefore, less sensitive to stress dependence. The oscillation of q_c^* in Table 3 is of smaller amplitude than that of q_c itself.

It is interesting to observe that about 20 percent of the subgrade elements are affected by stress dependence, compared to only 8 percent for the F-15 edge load. Subgrade stress dependence is predictably a more serious consideration under corner than under edge loading. The high values of σ_D are limited to the upper 5.5 feet of the subgrade, below which σ_D is less than 2 psi.

TABLE 3 EFFECT OF SUBGRADE STRESS DEPENDENCE: F-15 CORNER SWL

ITERATION	δ_c		q_c		q_c^*		σ_c	
	mils	%	psi	%	psi	%	psi	%
1	72.42	100	42.93	100	31.27	100	312.1	100
2	87.67	121	28.16	66	19.95	64	358.5	115
3	82.99	115	22.16	52	19.86	64	343.1	110
Avg. 2-3	85.33	118	25.21	59	19.81	64	350.8	112

Notes:

$E = 4 \times 10^6$ psi $\mu = 0.15$ $h = 12$ in.
$E_s = 7682$ psi ('SOFT') $\mu_s = 0.45$ $\ell_e = 49.64$ in.
Slab: 15 ft x 15 ft $(L/\ell_e) = 3.63$
Load: 30 kips @ 355 psi, converted to four work equivalent loads ($c = 9.193$ in.)

-Mesh (Slab extends between underlined coordinates):
x-coordinates = 0; 27.5; 29.167; 30; 30.833; 32.5; 35; 40; 45; 60 ft
y-coordinates = 60; 45; 40; 35; 32.5; 30.833; 30; 29.167; 27.5; 0 ft
z-coordinates = 1; 0.5; 0; -0.5; -1; -2.5; -6.5; -17.5; 40 ft

In slab: $(2a/h)_{min}$=0.833; χ=1.0; α_{max}=6.0; (c/2a)=0.92.

-Location and method of extrapolation of responses:
δ_c : at slab corner, at top of the slab;
σ_c : tension at top of slab, at some distance from corner: $\sigma_c = \sigma_1$, from values of σ_x, σ_y, τ_{xy}, extrapolated to the top, using linear orthogonal extrapolation;
q_c : compressive, at surface of subgrade under corner of slab: extrapolated up to surface of subgrade from values under corner region of slab, using linear orthogonal extrapolation.
q_c^* : compressive, at surface of subgrade, at x=5 in., y=5 in. from corner, under slab, extrapolated like q_c.

Comparison with Two-Dimensional Results

In view of the relatively coarse mesh employed in the GEOSYS runs, considerable discrepancies exist between three- and two-dimensional responses. GEOSYS gives a δ_c which is about 10 percent lower than the one predicted by ILLI-SLAB using a fine mesh. Differences in σ_c and q_c are even higher (+10 percent and −70 percent, respectively). According to the criteria developed above, GEOSYS results may be expected to be too low by less than 5 percent. Possible causes of the remainder of the gap between the two- and three-dimensional results were identified above as the coarseness of the GEOSYS mesh in the area of the load and the extrapolation involved in obtaining maximum stress values from the GEOSYS output. The latter is more important in the case of subgrade stress, in view of the high stress gradients existing near loaded slab edges and corners.

Figure 10 shows the distribution of subgrade stresses predicted by ILLI-SLAB and GEOSYS. These confirm that the two models are in good agreement, except in a region about 8 inches wide (or 0.2 l_e) along the slab edges. Pronounced subgrade stress gradients develop very close to the edges of the slab under all three fundamental loading conditions.

DISCUSSION AND CONCLUSIONS

Three-dimensional finite element analysis is shown in this paper to be a feasible and viable tool in pavement studies. Although this sophisticated numerical technique is unlikely to become a routine procedure in the near future, results presented herein indicate that it is possible to use a three-dimensional model to account for subgrade stress dependence, soil yielding, among other factors, as well as to accommodate multiwheel gears situated anywhere on the pavement surface. The GEOSYS model described is currently the only program that can be employed for analyzing both rigid and flexible pavements. Thus, it will be indispensable in future

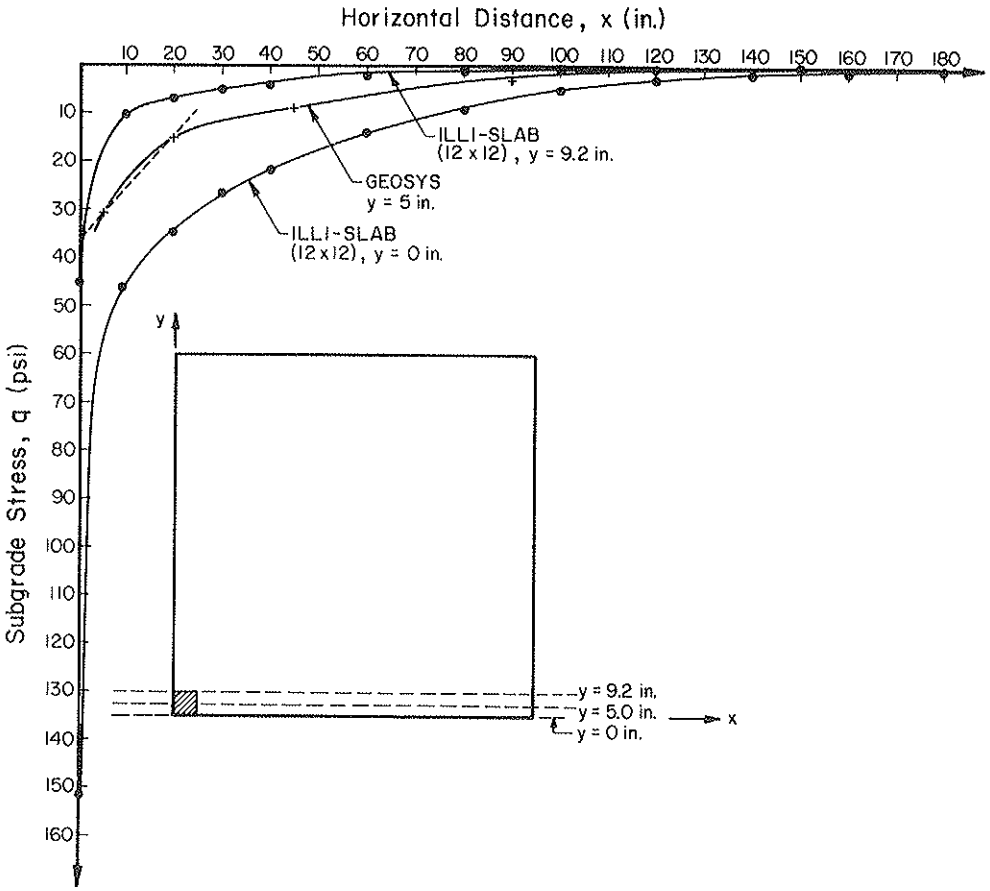

FIGURE 10 Comparison of GEOSYS and ILLI-SLAB surface subgrade stress distributions for F-15 corner SWL, under slab.

efforts to establish the elusive "unified" approach and to develop a generalized mechanistic design procedure.

A most significant conclusion reached, however, is that the three-dimensional investigations reinforce the validity and desirability of conventional two-dimensional analysis. In view of the relatively limited amount of three-dimensional results generated during this investigation, the accuracy of these results was often assessed by reference to the corresponding two-dimensional values. Where these disagreed, probable causes were considered and were usually found to be due to the coarse three-dimensional mesh used in these analyses.

This is not to deny the desirability of three-dimensional analysis as a means of checking and validating two-dimensional results. It does suggest, however, that for a meaningful utilization of the much more complex and demanding three-dimensional approach, adequate computer resources must be available. The rapid advances of computer technology in general, and the introduction of supercomputers in particular, provide reasons for optimism in this respect. Results from this study will be invaluable when considering the implementation of such a model on the mammoth machines anticipated in the near future.

From a more practical viewpoint, this study has shown that subgrade stress dependence may sometimes be important, primarily when considering heavy edge and corner loads. Subgrade stress dependence affects the maximum subgrade stress to a much greater extent than the maximum deflection or bending stress. When the load becomes more severe, for example, when it is placed near a corner rather than near an edge, the difference between the first and last iterations becomes much greater. These conclusions are similar to those reached using the two-dimensional K_R model (*10, 12*).

ACKNOWLEDGMENTS

The investigations for this paper were supported by a grant from the U.S. Air Force Office of Scientific Research, Air Force Systems Command, Bolling Air Force Base, Washington, D.C. The project manager was Lt. Col. L. D. Hokanson. M. R. Thompson and E. J. Barenberg were the project supervisors. Their advice and comments on the manuscript are greatly appreciated. The authors also acknowledge the cooperation of M. W. Salmon, formerly a graduate research assistant at the University of Illinois.

REFERENCES

1. A. M. Ioannides. *Analysis of Slabs-On-Grade for a Variety of Loading and Support Conditions.* Report TR-85-0083. U.S. Air Force Office of Scientific Research, Air Force Systems Command, USAF, Bolling AFB, Washington, D.C., Sept. 1984.
2. A. M. Ioannides, J. P. Donnelly, M. R. Thompson, and E.

J. Barenberg. *Three-Dimensional Finite Element Analysis of a Slab on Stress Dependent Elastic Solid Foundation*. Report TR-86-0143. U.S. Air Force Office of Scientific Research, Air Force Systems Command, USAF, Bolling AFB, Washington, D.C., Oct. 1986.
3. *Analytic Modeling of Rock-Structure Interaction*, Volumes 1–3. Reports AD-761-648, 649, 650, Advanced Research Projects Agency of U.S. Department of Defense and U.S. Bureau of Mines, April 1973.
4. A. M. Ioannides, M. R. Thompson, and E. J. Barenberg. Finite Element Analysis of Slabs-on-Grade Using a Variety of Support Models. *Proc., 3rd International Conference on Concrete Pavement Design and Rehabilitation*, Purdue University, West Lafayette, Ind., April, 1985, pp. 309–324.
5. A. M. Ioannides. Axisymmetric Slabs of Finite Extent on Elastic Solid. *Journal of Transportation Engineering*, ASCE, Vol. 113, No. 3, May 1987, pp. 277–290.
6. K. M. Marshek, H. H. Chen, R. B. Connell, and C. L. Saraf. The Effect of Truck Tire Inflation Pressure and Axle Load on Flexible and Rigid Pavement Performance. In *Transportation Research Record 1070*, TRB, National Research Council, Washington, D.C., 1986, pp. 14–21.
7. H. H. Chen, K. M. Marshek, and C. L. Saraf. The Effects of Truck Tire Contact Pressure Distribution on the Design of Flexible Pavements—A 3D Finite Element Approach. Presented at the 65th Annual Meeting of the Transportation Research Board, Washington, D.C., Jan. 1986.
8. A. M. Ioannides, Finite Difference Solution for Plate on Elastic Solid, *Journal of Transportation Engineering*, ASCE, Vol. 114, No. 1, Jan. 1988, pp. 57–75.
9. W. C. Kreger. Computerized Aircraft Ground Flotation Analysis—Edge Loaded Rigid Pavement. Research Report ERR-FW-572. General Dynamics Corp., Fort Worth, Tex., Jan. 1967.
10. A. M. Ioannides, E. J. Barenberg, and M. R. Thompson. Finite Element Model with Stress Dependent Support, In *Transportation Research Record 954*, TRB, National Research Council, Washington, D.C., 1984, pp. 10–16.
11. M. R. Thompson and Q. L. Robnett. Resilient Properties of Subgrade Soils. *Transportation Engineering Journal*, ASCE, Vol. 105, No. TE1, Jan. 1979, pp. 71–89.
12. M. R. Thompson, A. M. Ioannides, E. J. Barenberg, and J. A. Fischer. Development of a Stress Dependent Finite Element Slab Model. Report No. TR-83-1061. U.S. Air Force Office of Scientific Research, Air Force Systems Command, USAF, Bolling AFB, Washington, D.C., May 1983.
13. A. Losberg. *Structurally Reinforced Concrete Pavements*. Doktorsavhandlingar Vid Chalmers Tekniska Högskoła, Göteborg, Sweden, 1960.
14. A. M. Ioannides. Insights from the Use of Supercomputers in Analyzing Rigid and Flexible Pavements. Presented at 66th Annual Meeting of the Transportation Research Board, Washington, D.C., Jan. 1987.
15. A. M. Ioannides. Recent Findings Using Advanced Analysis Methods for Slabs-On-Grade. Presented at 65th Annual Meeting of the Transportation Research Board, Washington, D.C., Jan. 1986.

Publication of this paper sponsored by the Committee on Strength and Deformation Characteristics of Pavement Sections.

Verification of Backcalculation of Pavement Moduli

S. W. LEE, J. P. MAHONEY, AND N. C. JACKSON

This paper introduces a backcalculation computer program which can be used to estimate the elastic modulus for each pavement layer. This microcomputer program, EVERCALC, is based on the Chevron N-layer elastic analysis computer program and was developed primarily for flexible pavement analysis and falling weight deflectometer (FWD) data. The program is capable of estimating the elastic modulus for each layer of a pavement structure (up to a maximum of three layers) directly from surface deflection measurements. Further, the stress sensitivity coefficients for unstabilized layers (both base and subgrade) are estimated, as well as a "standard" asphalt concrete modulus analogous to a laboratory condition. Results from EVERCALC were verified in two ways. The first approach was to compare theoretical and backcalculated moduli for a range of three layer pavements. These comparisons showed modest differences among the moduli (about 8% for asphalt concrete, 6% for base course, and less than 2% for the subgrade soils). The second verification approach was to compare backcalculated and laboratory moduli based on FWD tests and field material sampling, along with appropriate laboratory testing. In general, the differences in moduli are significantly less than the "natural" variation of these materials within a relatively short pavement segment. (Pavement segments were originally selected for their apparent uniformity.)

The need to evaluate in situ pavement properties, such as layer moduli, is readily apparent to pavement engineers. The evolution of pavement structural characterization by use of both mechanistic analysis and nondestructive testing equipment, such as the falling weight deflectometer (FWD), has resulted in new pavement analysis tools.

This paper introduces a backcalculation computer program which can be used to estimate the elastic modulus for each pavement layer. This microcomputer program, EVERCALC, is based on the Chevron N-layer elastic analysis computer program. EVERCALC was developed primarily for flexible pavement analysis and the FWD. The program is capable of estimating the elastic modulus for each layer of a pavement structure (up to a maximum of three layers) directly from surface deflection measurements. Further, the stress sensitivity coefficients for unstabilized layers (both base and subgrade) are estimated, as well as a "standard" asphalt concrete modulus analogous to a laboratory condition. Comparisons of EVERCALC solutions to both theoretical and laboratory conditions are shown in an attempt to verify the backcalculation process. It is important to note that the backcalculation results presented in this paper were obtained in a "production" mode, i.e., the program was limited to a maximum of three iterations or a 10% cumulative error. (This will be more fully explained later.)

S. W. Lee and J. P. Mahoney, University of Washington, 121 More Hall, FX-10, Seattle, Wash. 98195. N. C. Jackson, Washington State Department of Transportation, Transportation Building, Olympia, Wash. 98504.

NONDESTRUCTIVE TESTING

Of the various nondestructive testing (NDT) devices available, the FWD was chosen as the primary focus of the reported work. There are a number of reasons for this. First, the FWD is the primary deflection measuring instrument used by the Washington State Department of Transportation (WSDOT). Second, it can provide variable and large impulse loadings to the pavement surface which to some degree simulate actual truck traffic.

With the FWD (Dynatest model 8000), a transient impulse load is applied through a set of rubber cushions, which results in a load pulse of 25 to 30 milliseconds. The pavement deflections are measured at up to seven locations with velocity transducers (*1, 2*). As with any NDT device, the FWD has a few (but generally minor) drawbacks. For example, the depth to a "rigid layer" in a pavement may affect the deflection basin and, hence, the backcalculation analysis (*3*). Further, the accelerations of the FWD load and moving wheel loads are different. (The FWD is higher.) Thus, the inertia of the pavement mass may play an important role for the FWD, while it is negligible for the moving wheel (*4, 5*).

Overall, the FWD has been shown to be a powerful, if not the best, NDT device currently available (*6, 7*).

CHARACTERISTICS OF PAVEMENT MATERIALS

General

A "typical" flexible pavement system consists of layers of both bituminous bound (asphalt concrete) and unbound (base and subgrade) materials. The treatments performed on these materials in the backcalculation process will be described in this section.

Asphalt Concrete

The stiffness of asphalt concrete is a function of numerous parameters, two of the most important being temperature and load duration (*8*). Based mostly on laboratory resilient moduli data for WSDOT class *B* asphalt concrete mixtures (tradi-

tional, dense mixes), the following regression relationship was obtained (*9*):

$$\log E_{ac} = 6.4721 - 1.4736 \times 10^{-4}(T)^2$$

where

E_{ac} = modulus of asphalt concrete (psi), and
T = pavement temperature (°F).

Thus, this straightforward relationship can be used to adjust a "backcalculated" modulus at a given field temperature to any other temperature (presumably to some "standard" temperature, such as 77°F). This adjustment is made by multiplying the backcalculated modulus by the ratio of the moduli at the desired (or standard) temperature and the field temperature (pavement temperature at the time of FWD testing).

The effect of different load durations for asphalt concrete mixtures is accounted for by use of an equation developed for the Asphalt Institute (*10*). This is necessary if one wishes to view backcalculated asphalt concrete moduli in terms of the "traditional" laboratory values, since the durations of laboratory load pulses are generally at the a level of 100 milliseconds and FWD load pulses closer to 25 to 30 milliseconds. Using normal WSDOT asphalt concrete mixture parameters, the differences in load durations (FWD vs. laboratory) and the Asphalt Institute relationship, the following regression equation was developed:

$$R = 0.791 + 0.00813\ (T)$$

where

R = ratio of FWD to laboratory moduli, and
T = pavement temperature (°F) during FWD testing.

This relationship adjusts the "field" backcalculated asphalt concrete modulus by multiplying the backcalculated modulus by $1/R$.

Clearly, pavement temperature is a significant factor for asphalt concrete stiffness. In the described backcalculation procedure, the pavement temperature at the time of FWD testing is required. To determine the pavement temperature, one can either measure it directly (which is time consuming) or use an approximate computational technique for estimation. Southgate and Deen's method (*11*) was chosen for the latter technique. Their procedure requires the pavement surface temperature, the previous five-day mean temperature, and pavement thickness to estimate the temperature at mid-depth in the asphalt concrete layer.

Base and Subgrade

The modulus of unbound (or unstabilized) materials is a function of numerous factors, such as degree of saturation, density, gradation, stress level, and load duration and frequency. Thus, most unbound base materials and subgrade soils exhibit a direct relationship between modulus and stress state (*8*). This relationship is generally as follows:

$$E_b = K_1(\Theta)^{K_2}$$

and

$$E_s = K_3(\sigma_d)^{K_4}$$

where

E_b = elastic (or resilient) modulus for base materials and/or coarse-grained soils (psi),
E_s = elastic (or resilient) modulus for fine-grained soils (psi),
Θ = bulk stress (psi),
σ_d = deviator stress (psi), and
K_1, K_2, K_3, K_4 = regression coefficients.

If varying load levels are obtained with the FWD at a specific pavement location, backcalculated moduli and associated stress states can be estimated and the K values obtained by simple linear regression.

EVERCALC

EVERCALC is a mechanistic-based pavement analysis computer program based on the Chevron N-layer program. This microcomputer program (which runs on an IBM AT or compatible computer) uses an iterative procedure of matching the measured surface deflections with the theoretical surface deflections calculated from assumed elastic moduli. The program produces a solution when the summation of the absolute values of the discrepancies between the measured and theoretical surface deflections falls within a preset allowable tolerance (generally 10%). Lower tolerance levels will produce more accurate solutions; however, the 10% tolerance results in modest computer run time (about 5 minutes for a three-layer pavement case). The program is primarily for the analysis of flexible pavement using FWD deflection measurements. The acquired input data for this program are six surface deflection measurements at the offsets of 0, 8, 12, 24, 36, and 48 inches from the center of the load (refer to Figure 1), pavement layer thicknesses, and appropriate temperature data.

The program is capable of evaluating a flexible pavement structure containing up to three layers. The program can be run with or without a "rigid base." The program estimates the initial "seed" moduli and performs backcalculation of the elastic modulus for each pavement layer. It also determines the stress sensitivity coefficients (K values) for the base materials and subgrade soil when the FWD data for at least two load levels are available at a given point. Further, the asphalt concrete moduli are adjusted to WSDOT laboratory standard conditions (77°F temperature and 100-millisecond load duration).

The seed moduli are estimated using internal regressions, which are algorithms developed using regression between pavement layer moduli, load, and various kinds of deflection basin parameters (*12*).

Prior studies have found that the Chevron N-layer computer program has a computational error in calculated pavement surface deflection as compared with those calculated by BISAR (*13, 14*). The problem appears to be more severe near the applied load and is exacerbated if a rigid base is used. To examine these surface deflection differences between Chevron N-layer and BISAR, surface deflections were calculated (without rigid base) by both computer programs for the following cases using an 11.8-inch diameter circular load area. (see Table 1).

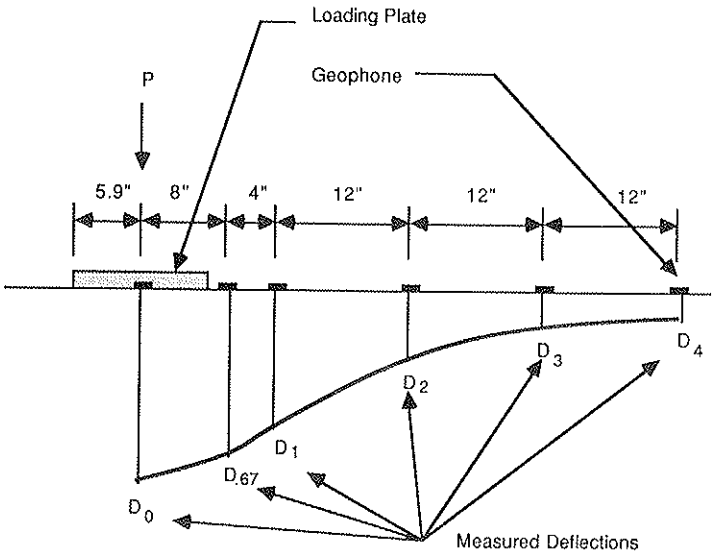

FIGURE 1 Present configuration of WSDOT FWD.

TABLE 1 COMPARISON OF CHEVRON N-LAYER AND BISAR CALCULATIONS OF SURFACE DEFLECTION DIFFERENCES

Asphalt Concrete	Stiffness (ksi):	50	500	1,000
	Thickness (in):	6	12	
	Poisson's ratio:	0.35		
Base	Stiffness (ksi):	10	20	40
	Thickness (in):	12	24	
	Poisson's ratio:	0.40		
Subgrade	Stiffness (ksi):	5	15	30
	Thickness (in):	semi-infinite		
	Poisson's ratio:	0.45		
Load levels (lb)	9,000 and 15,000			

The average surface deflection and associated standard deviation differences for 216 cases are shown in Table 2.

Further, the maximum deflection difference was 8.2% directly under the load (E_{ac} = 1,000 ksi, h_{ac} = 12 in., E_b = 40 ksi, h_b = 24 in., E_{subg} = 5 ksi), with only 12 of the 216 cases over 5%. Generally, the largest differences (2.0% or more) were for the thick, higher stiffness surfaces on lower stiffness subgrades.

The basic conclusion drawn from the above information is that the Chevron N-layer program is adequate for backcalculation of typical moduli for flexible pavements (given normally used convergence errors). However, backcalculation programs based on the Chevron N-layer should not be used on rigid pavements at this time.

ACCURACY OF BACKCALCULATION SOLUTIONS

A number of concerns about backcalculation of elastic moduli can be raised. These can include (1) nonunique solutions, (2) requirement for equivalent moduli for a limited number of layers (three or four), (3) differences between backcalculated and laboratory obtained elastic moduli, and (4) selection of the optimum number and location of surface deflection measurements.

Nonunique solutions simply mean that if different initial seed moduli are used, then different backcalculated moduli result in a final solution. The equivalent moduli problem arises from the fact that a limited number of pavement layers can

TABLE 2 AVERAGE SURFACE DEFLECTION AND ASSOCIATED STANDARD DEVIATION DIFFERENCES FOR 216 CASES

Statistics	Radial Offset (in.) 0	8	12	24	36	48
Mean (%)	1.1	0.4	0.2	0.0	0.1	0.1
Std. Dev. (%)	1.7	0.6	0.3	0.1	0.1	0.1

be used in the backcalculation process (in part limited by the number of measured surface deflections, computer run time, and theory associated with modeling complex materials). Thus, one must obtain (for example) a single modulus value for the asphalt concrete materials even though such a layer may be composed of different asphalt concrete mixtures, lifts, and hence moduli. Finally, backcalculated and laboratory moduli must show at least modest agreement in order for pavement engineers to become more confident in backcalculation procedures.

When the seed moduli are accurately estimated, the backcalculation process will produce solutions with less error in fewer iterations, thus minimizing the nonuniqueness problem. The seed moduli may be estimated by engineering judgment, temperature-stiffness relationships, and surface deflections, among others. EVERCALC contains internal regression equations (*12*), which are used to estimate the seed moduli (for up to three layers) from deflection basin parameters. This is done in an attempt to minimize nonuniqueness.

To address at least partially the nonuniqueness question for backcalculated solutions, EVERCALC backcalculated solutions were compared with theoretical elastic layer solutions. This was accomplished by calculating "theoretical" surface deflections for preselected layer moduli and thicknesses (for three layer pavements). These calculations were performed with the Chevron N-layer computer program for the following cases, shown in Table 3.

Surface deflections were calculated at six offsets of 0, 8, 12, 24, 36, and 48 inches from the load. The load was assumed to be 9,000 pounds, placed on a circular load plate 11.8 inches in diameter. The cases were excluded in which the asphalt concrete layer was of greater thickness than the base; thus, 384 cases were used. The surface deflections so calculated were then used as inputs into EVERCALC, and moduli for each of the three layers backcalculated. This enabled a straightforward comparison of the known moduli used originally to calculate the surface deflections (via Chevron N-layer program) to the backcalculated moduli obtained from those same surface deflection (via the EVERCALC program).

A maximum of five surface deflections can be used for direct backcalculation with EVERCALC; thus, two separate runs were made for surface deflections at 0, 8, 12, 24, and 36 inches (case A) and those at 0, 12, 24, 36, and 48 inches (case B). These two deflection sensor configurations have been commonly used by the WSDOT and appear to define the deflection basin reasonably. A maximum allowable tolerance of 10% was used for "matching" the deflection basins. The 10% tolerance is an absolute value (i.e., the sum of the absolute differences in surface deflections at all five locations). This tolerance level resulted in three backcalculation iterations or less to procure an "in tolerance" solution for the cases studied. Thus, the backcalculation results reported throughout this paper were obtained in a "production" mode representative of expected, everyday usage of EVERCALC.

The percent differences between the backcalculated and theoretical moduli were determined. The backcalculations performed for surface deflection measurements conforming to case A were slightly better than those for case B (i.e., better agreement between backcalculated and theoretical moduli). This is most likely due to the second surface deflection measurement being only 8 inches from the center of the load plate for case A, as opposed to 12 inches for case B, thus better defining a critical portion of the deflection basin.

A summary of the absolute percent differences (or errors) for the backcalculated and theoretical moduli is shown in Table 4 for case A surface deflection locations (i.e., sign conventions were ignored which result in higher average errors). Overall, the subgrade moduli have the closest agreement (about 1.5%). The base materials have an average difference of about 6.5% and the pavement surfacing (asphalt concrete) about 8.2%. Figure 2 is used to show the cumulative frequency distribution of the errors. Overall, most of the calculated errors were less than 10% for the subgrade moduli. For asphalt concrete and base layers, 82% of the comparisons had less than a 10% error; 90% had less than 20% error; and 95% had less than 30% error. Further, the errors tended to increase for thin, low stiffness (100,000 psi) asphalt concrete layers.

COMPARISON OF BACKCALCULATED AND LABORATORY MODULI

Comparisons between backcalculated (or in situ) and laboratory moduli are difficult because of variability of the materials, sampling, and testing. The results presented in this section will show the results of such an attempt.

Sixteen pavement test sites (Table 5) were used to compare the backcalculated and laboratory moduli. These test sites are typical of flexible pavement sections on the state-maintained route system in Washington. In part, however, they were selected for their apparent uniformity (for example, in construction, distress, and subgrade soils). Surface distress at these sites was observed to be mostly fatigue (alligator) cracking or its usual precursor, longitudinal cracking. Only five of the sixteen test sites were evaluated (for backcalculation pur-

TABLE 3 COMPARISON OF EVERCALC BACKCALCULATED SOLUTIONS WITH THEORETICAL ELASTIC LAYER SOLUTIONS PERFORMED WITH CHEVRON N-LAYER PROGRAM

Asphalt Concrete	**Stiffness (ksi):**	100	300	500	800
	Thickness (in):	3	5	8	
	Poisson's ratio:	0.35			
Base	**Stiffness (ksi):**	10	20	40	
	Thickness (in):	6	12	24	
	Poisson's ratio:	0.40			
Subgrade	**Stiffness (ksi):**	5	10	20	30
	Thickness (in):	semi-infinite			
	Poisson's ratio:	0.45			

TABLE 4 CALCULATED ERRORS FROM COMPARISON OF BACKCALCULATED AND THEORETICAL LAYER MODULI

Surface Thick. (in.)	Layer	Error (%) Theoretical Elastic Modulus (psi) 100,000 Mean	100,000 Std	300,000 Mean	300,000 Std	500,000 Mean	500,000 Std	800,000 Mean	800,000 Std	Average Mean	Average Std
3.0	ACP	18.5	31.8	6.8	12.2	5.0	9.5	5.8	9.8	9.7	13.4
	Base	3.9	6.0	3.7	4.4	4.0	4.8	4.8	6.4	4.6	4.7
	Subgrade	0.7	0.5	0.9	0.9	1.4	1.7	1.4	2.1	1.3	1.2
5.0	ACP	13.5	24.8	6.2	9.4	4.7	7.4	5.5	6.9	7.7	10.4
	Base	6.0	9.6	5.1	6.1	5.1	4.6	6.5	4.8	5.5	5.9
	Subgrade	1.0	0.9	1.1	1.0	1.6	1.5	1.3	1.1	1.2	1.2
8.0	ACP	9.8	24.3	6.2	9.2	3.6	5.2	5.5	11.0	7.2	9.9
	Base	8.6	10.7	8.0	11.3	8.0	7.8	11.0	11.7	9.5	9.4
	Subgrade	2.2	1.7	2.3	1.8	2.4	1.8	2.1	1.6	2.0	2.0

Note 1: Error (%) = $\left|\left(\frac{\text{Backcalculated modulus - theoretical modulus}}{\text{theoretical modulus}}\right)(100)\right|$

poses) as three-layer pavements. The remainder were evaluated as two-layer systems ("full-depth" cases).

The field material sampling required for laboratory testing included obtaining asphalt concrete cores at three locations (stations 0 + 50, 5 + 50, and 9 + 50) within the 1,000-foot-long test sites. This was done to estimate better the asphalt concrete modulus and thickness changes within each test site. Disturbed base course and subgrade soil samples were obtained at the pavement shoulder at approximately the middle of each test site (station 5 + 50). During this sampling in situ, moisture contents were made in the base and subgrade materials.

The laboratory testing of the asphalt concrete cores was conducted in accordance with ASTM D4123 at three temperature levels (41°, 77°, and 104°F) and a loading duration of 100 milliseconds. The base and subgrade materials were recompacted in the laboratory and tested in accordance with AASHTO T274. The remolding moisture content was kept as close as possible to those measured in the field at the time of sampling. The triaxial testing was performed on each sample with confining stresses of 1, 2, 4, and 6 psi and deviator stresses of 1, 2, 4, 6, 8, 10, and 12 psi. All laboratory testing was conducted by the WSDOT at its materials laboratory in Olympia, Washington.

Asphalt Concrete Comparisons

The comparisons of backcalculated (EVERCALC) and laboratory asphalt concrete moduli are shown in Table 6 for all sixteen test sites. All moduli values have been rounded off to the nearest 1,000 psi; however, the percent differences were calculated on the non-rounded values. Further, all backcalculated moduli values were adjusted to a "standard" loading duration (100 milliseconds) and temperature (77°F) to provide better comparisons with the laboratory moduli (for which a large amount of published modulus data is available).

Differences in the backcalculated and laboratory moduli range from being essentially identical to over 400%. Overall, differences of 20% to 50% were common. The largest differences were observed for test site 8, which had extensive, severe fatigue cracking observed at the pavement surface. Thus, the low backcalculated values (40,000 to 100,000 psi) should be expected. Naturally, when this test site was cored, only those cores were obtained which had no cracks. Therefore, the large differences between backcalculation and laboratory moduli are understandable. This same discussion applies to test site 10, since this site has extensive longitudinal cracking. If one views the moduli differences for the remaining test

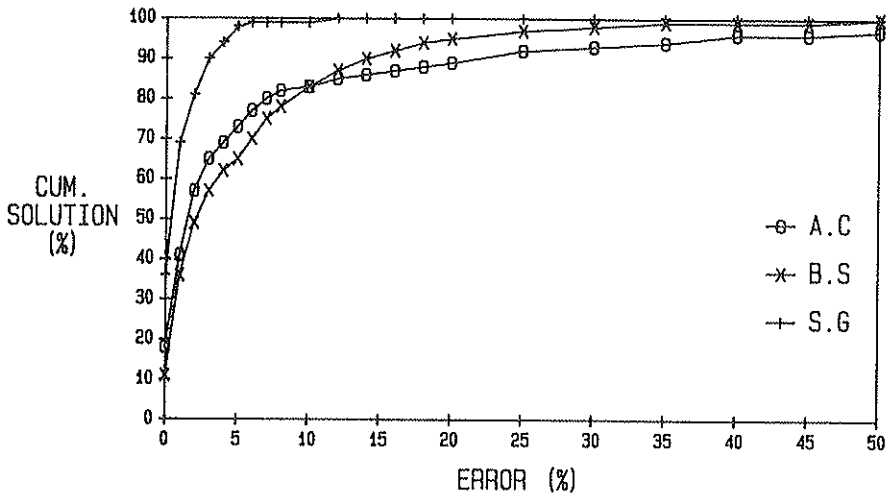

FIGURE 2 Accuracy of backcalculation.

TABLE 5 TEST SITE DESCRIPTIONS

Test Site No.	Route No.	Milepost	Year Original Construction (overlay year)	ACP Thick.	Base Thick.	Observed Surface Distress (if any)
1	SR 11	20.85	72	5.2	28.8	Long. cracking
2	SR 20	53.50	73	4.9	4.8	Long. cracking
3	SR 20	77.50	68 (85)	10.9	6.6	---
4	SR 20	108.20	78	3.5	9.0	---
5	SR 20	140.80	72	3.4	6.6	---
6	SR 167	17.80	68 (80)	11.2	---	---
7	SR 202	30.12	78	13.0	---	---
8	SR 410	9.60	68	7.3	3.6	Fatigue cracking
9	SR 5	35.80	73	16.4	---	---
10	SR 14	18.15	73	9.0	3.6	Long. cracking
11	SR 411	18.05	79	6.8	21.0	---
12	SR 500	3.20	79	6.3	8.4	---
13	SR 90	208.65	73	9.6	8.4	Long. & Trans. crack.
14	SR 90	208.85	73	9.6	8.4	Trans. cracking
15	SR 195	7.24	70 (85)	6.2	11.4	---
16	SR 195	63.80	76	8.5	12.0	---

sites (excluding test sites 8 and 10), then the differences are not alarming.

To put the asphalt concrete moduli differences into greater perspective, the backcalculated moduli for test sites 1 and 3 ("higher" and "lower" moduli test sites) were plotted and shown in Figure 3. The backcalculated moduli were determined from the FWD deflection basins taken every 50 feet within the 1,000-foot test sites. A quick inspection of Figure 3 shows that substantial variations in asphalt concrete moduli can be expected, which suggests the power that NDT pavement evaluation can provide.

Base Course Comparisons

The comparisons of backcalculated and laboratory base course moduli for five of the sixteen test sites are shown in Table 7. These five test sites were judged to have base course thicknesses which would provide for "reasonable" base moduli determination. In general, use of the EVERCALC program has led the authors to conclude (at this time) that the base course thickness should be about 1.5 times thicker (or more) than the surfacing layer in order to attempt a three-layer backcalculation.

The backcalculated and laboratory base course moduli were compared at similar stress states (i.e., the in situ stresses estimated during FWD testing and the laboratory triaxial stresses were similar). Overall, good agreement was found for four of the five test sites. The unusually high laboratory modulus for test site 5 (60,000 psi versus 38,000 psi for backcalculation) may be attributed largely to how the base course material was sampled.

Table 8 is provided to show comparisons between the stress sensitivity coefficients (K_1, K_2) for the backcalculated and laboratory moduli. These coefficients are automatically computed by the EVERCALC program if two or more FWD load levels are used at a test point. Overall, the agreement is modest at best; however, the poorest comparison is again for test site 5. Due to the small number of data points for determining these coefficients from FWD data and backcalculation, one

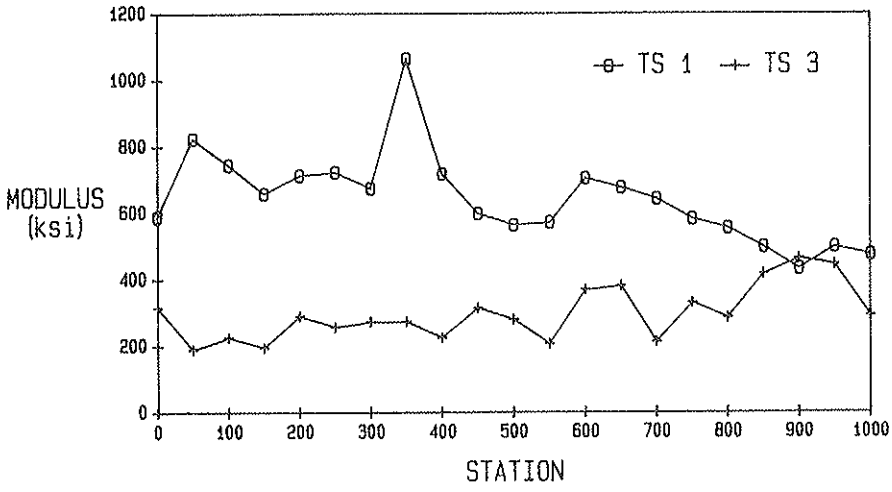

FIGURE 3 Variation of asphalt concrete modulus.

TABLE 6 COMPARISON OF BACKCALCULATED AND LABORATORY ASPHALT CONCRETE MODULI

Test Site No.	Solution Method	Modulus (psi) Station 0 + 50	Station 5 + 50	Station 9 + 50	Average
1	NDT/FWD	868,000	668,000	604,000	713,000
	Lab	426,000	469,000	387,000	427,000
	Difference (%)	-51	-30	-36	-40
2	NDT/FWD	725,000	498,000	487,000	570,000
	Lab	633,000	355,000	234,000	407,000
	Difference (%)	-13	-29	-52	-29
3	NDT/FWD	246,000	373,000	568,000	395,000
	Lab	333,000	557,000	334,000	408,000
	Difference (%)	+36	+50	-41	3
4	NDT/FWD	684,000	472,000	194,000	450,000
	Lab	346,000	215,000	244,000	268,000
	Difference (%)	-49	-54	+26	-40
5	NDT/FWD	531,000	494,000	740,000	588,000
	Lab	357,000	147,000	354,000	286,000
	Difference (%)	-33	-70	-52	-51
6	NDT/FWD	722,000	741,000	510,000	658,000
	Lab	171,000	489,000	464,000	355,000
	Difference (%)	-76	-34	-21	-46
7	NDT/FWD	460,000	577,000	757,000	598,000
	Lab	431,000	596,000	743,000	590,000
	Difference (%)	-6	+3	-2	-1
8	NDT/FWD	102,300	42,000	94,000	79,400
	Lab	200,000	227,000	215,000	214,000
	Difference (%)	+96	+438	+130	+170
9	NDT/FWD	455,000	657,000	578,000	563,000
	Lab	135,000	117,000	181,000	144,000
	Difference (%)	-70	-82	-69	-74
10	NDT/FWD	131,000	289,000	340,000	253,000
	Lab	779,000	687,000	527,000	664,000
	Difference (%)	+495	+137	+55	+162
11	NDT/FWD	215,000	243,000	358,000	272,000
	Lab	344,000	352,000	219,000	305,000
	Difference (%)	+60	+45	-39	+12
12	NDT/FWD	311,000	242,000	270,000	274,000
	Lab	343,000	414,000	380,000	379,000
	Difference (%)	+10	+71	+41	+38
13	NDT/FWD	264,000	232,000	344,000	280,000
	Lab	198,000	343,000	318,000	286,000
	Difference (%)	-25	+47	-8	+2
14	NDT/FWD	260,000	218,000	256,000	245,000
	Lab	289,000	240,000	188,000	239,000
	Difference (%)	+11	+10	-27	-2
15	NDT/FWD	404,000	262,000	495,000	387,000
	Lab	375,000	605,000	419,000	466,000
	Difference (%)	-7	+131	-15	+20
16	NDT/FWD	307,000	214,000	321,000	281,000
	Lab	202,000	166,000	164,000	177,000
	Difference (%)	-34	-22	-49	-37

should expect a wider range of coefficient values (as opposed to laboratory results).

To view these comparisons against the expected field base course moduli, backcalculated moduli for test site 1 were computed every 50 feet and plotted in Figure 4. Thus, within only 1,000 feet of a pavement structure, these moduli can easily vary by a factor of about 2.

Subgrade Soil Comparisons

The comparisons of backcalculated and laboratory subgrade soil moduli for all sixteen test sites are shown in Table 9. As was done for the base course comparisons, the moduli comparisons shown in Table 9 were made at similar stress states. The observed differences for these subgrade soils are the least

TABLE 7 COMPARISON OF BACKCALCULATED AND LABORATORY BASE COURSE MODULI

Test Site No.	Modulus (psi)			Moisture Content (%)		
	NDT/FWD	Lab	Diff. (%)	Field	Lab	Diff. (%)
1	23,000	23,000	0	3.7	4.7	+1.0
4	45,000	53,000	18	4.4	4.5	+0.1
5	38,000	60,000	60	5.0	4.3	-0.7
11	21,000	25,000	22	4.2	3.9	-0.3
15	22,000	31,000	36	4.4	4.9	+0.5
Average	30,000	38,000	28	4.3	4.5	+0.2
Std.Dev.	10,000	15,000		0.4	0.4	

TABLE 8 BASE COURSE STRESS SENSITIVITY COEFFICIENTS

Test Site No.	Solution Method	Stress Sensitivity Coefficients		
		K_1	K_2	R^2 (%)
1	NDT/FWD	4,680	0.68	98
	Lab	7,350	0.49	91
4	NDT/FWD	1,149	1.16	92
	Lab	11,529	0.48	91
5	NDT/FWD	280	1.44	96
	Lab	14,270	0.42	89
11	NDT/FWD	1,590	1.10	96
	Lab	9,010	0.44	90
15	NDT/FWD	11,700	0.32	2
	Lab	13,000	0.41	92

of the three pavement materials being compared. Overall, the percent differences range from a low of 2% to a high of 84%, with the average being 10%. The average backcalculated moduli for all sites is 29,000 psi, compared with an average laboratory modulus of 26,000 psi. (Recall that the laboratory moduli were for disturbed, or recompacted, samples.) These differences, again, should be viewed against the kind of variation one might expect in a relatively uniform, short length of pavement. Figure 5 shows the backcalculated subgrade soil moduli for FWD tests performed every 50 feet for two 1,000-foot long test sites (test sites 1 and 3). The illustrated subgrade can easily vary by a factor of 2.

Table 10 is provided to illustrate comparisons of the stress sensitivity coefficients (K_3, K_4) for the backcalculated and laboratory moduli. Overall, the agreement is somewhat better than that observed for the base course comparisons.

SUMMARY AND CONCLUSIONS

A backcalculation program (EVERCALC), which is used to determine pavement-layer elastic moduli, has been examined in two fundamental ways in an attempt to verify the results. The first verification approach was to compare theoretical and backcalculated moduli for a range of three-layer pavement systems. This was accomplished by using the Chevron N-layer

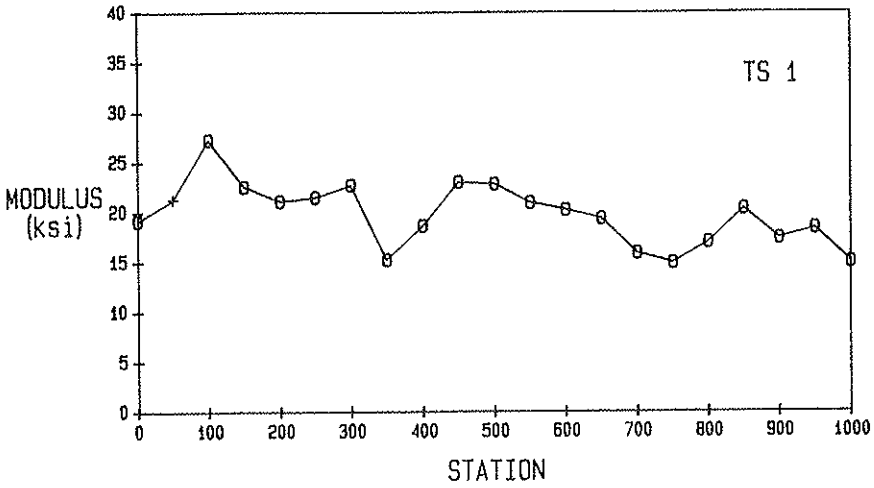

FIGURE 4 Variation of base modulus.

TABLE 9 COMPARISON OF BACKCALCULATED AND LABORATORY SUBGRADE SOIL MODULI

Test Site No.	Modulus (psi) NDT/FWD	Lab	Diff. (%)	Moisture Content (%) Field	Lab	Diff.
1	26,000	20,000	-21	5.6	7.3	+1.7
2	21,000	16,000	-23	2.4	6.0	+3.6
3	15,000	20,000	+32	3.7	6.4	+2.7
4	27,000	49,000	+84	3.8	4.7	+0.9
5	36,000	32,000	-11	3.5	4.8	+1.3
6	29,000	15,000	-47	9.6	6.0	-3.6
7	39,000	33,000	-14	5.6	5.5	-0.1
8	9,000	5,000	-36	21.5	15.7	-5.8
9	37,000	32,000	-14	12.2	12.6	+0.4
10	39,000	26,000	-32	7.8	9.2	+1.4
11	26,000	28,000	+8	6.9	11.1	+4.2
12	36,000	35,000	-2	8.2	9.0	+0.8
13	36,000	42,000	+17	10.4	8.2	-2.2
14	40,000	42,000	+4	10.4	8.2	-2.2
15	20,000	12,000	-42	13.6	15.1	+1.5
16	20,000	8,000	-59	11.8	12.1	+0.3
Average	29,000	26,000	-10	8.4	8.9	+0.5
Std. Dev.	10,000	13,000		5.0	3.6	

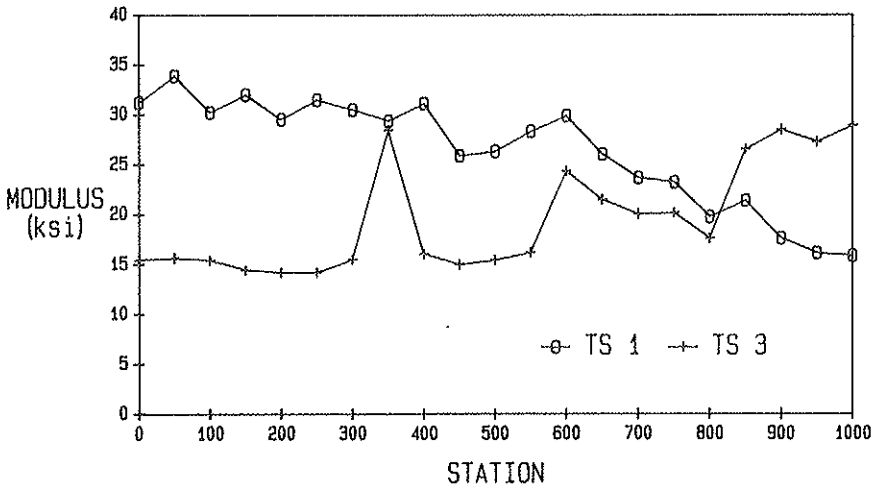

FIGURE 5 Variation of subgrade modulus.

elastic analysis program to generate deflection basins for specified layer moduli and thickness conditions. These comparisons showed modest differences (about 8% for asphalt concrete, 6% for base course, and less than 2% for the subgrade). The largest differences for asphalt concrete were observed for thin surfaces with low stiffness. As the asphalt concrete layer thickness increases, both the base and subgrade moduli differences increased.

The second verification approach was to compare backcalculated and laboratory moduli based on FWD tests and field material sampling along with appropriate laboratory testing. The results show the greatest range of differences for the asphalt concrete layers followed by the base and subgrade materials; however, large differences between backcalculated and laboratory asphalt concrete moduli should be expected for those test sites with extensive cracking. The observed differences between backcalculated and laboratory moduli do not offer a true verification, since laboratory test procedures of disturbed (recompacted) samples do not necessarily provide reference (or true) moduli. Further, these observed differences are generally much less than the variation of moduli expected within relatively uniform, short lengths of pavement (in this case, 1,000 feet).

The following conclusions are offered:

1. The backcalculation of layer moduli from measured pavement deflection basins appears to provide reasonable estimates of in situ pavement moduli. Further, moduli can be estimated for cracked asphalt concrete conditions.
2. The EVERCALC program is a backcalculation procedure which should be of value to the pavement research community and help meet the needs of road-owning agencies.

TABLE 10 SUBGRADE SOIL STRESS SENSITIVITY COEFFICIENTS

Test Site No.	Solution Method	Stress Sensitivity Coefficients		
		K_3	K_4	R^2 (%)
1	NDT/FWD	34,160	-0.24	89
	Lab	16,850	0.17	21
2	NDT/FWD	7,600	0.31	72
	Lab	3,140	0.50	6
3	NDT/FWD	20,610	-0.19	72
	Lab	16,360	0.13	17
4	NDT/FWD	59,050	-0.32	87
	Lab	32,680	0.16	54
5	NDT/FWD	48,710	-0.12	99
	Lab	20,410	0.16	16
6	NDT/FWD	48,670	-0.38	58
	Lab	11,750	0.20	14
7	NDT/FWD	49,176	-0.19	58
	Lab	27,360	0.16	42
8	NDT/FWD	11,910	-0.12	79
	Lab	7,290	-0.10	7
9	NDT/FWD	47,750	-0.21	59
	Lab	24,370	-0.21	68
10	NDT/FWD	37,270	0.02	20
	Lab	11,670	0.17	50
11	NDT/FWD	44,730	-0.44	97
	Lab	23,750	0.15	34
12	NDT/FWD	21,030	0.15	76
	Lab	4,640	0.56	53
13	NDT/FWD	65,390	-0.19	94
	Lab	26,480	0.18	21
14	NDT/FWD	39,260	-0.03	29
	Lab	26,480	0.18	21
15	NDT/FWD	28,760	-0.29	98
	Lab	17,460	-0.32	21
16	NDT/FWD	34,840	-0.30	96
	Lab	8,150	-0.01	21

3. The results of backcalculation analyses based on elastic solutions appear to be influenced by at least the following:
   (a) The backcalculation error is higher for asphalt concrete moduli with relatively thin, low stiffness surfaces.
   (b) The base course thickness should be about 1.5 times (or more) greater than the asphalt concrete surface course in order to achieve reasonable estimates of base moduli.
   (c) The two sensor configurations on the WSDOT FWD did not significantly alter the backcalculated moduli. (One of the two, however, did appear to have slightly smaller errors.)

ACKNOWLEDGMENTS

The study described in this paper was conducted on a Highway Planning and Research study with the Washington State Department of Transportation. The cooperation of WSDOT, the Federal Highway Administration, and the Washington State Transportation Center is deeply appreciated.

REFERENCES

1. R. E. Smith and R. L. Lytton. *Synthesis of Study of Nondestructive Testing Devices for Use in Overlay Thickness Design of Flexible Pavements*. Report FHWA-RD-83-/097, FHWA, Washington, D.C., April 1984.
2. A. J. Bush and D. R. Alexander. Pavement Evaluation Using Deflection Basin Measurements and Layered Theory. In *Transportation Research Record 1022*, TRB, National Research Council, Washington, D.C., 1985, pp. 16–29.
3. W. Udin, A. H. Meyer, and W. R. Hudson. Rigid Bottom Considerations for Nondestructive Evaluation of Pavements. In *Transportation Research Record 1070*, TRB, National Research Council, Washington, D.C., 1986, pp. 21–29.
4. M. S. Hoffman. Loading Mode Effects on Pavement Deflections. *Journal of Transportation Engineering*, Vol. 109, No. 5, Sept. 1983, pp. 651–668.
5. B. E. Sebaaly and M. S. Momlouk. *Dynamic Analysis of Falling Weight Deflectometer Data*. Paper presented at the Annual Transportation Research Board Meeting, Jan. 1986.
6. O. Tholen, J. Sharma, and R. L. Terrel. Comparison of Falling Weight Deflectometer with Other Deflection Testing Devices. In *Transportation Research Record 1007*, TRB, National Research Council, Washington, D.C., 1985, pp. 20–26.

7. M. S. Hoffman and M. R. Thompson. Backcalculating Nonlinear Resilient Moduli from Deflection Data. In *Transportation Research Record 852*, TRB, National Research Council, Washington, D.C., 1982, pp. 42–51.
8. Y. T. Chou. *Engineering Behavior of Pavement Materials: State of Art*. Report FAA-RD-77-37, U.S. Army Engineer Waterway Experiment Station, Vicksburg, Miss., Feb. 1977.
9. A. A. Bu-Bushait. *Development of Flexible Pavement Fatigue Model for Washington State*. Ph.D. dissertation, Department of Civil Engineering, University of Washington, Seattle, Wash., 1986.
10. J. F. Shook, F. N. Finn, M. W. Witczak, and C. L. Monismith. Thickness Design of Asphalt Pavement, The Asphalt Institute Method. In *Proc., 5th International Conference on the Structural Design of Asphalt Pavements*. Delft University of Technology, The Netherlands, Vol. 1, Aug. 1982, pp. 17–44.
11. H. F. Southgate and R. C. Dean. Temperature Distributions in Asphalt Concrete Pavements. In *Transportation Research Record 549*, TRB, National Research Council, Washington, D.C., 1975, pp. 39–46.
12. E. E. Newcomb. *Development and Evaluation of Regression Method to Interpret Dynamic Pavement Deflections*. Ph.D dissertation. Department of Civil Engineering, University of Washington, Seattle, Wash., 1986.
13. F. Parker, W. R. Barker, R. C. Gunkel, and E. C. Odem. *Development of a Structural Design Procedure for Rigid Airport Pavements*. Report FAA-RD-77-81. U.S. Army Waterways Experiment Station, Vicksburg, Miss., 1979.
14. H. J. Southgate, R. C. Deen, D. H. Cain, and J. G. Mayes. *Modifications to CHEVRON N-Layer Computer Program*. Report UKTRP-87-XX. University of Kentucky, Lexington, Ky., 1987.

Publication of this paper sponsored by Committee on Strength and Deformation Characteristics of Pavement Sections.

Dynaflect Evaluation of Layer Moduli in Florida's Flexible Pavement Systems

KWASI BADU-TWENEBOAH, BYRON E. RUTH, AND WILLIAM G. MILEY

Research conducted to investigate the nondestructive testing (NDT) characterization of in-place pavement materials has resulted in the development of a modified sensor spacing for the Dynaflect. The modified testing configuration provides the capability to separate the deflection response contributed by the subgrade, the stabilized subgrade, and the combination of base and asphalt concrete for typical Florida flexible pavement systems. Analysis of Dynaflect data for in-service pavements using an elastic layer computer program resulted in the development of simple power law regression equations to predict layer moduli from modified sensor deflections. This paper presents the development of the simplified layer moduli prediction equations, and the recommended testing and analytical procedures for pavement evaluation investigations. The use of this simplified approach allow a large number of test locations to be analyzed by eliminating the use of computer-iterative programs which are usually time consuming, expensive, and often subject to substantial errors.

Nondestructive testing (NDT) and deflection measurements are now universally recognized methods for the structural evaluation of road and airfield pavements. NDT of pavements has evolved from the very basic Benkelman Beam to the more refined equipment such as Dynaflect, Road Rater, and Falling Weight Deflectometer. The Dynaflect is presently the most commonly used NDT device in the United States for evaluation and design of pavement. Like the Benkelman Beam, a large number of data has been accumulated with the use of this device.

The Dynaflect is a steady-state vibratory device that is instrumented to measure peak-to-peak dynamic deflection on the pavement surface. It applies a load of 1000 lbs., at a frequency of 8 cycles per second, through two steel wheels that are 20 in. apart center to center. The resulting deflection basin is measured by five geophones spaced 12 in. apart, with the first geophone located midway between the loading wheels. These deflection measurements represent the stiffness of the entire pavement section.

Although some significant accomplishments have been made in separating the effects of major parts of the pavement structure, the separation of the effects of all of the various components of the structure with deflection basin measurements has not yet been accomplished. Thus, with the possible exception of the subgrade modulus, the moduli of the other layers are estimated using linear-elastic computer-iterative programs, graphical solutions, or nomographs. The major problems associated with the above solution techniques are that unique solutions cannot be guaranteed, solutions can be time consuming, and the expertise required for interpretation may not be available. The purpose of this paper is to present a simplified approach that would allow a layer-by-layer analysis of the Dynaflect deflection basin. Such a simplified approach would allow a large number of test points to be analyzed and consequently enhance our ability to carry out mechanistic pavement evaluation on a routine basis.

K. Badu-Tweneboah and B. E. Ruth, Department of Civil Engineering, University of Florida, Gainesville, Fla. 32611. W. G. Miley, Bureau of Materials and Research, Florida Department of Transportation, Gainesville, Fla. 32611.

BACKGROUND

The Florida Department of Transportation (FDOT) has for many years been interested in the use of NDT methods for pavement evaluation to typify pavement response and to provide information for structural characterization. The Benkelman Beam was used extensively into the 1970s for research projects and for "troubleshooting" distressed pavement sections. The first Dynaflect unit was purchased by the FDOT in 1966. Initially, it was used as a research tool in combination with Benkelman Beam and plate bearing tests on pavement layers. The Dynaflect evolved as a reliable device for assessment of structural response uniformity for Florida's highway pavement network.

In 1981, the FDOT's Bureau of Materials and Research pavement section under the direction of W. G. Miley developed and adopted a method of predicting the structural subgrade support value from Dynaflect sensor response. This was based on correlations between plate bearing moduli and the measured deflection at the fourth sensor (*1*). Subsequent use of the Dynaflect for pavement evaluation and to determine rehabilitation design thickness requirements has proven valuable to the FDOT. However, determination of layer moduli using elastic multilayered computer programs was time consuming and often yielded moduli that were outside the realm of possibility. Consequently, a research project was initiated in 1984 for the purpose of developing simplified methods for the determination of layer moduli using the Dynaflect.

This investigation involved computer simulation of Dynaflect response using ten different sensor positions (figure 1) for a parametric study of different layer thicknesses and moduli encompassing the range of values encountered in Florida. The results of the study indicated that modified sensor positions provided a unique capability for separation of the deflection response characteristics of asphalt concrete and limerock base from the underlying materials. Also, power law relationships for the fifth sensor was found to be reliable in assess-

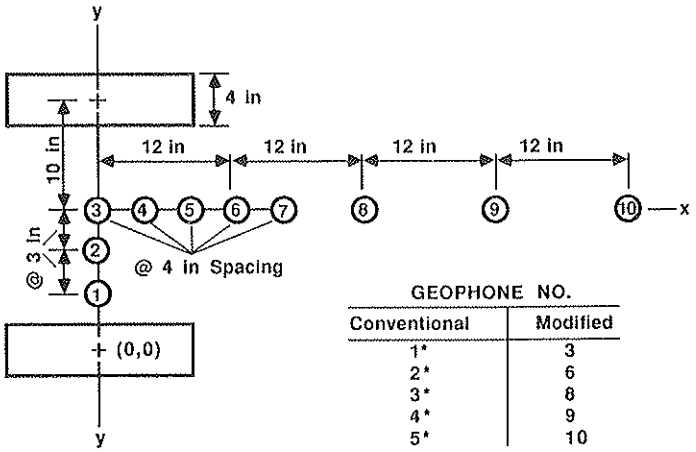

FIGURE 1 Dynaflect modified geophone positions.

ing the subgrade modulus. A series of prediction equations were developed from the computer-generated information for the estimation of the moduli in four layer pavement systems (*2, 3*). Although the prediction accuracy appeared to be good, the complexity of the equations and the dependency upon reasonable estimates of E_1 or E_2 to solve for E_2 or E_1, respectively, indicated that further research to simplify and improve the accuracy of layer moduli predictions would be desirable.

Field tests were conducted on asphalt concrete pavements using the Dynaflect, Falling Weight Deflectometer (FWD), cone penetration test (CPT), Marchetti Dilatometer test (DMT), and plate loading test (PLT). The CPT and DMT data were collected to evaluate the stratigraphy of the subsurface thatis valuable in tuning moduli for elastic layer analyses based on measured deflection basins (*4*). A thin layer of extremely low or high modulus subgrade soil close to the pavement structure can prevent the matching of measured NDT deflections when using the composite subgrade modulus (E_4).

The field test data provided Dynaflect deflection values for standard and modified sensor configurations. Regression analysis of the data, using moduli values that gave analysis program BISAR predicted deflections closely matching the measured deflections, resulted in simplified power law equations for prediction of layer moduli (E_{12}, E_3, and E_4). The composite modulus, E_{12}, of asphalt concrete and base course moduli can provide a direct means for evaluation of the adequacy of the upper pavement layers and separation from the influence of the underlying support layers (E_3 and E_4). The estimation of the asphalt concrete modulus (E_1) from correlations between the constant power viscosity for recovered asphalts and the resilient modulus (E_1) of the mix (*5*) allowed for direct computation of the base course moduli (E_2).

Pavement evaluation is simplified using the Dynaflect and these analysis procedures. This simplified approach enhances our ability to directly determine the adequacy of a pavement structure and to identify structural deficiencies. Also elastic layer analysis can be performed to assess wheel-loading conditions at critical temperatures (*6*) to aid in determining rehabilitation design requirements.

The ensuing discussion presents the results of Dynaflect tests on various pavements, the development of the simplified layer moduli relationships, and the recommended testing and analytical procedures for pavement evaluation investigations. Finally, an application example is provided.

TEST PAVEMENT SECTIONS

Most of the pavement sections used in the study had been scheduled for evaluation by the FDOT. These sections, as listed in table 1, are representative of pavement deflection response, type of construction, and soil moisture conditions. The thickness of the asphalt concrete layer ranges from 1.5 in. to 8.5 in., while the base course thicknesses vary from 6.0 in. to 24.0 in. The subbase thicknesses were generally found to be 12.0 in., except for the SR 24 and SR 80 test sites in which construction drawings indicated thicknesses of 17.0 in. and 36.0 in., respectively.

The base course material consisted of limerock except for SR 12 which was constructed with a sand-clay mixture. In most cases the subbase material was stabilized either mechanically or chemically with lime or cement. This layer is conventionally called stabilized subgrade by the FDOT. The underlying subgrade soils were generally sands with clay-silt layers often encountered at depth, as indicated from the penetration tests (*4*). In certain locations (SR 715 and SR 80), clay and organic soil deposits were the primary subgrade layer. Water table locations inferred from the CPT holes are also listed in Table 1.

Most of the pavement sections were uncracked or had limited (hairline) longitudinal and/or transverse cracking. However, US 441 test section did exhibit block cracking even though the pavement structure was very stiff. Some segments of SR 80, a recently constructed highway, were highly distressed due to construction problems that had resulted in potholes, ponding of water, and cracks in the asphalt concrete surface. Therefore, two segments of this roadway were included in this study: section 1, in which there was no visible surface distress, and section 2, in which cracks and potholes were present.

DESCRIPTION OF TESTING PROCEDURES

Testing with the Dynaflect was accomplished using the standard sensor spacing to identify segments of pavement with

TABLE 1 CHARACTERISTICS OF TEST PAVEMENTS

Test Road	County	Mile Post Number	Year*	Pavement Thickness (in.)		Water Table (in.)
				AC	Base	
SR 26A	Gilchrist	11.8-12.0	1930(1982)	8.0	9.0	62
SR 26B	Gilchrist	11.1-11.3	1930(1982)	8.0	7.5	44
SR 26C	Gilchrist	10.1-10.2	1930(1982)	6.5	8.5	33
SR 24	Alachua	11.1-11.2	1976	2.5	11.0	NE**
US 301	Alachua	21.5-21.8	1966	4.5	8.5	45
US 441	Columbia	1.2- 1.4	1960	3.0	9.0	NE
I-10A	Madison	14.0-14.1	1973(1980)	8.0	10.4	NE
I-10B	Madison	2.7- 2.8	1973(1980)	7.0	10.2	NE
I-10C	Madison	32.0-32.1	1973(1980)	5.5	10.2	NE
SR 15A	Martin	6.5- 6.6	1973	8.5	12.5	65
SR 15B	Martin	4.8- 5.0	1973	7.0	12.0	65
SR 715	Palm Beach	4.7- 4.8	1969	4.5	24.0	NE
SR 12	Gadsden	1.4- 1.6	1979	1.5	6.0	NE
SR 80	Palm Beach	Sec. 1 & 2	1986	1.5	10.5	NE

* Year represents the approximate date the road was built. Dates in parentheses are the latest year of reconstruction--overlay, surface treatment, etc.

** Water table not encountered at depth up to 18 ft. Measurements were made using a moisture meter inserted in the holes produced from cone penetration test (CPT).

TABLE 2 TYPICAL DYNAFLECT DEFLECTION DATA FROM TEST SECTIONS

Test Road	Mile Post Number	Deflections (mils)							
		D_1	D_3	D_4	D_6	D_7	D_8	D_9	D_{10}
SR 26A	11.912	0.87	0.81	0.77	0.68	0.61	0.53	0.45	0.39
SR 26B	11.205	1.28	1.18	1.23	1.12	0.99	0.90	0.77	0.68
SR 26C	10.168	0.89	0.77	0.77	0.62	0.53	0.37	0.24	0.16
SR 26C	10.166	0.90	0.77	0.78	0.68	0.54	0.44	0.27	0.17
SR 24	11.102	0.50	0.51	0.50	0.33	0.28	0.22	0.18	0.15
US 301	21.580	0.56	0.50	0.49	0.37	0.34	0.27	0.20	0.15
US 301	21.585	0.62	0.47	0.46	0.35	0.30	0.25	0.18	0.14
US 301	21.593	0.39	0.43	0.42	0.33	0.27	0.23	0.17	0.14
US 441	1.236	0.65	0.68	0.64	0.52	0.45	0.34	0.26	0.22
US 441	1.241	0.73	0.63	0.57	0.45	0.40	0.32	0.25	0.20
I-10A	14.062	0.30	0.29	0.28	0.18	0.16	0.10	0.07	0.05
I-10B	2.703	0.44	0.46	0.40	0.29	0.25	0.17	0.12	0.09
I-10C	32.071	0.70	0.46	0.43	0.30	0.29	0.22	0.18	0.15
SR 15B	4.811	1.10	1.03	1.04	0.91	0.92	0.82	0.75	0.66
SR 15A	6.549	1.50	1.46	1.48	1.40	1.36	1.27	1.14	1.04
SR 715	4.722	1.37	1.29	1.23	1.08	1.02	0.96	0.89	0.81
SR 715	4.720	1.45	1.38	1.36	1.15	1.19	1.07	1.00	0.91
SR 12	1.485	0.86	0.68	0.65	0.44	0.42	0.36	0.27	0.21
SR 80	Sec 1	2.11	2.02	1.89	1.61	1.48	1.37	1.07	0.85
SR 80	Sec 2	2.41	2.15	2.05	1.61	1.48	1.22	0.96	0.74

* Deflections are for both modified and standard geophone positions.

fairly uniform deflection response. Each segment was tested at 25 ft. spacings until three or more locations provided essentially identical deflection basins. The modified Dynaflect sensor array was then used to obtain deflection measurements. These sensors were positioned by hand at locations designated as 1, 4, 7, and 10 (see figure 1). These positions were derived from the analytical studies (*2, 3*) that provided the best response for layer separation. The initial part of the field testing involved placing the extra sensor at position 9 in the modified system (standard position 4). This procedure was later changed to placing one sensor near each Dynaflect loading wheel and the remaining sensors at modified positions 4, 7, and 10. In the latter case, an average value of D_1 was used in the analysis. Table 2 presents typical Dynaflect deflection data for the different test sections.

Temperature measurements were obtained for the ambient air, the surface of pavement, and in the middle of the asphalt concrete pavement layer using a temperature probe. The mean

TABLE 3 TEMPERATURE MEASUREMENTS OF TEST PAVEMENT SECTIONS

Test Road	Mile Post Number	Test Date	Temperature (°F)		
			Air	Surface	Mean
SR 26A	11.912	10-31-85	79	82	81
SR 26B	11.205	11-05-85	45	48	59
SR 26C	10.168	11-05-85	60	60	82
SR 24	11.102	12-03-85	57	55	57
US 301	21.580	2-18-86	63	65	69
US 441	1.236	2-26-86	51	56	79
I-10A	14.062	3-18-86	84	106	104
I-10B	2.703	3-25-86	80	101	88
I-10C	32.071	3-26-86	82	99	106
SR 15A	6.549	4-28-86	88	110	120
SR 15B	4.811	4-28-86	93	111	127
SR 715	4.722	4-29-86	80	88	111
SR 12	1.485	8-12-86	81	91	102
SR 80	Sec 1 & 2	8-19-86	84	96	94

asphalt pavement temperatures, listed in table 3, were taken using the probe to measure the temperature of motor oil that had been poured into a drilled hole in the pavement. The mean pavement temperature measurements were necessary for correction of prediction of asphalt concrete moduli from low temperature viscosity data of the asphalts recovered from pavement cores (*5*).

TUNING OF LAYER MODULI

Moduli for four layer pavement systems were used as input into an elastic layer analysis program (BISAR) for prediction of the Dynaflect deflection basin. Constant power viscosity (n_j) versus temperature relationships were developed using recovered asphalts tested by the Scheweyer Constant Stress Rheometer. The recovered asphalt viscosity corresponding to the average asphalt concrete pavement temperature during Dynaflect testing was used in previously established equations (*5*) to predict the modulus of the asphalt concrete layer (E_1). Values for E_2, E_3, and E_4 were estimated using equations developed from the analytical studies and reported by Ruth and Badu-Tweneboah (*2*) and Ruth et al. (*3*). These modulus values (E_1, E_2, E_3, and E_4) plus layer thicknesses and Poisson's ratios served as the input data for BISAR. The interface conditions between layers were represented as perfectly rough (complete bonding). The BISAR-predicted Dynaflect deflections were then compared to the measured values to determine if any adjustment of the input moduli was necessary to achieve a suitable match of the measured deflection basin. This process of juggling E values is referred to, in this discussion, as tuning.

Figure 2 illustrates measured and predicted deflection basins for US 441, SR 80, and SR 24 test sites. Most of the test sites gave results similar to that of US 441 and SR 80, although some adjustment in one or more of the layer modulus values was required. However, efforts to achieve a better fit between measured and predicted deflections on SR 24 proved to be fruitless. Evaluation of the stratigraphy using the cone penetration test (cone tip resistance and friction ratio) indicated that either variable foundation soils or nonvisible cracks had influenced the deflection response of the pavement. Tables 4 and 5 give the tuned layer moduli and BISAR predicted deflections, respectively, for each of the test sites.

Regression analyses were performed to evaluate the reliability of the BISAR predicted Dynaflect deflections. Figures 3, 4, 5, and 6 present the results of the regression analyses for deflections at modified sensor locations 1, 4, 7, and 10, respectively. In all cases, the high R^2 value ($R^2 > 0.96$) indicated an exceptionally good correlation between predicted and measured deflections. The regression equations for D_4 and D_7 (figures 4 and 5) provided an almost perfect correlation, with the intercept and slope being within 0.015 mils of zero and 0.018 mils of unity, respectively.

The D_1 values (figure 3) tended to yield a slightly higher intercept (0.065) and slope (1.107) which results in the predicted deflections being slightly greater than those measured. There were four test sites where predicted D_1 values were about 0.2 to 0.3 mils greater than the measured D_1 values. This difference may be due to sensor placement variation, the use of single D_1 measurement in the earlier tests, variation in measured D_1 response according to wheel positioning, or where complete tuning was not achieved (e.g., SR 24).

Except at one site, the D_{10} values provided an excellent, highly reliable relationship (figure 6). However, the slope of 0.95 suggests that predicted deflections are about 5 percent less than measured D_{10} values. The discrepancy occurs because the straight line log-log relationship for predicting E_4 from D_{10} (standard D_5) tends to be a curvilinear (hyperbolic) relationship for E_4 values which fall below 1,000 psi or above 200,000 psi (*2*).

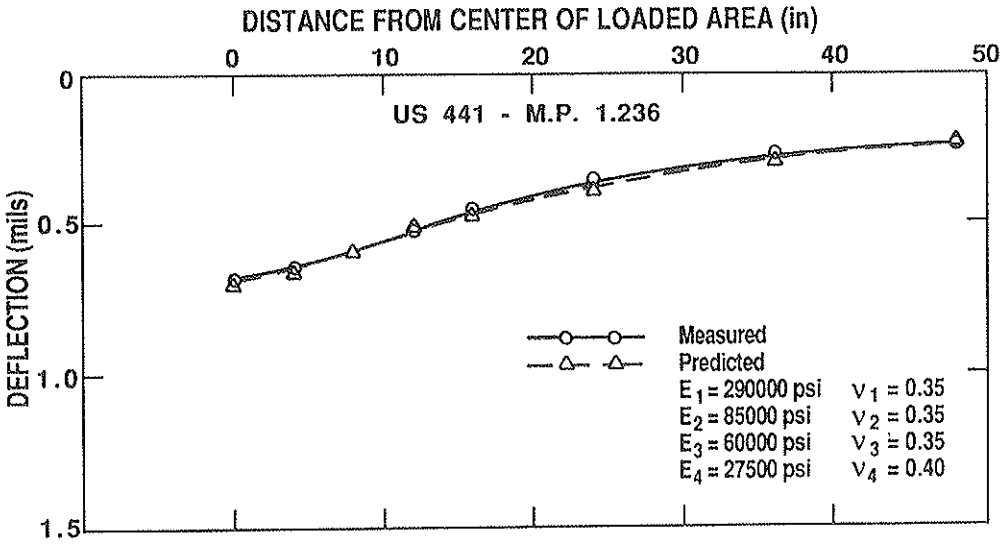

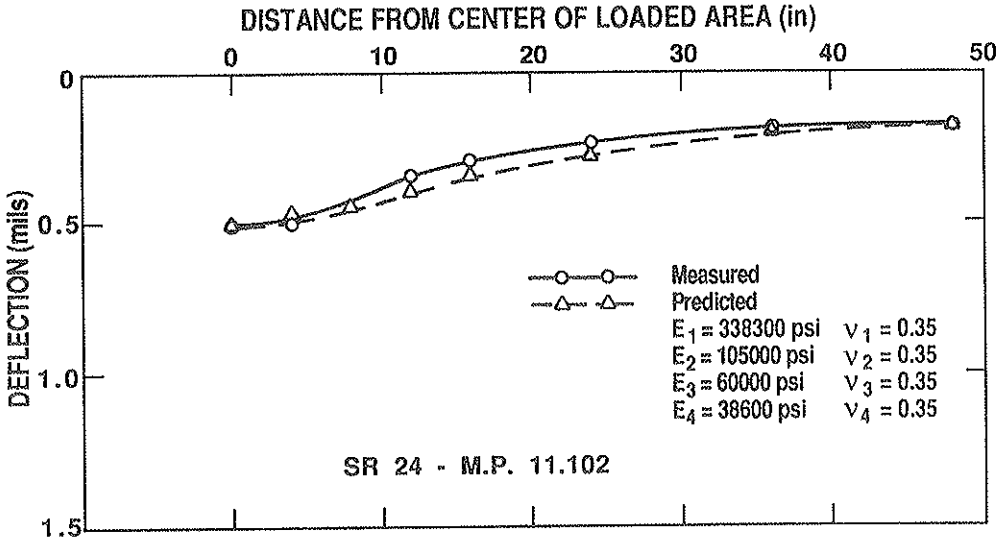

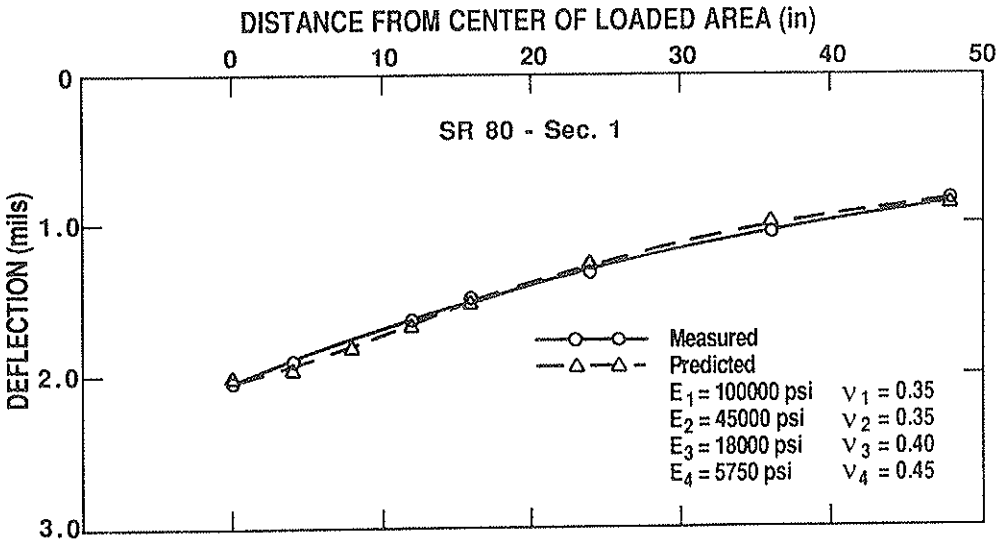

FIGURE 2 Comparison of measured and predicted deflection basins.

TABLE 4 TUNED LAYER MODULI FOR TEST SECTIONS

Test Road	Mile Post Number	Layer Moduli (psi)			
		E_1	E_2	E_3	E_4
SR 26A	11.912	171500	105000	70000	14600
SR 26B	11.205	360000	90000	60000	7900
SR 26C	10.168	171500	55000	35000	28500
SR 24	11.102	338260	105000	75000	38600
US 301	21.580	250000	120000	60000	38600
US 301	21.585	250000	120000	75000	42000
US 301	21.593	250000	130000	80000	44000
US 441	1.236	290000	85000	60000	27500
US 441	1.241	290000	120000	75000	28500
I-10A	14.062	65000	95000	89400	105000
I-10B	2.703	113000	80000	65000	60000
I-10C	32.071	67000	105000	85000	40000
SR 15B	4.811	150000	120000	75000	8100
SR 15A	6.549	150000	120000	40000	4800
SR 715	4.722	92600	75000	50000	6000
SR 715	4.720	92600	65000	45000	5500
SR 12	1.485	400000	120000	75000	26500
SR 80	Sec 1	100000	45000	18000	5750
SR 80	Sec 2	100000	26500	18000	5750

TABLE 5 PREDICTED DEFLECTIONS FROM TUNED LAYER MODULI

Test Road	Mile Post Number	Deflections (mils)									
		D_1	D_2	D_3	D_4	D_5	D_6	D_7	D_8	D_9	D_{10}
SR 26A	11.912	0.95	0.82	0.80	0.78	0.74	0.69	0.64	0.56	0.46	0.38
SR 26B	11.205	1.25	1.19	1.18	1.16	1.12	1.06	1.01	0.90	0.77	0.66
SR 26C	10.168	0.93	0.79	0.76	0.73	0.65	0.56	0.49	0.37	0.26	0.20
SR 24	11.102	0.62	0.50	0.47	0.45	0.40	0.35	0.31	0.25	0.19	0.15
US 301	21.580	0.65	0.54	0.52	0.50	0.45	0.39	0.34	0.27	0.19	0.15
US 301	21.585	0.59	0.49	0.46	0.44	0.40	0.35	0.31	0.24	0.18	0.14
US 301	21.593	0.56	0.46	0.44	0.42	0.38	0.33	0.29	0.23	0.17	0.13
US 441	1.236	0.85	0.71	0.68	0.64	0.58	0.51	0.45	0.36	0.27	0.21
US 441	1.241	0.73	0.62	0.59	0.57	0.52	0.46	0.42	0.34	0.26	0.20
I-10A	14.062	0.70	0.35	0.30	0.27	0.22	0.18	0.15	0.11	0.07	0.05
I-10B	2.703	0.66	0.45	0.42	0.39	0.34	0.28	0.24	0.18	0.13	0.10
I-10C	32.071	0.83	0.50	0.46	0.44	0.398	0.35	0.31	0.25	0.19	0.15
SR 15B	4.811	1.25	1.10	1.07	1.05	1.00	0.96	0.91	0.83	0.72	0.63
SR 15A	6.549	1.71	1.56	1.54	1.52	1.47	1.42	0.36	0.26	0.13	1.00
SR 715	4.722	1.57	1.31	1.27	1.23	1.17	1.10	1.05	0.96	0.86	0.76
SR 715	4.720	1.71	1.45	1.40	1.37	1.29	1.22	1.15	1.05	0.94	0.83
SR 12	1.485	0.87	0.73	0.70	0.67	0.61	0.54	0.48	0.38	0.29	0.22
SR 80	Sec 1	2.49	2.09	2.01	1.94	1.80	1.63	1.49	1.25	1.01	0.85
SR 80	Sec 2	2.92	2.30	2.16	2.07	1.87	1.67	1.50	1.25	1.01	0.86

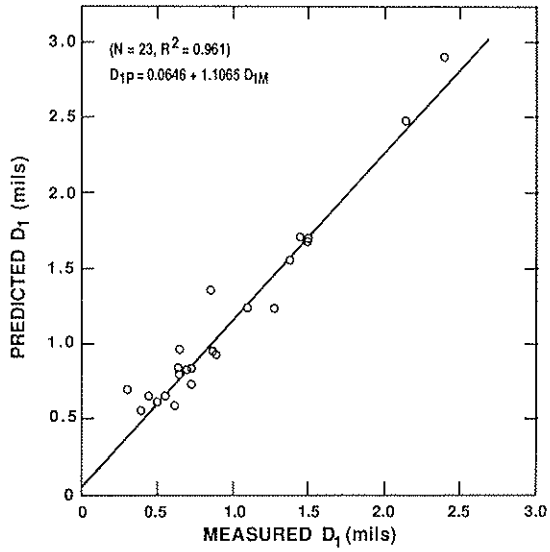

FIGURE 3 Relationship between predicted and measured sensor 1 deflections.

DEVELOPMENT OF SIMPLIFIED LAYER MODULI EQUATIONS

Since the tuned layer moduli provided predicted Dynaflect deflections that correlated exceedingly well with the measured deflections, regression analyses were performed to assess the relationship between

- Composite modulus of asphalt concrete and base course layers (E_{12}) and $D_1 - D_4$.
- Subbase or stabilized subgrade modulus (E_3) and $D_4 - D_7$, and
- Subgrade modulus (E_4) and D_{10}.

As mentioned previously, these sensor deflections were selected from the analytical studies (*2, 3*) because they were related to the moduli of specific layers. It was necessary to combine the asphalt concrete and base course moduli because the analyses had indicated that no sensor location or combination of sensor deflections was suitable for separation of E_1 and E_2. The series of equations (*2, 3*) developed for prediction of either E_1 or E_2 from $D_1 - D_4$, with a reasonable

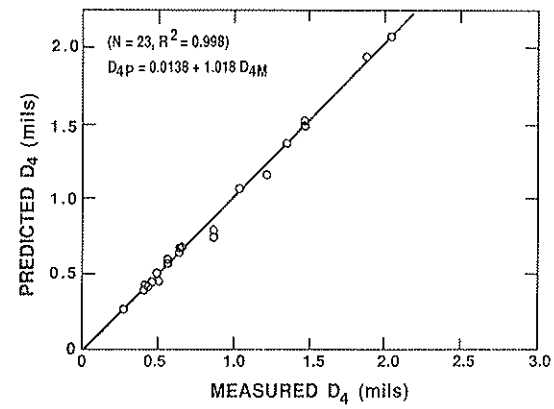

FIGURE 4 Relationship between predicted and measured sensor 4 deflections.

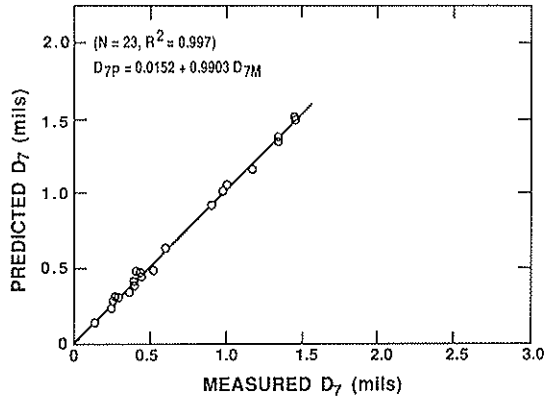

FIGURE 5 Relationship between predicted and measured sensor 7 deflections.

estimate of E_2 or E_1, respectively, albeit their high degree of prediction accuracy, were considered to be too complex for routine evaluation of pavements. Therefore two equations were employed to combine E_1 and E_2 to a composite E_{12} value. The first formula is essentially a weighted average formula, and is of the form

$$E_{12} = \frac{E_1 t_1 + E_2 t_2}{t_1 + t_2} \tag{1}$$

where

E_{12} = composite asphalt concrete and base course modulus,
E_1 = modulus of the asphalt concrete layer,
E_2 = modulus of the base course layer,
t_1 = the thickness of the asphalt concrete layer, and
t_2 = the thickness of the base course layer.

Equation 1, which is a commonly used weighting formula, has been previously utilized by Vaswani (*7*) to combine pavement layers over the subgrade. The second method used to combine E_1 and E_2 follows the approximation suggested by

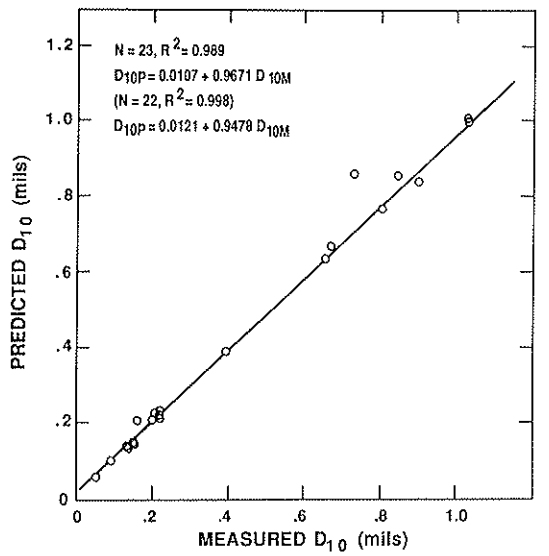

FIGURE 6 Relationship between predicted and measured sensor 10 deflections.

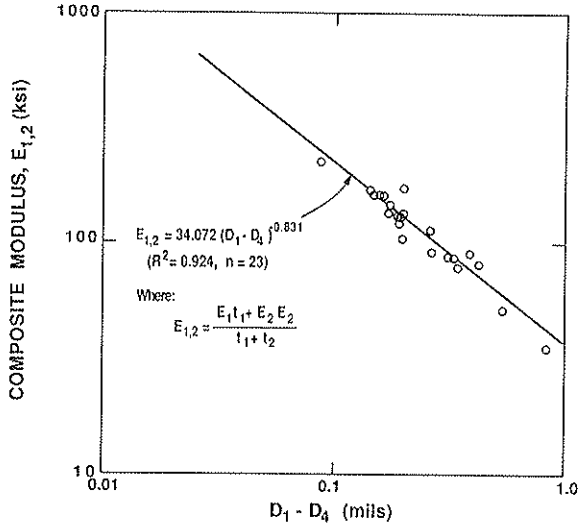

FIGURE 7 Relationship between $E_{1,2}$ (calculated using weighted average formula) and $D_1 - D_4$.

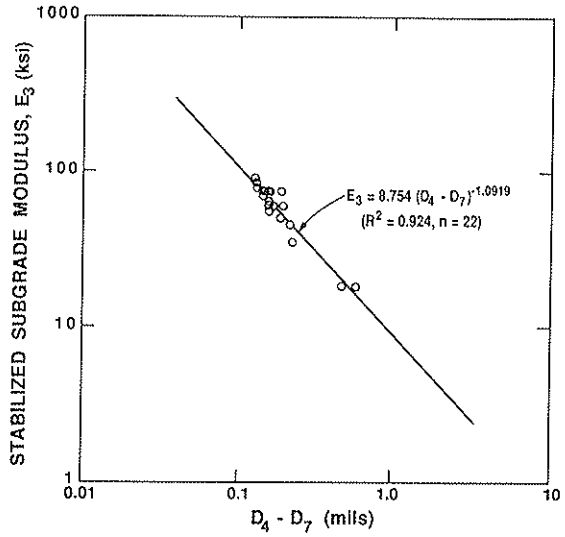

FIGURE 9 Relationship between E_3 and $D_4 - D_7$.

Thenn de Barros (*8*). The equation is of the form

$$E_{12} = \left(\frac{t_1 E_1^{1/3} + t_2 E_2^{1/3}}{t_1 + t_2}\right)^3 \quad (2)$$

where the variables are as previously defined.

Figures 7 and 8 present the relationships between E_{12} and $D_1 - D_4$ for each of the weighting methods. There is very little difference between modulus deflection relationship for the standard weighting method (Eqn. 1) and the Thenn de Barros formula (Eqn. 2), as shown in figure 7 and figure 8, respectively. It would appear that either method would be suitable for defining E_{12} although the difference between methods is greatest with low E_{12} values and high $D_1 - D_4$ values (e.g., $E_{12} < 34.0$ ksi, and $D_1 - D_4 > 1.0$ mil). As will be shown later, E_2 can be computed directly using E_{12} and either laboratory-measured E_1 values or E_1 values predicted from constant power viscosity (n_j).

The relationship between E_3 and $D_4 - D_7$ is illustrated in figure 9. The results of the regression analysis is fairly good except the range in E_3 values is narrow and limited to only two values below 20 ksi (SR 80). Additional test data in the lower range would be helpful in either verifying the validity of the E_3 prediction equation or modifying the regression equation.

Subgrade modulus prediction equations and the modified Dynaflect sensor 10 deflection values are shown in figure 10. The simplified equation was originally developed using data collected in Quebec, Canada, and Florida (*2*). The results from this earlier study are not included in figure 10. From a practical standpoint, there is very little difference between the E_4 prediction equations. This difference is not significant enough to warrant the use of one equation in preference to the other, except when D_{10} is less than 0.06 mil or much greater than 1.0 mil. Prior analyses (*2, 3*) using the simplified

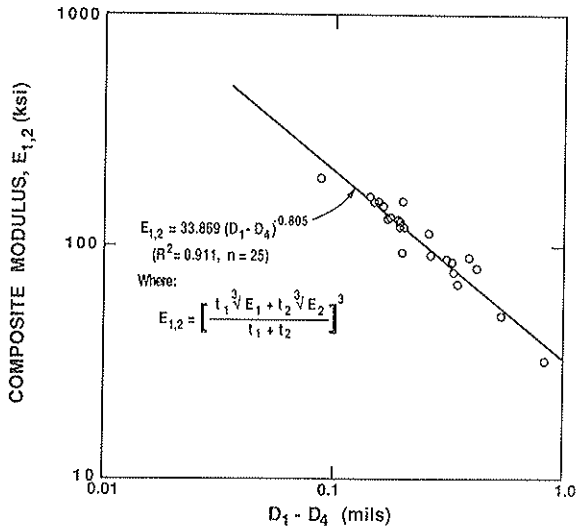

FIGURE 8 Relationship between $E_{1,2}$ (determined using Thenn de Barros' equations) and $D_1 - D_4$.

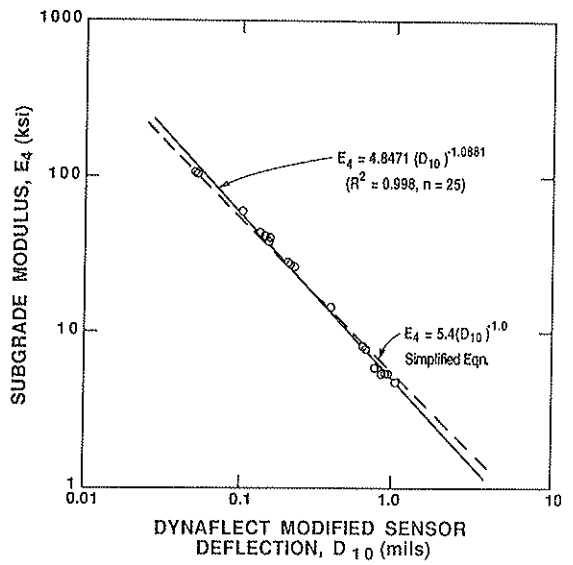

FIGURE 10 Relationship between E_4 and D_{10}.

E_4 prediction equation had indicated overprediction of weak subgrades ($E_4 < 10$ ksi) and underprediction of high or stiff subgrades ($E_4 > 100$ ksi).

The findings from this investigation indicated that separation of loaded areas produces "double bending" which allows for the optimization of sensors to separate layer response. Double bending occurs when two loads are spaced a sufficient distance apart to produce two interacting deflection basins. Proper selection of load and sensor spacing provides deflection measurements that are directly related to the stiffness (modulus) of each pavement layer. Therefore, the unique load-sensor configuration obtained in this study made it possible to develop simplified (power law) equations for prediction of layer moduli. If desired, the predicted layer moduli can be used as "seed moduli" in iterative elastic multilayer computer programs. The results of another investigation demonstrated that predicted E_1 and E_4 values are reliable and seldom require much adjustment or tuning to match the measured deflection basin (*9*). It appears that the most desirable approach in computer simulation is to use E_1 and E_4 as fixed values with predicted E_2 and E_3 values as "seed moduli" for iterative or judgment modified analysis.

RECOMMENDED TESTING AND ANALYSIS PROCEDURES

General testing requirements and procedures for analysis of Dynaflect data for pavement evaluation studies follow:

1. Pavement and air temperature data: Air and pavement surface temperatures can be obtained at suitable intervals during Dynaflect testing using handheld or pocket probe, thermister, thermocouple, or other temperature measuring devices. The mean pavement temperature can be determined by recording the temperature of oil poured into a ⅜- or ½-inch-diameter hole drilled with a masonry bit into the pavement within about a half-inch of the total thickness of the asphalt concrete. One location for a segment of roadway may be sufficient provided that solar radiation and wind effects are fairly uniform and do not vary enough to alter the average temperature more than ±2°F.

It is recommended that conventional pavement response measurements (e.g., Dynaflect) be obtained when pavement temperatures are between 30°F and 85°F. High pavement temperatures may affect the deflection measurements and make it difficult to achieve reliable results. This is particularly true where binder viscosity and E_1 are very low, resulting in excessive volume changes near the loaded area and erroneous deflection measurements.

2. Conduct Dynaflect tests at the desired interval (longitudinal distance) with the sensors at locations conforming to those shown in figure 11. Due to the potential for eccentric loading and variations in pavement response for sensors 1 and 2, it is required that the average value be used in the analysis.

3. Check whether measured deflections are within these limits:

$$0.56 \leq D_1 \text{ or } D_2 \leq 2.92 \text{ mil}$$

$$0.27 \leq D_3 \leq 2.07 \text{ mil}$$

$$0.15 \leq D_4 \leq 1.50 \text{ mil}$$

$$0.05 \leq D_5 \leq 1.00 \text{ mil}$$

and also that the following criteria are met:

$$0.09 \leq D_1 + D_2 - 2D_3 \leq 0.85 \text{ mil}$$

$$0.12 \leq D_3 - D_4 \leq 0.57 \text{ mil}$$

These criteria conform approximately to the following range of layer moduli and thicknesses:

$65.0 \leq E_1 \leq 400$ ksi	$1.5 \leq t_1 \leq 8.5$ in.
$26.0 \leq E_2 \leq 130$ ksi	$6.0 \leq t_2 \leq 24.0$ in.
$18.0 \leq E_3 \leq 90.0$ ksi	$12.0 \leq t_3 \leq 36.0$ in.
$5.0 \leq E_4 \leq 105$ ksi	t_4 = semi-infinite

Note that for the prediction equations, E_i is in ksi, t_i in in., and D_i in mils. Also extremely high or low D_5 values, outside the stipulated range, may be used for estimates of E_4 from 1.0 to 200 ksi.

4. If the above conditions are satisfied proceed to step 5. If not, check deflection measurements and then go to step 3. If the checked deflections do not meet conditions in step 3, proceed to step 5 considering that the predictions may be approximate or significantly in error.

5. Obtain pavement layer thicknesses from construction drawings or by coring.

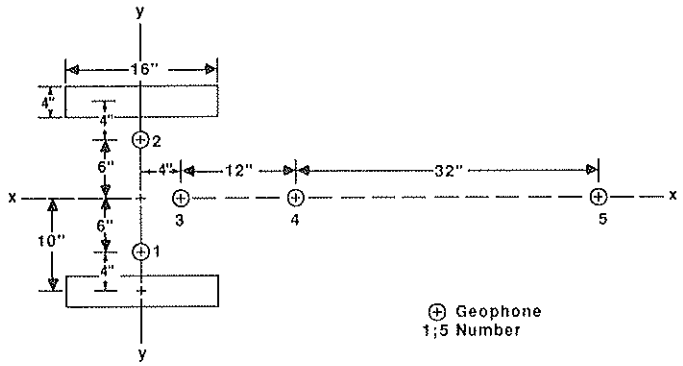

FIGURE 11 Schematic of Dynaflect loading and sensor positions in the modified system.

6. Calculate composite modulus, E_{12} using Equations 3 and 4.

$$E_{12} = 60.611(D_1 + D_2 - 2D_3)^{-0.831} \quad (3)$$

$$E_{12} = 59.174(D_1 + D_2 - 2D_3)^{-0.805} \quad (4)$$

7. Estimate E_1 from recovered asphalt viscosity-temperature-modulus relationships or from dynamic indirect tensile tests on pavement cores (*5, 9*). In Florida, E_1 can be estimated using the relationships illustrated in figure 12. The relationship for pavements with no visible cracks can be used to determine E_1 for the average pavement temperature during Dynaflect testing. If the pavement exhibits extensive cracking (e.g., alligator cracking), E_1 will be reduced considerably, even approaching the modulus (E_2) of the granular base course. It may be impossible to estimate a realistic E_1 value that would simulate the measured deflection basin using elastic layer computer programs.

The relationship for considerable cracking in figure 12 can be used when pavement cracks are spaced sufficiently to eliminate their influence on the Dynaflect deflections. This would apply to pavement sections that have uncracked segments within cracked segments. In this situation higher deflections and lower subgrade or stabilized subgrade moduli may cause the overstressing of these cracked segments. Analysis of the cracked pavements using the E_{1max} relation from uncracked segments could be performed using the E_3 and E_4 values predicted for cracked segments to verify high stress levels and the cause of cracking.

8. If E_1 is known, calculate E_2 using E_{12} from Equation 3 and the explicit form of Equation 1 as follows:

$$E_2 = \frac{E_{12}(t_1 + t_2) - E_1 t_1}{t_2} \quad (1a)$$

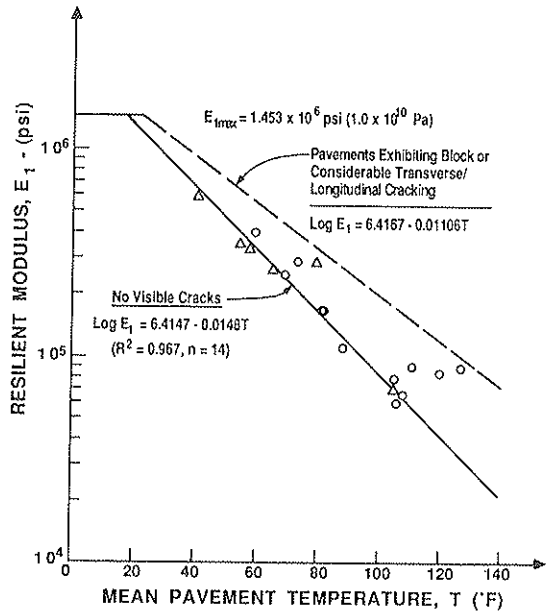

FIGURE 12 Relationship between asphalt concrete modulus E_1 and mean pavement temperature.

9. If E_1 is known, calculate E_2 using E_{12} from Equation 4 and the explicit form of Equation 2 as follows:

$$E_2 = \left[\frac{(t_1 + t_2)(E_{12})^{1/3} - t_1(E_1)^{1/3}}{t_2}\right]^3 \quad (2a)$$

10. Compare E_2 from steps 8 and 9; use an average if possible.

11. If E_1 is unknown, use an average value of E_{12} calculated from Equations 3 and 4, if possible, and $t_1 + t_2$ as composite layer thickness.

12. Calculate E_3 using Equation 5:

$$E_3 = 8.7541\ (D_3 - D_4)^{-1.0919} \quad (5)$$

13. Calculate E_4 from Equation 6:

$$E_4 = 5.40\ (D_5)^{-1.0} \quad (6)$$

Note that in Equations 1 through 6 modulus E_i is in ksi, deflection D_i is in mils, and thickness, t_i in in.

14. Use E_1, E_2, or E_{12}; E_3; and E_4 in an elastic layer computer program to calculate Dynaflect deflections, D_1 through D_5 with coordinates corresponding to that of figure 11. Reasonable values of Poisson's ratio can be assumed without much error on the predicted deflections.

15. Compare measured with predicted deflections; adjust layer moduli to match measured deflections, as required.

The above steps or algorithms have been incorporated into the BISAR elastic layer computer program to perform the iteration after the initial computation of the "seed moduli." The iteration process is interactive and user-specified with respect to the modulus value to be adjusted to achieve the desired tuning.

The FDOT currently has three Dynaflect units, one of which has been modified to meet the system described in this paper. Current plans are to use the standard and modified systems side by side in their research and routine pavement evaluation studies. The Department has also installed microcomputers in the Dynaflect vehicles to allow for on-site assessment of measured data and analysis. With the accumulation of a sufficient data base, it is hoped that the modified system will eliminate the many hassles associated with the interpretation of Dynaflect deflection basins.

APPLICATION EXAMPLE

The following example is provided to illustrate the use of the pavement layer moduli prediction procedures. Dynaflect tests were conducted on SR 24 in Alachua County on January 30, 1987. The air, surface, and mean pavement temperatures during testing were 65°, 62°, and 60°F, respectively. Sensor deflections in the modified system (figure 11) for Milepost 11.122 were 0.83, 0.63, 0.56, 0.32, and 0.16 mils. Pavement layer thicknesses for the asphalt concrete, limerock base, and the stabilized subgrade was determined to be 2.5, 11.0, and 17.0 inches, respectively.

The composite modulus E_{12} was found from Equations 1 and 2 to be 148.6 and 141.0 ksi, respectively, resulting in an average value of 144.8 ksi. The stabilized subgrade and subgrade moduli were computed to be 41.6 ksi and 33.75 ksi, respectively. From figure 12, using a temperature of 60°F, E_1 was

TABLE 6 LAYER MODULI AND PREDICTIONS IN EXAMPLE PROBLEM

a) Layer Moduli

Layer	Modulus (psi)		
	3-Layer*	4-Layer	Tuned
Asphalt Concrete	144790	336000	336000
Limerock Base		108547	95000
Stabilized Subgrade	41587	41587	55000
Subgrade	33750	33750	34000

b) Sensor Deflections

Sensor Number	Measured Deflections	Predicted Deflections (mils)		
		3-Layer	4-Layer	Tuned
1**	0.73	0.755	0.750	0.733
2**	0.73	0.755	0.750	0.733
3	0.56	0.555	0.569	0.534
4	0.32	0.399	0.394	0.365
5	0.16	0.171	0.170	0.167

* Composite modulus, E_{12} is calculated for E_1 and E_2 in the 3-layer case.

** An average value of D_1 and D_2 is used in the analysis.

estimated to be 336.0 ksi. The value of E_2 was then calculated from Equations 1a and 2a to be 105.9 and 111.1 ksi, respectively, with an average of 108.5 ksi being used in the analysis. Table 6 summarizes the layer moduli and BISAR deflection predictions for the calculated or "seed" moduli and the "final" moduli after tuning.

The BISDEF computer program (*10*) was used to compute the moduli of the pavement for comparison purposes. It was not feasible to model the modified sensor configuration (figure 11) in BISDEF, so the corresponding standard array deflections were used. The use of the iterative program required that a rigid layer (E = 1,000,000 psi) be placed at some user-specified depth below the subgrade. The reason for using a finite subgrade thickness, and hence a five-layer system, is to limit the lateral extent of the calculated deflection basins, and presumably it approximates the response of a more realistic subgrade with a modulus of elasticity that increases with depth. Although BISDEF (*10*) recommends a subgrade thickness of 240 in., a value of 999 in. was used in the analysis. It was necessary to simulate the BISAR four-layer solution presented in table 6 as much as possible, and sensitivity analysis (*9*) had shown that there was negligible difference in deflections if a subgrade thickness of 30 ft. or more is used. Also, cone penetration tests (*4*) conducted on that section of highway to a depth of 22 ft. did not indicate the presence of bedrock or a hard layer.

Table 7 lists BISDEF solution using the standard Dynaflect deflections for three input conditions. Case 1, in which BISDEF used its default moduli to determine the four modulus values, predicted unreasonably high E_1 and E_3 values. In case 2, the E_1 value from figure 12 was input into BISDEF and maintained constant, and the iteration process was seeded with the calculated modulus values from the prediction equations for the other layers. The third case is similar to case 2 except that both E_1 and E_4 were kept fixed. It is interesting to note that in all cases, BISDEF predicted higher E_3 than E_2. CPT logs on this site did not indicate any possible weakness of the base course layer.

CONCLUSIONS

A nondestructive testing procedure using a modified Dynaflect sensor configuration has been developed and recommended for flexible pavement evaluation studies in Florida. This technique provides the capability of separating the deflection response of each layer in a four-layer asphalt concrete pavement system. Analyses of Dynaflect data from test pavements with a wide variety of subgrade soils (muck to rock) resulted in the development of simple power law regression equations. The layer modulus prediction equations presented in this paper are applicable to the following range of parameters:

$65.0 \leq E_1 \leq 400$ ksi $\quad 1.5 \leq t_1 \leq 8.5$ in.

$26.0 \leq E_2 \leq 130$ ksi $\quad 6.0 \leq t_2 \leq 24.0$ in.

$18.0 \leq E_3 \leq 90.0$ ksi $\quad 12.0 \leq t_3 \leq 36.0$ in.

$5.0 \leq E_4 \leq 105$ ksi $\quad t_4$ = semi-infinite

TABLE 7 BISDEF SOLUTION FOR EXAMPLE PROBLEM

a) Layer Moduli

Layer	Modulus (psi)		
	Case 1[(a)]	Case 2[(b)]	Case 3[(c)]
Asphalt Concrete	1000000	336000	336000
Limerock Base	59711	62330	67767
Stabilized Subgrade	150000	80000	80000
Subgrade	28998	35604	34000

b) Sensor Deflections

Sensor Number	Measured Deflections	Predicted Deflections (mils)		
		Case 1[(a)]	Case 2[(b)]	Case 3[(c)]
1	0.55	0.5	0.5	0.5
2	0.35	0.4	0.4	0.4
3	0.23	0.3	0.2	0.3
4	0.19	0.2	0.2	0.2
5	0.16	0.2	0.1	0.2

(a) Using BISDEF's default moduli in the iteration process.

(b) E_1 value fixed and calculated E_2, E_3 and E_4 values (Table 6) used as seed moduli.

(c) E_1 and E_4 fixed, calculated E_2 and E_3 values used as seed moduli in BISDEF.

The advantages of the technique are:

1. An on-board computer (PC) can compute predicted moduli for a four-layer pavement system and print out deflection response and layer moduli profiles superimposed in graphic format for visual interpretation of lineal segments of highway pavement.
2. The deflection response of sensors 1, 2, and 3 (see figure 11) separates the stiffnesses of the asphalt concrete and base course from the underlying support layers. Changes or differences in the average D_1 and D_2 values can be assessed to determine if E_3 or E_4 has produced the change, or if E_{12} indicates stronger or weaker pavement structure.
3. Predicted E_1, E_2, E_3, and E_4 values appear to be more reliable than a four-layer iterative approach.
4. Improved results from iterative procedures seem feasible using predicted layer moduli as "seed moduli" or E_1 and E_4 being fixed with predicted E_2 and E_3 values as the "seed moduli" in the computer iteration process.

REFERENCES

1. H. F. Godwin, and W. G. Miley. Pavement Deflection to Estimate Soil Support Value for Overlay Design. *Proc. First International Symposium on Bearing Capacity and Airfields*, Trondheim, Norway, 1982, pp. 684–691.
2. B. E. Ruth, and K. Badu-Tweneboah. *Non-Destructive Testing for the Structural Characterization of In-Place Pavement Materials*. Final Report: Project 245-D29, Department of Civil Engineering, University of Florida, 1986.
3. B. E. Ruth, E. Puyana, and K. Badu-Tweneboah. Pavement Layer Moduli Evaluation Using Dynaflect. *Proc., Second International Conference on the Bearing Capacity of Roads and Airfields*, Plymouth, England, 1986, pp. 299–308.
4. K. Badu-Tweneboah, J. L. Davidson, B. E. Ruth, and W. G. Miley. Evaluation of Flexible Pavement Substructure. *Proc., VIII Pan-American Conference on Soil Mechanics and Foundation Engineering*, Cartegena, Columbia, 1987, Vol. 3, pp. 27–38.
5. K. Badu-Tweneboah, M. Tia, and B. E. Ruth. Procedures for Estimation of Asphalt Concrete Pavement Moduli at In Situ Temperatures. Presented at 66th Annual Meeting of the Transportation Research Board, Washington, D.C., 1987.
6. B. E. Ruth, M. Tia, and K. Badu-Tweneboah. Factors Affecting the Cracking of Asphalt Concrete Pavements. *Proc., Canadian Technical Asphalt Association*, 1986, Vol. XXXI, pp. 96–109.
7. N. K. Vaswani. Method for Separately Evaluating Structural Performance of Subgrades and Overlying Flexible Pavements. In *Highway Research Record 362*, HRB, Washington, D.C., 1971, pp. 48–62.
8. S. Thenn de Barros. Deflection Factor Charts for Two- and Three-Layer Elastic Systems. In *Highway Research Record 145*, HRB, National Research Council, Washington, D.C., 1966, pp. 83–108.
9. B. E. Ruth, M. Tia, and K. Badu-Tweneboah. *Structural Characterization of In-Place Materials by Falling Weight Deflectometer*. Final Report Project 245-D51. Department of Civil Engineering, University of Florida, 1986.
10. A. J. Bush III, and D. R. Alexander. Pavement Evaluation Using Deflection Basin Measurements and Layered Theory. In *Transportation Research Record 1022*, TRB, National Research Council, Washington, D.C., 1985, pp. 16–28.

Publication of this paper sponsored by Committee on Strength and Deformation Characteristics of Pavement Sections.

Compaction Specification for the Control of Pavement Subgrade Rutting

HANI A. LOTFI, CHARLES W. SCHWARTZ, AND MATTHEW W. WITCZAK

Soil compaction is a primary measure for controlling permanent deformations of pavement subgrade materials. Major parameters in any compaction specification include the compaction moisture content, compacted density, and depth of compaction. An analytical procedure for predicting subgrade rut depth (permanent deformation) based on the resilient and permanent deformation characteristics of the subgrade is presented. Rut depths associated with a range of values for the major compaction parameters are evaluated for highway pavements using this new procedure. The analytical results suggest a new criterion for compaction moisture content that minimizes subgrade rutting. Contour plots illustrating the trade-offs among compaction level, compaction depth, and natural subgrade conditions are also presented

Accurate assessment of pavement performance throughout its service life is an essential component of pavement design. One of the key factors governing the performance of flexible pavements is the permanent deformation or rutting of the pavement layer materials.

The subgrade is often responsible for much of the permanent deformation in flexible pavements. In many cases where the in situ soil can withstand a specific vehicle-pavement-traffic combination without failure or excessive deformation, it can be used directly as the subgrade material. If, on the other hand, the in situ soil is not suitable or is below the required elevation, imported subgrade materials may be required to support the pavement structure. The compaction process used in placing this imported subgrade soil then becomes an important step in the design process.

A primary objective of compaction for highway and airfield pavements is minimization of the deformations of the subgrade soil, especially those caused by the initial load repetitions. Current subgrade compaction specifications from different highway agencies are summarized in table 1. These specifications are largely empirical, relying heavily upon previous engineering experience. The data in table 1 indicate some disagreement between use of the AASHTO T-180 (modified Proctor compaction energy) and the AASHTO T-99 (standard Proctor compaction energy) test specifications.

One quantitative criterion for comparing existing empirical compaction specifications or for developing new specifications is the rut depth at the top of the subgrade layer. Rut depth magnitude can be evaluated either by structural analysis of the layered pavement system or by statistical analysis of past performance data. The present study is an example of the first approach.

H. A. Lotfi, Cairo University, Giza, Egypt. C. W. Schwartz and M. Witczak, University of Maryland, College Park, Md. 20742.

In this study, a nonlinear analytical methodology for calculating subgrade rut depth is presented and used in a series of analytical studies to evaluate the influence of various compaction parameters on subgrade rutting. Four specific compaction parameters are explicitly considered: (a) compaction moisture content; (b) compacted density (defined here as the percent compaction relative to the modified Proctor maximum density); (c) compaction depth; and (d) natural subgrade condition. A widely used empirical compaction specification for highways is evaluated using this methodology. Finally, some guidelines for more rational compaction specification for cohesive subgrade soils are drawn from the analysis results.

SUBGRADE RUTTING MODEL

In pavement structures subjected to cyclic loading, the cumulative permanent vertical strain after N cycles of loading, $\varepsilon_{pc}(N)$, can be calculated as the summation of the incremental permanent strains developed in each cycle:

$$\varepsilon_{pc}(N) = \sum_{I=1}^{N} \varepsilon_p(I) \tag{1}$$

in which $\varepsilon_p(I)$ is the incremental permanent strain for the Ith loading cycle. Equation 1 is represented graphically in figure 1, where linear behavior is assumed. Because of the plastic nature of pavement and subgrade materials, the loading modulus, E_{lo}, is in general not equal to the unloading resilient modulus, M_r.

A relationship between E_{lo} and M_r (*10*) can be developed based on the following the typical relationship between $\varepsilon_{pc}(N)$ and N suggested by Monismith (*8*) and Barksdale (*3*):

$$\varepsilon_{pc}(N) = aN^b \tag{2}$$

in which a and b are empirical material constants determined from a plot of log $\varepsilon_{pc}(N)$ vs. log N. The incremental permanent strain caused by the Nth load repetition is obtained by differentiating Eq. 2:

$$\frac{d\varepsilon_{pc}(N)}{dN} = \varepsilon_p(N) = abN^{b-1} \tag{3}$$

The resilient vertical strain due to unloading during the Nth cycle, $\varepsilon_r(N)$, is commonly assumed to be independent of the number of cycles (*10*), i.e.:

$$\varepsilon_r(N) = \varepsilon_r \tag{4}$$

Dividing Eq. 3 by ε_r:

$$\frac{\varepsilon_p(N)}{\varepsilon_r} = \frac{ab}{\varepsilon_r} N^{b-1} \tag{5}$$

TABLE 1 EXAMPLES OF COMPACTION LEVELS SPECIFIED BY VARIOUS HIGHWAY AGENCIES

Agency	Specified Compaction Level
Federal Highway Administration (4)	90% AASHTO T-99
AASHTO (1)	95% AASHTO T-99
Asphalt Institute (2)	95% AASHTO T-180 (top 12 in.) 90% AASHTO T-180 (below)
Maryland State Highway Administration (7)	95% AASHTO T-180 (top 12 in.) 92% AASHTO T-180 (below)
Indiana State Highway Administration (5)	95% AASHTO T-99
Colorado State Highways (9)	95% AASHTO T-99 or 90% AASHTO T-180

Note: AASHTO T-99 = standard Proctor test
AASHTO T-180 = modified Proctor test

For convenience, Eq. 5 can be simplified by defining two new material parameters:

$$\mu = \frac{ab}{\varepsilon_r} \tag{6}$$

$$\alpha = 1 - b \tag{7}$$

Eq. (5) then becomes:

$$\varepsilon_p(N) = \varepsilon_r \mu N^{-\alpha} \tag{8}$$

On the other hand, as shown in figure 1:

$$\varepsilon_p(N) = \varepsilon_t(N) - \varepsilon_r \tag{9}$$

in which $\varepsilon_t(N)$ is the total loading vertical strain developed during the Nth load cycle. By assuming linear stress-strain behavior during loading and unloading with different moduli

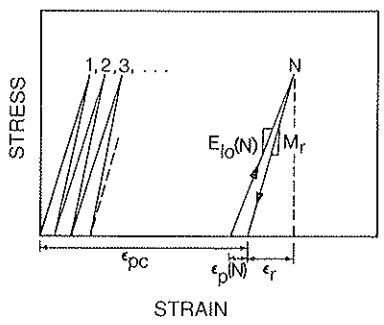

FIGURE 1 Strains developed during cyclic loading.

E_{lo} and M_r, the total and resilient strains in the vertical or z-direction can be represented respectively as

$$\varepsilon_{t_z} = \frac{1}{E_{lo}(N)}[\sigma_z - \nu(\sigma_x + \sigma_y)] = \frac{\sigma_z^*}{E_{lo}(N)} \tag{10}$$

and

$$\varepsilon_{r_z} = \frac{1}{M_r}[\sigma_z - \nu(\sigma_x + \sigma_y)] = \frac{\sigma_z^*}{M_r} \tag{11}$$

in which $\sigma_z^* = \sigma_z - \nu(\sigma_x + \sigma_y)$ and ν is assumed the same for both loading and unloading. Combining Eqs. 8, 9, 10, and 11:

$$\varepsilon_p(N) = \frac{\sigma_z^*}{E_{lo}(N)} - \frac{\sigma_z^*}{M_r} = \frac{\sigma_z^*}{M_r}\mu N^{-\alpha} \tag{12}$$

Rearranging Eq. 12:

$$E_{lo}(N) = \frac{M_r}{1 + \mu N^{-\alpha}} \tag{13}$$

Based on Eqs. 1 and 13, the following procedures can be used to calculate rut depth:

(1) Determine the stress-dependent unloading (resilient) modulus, M_r;
(2) Use M_r in a multilayer elastic solution to calculate the pavement recovery deformation during unloading, δ_{unlo} (constant for all N);
(3) For a specific load cycle N, determine $E_{lo}(N)$ using Eq. 13;

(4) Use $E_{lo}(N)$ in a multilayer elastic solution to calculate the pavement deformation during loading at cycle N, $\delta_{lo}(N)$;
(5) Determine the incremental permanent deformation at load cycle N, $\delta_p(N) = \delta_{lo}(N) - \delta_{unlo}$;
(6) Repeat steps 3 to 5 for various N values;
(7) Determine the total accumulated rut depth at load cycle N by numerical integration of the values obtained in step 5.

COMPUTER SOLUTION ALGORITHM

The computer program ERHAP (Evaluation of Rutting for Highway and Airfield Pavements) follows the procedure described in the preceding section to calculate the rut depth at the top of the subgrade layer for flexible pavement systems. The unloading deformation is computed from the cyclic stresses and the resilient modulus using the following equations to represent the stress dependency of the pavement layers:

For cohesive soils:

$$M_r = k_1 \sigma_d^{-k2} \tag{14}$$

For cohesionless soils:

$$M_r = k_1 \theta^{k2} \tag{15}$$

in which k_1 and k_2 are material coefficients, σ_d is the cyclic deviator stress, and θ is the bulk stress.

Stress states cannot be computed without specification of the moduli for the various soil layers in the pavement, and the moduli cannot be determined without knowledge of the existing stress states. Consequently, the solution must be obtained through an iterative procedure. Starting with an initial assumed value of modulus for each stress dependent layer, stress states due to a specific load configuration are evaluated using multilayer linear elastic theory. Updated moduli values are obtained from these computed stresses using Eqs. 14 and 15. The process is repeated until the differences between the calculated stresses at successive iteration cycles are within a specified tolerance level.

The computer program BISAR (*11*), developed by the Shell Oil Company, is incorporated in ERHAP as a subprogram for calculating the stresses at the mid-depth of each layer. The BISAR program is based on multilayer linear elastic theory and is capable of analyzing stresses, strains, and deformations for multiple load conditions.

For rut depth calculation, ERHAP again employs the BISAR program as a subprogram to compute the vertical deformation at the top of the subgrade soil. The nonlinear resilient moduli, calculated iteratively as described above, are used as unloading moduli for the calculation of the unloading recoverable deformation, δ_{unlo}. The value of the loading modulus is determined at each load cycle for each subgrade layer using Eq. 13, and the incremental loading deformation $\delta_{lo}(N)$ is calculated by BISAR. Note that the stress dependence of the loading modulus is incorporated through the M_r material parameter in Eq. 13. The incremental permanent deformation $\delta_p(N)$ is then:

$$\delta_p(N) = \delta_{lo}(N) - \delta_{unlo} \tag{16}$$

Values of $\delta_p(N)$ are calculated at various values of $N = N_i$ and the cumulative permanent deformation or rut depth, RD, is evaluated at the final load cycle by numerical integration:

$$RD = \sum_{i=1,2,3} \frac{\delta_p(N_i) + \delta_p(N_{i+1})}{2} (N_{i+1} - N_i) \tag{17}$$

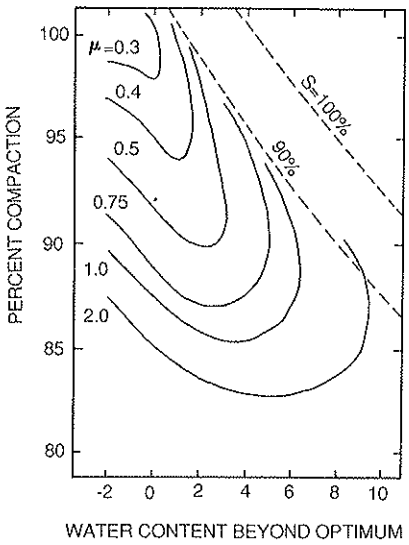

FIGURE 2 Values of μ at different dry density-compaction moisture combinations (soaked condition).

INFLUENCE OF COMPACTION PARAMETERS ON SUBGRADE RUTTING

The permanent deformation at the top of the subgrade is used in this study as the principal criterion for evaluating compaction specifications for subgrade soils. The soil parameters μ, α, and CBR for a typical cohesive soil at different compaction conditions are shown in figures 2 through 4 (*6*). Other soil properties are summarized in table 2. The μ and α parameters will in general be functions of soil type, moisture content, and compacted density. The influence of stress level on these parameters for this soil is negligible (*6*). The μ and α coefficients are used as input to ERHAP to calculate rut depths for different compaction conditions. The CBR values are used

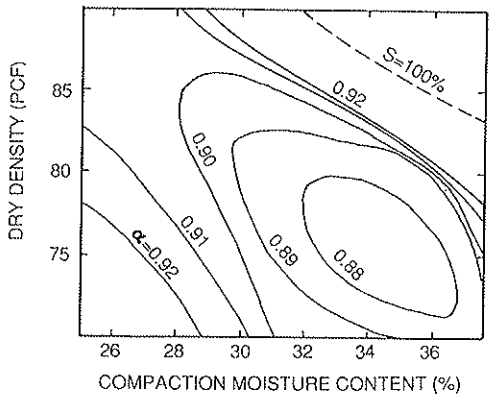

FIGURE 3 Values of α at different dry density-compaction moisture combinations (soaked condition).

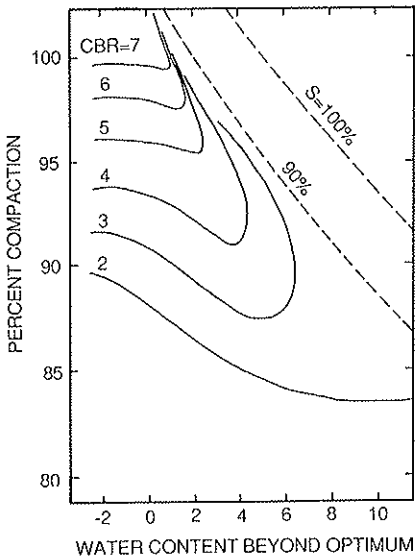

FIGURE 4 Values of CBR at different dry density-compaction moisture combinations (soaked condition).

to predict the nonlinear resilient modulus using the empirical relation (*6*):

$$\log M_r = 1.0016 + 0.0430(\text{CBR}) - 1.9557\left(\frac{\log \sigma_d}{\text{CBR}}\right) - 0.1705 \log \sigma_d \quad (18)$$

in which M_r is in ksi, δ_d is in psi, and CBR is in percent.

As the soaked CBR condition is the critical case for evaluating subgrade strength in highway pavement design, values of μ and α at the soaked condition were accordingly used in all analyses reported here. Note that even if a flexible pavement section is located in a dry environment, the permanent deformation that occurs during a short wet season is substantial and will often control the design.

As noted earlier, there is wide variation among the compaction specifications of different highway agencies. The Asphalt Institute compaction specification (*2*) was chosen for investigation in this study because it is the most comprehensive, i.e., all four major compaction parameters are considered: compacted density, compaction moisture content, depth of compaction, and natural subgrade condition. The Asphalt Institute compaction criteria for cohesive soils require a density not less than 95 percent of the AASHTO T-180 (modified Proctor) density for the top twelve inches of subgrade and 90 percent for below. The compaction moisture content must be within one to two percentage points below the modified Proctor optimum water content.

TABLE 2 PROPERTIES OF COHESIVE SOIL USED IN STUDY (*6*)

Soil description:	"EPK" Kaolinite (available from The Feldspar Corp., Spruce Pine, N.C.)
USCS Class:	ML
Plastic Limit:	41.9%
Liquid Limit:	48.2%
Clay content:	34% (particles smaller than 0.002 mm.)

Typical highway loads are represented in the analyses by a standard 18-kip single axle load (18 KSAL) with one million repetitions. This loading condition was used in conjunction with the AASHTO flexible pavement design procedures in all cases analyzed. A schematic pavement section is shown in figure 5. This pavement section, together with the standard highway loading, was used to investigate the influence of the various compaction parameters.

Compaction Water Content

As shown in figure 3, each compaction level has an associated compaction water content at which μ is minimized. Conceptually, this should also represent the optimum condition for minimizing subgrade rutting. The relationship between compaction level and water content for minimizing μ can be represented by the regression equation:

$$w_o = 32.1 - 0.332(PC) \qquad (R^2 = 0.97) \qquad (19)$$

in which w_o is the percentage point difference between the compaction moisture content and the modified Proctor optimum moisture content and PC is the relative compaction in percent based on the modified Proctor maximum dry density.

From figure 4, a different PC vs. w_o relationship is found to maximize CBR. This relationship can be represented by the regression equation:

$$w_o = 39.6 - 0.392(PC) \qquad (R^2 = 0.99) \qquad (20)$$

Both CBR and μ affect rutting magnitude. To investigate the relative importance of these two parameters, rut depth was calculated at different values of w_o for two pavement sections, one resting on a uniform subgrade with $PC = 95$ percent and the other on a subgrade with $PC = 90$ percent. One million 18-KSAL load repetitions were assumed in each case. As is clearly shown in figure 6, the compaction moisture content corresponding to the minimum μ-value produces less rutting than does the compaction moisture content corresponding to the maximum CBR. Consequently, the relation-

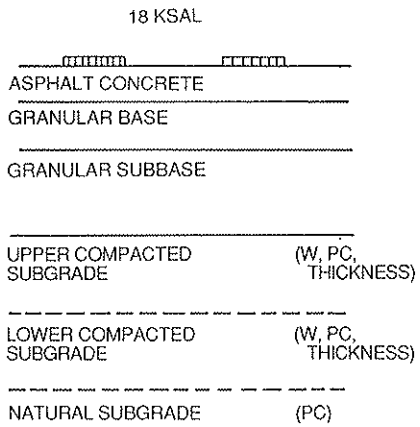

FIGURE 5 Pavement section schematic for rut depth analyses.

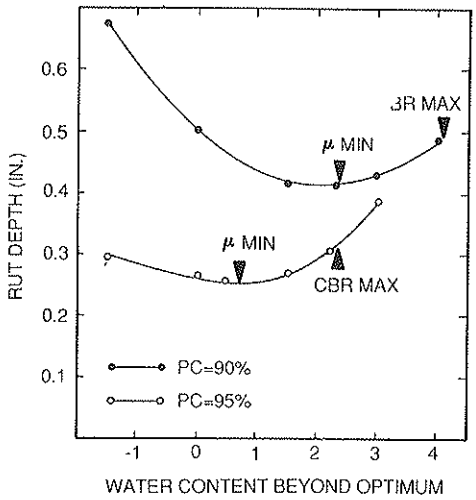

FIGURE 6 Influence of compaction moisture content on rut depth at different compaction levels.

ship between compaction moisture content and percent compaction given in Eq. 19 is the more suitable criterion for compaction moisture control.

The reduction in rutting resulting from this proposed compaction moisture criterion can be illustrated by calculating the rut depth at the top of a subgrade compacted to the Asphalt Institute's minimum compaction level requirements (95 percent for the top twelve inches and 90 percent below). For compaction moisture contents based on Eq. 19 (w_o = 0.6 percentage points for PC = 95 percent and 2.3 points for PC = 90 percent; see Eq. 19), the calculated rut depth is 0.382 inches. For comparison, rut depths were calculated at the same compaction levels but at a variety of uniform moisture contents. A normalized rut depth factor RF is defined as

$$RF = \text{(Computed Rut Depth)} / 0.382 \text{ in.} \quad (21)$$

The relation between RF and w_o is shown in figure 7. The RF values are always greater than one, implying that the lowest rut depth is obtained by varying w_o with PC as proposed in Eq. 19. Compacting wet of optimum as specified by Eq. 19 reduces the rut depth by 35 percent from that obtained using the Asphalt Institute specification of 1.5 percentage points dry of optimum (i.e., $w_o = -1.5$).

Compaction Level

Rut depths corresponding to five different compaction levels and three different thicknesses for the top subgrade layer were calculated. The five compaction combinations considered were as follows:

1. As specified by the Asphalt Institute (95 percent compaction for the top layer and 90 percent below)
2. Three percentage points dry of specifications (92 percent compaction for the top layer and 87 percent below)
3. Five percentage points dry of specifications (90 percent compaction for the top layer and 85 percent below)
4. Two percentage points wet of specifications (97 percent compaction for the top layer and 92 percent below)
5. Five percentage points wet of specifications (100 percent compaction for the top layer and 95 percent below)

The three different thickness values (d_1) considered for the top subgrade were 6, 12, and 24 inches; recall that the Asphalt Institute specifies 12 inches. The AASHTO design procedure was used to determine the required thicknesses for the pavement layers. In this procedure, the total pavement thickness is dependent on the compaction level of the top subgrade layer. The μ, α, and CBR values for each subgrade layer were taken from figures 2, 3, and 4 while M_r was calculated from Eq. 18.

Subgrade rut depth was calculated at one million 18-KSAL load repetitions for each of the 15 combinations of compaction

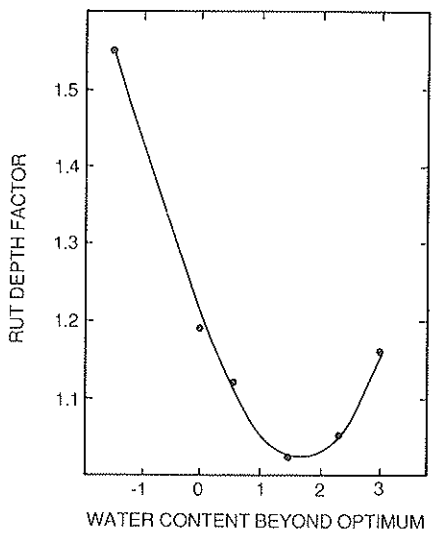

FIGURE 7 Influence of compaction moisture content on rut depth factor for Asphalt Institute compaction specification.

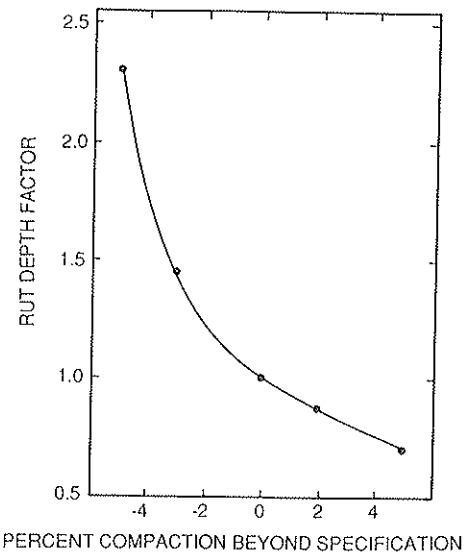

FIGURE 8 Influence of compacted density of top compacted subgrade layer on rut depth factor.

level and compaction depth (5 values of PC and 3 values of d_1). The normalized rut depth factors determined using Eq. 20 are summarized in figure 8 for d_1 = 12 inches. The rut depth factor increases significantly for negative PC_o values (PC_o is defined as the percentage point difference between the actual percent compaction and that specified by the Asphalt Institute). An increase in compaction level by 5 percentage points reduces RF from 1.0 to 0.7 while a decrease in compaction level by the same amount increases RF to 2.3.

The results to this point are all based on traffic levels of one million repetitions of the standard 18-KSAL vehicle. The influence of the number of load repetitions on the RF-PC_o relationship was investigated by analyzing repetition levels of 50 thousand and 20 million. The variation in normalized RD with PC_o for different numbers of repetitions is shown in figure 9; the normalization factor used in the denominator of Eq. 21 in these cases is the rut depth computed for the specified traffic conditions and based upon a pavement design and compaction conditions as specified by AASHTO and the Asphalt Institute. The normalization process largely compensates for the effect of load repetitions. Therefore, the analysis of a single repetition level may be sufficient for investigating the influence of the compaction parameters on the rut depth factor.

Depth of Compaction

The thickness of the upper compacted subgrade layer (d_1) specified by the Asphalt Institute is 12 inches. Contours of various PC_o-d_1 combinations producing the same subgrade rut depth are illustrated in figure 10. For example, a point on the RF = 1 contour represents a PC_o-d_1 combination that is equivalent to the Asphalt Institute specifications, at least in terms of subgrade rutting. The contours graphically illustrate

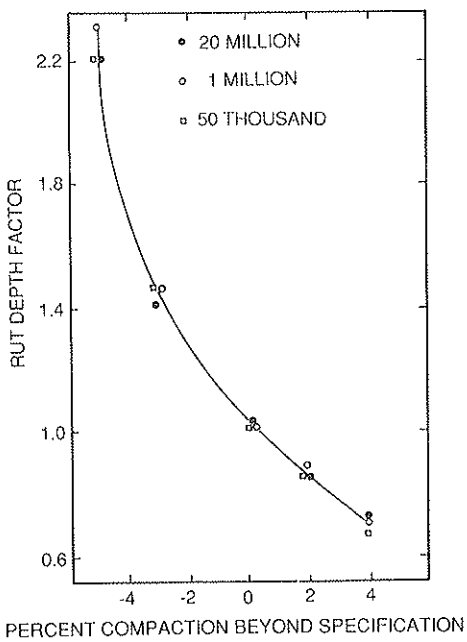

FIGURE 9 Variation of rut depth factor with compacted density for all repetition levels.

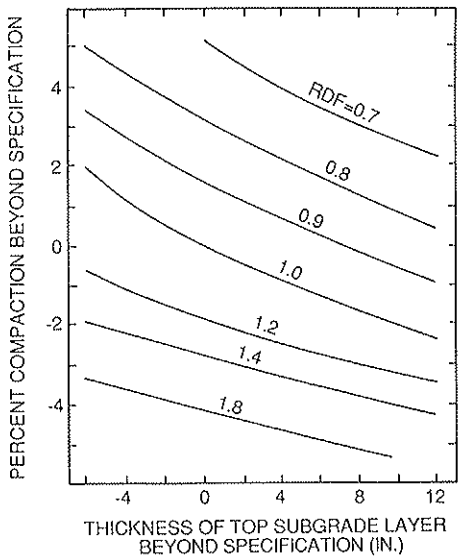

FIGURE 10 Combined influence of d_1 and PC_o on rut depth factor.

the relative gains and losses in rut depth that result from any PC_o-d_1 combination.

Natural Subgrade Condition

The Asphalt Institute compaction specification implicitly assumes an infinite thickness for the lower compacted subgrade layer. In effect, the Asphalt Institute specifications require that the natural subgrade have an in situ density corresponding to a compaction level of 90 percent. Clearly, this is not always the case. The influence of the natural subgrade condition on rut depth is illustrated through analyses of a pavement section composed of three subgrade layers. The top two layers are compacted layers and the bottom layer represents the natural subgrade. Three natural subgrade conditions were investigated: well compacted, defined as PC = 90 percent; moderately compacted, defined as PC = 87 percent; and poorly compacted, defined as PC = 85 percent.

It is clear that if the thickness of the middle subgrade layer is increased to the limit where the induced stresses at the bottom layer approach zero, then the natural subgrade condition will have no effect on rut depth. Alternatively, when the natural subgrade is well compacted (PC = 90 percent), the middle compacted subgrade layer is equivalent to the natural subgrade and only the top compacted subgrade layer influences rut depth. Figure 11 shows the trade-offs for the intermediate conditions where the natural subgrade is moderately to poorly compacted for different thicknesses of a middle subgrade layer (d_2) compacted to the specified 90 percent level. For example, a poorly compacted natural subgrade requires a 50-inch middle subgrade layer to achieve a RF of 1.0, while a moderately compacted natural subgrade requires only 36 inches for the middle subgrade layer.

Because of the relatively large layer thicknesses needed to overcome the influence of inferior natural subgrades, it is worthwhile investigating the compaction levels for the upper two subgrade layers required to achieve a rut depth factor of 1.0 at smaller d_2 values. Figure 12 illustrates computed rut

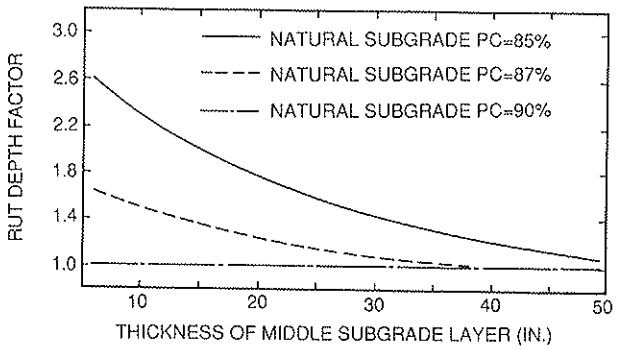

FIGURE 11 Influence of depth of middle compacted subgrade layer on rut depth factor for various natural subgrade conditions.

depth factors at different combinations of d_2 and subgrade compaction levels for a moderately compacted natural subgrade. For example, any point on the $RF = 1$ line in figure 12 represents a PC_o-d_2 combination that can be used with a moderately compacted natural subgrade as a substitute for the natural subgrade conditions implicitly assumed in the Asphalt Institute specifications.

SUMMARY AND CONCLUSIONS

A methodology for calculating the rut depth at any point throughout a pavement subgrade has been presented. This approach considers the stress dependency of the resilient modulus as well as the plastic behavior (as manifested by the difference between loading and unloading moduli) of cohesive soils. The approach can treat any loading configuration (single or multiple loads) and the effect of overburden stresses on the nonlinear moduli. A computer program based on the BISAR multilayer elastic analysis algorithms has been developed for performing these calculations.

A series of analytical studies was performed using the rutting model to provide guidance for more rational compaction specifications. Four major compaction parameters were considered in these studies: compaction moisture content; compaction level (percent compaction); depth of subgrade compaction; and the natural subgrade condition. Soil properties were based upon a single but typical cohesive soil type. The soaked condition was assumed in all analyses as it represents the critical case for rutting. Conclusions regarding the influence of each of the four compaction variables are as follows:

1. *Compaction Moisture Content.* For a given compaction level, there exists a specific compaction moisture content that minimizes subgrade rutting. The relationship between compaction level and moisture content for minimum rutting is given by Eq. 19 for the cohesive subgrade soil considered in this study.
2. *Compaction Level.* Results from this study confirm the reasonableness of the compaction levels recommended by The Asphalt Institute for highway loads. It was found that a decrease in compaction level from the specified values caused a significant increase in subgrade rutting while increases in compaction level beyond the recommended values produced negligible improvements. For example, calculated rut depth increased by 130 percent when the compaction level was decreased by 5 percentage points from the Asphalt Institute's recommendations; however, rut depth decreased by the comparatively smaller value of 30 percent when the compaction level was increased by 5 percentage points over the recommended values.
3. *Depth of Subgrade Compaction.* The thickness of the upper compacted subgrade layer was found to significantly influence rut depth. For example, increasing the thickness of the top subgrade layer from 6 to 24 inches reduced the computed rut depth by approximately 30 percent. Contours showing the variation of rut depth for different compaction level and compaction depth combinations are provided for highway loads.
4. *Natural Subgrade Condition.* The Asphalt Institute compaction specifications implicitly assume that the natural subgrade is compacted to 90 percent of the AASHTO T-180 maximum. In reality, this condition often does not occur. Contour lines have been developed to illustrate the combinations of compaction level and thickness for the middle subgrade layer that can be used to overcome the influence of moderately or poorly compacted natural subgrades.

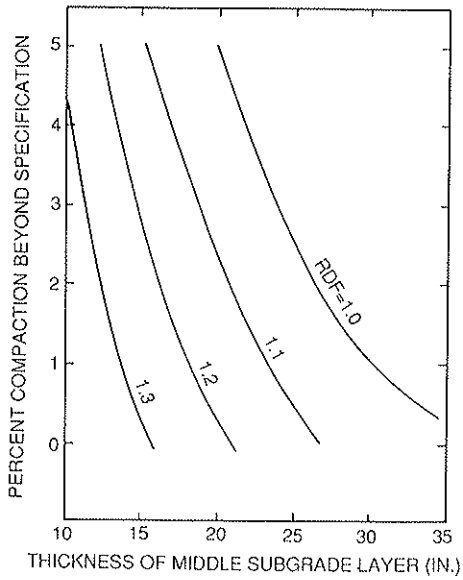

FIGURE 12 Combined influence of d_2 and PC_o on rut depth factor for moderately compacted natural subgrade.

The number of load repetitions was found to have a negligible influence on all of the general conclusions summarized above.

Although the results from these analyses have produced many interesting and useful observations regarding subgrade compaction criteria, it must be kept in mind that the analyses are all based upon properties for a single cohesive soil type. While it is expected that other cohesive subgrade soils will exhibit similar qualitative behavior, generally applicable quantitative conclusions will require additional studies that consider a range of cohesive soil properties.

ACKNOWLEDGMENT

The computations in this study were performed using resources provided by the Computer Science Center at the University of Maryland. This support is gratefully acknowledged.

REFERENCES

1. American Association of State Highway and Transportation Officials. *AASHTO Material Specifications, M57-64*, AASHTO, Washington, D.C., 1978.
2. Asphalt Institute. *Asphalt Paving Manual*, Series No. 8. College Park, Md., 1978.
3. R. D. Barksdale. Laboratory Evaluation of Rutting in Base Coarse Materials, Proc., *Third International Conference on Structural Design of Asphalt Pavement*, Ann Arbor, Mich., 1972.
4. Federal Highway Administration. *Standard Specifications for Construction of Roads and Bridges on Federal Highway Projects*. Section 203.19. Washington, D.C., 1975.
5. Indiana State Highway Administration. *State Highway Standard Specifications*, Section 203.23. 1978.
6. H. A. Lotfi. *Development of a Rational Compaction Specification for Cohesive Soils*. Ph.D. dissertation. University of Maryland, College Park, 1984.
7. *Specificatons for Materials, Highways, Bridges, and Incidental Structures*. Maryland State Road Commission, 1968.
8. C. L. Monismith, K. Inkabi, C. R. Feem, and D. B. McLean. A Subsystem to Predict Rutting in Asphalt Concrete Pavement Structures. *Proc., Fourth International Conference on the Structural Design of Asphalt Pavement*, Ann Arbor, Mich., 1977.
9. State of Colorado. *Standard Specification for Road and Bridge Construction*, Section 203.11, Denver, Co, 1976.
10. J. Uzan. *Permanent Deformation in Pavement Design and Evaluation*. Technion-Israel Institute of Technology, 1982.

Publication of this paper sponsored by Committee on Strength and Deformation Characteristics of Pavement.

Resilient Modulus and AASHTO Pavement Design

ROBERT P. ELLIOTT AND SAM I. THORNTON

In the 1986 *AASHTO Guide for the Design of Pavement Structures*, subgrades and granular base layers are evaluated by the resilient modulus test. Inclusion of the resilient modulus test was prompted by the need for a rational evaluation method. Resilient modulus is a measure of a material's deflection behavior. Since pavement life and surface deflection are strongly related, resilient modulus is a fundamental and rational material property that needs to be included in pavement design. The effects of variations in subgrade resilient modulus on various design parameters and on the AASHTO design thickness are examined. The seasonal variations of subgrade resilient modulus with moisture fluctuation and freezing and thawing are discussed; and methods for selecting a single design resilient modulus are examined. However, resilient modulus does not measure all of the material properties that can influence pavement behavior. Consequently, resilient modulus should not be the only property used in selecting a pavement material or in judging the material's structural contribution to the pavement.

The 1986 *AASHTO Guide for the Design of Pavement Structures* (*1*) requires the use of the subgrade resilient modulus to design a flexible pavement. Resilient modulus is also included as the test for establishing the structural layer coefficient for base and subbase materials.

What is resilient modulus? How does resilient modulus relate to the "real world" structural capacity and performance of flexible pavements? How is a resilient modulus value selected for design? How is resilient modulus used in design? These are questions being asked by many experienced highway designers and materials engineers. The questions are particularly bothersome because the standard resilient modulus test (AASHTO T-274) is quite time consuming.

Before trying to understand the resilient modulus, the need to replace the soil support scale that was used in the previous *AASHTO Interim Guide for Design of Pavement Structures* (*2*) should be recognized. The fundamental basis for both guides is the AASHO Road Test that was conducted in 1958–1960. Although the Road Test is the most comprehensive pavement research project ever undertaken, it did not (and could not) include all variables that can affect the performance of a pavement. One major factor not examined was subgrade soil strength. Only one type of soil was used in the Road Test.

Following the Road Test, pavement design procedures were developed from the research findings. The design procedures required some method for considering different subgrade soil types. For rigid pavements, a rational method for including subgrade soil was available that involved incorporating Westergaard's modulus of subgrade reaction (k-value) and Spangler's theoretical formula for corner stresses (*3*). However, no similar approach was available for flexible pavements.

For flexible pavements, a "soil support" scale was established using engineering judgment supplemented with limited data from Road Test sections having the greatest thickness of crushed stone base. This scale was not based on any particular method of test. Each highway agency was left to adopt a test method and establish or select a relationship between that test and the "soil support" scale. Without an analytical basis and a unified method of test, there was little possibility of improving the soil support scale.

Department of Civil Engineering, University of Arkansas, Fayetteville, Ark. 72701.

WHAT IS RESILIENT MODULUS?

Resilient modulus is a fundamental material property that is similar in concept to the modulus of elasticity. That is, resilient modulus is a stress-strain relationship. However, it differs from the modulus of elasticity in that it is determined from a repeated-load, triaxial-compression test ("unconfined compression" is used by some investigators) and is based on only the resilient (or recoverable) portion of the strain. Resilient modulus is defined as:

$$\text{Resilient modulus} = \frac{\text{stress amplitude}}{\text{strain amplitude}}$$

where

stress amplitude = load/area of the specimen
strain amplitude = recoverable deformation/original height

The general stress-strain behavior of a soil or granular material is illustrated in Figure 1. As the load is applied, the stress increases as does the strain. When the stress is reduced, the strain also reduces but all of the strain is not recovered after the stress is removed. The total strain, therefore, is composed of both a permanent (or plastic) component and a recoverable (or resilient) component. The plastic strain is not included in the resilient modulus.

The resilient modulus test is designed to simulate the behavior of soils and granular materials when subjected to traffic loading within a pavement system. Consequently, the sample preparation, conditioning, and testing are conducted so as to simulate field conditions. The standard method of test is prescribed by AASHTO T-274.

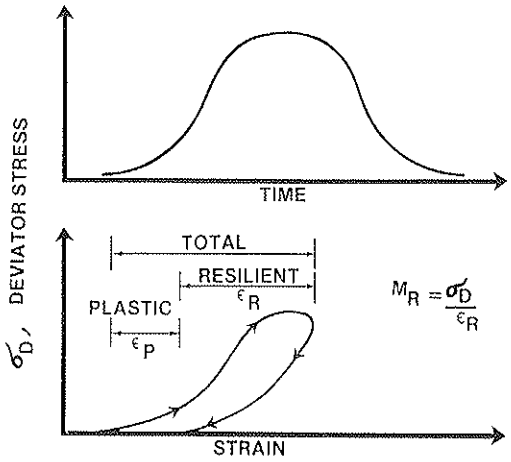

FIGURE 1 Typical load response in the resilient modulus test.

BASIS FOR RESILIENT MODULUS TESTING

The AASHO Road Test demonstrated that pavement surface deflection under load is a strong indicator of how well a pavement will perform (*4*): "The performance of the flexible pavements was predicted with essentially the same precision from load-deflection data as from load-design information."

Other studies (*5–9*) found similar relationships between pavement deflection and performance (Figure 2).

Surface deflection results from the accumulation of load-induced strain within the pavement and subgrade with the subgrade being the major contributor. At the AASHO Road Test (*4*), 60 to 80 percent of the deflection measured at the surface was found to develop within the subgrade. Consequently, the stress-strain relationship for the subgrade (resilient modulus) is a major factor contributing to surface deflection. It follows that subgrade resilient modulus is also a major factor in flexible pavement performance.

SIGNIFICANCE OF SUBGRADE RESILIENT MODULUS

Surface deflection is not itself detrimental to the pavement. However, deflection is an indicator of the factors that are detrimental. There are two major types of load-induced flexible pavement failure—fatigue cracking and rutting. Figure 3 illustrates the two prime structural parameters contributing to failure: the tensile strain that develops in the bottom of the asphalt (AC) layer and the stress or strain applied to the top of the subgrade.

Figures 4 and 5 illustrate the effect of subgrade resilient modulus on the AC tensile strain and the subgrade stress. These plots were developed using the ILLI-PAVE design algorithms developed by Thompson and Elliott (*11*). They represent the structural response of a conventional flexible pavement having a 3-inch AC surface and a 12-inch aggregate base when subjected to a 9,000-pound wheel load. The effects would be similar for other designs and other loads.

In Figure 4, the AC strain decreases as the resilient modulus of the subgrade increases. A strain decrease increases the fatigue life (load applications before cracking) for the AC surfacing.

Figure 5 shows the change in subgrade stress ratio with resilient modulus. The stress ratio is the load-induced deviator stress on the subgrade divided by the unconfined compressive strength of the soil. In analyzing the performance of the AASHO Road Test pavements, Elliott and Thompson (*12*) found a strong relationship between subgrade stress and load applications prior to cracking. As a result, the stress ratio was selected as the design parameter to guard against overstressing the subgrade. In Figure 5, the stress ratio decreases as the resilient modulus increases indicating an increasing pavement life.

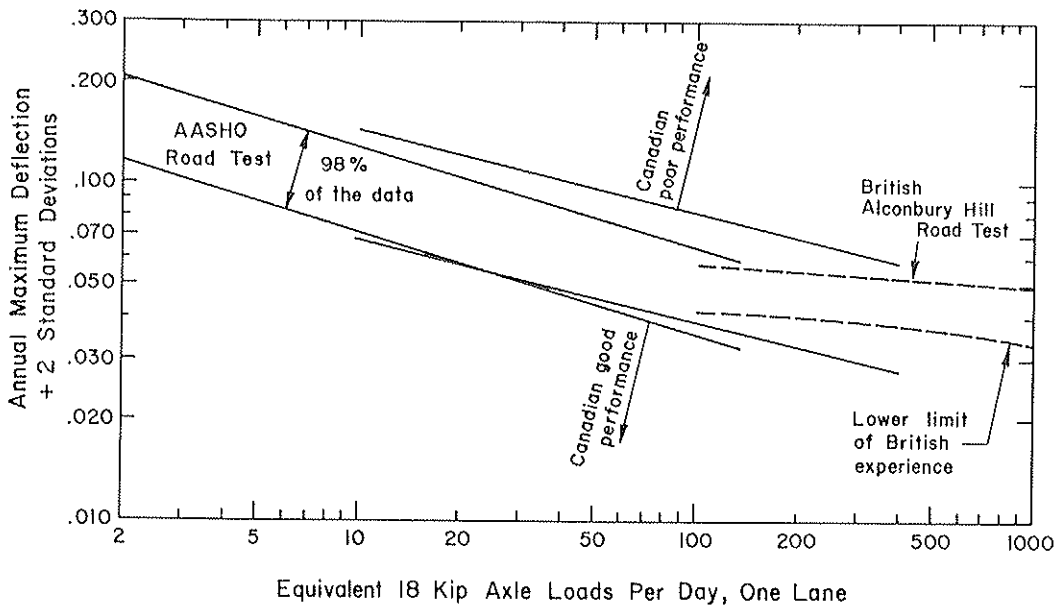

FIGURE 2 Reported deflection-life relationships (*10*).

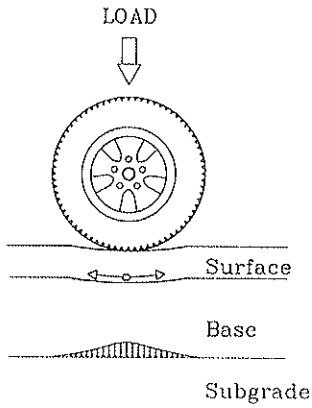

FIGURE 3 Primary structural responses that control pavement performance.

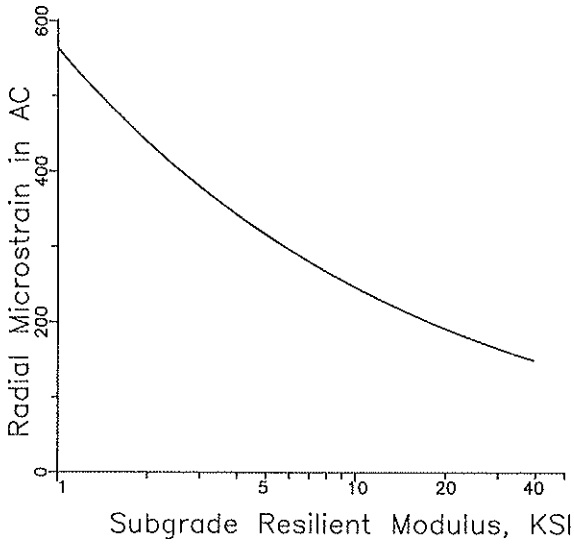

FIGURE 4 Effect of subgrade resilient modulus on asphalt radial strain.

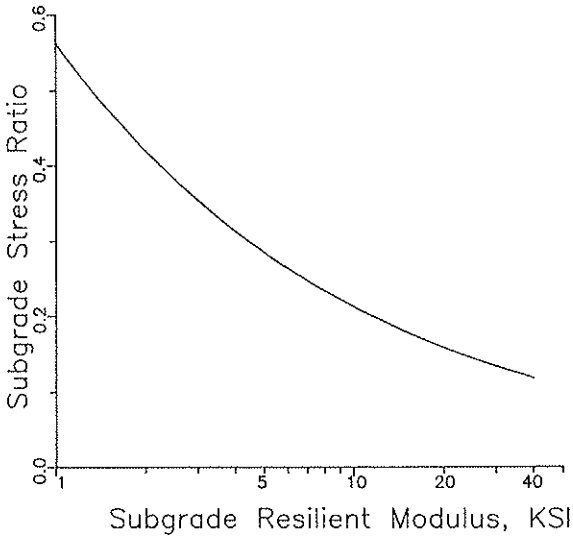

FIGURE 5 Effect of subgrade resilient modulus on subgrade stress ratio.

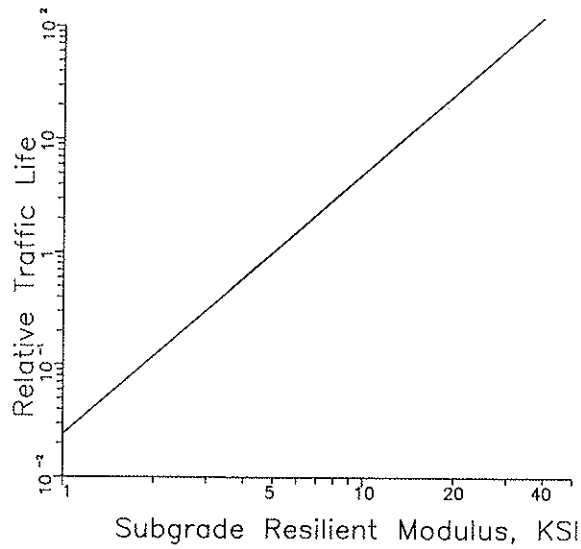

FIGURE 6 Effect of subgrade resilient modulus on relative traffic life.

EFFECT ON DESIGN BY AASHTO

Figures 6, 7, and 8 illustrate the effect of subgrade resilient modulus based on the 1986 AASHTO Guide.

Figure 6 is the relationship between resilient modulus and design traffic life. Relative traffic life is expressed as the total 18-kip equivalent single axle loads (ESALs) for any given resilient modulus divided by a base value. For this figure, the base value is the ESAL's for a resilient modulus of 5 ksi. For example, a pavement constructed on a subgrade having a resilient modulus of 10 ksi will carry nearly 5 times the traffic that the same pavement could carry if the resilient modulus were 5 ksi. Similarly, the 5-ksi soil would permit the pavement to carry approximately 8 times as much traffic as it could if built on a soil having a resilient modulus of 2 ksi.

Figure 7 shows the relationship between resilient modulus and the design structural number. For Figure 7, a structural

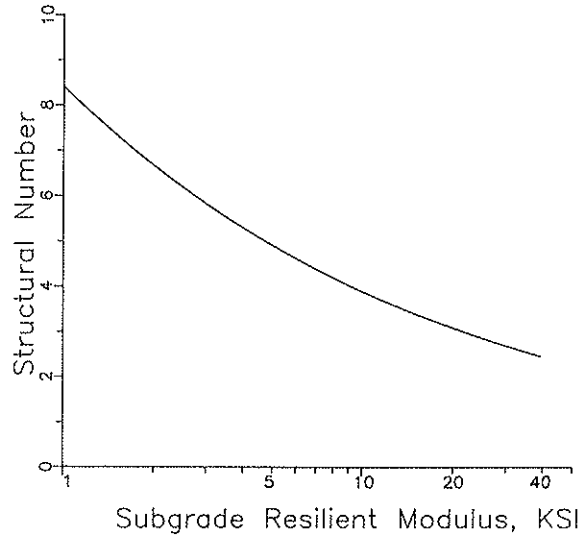

FIGURE 7 Effect of subgrade resilient modulus on design structural number.

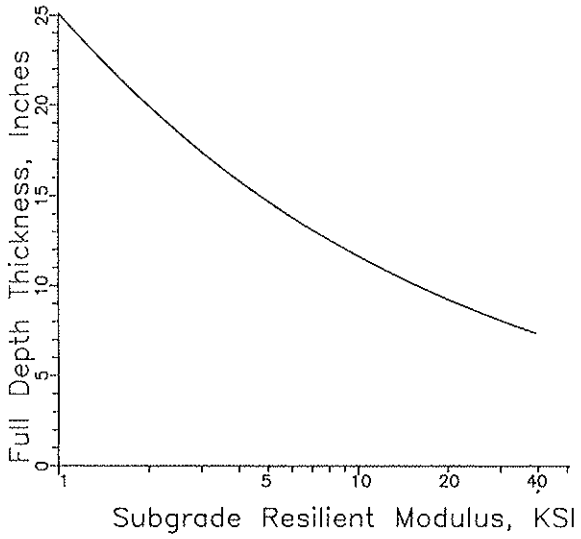

FIGURE 8 Effect of subgrade resilient modulus on design thickness.

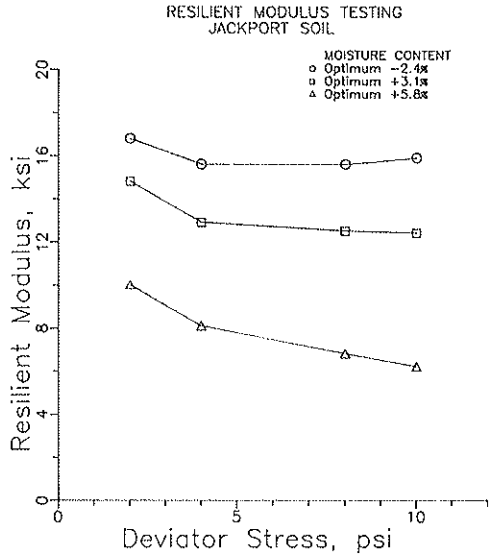

FIGURE 9 Effect of stress level and moisture content on the resilient modulus of a typical cohesive subgrade soil.

number of 5.0 was used with a resilient modulus of 5 ksi as the base. For the same traffic conditions, a structural number of 6.6 would be needed on a subgrade having a resilient modulus of 2 ksi. If the resilient modulus were 10 ksi, the required structural number would be 4.0.

Figure 8 was prepared to show the effects of resilient modulus on pavement thickness. The structural numbers from Figure 7 are converted to equivalent full-depth asphalt thicknesses. The conversion was made using structural layer coefficients of 0.44 and 0.30 for the AC surface and bituminous base, respectively; and assuming that the base thickness would be 3 times the surfacing thickness. For this example, the full-depth thickness would range from 20 to 15 to 12 inches for resilient moduli of 2, 5, and 10 ksi, respectively. In practical terms, figures 7 and 8 indicate that a 30 percent error in the resilient modulus will result in an error of 1 to 1.5 inches in selecting the appropriate total asphalt thickness.

SEASONAL VARIATIONS

Unfortunately, there is no simple test that will give the resilient modulus of a soil. In fact, the subgrade resilient modulus is not a single, fixed value. Rather, the resilient modulus changes due to a number of factors throughout the pavement's life.

There are several factors that affect the resilient modulus of a soil. Among these are moisture content, stress levels, and freeze-thaw cycles. Figure 9 illustrates the effects of stress level and moisture content on a typical cohesive soil. Of particular concern to the pavement designer is how these factors can influence the seasonal variation of the subgrade. A seasonal variation is to be expected because, in most areas of the country, roadbeds are softer in the spring than they are at other times of the year. This is demonstrated by the seasonal variation in pavement surface deflections. However, the seasonal variation is more pronounced for some soils than it is for others. This is shown by Figure 10, which is a plot of deflection test data from conventional flexible pavements in the vicinity of the AASHO Road Test.

Much of the variation in resilient modulus can be attributed to seasonal moisture changes. However, the springtime peak deflection commonly noted in northern states is also indicative of the effect of freeze-thaw. Figure 11 illustrates the dramatic reduction in resilient modulus following a single freeze-thaw cycle. Similar tests conducted on several Arkansas soils indicate that a resilient modulus reduction on the order of 50 percent can be expected as a result of freeze-thaw action.

SUBGRADE RESILIENT MODULUS SELECTION—AASHTO METHOD

Design by the AASHTO Guide requires the selection of an "Effective Roadbed Soil Resilient Modulus." Since the seasonal variation of resilient modulus is quite complex, the selection of a single resilient modulus value for use in design can be quite complex. The object, of course, is to select a single value that is representative of the entire year.

The 1986 Guide contains a specific recommended method for selecting the subgrade resilient modulus. It consists of estimating seasonal variations in resilient modulus and assigning relative damage factors on a monthly or bimonthly basis. The damage factors are summed and the average determined. The resilient modulus corresponding to the average damage factor is then used for design. The following steps are involved in selecting the subgrade resilient modulus.

Step 1. Develop a relationship between resilient modulus and subgrade moisture content. This involves conducting resilient modulus tests on the subgrade soil at various moisture contents representing the range of moisture variation expected. For example, using the resilient modulus for the 6-psi deviator stress data from Figure 9, a relationship between resilient modulus and moisture content is developed (Figure 12).

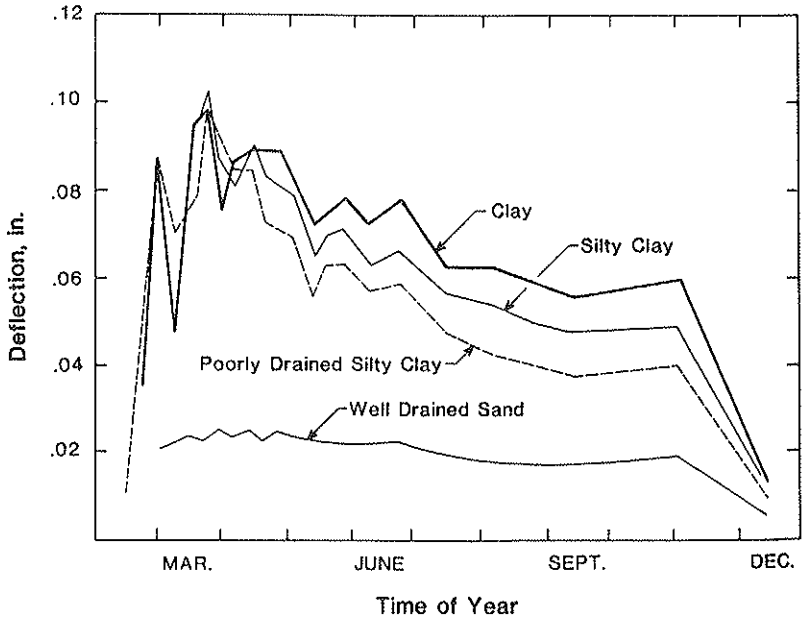

FIGURE 10 Seasonal variations in pavement deflections on various soils (data from Illinois Department of Transportation).

Step 2. Estimate the seasonal variation in moisture content. Although there is no standard approach for making this estimate, a practical approach might be to sample a similar subgrade. For this example it is assumed that moisture contents were determined four times during the year on a similar subgrade soil from a nearby pavement. From these a seasonal variation has been estimated as shown in Figure 13.

Step 3. Determine the monthly (or bimonthly) resilient modulus. Figures 12 and 13 are used to estimate the resilient modulus for each month of the year. The monthly values are entered on the AASHTO form (Figure 14). For example, the moisture content in March is about 25 percent. From Figure 12, the resilient modulus for 25 percent moisture content is 9,500 psi. Except for January and February, the resilient moduli for other months are found in a similar fashion. For January, it is assumed that the subgrade will be frozen resulting in a very high resilient modulus. February is assumed to be a period of thawing. To account for the freeze-thaw effect (Figure 11), the resilient modulus is determined in the normal fashion and reduced by 50 percent.

Step 4. Select a relative damage factor for each resilient modulus. Relative damage factors corresponding to the monthly resilient modulus values are selected using the scale on the right side of Figure 14. For the frozen subgrade (January), the resilient modulus would be high resulting in a low relative

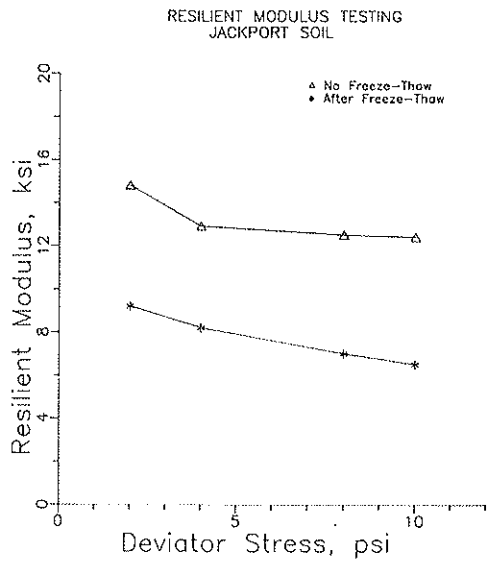

FIGURE 11 Effect of freeze-thaw on the resilient modulus of a typical cohesive subgrade soil.

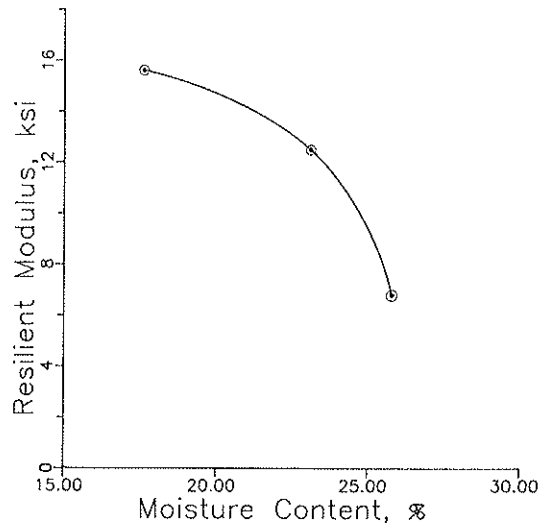

FIGURE 12 Moisture content-resilient modulus relationship for soil used in example.

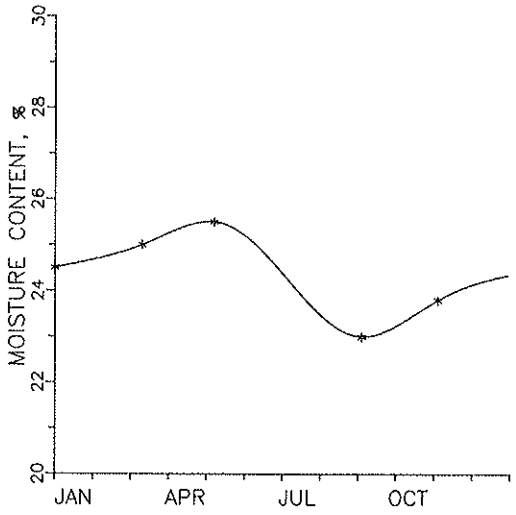

FIGURE 13 Seasonal moisture variation used in example.

damage factor. For practical purposes, a damage value of 0.0 is assigned.

Step 5. Use the average monthly relative damage factor to select the Effective Roadbed Soil Resilient Modulus. The average damage value (.063) is used with the scale on the right side of Figure 14 to select the Effective Roadbed Soil Resilient Modulus (9,900 psi) to be used in design.

ALTERNATIVE SELECTION APPROACH

The above method requires testing each soil at several different moisture contents. An alternative approach would be to test each soil at a single representative "time-of-year" moisture content. Elliott and Thompson (*12*) conducted an analysis to find the appropriate "time-of-year" condition that would be representative of the entire year for the AASHO Road Test pavements. The study included (a) an investigation of the seasonal variation of resilient modulus at the AASHO Road Test, and (b) a determination of the seasonal load dam-

Month	Roadbed Soil Modulus, M_R (psi)	Relative Damage, u_f
Jan.	30,000	.005
Feb.	5,500	.25
Mar.	9,500	.070
Apr.	8,900	.081
May	8,600	.088
June	11,000	.050
July	12,700	.038
Aug.	13,000	.034
Sept.	13,100	.033
Oct.	12,800	.035
Nov.	12,700	.036
Dec.	12,300	.038
Summation: Σu_f =		.758

Average: $\bar{u}_f = \frac{\Sigma u_f}{n} =$ .063

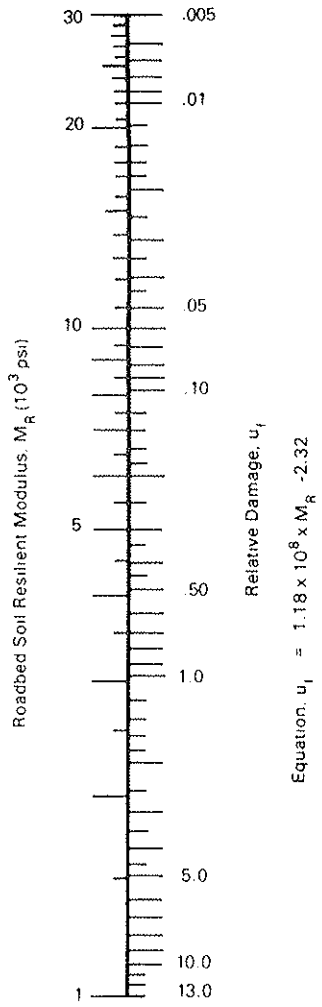

Effective Roadbed Soil Resilient Modulus, M_R (psi) = 9,900 (corresponds to $\bar{u}_f$)

FIGURE 14 Example determination of design resilient modulus by the AASHTO method.

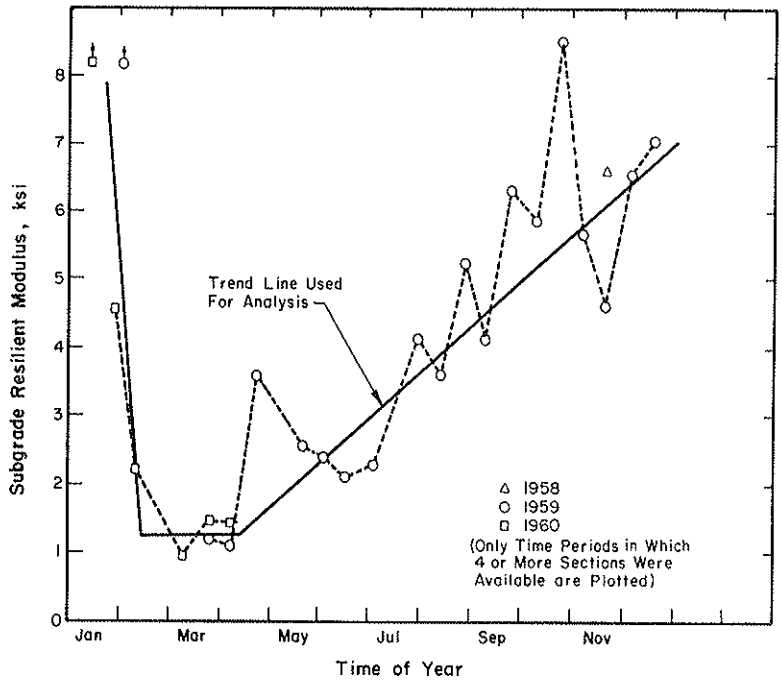

FIGURE 15 Seasonal subgrade resilient modulus variation at the AASHO Road Test (*12*).

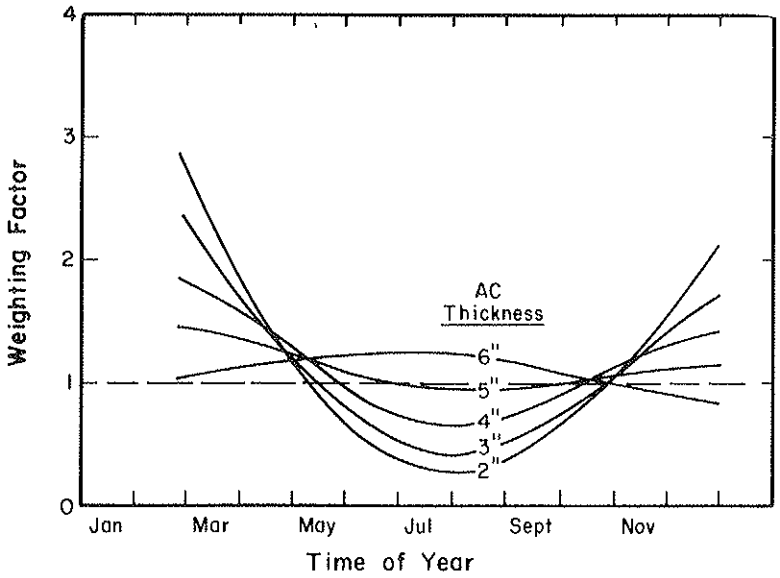

FIGURE 16 Seasonal weighting factors for various thicknesses of asphalt surfacing (*12*).

age effects for pavements with various thicknesses of asphalt. Their study was based on asphalt fatigue damage effects and included consideration of seasonal variation in the AC stiffness modulus as well as the subgrade resilient modulus.

The seasonal subgrade resilient modulus variation (based on analysis of deflection measurements taken during the AASHO Road Test) is shown on Figure 15. Figure 16 is the seasonal load damage effects expressed as a Weighting Factor. Elliott and Thompson concluded that no single resilient modulus could truly represent all pavement thicknesses. However, since all curves intersected in a fairly tight pattern in late April and mid-October, they stated that conditions during either of those periods should be acceptable for design purposes.

The disadvantage of using this alternative selection approach is the need to identify the representative "time-of-year" conditions. Limited analyses suggest that late spring conditions should be reasonable for most areas of the United States and probably no worse an approximation than the seasonal moisture variation estimate required by the AASHTO method. The advantage of this approach would be a significant reduction in the amount of testing needed for an individual soil

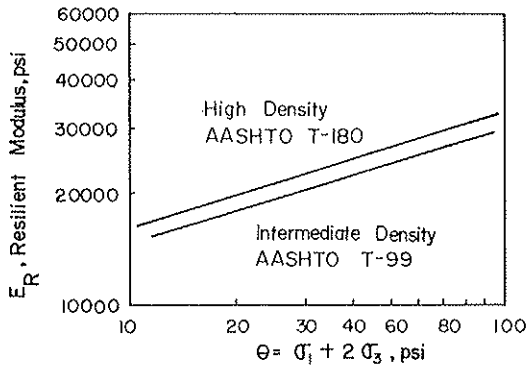

FIGURE 17 Effect of density on resilient modulus of a granular base material (*13*).

sample. This would permit testing more soils for the same testing effort.

RESILIENT MODULUS IN PERSPECTIVE

Resilient modulus is a significant and rational material property that needs to be included in the pavement design process. However, the resilient modulus does not represent all properties of a subgrade or granular layer that can affect the performance of a pavement.

The most direct evidence that other properties are also significant comes from the AASHO Road Test (*4*). Two granular materials were used—crushed stone and gravel. Of these, the gravel base sections deflected less. Inch for inch, the gravel was more effective in reducing the deflections. This suggests that the gravel possessed the higher resilient modulus. Nevertheless, the crushed stone sections had the superior performance. As stated in the Road Test report: "Perhaps the gravel possessed less internal stability than the stone; yet it may have been somewhat less resilient (i.e., higher resilient modulus)."

Similarly, Figure 17 indicates that density has only a limited effect on resilient modulus of a granular material. This could lead one to conclude that density is not significant. However, Figure 18 shows that density is quite significant relative to permanent deformation (strain).

Resilient modulus reflects only the rebound or resilient deformation behavior of the material. In so far as this relates to the load-induced stresses, strains, and deflections, resilient modulus is important and significant. However, the resilient modulus is not a good indicator of rutting potential. For many materials, the permanent deformation (rutting) behavior may well be the factor controlling pavement life. Therefore, resilient modulus must not be the only property considered in designing and selecting materials for a flexible pavement; layer coefficients based solely on resilient modulus can be misleading.

CONCLUSIONS

1. Resilient modulus is a fundamental material property. It relates to pavement design and performance for the same reason that surface deflection relates. It provides a measure of the load-induced stress-strain behavior of the soil and granular base layers which in turn governs the load response of the pavement system.
2. Resilient modulus should not be the only property considered in judging the acceptability of a soil or granular material. Because resilient modulus provides no measure of the permanent deformation (rutting) behavior, the selection of a granular material and assignment of layer coefficients based solely on resilient modulus can be misleading.
3. Many factors affect the resilient modulus causing it to vary seasonally throughout the life of the pavement. Conse-

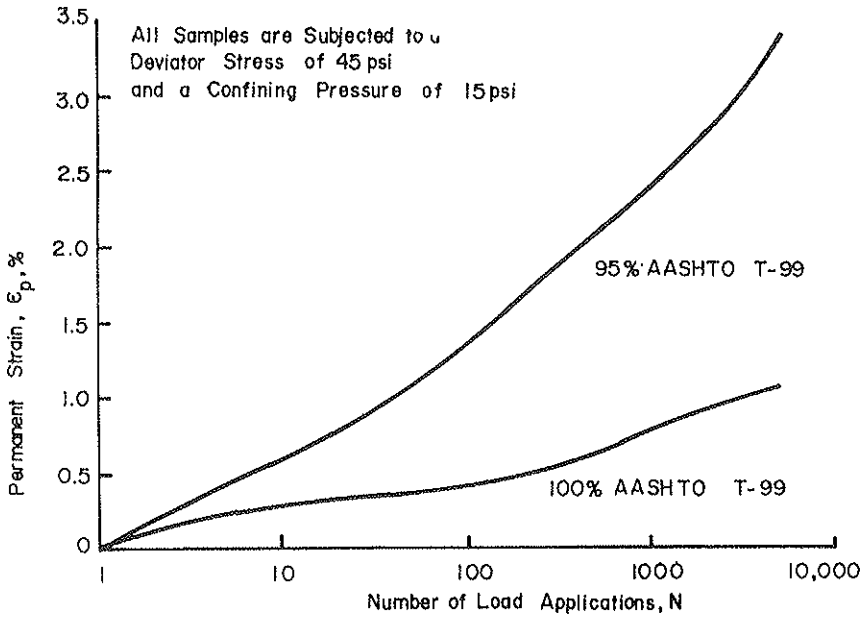

FIGURE 18 Effect of density on permanent deformation behavior of a granular base material (*13*).

quently, the selection of a single soil resilient modulus for use in design can be complicated.

4. While on paper the AASHTO Guide selection procedure is rational and straightforward, the estimation of seasonal moisture variation can be quite nebulous and the amount of testing required very time consuming. Consequently, a more practical approach is to test under a single, representative time-of-year condition. Late spring is a reasonable first approximation of the appropriate time of year for most of the United States.

ACKNOWLEDGMENTS

This paper is in part based on Project TRC-94, "Resilient Properties of Arkansas Soils," which is being conducted by the Arkansas Highway and Transportation Research Center. TRC-94 is sponsored by the Arkansas State Highway and Transportation Department and the U.S. Department of Transportation (Federal Highway Administration).

REFERENCES

1. *AASHTO Guide for Design of Pavement Structures*. American Association of State Highway and Transportation Officials, Washington, D.C., 1986.
2. *AASHO Interim Guide for Design of Pavement Structures*. American Association of State Highway Officials, Washington, D.C., 1972.
3. G. Langsner, T. S. Huff, and W. J. Liddle. Use of Road Test Findings by AASHO Design Committee. In *Special Report 73: The AASHO Road Test*, HRB, National Research Council, Washington, D.C., 1962, pp. 399–438.
4. *Special Report 61E—The AASHO Road Test, Report 5: Pavement Research*. HRB, National Research Council, Washington, D.C., 1962.
5. M. E. Burt. *Progress in Pavement Design*. TRRL Report LR 508. Transport and Road Research Laboratory, Department of the Environment, England, 1972.
6. Canadian Good Roads Association. Field Performance Studies of Flexible Pavements in Canada. *Proc., 2nd International Conference on the Structural Design of Asphalt Pavements*, Ann Arbor, Mich., 1967.
7. F. N. Hveem. Pavement Deflections and Fatigue Failures. *Bulletin 114*, HRB, National Research Council, Washington, D.C., 1955.
8. F. P. Nichols. Deflections as an Indicator of Flexible Pavement Performance. In *Highway Research Record 13*, HRB, National Research Council, Washington, D.C., 1963.
9. *Special Report 22: The WASHO Road Test, Part 2, Test Data, Analysis, Findings*. HRB, National Research Council, Washington, D.C., 1955.
10. R. I. Kingham. *Development of the Asphalt Institute's Deflection Method for Designing Asphalt Concrete Overlays for Asphalt Pavements*. Research Report 69-3, The Asphalt Institute, 1969.
11. M. R. Thompson and R. P. Elliott. ILLI-PAVE-Based Response Algorithms for Design of Conventional Flexible Pavements. In *Transportation Research Record 1043*, TRB, National Research Council, Washington, D.C., 1985.
12. R. P. Elliott and M. R. Thompson. ILLI-PAVE Mechanistic Analysis of AASHO Road Test Flexible Pavements. In *Transportation Research Record 1043*, TRB, National Research Council, Washington, D.C., 1985.
13. *Techniques for Pavement Rehabilitation*. National Highway Institute, FHWA, 1984.

Publication of this paper is sponsored by the Committee on Strength and Deformation Characteristics of Pavement.

Direct Calculation of Maximum Curvature and Strain in Asphalt Concrete Layers of Pavements from Load Deflection Basin Measurements

FRIEDRICH W. JUNG

Deflection measurements under impulse load carried out with the Falling Weight Deflectometer (FWD) are usually processed by using elastic layer analysis programs, back-calculating layer moduli from measured deflections, and then forward-computing critical performance parameters such as stresses and strains at locations under the load. Presented here is a direct, and more reliable way, of computing the important value of horizontal strain at the bottom of the asphaltic layer. The measured deflections from an FWD test, the radius of load distribution, and the thickness under the load are the only data needed to calculate, first, the curvature, and then, the strains in the top (asphaltic) layer of a pavement structure, in the center under the load. Corresponding stresses can also be calculated but additional information is needed, namely, the elastic stiffness of the first layer, Poisson's ratio, and the load-induced vertical stress. It is shown that strains and stresses in the immediate vicinity of the load position as computed with elastic layer analysis methods via back-calculated moduli are not as reliable as this new proposed strain criterion. At this time, the proposed new method of calculating strain directly is derived, presented, and discussed as a theory, without experimental field verification.

To determine the strength and predict the performance of asphalt pavements from some kind of deflection measurement has been the subject of major efforts in research for many years. The Falling Weight Deflectometer (FWD) test is only one of many methods to measure deflections of pavements; however, it is a very recent one and it is widely accepted in the U.S. The FWD test accurately measures a set of deflections of a deflection bowl under an impulse load of circular distribution, simulating the transient load of a passing wheel (*1, 2*). In this method there is a choice of several levels of impulse load, corresponding to variations in axle weight of actual vehicles. Deflections are measured at various distances from the load, including at the load axis itself. In operation, the test equipment is fast, economical, and very simple to use.

The state-of-the-art in processing data from FWD measurements is as follows. Asphalt concrete pavements with known layer thicknesses are analyzed by using a set of deflections measured along the wheel path, typically in the center underneath the circular loading plate and at six adjacent locations outside the plate, spaced over 1.5 to 2 m. These deflections (together with known layer thicknesses) are used to back-calculate the elastic stiffness (Young's modulus) of all pavement layers, including the subgrade, using certain computer programs for elastic layer analysis. Once the elastic stiffnesses are known, any stresses, strains, and deflections can be computed by the same or similar compatible programs in forward mode. This paper is concerned with the maximum horizontal strains and stresses in the first, usually asphaltic layer, of a multi-layered pavement structure. It is customary to regard strains or stresses at certain locations under wheel loads as critical. One of these locations is at the bottom of the asphaltic layer underneath the load, where horizontal stresses and/or strains are regarded as critical distress parameters, being related to fatigue strength (*3, 4*). In this context it can be shown that there is a more direct and simpler way to calculate the horizontal strains and stresses, which can supplement the aforementioned methods.

For reasons of pure geometry, the horizontal strains in any top layer of a pavement structure can be calculated directly from measured deflections, based on the theory of elastic plates, using the (partial) second derivatives or radii of curvatures directly obtained from the deflection basin. This basin is given by discrete values from the FWD testing. Through these points of measurement a suitable curve must be fitted. However, this approach is hampered by a lack of data points in the immediate vicinity of the load axis. The critical maximum curvature is underneath the load, and the difficulty is to find a sufficiently accurate value of it, representing the deflection basin in the center under the circular contact pressure area. From such a curvature value (and the given thickness) the strains in the asphalt layer can be calculated without knowing the modulus of elasticity or Poisson's ratio. The thickness of the asphaltic layer underneath the load must be known, but need not be so widely uniform as assumed in elastic layer analysis methods. In turn, corresponding stresses can be calculated from those strains, if additional information is available, such as vertical stresses, elastic modulus of the asphaltic layer, and Poisson's ratio.

Ministry of Transportation and Communications, Central Building, 1201 Wilson Avenue, Downsview, Ontario M3M 1J8, Canada.

STRESSES AND STRAINS FOR CIRCULARLY DISTRIBUTED LOADS

For such a single load, well inside a (non-cracked) pavement, the second derivative or curvature of the deflection basin under the load axis can be assumed to be a maximum, and equal in all directions because of the circular contact pressure area. The following equations apply:

Plate stiffness

$$K = \frac{EH^3}{12(1 - \mu^2)} \tag{1}$$

Bending moment

$$M = -KW''(1 + \mu) \tag{2}$$

Horizontal stress

$$S = 6M/H \tag{3}$$

Horizontal strain

$$e = S(1 - \mu)/E \tag{4}$$

where

K = bending stiffness of plate,
E = elastic stiffness of asphaltic layer(s),
H = (total) thickness of asphaltic layer(s),
μ = Poisson's ratio,
W = deflection as a function of distance,
W'' = second derivative of deflection at zero distance,
M = bending moment under the load at zero distance,
S = maximum stress at bottom of asphaltic layer, and
e = maximum strain at bottom of asphaltic layer.

Note: The second derivative is negative. Bending moments, stresses and strains are equal in all directions.

Without a knowledge of the material properties of the first layer (the modulus, E, and Poisson's ratio), the strain, e, can still be calculated from pure geometrical conditions:

either

$$e = W''H/2 \tag{5}$$

or

$$e = H/(2R) \tag{6}$$

The stress is then

$$S = eE/[(1 - \mu)(1 + S_v/S)] \tag{7}$$

where

R = radius of curvature in mm, and
S_v = vertical stress in MPa.

At this stage, in order to calculate corresponding stresses from strains, additional information is required, namely the elastic stiffness (E) of the first asphaltic or concrete layer, the Poisson's ratio of this layer, and the vertical stress (S_v) at the particular point. This vertical component of stress must be obtained by an elastic layer analysis program; however, a simple version based on equivalent layer thickness would be sufficient for an estimate of such stress.

The equations quoted above are based on the concept of regarding the asphaltic layer as an elastic plate. This plate, as a free body, deforms or deflects under two forces, the applied wheel load or falling weight impulse load acting more or less concentrated from above, and the corresponding reactions of soil pressure from the layers underneath, acting onto the plate from below in a more distributed fashion (Figure 1a). For a given load, the deflection bowl, its depth and largeness, depends on the stiffness of the plate and the relative stiffness or strength of the base or soil layers underneath.

Equations 5, 6, and 7 constitute a direct calculation of horizontal strain and stress in the A.C. layer. However—and this is the difficult part—it is now necessary to find an expression for the curvature or second derivative from an accurate deflection function.

CURVATURE CALCULATION INSIDE THE CONTACT PRESSURE AREA

The maximum value of the second derivative (W'') or curvature ($1/R$) of the asphaltic layer, for a circular, uniformly distributed load (p), is located in the center of this circular contact pressure area. The value, W'', can be derived in accordance with elastic plate theory. For the derivation, the following general assumptions should be noted:

1. Single tire loads and impulse loads from the FWD test are uniformly distributed over a circular area.
2. The resultant load per unit area on the circular part of the asphaltic layer "plate" has a paraboloidal distribution, for the following reason. Within the loaded area, from $-a$ to $+a$, the tire or plate contact pressure must be combined with the soil pressure acting from below, resulting in a reduced diagram of parabolically distributed load as shown in Figure 2. The resultant area load (i.e., load per unit area) on the asphaltic layer plate in this region is actually assumed to be distributed in the form of a square paraboloid. (The derivation of the exact solution for this case from the differential equation of circular plates is not presented here.) The result for maximum curvature is:

$$W''(0) = -\frac{2(Y_1 - Y_a)}{a^2} - \frac{a^2(8p_o + p_a)}{288K} \tag{8}$$

where

$W''(0)$ = second derivative in the center, in 1/mm;
Y_1 = maximum deflection in the center, in mm;
Y_a = deflection at the edge of the loaded area, in mm;
a = radius of the loaded area, in mm;
p = circular contact pressure from load, in MPa;
p_o = resultant pressure in the center, in MPa;
p_a = resultant pressure at the edge, at a, in MPa;
K = plate stiffness (Equation 1); and
r = distance from the center, in mm.

A better understanding of the curvature function or second derivative, W'', within the circular contact pressure area can be achieved by studying W'' as a function of distance, r:

$$W(0) = -\frac{2(Y_1 - Y_a)}{a^2} - \frac{p_o}{32K} \times (a^2 - 6r^2) - \frac{p_a - p_o}{288Ka^2}(a^4 - 15r^4) \tag{9}$$

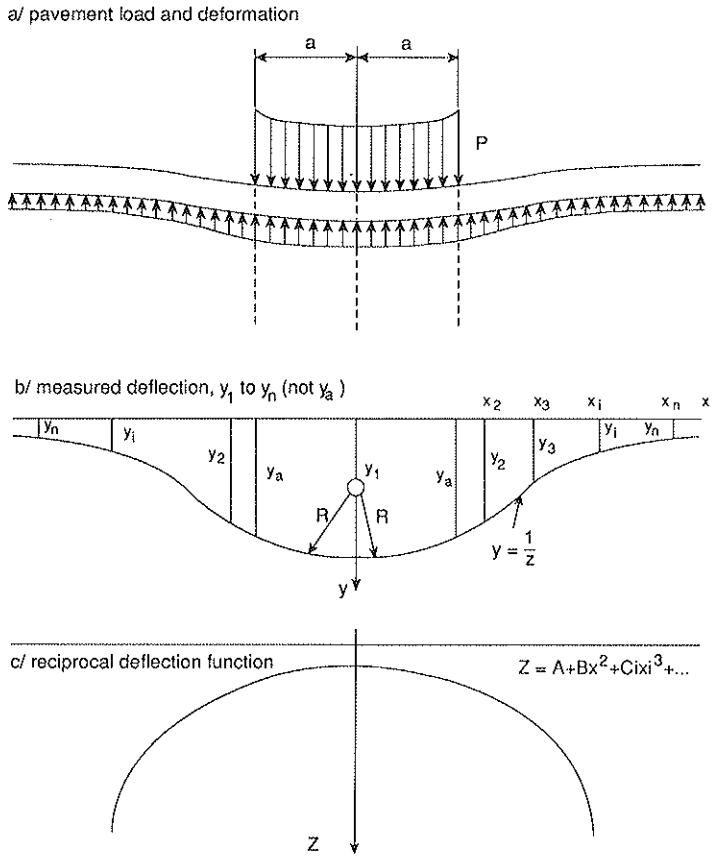

FIGURE 1 Deflection basin geometry.

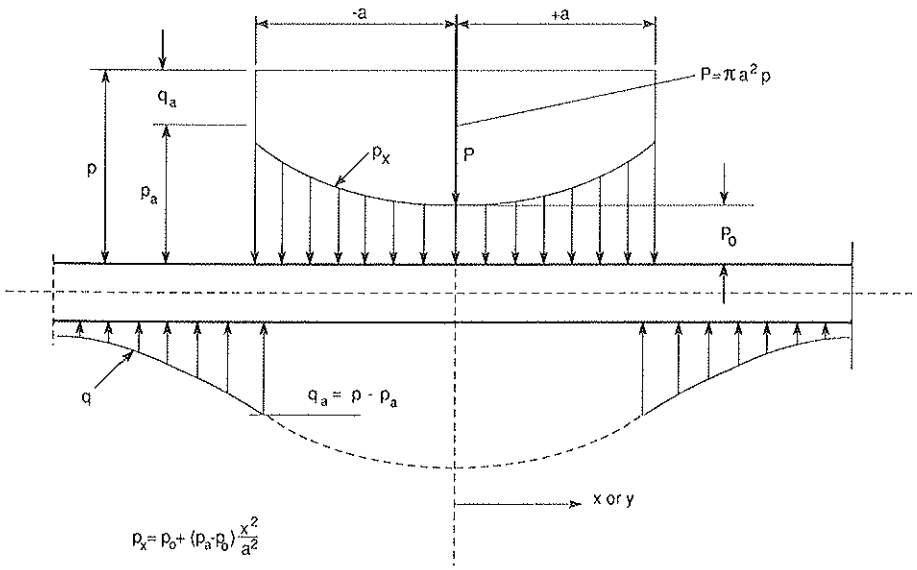

FIGURE 2 Load distribution between $-a$ and $+a$.

Equation 9 is plotted for a typical example as illustrated in Figure 3. Note, the maximum curvature is at $r = 0$, namely $5.422*10^{-6}$(1/mm). The first term of Equation 8, by itself, would lead to a value of $4.764*10^{-6}$ (1/mm), which can be interpreted as an average within a distance, r, of about 100 mm. This slightly lower value of average curvature agrees fairly well with values obtained from manual curvature calculations using simulated Chevron deflection output, as shown below. Thus, the first term of Equation 8 or 9 constitutes an approximate calculation of curvature compatible with elastic layer analysis programs, a smaller value than the actual maximum. This first term would be an exact solution for a hypo-

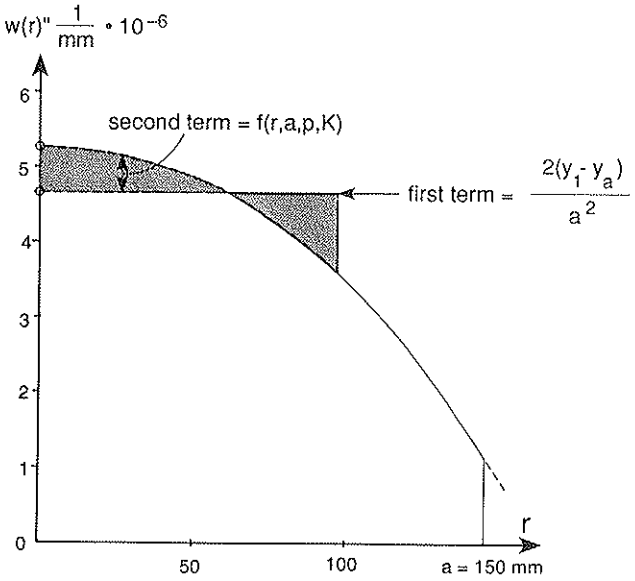

FIGURE 3 Radial curvature in the asphaltic layer.

thetical case in which the soil pressure, q, and the contact pressure, p, were removed, and the plate were loaded via a circular ring of radius, a.

Unfortunately the deflection, Y_a, cannot be measured, but must be calculated by interpolation using the other measured deflections. The ensuing error is positive, i.e., in the direction of higher values, being closer to the theoretical maximum (tables 1 and 2). Further, the deflection basin consists of two different parts, i.e., of two curves not continuous in all derivatives. The inner part ($-a$ to $+a$) has been accurately derived, resulting in Equation 9. The outer part only is empirically given by the measurements of outside sensors.

The curve-fitting function chosen is a reciprocal polynomial (Z) (Figure 1). It is used only to calculate the very influential and important value of the deflection, Y_a, at the edge of the loaded area (i.e., at $x = a$) by interpolation.

The curve-fitting and interpolation procedure to compute an approximate substitute for the theoretical value of Y_a becomes more reliable, thus leading to less erratic results, when the first outside sensor (Y_2) is as close to the circular disk as possible and when the center point deflection is included as part of the curve (as illustrated in Figure 1b and 1c), in

TABLE 1 COMPARISON OF STRAIN R WITH CHEVRON/ELSYM5

DESCRIPTION	CURVATURES * 10^{-6} 1/mm		STRAIN * 10^{-6}		
	DIRECT	ELSYM5/ CHEVRON	DIRECT	ELSYM5/CHEVRON bottom	average
Typical 3-layer case a = 150 mm, H = 100 mm	-5.160	-4.80	258.0	170.4	193
Typical 4-layer case a = 150 mm, H = 100 mm	-5.426	-5.28	271.3	185.7	255
Overload case, 2.5x a = 150 mm, H = 100 mm	-14.46	-13.8	642.6	423.0	520
Deep strength 140 mm on weak soil	-4.334	-4.53	302.7	278.2	278
Reduced area a = 102 mm high pressure 400 psi	-26.97	-26.75	1198.9	786.4	860
Wider area, a=203 mm normal pressure	-8.753	-8.66	389.0	243.2	341
Typical 3-layer case average deflection	-5.066	-5.18	253.3	208.2	204
Very soft layer inserted under asphalt	-8.438	-8.74	421.9	383.8	385

Note: In the last column, "average" means the average of the absolute value of the top and bottom strains of the first layer from the output listing of CHEVRON or ELSYM5. These values in the last column ought to be close to or equal to H/2 times the curvature values in the second column. This identity check would establish consistency within the CHEVRON or ELSYM5 programs themselves, not involving the STRAINR model. Note that the check fails except in the case of a very soft inserted layer in the last line.

TABLE 2 CURVATURE BY SECOND DIFFERENCES VERSUS EQUATION 8

CASE (see also Table 1)	SECOND DIFFERENCES [1/mm]*10^{-6}	EQUATION 8 [1/mm]*10^{-6}
1/ Typical 3-layer case	-4.80	-5.475
2/ 4-layer case, example	-5.28	-6.018
3/ Overload case, 2.5 x	-13.78	-15.535
4/ Deep strength, weak soil	-4.53	-4.603
5/ Reduced area, high pr.	-26.75	-28.931
6/ Wide area, normal pr.	-8.66	-9.722
7/ 3-layer case, av. defl.	-5.182	-5.562
8/ Soft 2nd layer inserted	-8.744	-8.875

spite of the fact that it belongs to the inner part which is mathematically different. Nevertheless, a useful solution has been established which has been verified as follows:

The first term of both Equations 8 and 9, using the accurate value of Y_a, leads to practically the same curvatures as obtained by using the method of second differences, for the same data from Chevron or ELSYM5 simulation examples.

Comparative computations show that the exact calculation of curvature by Equation 8 results in larger values (up to 15 percent) than the second differences from Chevron or ELSYM5. These results from second differences compare much better with the first term of Equations 8 or 9, omitting the second term. Thus there is a valid argument to dispense with this term which requires additional information about the asphaltic layer. Thus, the following Equation 10 can be used to calculate the minimum radius of curvature, R:

$$R = -\frac{(Y_1 - Y_a)^2 + a^2}{2(Y_1 - Y_a)} \tag{10}$$

where

Y_1 = maximum deflection in the center, in mm;
Y_a = deflection at the edge of the load disk, in mm;
a = radius of the circular loading area, in mm; and
R = radius of curvature, in mm.

Note that the first term in the numerator is very small and can be set to zero; then $1/R$ becomes exactly the first term of the second derivative, W'', in Equations 8 and 9.

A small computer program can be written to calculate curvatures and strains of the asphaltic layer, based on Equation 10, using a substitute value of Y_a found by interpolation of the deflection basin function shown in Figure 1, which is curve-fitted from relevant FWD measurements.

Alternatively, one can take into account the second term of Equation 9. This solution could ultimately be useful in conjunction with a simplified elastic layer analysis program based on Odemark, using the concept of equivalent layer thickness.

EXAMPLE

The following example illustrates one of the verification tests of the proposed method, comparing the new proposed calculations (based on Equation 11) with those from a corresponding case calculated by the Chevron program. For running the small program of the proposed method, calculated Chevron deflections were selected as input, simulating feasibly-spaced FWD measurements, in the center and at four other points outside the circular load area. In addition to these measurements, the following data are needed to run the new program:

Radius of load area: $a = 150$ mm; layer thickness: $H = 100$ mm

The deflections chosen from the Chevron example output, used as simulated input into the new program, are as follows:

at 0.0 m 0.4903 mm

at 0.2 m 0.3951 mm

at 0.3 m 0.3394 mm

at 0.4 m 0.2949 mm

at 0.5 m 0.2585 mm

The following values were calculated by the proposed method:

Deflection at the edge of the loaded area: $Y = 0.4293$ mm (the actual Chevron value is 0.4305, an inevitable error in curve-fitting and interpolation)
Radius of curvature at the center: $R = -184.3$ m
Second derivative at center: $W'' = -5.43 * 10^{-6}$ (1/mm)
Strain at bottom of asphaltic layer: $e = +271 * 10^{-6}$

More information was needed to run the Chevron program, namely:

Load: 40.01 kN, tire pressure: 566.00 kPa, load radius: 150 mm
Layer values:

(1) Modulus: 3000 MPa, Poisson's ratio: 0.35, Thickness: 100 mm
(2) Modulus: 500 MPa, Poisson's ratio: 0.35, Thickness: 200 mm
(3) Modulus: 80 MPa, Poisson's ratio: 0.35, Thickness: infinite

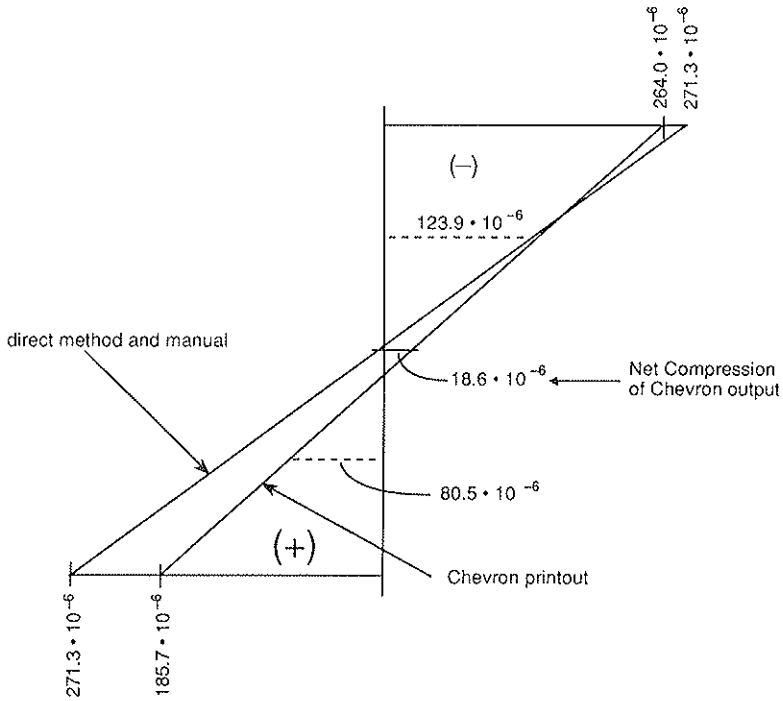

FIGURE 4 Comparison of strain calculation (Chevron example).

Note: (1) = surface course, (2) = base course, (3) = subgrade.

Using these input values for the Chevron program, the deflections were calculated every 50 mm. Then the finite difference method was used to manually compute the second derivatives between $X = 0$ and 150 mm.

The results fluctuate somewhat inconsistently, and the average was found to be -5.37, with a slightly smaller value at $X = 0$ of -5.28. This compares fairly well with the computed value of -5.43 of the output listed above, being slightly larger and therefore closer to the theoretical maximum.

Figure 4 shows a comparison of the corresponding strain calculations. The strain diagram from the direct Chevron printout is slightly curved at the top; it also exhibits a small net compressive strain. The strains of the direct output ($+185.7 * 10^{-6}$ and $-246.0 * 10^{-6}$) are smaller, especially at the bottom (+), and the steeper slope of this strain diagram seems to be inconsistent with the second derivative, manually computed from the same output (-5.37). At least the slope of the printed-out strain diagram of Chevron should concur with the manually calculated curvature from the same printout (calculated by second differences).

With the strain calculated in the printout above, the stress at the bottom of the asphalt layer can be computed by means of Equation 7. Setting $S = 0$, the result would be:

$$S = 0.000271 * 3000/0.65 = 1.25 \text{ MPa (tensile stress)}$$

The vertical stress, S, under the load is not zero but rather is negative, a fraction of the vertical contact pressure. Let us estimate the ratio of Sv/S to be -0.5; the value of the last term in the bracket of Equation 7 is then reduced to $0.5 * 0.35 = 0.175$, and the factor $e * E$ must be divided by 0.825 instead of 0.65. The result is:

$$S = 0.000271 * 3000/0.825 = 0.99 \text{ MPa}$$

The corresponding value printed out from Chevron is only $S = 0.6975$ MPa

The example illustrates that curvatures or second derivatives ($1/R$ or W'') can be calculated with great confidence and sufficient accuracy. The strain computed either as $e = W'' * H/2$, or as $e = H/2R$ is certainly more reliable than the inconsistent output of the Chevron program. The stress, on the other hand, is dependent not only on layer material constants (E and μ), but also on the vertical stress component, which can be significant in the vicinity of the applied load.

Note: In the last column of Table 1, "average" means the average of the absolute value of the top and bottom strains of the first layer from the output listing of Chevron or ELSYM5. These values in the last column ought to be close to or equal to $H/2$ times the curvature values in the second column. This identity check would establish consistency within the Chevron or ELSYM5 programs themselves, not involving the new direct method. Note that the check fails except in the case of a very soft inserted layer (Table 1).

TESTING OF THE PROPOSED NEW METHOD

Many different cases have been calculated by the Chevron or the ELSYM5 program to verify the new proposed method. The results are listed in Tables 1 and 2. In both tables curvatures were first calculated manually from densely spaced deflection printouts from selected cases computed by elastic layer analysis (Chevron or ELSYM5). The second differences of the deflections were divided by the square of the selected space increments (50 or 25 mm). These manually calculated curvature values are listed under "Chevron/ELSYM5" in Table 1, and under "second differences" in Table 2. Then, another set of deflection printouts was selected in order to simulate FWD measurements, namely the deflection in the center and

some deflections outside the circular disk. These were used to calculate curvatures in accordance with Equation 10 for Table 1, and Equation 8 for Table 2. The second term of Equation 8 required the use of further printout values of vertical pressures.

With regard to Table 1, it should be noted that there is a fair agreement between manually calculated curvatures and those calculated by the proposed direct method, listed under "direct". However, the horizontal strains at the bottom of the asphaltic layer do not agree (Table 1, second and third column from the right). Naturally, agreement cannot be expected because the elastic layer analysis programs assume full friction between the asphaltic and granular base layer, whereas the proposed direct method assumes zero friction. However, the slopes of the deflection diagrams ought to agree, concordant with the agreement in curvature.

In order to test this, the last column of Table 1 contains the average of the absolute values of strains from top and bottom, printed out by Chevron or ELSYM5. It shows improvement, but most of these average strains from printouts are still too low. It seems that the elastic layer analysis programs suffer from the phenomenon of quasi-singularity, which results in underestimating the maximum horizontal strain in the first top layer. The assumption of full friction aggravates the situation. The assumption of zero friction in the proposed direct method may not be quite correct either, however, it may still be closer to reality to overestimate the tensile strain in this way because it may counteract neglecting the second term in Equation 8. With regard to Table 2, for the region under the distributed load, from $-a$ to $+a$, the curvature or second derivative has been independently derived by solving the differential equation of elastic circular plates, resulting in Equations 8 and 9. Using Equation 8, we can calculate maximum curvatures and compare them with corresponding results from using the second differences of the deflections printed out by Chevron or ELSYM5. Eight cases, the same as in Table 1, have been calculated and compared in this way, and are listed in Table 2. The comparison shows that the manual calculations of curvature from printouts fall short of the theoretical maxima. This proves the advantage of assuming zero friction in the proposed direct method.

The curvatures calculated by Equation 9 are higher, and the corresponding strains are again higher than the ones printed out by Chevron or ELSYM5.

These verification tests reveal that loads on pavements, distributed over a relatively small circular area, constitute a point of quasi-singularity of the asphaltic "plate." This is the main reason why elastic layer analysis programs cannot catch the true maxima of strain and curvature and why they compute horizontal strains and stresses under the load axis (close to the load) too low.

Better results might be expected by finite element techniques with densely spaced grids around the contact pressure area.

CONCLUSIONS AND RECOMMENDATIONS

For single loads on asphalt pavements, which can be assumed to be distributed over a circular area, the curvature of the asphaltic layer and the horizontal strain at the bottom of this layer can be calculated directly from some measured values of the deflection basin near the center. Other values needed are the radius of the contact pressure area, and the thickness of the asphaltic layer at the load position. Because no other information is needed (about layer materials and thicknesses of lower base layers), the horizontal strain calculated in this particular way is a very potent parameter for pavement design.

The bottom strain in the asphalt layer so calculated is larger than the strain from elastic layer analysis, where full friction between asphaltic and granular layers is assumed, which causes tensile stresses at the top of the granular base.

Contrary to the proposed calculation of strain (based on pure geometry), the corresponding horizontal stresses are affected by the usual uncertainties of determining material parameters such as elastic stiffness, and Poisson's ratio.

The direct calculation of curvature and strain by this new approach has been verified against more detailed computations and output from Chevron or ELSYM5 programs. The second derivatives of the deflections in the center, the maximum curvatures, were found to agree fairly well, but the corresponding printed-out strains were found to be inconsistent with Chevron's or ELSYM5's own deflections and curvatures. The slopes of printed-out strain diagrams from Chevron and ELSYM5 did not concur (as they should have) with the manually computed curvatures from the same runs of the programs; thus, the maximum horizontal strains were much too low. The new method has also been verified through an independently derived formula, based on a solution of the differential equation of elastic plates for the region under the circular load. The variability or function of curvature within the loaded area has been studied and discussed: Chevron and ELSYM5 deflection print-outs, via second differences, seem to closely approximate an average curvature between the maximum value at the load axis and the much lower value at a distance from the axis about equal to the layer thickness. This average curvature is somewhat smaller than the maximum curvature in the center, but sufficiently close to it (Figure 3).

Since the strain parameter is generally conceived to be correlated to the fatigue strength of asphaltic pavement layers, routinely processing data from Falling Weight Deflectometer tests by this new strain criterion is recommended, in addition to other current FWD processing methods.

There is as yet no immediate verification by field experiments of the new method proposed here. Theoretical derivation within an accepted theory of structural analysis and comparison with elastic layer analysis methods can only go so far. Thus carrying out experiments with various sizes of FWD disks and various types and sizes of tires which may not have exactly circular contact pressure areas is suggested. Can we use an equivalent radius for noncircular pressure areas, and what would that radius be? Can we use a similar approach for dual tires? If field experiments should prove too "rough" with respect to quality control, this might be an area for laboratory tests.

REFERENCES

1. O. Tholen. Falling Weight Deflectometer—A Device for Bearing Capacity Measurement: Properties and Performance. *Department of Highway Engineering Bulletin*, Vol. 1, 1980, The Royal Institute of Technology, Stockholm.
2. B. E. Sebaaly, et al. Dynamic Analysis of Falling Weight

Deflectometer Data. In *Transportation Research Record 1070*, TRB, National Research Council, Washington D.C., 1986.
3. J. B. Rauhut, et al. *Pavement Damage Functions for Cost Allocation*. Report FWHA/RD-84/019. FHWA, U.S. Department of Transportation, 1984 Vol. 2, Chapter 3.
4. R. B. Kulkarni, et al. Use of Falling Weight Deflectometer Data in Predicting Fatigue Cracking. In *Transportation Research Record 1070*, TRB, National Research Council, Washington, D.C., 1986.

Publication of this paper sponsored by Committee on Strength and Deformation Characteristics of Pavement.

Determination of Pavement Layer Thicknesses and Moduli by SASW Method

SOHEIL NAZARIAN, KENNETH H. STOKOE II, ROBERT C. BRIGGS, AND RICHARD ROGERS

Nondestructive tests are being used more than ever in evaluating the integrity of existing pavement systems. The nondestructive tests can be divided into two main categories: (1) deflection-based methods, in which devices such as the Falling Weight Deflectometer (FWD) and dynaflect are used, and (2) wave propagation methods such as the Spectral-Analysis-of-Surface-Waves (SASW) method. The SASW method has several significant advantages over deflection-based methods. One advantage is that moduli of thin pavement layers in the upper portion of the pavement system can be easily and accurately measured. A second advantage is that variations in moduli within different layers, especially in the lower portions of the base and in the subgrade, can be evaluated. This feature is particularly beneficial when bedrock is close to surface. A third advantage is that layering in the pavement system does not have to be known. In fact, the thickness of the layers can be determined as illustrated in the modulus profiles presented in the paper. A series of tests was performed at nine flexible pavement sections with significantly different profiles to evaluate the accuracy of layer thickness determination by the SASW method. The thicknesses of the asphaltic-concrete surface layer varied between 1 and 5 inches. The base and subbase materials consisted of substantially different materials. No information regarding the types or thicknesses of the layers was provided during data collection or reduction. Only after the results were reported to the Texas State Highway Department were the pavement profiles known. It was found that the SASW method predicted the thicknesses of the layers quite closely. In addition, moduli determined by the SASW method were compared with moduli back-calculated from FWD tests performed at the same sites. The variation in moduli of similar materials used at different sections exhibit somewhat less scatter when obtained from SASW tests. However similar trends were found with both methods.

The Spectral-Analysis-of-Surface-Waves (SASW) method is a field seismic method for determining moduli and thicknesses of pavement systems. As with any in situ method, limitations in terms of accuracy in the final modulus profiles should be understood. The sources of these limitations can be varied. For instance, limitations can result from--

- The degree of sensitivity of the parameter being measured to the moduli,
- The amount of simplification introduced in the theoretical model used for data reduction,
- The degree to which the field data collection deviates from the assumptions made in developing the theoretical model,
- Inevitable scatter in the data collected in the field, and
- Any dependency of the method on personnel skills in data collection and/or reduction.

To better understand the limitations of the SASW method, a series of theoretical, parametric, and sensitivity studies, as well as extensive field investigations, have been conducted at The University of Texas during the last several years. This paper presents the results of one of the field studies.

The SASW method was used at nine sites at the Pavement Test Facility of Texas A&M University in Bryan, Texas, in March 1986. The primary objective of the tests was to evaluate the effectiveness of the SASW method in determining the thicknesses of various layers of different materials comprising the pavement systems. A secondary objective was to study moduli variations in similar materials at carefully controlled pavement sites. The results are reported herein, along with brief background information on the SASW method and an explanation of the procedures and data analyses. In addition, moduli obtained from FWD tests performed on the same sections are included for comparison purposes.

It should be noted that no information pertaining to the types of materials or thicknesses of the layers was provided at the time of testing or data reduction (except for Site 7). The material profiles reported herein were provided after Young's modulus profiles of the different sites were reported to the Texas State Department of Highways and Public Transportation.

SPECTRAL-ANALYSIS-OF-SURFACE-WAVES TESTING

General Background

The Spectral-Analysis-of-Surface-Waves (SASW) method is a method of seismic testing developed for determining small-strain Young's modulus profiles at pavement sites and small-strain shear modulus profiles at soil sites (*1, 2*). The SASW method is a nondestructive method in which both the source and receivers are located on the pavement surface. The source is simply a transient vertical impact that generates surface waves of various frequencies, which the medium transmits. Two vertical receivers, located on the surface, monitor the

S. Nazarian, Department of Civil Engineering, The University of Texas, El Paso, Tex. K. H. Stokoe, II, Geotechnical Engineering, The University of Texas, Austin, Tex. R. C. Briggs and R. Rogers, Pavement Management Section, Texas Department of Highways and Public Transportation.

propagation of surface wave energy past them. By analysis of the phase information of the cross power spectrum for each frequency determined between the two receivers, phase velocity, shear wave velocity, and elastic moduli are determined.

The terms elastic or small-strain are generally used to describe moduli evaluated by SASW testing. These terms are used (or their use is implied) because stress waves generated in this type of seismic testing create strains in the medium that are less than 0.001 percent. Moduli measured at these strain levels are essentially constant and, hence, independent of strain amplitude (*3, 4*). Therefore, the medium being tested behaves like an elastic material. This low stress level also allows for truly nondestructive testing.

Two key points in SASW testing are the generation of primarily first-mode surface wave energy and the measurement of surface waves (Rayleigh waves) at significant distances from the source. Rayleigh wave velocity, V_R, is constant in a homogeneous half-space and independent of the frequency. Each frequency, f, has a corresponding wavelength, L_R, according to:

$$V_R = fL_R \tag{1}$$

Rayleigh wave and shear wave velocities are related by Poisson's ratio. In an isotropic elastic half-space, the ratio of Rayleigh-wave-to-shear-wave velocity increases as Poisson's ratio increases. This ratio varies from 0.90 to 0.96 for values of Poisson's ratio ranging from 0.15 (concrete) to 0.5 (saturated subgrade).

If the stiffness of a site varies with depth, then the velocity of the Rayleigh wave (R-wave) will vary with frequency. The variation of R-wave velocity with frequency (wavelength) is called dispersion. The dispersive characteristic of surface waves is the key to the SASW method. A plot of surface wave velocity versus wavelength is called a dispersion curve. The dispersion curve is developed from phase information of the cross power spectrum. This information provides the relative phase between two signals (two-channel recorder) at each frequency in the range of frequencies excited in the SASW test. For a travel time equal to one period of the wave, the phase difference is 360 degrees. Thus, for each frequency the travel time between receivers can be calculated by

$$t(f) = \phi(f)/(360f) \tag{2}$$

where:

f = frequency,
$t(f)$ = travel time for a given frequency, and
$\phi(f)$ = phase difference in degrees for a given frequency

The distance between the receivers, D, is a known parameter. Therefore, R-wave velocity at a given frequency, $V_R(f)$, is simply calculated by

$$V_R(f) = D/t(f) \tag{3}$$

and the corresponding wavelength of the R-wave is equal to

$$L_R(f) = V_R(f))/f \tag{4}$$

By repeating the procedure outlined by equations 2 through 4 for every frequency, the R-wave velocity corresponding to each wavelength is evaluated, and the dispersion curve is determined. Several studies have been performed recently to evaluate the optimum source/receiver array. The general array

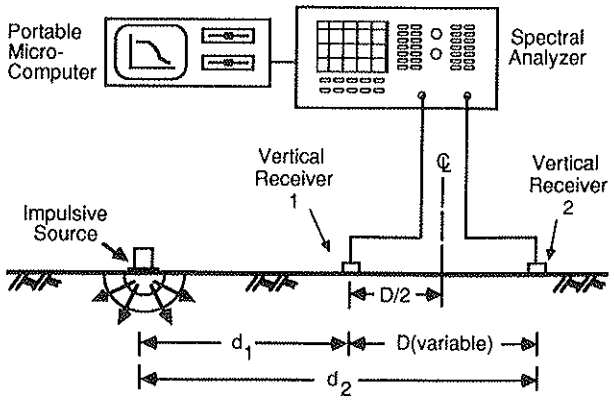

FIGURE 1 General configuration of SASW testing.

configuration is shown in figure 1. The distances are expressed as follows: source to near receiver = d_1, source to far receiver = d_2, and receiver to receiver = D. Analytical studies by Sanchez-Salinero (*5*) show that a desirable array configuration can be expressed as:

$$d_2/d_1 = 2 \tag{5}$$

Sheu et al. (*6*) combined experimental studies on pavements with the analytical work of Sanchez-Salinero (*5*) to determine the range of wavelengths that can be accurately obtained with a fixed source/receiver spacing. They found that for an array with $d_2/d_1 = 2$ the distance between receivers can be related to useable wavelengths as

$$L_R < 3D \tag{6}$$

As the velocities of different layers are unknown before testing, it is difficult to know if the limit expressed in equation 6 is satisfied. Practically speaking, it is more appropriate to test with various distances between the receivers in the field and then evaluate the range of wavelengths over which reliable measurements were made. The procedure is to select a spacing between receivers, perform the test, and reduce the data to determine the wavelengths and associated velocities. The next step is to eliminate the points that do not satisfy equation 6.

Rayleigh wave velocities determined by this method are not actual velocities of the layer, but apparent R-wave velocities (known as phase velocities). Existence of a layer with high or low velocity at the surface of the medium affects measurement of the velocities of the underlying layers. Therefore, a method for distinguishing shear-wave velocities from phase velocities is necessary in SASW testing.

Inversion of the dispersion curve, or (in short) inversion, is the procedure of determining the shear-wave velocity profile from the dispersion curve. Inversion consists of determination of the depth of each layer and the actual shear-wave velocity of each layer from the apparent R-wave velocity versus wavelength information.

The inversion process used herein is based on a modified version of Thomson's (*7*) and Haskell's (*8*) matrix solution for elastic surface waves in a layered solid media. To simplify the process of inversion, some assumptions were made. These assumptions include—

- The layers are horizontal,

- The velocity of each layer is constant, and
- The layers are homogeneous and linearly elastic.

The inversion process is an iterative process in which a shear-wave velocity profile is assumed and a theoretical dispersion curve is constructed. The experimental and theoretical dispersion curves are compared and necessary changes are made in the assumed shear-wave velocity profile until the two curves (experimental and theoretical dispersion curves) match within a reasonable tolerance.

Once the shear-wave velocities are determined, the following formulae are used to calculate shear and Young's moduli:

$$G = \rho V_s^2 \tag{7}$$

and

$$E = 2G(1 + \nu) \tag{8}$$

where

G = shear modulus
E = Young's modulus
ρ = mass density and
ν = Poisson's ratio

As mentioned earlier, moduli obtained in this manner are the elastic, or small-strain, moduli. A methodology to account for non-linear behavior of moduli obtained for different layers utilizing the SASW method is suggested by Nazarian et al. (*9*). This methodology is the same as that employed in geotechnical earthquake engineering where small-strain moduli evaluated by in situ seismic tests are adjusted to values appropriate for large-strain earthquake excitation by combining (linear) field and (nonlinear) laboratory moduli.

Field Procedure

The general configuration of the source, receivers, and recording equipment is shown in figure 1. Accelerometers were used as receivers for close receiver spacings ($\leq$4 feet), and geophones with a natural frequency of 4.5 Hz were used as receivers for greater spacings. This was done to optimize recording of the wave passage; that is, accelerometers produce more output at closer receiver spacings where high frequencies are present, while geophones produce more output at larger receiver spacings where low-frequency *R*-waves are excited.

The common receivers midpoint (CRMP) geometry (*10*) was used for testing. With this geometry the two receivers were each moved an equal distance away from an imaginary center line between the receivers, and the source was moved so that the distance between the source and near receiver was equal to or greater than the distance between the two receivers. In addition, the location of the source was reversed for each receiver spacing so that forward and reverse profiles were run. This testing sequence is illustrated in figure 2. Distances between receivers of 0.5, 1, 2, 4, and 8 feet were used at each site.

Different sources were used. For close receiver spacings, a 4-oz hammer was used. For greater distances, 2.5- and 5-lb sledge hammers were employed, with the largest hammer generally used at the 8-ft spacing.

The recording device was a Hewlett-Packard 3562A Fourier spectral analyzer. This analyzer is a digital oscilloscope combined with a micro-processor that can perform directly in either the time or the frequency domain.

It is worthwhile noting here that the field procedure outlined above results in the performance of essentially two tests, one for the forward profile and one for the reverse profile. The results (in terms of dispersion curves) are typically very close, so that an average dispersion curve is calculated from the forward and reverse tests. One can think of this type of testing as a 1-test run at each site for the SASW method. However, the SASW method is very repeatable at the same site, with typically less than a five percent scatter among three or more tests (*6, 11*). Therefore, duplicate SASW tests were not performed in this study.

PRESENTATION OF RESULTS

Description of Sites

The general layout of the pavement test facility constructed at Texas A&M University in the mid-1960s is shown in figure 3. This facility, which is 460-ft long and 50-ft wide, consists

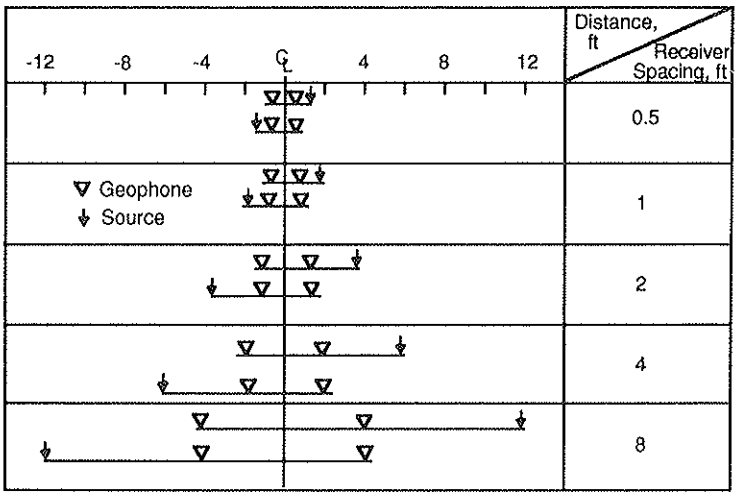

FIGURE 2 Schematic of experimental arrangement for SASW tests.

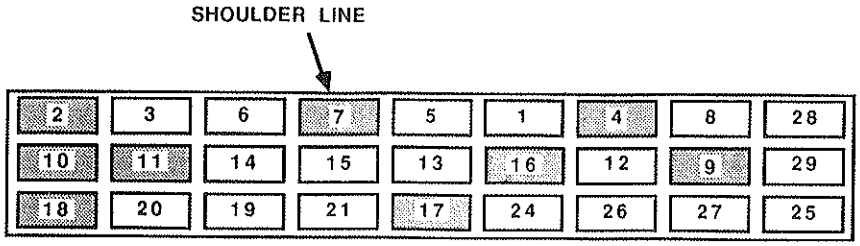

SASW Tests were Performed at the Nine Highlighted Sections (Nos. 2, 4, 7, 9, 10, 11, 16, 17 and 18).

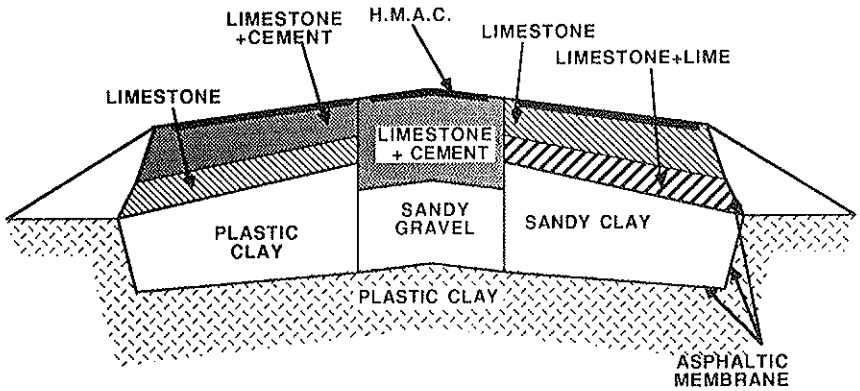

FIGURE 3 General layout of pavement test facility at Texas Transportation Institute.

TABLE 1 MATERIAL PROFILES OF TTI PAVEMENT TEST FACILITY (*12*)

Section	Thickness (in.)				Material Type			
	Surface	Base	Subbase	Embank.	Surface	Base	Subbase	Embank.
2	1	12	4	36	AC	LS+C	LS	PC
4	5	12	12	24	AC	LS+C	LS	PC
7	1	4	12	36	AC	LS	LS+C	PC
9	5	4	4	40	AC	LS	LS	GR
10	1	12	4	36	AC	LS	LS	GR
11	1	4	12	36	AC	LS	LS	GR
16	5	12	12	24	AC	LS+C	LS+C	GR
17	3	8	8	34	AC	LS+L	LS+L	SC
18	1	8	8	36	AC	LS+L	LS+L	SC

AC: Hot Mix Asphaltic Concrete
LS+C: Crushed Limestone mixed with 4% Cement
LS+L: Crushed Limestone mixed with 2% Lime
LS: Crushed Limestone
GR: Sandy Gravel
SC: Sandy Clay
PC: Plastic Clay

of 27 different pavement sections. Each section is approximately 40-ft long and 12-ft wide. Some of the sections in the facility do not represent typical pavement sections encountered on roads, since the main function of the facility was to determine the limitations and versatility of nondestructive testing methods.

Nine randomly selected sections were tested in March 1986. The nine sections are marked in figure 3. Material profiles of all sections, as reported by Scrivner and Michalak (*12*), are included in table 1. The top layer is always asphaltic-concrete pavement. Base and subbase materials are either crushed limestone or a mixture of crushed limestone with lime or

TABLE 2 ENGINEERING PROPERTIES OF MATERIALS USED IN CONSTRUCTION OF TTI PAVEMENT FACILITY (*12*)

Description	Abbreviation Used In Table 1	AASHO Class	Unified Soil Class	Texas Triaxial Class	Compressive Strength (psi)*
Plastic Clay	PC	A-7-6(20)	CH	5.0	22
Sandy Clay	SC	A-2-6(1)	SC	4.0	40
Sandy Gravel	GR	A-1-6	SW	3.6	43
Crushed Limestone	LS	A-1-a	GS-GM	1.7	165
Crushed Limestone + 2% Lime	LS+L	A-1-a	GW-GM	1.0	430
Crushed Limestone + 4% Cement	LS+C	A-1-a	GW-GM	1.0	2270
Hot Mix Asphalt Concrete	AC				

*By Texas triaxial procedure at a lateral pressure of 5 psi

Note: The natural material below the embankments was plastic clay similar to that described above, changing to a denser clay at a depth of about 90 inches below the surface of the pavement. The dense clay is abbreviated DC; its properties were not determined in the laboratory.

cement. Subgrade materials consist of three different sands or clays. Engineering properties of each material determined by laboratory tests are given in table 2.

Dispersion Curves

Typical dispersion curves from SASW testing at two of the nine sites (Sites 4 and 11) are shown in figures 4 and 5. (These curves represent the average values for the forward and reverse profiles at each site.) Spectral analysis functions measured at these sites are not presented for the sake of brevity. Typical functions can be found in Nazarian and Stokoe (*2*). However, the quality of the data collected in the field was very good.

Shear-Wave Velocities

Typical shear-wave velocity profiles after inversion of the dispersion curves are given in tables 3 and 4 for sites 4 and 11,

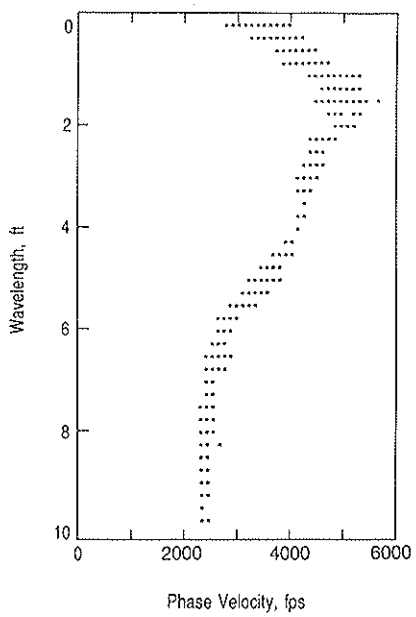

FIGURE 4 Dispersion curve from SASW tests at section 4.

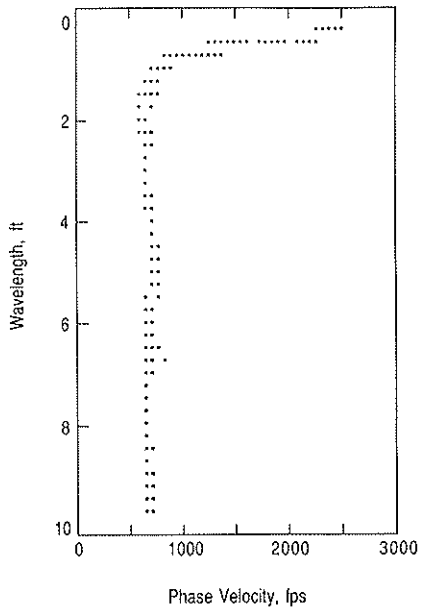

FIGURE 5 Dispersion curve from SASW tests at section 11.

TABLE 3 VARIATION OF SHEAR-WAVE VELOCITY AND YOUNG'S MODULUS WITH DEPTH AT SECTION 4

Layer Number	Layer Thickness	Layer Depth[1]	Shear Wave Velocity	Young's Modulus	Assumed Poisson's Ratio	Assumed Total Unit Weight
	in.	in.	fps	ksi		pcf
1	1.20	0.60	2239	337.9	0.25	125
2	1.20	1.80	2239	337.9	0.25	125
3	1.20	3.00	2239	337.9	0.25	125
4	1.20	4.20	2508	421.2	0.15	135
5	1.20	5.40	6261	2625.0	0.15	135
6	1.20	6.60	7115	3390.0	0.15	135
7	2.40	8.40	7115	3390.0	0.15	135
8	2.40	10.80	7115	3390.0	0.15	135
9	2.40	13.20	7115	3390.0	0.15	135
10	2.40	15.60	7043	3322.0	0.15	135
11	2.40	18.00	3005	604.7	0.15	135
12	2.40	20.40	2757	509.1	0.15	135
13	4.80	24.00	2757	509.1	0.15	135
14	4.80	28.80	2757	509.1	0.15	135
15	4.80	33.60	1366	125.8	0.25	125
16	4.80	38.40	1335	120.1	0.25	125
17	4.80	43.20	1333	119.8	0.25	125
18	4.80	48.00	977	60.4	0.33	110
19	H-S	H-S[2]	718	32.6	0.33	110

[1] Depth to the midheight of the layer
[2] Denotes Half-Space

TABLE 4 VARIATION OF SHEAR-WAVE VELOCITY AND YOUNG'S MODULUS WITH DEPTH AT SECTION 11

Layer Number	Layer Thickness	Layer Depth[1]	Shear Wave Velocity	Young's Modulus	Assumed Poisson's Ratio	Assumed Total Unit Weight
	in.	in.	fps	ksi		pcf
1	1.20	0.60	3005	604.7	0.25	125
2	1.20	1.80	1589	170.2	0.25	125
3	1.20	3.00	732	33.9	0.33	110
4	1.20	4.20	715	32.3	0.33	110
5	1.20	5.40	688	29.9	0.33	110
6	1.20	6.60	677	29.0	0.33	110
7	2.40	8.40	713	32.2	0.33	110
8	2.40	10.80	708	31.7	0.33	110
9	2.40	13.20	708	31.7	0.33	110
10	2.40	15.60	714	32.3	0.33	110
11	2.40	18.00	733	34.0	0.33	110
12	2.40	20.40	612	23.7	0.33	110
13	4.80	24.00	612	23.7	0.33	110
14	4.80	28.80	612	23.7	0.33	110
15	4.80	33.60	660	27.6	0.33	110
16	4.80	38.40	582	21.4	0.33	110
17	4.80	43.20	582	21.4	0.33	110
18	4.80	48.00	660	27.6	0.33	110
19	H-S	H-S[2]	687	29.9	0.33	110

[1] Depth to the midheight of the layer
[2] Denotes Half-Space

respectively. Nineteen layers were used in the inversion process for each site. The thicknesses of the layers ranged from about 1 inch (near the surface) to about 5 inches for subgrade material. To simplify data reduction, the same profiles of thicknesses were used at all sites as follows: six 0.1-ft-thick layers, underlain by six layers each 0.2-ft thick, underlain by six 0.4-ft-thick layers, and a final layer that was assumed to extend to infinity. The more refined the layering selected in inversion, the better determined are the thicknesses of different layers. Also, if only a few layers are assumed (say 3 or 4), it may be impossible to match the theoretical and experimental dispersion curves.

For each site the inversion process consisted of the following steps:

1. The experimental dispersion curve based on the field data was obtained.
2. This experimental dispersion curve was compared with the ones from the previous sites and

- If a similar dispersion curve could be found, the shear-wave velocity profile from that site was used as the starting point to invert the shear-wave velocity profile of the present site;
- Otherwise, a rough inversion using a five-layer system was first performed after which that profile was again inverted using the refined 19-layer system described above.

In the rough inversion process, values of Poisson's ratio and total unit weight of 0.33 and 110 pcf were assumed for all layers. Mis-estimations of Poisson's ratio and total unit weight have minimal effects on the shear-wave velocities obtained by the inversion process (*11*). However, for the final inversion, the values of Poisson's ratio and total unit weight were modified, based on the shear-wave velocity as shown below (except for the asphaltic-concrete top layer where Poisson's ratio and total unit weights of 0.25 and 125 pcf were used, respectively):

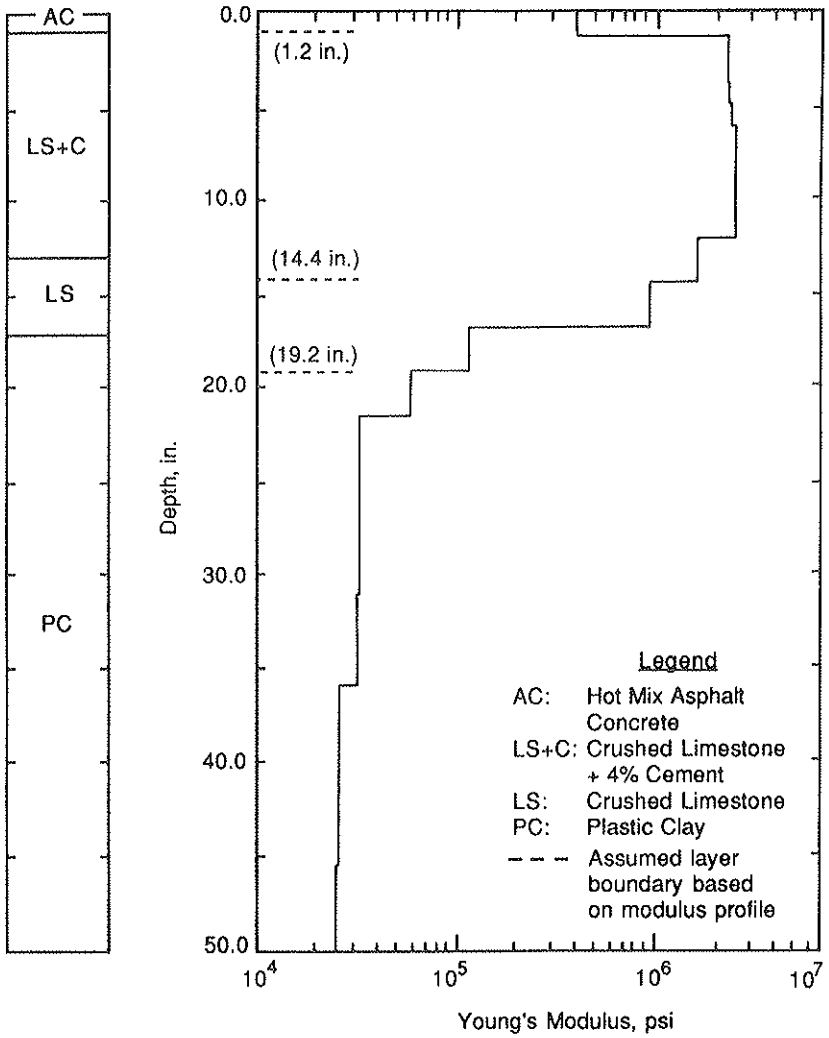

FIGURE 6 Composite profile of section 2.

Shear Wave Velocity (fps)	*Poisson's Ratio*	*Total Unit Weight (pcf)*
<1000	0.33	110
>1000 and <2500	0.25	125
>2500 (except for AC)	0.15	135

The reason for categorizing total unit weight and Poisson's ratio was that no insight into the nature of the materials at each site was given to the first two authors at the time of data reduction. Based on previous experience with pavement materials, these values of Poisson's ratio and total unit weight seem most reasonably associated with the different materials divided upon the basis of material stiffness (wave velocity).

The material profile of Site 7 was known during data reduction because of initiation of a cooperative project on that section between the time data were collected and the modulus profile was reported.

Young's Modulus

Based on the shear-wave velocity profiles, Young's moduli at different depths were calculated utilizing equations 7 and 8. The resulting Young's modulus profiles are presented in figures 6 through 14. The total unit weights used in determining Young's moduli are reported in the above table.

DISCUSSION OF RESULTS

SASW Tests

Although the primary intent of this study is to evaluate the sensitivity of the SASW method in determining layer thicknesses, it is interesting and informative to begin by looking at the range in values of moduli determined for similar mate-

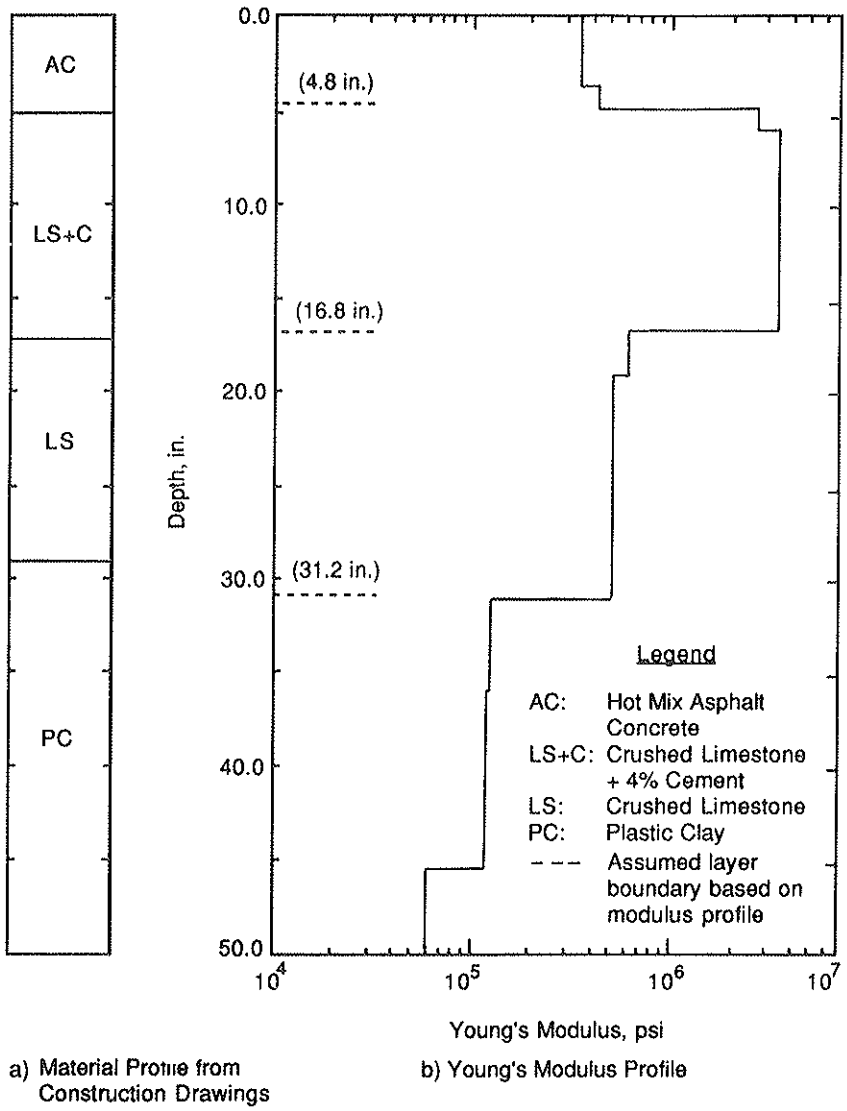

FIGURE 7 Composite profile of section 4.

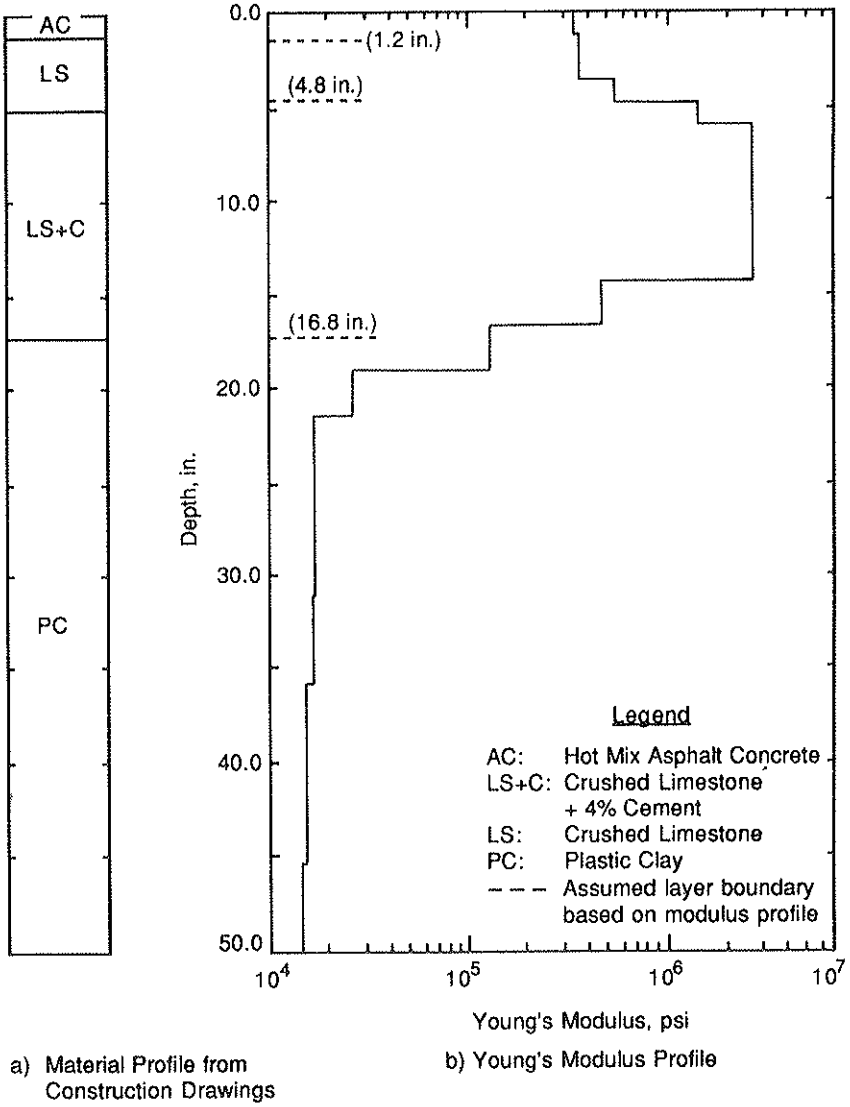

FIGURE 8 Composite profile of section 7 (material profile was known before inversion).

rials at the nine sites. To simplify this comparison, only average values of moduli near the center of each layer are used. These average modulus values are summarized in table 5.

The modulus of the AC layer ranges from 338 to 1,392 ksi which seems to be a rather large range. However, if Site 9 is deleted from this comparison, the modulus ranges from 338 to 605 ksi, a very reasonable range. The value of the modulus of the AC layer at Site 9 seems unusually high, but additional testing reconfirmed this value. The reason or reasons for this high value are unknown. The results do point out, however, the range in modulus, which can occur even under the carefully controlled conditions at this test facility.

Ranges in moduli for the base, subbase, and subgrade materials are as follows:

Crushed Limestone: 32–509 ksi
Crushed Limestone + 4% Cement: 2500–3390 ksi
Crushed Limestone + 2% Lime: 1200–1340 ksi
Sandy Gravel: 25–33 ksi
Sandy Clay 50–51 ksi
Plastic Clay: 17–34 ksi

Except for the plain crushed limestone base and the sandy clay subgrade, these materials all exhibit reasonable values and ranges in values, with ranges in moduli on the order of two or less. The sandy clay exhibits rather high moduli which are still possible based on the authors' experience. On the other hand, the range in modulus for the limestone base seems too large. The LS base exhibits a very low modulus at Site 9, as if the base did not exist. On the other hand, the limestone base exhibits very high modulus values at Sites 4 and 7. The reason(s) for these low and high modulus values of the LS base is unknown. It is hoped that some of the sites can be cored to determine the precise materials and profiles in the near future.

Prediction of layer thicknesses from the modulus profiles

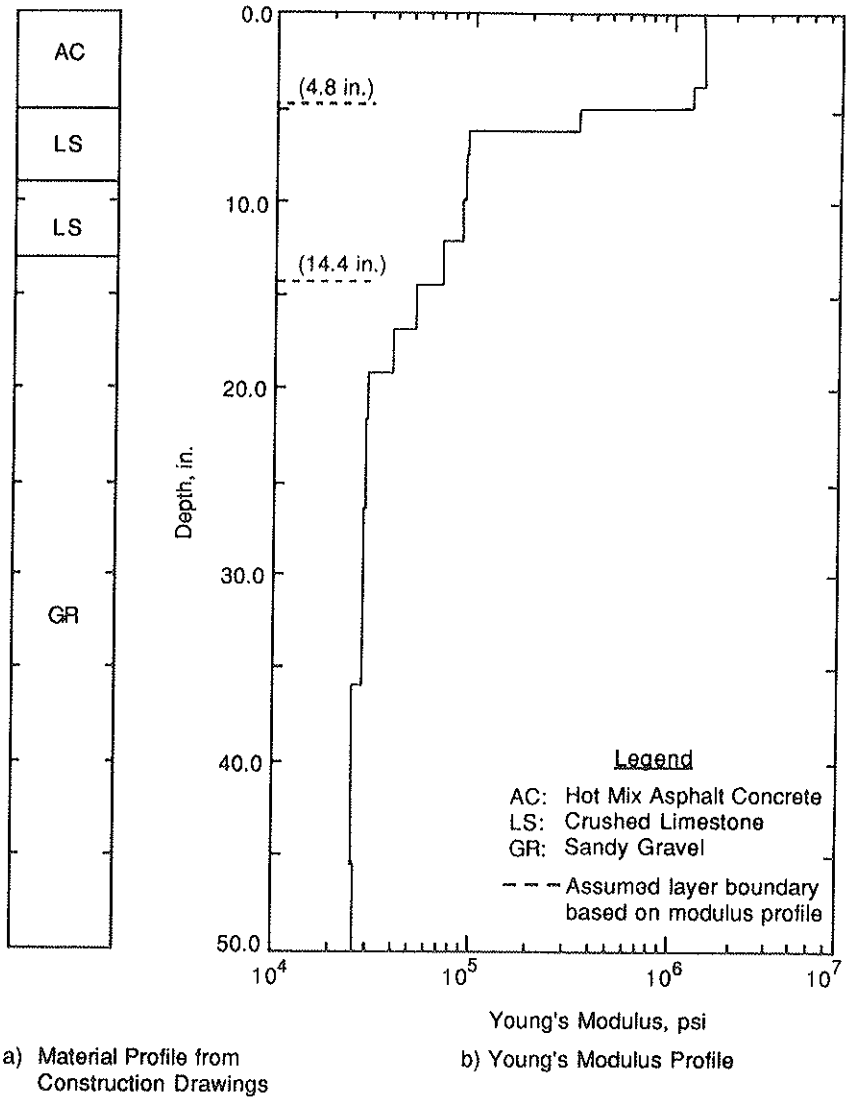

FIGURE 9 Composite profile of section 9.

is quite good at these sites, as summarized in table 6. Depths where the boundaries of different layers were selected are marked on the corresponding Young's modulus profiles presented in figures 6 through 14.

At six sections (Sections 9, 10, 11, 16, 17 and 18) the base layers are subdivided into two sublayers of similar materials simply because of the experimental design procedure employed to determine material types and thicknesses of different layers at each section [see Scrivner and Michalak (*12*)]. These six sections represent nothing but two-layer pavement systems.

It can be seen in figures 6 through 14 that when the base and/or subbase materials are lime or cement stabilized, determination of thicknesses is quite straightforward because of abrupt changes in the modulus profiles as shown at Sites 4, 16 and 17. However, for other types of base and subbase materials, a transition zone occurs in the modulus profile at layer boundaries which complicates definition of the layer boundaries (such as Site 2 at 19.2-in and Site 9 at 14.4-in). Intuitively, occurrence of this transition zone is logical because of possible mixing or intrusion of materials on different sides of the boundaries.

One important point when estimating layer thicknesses from modulus profiles is that when the stiffness of two adjacent layers is quite similar, it is not possible to distinguish between these two layers. A good example of this result is the profile of Site 7 where the stiffness of the AC and LS layers is very similar down to a depth of about 5 inches. It is not possible to identify the thickness of the AC layer at this site. From a pavement design standpoint, however, the AC and LS layers will act as one 5-in thick layer with a modulus of about 360 ksi.

The following specific comments can be made about the various profiles:

- At Sites 2, 4, 9, 16 and 17, the thicknesses of the layers estimated from the SASW modulus profiles agree closely with the thicknesses described in the construction drawings. The AC layer thickness is within 0.2 inch, and the base layer

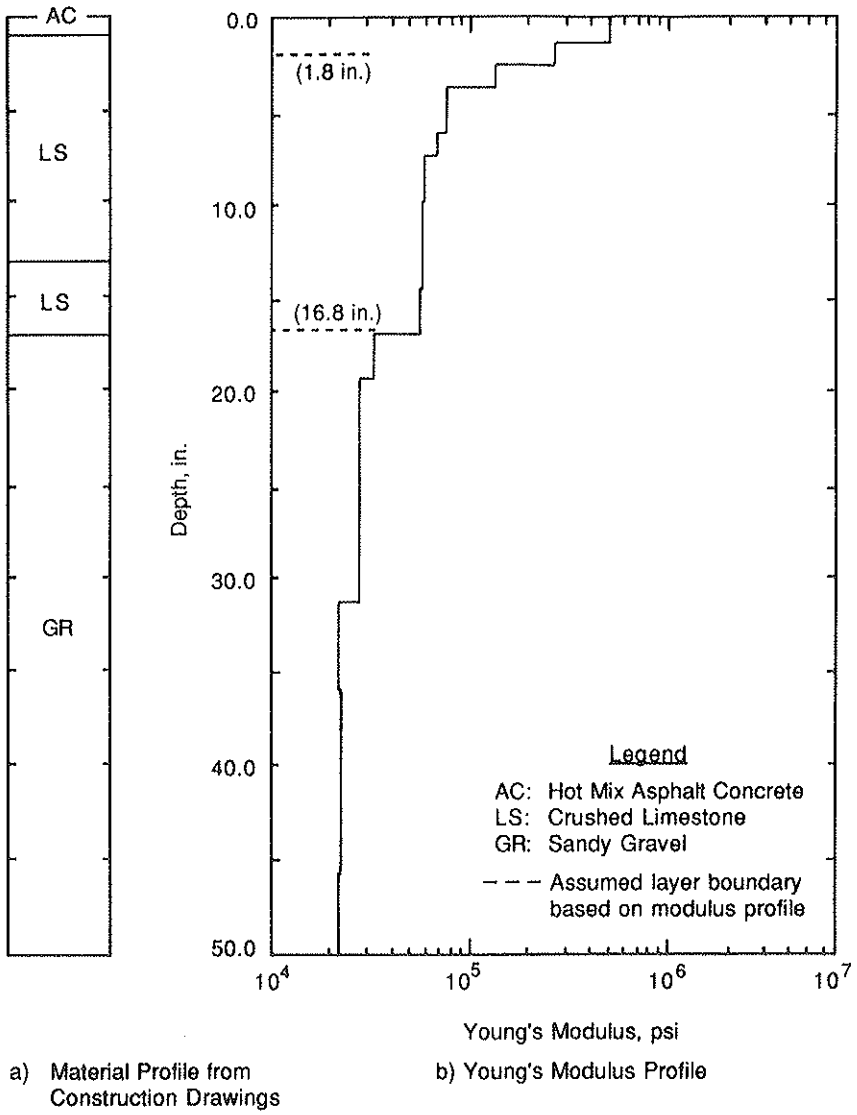

FIGURE 10 Composite profile of section 10.

thickness is generally within about one inch. There is, however, a gradual transition area in the subbase and subgrade layers. These can be due to a gradual change in the property of the subgrade-subbase interface.

- The layer thicknesses at Site 7 were known in advance. However, a transition zone between the subbase and subgrade is detected in the SASW tests, which was unknown but seems possible.
- At Site 9, the modulus of the base layer (LS) is less than similar materials at Sites 4 and 7 and is more similar to the base layer at Sites 2 and 10.
- It seems that the crushed limestone used as a base has a low modulus at Site 10. Once again, a transition zone between the AC and base layers is evident at Site 10. This transition zone seems quite reasonable and thus (probably) represents the actual profile.
- Site 11 has been reported to have an identical profile to Site 10. The SASW profile shows that the layering is quite close for the two sites, but the crushed limestone base at Site 11 is much less stiff than at Site 10. (This matter is also reflected in FWD deflections from the two sites (see table 7). As a result, the depth of the bottom of the base at Site 11 is less well defined than at Site 10. Those sites show that it becomes difficult to select boundaries whenever stiffness contrasts between layers is less than about a factor of 2.
- At Site 18 the boundary of base and subgrade is predicted quite well. However, the boundary between the asphalt and the base layer indicates a gradual change in stiffness, which may or may not exist in the actual profile.

Falling Weight Deflectometer Tests

On the same day that the SASW tests were carried out, deflection data were collected using the FWD device. At each section, one FWD test was performed at a nominal load of 9 kips. (Other nominal loads were also applied but were not considered in this study.)

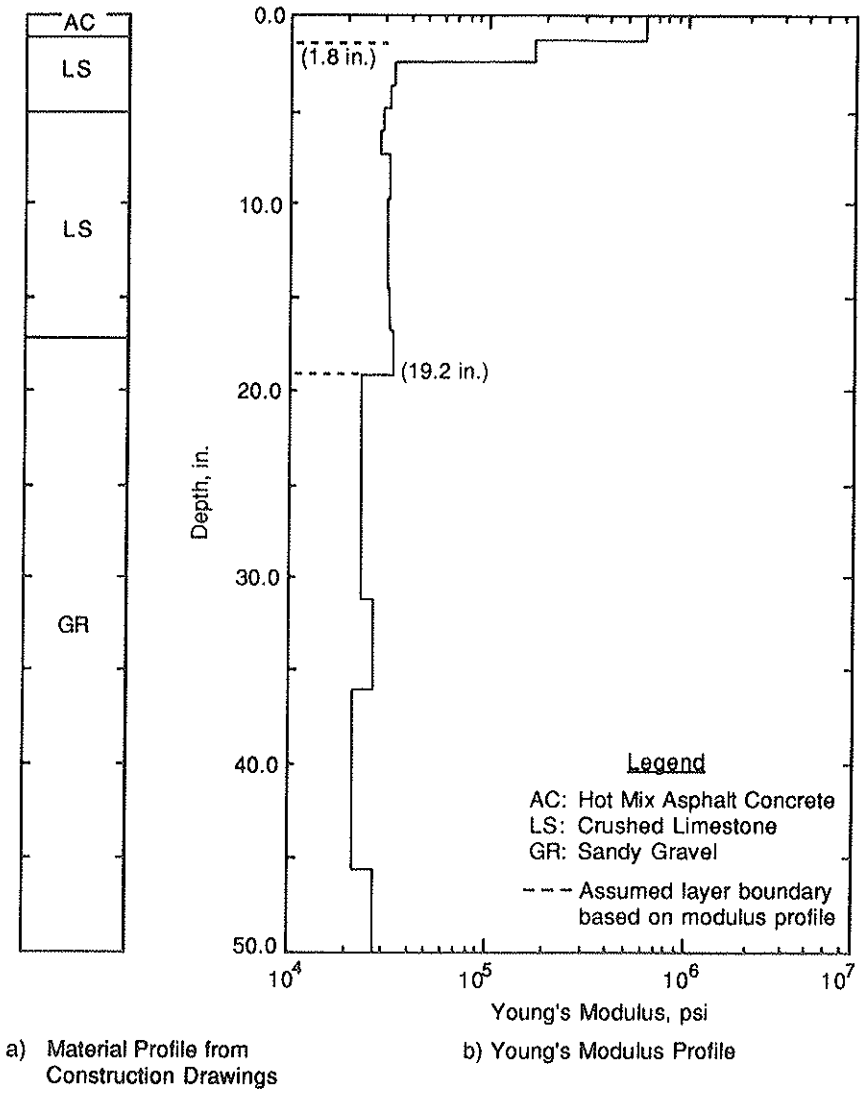

FIGURE 11 Composite profile of section 11.

The actual deflection basins measured in the field are presented in table 7. Preliminary modulus profiles back-calculated by personnel of the Texas Transportation Institute using Program CHEVDEF (*13*) (see acknowledgements) are reported in table 8. Also included in table 8 is the absolute sum of differences between the measured and calculated deflections. Bush (*13*) recommends that the absolute sum of the differences should be less than 10 percent for an acceptable fit. It can be seen that in all cases except one (Site 4) the absolute sum of differences is greater than this recommended value. Program BISDEF was also used for back-calculation of moduli. Overall, the absolute sum of the differences between the measured deflection and with BISDEF calculated were similar to those reported for CHEVDEF.

The main reason for the lack of ability in obtaining a better match between the field and theoretical deflection basins can be due to several factors, such as variations in moduli within different layers cannot be considered. A good example is the subgrade, which consists of two distinct sublayers of fill material and a natural soil layer.

Comparison of Moduli from SASW and FWD Tests

In the last section it was mentioned that back-calculated moduli obtained from FWD devices are preliminary because of somewhat large variation between the measured and calculated deflection basins. Therefore, the discussion presented herein is very general in nature.

Moduli of the asphaltic concrete layers obtained by preliminary work on basin-fitting of the FWD data exhibit, in general, greater variation than those of the SASW tests. This is expected because of the lack of sensitivity of the FWD method to the stiffness of the top thin layer, while the SASW method is quite sensitive in this region. It is, however, interesting to

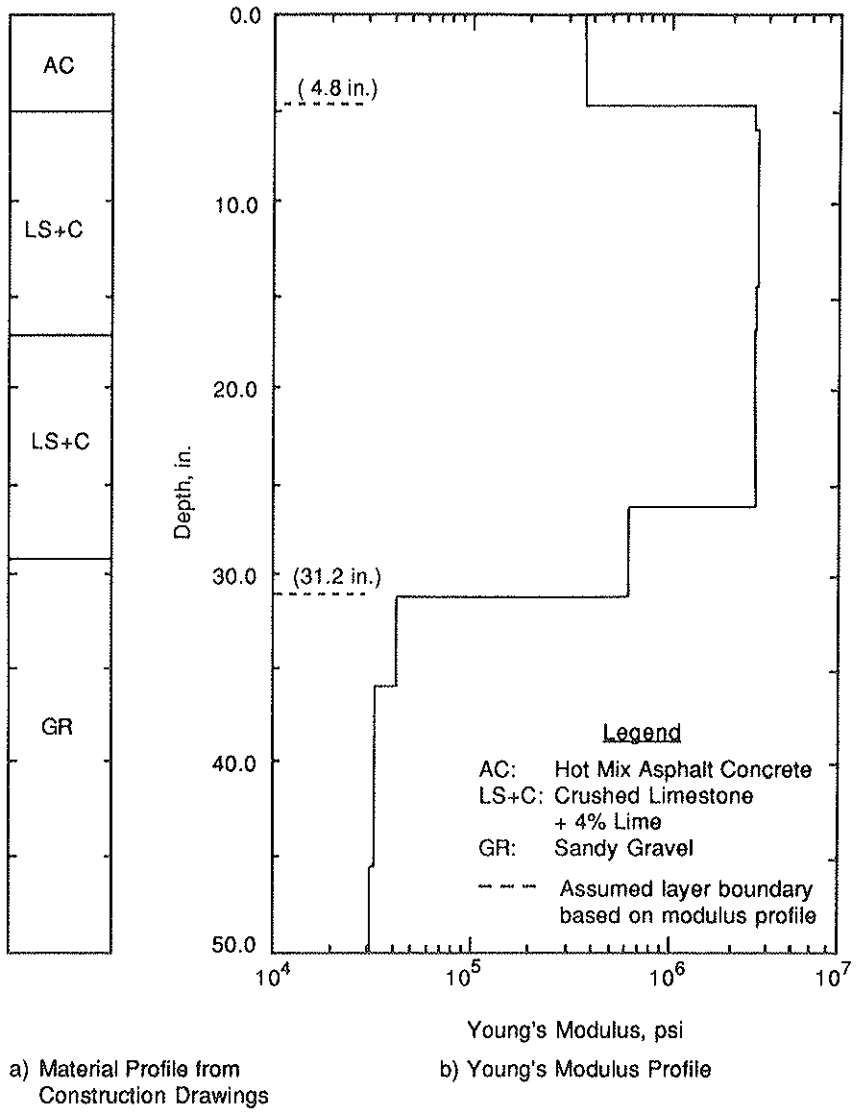

FIGURE 12 Composite profile of section 16.

note that in the FW0 results the AC layer at Site 9 exhibits the highest value of modulus, as do the SASW results.

Moduli of the crushed limestone used as the base and/or subbase vary greatly from one section to another as obtained by both methods. At Sites 7 and 10, the moduli are within about 20 percent by both methods. However, for the other sites, modulus values from the two testing methods vary by a factor ranging from 2 to about 20, a poor comparison which is under further study.

Moduli of the cement-stabilized crushed limestone are relatively constant as determined by the SASW tests, with a maximum variation of about 20 percent from the average. A much larger variation in modulus values exists in the FWD results. However, at Sites 2, 4, and 16, the average moduli of this material are within about 15 percent of each other, a good comparison.

Only two sites were tested which have bases of lime-stabilized crushed limestone. The modulus values of this material do not vary much, as shown in table 5. However, moduli obtained by the SASW method average about 75 percent higher than those obtained by the FWD method.

The three fill materials (sandy gravel, sandy clay, and plastic clay) exhibit the same trends from the two testing methods. The moduli of the plastic clay and sandy gravel are generally within about 25 percent. However, the modulus values of the sandy clay fill from the SASW tests are about twice as large as those obtained by the FWD tests.

Another way of comparing moduli from the two methods consists of inputting the SASW modulus profiles in a layered-theory algorithm (such as BISAR) and determining theoretical deflection bowls. The theoretical deflection bowls can then be compared with the field deflection bowls obtained from the FWD tests. This approach is not very feasible in this study, however, because the SASW modulus profiles are quite shallow. Since the main goal of this project was to obtain the thicknesses of different layers in the upper portion of the

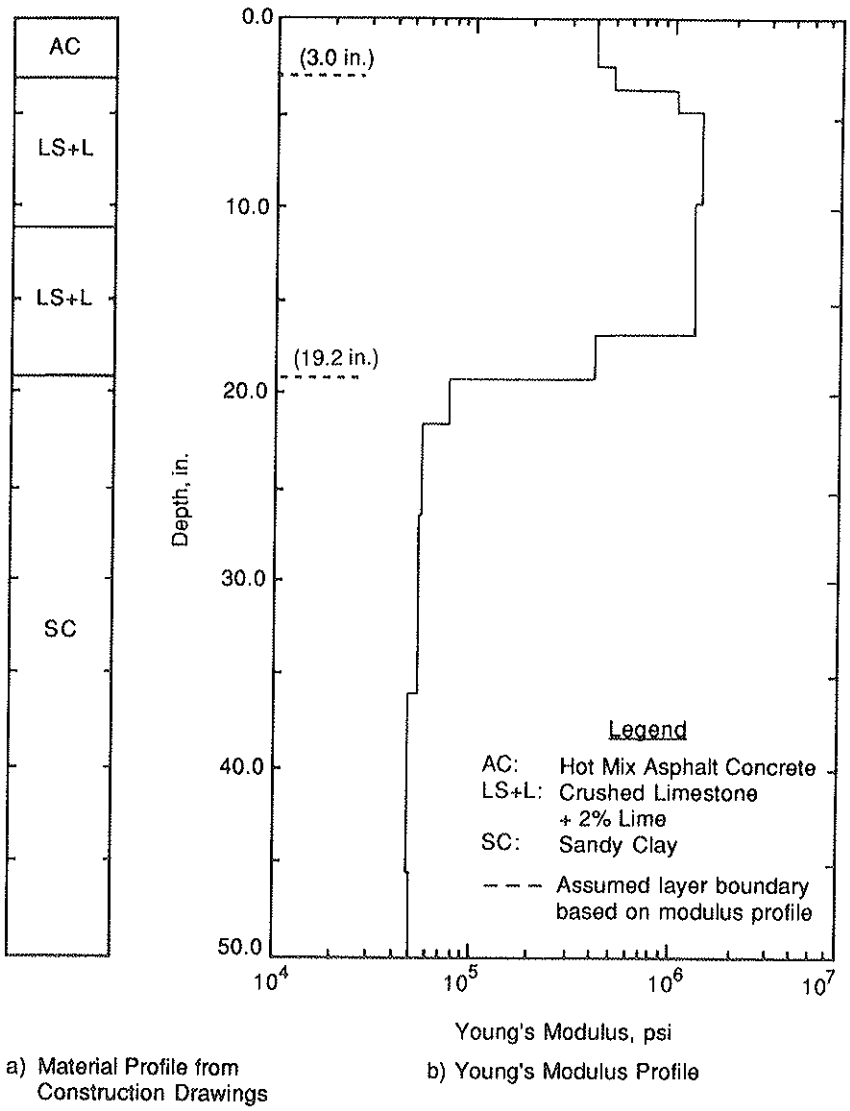

FIGURE 13 Composite profile of section 17.

pavement systems, many layers were placed near the surface, and the moduli were determined accurately to a depth of only about 50 inches.

CONCLUSIONS

Overall, moduli and thicknesses determined by the SASW tests seem very reasonable. The accuracy of the layer boundaries determined from the SASW profiles can be further improved by assuming more layers. However, the value of more detailed profiles than presented herein is questionable in the design process. On the other hand, more detailed layer boundaries could be important for construction control, and this result is quite feasible but requires more data-reduction time, which constitutes no problem, and this occurrence should be studied more rigorously. Most importantly, however, the strength of the SASW method in terms of determining complex stiffness profiles with numerous layers is clearly demonstrated by these tests.

Comparison of modulus values from the SASW and FWD tests at the same sites show several general points. First, moduli of the top pavement layer exhibit less scatter in SASW tests than in FWD tests because of the higher sensitivity of the SASW method to properties in this region of the pavement. Second, moduli of other pavement layers, especially thick, stiff layers such as at Site 16, are generally within about 30 percent by the two types of tests. Third, moduli of the subgrades at six of the nine sites are also within about 30 percent.

Moduli from SASW tests are low-strain moduli. On the other hand, moduli back-calculated from FWD deflection basins may contain manifestations of nonlinear behavior induced by

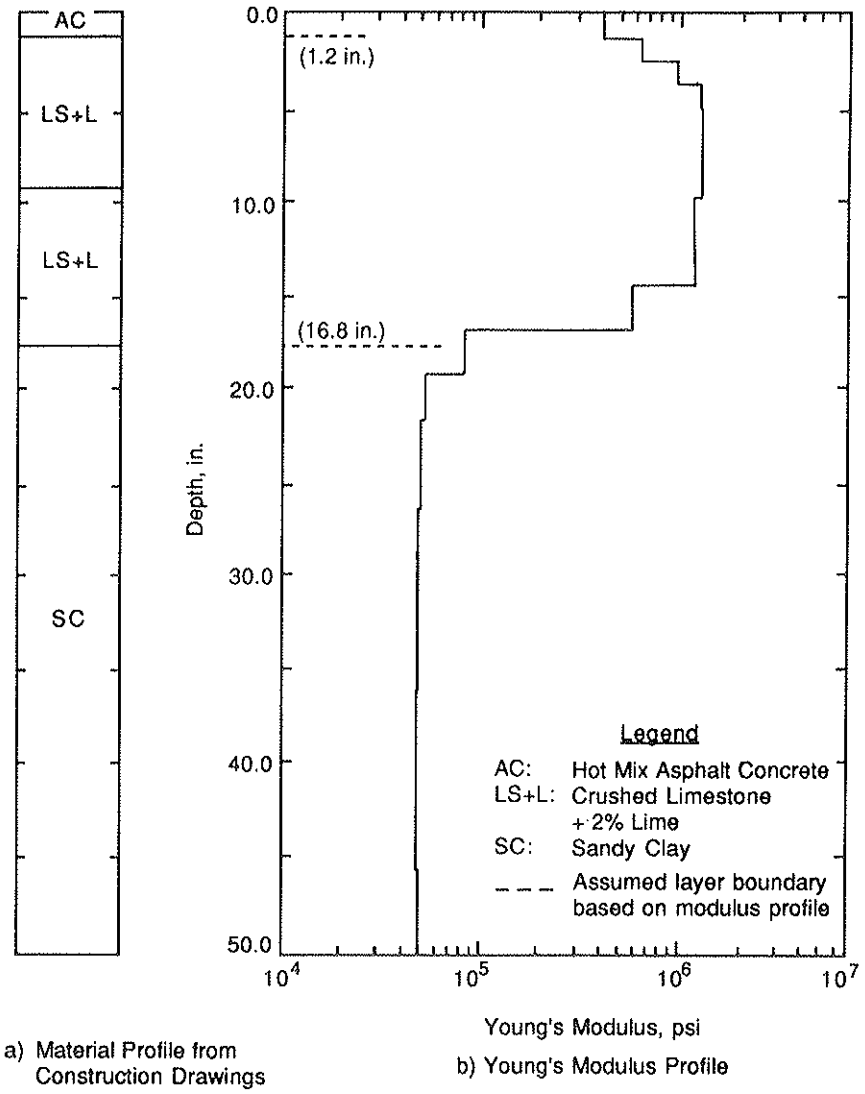

FIGURE 14 Composite profile of section 18.

the heavy loads imparted to the pavement surface. In theory, both tests should yield the same moduli if the boundary conditions for both methods are similar and satisfied properly in the back-calculating procedures. Moduli obtained by the two methods compare well when the predominant pavement layers are thick and stiff. It seems that in these cases both tests are performed in the linear range and the pavement structure is relatively simple.

ACKNOWLEDGMENTS

This work was supported by the Texas State Department of Highways and Public Transportation under Contract Number IAC(86-87)0936. The preliminary modulus values obtained from the FWD device were provided by Tom Scullion of the Texas Transportation Institute, whose cooperation is appreciated.

TABLE 5 SUMMARY OF AVERAGE MODULUS VALUES OF MATERIALS DETERMINED FROM SASW TESTS

Section	Average Modulus of Each Material, ksi						
	AC*	LS	LS+C	LS+L	GR	SC	PC
2	409	85	2500	--	--	--	34
4	338	509	3390	--	--	--	33
7	338	362	2727	--	--	--	17
9	1392+	99	--	--	29	--	--
10	500	60	--	--	25	--	--
11	605	32	--	--	25	--	--
16	371	--	2700	--	33	--	--
17	395	--	--	1340	--	51	--
18	395	--	--	1200	--	50	--

*AC: Hot Mix Asphalt Concrete
LS: Crushed Limestone
LS+C: Crushed Limestone + 4% Cement
LS+L: Crushed Limestone + 2% Lime
GR: Sandy Gravel
SC: Sandy Clay
PC: Plastic Clay
+ Unusually high value has been confirmed by additional tests

TABLE 6 COMPARISON OF THICKNESSES ESTIMATED FROM SASW TESTS AND CONSTRUCTION DRAWINGS

Section	Thickness from Construction Drawings, in.			Thickness from SASW Profile, in.			Difference in Layer Thicknesses, in.		
	AC	Base	Subbase	AC	Base	Subbase	AC	Base	Subbase
2	1	12	4	1.2	13.2	5.0	0.2	1.0	1.0
4	5	12	12	4.8	12.0	14.4	0.2	0	2.4
7	1	4	12	1.2+	3.6+	12.0	0.2	0.5	0
9	5	8*	--	4.8	9.6*	--	0.2	1.6	--
10	1	16*	--	1.8	15*	--	0.8	1	--
11	1	16*	--	1.8	17.4*	--	0.8	1.4	--
16	5	24*	--	4.8	26.4*	--	0.2	2.4	--
17	3	16*	--	3	16.2*	--	0	0.2	--
18	1	16*	--	1.2	15.6*	--	0.2	-0.4	--

* Subbase and Base were constructed from the same materials.
+ AC Layer and Base have about the same modulus and would be interpreted as one layer with a thickness of 4.8 in. if the material profile was never known.

TABLE 7 DEFLECTION BASINS MEASURED AT TTI PAVEMENT TEST FACILITIES

Section	Load, lbs	Deflection, mils						
		Sensor Number*						
		1	2	3	4	5	6	7
2	9480	6.8	5.7	4.7	3.9	3.0	2.4	1.8
4	9392	3.2	2.3	2.3	2.0	1.7	1.5	1.3
7	9376	11.5	6.2	5.5	4.6	3.8	3.0	2.5
9	9368	9.3	5.9	3.6	2.4	1.7	1.3	1.2
10	9432	16.2	7.6	4.1	2.9	2.2	1.8	1.4
11	9176	19.7	7.6	3.6	2.5	1.9	1.6	1.2
16	9288	2.1	1.4	1.4	1.3	1.1	1.0	0.9
17	9384	6.3	5.2	4.3	3.5	2.8	2.2	1.8
18	9392	5.0	4.2	3.7	3.1	2.6	2.2	1.7

* Sensor Number 1 was located directly under the load and the other 6 sensors were placed one foot apart.

TABLE 8 SUMMARY OF MODULUS VALUES BACK-CALCULATED FROM FWD TESTS

Section	Average Modulus of Each Material, ksi							
	AC*	LS	LS+C	LS+L	GR	SC	PC	ASD[a], percent
2	947	23	3119	--	--	--	24	18.7
4	609	87	4491	--	--	--	32	4.1
7	864	293	797	--	--	--	19	19.6
9[b]	1000	100	--	--	23	--	--	61.8
10	885	69	--	--	27	--	--	24.8
11	475	65	--	--	32	--	--	25.4
16	302	--	2125	--	46	--	--	12.6
17	570	--	--	851	--	22	--	35.0
18	320	--	--	631	--	21	--	24.6

[a] ASD denotes Absolute Sum of Percent Difference between the measured and backcalculated deflection basins.

*AC: Hot Mix Asphalt Concrete
LS: Crushed Limestone
LS+C: Crushed Limestone + 4% Cement
LS+L: Crushed Limestone + 2% Lime
GR: Sandy Gravel
SC: Sandy Clay
PC: Plastic Clay

[b] Modulus values for Site 9 backcalculated by personnel at The University of Texas at Austin

REFERENCES

1. S. Nazarian and K. H. Stokoe, II. *In Situ Determination of Elastic Moduli of Pavement Systems by Spectral-Analysis-of-Surface-Waves Method (Practical Aspects)*. Research Report 368-IF. Center for Transportation Research, The University of Texas at Austin, 1985.
2. S. Nazarian and K. H. Stokoe, II. *In Situ Determination of Elastic Moduli of Pavements Systems by Spectral-Analysis-of-Surface-Waves Method (Theoretical Aspects)*. Research Report 437-2. Center for Transportation Research, The University of Texas at Austin, 1986.
3. B. O. Hardin and V. P. Drnevich. Shear Modulus and Damping in Soils: Measurement and Parameter Effects. *Journal of the Soil Mechanics and Foundations Division*, ASCE, Vol. 95, No. SM6, 1972, pp. 602–624.
4. R. D. Barksdale and R. G. Hicks. Material Characterization and Layered Theory for Use in Fatigue Analysis. In *Special Report 140: Structural Design of Asphalt Concrete Pavements To Prevent Fatigue Cracking*, HRB, National Research Council, Washington, D.C., 1973, pp.20–49.
5. I. Sanchez-Salinero. *Analytical Investigation of Seismic Methods Used for Engineering Applications*. Ph.D. dissertation. The University of Texas at Austin, 1987.
6. J. C. Sheu, I. Sanchez-Salinero, J. M. Roesset, and W. R. Hudson. *Investigation of Variables Affecting In Situ Determination of Elastic Moduli of Pavement Systems by Surface Wave Method*. Research Report 437-3F. Center for Transportation Research, The University of Texas at Austin, November 1986.
7. W. T. Thomson. Transmission of Elastic Waves through a Stratified Solid Medium. *Journal of Applied Physics*, Vol. 21, 1950, pp. 89–93.
8. N. A. Haskell. The Dispersion of Surface Waves on Multilayered Media. *Bulletin of the Seismological Society of America*, Vol. 43, No. 1, 1953, pp. 17–34.
9. S. Nazarian, K. H. Stokoe, II, and R. C. Briggs. Nondestructively Delineating Changes in Modulus Profiles of Secondary Roads. In *Transportation Research Record 1136*, TRB, National Research Council, Washington, D.C., 1987, pp. 96–108.
10. S. Nazarian, K. H. Stokoe II, and W. R. Hudson. Use of Spectral-Analysis-of-Surface-Waves Method for Determination of Moduli and Thicknesses of Pavement Systems. In *Transportation Research Record 930*, TRB, National Research Council, Washington, D.C., 1983, pp. 38–45.
11. S. Nazarian. *In Situ Determination of Elastic Moduli of Soil Deposits and Pavement Systems by Spectral-Analysis-of-Surface-Waves Method*. Ph.D. dissertation. The University of Texas at Austin, 1984.
12. F. Scrivner and C. H. Michalak. *Linear Elastic Layered Theory as a Model of Displacements Measured within and beneath Flexible Pavement Structures Loaded by the Dynaflect*. Research Report 123-25. Texas Transportation Institute, Texas A&M University, College Station, Tex., 1974.
13. J. A. Bush. *Nondestructive Testing for Light Aircraft Pavements, Phase II, Development of Nondestructive Evaluation Methodology*. Report No. FAA-RD-80-9-II. U.S. Army Corps of Engineers, Vicksburg, Miss., 1980.

Publication of this paper sponsored by Committee on Strength and Deformation Characteristics of Pavement.

Load-Associated Crack Movement Mechanisms in Roads

F. C. RUST AND V. P. SERVAS

The increasing use of modified binders to inhibit reflection cracking, and the fact that these materials are sometimes unsuccessful, highlights the need to investigate the mechanisms of load-associated crack movement and crack reflection. The Crack-activity Meter (CAM), developed to measure load-associated crack movement, is discussed in this paper. Heavy Vehicle Simulator (HVS) tests, incorporating crack-movement measurements are discussed, as well as various types of crack-movement behavior. Four typical mechanisms of crack and joint movement are identified and discussed. This work has led to an improved understanding of the mechanisms of crack movement and crack reflection and to a procedure, based on the measurement of crack movement, that can be used to aid rehabilitation design.

The reflection of primary cracks through overlays and seals on roads is recognized as a serious problem. The ingress of rainwater through such surface cracks can cause pumping, leading to forms of distress such as pot-holing and/or deformation. This can, in turn, lead to the premature failure of an otherwise sound pavement.

Asphaltic overlays are often used to rehabilitate both flexible and rigid pavements. However, such efforts can be invalidated by the reflection of cracks through overlays and seals. Special or innovative materials such as bitumen-rubber, geofabrics and low-viscosity asphalt have been used in attempts to solve this problem with varying degrees of success (*1*). This emphasizes the fact that the mechanisms of crack movement and crack reflection are not yet fully understood.

Cracks in a pavement can reflect due to thermal effects, as well as wheel load effects. Extensive investigation has been done regarding crack reflection due to thermal effects on concrete pavements. In South Africa there are relatively few concrete pavements, and the thermal changes are not as severe as in some countries. Furthermore, many pavements contain cemented bases where thermal movements are relatively low and, therefore, wheel load-associated crack reflection is of more importance.

In order to investigate and measure load-associated crack movement in the field a new instrument, the Crack-activity Meter (CAM), was developed (*2*). The CAM has been used extensively with the Heavy Vehicle Simulator (HVS) during the accelerated testing of various types of pavements. The measurement of crack movement and changes in crack movement with pavement deterioration has led to the identification of four typical mechanisms of crack and joint movement. Crack-movement measurements and the analysis of crack-movement mechanisms has led to better understanding of how and why cracks move under heavy wheel loads. This improved understanding has laid the foundation for more meaningful research into the problems of and possible solutions to crack reflection.

Division for Roads and Transport Technology, P.O. Box 395, Pretoria, 0001, South Africa.

THE CRACK-ACTIVITY METER (CAM)

The Crack-activity Meter (CAM) can measure both relative vertical and horizontal crack movement simultaneously. Figure 1 shows a schematic diagram of the CAM. Data are recorded continuously as a wheel approaches the point of measurement and passes over it. A plot of crack movement versus the distance of the wheel from the measuring point is, therefore, the influence line of crack movement.

The CAM was specifically designed to measure the relative crack movements directly and with reasonable accuracy. The CAM has the following features:

- Its reference point is as close as possible to the point of measurement. This minimizes the risk of errors resulting from calculating crack movement from two deflection measurements (*1*).
- It is small enough to fit between the dual wheels of the HVS or a truck. Measurements can therefore be taken between the tires of a dual wheel where the maximum crack movement and surface deflection occur.
- The contact area between the CAM and the road surface is as small as possible; this minimizes errors caused by the possible tilting of its frame.
- The effect of the curvature of the road surface on the accuracy of measurements is minimal. The ratio between the distance above the road surface where crack movement is measured (10 mm) and the radius of curvature (say 100 m) is so small that its influence can be ignored.
- The data are recorded on a microcomputer, thus simplifying data validation and processing, and allowing the recording of total influence lines of data rather than only peak values.

The CAM can be used to measure crack movements on a pavement at different stages during its structural life. Typical influence lines of crack movement recorded on a cemented base pavement are shown in figure 2; the structure of this pavement is shown in figure 3. These influence lines show that, on this pavement, a crack goes through an opening-closing-opening cycle for one pass of a wheel. It is interesting

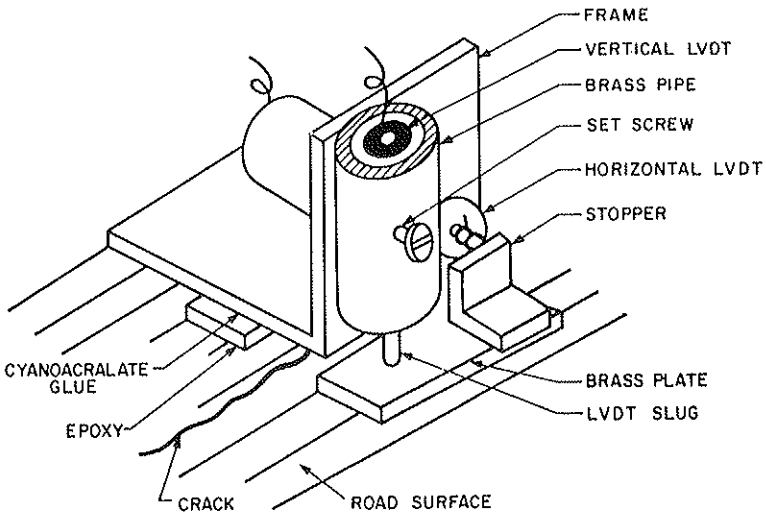

FIGURE 1 The crack-activity meter (CAM).

to note that, on this pavement, the horizontal load-associated crack movement was much larger than the vertical crack movement. This contradicts previous assumptions that horizontal crack movement is mainly due to thermal effects and that wheel loads cause only vertical movement.

Naturally, the crack movements can change if the factors influencing them change. Changes in crack movement are brought about artificially during HVS testing when accelerated trafficking causes changes in parameters such as the shape of the deflection basin or the size of the blocks defined by the cracks. The peak crack movements recorded at various stages of an HVS test can be plotted against trafficking to produce a crack movement behavior curve (see figure 4). The CAM can thus be used in conjunction with the HVS to determine how the crack movement will change as a pavement deteriorates.

CRACK MOVEMENT BEHAVIOR

The CAM has been used extensively to measure crack movements on various types of pavements as part of HVS test programs to investigate typical mechanisms of crack movement and the crack movement behavior of various types of pavements. These included a flexible pavement, a cracked Jointed Concrete Pavement (JCP) and rigid pavements (uncracked JCPs and Continuously Reinforced Concrete pavements). On the uncracked JCPs the movement of the joints was monitored to establish their mechanisms of failure. The crack movement behavior and their controlling mechanisms on these pavements are discussed below.

Crack Movement Behavior on a Flexible Pavement

The MR27 is a cemented base pavement near Cape Town; the structure of this pavement is shown in figure 3. At certain locations the pavement displayed severe signs of distress; this took the form of cracking (block sizes two to three meters), rutting and pumping from the cemented base.

In order to aid the rehabilitation design for this pavement an HVS test was conducted on a section in the fast lane of the pavement where the pavement structure was still in a reasonable state. Crack movements were measured at two points on the test section. Figure 4 shows the crack movement behavior recorded during the HVS test. The crack movement reached a maximum of 200 μm and then decreased again. Figure 5 shows the recorded surface deflections. The crack

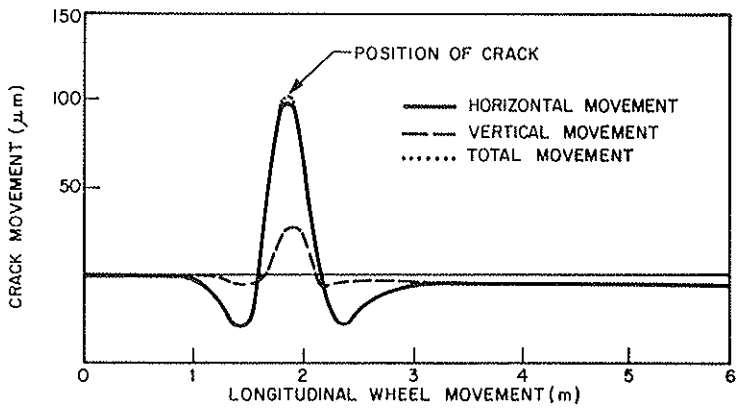

FIGURE 2 Typical influence lines of crack movement obtained on the MR27.

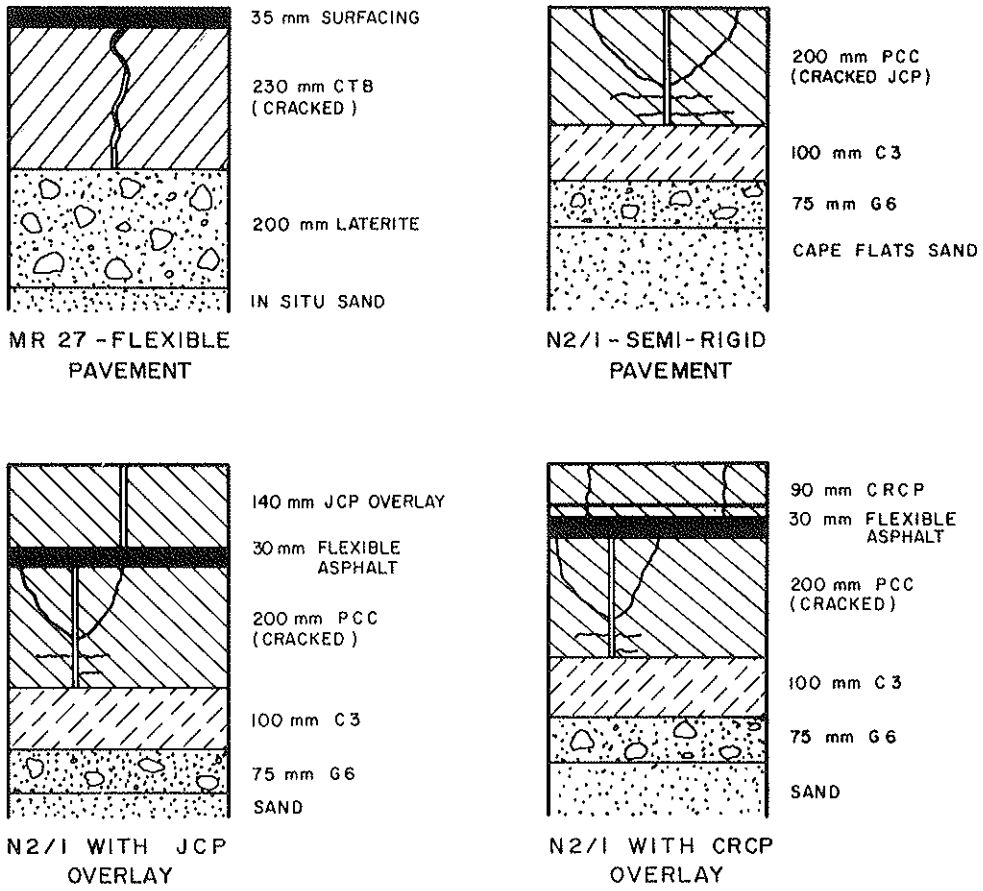

FIGURE 3 Structures of pavements on which crack movement behavior was determined.

movement as well as the surface deflection increased initially due to the ingress of rainwater. After the pavement dried the surface deflection decreased, as did the crack movement. A test pit opened on completion of the HVS test revealed that the blocks had not broken down further under HVS traffic. The crack movement behavior on this pavement section was therefore influenced by and correlated reasonably well with surface deflection.

Crack Movement Behavior on a Semi-Rigid Pavement

The N2 between Cape Town and Somerset West is a jointed concrete pavement (JCP); it shows unusual distress in the vicinity of the joints. Alkali-aggregate reaction in this pavement initiated cracking which, under the action of traffic loading, cyclic temperature, and moisture changes, led to structural distress such as progressive spalling. The size of the blocks defined by the cracks ranged from 350 mm to 450 mm in the vicinity of the joints. The frequency of the cracking was such that, for the purpose of analyzing crack movements, the pavement could no longer be regarded as a rigid pavement but rather as a semi-rigid pavement. The HVS was used to test several experimental overlays placed on this pavement. These included the use of bitumen-rubber modified asphalts, geofabric interlayers, a bitumen-rubber interlayer with a gap-graded asphalt overlay, granular layers, and concrete overlays. Viljoen et al. (*3*) discussed the behavior of a number of these overlays under HVS traffic.

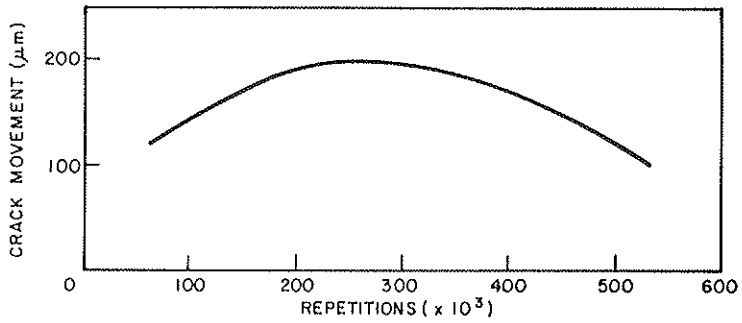

FIGURE 4 Crack movement behavior on the MR27 at measuring point 6.

As part of the above work, crack movements were measured in order to investigate the ability of the bitumen-rubber modified asphalt overlay to retard reflection cracking on cracks with a known activity. These measurements were taken on cracks in the vicinity of two joints in the pavement (joint 131 and joint 132). Joint condition ratings determined before the pavement was overlaid (*4*) indicated that joint 131 was in a more deteriorated state than joint 132. Figure 6 shows the crack movement behavior. At joint 132 the crack movement increased markedly to a maximum of approximately 600 μm as the test progressed and the blocks between the cracks broke down to a critical block size. Further block breakdown led to

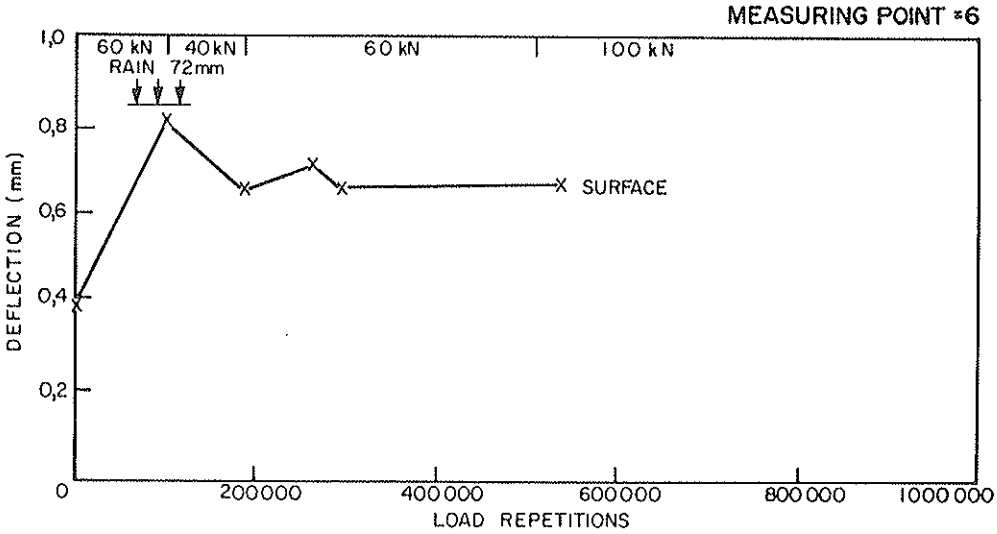

FIGURE 5 Average surface deflection on the MR27 at measuring point 6 under a 40-kN wheel load.

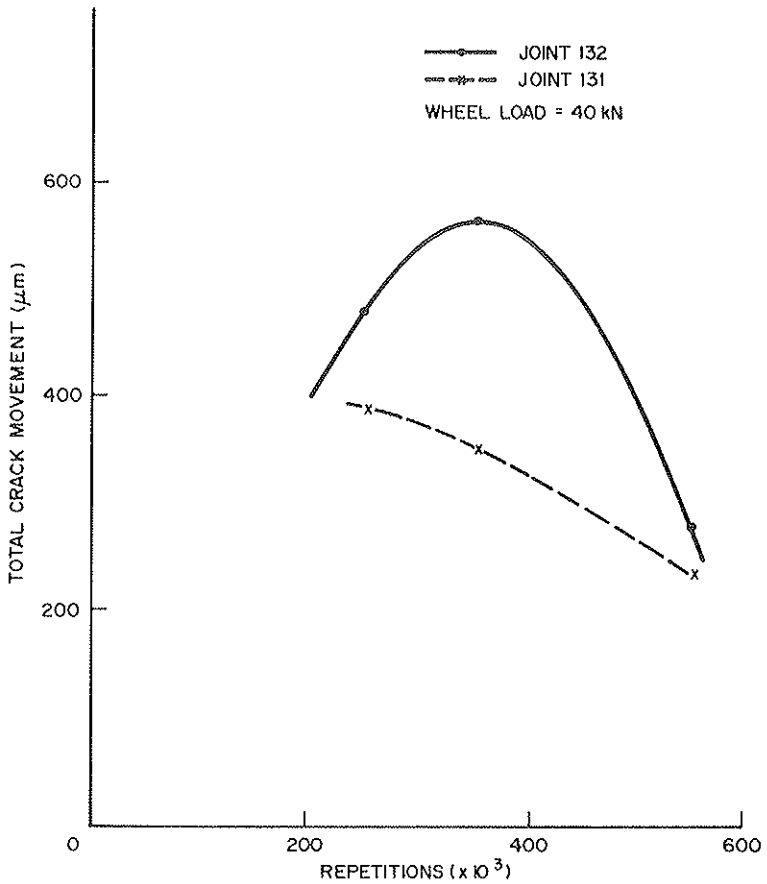

FIGURE 6 Crack movement behavior of cracks in the vicinity of two joints in the cracked JCP—Section 1.

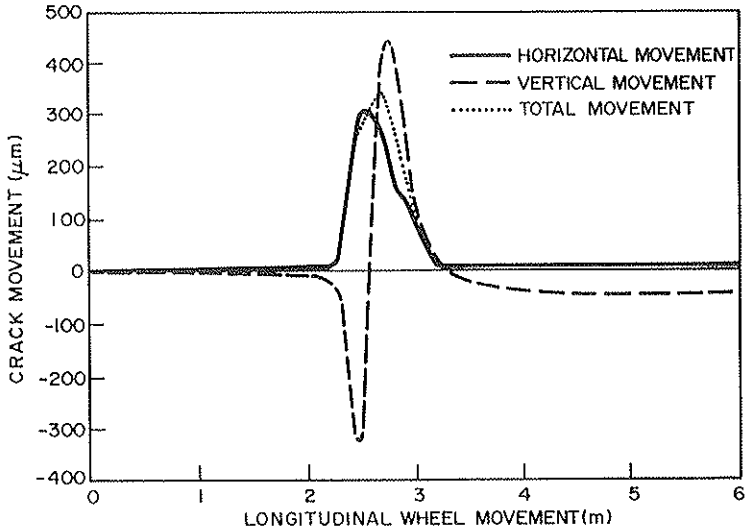

FIGURE 7 Typical influence lines of joint movement recorded on the thin JCP overlay—N2/1.

a decrease in crack movement. In the case of joint 131 the crack movement decreased from the beginning of the test. The difference in crack movement behavior between the two joints confirms their different states before commencement of the test.

A test pit opened at joint 132 after completion of the test showed signs of granulation of the top part of the concrete layer confirming that block breakdown had indeed taken place. Cracks that developed in the concrete after deterioration of the blocks did not reflect through the rubberized overlay, thus confirming that the crack movement had decreased after the blocks deteriorated.

Crack movement can be caused by the tilting or rocking of the blocks under a wheel load. High-crack movements were therefore still present in the case of this relatively stiff pavement with low deflections. The crack movement increased with block breakdown until the critical block size was reached. Further block breakdown led to a decrease in crack movement as the blocks became too small to tilt under the wheel. For this pavement, therefore, there was a clear correlation between block size and crack movement. Block size can therefore be very important if tilting is the major mechanism of crack movement.

Crack Movement Behavior on Rigid Pavements

The CAM was also used to measure the joint movement of rigid pavements to investigate their mechanisms of failure. This was especially successful on experimental JCP and continuously reinforced concrete pavement (CRCP) overlays placed on the cracked JCP discussed above. The crack movement behavior of these two pavement types, monitored during HVS testing, is discussed below.

A thin and a thick unbonded JCP overlay (115 mm and 145 mm respectively) were placed on the cracked JCP with an asphaltic bond-breaking layer separating them. Figure 3 shows the pavement structure after the placing of the new JCP. The thin JCP carried approximately 12 million equivalent axle loads (E80s) in the dry state before cracking. In the case of the thick JCP the pavement lasted approximately 30 million E80s before it started cracking. Crescent-shaped cracking appeared at distances of 600 mm to 700 mm away from the joint in the new JCP. Secondary cracking developed with further trafficking of the pavement. In the wet state the thin JCP (115 mm) started cracking after only 3 million E80s, and the thick JCP (145 mm) after only 7 million E80s. It is evident that the ingress of water into the pavement considerably shortened its life.

CAM measurements were taken on the joints of the new JCP during testing of the thin as well as the thick overlay. Figure 7 shows typical influence lines of joint movement. The high vertical movement (greater than the horizontal movement) is typical of an uncracked JCP—the slabs between the joints are too large to rock under the wheel load.

Figure 8 shows the joint movement behavior recorded during HVS testing of the thin JCP in the dry state. The vertical joint movement was, at first, relatively low but increased quickly to a level of approximately 200 μm after approximately 80,000 repetitions of a 100-kN dual wheel load. The crack movement remained constant at 200 μm up to approximately 320,000 repetitions. At this stage the JCP developed D-cracking about 600 mm away from the joint. Shortly after commencement of the test, a small void developed directly underneath the JCP in the vicinity of the joint; this explains the initial increase in joint movement. The high vertical movement caused tensile strains to develop at the surface of the slab. The joint movement then remained constant for a number of repetitions, while the slab was bending in a cantilever motion because of the loss of support. The concrete eventually fatigued and D-cracking developed at the position where the maximum bending moment (and tensile strain) occurred in the slab. After cracking, the joint movement increased markedly as the blocks between the cracks tilted or rocked under the wheel.

In the case of the wet test, the high vertical movement and the presence of water created an aggressive pumping action, which caused erosion of the asphaltic bond-breaking layer, leading to a larger void and a correspondingly higher vertical movement. The concrete was therefore subjected to much

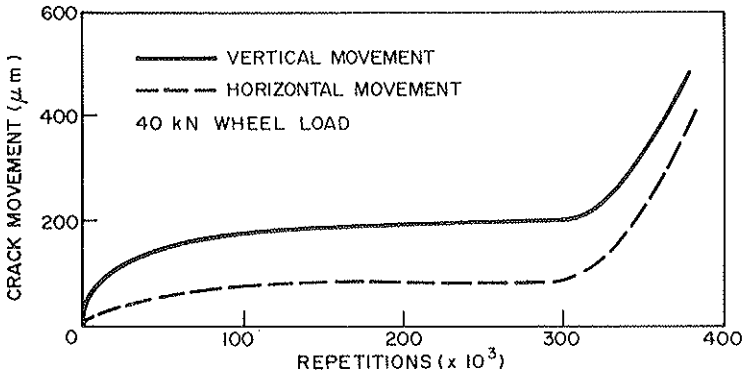

FIGURE 8 Joint movement behavior recorded during HVS testing of the thin JCP overlay in the dry state—N2/1.

higher levels of strain and lasted fewer repetitions. The thicker JCP (145 mm) lasted longer because of its greater strength when subjected to bending or cantilever action.

The CRCP experimental overlays on the cracked JCP consisted of 90 mm and 125 mm continuously reinforced concrete with 0.67 percent longitudinal reinforcement and a flexible asphalt levelling layer. The thin CRCP was tested both in the slow lane and on the shoulder. In the wheel path, the CRCP was well supported by the levelling layer and the cracked JCP. On the shoulder, the support consisted of a thin asphalt surfacing on top of a granular layer and Cape Flats sand. During HVS testing of both sections under dry as well as wet conditions the structure performed extremely well. In the wheel path, approximately 40 million equivalent standard axles (E80s) were applied with no apparent distress becoming visible. Figure 9 shows the crack movement behavior during HVS testing. The mechanism of crack movement on a CRCP is mainly that of a hinging action of the blocks (defined by the shrinkage cracks) on the reinforcement steel. This results in very low vertical and horizontal crack movements (generally below 30 μm). The aggressive pumping action, found under the JCP overlays, did not therefore develop in this case. The result is that the thin CRCP lasted much longer than even the thick JCP. Figure 10 shows a summary of the crack movement behavior curves obtained during HVS testing.

The load-associated joint movements on JCPs are also influenced by thermal change. Under a 40-kN wheel load the vertical joint movement of a JCP has decreased by 30 percent and increased by 47 percent during a 24-hr cycle of HVS testing.

CRACK MOVEMENT MECHANISMS

The crack movement measurements in conjunction with HVS testing indicate that cracks or joints on a pavement will move due to various mechanisms. Furthermore, there are various reasons for changes in crack movement. In particular, the following were noted:

- The cracks on a flexible pavement can move due to their position in the deflection basin.
- Crack movement on a flexible pavement can change due to a change in either the shape of the deflection basin or the block size.
- The cracks in a semi-rigid pavement can move due to the tilting of the blocks under a wheel load; this crack movement can change with the size of the blocks.
- On a rigid pavement (such as a JCP) the joints may move

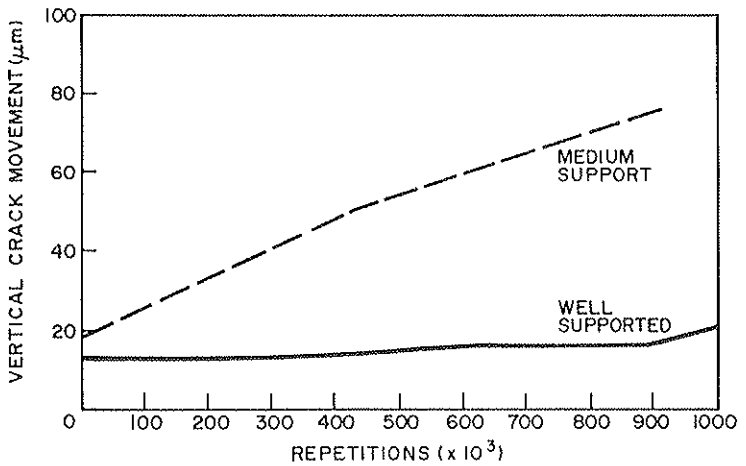

FIGURE 9 Crack movement behavior recorded on the thin CRCP overlay on the N2/1.

vertically due to a cantilever action of the slabs if a void is present under the slab.

- On a CRCP the cracks can move due to the hinging of the blocks on the reinforcement steel.

Four mechanisms of crack movement and changes in crack movement will be discussed below. The understanding of these mechanisms has been instrumental in the explanation of crack movement behavior on flexible pavements, as well as in the explanation of the mechanisms of failure on rigid pavements.

Crack Movement Resulting from the Shape of the Deflection Basin

The deflection basin of a flexible pavement under a heavy wheel load will normally be as shown in figure 11. The middle portion of the deflection basin will be concave and toward the end of the basin its shape at the surface will tend to be convex. A typical deflection basin on a flexible pavement will therefore have one concave portion and two convex portions. The magnitude of the peak deflection is indicative of the support conditions of the pavement, and the degree of curvature in the deflection basin is indicative of the state of the layers closer to the surface. Horak (5) has indicated that analysis of the deflection basin can be used to assess the state of the structural layers in a pavement. The above indicates that the shape of the deflection basin can change with the support conditions or with the state of the structural layers.

Figure 11 also shows that cracks on the surface of a pavement will be open or closed, depending on their position in the deflection basin. A particular crack will go through a cycle of opening-closing-opening for every wheel that passes over it. The magnitude of the peak crack movement will depend on the degree of curvature of the deflection basin as well as on the size of the blocks defined by the cracks. Figure 12

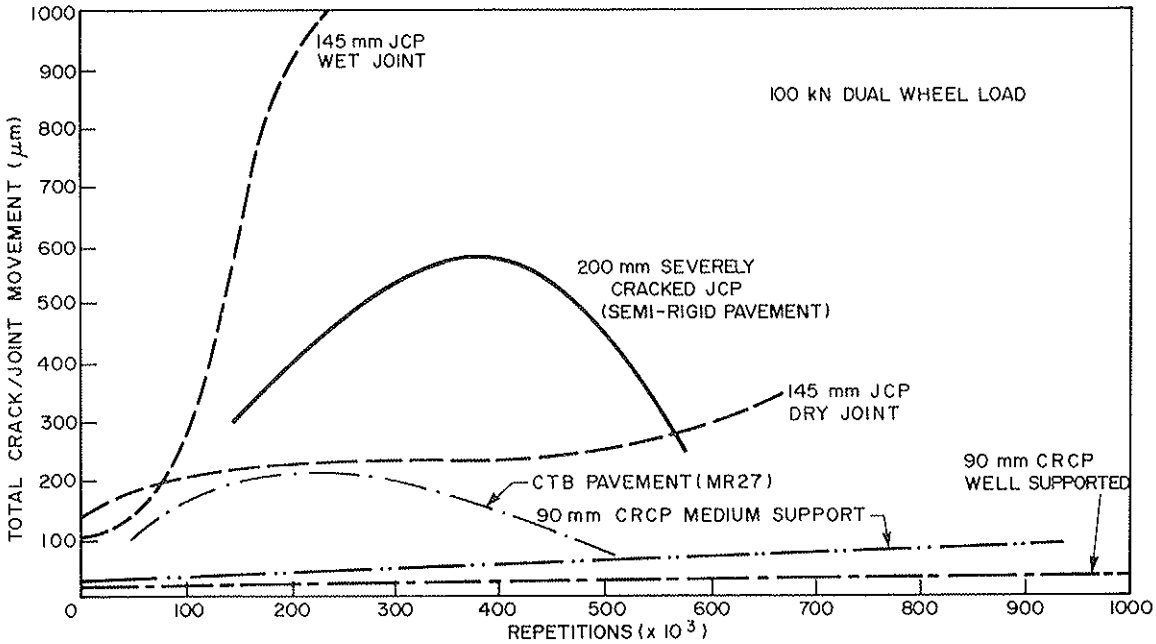

FIGURE 10 Crack movement behavior curves obtained during HVS testing.

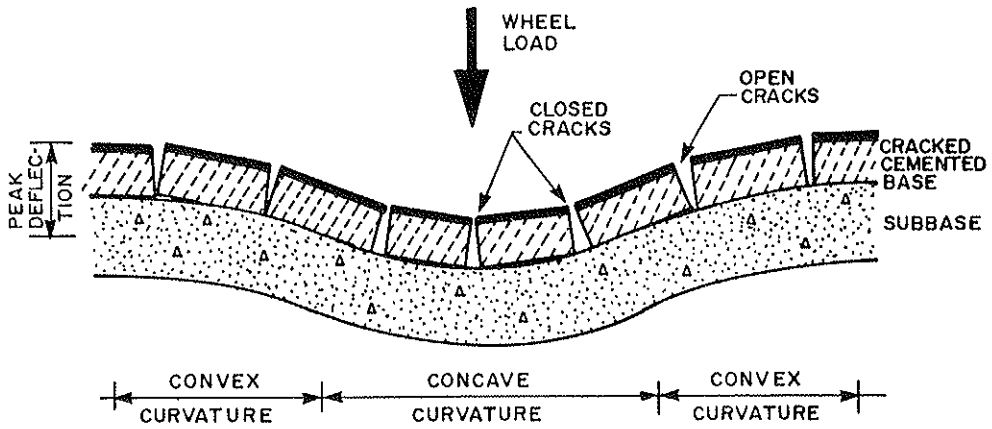

FIGURE 11 Typical deflection basin of a flexible pavement.

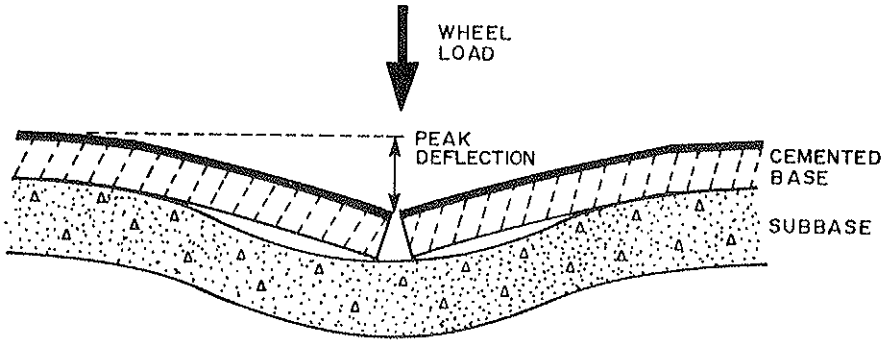

FIGURE 12 Large blocks in a typical deflection basin—crack movement due to downward deflection.

shows a large block in a typical deflection basin. If the blocks are very large, the crack movement will result from the cantilever action of these blocks under the wheel load. This implies that in the case of large blocks the magnitude of the peak crack movement will relate to the peak deflection. This fact was illustrated during the HVS test on the MR27 discussed above.

If the block sizes are in the order of 0.5 m to 1.0 m the cantilever action will be a minimum as the blocks are more rigid. In this case the shape of the deflection basin as well as the block size will influence the magnitude of crack movement. On the other hand, if the blocks are very small the crack movement will be very low (see figure 13). The above implies that the crack movement can change during flexible pavement life with changes in the deflection basin or the block size.

Crack Movement Resulting from the Tilting of the Blocks

The HVS test on the semi-rigid pavement discussed above showed that the crack movement can be significantly high even if the peak deflection recorded is relatively low. This fact indicates that crack movement can be caused by tilting or rocking of the blocks defined by the cracks under a heavy wheel load. Figure 14 illustrates this phenomenon. In this case the peak deflection and the shape of the deflection basin will have only a minor influence on the crack movement. If the blocks are very large they will not be tilted by the wheel load, and the cantilever action will cause only small crack movements. If the blocks are very small the wheel load will also not be able to tilt them. In the case of semi-rigid pavements, the crack movement will be mainly due to the tilting of the blocks and can change with the block size. However, the deflection basin, being relatively shallow, will have little influence on the crack movement.

The HVS test on the semi-rigid pavement illustrated the above. On this pavement the crack movement was initially in the order of 300 μm and the block size in the order of 300 mm to 400 mm. The breaking up of the blocks led to an increase in the crack movement to a maximum of approximately 600 μm with eventual decrease as the blocks became to small to be tilted under the wheel load.

Joint Movement due to Cantilever Action on Rigid Pavements

The CAM can also be used to measure the movement of the joints in JCPs. HVS testing of these pavements has shown that the vertical movement of the joint was generally larger than the horizontal movement. This is unusual and was caused by the existence of a small void under the slab in the vicinity of the joints. This void led to very high vertical movements generated by a cantilever action of the concrete slab. Figure 15 shows the cantilever action due to the loss of support under the slab.

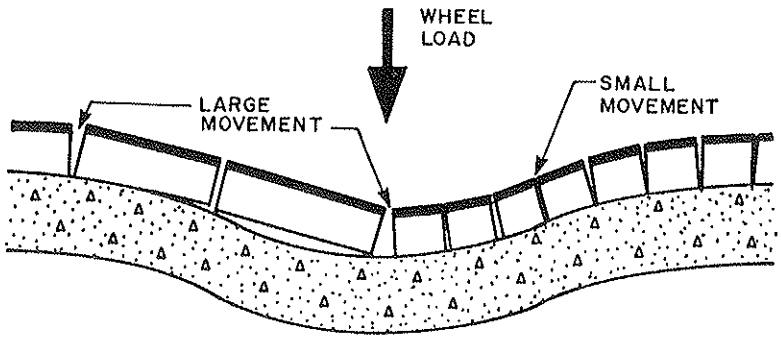

FIGURE 13 Crack movement related to the size of the blocks.

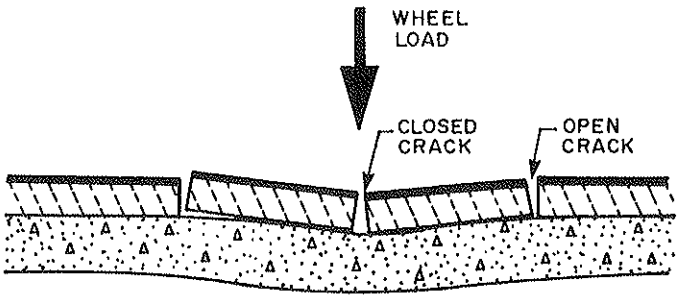

FIGURE 14 Crack movement due to the tilting of the blocks.

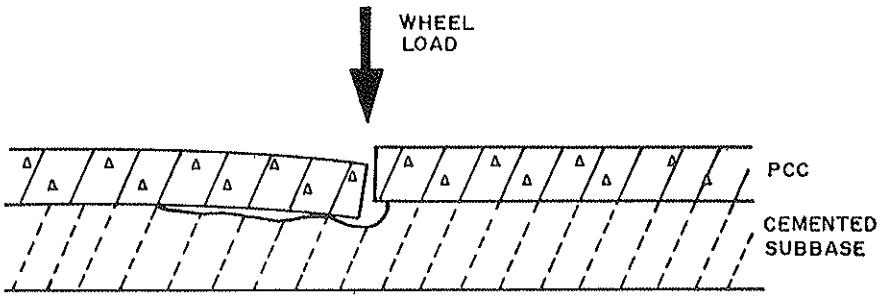

FIGURE 15 Movement of a joint in a JCP due to a void under the slab—cantilever action.

Crack Movement due to Hinging Action

On CRCPs the crack movement mechanism is mainly one of hinging of the blocks on the reinforcement. The reinforcement steel in the concrete prevents excessive vertical crack movement. The crack movements are therefore very low and the aggressive pumping action is absent. This mechanism is shown in figure 16.

CONCLUSIONS

The phenomenon of the reflection of primary cracks through overlays and seals is partly due to repetitive thermal and/or load-associated crack movement. The development of the Crack-activity Meter (CAM) provides a means of measuring load-associated crack movements accurately and effectively. The CAM has been used extensively in conjunction with Heavy Vehicle Simulator (HVS) testing.

The measuring and analysis of crack movements has led to a better understanding of the mechanisms of crack reflection. Four typical mechanisms of crack movement have been defined:

- Crack movement caused by the shape of the deflection basin,
- Crack movement caused by the tilting of blocks under a heavy wheel load,
- Joint movement on uncracked JCPs caused by the cantilever action of the slabs, and
- Crack movement on CRCPs caused by the hinging of the blocks on the reinforcement steel.

In the case of the deflection basin mechanism the crack movement during pavement life can change should the shape of the deflection basin or the block size change. In the case of the block-tilting mechanism the deflection basin has a minor influence on the magnitude of the crack movement. This mechanism is, however, influenced by a change in the block

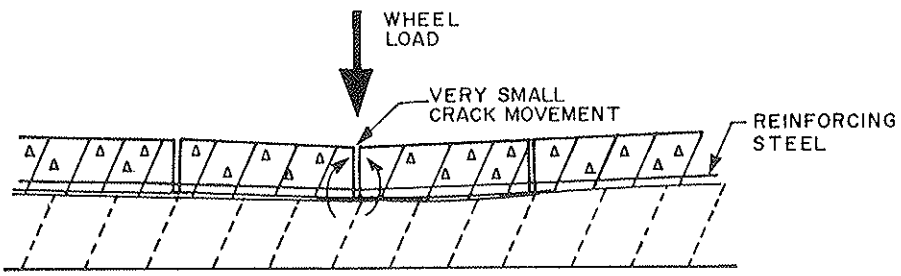

FIGURE 16 Crack movement on a CRCP—hinging of blocks on reinforcement steel.

size. On JCPs it was found that the vertical movement of joints can be very high due to cantilever action if a void is present directly under the slab. In the presence of water, this cantilever action can lead to a very aggressive pumping action, which aggravates the joint movement and leads to very rapid failure. On CRCPs the crack movements are generally low and therefore no pumping takes place.

The analysis of the mechanisms of crack movement has also led to an improved understanding of how and why cracks on pavements move. This work has not only led to an improved understanding of the mechanisms of load-associated crack and joint movement but has also laid the foundation for research which has led to a procedure, based on the measurement of crack movement, that can be used to aid the rehabilitation design of cracked pavements.

ACKNOWLEDGMENT

The work described in this paper was done at the National Institute for Transport and Road Research, CSIR, in Pretoria, South Africa, and is published with the permission of the Chief Director of the NITRR.

REFERENCES

1. F. C. Rust. *State of the Art of Rehabilitating Reflection Cracking in Cemented Pavements*. NITRR Technical Report RP/29. CSIR, Pretoria, South Africa, 1986.
2. F. C. Rust. *A Detailed Description of the Working of the Crack-activity Meter (CAM)*. NITRR Technical Report RP/36. CSIR, Pretoria, South Africa, 1986.
3. A. W. Viljoen, C. R. Freeme, V. P Servas and F. C. Rust. Heavy Vehicle Simulator Aided Evaluation of Overlays on Pavements with Active Cracks. Presented at the Sixth International Conference on Asphalt Pavements, Ann Arbor, Michigan, 1987.
4. P. S. Strauss, O. Schnitter and C. P. Du Toit. *National Route 2, Section 1 near Somerset West: Experimental Sections Construction Report*. Directorate Land Transport reference N16/4/6-02-010-06. South Africa, November 1983.
5. E. Horak. The Use of Surface Deflection Basin Measurements in the Mechanistic Analysis of Flexible Pavements. *Proceedings of the Sixth International Conference on Asphalt Pavements*, Ann Arbor, Michigan, 1987.

Publication of this paper sponsored by Committee on Strength and Deformation Characteristics of Pavement.

Analyzing the Interactions Between Dynamic Vehicle Loads and Highway Pavements

MICHAEL J. MARKOW, J. KARL HEDRICK, BRIAN D. BRADEMEYER, AND EDWARD ABBO

Mechanistic models to predict structural performance and deterioration have been developed for both flexible and rigid pavements. However, many of these models retain a simplified and idealized depiction of tire loads, and none really incorporates a true representation of a moving, dynamic force along the pavement surface. Thus, attempts to model the impacts to pavements of new types of heavy vehicles have at best been approximate and have often had to be supplemented by empirical data. In this paper we develop analytic models to study the interactions between moving, dynamic loads and highway pavements. One set of models simulates the dynamic behavior of heavy vehicles, including their body configuration and mass distribution, axle spacing and configuration, nonlinear suspension characteristics, and nonlinear tire behavior. The second set of models simulates the primary responses (stresses, strains, etc.) of pavements to vehicle forces, and translates primary responses into pavement damage. Existing mechanistic models are modified specifically to treat moving, dynamic loads for both flexible and rigid pavements. This paper presents examples of results (in terms of both dynamic forces and pavement damage) for rigid pavements, although the concepts apply as well to flexible surfaces. A parametric study is summarized, considering variations in both vehicle and pavement characteristics. Those characteristics most important to dynamic loading include vehicle suspension type and characteristics, speed, height of pavement faults, and joint spacing. Other factors (such as tire pressure) contribute smaller effects (although tire pressures are more important on flexible pavements). Results indicate that under certain conditions, dynamic loads are 40 percent higher than static loads and affect the mid-region of PCC slabs most significantly.

Current models of vehicle-pavement interaction employ simplified models of vehicle loading, such as static or pseudo-moving loads. However, instantaneous dynamic vehicle loads may be considerably higher than static loads (*1*, *2*); thus, dynamic loading can have a considerable impact on pavement performance (*3*). Current models cannot account for this effect. The prediction of pavement deterioration and serviceability under dynamic vehicle loading becomes particularly important when pavement design and analysis methods must be extended to encompass changing vehicle and pavement technology responding to new road design, construction, and regulatory practices. The purpose of this paper is to describe and illustrate a general methodology to analyze pavement responses to moving, dynamic vehicle loads, which may be used to predict pavement performance.

M. J. Markow, Center for Construction Research and Education, Department of Civil Engineering, Massachusetts Institute of Technology, Cambridge, Mass. J. K. Hedrick, Vehicle Dynamics Laboratory, Department of Mechanical Engineering, Massachusetts Institute of Technology, Cambridge, Mass. B. D. Brademeyer, Center for Construction Research and Education, Department of Civil Engineering, Massachusetts Institute of Technology, Cambridge, Mass. E. Abbo, Vehicle Dynamics Laboratory, Department of Mechanical Engineering, Massachusetts Institute of Technology, Cambridge, Mass.

DYNAMIC VEHICLE-PAVEMENT INTERACTIONS

The interaction between vehicle loads and pavement responses is frequently characterized as a one-way interaction, wherein the vehicle loads influence pavement responses but not vice versa. In reality, a mutually sustaining process occurs. The roughness of the pavement surface excites dynamic forces within the vehicle. These dynamic tire forces induce primary responses (stresses, strains, deflections) within the pavement, which affect the amount of distress produced by the vehicle, which in turn affects the dynamic tire forces experienced by subsequent vehicles, and so on in a two-way interaction between vehicles and pavements.

Analysis by Simulation Models

The study of this two-directional interaction between vehicles and pavements is a fundamental tenet of the research project described in this paper. The objective of this study is to assess the impacts of moving, dynamic vehicle loads on both flexible and rigid surfaces. Furthermore, an underlying premise is to generalize the problem description and analytic procedures so that, for example, new axle configurations, new tire designs, variations in tire pressures, as well as changes in pavement design and construction may be analyzed simultaneously. To do this, the study employs two sets of simulation models.

One set of models simulates the behavior of several commercial vehicles, including their configuration and mass distribution, axle spacing and configuration, suspension characteristics, and tire behavior. Each of these models simulates the movement of a given vehicle along a pavement profile;

any roughness inherent in the profile excites the dynamic elements of the simulated vehicle, as a function of the amplitude and frequency of the surface irregularities, the vehicle characteristics described above, and vehicle speed. The result of this simulation is a vehicle force profile containing digitized values of tire forces over distance (or time), representing the combined effects of all dynamic motions simulated. (Vehicle motions are simulated in a vertical plane through the vehicle's longitudinal axis (a "bicycle model"). The models therefore simulate bounce and pitch of the vehicle body, suspension, and tires, but not roll from side to side.)

The second set of models simulates the response of a pavement to the dynamic force profile of a moving vehicle developed above. The models used have been selected from the available mechanistic models for flexible and rigid pavements and adapted specifically to handle moving, dynamic loads. The objective was not to improve the modeling of pavement responses per se, but rather to build in the coupling with the vehicle force profile and to modify the response calculations to account for axle groupings (tandems, tridems, etc.). A requirement placed on the models selected was that they predict both primary responses (stresses, strains, and deflections), as well as ultimate responses: both distress (cracking, rutting, spalling, faulting, etc.) and serviceability. Since distress accumulates with the number of load repetitions and is also influenced by the magnitude, duration, and configuration of loading, as well as environmental and time-dependent conditions, the behavioral response predicted by these models should also be time- and temperature-dependent.

Separate analyses have been conducted for flexible and rigid pavements to account for inherent differences in mechanistic behavior, boundary conditions, and design characteristics. For flexible pavements, a modified version of Federal Highway Administration (FHWA) VESYS system has been used to represent pavement responses to moving, dynamic vehicle loads; for rigid pavements, a modified version of PMARP (also developed for FHWA) has been used. For purposes of illustration, this paper examines a case study of rigid pavements; the modifications to the PMARP pavement model are described in a subsequent section.

General Analytic Approach

Although separate models are used to simulate flexible and rigid pavements, the general approach is the same in each case. The force profile generated by the vehicle models simulates a moving, dynamic load along the pavement. At one or more points of measurement in the pavement, these dynamic forces are translated into primary responses and the maximum response computed. Where axle groups are encountered, appropriate superposition of responses is performed, and the maximum total response is identified. The maximum response is then translated into the appropriate components of pavement distress. Increments of distress are accumulated through repeated vehicle passes and the results compiled. Thus, the result of this simulation is a progression of damage in the pavement as a function of the pavement surface roughness (which increases over time as a function of the thickness and materials properties of the pavement layers, subgrade strength, environmental factors, etc.), vehicle characteristics (as represented by the dynamic tire force profile), and vehicle speed.

In theory, the two analytic steps above should be performed in an iterative process in which vehicle forces are generated and applied to a pavement, the increment in pavement damage (specifically, roughness) due to this force profile computed, that new force profile applied to the pavement, the new increment in roughness computed, and so forth. Since this procedure would be extremely expensive in computer time, a close approximation is employed: vehicle force profiles are computed in the vehicle simulation for several discrete levels of pavement roughness. These results are interpolated for any other levels of roughness encountered in the subsequent simulations of pavement deterioration.

Dynamic Vehicle Behavior

Models to simulate the behavior of moving vehicles have been developed for several commercial trucks and buses and are described by O'Connell, Abbo, and Hedrick (*4*); Hedrick, Cho, Gibson, et al. (*5*); Hedrick, Markow, Brademeyer et al. (*6*); and Abbo (*7*). These models represent analytically the dynamic behavior of the component rigid bodies, axle suspensions, and tires as the vehicle moves along a pavement of specified roughness at a specified speed. The result is a force vs. time or force vs. distance profile, again as a function of (assumed constant) speed and pavement roughness. Separate force profiles are produced for each axle of the vehicle, for each speed and roughness. These force profiles are used as inputs to the models of pavement response.

Influence Functions to Reflect Moving Loads

For vehicle speeds of interest, the dynamic effect on pavement mass or inertia is negligible, as shown by Delatte (*8*). There-

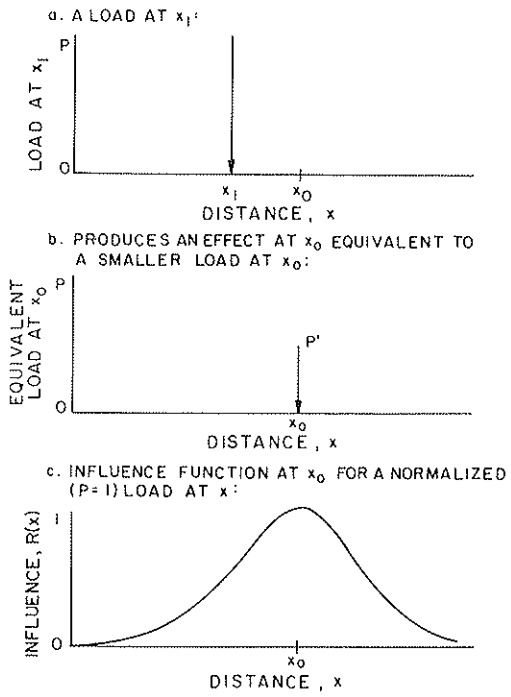

FIGURE 1 Load influence.

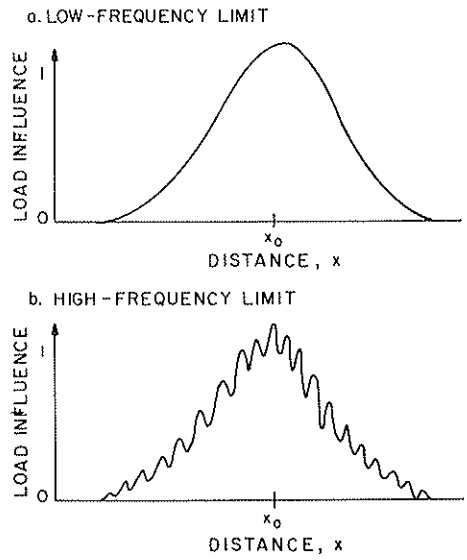

FIGURE 2 Variation of load influence with dynamic loads.

fore, one may represent the pavement response to a moving vehicle load as a quasi-static phenomenon, as shown in figure 1 (where pavement response refers to stress, strain, or deflection at a point in the pavement structure). Given this premise, the pavement response to a load P at a distance $x = x_0 - x_1$ is assumed to be equivalent to the response to a lesser load ($P' < P$) placed directly above the point of interest (x_0). This effect can be captured by influence functions relating the effect at x_0 of a load P at x_1. For a unit load ($P = 1$), the primary response at x_0 due to the load P at x_1 is characterized by the instantaneous static (or elastic) response $I(x_0 - x_1)$, where the function $I(x_0 - x_1)$ is the influence function. As an arbitrary load traverses the pavement, the response at x_0, $R(x_0)$, due to the force $F(x)$ imposed by this load at an arbitrary location x is given by the response function:

$$R(x_0) = I(x_0 - x)\, F(x) \tag{1}$$

The influence function in figure 1 is appropriate for a load of constant (unit) magnitude traversing the pavement. In the general case, however, the load will fluctuate, reflecting the dynamic vehicle forces discussed above. Thus, a dynamically varying component will be superimposed on the influence function in figure 1. The result of this superposition is illustrated in figure 2 (at the low-frequency and high-frequency limits). Therefore, the maximum influence a moving load can exert in the vertical plane at x_0 is a function of both the shape of the basic influence function in figure 1 and the dynamic effects superimposed on the basic function, as shown in figure 2. It is this maximum influence (or, if appropriate, the mean and variance of the maximum influence) that is used as the basis of pavement damage prediction.

Observe that the maximum influence a moving, dynamic load may have on x_0 does not necessarily occur when the load is directly above x_0. First, because of viscoelastic behavior, pavement responses may exhibit a delay in relation to the moving load. Second, the dynamic effects illustrated in figure 2 may shift the peak influence some distance from x_0. The magnitude of this distance depends on the frequency of the dynamic load variation.

Pavement Damage

Different response functions (equation 1) may be defined for stress, strain, strain-energy, or deflection and are obtained from the particular mechanistic model used in the analysis. For purposes of illustration, rigid pavements have been selected as examples in this paper. Solutions yielding the primary responses in portland cement concrete pavements that have joints or cracks have been developed over the past ten years. These solutions rely on finite element methods to treat the rigid behavior of the slab and the discontinuities (joints) between slabs. Several candidate models were available for consideration for this project, as reviewed by Abbo (*7*). The one selected for this project was the PMARP program (*9*).

In its original form, the PMARP program computes stresses and strains due to a static point load at a critical slab location. Miner's hypothesis is used to determine fatigue cracking at the individual nodes of the slab. Although the Miner's Law calculation is retained in the version used in this research, several changes were made to PMARP to improve its simulation of a moving, dynamic load. First, influence functions were introduced to model the travel of the load along the slab. Second, new equations were included (and some corrections made to existing equations in the model) to improve its predictions of pavement damage. A summary of the major additions is given below.

Joint Faulting Model

The joint faulting model used is the one adapted from PCA research for use in the EAROMAR-2 program developed for Federal Highway Administration (*10*). This model considers jointing as a function of traffic, pavement age, joint spacing, subgrade drainage, and type of subbase. For undoweled pavements the equation for jointing is as follows:

$$JF = 0.0403 + \frac{1.53(DTN \cdot A^2)^{0.465}}{H^{3.9}} S^{0.61} (J - 13.5)^b \tag{2}$$

where

JF = joint fault magnitude (in.),
DTN = daily traffic number, or the number of vehicle passes per day,
A = age of pavement (yrs),
H = slab thickness (in.),
S = subgrade type (good = 1, poor = 2),
J = joint spacing (ft.), and
b = factor depending upon subbase characteristics, equaling 0.241 for granular subbases and 0.037 for stabilized subbases.

The faulting model for doweled pavements is

$$JF_{LTD} = \frac{1}{(1 + A)^{1/2}} JF \tag{3}$$

Thermal Gradient in the Slab

A difference in temperature between the top and bottom of the slab introduces thermal stresses that are superimposed on

(either constructively or in opposition to) the stresses caused by traffic loads. The thermal gradient in the slab may be represented in the finite element model as an equivalent moment applied along the edge of the slab. The resulting stress may be represented as follows:

$$M^* = \frac{\alpha g E t^3}{12} \quad (4)$$

where

M^* = equivalent moment induced by thermal stresses (psi),
α = coefficient of thermal expansion (in./in./deg-F),
g = thermal gradient (deg-F/in.),
E = Young's Modulus of Elasticity of concrete (psi), and
t = thickness of the slab (in.).

Additional Assumptions

In applying the modified PMARP model to the analysis of dynamic loads, the following assumptions were made to simplify the computations and reduce computer time:

- The elastic modulus of concrete and the modulus of rupture were assumed to remain constant over the life of the pavement and were taken as average values.
- Subgrade weakening due to pumping was neglected.
- The major contribution to roughness was taken to be the faults at joints, rather than surface roughness in the interior of the pavement slab.

RESULTS

Parametric Studies

These procedures were applied in a set of parametric studies, in which the following parameters were varied:

1. Suspension Type:
   - Single-Leaf
   - Four-Leaf Tandem
   - Walking-Beam Tandem
2. Suspension Stiffness, k
3. β-parameter for Leaf-Springs
4. Vehicle Speed
5. Tire Pressure
6. Axle Load Sharing Coefficient
7. Tandem Axle Spacing
8. Pavement Roughness (i.e., Fault Height)
9. Joint Spacing
10. Slab Warping
11. Slab Interior Roughness

The results of these studies are summarized below, with a more complete presentation by Abbo (*7*).

Effects of Pavement Characteristics on Dynamic Loads

First it is useful to understand the pattern of dynamic loading and how that pattern is influenced by pavement characteristics. To do so we have used a base case comprising a jointed, undoweled pavement having a slab length of 30 feet. Undoweled pavements have been simulated because they exhibit greater faulting and permit a fuller study of the effects of faults on vehicle dynamics. For the base case, a uniform fault height of 0.5 inch has been assumed. (Doweled pavement joints generally maintain faulting within 0.2 inch over the pavement service life, according to the faulting model used in equation 3. At these relatively small fault heights, less than 0.25 inch, there is no significant variation in vehicle dynamics with respect to the parameters tested. This will be illustrated in the results below.) The vehicle used in testing the sensitivity to pavement parameters is a 2S1 combination with single-leaf spring suspensions, travelling at 35 mph.

Loading and Responses Due to Multiple Axles

Although the outputs of the vehicle and pavement models permit detailed analyses by axle, more aggregate and concise measures of results make it easier to display the sensitivity of dynamic loading to pavement and vehicle parameters. These measures embody the effects of the vehicle overall, rather than of any given axle combination. One such measure pertains to the force imposed by the vehicle, the second to the pavement response. To compute these measures, the pavement slab is divided into equal-size sections sufficiently small to enable resolution of the peak forces up to the highest frequencies of interest. The aggregate force at a particular point K is defined by:

$$F_K = \sum_{j=1}^{N_a} P_{jk} \quad \text{for } k = 1, 2, 3, \ldots, N_s \quad (5)$$

where

N_a = number of vehicle axles j,
P_{jk} = force imposed by axle j at slab location k, and
N_s = total number of stations k along the slab length.

The mean aggregate load is determined by averaging the aggregate load in equation 5 over several slabs (typically 20) to suppress any transient dynamic effects. The mean aggregate load is then normalized by the vehicle static load, and it is this value that is displayed in the results below. It is important to bear in mind that the aggregate force at a point depends on the cumulative effect of all vehicle axles that pass over it. Therefore, the maximum aggregate force will not necessarily occur at the same location as the maximum force generated by any individual axle. Analogously, the aggregate response of the pavement $R_T(x)$ at some point x is the sum of the responses due to the individual vehicle axles:

$$R_T(x) = \sum_{j=1}^{N_a} R_j(x) \quad (6)$$

where $R_j(x)$ is the response function at x due to axle j (as computed in equation 1). In applying equations 5 and 6, account is taken of the proper spacing of the axles on a vehicle.

Effect of Slab Length

Four slab lengths, ranging from 10 feet to 45 feet, were investigated. The vehicle behavior due to these varying intervals

between faults was investigated (for example, by changes in the power spectral density functions of the vehicles, as documented in (7)), as well as the effects on dynamic loads. A summary of these results follows.

The vehicle simulated in these examples has a steer-to-drive wheelbase of about 11.5 feet and a drive-to-rear wheelbase of 19.5 feet. Therefore, the 10-ft joint spacing results in almost simultaneous excitation of each of the three axles, stimulating primarily the vehicle bounce mode. For a joint spacing of 20 feet, there is a small time delay between inputs to the drive and rear axles, which excites the trailer bounce and tractor pitch modes, resulting in the largest pavement loads observed in this study. The 30-ft and 45-ft joint spacings do not excite the out-of-phase tractor-trailer pitch motions as much.

The effects of this behavior on aggregate vehicle load along the length of the slab can be seen in figure 3 for three of the joint spacings (20, 30, and 45 feet). A joint spacing of 20 feet produces a 12 percent increase in aggregate loading, with the peak load occurring roughly 10 feet after the faulted joint. Note, however, that the load imposed on the subsequent slab just after the joint is 20 percent lower for the 20-ft slab length than it is for the other slab lengths.

Effect of Height of Joint Fault

For the base case used (30-ft joint spacing, 35-mph vehicle speed) the height of joint faults did not affect the location of peak loads but did affect their magnitude. For example, considering just the drive axle of the vehicle, the normalized dynamic load (dynamic force divided by static force) measured at the peak load location 10 feet past the slab joint increased from about 1.05 for a 0.1-in fault to over 1.25 for a 0.75-in fault.

On an aggregate vehicle basis the impacts of joint faults can be seen in figure 4. There is a very small (about 3 percent) difference in the pattern and magnitude of loads for joint faults less than 0.25 inch. However, there is up to a 20 percent increase for a change in fault height from 0.25 inch to 0.75 inch. This illustrates the point mentioned above: relatively small fault heights (as might be expected on new pavements or those with good load transfer devices) result in insignificant changes in dynamic loadings. The increase in dynamic force that does take place when faulting becomes substantial supports the earlier contention that the two-way interaction between vehicles and pavements does indeed result in an accelerating, progressive cycle of vehicle load and pavement damage.

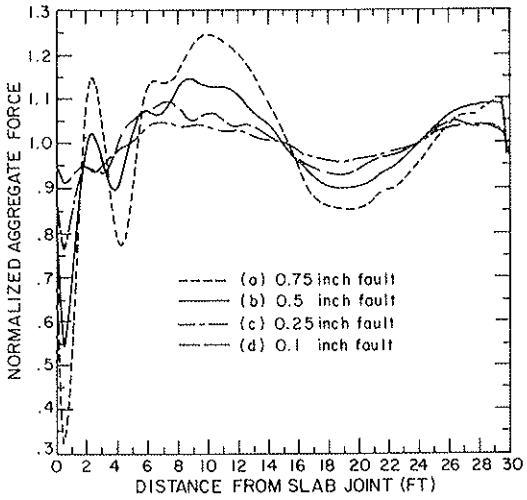

FIGURE 4 Effect of fault height on aggregate load.

Effect of Slab Warping

For a vehicle speed of 35 mph and a slab length of 30 feet, the warping of the slab corresponds to an input to the vehicle of 1.7 Hz. This frequency coincides with the natural frequency of the tractor bounce and pitch modes, which influences the changes in dynamic loading observed in figure 5. Specifically, the peak load regions of all the axles shift further away from the slab joint as the slab warping increases. The heaviest

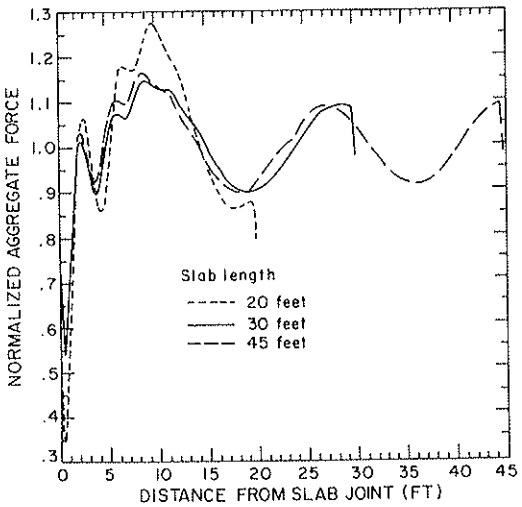

FIGURE 3 Effect of slab length on aggregate load.

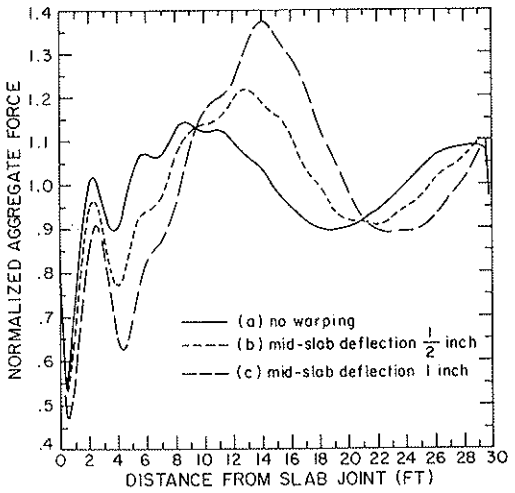

FIGURE 5 Effect of slab warping on aggregate load.

loading is sustained in the middle third of the slab, due to the excitation of the lower frequency body modes. This increase in aggregate loading is up to 25 percent for a slab radius of curvature of 1350 feet (equivalent to a 1-in deflection at the center of a 30-ft slab).

Effect of Slab Roughness

The interior roughness of the slab was varied by adjusting the assumed slope variance between 1.7×10^{-6} and 22×10^{-6} in.^{2}. Changes in the magnitudes of the resulting peak forces were no more than 4 percent and were judged to be insignificant over the range of roughnesses typically associated with rigid pavements. The primary excitation of vehicle dynamics was, therefore, taken to be the faults at rigid pavement joints.

Effects of Vehicle Parameters on Pavement Damage

The effects of vehicle parameters were also investigated. Although the results could again be expressed in terms of aggregate load, we now take them one step further to use the modified PMARP model (including equations 2 through 4) to consider the impacts on pavement damage. In these runs, damage has been limited to fatigue cracking, which is presented in two ways: (1) as a probability of occurrence over time, taken as a weighted average of the Miner's Law calculations for all nodes in the slab, and (2) as the amount of damage (in square inches) occurring by region of the slab. (Five regions have been defined, where the load traverses the slab from region 1 to region 5.)

Static Versus Dynamic Moving Load

Damage due to dynamic loading was compared to the simulated case of a moving constant load for the reference vehicle (a 2S1 tractor-semi-trailer) and the base case pavement conditions (30-ft slab length, 0.5-in fault height, 35-mph vehicle speed). The results are illustrated in figures 6 and 7.

The moving dynamic load produces approximately 38 percent greater fatigue cracking damage than the static moving case after 15 years of pavement service, as shown in figure 6. This indicates the importance of considering vehicle dynamic loading when assessing pavement performance. A somewhat unexpected result is that the rate of additional damage accumulation is linear, rather than accelerating as had been hypothesized. This result may be due to some of the simplifying assumptions made earlier, in particular the constant values of the concrete elastic modulus. (Note that these results differ from those discussed for faults earlier.)

Figure 7 illustrates the distribution of cracking along the slab length for the constant and dynamic moving load cases. For constant (or moving static) loads we obtain a symmetrical distribution of cracking over the slab, with the most severe cracking occurring in the regions close to the joints. Comparing this to the dynamically moving load, we note that there is a 15 percent decrease in the cracking that occurs in the regions close to the joints. Furthermore, there is a large increase in the cracking in the mid-slab regions, which is

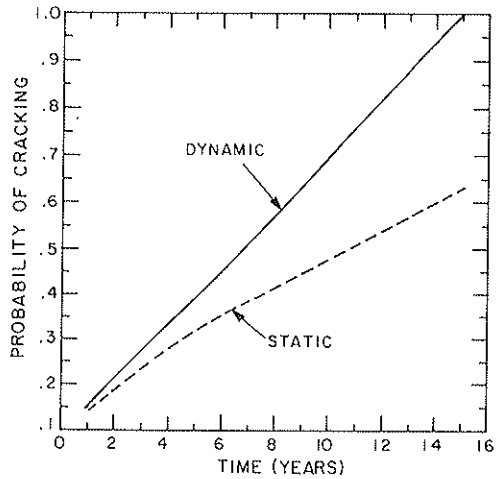

FIGURE 6 Growth in the probability of fatigue damage: moving dynamic load vs. moving constant load.

attributable directly to the body mode contribution to the tire force. The importance of the body mode contribution to total dynamic loading on rigid pavements has already been alluded to in the discussion of the role of pavement faults and joint spacing in exciting this mode; this finding will be reinforced in the analysis of vehicle characteristics below.

Single Leaf-Spring Suspension (2S1)

Effect of Leaf-Spring Stiffness The effect of increasing the leaf-spring stiffness is to reduce the wheel mode and increase the body mode contribution to the tire force on the pavement. (Wheel-mode forces are of higher frequency, about 10–15 Hz; body-mode forces are of lower frequency, about 2–3 Hz.) The resulting effect on pavement cracking over a 15-yr simulated period is a 10 percent reduction in the cracking damage when the leaf-spring stiffness is halved. Furthermore, mid-slab cracking is lowered by a reduction in the leaf-spring stiff-

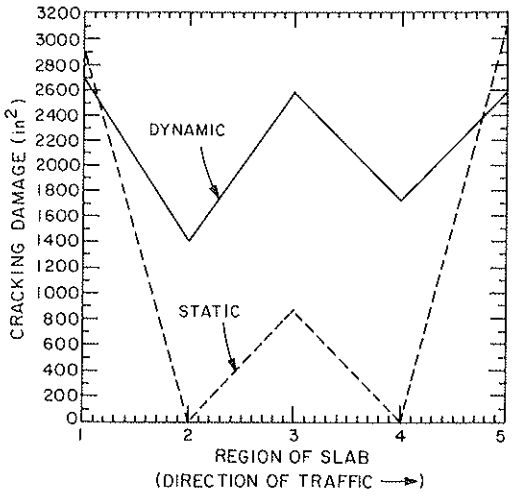

FIGURE 7 Cracking damage (in.^{2}) along slab length: moving dynamic load vs. moving constant load.

ness. However, these savings are somewhat offset by the increase in cracking in the region close to the joint, due to an increase in the wheel mode contribution to the tire force with the softer suspension.

Effect of β-Parameter β is a friction parameter that describes the hysteretic nature of the leaf-spring. The nominal (base-case) value of β is 4×10^{-3} feet. The effect of decreasing the leaf-spring damping (increasing β) is to increase the wheel mode contribution and reduce the body mode contribution. The reduction in the cracking occurs in the mid-slab region, similar to the case described above for suspension stiffness. The results show that a larger value of β, or reduction in leaf-spring damping, produces a reduction in cracking (approximately 12 percent) over the entire slab, due to the reduction in the body mode contribution.

Effect of Speed Vehicle loading was simulated at three different speeds: 35, 55, and 70 mph. For the particular vehicle and pavement characteristics used, 55 mph was determined to be the speed at which tire forces are maximum (in other words, the speed at which vehicle dynamics are reinforced by the pavement characteristics). At speeds other than this critical value the excitation of dynamic forces is reduced. For vehicle speeds of about 35 mph the effect of dynamics become less important, and the damage distribution resembles that of a static moving load. When speed is increased from 55 to 70 mph, pavement damage is reduced over most of the slab, but is increased in the latter part of the slab (where the vehicle leaves the slab).

Due to the coincidence of (1) the dimensions of the vehicle wheelbases, and (2) the slab length simulated, the vehicle experiences simultaneous inputs to the steer and rear axles. On an actual pavement, the frequency at which the vehicle experiences these inputs should be adjusted so it is not in the range of the body mode frequency. The adjustment can be made either by regulating vehicle speed or by changing the slab length.

Walking-Beam Tandem Suspension (3S2)

Analyses of the walking-beam suspension were conducted in a way similar to that described for the single leaf-spring suspension described above. Of the three speeds tested (35, 55, and 70 mph), 55 mph was the most critical (as it was for single axles) because of the excitation of the lightly damped out-of-phase axle pitch mode (approximately 10 Hz). Damage at 55 mph can be mitigated by reducing the tandem axle spacing from the standard of 52 inches simulated in these runs. However, the walking-beam suspension performs better than the single-axle suspension at low speeds, since it has the ability to filter out the faults in the pavement. This filtering occurs without excessively exciting the axle pitching mode at low speeds.

Four-Leaf Tandem Suspension (3S2)

In comparison to other axle groups, the four-leaf tandem does damage equivalent to the walking-beam (and more than the single-axle) at the slab joints, but it does no more damage than the single-axle suspension (and much less than the walking-beam) in the mid-slab regions. The reason that the four-leaf suspension does less damage than the walking-beam overall is that the out-of-phase pitching mode of the suspension is more restricted by the inherent coulomb friction in the leaf springs.

Effect of β-Parameter

The amount of cracking simulated is relatively sensitive to the β parameter. There is an optimal value of leaf-spring damping around $\beta = 4 \times 10^{-3}$ ft. (Recall that for single-axle suspensions, however, higher values of β were preferable.) The difference in response to β between these two axle groups is due to the coupling of the tandem axles (through the short-rocker). A lower value of β in the single-axle suspension translates to a larger contribution of the body mode, resulting in greater cracking damage (refer to the discussion of the single leaf-spring axle). In the tandem-axle case a very low value of β (high coulomb friction) results in increasing the contribution of the body mode to the tire force, thereby increasing the damage. On the other hand, too high a value of β excites the axle out-of-phase pitching mode, also increasing damage. Therefore, there exists an optimum value of β for the four-leaf tandem, lying between these extremes.

Effect of Tire Pressure

The effects of tire pressures were investigated for all the suspension types; the results for the four-leaf tandem will illustrate the trends observed. Tire pressure has some effect on vehicle dynamics, since lower pressures filter the input to the leaf-spring suspension, thereby attenuating the wheel mode contribution to the tire force. Also, lowering the tire pressure leads to a larger surface contact area, reducing the primary response (for example, stress) of the pavement. This would reduce the rate of crack initiation and propagation through the slab.

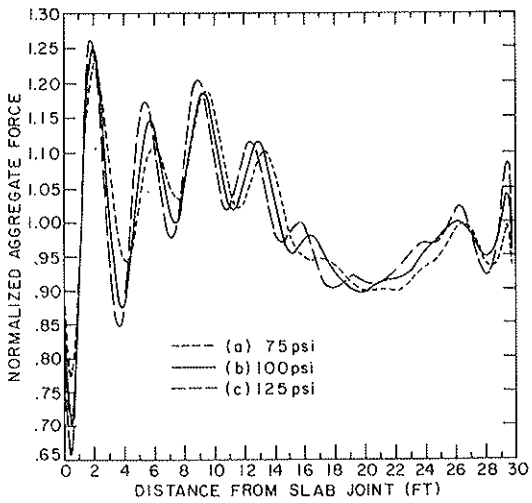

FIGURE 8 Effect of tire pressure, four-leaf tandem axle.

The analysis of tire pressure effects are shown in figure 8, where the aggregate dynamic force is shown for tire pressures of 75, 100, and 125 psi. These plots show that the greatest effect of tire pressure occurs at the second peak load, where a 5.5 percent increase in load magnitude is attained by raising the tire pressure from 75 to 125 psi. Tire pressure thus appears to have a small effect on vehicle dynamics and, therefore, a small effect on rigid pavement damage for the conditions tested in this study. This result differs from that observed for flexible pavements, where the influence functions tend to be narrower or tighter (the rigidness of the PCC slab renders it less sensitive to greater stress that may result from higher tire pressures).

Other Impacts

Other impacts are summarized below, with additional details in Reference 7:

- Increasing the leaf-spring stiffness by 50 percent produces a 6 percent reduction in the overall damage produced. This trend is the opposite of that for the single-axle leaf-spring, where softer suspensions are more favorable.
- Reducing the axle spacing from 52 to 40 inches increases the pavement damage by 9 percent. This is opposite to the effect produced in the walking-beam suspension, where the higher stress produced by bringing the axles together is far out-weighed by the reduced dynamics.
- Changing the load sharing coefficient (LSC) from perfect load sharing (LSC = 1.0) to LSC = 0.9 does not result in a significant change in damage overall but does redistribute damage somewhat, increasing the amount of cracking near the approach joint.

CONCLUSION

New analytic procedures have been developed to study in a very general way the interaction between vehicle dynamic loads and pavement damage. Detailed simulation programs of heavy truck dynamics have been created, and an existing rigid pavement program (PMARP) has been modified to account for dynamic tire loads on PCC slabs. To date, single and tandem axles have been investigated, with the following results:

- The static load case indicates that the mid-slab region has lower fatigue damage than the transverse joint regions. For the dynamic loading case, however, the mid-slab and transverse joint regions have similar fatigue damage values. Furthermore, fatigue damage due to dynamic moving loads in particular slab locations is up to 40 percent greater than that due to static loads.
- The mid-slab regions are more sensitive to dynamics than are the transverse joint regions. This results from the finding that the body mode contribution to the tire mode is more detrimental to cracking damage than the wheel mode contribution.
- For the particular combination of factors that was tested, the walking-beam suspension produces the most damage at highway speeds, followed by the four-leaf tandem and the single-axle suspension as the least damaging. These results may vary for other combinations of pavement and vehicle characteristics.

The factors that have been shown to be most critical in affecting dynamic loads on rigid pavements are

- Vehicle and axle configuration, and vehicle load,
- Suspension characteristics (stiffness, hysteresis),
- Vehicle speed, and
- Pavement roughness, faults, joint spacing, and slab warping.

Other factors are also important, although they were not specifically tested in the parametric study (for example, pavement design and environmental conditions, which affect the rate of pavement faulting and deterioration). Weakening of the pavement subgrade due to pavement pumping was not included in this set of analyses, and its inclusion might alter the conclusions obtained above. Tire pressure was investigated but not found significant in affecting dynamic loads; this conclusion is different from that obtained in earlier simulation of flexible pavements.

An important implication of these findings is the importance of the vehicle itself in influencing dynamic loads, implying that future policies governing the maintenance and rehabilitation of highway infrastructure may need to look at the vehicle as well as the pavement (and bridges). Furthermore, regulating heavy vehicles simply by gross weight and axle load may not be sufficient; the dynamic loads actually imposed by different axle configurations, suspensions, and tires may need to be accounted for. Finally, pavement management should be coordinated with the evolution in vehicle technology, since dynamic loads arise through the interaction of factors such as slab length, vehicle wheelbase, fault height, suspension damping, and axle spacing.

ACKNOWLEDGMENTS

This work has been supported by the U.S. Department of Transportation, Office of University Research. Technical supervision has been performed by the Federal Highway Administration. The authors wish to thank particularly William J. Kenis, Jr., who has served as Technical Monitor for this research and has provided very helpful suggestions and guidance.

REFERENCES

1. P. F. Sweatman. *A Study of Dynamic Wheel Forces in Axle Group Suspensions of Heavy Vehicles*. Special Report 27. Australian Road Research Board, June 1983.
2. A. P. Whittemore, J. R. Wiley, P. C. Schultz, and D. E. Pollock. *Dynamic Pavement Loads of Heavy Highway Vehicles*. National Cooperative Highway Research Program Report 105. HRB, National Research Council, Washington, D.C., 1970.
3. P. Ullidtz and B. K. Larsen. Mathematical Model for Predicting Pavement Performance. In *Transportation Research Record 949*, TRB, National Research Council, Washington, D.C., 1984, pp. 45–55.

4. S. P. O'Connell, E. Abbo, and J. K. Hedrick. Analyses of Moving Dynamic Loads on Highway Pavements: Part 1: Vehicle Response. *Proceedings, International Symposium on Heavy Vehicle Weights and Dimensions*, Kelowna, British Columbia, June 1986.
5. K. Hedrick, D. Cho, A. Gibson, J. Isaacson, and S. O'Connell. *Determination of Road Stress Factors for Buses*. Interim Report. U.S. DOT, February 1985.
6. J. K. Hedrick, M. Markow, B. Brademeyer, S. O'Connell, N. Delatte, and A. Gibson. *Predicting Models for Evaluating Load Impact Factors of Heavy Trucks on Current Pavement Conditions*. Interim Report. U.S. DOT, December 1985.
7. E. Abbo. *The Influence of Heavy Vehicle Dynamics on Rigid Pavements*. Master's thesis. Massachusetts Institute of Technology, January 1987.
8. N. J. Delatte. *Characterization of Dynamic Vehicle-Pavement Interaction*. Master's thesis. Massachusetts Institute of Technology, June 1986.
9. J. Larralde, W. F. Chen, C. W. Lovell, and C. D. Sutton. *Purdue Method for Analysis of Rigid Pavements: Users' Guide*. Purdue University; Federal Highway Administration, U.S. DOT, December 1984.
10. M. J. Markow and B. D. Brademeyer. *EAROMAR Version 2: Final Technical Report*. FHWA/RD-82/086. Federal Highway Administration, U.S. DOT, April 1984.

Publication of this paper sponsored by the Committee on Strength and Deformation Characteristics of Pavement.

LEF Estimation from Canroad Pavement Load-Deflection Data

L. R. RILETT AND B. G. HUTCHINSON

Load equivalency factors (LEFs) versus axle-load regression equations are reported for single-, tandem-, and tridem-axle groups. These functions have been developed from truck loading test data collected at nine sites across Canada in 1985 by the Canroad Transportation Research Corporation. While the load on the axle groups dominated the regression equations, pavement temperature, axle spacing, and vehicle velocity were found to be statistically significant for the tandem-axle groups at a number of the sites. Regression analysis of the pooled tandem data showed that load and axle spacing were significant. Analysis of the pooled tridem-axle group data showed that load, axle spacing, structural number, and vehicle speed were significant. The load equivalency functions are compared with the AASHTO functions and the differences highlighted.

A comprehensive set of field measurements of pavement surface deflections and surface course interfacial strains were obtained at fourteen test sites across Canada in 1985. These measurements have been reported by Christison (*1*) and were part of a major study of vehicle weights and dimensions conducted by the Canroad Transportation Research Corporation. Christison (*2*) analyzed these data and developed a set of response-type load equivalency factors (LEFs) for single-, tandem-, and tridem-axle groups, and these LEFs form the basis of a set of draft regulatory principles for interprovincial trucking in Canada (*3*).

Hutchinson et al. (*4*) have reanalyzed the pavement deflection data collected in this study using the ASTM Standard Practice for Counting Damage Cycles (*5*), instead of the method used by Christison (*2*), to extract the pavement damage cycles. This alternative method of analysis produced LEFs that were, on the average, 8 percent higher than those calculated by Christison (*2*) for the tandem-axle groups and 16 percent higher for the tridem-axle groups.

Neither of the analyses cited above conducted an exhaustive statistical analysis of this very rich data base. Variations in LEFs with vehicle speed, intra-axle spacing, pavement temperature, and pavement structural characteristics were not comprehensively analyzed. This paper describes the results of a comprehensive regression analysis of the influence of these factors on the LEFs, using the surface deflection data. The surface course-base course interfacial strain data have not been analyzed because they are not readily available to outside users at this time.

University of Waterloo, Waterloo, Ontario N2L 3G1, Canada.

DATA BASE

Surface deflections and interfacial (surface-base) strains were observed at fourteen test sites for a variety of test conditions. The Canroad Transportation Research Corporation developed a test vehicle that allowed a variety of tandem- and tridem-axle configurations to be developed and tested under a range of axle-group loads. Tests were also conducted at speeds of 6, 13, and 50 km/h. Each test run consisted of pairs of pavement response measurements under a standard Benkleman Beam truck with an 8,160 kg single-axle load on dual tires and under the candidate axle group. Three test runs were conducted at each velocity, and the published deflection data consist of the average, minimum, and maximum deflections under each axle of an axle group as well as the inter-axle residual deflections for multiple-axle groups. Christison (*1*) provides a detailed description of the data base in terms of the test program and pavement properties.

Figure 1(a) shows a typical deflection profile under the passage of a tridem-axle group. The load on the axle group was 26,036 kg, the axle spacing 3.7 m, the truck speed 12.9 km/h, and the pavement temperature 23.6°C. The diagram shows that the measured surface deflection increased from 0.442 mm through 0.498 mm to 0.503 mm under the passage of this tridem. The inter-axle residual deflection increased from 0.119 mm to 0.130 mm between the second and third axles. The deflection under the Benkleman beam truck was 0.422 mm. The maximum deflection tended to occur under the last axle of both the tandem and tridem groups at most test sites.

ESTABLISHING LOAD EQUIVALENCY FACTOR FUNCTIONS

The LEF for a particular load on a candidate axle group is usually defined as the ratio of the number of passes of a standard axle load to the number of passes of a candidate axle load to create the same amount of pavement damage. There are three broad approaches to establishing the LEF functions for different axle groups, and these are frequently referred to as the empirical approach, the theoretical approach, and the mechanistic approach.

EMPIRICAL APPROACH

The principal source of information for empirically determined LEF functions is the AASHO Road Test, where the

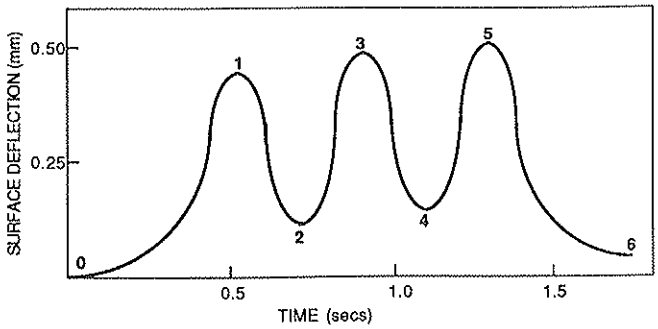

(a) SURFACE DEFLECTION PROFILE UNDER 26 036 KG TRIDEM

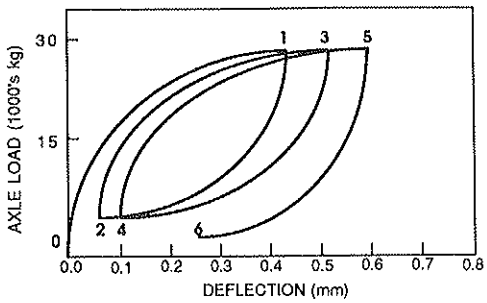

(b) LOAD - DEFLECTION HISTORY UNDER TRIDEM PASS

$$LEF = \left(\frac{0.503}{0.422}\right)^{3.8} + \left(\frac{0.498-0.130}{0.422}\right)^{3.8} + \left(\frac{0.422-0.119}{0.422}\right)^{3.8}$$

(c) LEF CALCULATION FOR TRIDEM PASS

FIGURE 1 Calculation of LEF for tridem axle pass.

deterioration of pavement sections of various thicknesses under homogeneous truck loads on single axles and on tandem axles were measured. It is well known that LEFs calculated for different loads on single- and tandem-axle groups vary with the PSI chosen to define failure and with the structural characteristics of a pavement. The AASHO Road Test analyses suggested that the LEF of a candidate axle group could be approximated by the fourth power of the ratio of a candidate axle load to the standard axle load. The results obtained from the AASHO Road Test are difficult to apply directly to current legal axle group loads and to axle groups other than singles and tandems, since this involves extrapolation of the results outside the range for which they were developed. For instance, the AASHTO LEF functions for tridems assumes that a tridem-axle group pass is equivalent to a single plus a tandem pass (*6*). This assumption is not supported by theoretical considerations or field observations.

THEORETICAL APPROACH

The theoretical approach to LEF function estimation proceeds by calculating the deformations or stresses in a pavement structure in combination with a fatigue damage law to establish the relative damage created by different axle groups and configurations.

Deacon (*7*) used maximum principal tensile strain as the fatigue damage parameter and compared his theoretical LEF magnitudes with those established at the AASHO Road Test. The recommended AASHO tandem equivalences were 80 percent of the theoretical values for pavements with structural numbers greater than 3, while the equivalences for single axles were approximately equal. Deacon suggested that for pavements with structural numbers of less than 3 the primary failure mechanism was not fatigue, and his approach might not be appropriate.

Ramsamooj et al. (*8*) used theoretical fracture mechanics to derive load equivalency factors from longitudinal stress intensity factors. They defined the LEF for single axles as the ratio of the maximum rise in the influence line for the stress intensity factor K for the candidate axle load to the maximum rise in K for the standard load, raised to the fourth power. For tandem axles the ratio of the peak-to-trough value of the stress intensity factor to that of the standard axle raised to the fourth power was also calculated. The accumulation of the damage cycles caused by each axle in the tandem was accomplished by adding these two calculations. This method of damage accumulation is adopted in this paper.

Treybig (*6*) developed fundamental relationships between damage related factors and performance based equivalency factors through the analysis of AASHO pavements. Subgrade compressive strain was found to have the best relationship with observed pavement performance as compared with surface tensile strain at the surface course-base course interface and surface deflection. This is rational since most of the Road Test pavements failed in rutting. Elastic layer theory was used for computing strains, and these were used for calculating LEFs for axle configurations other than single and tandem over a wide range of loads. These were then used to extend the equivalency factor concept to new size and weight configurations.

MECHANISTIC APPROACH

The mechanistic approach is similar to the theoretical approach, with the primary difference being that the distress indicators are measured in situ and not calculated. Christison (*2*) applied the cycle damage-pavement distress procedures adopted by Deacon and used measured surface deflection and interfacial tensile strain to predict LEF. For single axle loads the defection-based LEF was calculated using equation 1:

$$LEF_i = \left(\frac{d_i}{d_b}\right)^C \tag{1}$$

where d_i and d_b are the surface deflections under various single-axle loads and under the 80 kN (18 kip) single-axle, dual-tire loads, respectively.

The exponent C is the slope of the deflection-anticipated traffic loading relationship and was set equal to 3.8 following the recommendation by the Pavement Advisory Committee of the Canroad study.

Tandem-axle LEFs were calculated using equation 2:

$$F_i = \left(\frac{d_i}{d_b}\right)^C + \left(\frac{e_i}{d_b}\right)^C \tag{2}$$

where d_i equals the maximum surface deflection under each leading axle, and e_i equals the difference between maximum deflection under the second axle and the intermediate deflection between axles.

It is assumed that a linear summation of cycle ratios will govern the behavior of the pavement. This method has been used by a variety of authors to develop LEF functions based on fatigue analysis principles. For the most part, these functions have been fairly close to the AASHO relationships even though the latter are based on a PSI index, which attempts to combine cracking, shear deformation, and longitudinal profile into a single term. These theoretical methods do allow for the development of LEFs for conditions that were not studied in the AASHO Road Test, and they allow for the analysis of various influential variables that may affect pavement performance. In reviewing the LEF functions developed in this paper is must be remembered that they are based on these assumptions.

ISOLATION OF DAMAGE CYCLES

The calculation of the pavement damage implied by passages of particular axle groups consisted of two steps; these are (1) the isolation of the load-deformation cycles under each axle group and (2) the accumulation of the damage created by each cycle, which was estimated by dividing the maximum deflection observed in a load-deformation cycle by the deflection observed under the standard Benkleman beam truck, raising this ratio to 3.8, and summing the result across all load-deformation cycles induced by an axle group. This procedure is illustrated in figure 1 for the surface deflections observed under a tridem-axle group pass.

Figure 1(b) shows the load-deformation history of the surface course induced by the passage of the tridem. The ASTM Standard Practice for Cycle Counting in Fatigue Analysis (*5*) has been used to isolate the following load-deformation cycles:

Cycle	*Load-Deformation Path*	*Deflection (mm)*
Largest	0-5-6	0.503
Second largest	3-4-3	0.368
Third largest	1-2-1	0.323

Figure 1(c) shows that this results in an LEF of 2.97. The method used by Christison (*2*) results in an LEF of 2.5. This method of analysis is described in more detail by Hutchinson et al. (*4*) and compared with the method of damage accumulation used by Christison (*2*).

SITE-SPECIFIC LEF FUNCTIONS FOR TANDEM-AXLE GROUPS

The LEFs calculated for nine sites have been subjected to a comprehensive regression analysis in an attempt to isolate the influences of pavement temperature, vehicle speed, and axle spacing on LEF with equations of the following form being estimated:

$$\text{LEF} = \text{CONSTANT} * \text{LOAD}^l * \text{TEMP}^t * \text{SPEED}^s * \text{AXLE-SPACING}^a \tag{3}$$

where:

LOAD = load on tandem-axle group (1000 kg),
TEMP = average pavement temperature recorded during test run (°C),
SPEED = velocity of test vehicle (km/h), and
AXLE-SPACING = front-to-rear axle spacing in tandems and tridems (m).

The parameters of equation 3 have been estimated using multiple linear regression analysis of a natural logarithmic transformation of the data. Table 1 summarizes the results for the nine test sites analyzed. Sites 2 and 12 were not included, as preliminary results seemed to indicate that the deflection measurements contained excessive residuals. Similarly, site 3B was excluded, as the site was damaged during testing, and site 8 was excluded because the subbase consists of an old road. The number in brackets under each test site number is the structural number of the pavement at that site. The t-magnitudes are shown in brackets below the parameter magnitudes, and the parameters are significant at the 1 percent level except for those identified with an asterisk, which are significant at the 5 percent level. The second equation listed for each site is a simple regression equation relating LEF to load on the tandem-axle group.

TABLE 1 REGRESSION EQUATIONS FOR TANDEM-AXLE GROUPS

SITE	CONSTANT	l	s	t	a	R^2	n
1 (6.3)	.01174885	2.266 (29.8)	0.259 (8.8)	-0.574* (2.6)		.94	69
	.00367574	2.300 (21.0)				.87	
3 (6.1)	.00252883	2.380 (28.1)	0.072* (2.2)			.92	60
	.00308872	2.380 (27.3)				.92	
4 (3.6)	.00048663	3.127 (28.3)			-0.762* (-2.4)	.93	60
	.00034950	3.158 (27.2)				.93	
5 (4.2)	.00039922	2.876 (30.2)	-0.263 (-7.7)	0.497* (2.2)	-0.956 (-3.4)	.95	60
	.00066349	2.902 (20.9)				.88	
6 (4.3)	.00012768	2.774 (43.6)	-0.136 (-5.4)	0.676 (5.7)		.97	69
	.00082758	2.804 (32.8)				.94	
7 (5.1)	.00003884	2.974 (26.9)		0.707* (2.4)		.95	42
	.00043420	2.977 (25.5)				.94	
9 (3.6)	.00116971	2.74 (32.4)	0.207 (6.1)		-1.34 (-4.8)	.94	71
	.00115345	2.755 (24.2)				.89	
10 (3.4)	.00034395	2.869 (42.7)		0.300 (2.7)	-0.460* (-2.1)	.97	71
	.00095672	2.829 (41.3)				.96	
11 (6.6)	.00066150	2.844 (34.8)				.97	44
13 (6.9)	.00257733	2.394 (23.6)				.93	42

n = number of observations

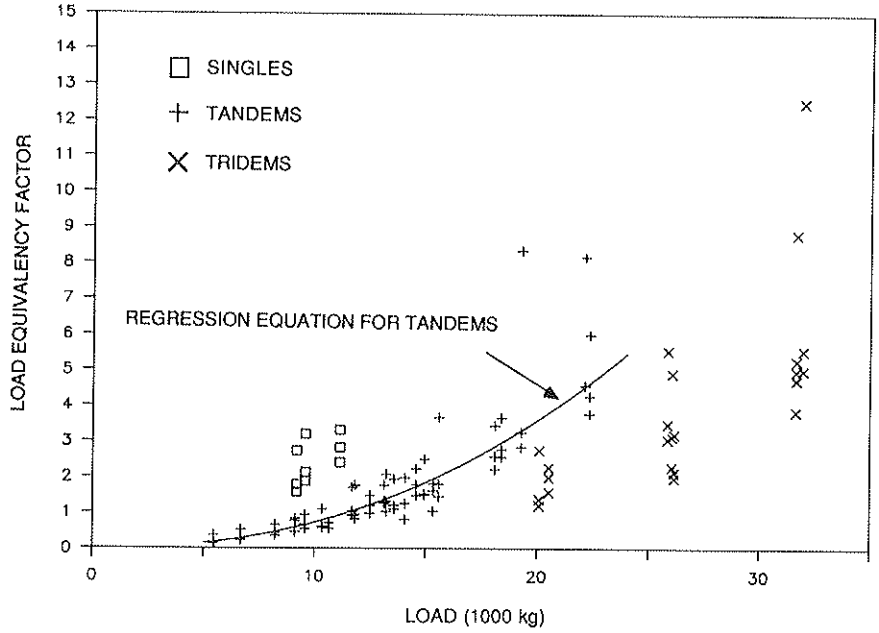

FIGURE 2 LEF vs. load on axle group for site 1.

Figure 2 shows the relationship between calculated LEF and load on axle group for site 1 for the three axle groups. The regression equation estimated for the tandems is also plotted on the diagram. Insufficient data are available to allow meaningful regression equations to be estimated for the single- and tridem-axle groups.

In interpreting these regression equations it should be remembered that the LEFs have been calculated from the ratios of deflections observed under the test vehicle to those observations under the Benkleman beam vehicle. That is, speeds, temperature, and structural number are effectively constant for each pair of test runs.

Inspection of the exponent of the load term shows that it varies only marginally between the two equations for each site and that there are some differences in the magnitudes of the exponent between sites. For example, site 1 has an exponent of 2.266, while site 4 has a magnitude of 3.127. A comparison of the coefficients of determination of the two models developed for each site show that the load term dominates the explanation of the variation in LEF.

Further inspection of the entries in table 1 shows that speed has a significant effect at five of the sites but that the sign of speed is not consistent. Flexible pavement deflection decreases as vehicle speed increases, and the results from the AASHO Road Test indicate that the percentage reduction in deflection is less for heavier vehicles than for lighter ones. Given that the LEF calculation is based on a ratio, one might hypothesize that increasing vehicle speed would result in an increase of the LEF, all things being equal. This would result in a positive coefficient for single-axle calculations.

This question is a little more complex for the tandem axles as there are two elements to the LEF calculation. The dominant factor is the maximum deflection term, and this is always lower for the higher speeds. However, given that the loading sequence is faster at higher speeds, the pavement does not have as much time to recover before the second axle loading occurs. It could be argued that this increase in the maximum deflection relative to the Benkleman beam deflection would result in a higher LEF. The second term could lower or raise the LEF when comparing LEFs across speeds, but since this value is usually less than unity, and it is raised to the 3.8th power, its effect is minimal. For those sites that exhibited positive coefficients for the speed variable, the ratios of maximum deflection over the Benkleman beam deflection increased with speed, while the opposite was true for those with negative coefficients.

Temperature was found to be significant at five sites and the exponents of temperature varied from 0.300 to 0.707 and were all positive, except for site 1. The range of average pavement temperatures at which the majority of tests were conducted at the sites that did not experience a significant temperature effect was about 10°C. The only exception to this was site 9, where the range was approximately 16°C to 30°C. The other sites experienced pavement temperature ranges of about 15°C, except for site 1, where the majority of the temperatures were between 18°C and 28°C. The testing process was not designed to isolate the effects of temperature; and, therefore, at those sites where pavement temperature was relatively constant, it would be expected that temperature would not have a significant influence.

Deflection tends to increase with increasing pavement temperature. A positive coefficient for a single-axle load would indicate that this increase in deflection is not the same percentage for all loads. More specifically, as temperature increases the deflections caused by larger loads increase faster than those for smaller loads. For tandem axles it may be hypothesized that the maximum deflection will increase with increasing pavement temperatures at a greater rate than for the lower load of the Benkleman beam truck. This would explain the positive signs of the pavement temperature variable.

It should also be noted that when the temperature effect was not significant (sites 3a and 9), the speed coefficient was positive. When the exponent of temperature was significant the exponent of speed had the opposite sign. Sites 5 and 6 have negative temperature exponents, while site 1 has a positive temperature exponent.

This change in the sign of the speed variables might indicate a temperature × speed interaction in terms of load equivalency factors. For relatively constant temperatures the load equivalency factor increases with increasing speed. However, when temperature is not constant there seems to be a decrease in LEF with increasing speed. This interaction is accounted for implicitly in the multiplicative forms of the model used in this analysis and would account for the differences found.

Perhaps more interesting are the results from the axle spacing variable. The coefficients were found to be significant only at four sites (4, 5, 9, and 10) and they ranged from −0.46 to −1.34. This means that as axle spacing increases the calculated load equivalency factor decreases. It should be noted that the sites that had the lowest calculated structural number were the ones where axle spacing was significant. This makes sense in that for the larger spacings, the pavement would have time to recover from the deformation caused by the first wheel load before the arrival of the second. Due to the nature of the load equivalency factor calculations the maximum deflection used would not be as high for the larger axle spacings. Conversely, the intermediate deflection used would be higher for the larger axle spacings. However, the maximum deflection term dominates, and this difference tends to yield lower LEF factors and hence the negative exponent of axle spacing.

POOLED LEF FUNCTIONS FOR TANDEMS

The data for the tandems were pooled for all of the test sites, the structural number was added as the fifth independent variable in equation 3, and the following equation resulted:

$$LEF = 0.0013563 \cdot \underset{(73)}{\text{LOAD}^{2.698}} \times \underset{(-3.4)}{(\text{AXLE SPACING})^{-0.396}} \quad (4)$$

$R^2 = 0.90$

No. observations = 597

$$LEF = 0.0011420 \cdot \underset{(72)}{\text{LOAD}^{2.704}} \quad (5)$$

$R = 0.90$

Figure 3 shows the LEF versus load on axle group for the 1.5-m tandems, while figure 4 shows the results for 1.2-m and 1.8-m tandems. In addition, the regression lines for each axle spacing are also shown. Equation 4 indicates that axle spacing is the only significant independent variable in addition to load on the tandem-axle group. The exponent of axle spacing means that the LEF decreases with increasing axle spacing. It should be recalled that the maximum deflection normally occurs under the second axle and that this maximum decreases with increasing axle spacing, since the pavement has more time to recover from the deflection induced by the lead axle. For a 16,000-kg tandem-axle load, equation [4] implies that the LEF would decrease from 2.2 at an axle spacing of 1.2 meters to 1.9 at a spacing of 1.8 meters, a reduction of about 14 percent. Sufficient data existed for the tests involving tandems with 1.5-m axle spacing to explore further the impacts of each of the variables and the following equation was estimated:

$$LEF = 0.0008665 \cdot \underset{(53)}{\text{LOAD}^{2.692}} \cdot \underset{(3.2)}{\text{SN}^{0.191}} \quad (6)$$

$R^2 = 0.87$

No. observations = 433

Equation 6 indicates that LEF increases with increasing structural number. From the previous discussion it might be expected that as pavement strength increased, there would be a relative decrease in maximum deflection resulting in a lower LEF. Inspection of equation 6 shows that the exponent of structural number is positive, although the magnitude is small and has little absolute impact on the LEF.

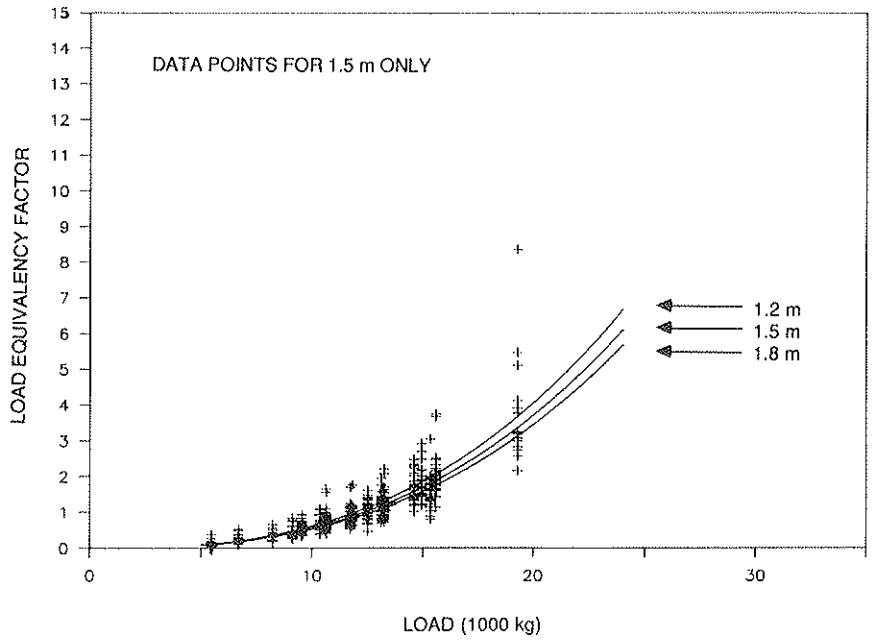

FIGURE 3 LEF vs. load on axle group for 1.5-m tandem.

POOLED LEF FUNCTIONS FOR SINGLE AXLES

Data were pooled for the single axles, as there were insufficient data to establish site-specific LEF functions. The following regression equation was estimated:

$$LEF = 0.0153598 \cdot \text{LOAD}^{2.159} \quad (7)$$

$R^2 = 0.43$ (75)
No. observations = 75

Equation 7 shows that only load is significant for single axles. Figure 5 shows the LEFs plotted against load on the single axle, along with equation 7. The coefficient of determination of the model is rather low, and this reflects the narrow load range for the single axles, which were only tested at three loads, all of which were very close to the standard axle load. This tends to reduce the influence of the loading variable and helps to explain why the load coefficient value is not closer to the theoretical value of 3.8.

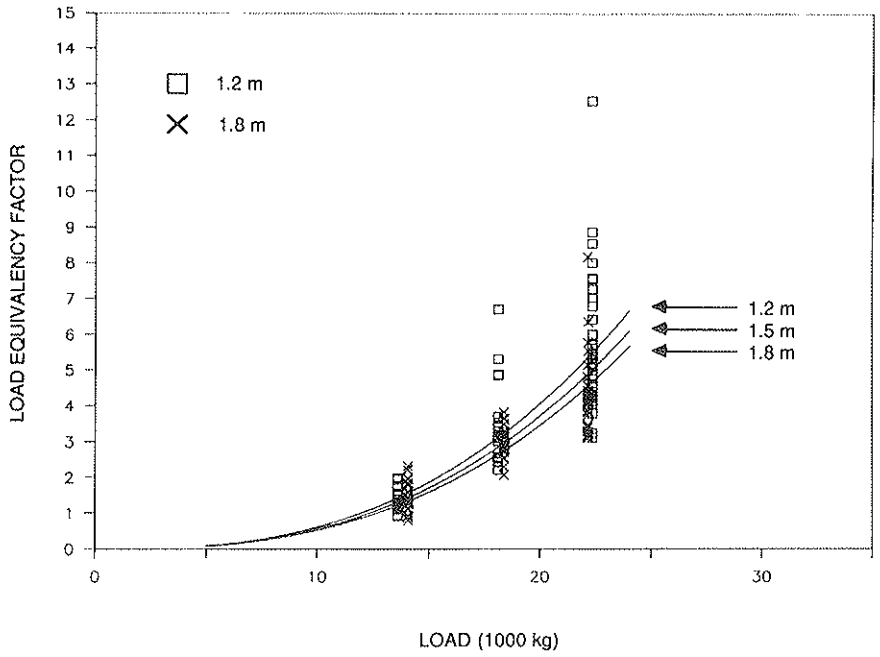

FIGURE 4 LEF vs. load on axle group for 1.2-m and 1.8-m tandems.

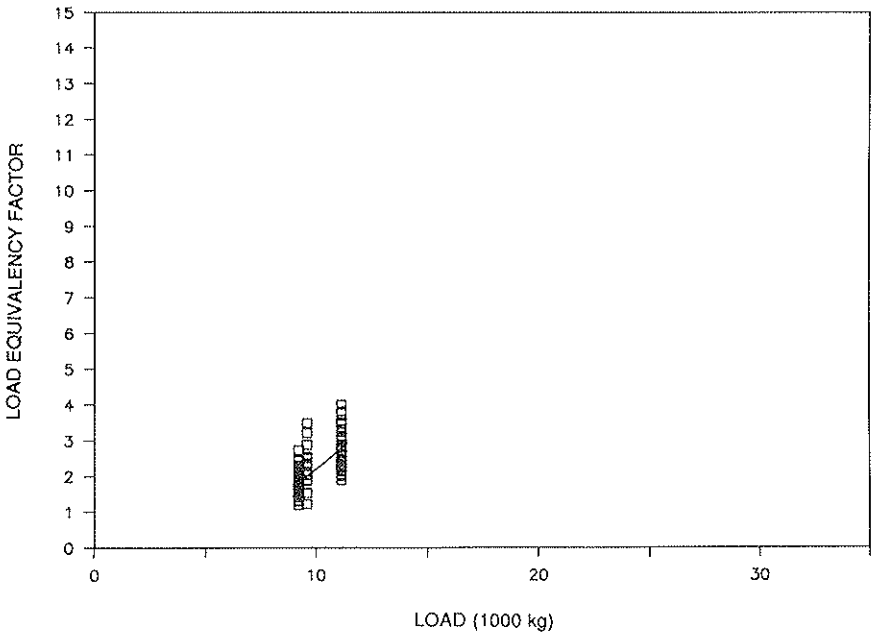

FIGURE 5 LEF vs. load for single axles.

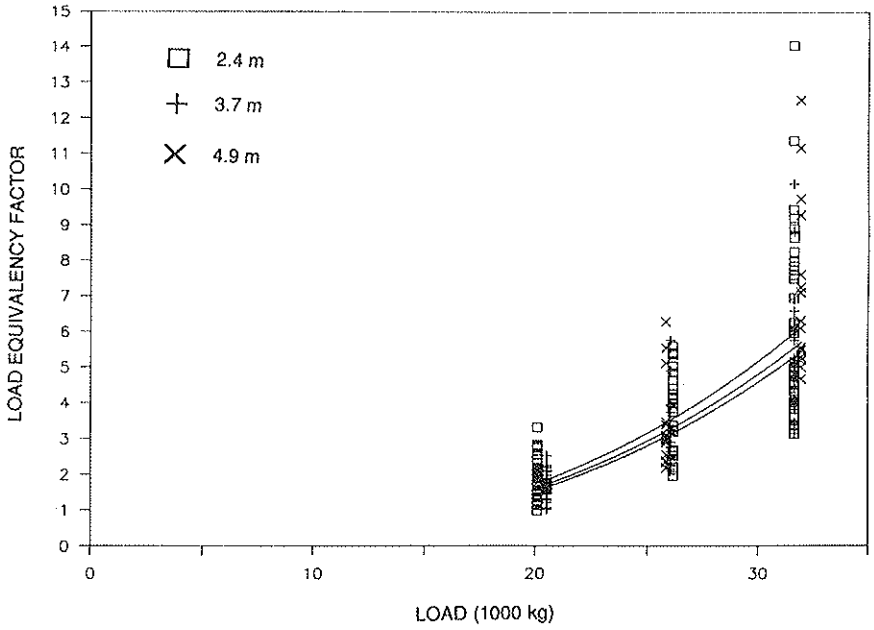

FIGURE 6 LEF vs. load on axle group for tridems.

POOLED LEF FUNCTIONS FOR TRIDEMS

The data available for the tridems were pooled, and the following regression equations were estimated:

$$LEF = 0.0008276 \cdot \text{LOAD}^{2.669} \cdot \text{AXLE-SPACING}^{-0.168} \times \text{SN}^{-0.251} \cdot \text{SPEED}^{.074} \quad (8)$$

(2.9) (22) (2.9) (−2.9)

$R^2 = 0.74$

No. observations = 190

$$LEF = .0006205 \cdot \text{LOAD}^{2.639} \quad (9)$$

(21)

$R^2 = 0.71$

The LEFs are plotted against the load on the axle group for tridems in figure 6, along with equation 8 for axle spacings of 2.4, 3.7, and 4.9 meters. Equation 8 shows that axle spacing, structural number, and vehicle speed are significant. The exponent of axle spacing is negative, indicating that as axle spacing increases the calculated LEF decreases. This is the same trend found for the tandem axles. The structural number exponent is also negative, which is opposite to the sign found for the tandem analysis. The LEFs reported for singles and tandems in the AASHTO interim guide show that they change in different ways with load, structural number, and terminal PSI. The vehicle speed coefficient is positive, but it is of such a low value that its impact on LEF is minimal.

COMPARISON WITH AASHTO LEF FUNCTIONS

Figure 7 compares some of the LEF functions reported in this paper with the AASHTO load equivalency functions. The tandem-axle function is for an axle spacing of 1.5 meters and an SN of 5. The tridem function is for a spacing of 3.7 meters, an SN of 5, and a velocity of 50 km/h. Inspection of the single-axle LEF function shows that it diverges significantly from the AASHTO function either side of an axle load of 10,000 kg. This divergence reflects the lower exponent of load shown in equation 7. It must be remembered that the range of single-axle loads tested was quite narrow. A comparison of the LEF functions for tandem axles shows that the LEFs calculated in this paper are significantly higher than the AASHTO functions for the range of axle groups between 10,000 and 20,000 kg. The relative positions of the two tandem LEF functions will change with changing assumptions about axle spacing and structural number. The LEF functions for the tridems have similar slopes, but the LEF function reported in this paper produces significantly higher LEFs than the AASHTO function. At a 25,000 kg axle group load the AASHTO LEF is about 1.6 compared with about 3.

CONCLUDING REMARKS

The LEF functions described in this paper are based on the the very strong assumption that load-associated pavement damage is governed by the load-deformation cycles observed under different axle groups. Load-deformation cycles have been extracted using ASTM standard practice. The LEF functions described in this paper may be described as response type functions in contrast to those that might be developed from field trials. The site-specific LEF functions for tandem-axle groups are dominated by the load term, but speed, temperature, and axle spacing also had significant impacts at many of the sites. Inconsistencies in the signs of the exponents for speed and temperature between sites suggest that a speed × temperature interaction effect exists. It is difficult to isolate this effect because the test pavement temperatures were not

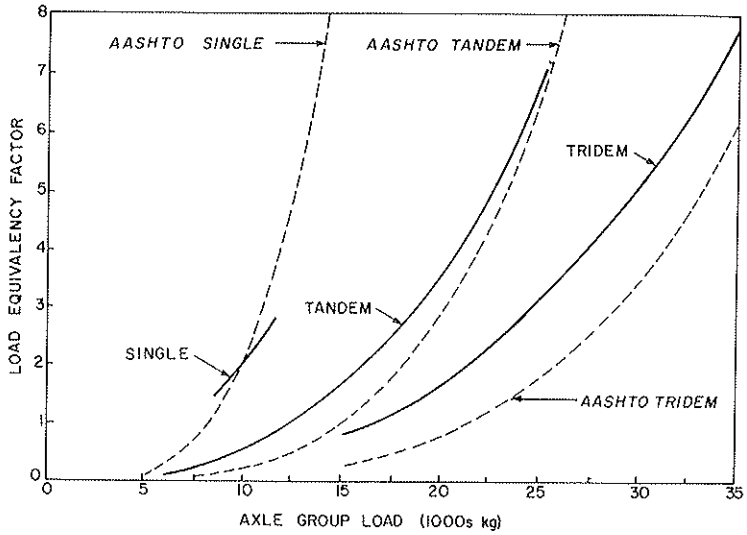

FIGURE 7 Comparison of LEF functions with AASHTO functions.

consistent between sites. Increasing axle spacing on the tandems produced statistically significant reductions in the LEFs at four sites, and these sites had the smallest structural numbers. A regression analysis of the pooled data for all tandems resulted in significant exponents for load and axle spacing but with load dominating the regression equation. Analysis of the pooled data for the 1.5-m tandems resulted in significant exponents for load and structural number, although the exponent of the structural number is small. The LEF function for the single axles had a rather low explanatory power, but this reflects the narrow range of loads tested.

Analyses of the pooled data for the tridems resulted in statistically significant exponents for load, axle spacing, structural number, and speed. The signs of axle spacing and structural number are negative while that of speed is positive, although small. Comparisons of the LEF functions developed in this paper with those of AASHTO showed some important differences. The tandem LEF function produces significantly higher LEF magnitudes than AASHTO and the single and tridem LEF functions had smaller slopes but produced similar magnitudes around LEFs of two.

REFERENCES

1. J. T. Christison. *Pavements Response to Heavy Vehicle Test Program: Part 1*. Canroad Transportation Research Corporation, 1986.
2. J. T. Christison. *Pavements Response to Heavy Vehicle Test Program: Part 2*. Canroad Transportation Research Corporation, 1986.
3. *Recommended Regulatory Principles for Interprovincial Heavy Vehicle Weights and Dimensions*. Joint RTAC/CCMTA Committee on Heavy Vehicle Weights and Dimensions, June, 1987.
4. B. G. Hutchinson, R. C. G. Haas, P. Meyer, K. Hadipour, and T. Papagiannakis. Equivalencies of Different Axle Load Groups. *Proceedings, 2nd North American Conference on Managing Pavements*, Toronto, 1987, pp. 3.191–3.202.
5. ASTM Standard E 1049-85: Standard Practices for Cycle Counting in Fatigue Analysis. *Annual Book of ASTM Standards*, Vol. 03.01, American Society for Testing and Materials, 1986.
6. H. J. Treybig. Equivalency Factor Development for Multiple Axle Configurations. In *Transportation Research Record 949*, TRB, National Research Council, 1983, pp. 32–44.
7. J. A. Deacon. Load Equivalency in Flexible Pavements. *Proceedings, AAPT*, 38, 1969, pp. 465–494.
8. D. V. Ramsamooj, K. Majidzadeh, and E. M. Kauffmann. The Analysis and Design of the Flexibility of Pavement. *Proceedings, International Conference on the Structural Design of Asphalt Pavements*, 1972, pp. 692–704.

Publication of this paper sponsored by Committee on Strength and Deformation Characteristics of Pavement Sections.

Field Evaluation of Bonded Concrete Overlays

SHIRAZ D. TAYABJI AND CLAIRE G. BALL

A field program of strain and deflection measurements was conducted by the Construction Technology Laboratories (CTL) for the Iowa Department of Transportation. The objective of the field measurement program was to obtain information on bonded concrete resurfaced pavements that can be used as a data base for verifying bonded resurfacing thickness design procedures. Data gathered during the investigation included a visual condition survey, engineering properties of the original and resurfacing concrete, load related strain and deflection measurements, and temperature-related curl (deflection) measurements. Field load testing was conducted by CTL at five sites in Iowa during April 1986. This report presents the results of field testing, analysis of results, and recommendations to incorporate study results in Iowa design procedures for bonded concrete overlays. Results of the investigation indicate that the four overlaid pavement sections evaluated as part of the reported study are performing as monolithic pavements with high interface shear strength at the interface. The strength of the existing pavement at all of the four overlaid test sections was high. In addition, cores obtained from sections 4 and 5 did not indicate D-cracking related damage in the overlay concrete. Comparison of the condition surveys for Section 1 (non-overlaid JRCP) and Section 2 (overlaid JRCP) indicate that all cracking in the existing pavement is not reflected through the overlay and that the cracks that did reflect through have remained tightly closed. Similarly, the condition survey of sections 4 and 5 indicate that cracks reflected through the overlay continue to remain tightly closed even after almost seven years of service. The field investigation conducted by CTL verifies that for properly constructed bonded overlays, pavement strengthening is achieved and that the overlaid pavement behaves monolithically as a full-depth concrete pavement.

A field testing program to measure strains and deflections was conducted by the Construction Technology Laboratories (CTL) for the Iowa Department of Transportation. The objective of the field measurement program was to obtain information on bonded concrete resurfaced pavements that could be used as a data base for verifying bonded resurfacing thickness design procedures. Data gathered during the investigation included a visual condition survey, engineering properties of the original and the overlay concrete, load related strain and deflection measurements, and temperature-related curl (deflection) measurements.

Resurfacing is basically the addition of a surface layer to extend the life of an existing pavement. Portland cement concrete has been used to resurface existing pavements since about 1913.

Transportation Systems Section, Construction Technology Laboratories, Inc., Skokie, Ill.

For many years concrete overlays were designed based on experience or engineering judgment. Use was also made of the Corps of Engineers procedure for design, which requires a coefficient that rates the condition of the existing pavement. However, since the rating for this procedure is based on the amount of surface cracking, it is subjective. In the last few years, several more rational procedures have been developed for concrete overlays. These procedures incorporate an evaluation of the existing pavement by nondestructive load testing and/or use the finite element methods of analysis to establish overlay thickness requirements. A recent design procedure for bonded overlays developed by the Portland Cement Association (PCA) is based on the finite element method of analysis (*1*). This procedure incorporates the strength characteristics of the existing and overlay pavement to compute overlay thickness. The procedure currently used by the Iowa DOT to establish bonded overlay thickness requires use of the Road Rater equipment to evaluate the existing pavement.

Field load testing was conducted by CTL at five sites in Iowa during April 1986. This paper presents the results of field testing, analysis of results, and recommendations to incorporate study results in Iowa's design procedure for bonded concrete overlays.

RESEARCH OBJECTIVES

Objectives of the study were as follows:

1. Perform condition survey and load testing of the overlaid pavement sections.
2. Analyze field data.
3. Prepare a report containing a discussion of use of the field data to verify design procedures for bonded concrete overlays.

PAVEMENT TEST SECTIONS

Field measurements were obtained at five pavement sections located in the State of Iowa. A brief description of each pavement section follows:

Section 1

This test section, located along the westbound lanes near mile post 190 on I-80, is a 24-ft wide roadway. The original pavement, constructed in 1964, is jointed reinforced concrete with

joints spaced at 76 feet 6 inches. This pavement is nominally 10-in thick and has not been overlaid. The outside shoulder consists of a granular base and asphalt concrete wearing surface.

Section 2

This test section is located adjacent to (just west of) section 1 and is also a 24-ft wide roadway. The pavement is jointed reinforced concrete with joints spaced at 76 feet 6 inches. The pavement section had been overlaid with portland cement concrete. The original pavement, constructed in 1964, is nominally 10-in thick. The overlay was constructed in 1984 and is nominally 4-in thick. The outside shoulder consists of a granular base and asphalt concrete wearing surface.

Section 3

This test section is located along the northbound lane near station 435 + 20 on County Road T-61, just south of Eddyville along the Monroe and Wapello County Line. The original pavement, constructed in 1972, is reinforced concrete with joints spaced at 40-ft intervals. The pavement section has been overlaid with portland cement concrete. The overlay, constructed in 1985, is plain concrete. In the overlay, transverse joints were provided to match the joints in the existing pavement at 40-ft intervals and intermediate joints were provided at 20-ft intervals. The original pavement is nominally 6-in thick and overlay is about 4-in thick. The shoulder consists of a granular base.

Section 4

This test section is located along the eastbound lanes of I-80 near mile post 39, just west of the Avoca interchange. The pavement is continuously reinforced concrete (CRC) and is overlaid. The existing pavement is nominally 8-in thick and overlay is nominally 3-in thick. The outside shoulder consists of a granular base and asphalt concrete wearing surface.

The original pavement was constructed in 1966 and exhibited D-cracking deterioration at time of overlay in 1979.

Section 5

This test section is located adjacent to (just east of) section 4. The original pavement is jointed reinforced concrete with joints spaced at 76 feet 6 inches. The pavement is overlaid with portland cement concrete. Thickness of the original pavement is nominally 10 inches, and the overlay is nominally 3-in thick.

The original pavement was constructed in 1965 and exhibited D-cracking deterioration at time of overlay in 1979.

BONDED OVERLAY CONSTRUCTION

When a bonded concrete overlay is used, steps are taken to ensure complete bond with the existing pavement so that the overlay becomes an integral part of the base slab. A schematic of a bonded overlay is shown in figure 1.

This section summarizes Iowa construction procedures for bonded overlays. The procedures described were used for the overlay construction at sections 4 and 5 along the eastbound lanes of I-80 in Pottawattawie County just west of Avoca.

A 4½-mi section of I-80 was resurfaced in 1979 with nominally 3-in thick bonded plain concrete. The resurfaced pavement was an 8-in thick CRC except for about 2,100 feet of 10-in thick jointed reinforced concrete near the east end of the project. The resurfaced pavement exhibited considerable D-cracking along joints and cracks.

The existing surface, milled to a depth of about ¼ inch, was cleaned by sandblasting and air-blasting. A cement grout was sprayed onto the cleaned surface just ahead of the overlay placement. Work also included installing edge drains and pressure relief joints in the existing pavement and the overlay. Transverse joints were provided in the bonded overlay to match joints in the existing pavement along the jointed portion of the project.

CONDITION SURVEY OF TEST SECTIONS

A visual condition survey was conducted at each test section. For sections 1, 2, and 5, the length surveyed was about 300 to 350 feet. For sections 3 and 4, the length surveyed was about 100 feet. Extent and severity of visible cracking was noted. For jointed pavements, severity of faulting was also noted. It should be noted that sections 1, 2, 4, and 5 carry heavy truck traffic. The average daily traffic (ADT) in each direction exceeds 6,000 vehicles and includes about 35 percent trucks. Results of the condition survey are presented in the following paragraphs.

Test Section 1

The condition survey for section 1 is given in figure 2. As seen in figure 2, there is a large amount of transverse cracking

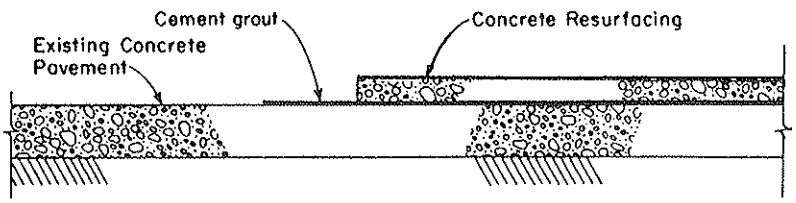

FIGURE 1 Bonded concrete overlay.

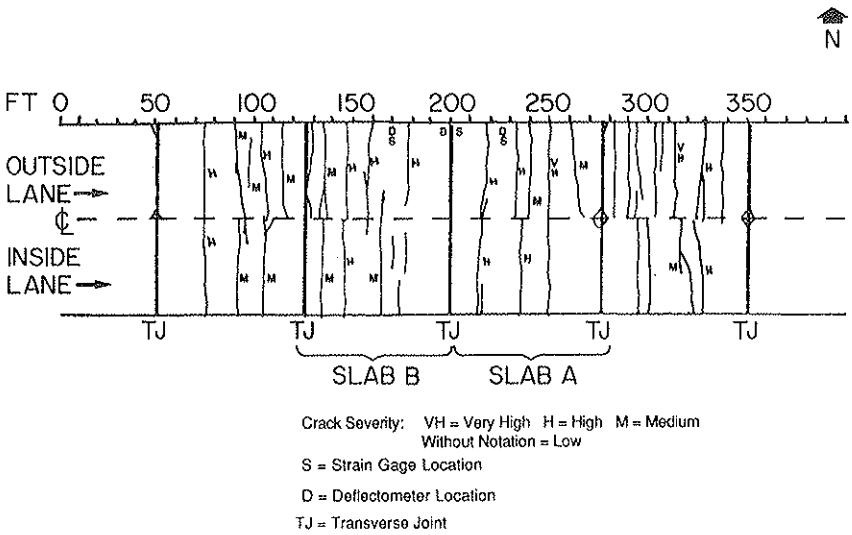

FIGURE 2 Condition survey for section 1.

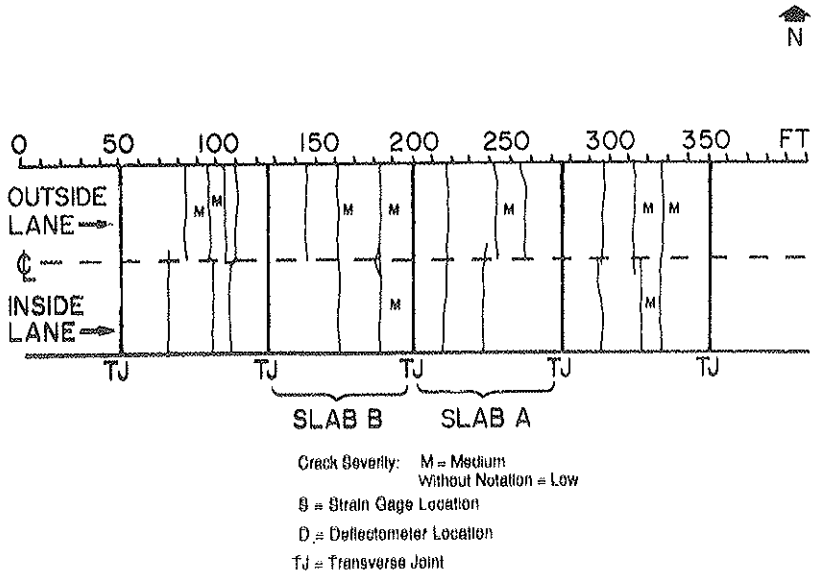

FIGURE 3 Condition survey for section 2.

within the test section area. Cracking was generally of low-to-medium severity. A few cracks did exhibit high severity. Transverse joints were faulted about ¼ to ⅜ inches.

Two slab panels, denoted Slab A and Slab B, selected for instrumentation are also indicated in figure 2.

Test Section 2

The condition survey for section 2 is given in figure 3. Cracking in section 2 is not as extensive as for section 1. Cracking was generally of low-to-medium severity. Faulting was not evident at the transverse joints within and near the test section.

Two slab panels, denoted Slab A and Slab B, selected for instrumentation are also indicated in figure 3.

Test Section 3

No cracking or damage was visually evident at section 3. Joint spacing at this location is 20 feet for the overlay and 40 feet for the existing pavement. There was no mid-slab cracking for faulting at joints.

Test Section 4

Section 4 is a continuously reinforced concrete pavement. The condition survey for section 4 is given in figure 4. Crack spacing within the length of pavement surveyed ranged from 1 foot to about 12 feet, with most cracks spaced 5 feet or more. All cracks were tight.

Locations of instruments (strain gages and deflectometers) are also identified in figure 4.

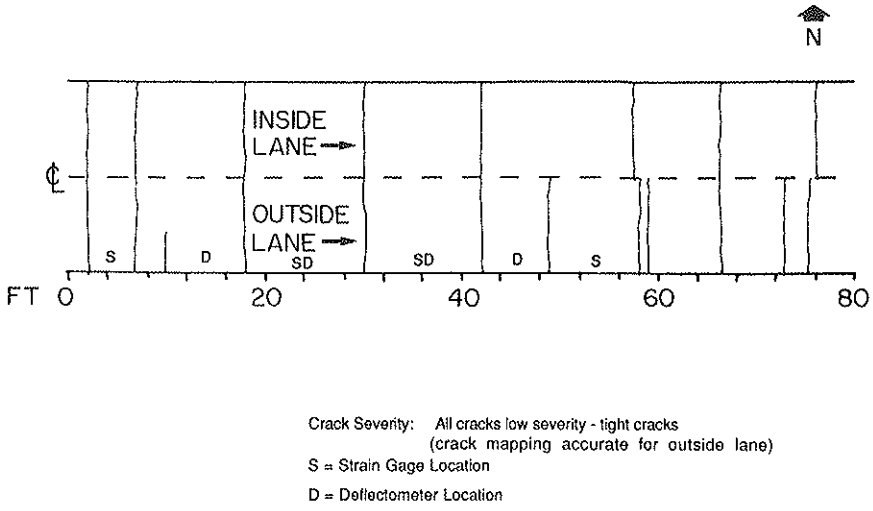

FIGURE 4 Condition survey for section 4.

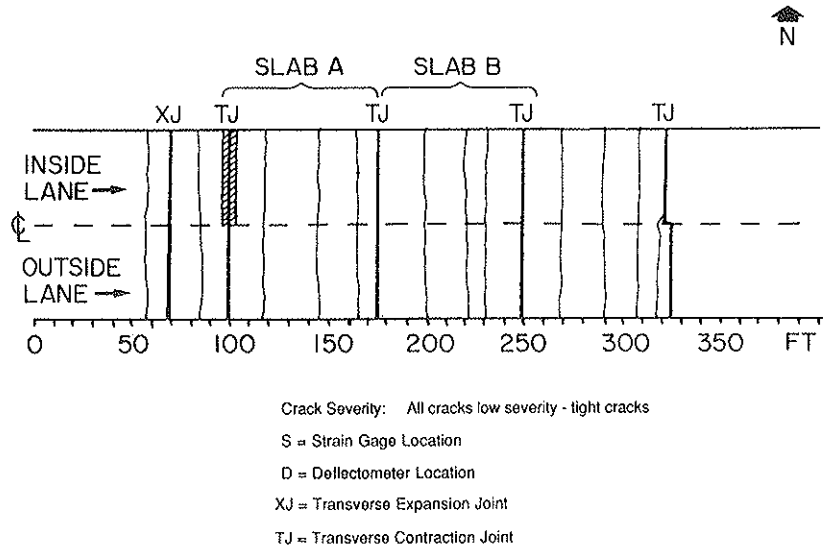

FIGURE 5 Condition survey for section 5.

TABLE 1 RESULTS OF CORE TESTS

Item	Test Section 1	2	3	4	5
Compressive Strength of Original Concrete, psi	8,590	8,160	6,860	6,920	6,770
Split Tensile Strength of Original Concrete, psi	630	730	680	600	660
Split Tensile Strength of Overlay Concrete, psi	---	660	670	730	780
Interface Shear Strength, psi	---	490	550	370	500
Overlay Thickness, in.	---	4.3	4.5	4.3	4.0
Original Pavement Thickness	10.5	10.0	6.0	8.0	10.0

Test Section 5

The condition survey for section 5 is given in figure 5. Cracking was generally of low severity. Faulting was not evident at transverse joints within the length of pavement surveyed.

Two slab panels, denoted as Slab A and Slab B, selected for instrumentation are also indicated in figure 5.

CORE TESTING

The installation of deflectometers used to measure slab deflections required coring 4¼-in diameter holes along the pavement edge. The 4-in diameter cores recovered were used for compressive, split-tensile, and shear strength testing. Test results are summarized in table 1.

Results of core tests indicate that strength of the original pavement concrete at all test sections was very high. For the original pavement core concrete compressive strength ranged from 6,770 to 8,590 psi and split-tensile strength ranged from 600 to 730 psi. For the overlay concrete, split-tensile strength ranged from 660 to 780 psi. The interface shear strength for the four sections with the bonded overlay ranged from 370 to 550 psi.

Assuming that the 28-day concrete compressive strength of concrete (at time of construction) was about 5,000 psi, test results indicate a compressive strength gain of about 35 to 72 percent in a period of about 20 years for the original concrete.

INSTRUMENTATION

All pavement test sections were instrumented to measure load-induced strains and deflections at the pavement surface. In addition, pavement temperature and slab curl were monitored with respect to time. Curl is the change in the vertical profile of the slab resulting from a change in the slab temperature.

For test sections with jointed pavement two adjacent slab panels were instrumented. Each slab panel was instrumented to obtain strains and deflections at mid-slab edge and deflection at a joint corner. For section 4, with the continuously reinforced concrete pavement, several cracked segments of the pavement were instrumented to obtain four replicate readings of edge longitudinal and interior transverse strains and edge deflection.

Typical strain gage and deflectometer locations for the jointed pavements of sections 1, 2, 3, and 5 are shown in figure 6. Exact locations of the gages and deflectometers for sections 1, 2, and 5 are shown in figures 2, 3, and 5, respectively. Instrumentation for section 4 is shown in figure 7. The instrumentation plan was established to provide maximum values of strains and deflection due to edge loading.

A brief description of instrumentation procedures used at the test sections follows.

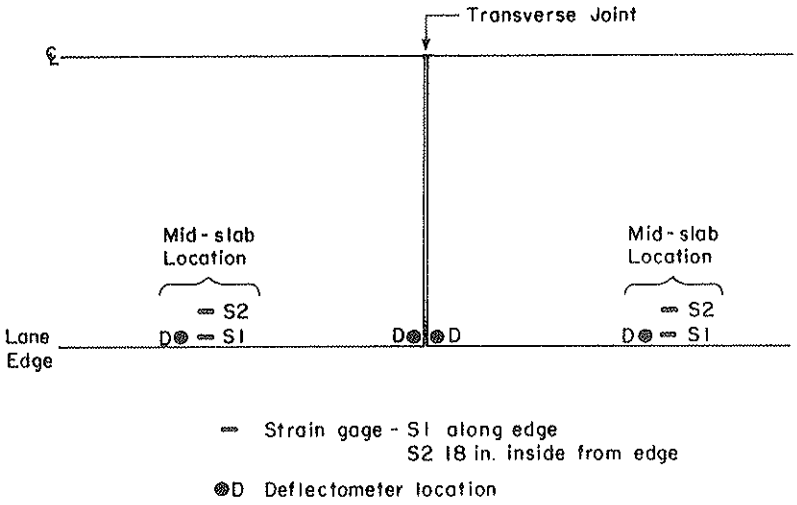

FIGURE 6 Typical instrumentation for sections 1, 2, 3, and 5.

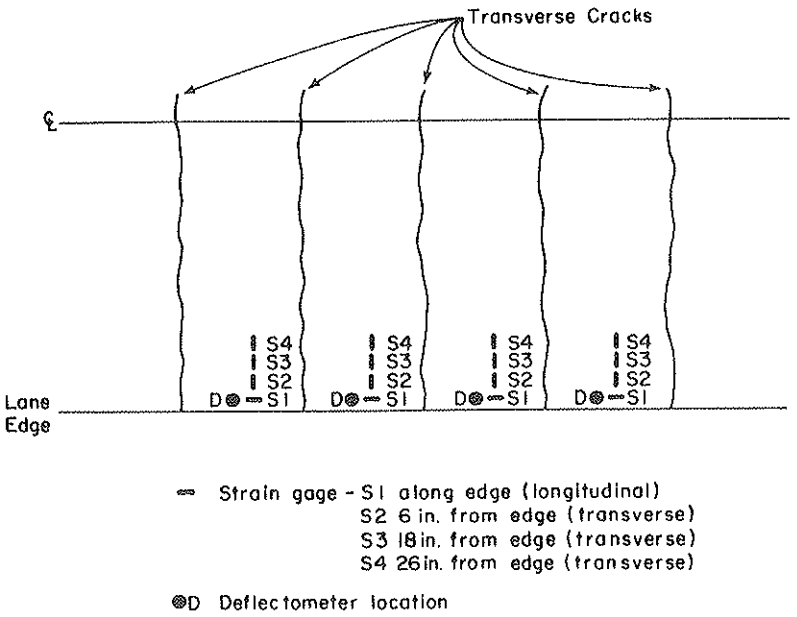

FIGURE 7 Instrumentation for section 4.

Load Strains

Load strains were measured with 4-in long electrical-resistant strain gages bonded to the pavement surface. All gages were placed in recessed grooves to protect them from direct application of wheel loads. The procedure for applying gage was:

- Grind a recess sufficient to remove the texture grooves in the pavement surface.
- Heat the concrete surface, when necessary.
- Clean the recess with acetone.
- Apply a thin coat of adhesive.
- Place the gage in the adhesive and remove all air bubbles.
- Connect lead wires to the gage.
- Run lead wires in recessed grooves to the pavement edge.
- Waterproof the gage.
- Fill gage and lead wire recesses with silicon rubber.

Load Deflections

Load deflections were measured with resistance-bridge deflectometers mounted in core holes located near the pavement edge. Readings were referenced to encased rods driven in the subgrade to a depth of 6 feet. The installation procedure used for the deflectometers allowed passage of the trucks directly over the deflectometer locations.

Curl Measurements

Pavement curl was measured with 0.001-in indicators placed at the same locations as the deflectometers. Curl readings were referenced to the encased rods placed in the subgrade. Curl readings were taken approximately once an hour.

Temperature Measurements

Changes in pavement temperature were measured with copper-constantan thermocouples placed at the surface of the concrete pavement and at the bottom of the pavement in the core holes used for placing deflectometers. Air temperature was monitored with a thermocouple shaded from direct sun.

Monitoring Equipment

Data were monitored and recorded with equipment carried in Construction Technology Laboratories' field instrumen-

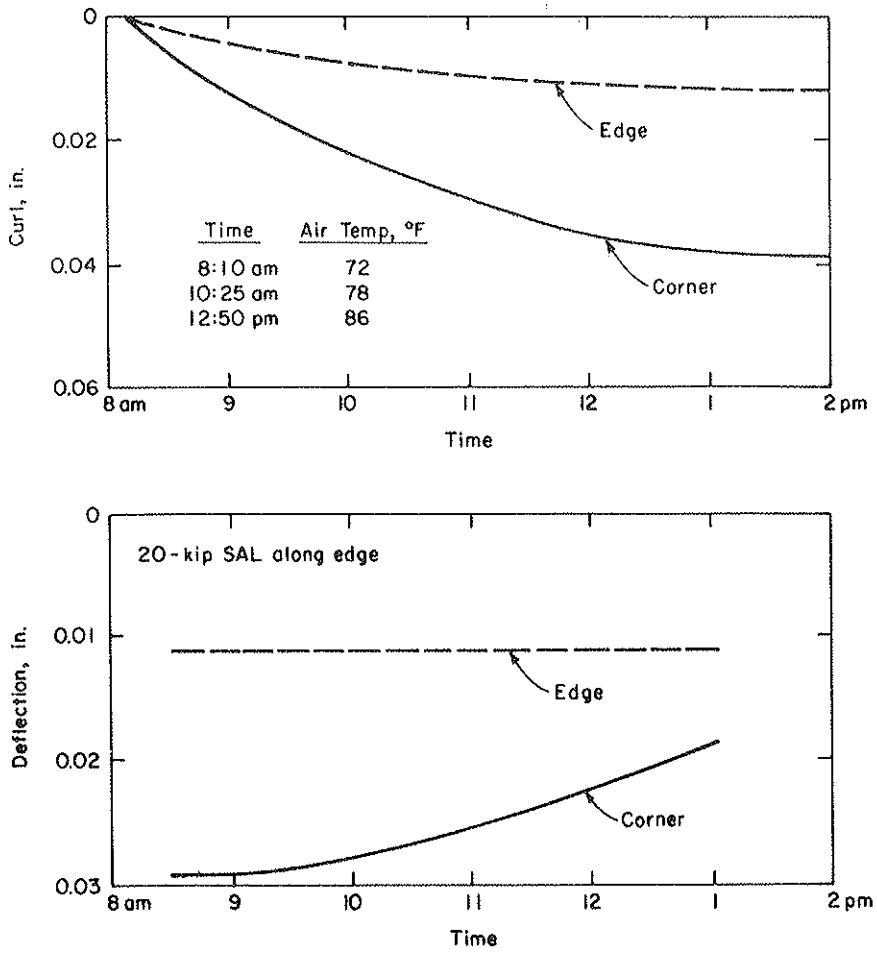

FIGURE 8 Variation of curl and deflection with time at section 1.

tation van. Strain and deflection data were recorded with a high-speed computer-based data acquisition system. Up to twenty channels of instrumentation were monitored and recorded simultaneously for each vehicle loading. Computer programs were written to monitor, record, and tabulate all field data. All analog data from strain gages and deflectometers were digitized and stored on computer floppy disks. Readings from each item of instrumentation were digitized simultaneously at the rate of approximately 200 points per second. Detailed loading curves for each strain gage and deflectometer were stored on computer floppy disks for future examination.

All monitoring and recording instruments were calibrated prior to testing.

LOAD TESTING

Loading was applied using two trucks supplied by Iowa DOT. One truck was loaded to provide a 20-kip nominal single-axle load (SAL). The second truck was loaded to provided a 34-kip nominal tandem-axle load (TAL).

It had been planned to use Iowa DOT Model 400 Road Rater equipment in conjunction with CTL load testing. This was planned to establish a correlation between Road Rater deflections and measured responses under the 20-kip SAL and 34-kip TAL. The Road Rater unit is an electronically controlled, hydraulically powered unit mounted in the rear of a van. A dynamic load is applied at a fixed frequency. The actual dynamic load applied is a function of displacement of the mass used to impart the loading. For rigid pavement, Iowa DOT uses peak-to-peak dynamic load of about 2,000 lb at a frequency of 30 cycles per second. The Road Rater has been used by Iowa DOT to determine AASHTO structural numbers for flexible pavements, to determine subgrade support values for rigid pavements, and to determine overlay requirements for both rigid and flexible pavements (*2, 3*).

The Road Rater unit was available only for testing at sections 1, 2, and 3 at the end of the CTL field testing program.

Strains and deflections were recorded for the 20-kip single axle and 34-kip tandem-axle loadings with the trucks moving at creep speed. Two wheel paths were used. For one wheel path, tire placement was 2 inches from the pavement edge. For the second wheel path, tire placement was 18 inches from the pavement edge. The tire placement distance is the distance from the pavement edge to the outside edge of the outside tire sidewall. Care was taken to ensure that wheel paths of the trucks coincided with the desired paths painted on the pavement.

Sections 1 and 2 were tested on April 25, 1986, section 3 was tested on April 26, 1986, and sections 4 and 5 were tested on April 23, 1986. Each day, testing was generally started between 8:00 and 9:00 am, and testing was repeated several times until about 2:00 pm. Specific testing times were governed by traffic control requirements and preparation times required at each test section.

TABLE 2 MEASURED RESPONSES AT SECTION 1

Response Type	Axle Load	Test Time 8:30 a.m.	9:30 a.m.	10:30 a.m.	11:30 a.m.	1:00 p.m.
WHEEL PATH: 2 in. from edge						
Edge Strain	SAL	30	27	27	26	26
	TAL	16	19	19	19	20
Long. Strain	SAL	29	32	30	28	28
@ 18 in.	TAL	14	15	15	15	18
Edge	SAL	0.012	0.013	0.012	0.012	0.012
Deflection, in.	TAL	0.020	0.018	0.017	0.015	0.015
Corner	SAL	0.029	0.029	0.026	0.024	0.018
Deflection, in.	TAL	0.033	0.028	0.026	0.024	0.022
WHEEL PATH: 18 in. from edge						
Edge Strain	SAL	16	16	14	13	13
	TAL	11	10	9	10	10
Long. Strain	SAL	16	16	13	13	16
@ 18 in.	TAL	10	8	9	8	10
Edge	SAL	0.008	0.009	0.009	0.008	0.008
Deflection, in.	TAL	0.014	0.012	0.012	0.011	0.011
Corner	SAL	0.021	0.019	0.019	0.017	0.013
Deflection, in.	TAL	0.023	0.021	0.020	0.019	0.017

NOTES: 1. SAL = 20-kip single-axle load
TAL = 34-kip tandem-axle load
2. For TAL, strain values listed are the larger of the two peak values under the two axles
3. Strain readings are in millionths.

DATA ANALYSIS

This section presents a summary of the field data and comparison of field data with results of theoretical analysis of bonded overlay sections. As stated previously, curl was measured at each deflectometer location generally between 8:00 am and 2:00 pm. Because of variations in slab curl with changes in temperature, measured deflections due to load along a slab edge or corner are affected by the time of testing. In addition, measured slab strains may also be affected by time of testing but at a lower level. Therefore, care has to be exercised in interpreting deflection and strain measurements if these measurements are made at different times of a day or on different days.

Curling and Warping Effects

Soon after concrete is placed, drying shrinkage of the concrete begins. Drying shrinkage in a slab-on-grade occurs at a faster rate at the slab surface than at the slab bottom. In addition, because the subgrade and subbase may remain wet, the slab bottom remains relatively moist. Thus, total shrinkage at the bottom is less than at the top. This differential in shrinkage results in a lifting of the slab from the subbase at edges and corner. Movements of this type resulting from moisture differentials are referred to as warping. Over a period of time, the warping behavior is modified by creep effects. However, warping is almost never recoverable.

In addition to warping, a slab-on-grade is also subjected to curling. Curling is the change in the slab profile due to temperature differential between slab top and bottom. Curling is a daily phenomenon. Slabs are curled upward from their warped shape during the night when temperatures are low and curled downward from their warped shape during the midday period when temperatures are higher.

Typical variations with time of pavement curl and deflections under load at slab edge and corner are shown in figure 8 for section 1. As shown in figure 8, corner curl was highest for jointed pavement sections 1, 2 and 5 with joint spacing of 76 feet 6 inches. Edge curl at all sections was low and thus had almost no effect on deflections due to truck loading over a period of time.

Summary of Measured Strains and Deflections

Pavement responses (strains and deflections) measured at sections 1 through 5 are listed in tables 2 through 6, respectively. Responses listed are generally an average of two readings (from Slab A and Slab B) for sections 1, 2, 3, and 5. For section 4, responses listed are generally an average of four readings.

The strains reported in the tables are those measured at

TABLE 3 MEASURED RESPONSES AT SECTION 2

Response Type	Axle Load	Test Time 9:00 a.m.	9:50 a.m.	11:00 a.m.	11:50 a.m.	1:20 p.m.
WHEEL PATH: 2 in. from edge						
Edge Strain	SAL	10	11	11	12	13
	TAL	11	11	10	9	12
Long. Strain	SAL	12	13	14	14	13
@ 18 in.	TAL	15	13	13	14	15
Edge	SAL	0.010	0.009	0.009	0.009	0.008
Deflection, in.	TAL	0.015	0.014	0.013	0.013	0.012
Corner	SAL	0.014	0.013	0.012	0.012	0.011
Deflection, in.	TAL	0.018	0.016	0.015	0.014	0.014
WHEEL PATH: 18 in. from edge						
Edge Strain	SAL	7	5	5	5	6
	TAL	5	5	6	6	6
Long. Strain	SAL	9	10	9	10	9
@ 18 in.	TAL	7	8	9	8	9
Edge	SAL	0.007	0.007	0.007	0.007	0.006
Deflection, in.	TAL	0.011	0.010	0.010	0.010	0.009
Corner	SAL	0.010	0.009	0.009	0.008	0.008
Deflection, in.	TAL	0.014	0.012	0.011	0.011	0.010

NOTES: 1. SAL = 20-kip single-axle load
TAL = 34-kip tandem-axle load
2. For TAL, strain values listed are the larger of the two peak values under the two axles.
3. Strain readings are in millionths

TABLE 4 MEASURED RESPONSES AT SECTION 3

Response Type	Axle Load	Test Time 8:00 a.m.	8:50 a.m.	9:55 a.m.	10:35 a.m.	11:20 a.m.
WHEEL PATH: 2 in. from edge						
Edge Strain	SAL	42	38	37	35	34
	TAL	33	32	29	27	28
Long. Strain	SAL	34	33	31	30	28
@ 18 in.	TAL	26	28	25	26	26
Edge	SAL	0.016	0.015	0.014	0.014	0.014
Deflection, in.	TAL	0.020	0.022	0.022	0.021	0.021
Corner	SAL	0.018	0.017	0.017	0.017	0.017
Deflection, in.	TAL	0.024	0.024	0.024	0.024	0.023
WHEEL PATH: 18 in. from edge						
Edge Strain	SAL	23	23	20	20	20
	TAL	22	21	21	20	20
Long. Strain	SAL	22	24	24	22	22
@ 18 in.	TAL	22	20	20	20	20
Edge	SAL	0.010	0.011	0.010	0.010	0.010
Deflection, in.	TAL	0.017	0.016	0.016	0.016	0.016
Corner	SAL	0.012	0.012	0.012	0.012	0.012
Deflection, in.	TAL	0.018	0.018	0.017	0.017	0.017

NOTES: 1. SAL = 20-kip single-axle load
TAL = 34-kip tandem-axle load
2. For TAL, strain values listed are the larger of the two peak values under the two axles.
3. Strain readings are in millionths

TABLE 5 MEASURED RESPONSES AT SECTION 4

Response Type	Axle Load	Test Time 9:45 a.m.	11:15 a.m.	1:15 p.m.	2:15 p.m.
WHEEL PATH: 2 in. from edge					
Edge Strain	SAL	30	29	26	27
	TAL	21	20	23	20
Trans. Strain	SAL	-9	---	-15	-16
(at 18 in.)	TAL	-12	-23	-23	-22
Trans. Strain	SAL	-13	--	25	-24
(at 26 in.)	TAL	-13	-18	-22	-23
Edge	SAL	0.013	0.012	0.011	0.011
Deflection, in.	TAL	0.016	0.016	0.015	0.015
WHEEL PATH: 18 in. from edge					
Edge Strain	SAL	16	14	16	15
	TAL	14	14	15	15
Trans. Strain	SAL	-2	-6	-6	-7
(at 18 in.)	TAL	-5	-10	-9	-8
Trans. Strain	SAL	-7	-9	-9	-7
(at 26 in.)	TAL	-9	-12	-15	-11
Edge	SAL	0.008	0.008	0.008	0.008
Deflection, in.	TAL	0.013	0.012	0.012	0.011

NOTES: 1. SAL = 20-kip single-axle load
TAL = 34-kip tandem-axle load
2. For TAL, strain values listed are the larger of the two peak values under the two axles.
3. Negative value of strain indicates tensile strain at slab surface.
4. Strain readings are in millionths

TABLE 6 MEASURED RESPONSES AT SECTION 5

Response Type	Axle Load	Test Time 10:15 a.m.	11:40 a.m.	1:35 p.m.	2:40 p.m.
WHEEL PATH: 2 in. from edge					
Edge Strain	SAL	22	22	21	23
	TAL	19	21	20	20
Long. Strain @ 18 in.	SAL	12	11	10	10
	TAL	10	9	10	12
Edge Deflection, in.	SAL	0.012	0.011	0.011	0.010
	TAL	0.017	0.016	0.015	0.015
Corner Deflection, in.	SAL	0.023	0.018	0.016	0.014
	TAL	0.024	0.019	0.017	0.017
WHEEL PATH: 18 in. from edge					
Edge Strain	SAL	16	12	13	15
	TAL	14	14	11	11
Long. Strain @ 18 in.	SAL	15	14	16	16
	TAL	12	14	12	14
Edge Deflection, in.	SAL	0.009	0.008	0.007	0.007
	TAL	0.012	0.012	0.012	0.012
Corner Deflection, in.	SAL	0.015	0.011	0.010	0.010
	TAL	0.019	0.014	0.012	0.012

NOTES: 1. SAL = 20-kip single-axle load
TAL = 34-kip tandem-axle load
2. For TAL, strain values listed are the larger of the two peak values under the two axles.
3. Strain readings are in millionths

the slab surface. It is assumed that strains at the slab bottom are equal in magnitude but opposite in sign. Thus, a reported value of 20 millionths compressive strain at the slab surface would imply a 20 millionths tensile strain at the slab bottom. Typical graphical recordings of edge strain at section 2 are shown in figure 9 for 20-kip single-axle and 34-kip tandem-axle loadings.

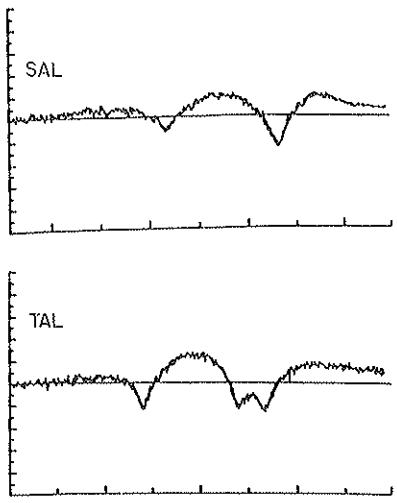

FIGURE 9 Typical recordings for edge strain.

A summary of the measured responses is presented for all test sections in table 7 for the 20-kip SAL and 34-kip TAL along the lane edge.

It is seen from table 7 that measured responses were much lower at section 2 with a total nominal slab thickness of 14 inches compared to responses at section 1 with a total nominal slab thickness of 10 inches. Measured strain values at section 2 were less than half of those at section 1. Measured deflection values at section 2 were also much lower, indicating the beneficial effects of the 4-in thick (nominal) overlay at section 2.

Measured responses at section 4 (overlaid CRCP) were a little larger than at section 5 (overlaid JRCP). This difference is accounted for by the larger thickness of the existing pavement at section 5. Section 3 had generally the highest measured responses with strains under a 20-kip SAL ranging from 34 to 42 millionths. Edge deflection, under the 20-kip SAL at section 3 ranged from 0.014 to 0.016 inches.

Corner deflections at the sections with jointed pavement generally were about 30 to 60 percent greater than edge deflections.

For section 4 (overlaid CRCP), the magnitudes of tensile transverse strains measured at the slab surface at 26-in inward from the edge were almost equal to edge longitudinal strains.

It should be noted that the Road Rater unit was used at sections 1, 2, and 3. At section 2, the Road Rater was used at mid-slab, and at 2-in and 18-in intervals in from the edge. At section 3, the Road Rater was used at mid-slab, at 7 inches from the edge, and at a joint location at 9 inches inside from the edge. Because the Road Rater was not placed directly

TABLE 7 SUMMARY OF MEASURED RESPONSES

Response Type	Test Section 1	2	3	4	5
20-kip SAL at edge					
Edge Strain	26-30	10-13	34-42	36-30	21-23
Long. Strain (@ 18 in.)	28-32	12-14	28-34	—	10-12
Trans. Strain (@ 18 in.)	—	—	—	(-9)-(16)	—
Trans. Strain (@ 26 in.)	—	—	—	(-13)-(-25)	—
Edge Deflection, in.	0.012-0.013	0.008-0.010	0.014-0.016	0.011-0.013	0.010-0.012
Corner Deflection, in.	0.018-0.029	0.012-0.015	0.017-0.018	--	0.014-0.023
34-kip TAL at edge					
Edge Strain	16-20	9-12	28-33	20-23	19-20
Long. Strain (@ 18 in.)	14-18	13-15	25-28	—	9-12
Trans. Strain (@ 18 in.)	--	—	--	(-12)-(-23)	—
Trans. Strain (@ 26 in.)	—	--	--	(-13)-(-23)	—
Edge Deflection, in.	0.015-0.020	0.012-0.015	0.020-0.022	0.015-0.016	0.015-0.017
Corner Deflection, in.	0.022-0.033	0.014-0.018	0.023-0.024	--	0.017-0.024
Total Slab Thickness, in. (nominal/actual)	10.5/10.5	14.0/14.3	10.0/10.5	11.0/12.3	13.0/14.0

NOTES: 1. Negative value of strain indicates a tensile strain at slab surface.
2. Ranges of values given for different times of testing.
3. Strain readings are in millionths.

over the CTL instrumentation, and because deflections measured by the Road Rater are generally of low magnitude (about 0.001 to 0.002 inches), the CTL data acquisition system was not able to provide usable data for the case of the Road Rater loadings.

Analysis of Results

A comparison was made between measured responses and calculated theoretical responses. Pavement responses (edge stresses and edge deflections) were calculated using a finite element computer program, Program JSLAB. Program JSLAB, developed by the Construction Technology Laboratories for the Federal Highway Administration, can analyze jointed slabs (*4*). Load input is in terms of wheel loads at any location on the slabs. Loss of support, variable support or material properties, as well as bonded and unbonded concrete overlays, can be considered. In the program, the subbase/subgrade support is characterized by the modulus of subgrade reaction.

Analysis was conducted for various thicknesses of pavement slabs subjected to 20-kip SAL and 34-kip TAL at the mid-slab pavement edge. Analysis was conducted for a single slab 12-ft wide and 20-ft long. Values of modulus of subgrade reaction used were 100, 300, and 500 pci. The overlaid sections were assumed to behave monolithically.

The measured strains were converted to stresses by assuming that the modulus of elasticity of concrete was 5,000,000 psi. Use of this value of the modulus of elasticity is justified considering the high compressive and split-tensile strengths of the concrete at the test sections. In addition, it is assumed that the overlaid pavements at sections 2 to 5 behave monolithically as evidenced by the high interface shear strengths between the overlay and the existing pavement.

The measured and computed edge stresses and deflections are compared in figure 10 for the 20-kip SAL and in figure

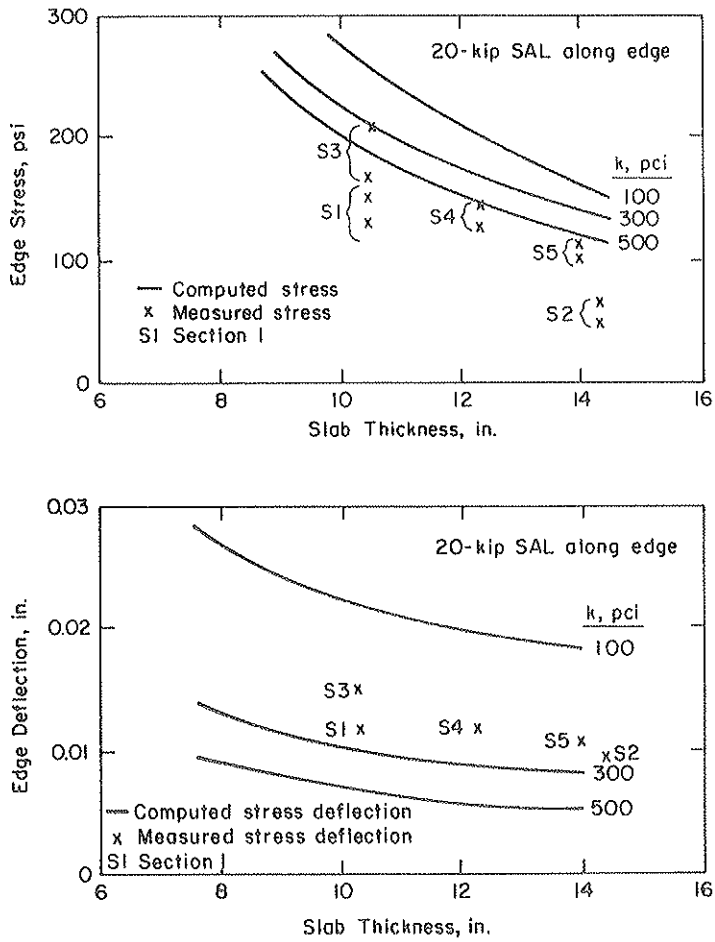

FIGURE 10 Comparison of measured and calculated responses for the 20-kip single-axle loading.

11 for the 34-kip TAL. It is seen that the measured stresses as well as deflections are a function of the total pavement thickness. Measured deflections are lower for larger total pavement thickness.

The modulus of subgrade reaction, k, values at the five test sections were reported to be about 200 pci. It is seen that the measured edge deflections correspond well with computed edge deflections at a k-value of about 200 pci for both the SAL and the TAL. Measured edge stresses also correspond well with computed edge stress except for sections 1 and 2. Measured edge stresses at sections 1 and 2 are much lower than would have been anticipated, especially considering reasonably good agreement between measured and computed edge deflections at these sections. One reason for lower measured edge stresses could be that the effective panel length (distance between transverse cracks) in the existing pavement is much shorter than the 20 feet assumed in the theoretical analysis. The condition survey for section 1, shown in figure 2, indicates an effective panel length of about 15 feet in the panels containing the instrumentation. The condition survey for section 2, shown in figure 3, indicates an effective panel length of about 20 feet in the overlay in the panels containing the instrumentation. However, the effective panel length in the existing pavement at section 2 may be less than 20 feet.

Based on the comparisons shown in figures 10 and 11, it is seen that the overlaid pavements are behaving monolithically and that the overlaid pavements are responding as full-depth pavement.

Effect of Wheel Path

The field investigation was planned to also provide information on the effect of wheel path. As discussed previously wheel paths used for both the SAL and the TAL were 2-in and 18-in inside from the edge. The 2-in wheel path simulated the edge loading condition. The effect of having a wheel path just 18 inches away from the edge is shown in figure 12. There is a significant reduction in measured edge stresses and edge deflections at all five sections for the wheel path at 18 inches compared to the wheel path at 2 inches. Similar reductions were also measured for joint deflections.

Thus, lane widening at time of overlay, if practical, and lane widening at time of new construction if a tied-concrete shoulder is not used, should be given serious consideration. Keeping truck traffic away from the free lane edge can significantly improve pavement performance by reducing critical stresses and deflections.

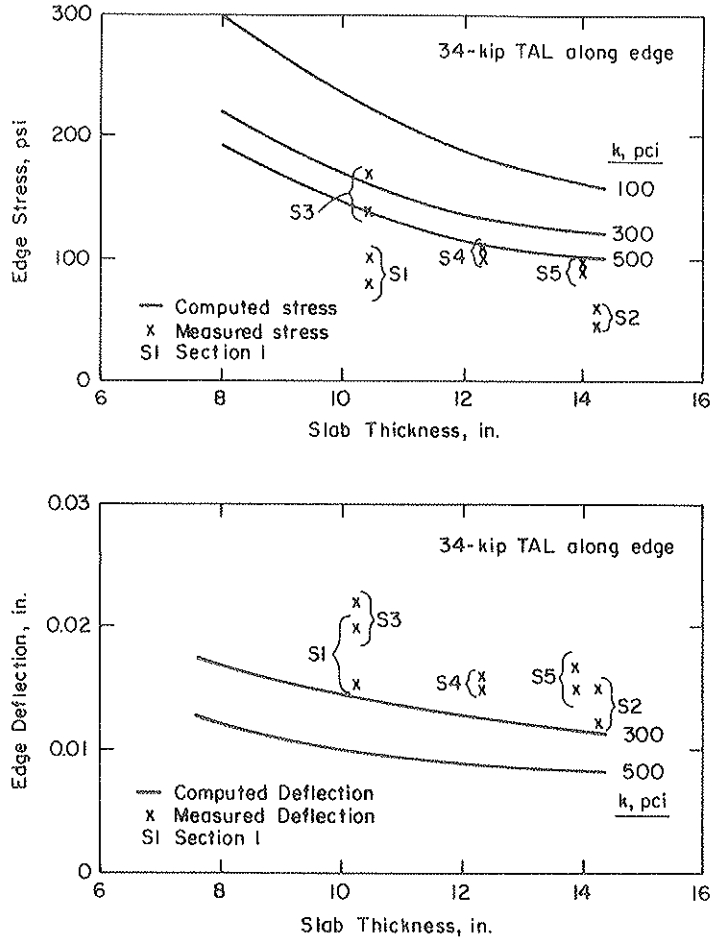

FIGURE 11 Comparison of measured and calculated responses for the 34-kip tandem-axle loading.

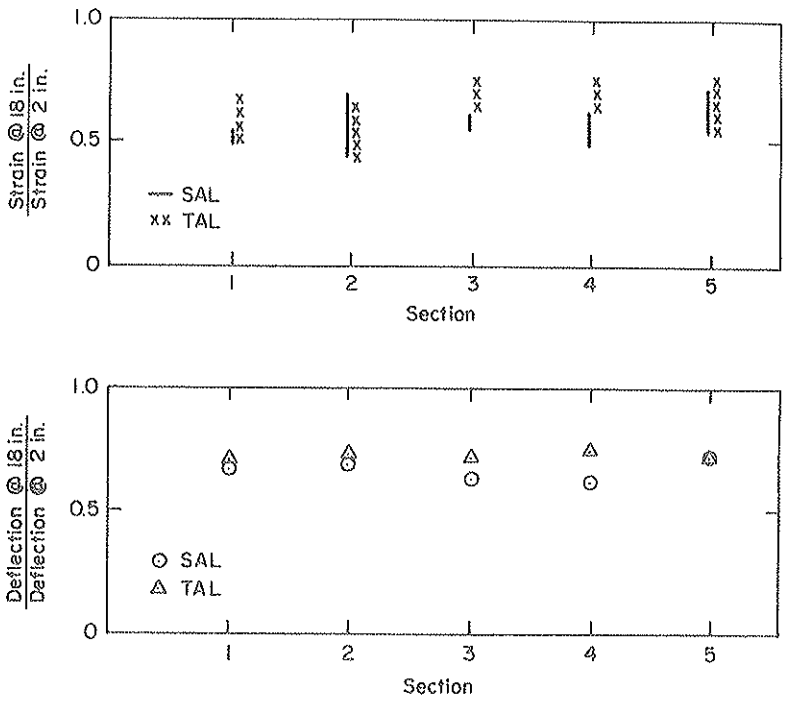

FIGURE 12 Comparison of responses for wheel paths of 18-in. and 2-in. inside from the edge.

SUMMARY

Results of the investigation indicate that the four overlaid pavement sections evaluated as part of the reported study are performing as monolithic pavements with high interface shear strength at the interface. The strength of the existing pavement at all of the four overlaid test sections was high. In addition, cores obtained from sections 4 and 5 did not indicate D-cracking related damage in the overlay concrete.

Comparison of the condition surveys for section 1 (non-overlaid JRCP) and section 2 (overlaid JRCP) indicate that all cracking in the existing pavement is not reflected through the overlay and that the cracks that did reflect through have remained tightly closed. Similarly, the condition survey of sections 4 and 5 indicate that cracks reflected through the overlay continue to remain tightly closed even after almost seven years of service.

The field investigation conducted by CTL verifies that for properly constructed bonded overlays, pavement strengthening is achieved and that the overlaid pavement behaves monolithically as a full-depth concrete pavement.

ACKNOWLEDGMENTS

Work was conducted by the Construction Technology Laboratories under the direction of W. G. Corley, Vice-President, Engineering Development Division. Vernon J. Marks of the Iowa Department of Transportation provided technical coordination. The cooperation by the many personnel of the Iowa Department of Transportation is gratefully acknowledged.

The opinions and findings expressed or implied in the paper are those of the authors. They are not necessarily those of the Iowa Department of Transportation.

REFERENCES

1. S. D. Tayabji and P. A. Okamoto. Thickness Design of Concrete Resurfacing. *Proceedings of the Third International Conference on Concrete Pavement Design and Rehabilitation*, Purdue University, April 1985.
2. D. Heins. *Dynamic Deflections for Determining Structural Rating of Flexible Pavements*. Project HR-178 Report, Iowa Highway Research Board, Iowa Department of Transportation, Ames, Iowa, February 1979.
3. V. J. Marks. *Improving Subgrade Support Values with Longitudinal Drains*. Project MLR-B4-3 Interim Report. Iowa Department of Transportation, Ames, Iowa, January 1984.
4. S. D. Tayabji and B. E. Colley. *Improved Rigid Pavement Joints*. Report FHWA-RD-B6-040, Federal Highway Administration, U.S. DOT, February 1984.

Publication of this paper sponsored by Committee on Pavement Rehabilitation.

Application of Deflection Testing to Overlay Design: A Case Study

CHERYL ALLEN RICHTER AND LYNNE H. IRWIN

In the fall of 1985, the Engineering Research and Development Bureau (ERDB) of the New York State Department of Transportation (NYSDOT) and the Cornell University Local Roads Program undertook a case study involving the application of the falling weight deflectometer (FWD) to pavement evaluation and overlay design. The site for the case study was a 1-mi section of state highway in the Finger Lakes Region of Central New York State, which had already been scheduled to receive an overlay during the 1986 construction season. Nondestructive pavement testing was conducted in December 1985 and May 1986. Pavement layer moduli were back-calculated from the FWD data using the computer program MODCOMP 2. As a part of the study, a mechanistically based computer program, called PAVMAN, was developed to calculate remaining pavement life and required overlay thickness. The pavement layer moduli determined using MODCOMP 2 were used with the PAVMAN program to estimate the remaining life of the existing pavement and determine the required overlay thickness. The results obtained with PAVMAN compared well with design overlay thicknesses determined using more traditional methods of overlay design (such as engineering judgement and the Asphalt Institute's deflection based method).

In the fall of 1985, the Engineering Research and Development Bureau (ERDB) of the New York State Department of Transportation (NYSDOT) and the Cornell Local Roads Program (CLRP) undertook a joint project concerned with the application of the falling weight deflectometer (FWD) to pavement evaluation and overlay design. The project took the form of a case study involving a 1-mi section of state highway in the Finger Lakes Region of central New York State. The decision to place an overlay at the project site during the 1986 construction season had been made prior to its selection as the site for the case study. The thickness of that overlay had also been decided prior to the selection of the project site.

The case study was the initial phase of a project undertaken by ERDB for the purpose of assessing the capabilities and applications of the falling weight deflectometer and the data it generates. Goals of the case study included:

- To give ERDB personnel an opportunity to become acquainted with the falling weight deflectometer and its use.
- To investigate potential applications of the FWD and the data it generates.
- To investigate the use of mechanistically-based analysis procedures with nondestructive test data.
- To assess the relative merits of different testing approaches (in terms of number and spacing of test points) for routine pavement evaluation.

C. A. Richter, Strategic Highway Research Program (SHRP), 818 Connecticut Ave., N.W., Washington, D.C. 20006. L. H. Irwin, Cornell University Local Roads Program, Riley Robb Hall, Ithaca, N.Y. 14853.

PROJECT SITE

The site for the case study was a 1-mi section of State Route 96 in Seneca County, New York. Route 96 is a two-lane, rural highway, running basically north-south, with no access control. Traffic data for the project area are given in tables 1 and 2. Because the terrain in the area is very flat and the soils are fairly shallow, drainage in the project area is generally poor.

The pavement in the project area at the time of the testing for the case study consisted of several surface treatments interlayered with two asphalt concrete overlays (nominal combined thickness, three inches) over a bituminous macadam pavement (3-in tar-bound crushed limestone top over a 7-in layer of crushed stone) placed in 1914. The most recent overlay was a 1-in armor coat placed in 1965.

At the time of the deflection testing, the condition of the pavement varied greatly. Some portions of the pavement were intact and exhibited little or no distress. Other portions, particularly sections of the northbound outer wheel path, were badly rutted (rut depths of up to 3½ inches) and/or exhibited severe alligator cracking. Recent pavement condition ratings for the project site are summarized in table 3. The surface and base ratings are on a ten-point scale, where a score of 9 or 10 indicates that the pavement is in excellent condition, while a score less than 6 indicates poor condition, and a score of 1 indicates the worst condition (*1*).

TESTING PROGRAM

Nondestructive Testing

Nondestructive pavement testing for the case study was conducted in December 1985 and May 1986. The testing in December 1985 consisted of FWD and Benkelman beam tests in the inner and outer wheel paths of both lanes. These par-

TABLE 1 TRAFFIC VOLUMES

Year	1960	1970	1973	1976	1977	1980	1986
AADT	1585	1723	1800	1850	2000	1800	3190

TABLE 2 VEHICLE CLASSIFICATION DATA (MARCH 1986)

Vehicle Class	Percentage of AADT
Passenger Cars and Pickup Trucks	88
2-Axle, 6-Tire Single Unit Trucks	6
Single Unit Trucks Having 3 or More Axles	1
3-Axle Tractor/Trailer Combinations	0
4-Axle Tractor/Trailer Combinations	1
Tractor/Trailer Combinations With 5 or More Axles	4

allel tests were conducted at 50-ft intervals on two 500-ft sections, one at each end of the project site.

In addition, FWD tests were conducted at intervals of 250 feet over the full 1-mi section in the two outer wheel paths and in the middle of the northbound lane, so that comparisons of the two test strategies (testing at short intervals over subsections of the pavement in question and testing at uniform intervals over the full length of the pavement section) could be made. Each of the test strategies resulted in about 22 tests per mile along each line of test points. In May 1986, only the two 500-ft sections were tested, again with both devices, at 50-ft intervals in the inner and outer wheel paths of both lanes. In all, FWD tests were conducted at 136 points in December 1985 and at 88 points in May 1986.

Three or four FWD drops from one height were conducted at each test point. After discarding data indicative of sensor overflow or other anomalies, the data for each test point were averaged (on a sensor by sensor basis), so that the effects of random error in deflection measurement would be minimized.

Supplementary Testing

In addition to the nondestructive deflection testing, a limited amount of pavement coring, soil boring, and seismographic testing was conducted. The pavement coring and soil boring were done to verify pavement layer thicknesses and to provide samples for laboratory testing. The laboratory tests (including sieve analyses, Proctor densities, sand equivalent tests, and Atterberg limits for the unbound materials and resilient modulus tests, asphalt extractions, and penetration tests for the asphalt concrete) were conducted to characterize the pavement materials for research purposes and would not be needed for routine pavement evaluation. Seismographic testing was conducted to determine the depth to bedrock in the project area, so that the subgrade could be more accurately modeled in subsequent analyses. Seismographic testing would generally not be required unless the depth to bedrock is relatively shallow (less than 30 feet, or so).

TABLE 3 PAVEMENT CONDITION RATINGS

Year	Surface	Base
1981	8	8
1982	7	7
1983	7	7
1984	7	7
1986	6	6

ANALYTICAL METHODS

Back-Calculation of Pavement Layer Moduli

Pavement layer moduli were back-calculated using the computer program MODCOMP 2 (*2*). The assumptions on which MODCOMP 2 is based include the following:

- Pavement layers are homogeneous and isotropic, and extend infinitely in the horizontal plane.
- The deepest pavement layer is semi-infinite.
- The load on the pavement is uniformly distributed over a circular area, and the direction of the force is perpendicular to the pavement surface.
- Full friction exists at the pavement layer interfaces (in other words, there is no lateral slippage of the pavement layers relative to each other).

Using MODCOMP 2, it was possible to obtain reasonable sets of layer moduli for 128 (94 percent) of the December 1985 test points, and 82 (93 percent) of the May 1986 test points. The failure to obtain reasonable solutions for the remaining test points was most likely due to inaccuracies in the pavement model (for example, incorrectly defining the depth to a bedrock layer, the use of a linear model for stress-dependent materials, inaccurate layer thicknesses, boulders at shallow depths in the subgrade, etc.).

Remaining Life and Required Overlay Thickness Calculations

A computer program, called PAVMAN (for PAVement MANagement), was developed to facilitate mechanistically-based analyses of remaining pavement life and required overlay thickness (*3*). PAVMAN was written in the FORTRAN programming language to run on IBM-PC microcomputers.

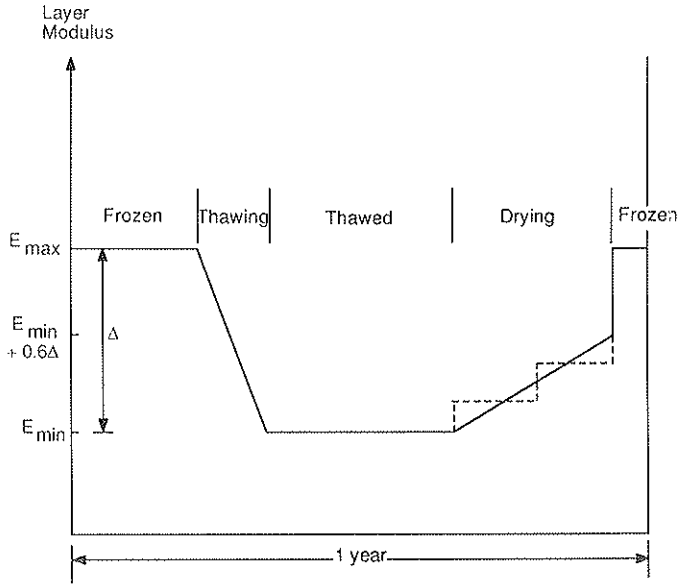

FIGURE 1 Freeze-thaw seasonal variation model.

Selected characteristics of PAVMAN are as follows:

- The pavement is modeled as a layered elastic system, using the same assumptions articulated above for MODCOMP 2.
- Pavement materials may be modeled as being either linear or stress-dependent in their response to load.
- Traffic is considered in terms of an eighteen-kip equivalent single axle load.
- The computer program NELAPAV (*4*) is used as a subroutine to calculate the critical strains induced in the pavement system by a 9-kip dual wheel load.
- Subgrade rutting and surface fatigue are considered as potential failure modes. The fatigue was summed for both the overlay material and the existing surface.
- The revised Shell subgrade strain criteria (*5*) are used to estimate the allowable number of strain repetitions for the subgrade.
- The Shell asphalt concrete fatigue criteria (*6, 7*) are used to estimate the allowable number of strain repetitions for an asphalt concrete surface or overlay.
- The user may select one of three seasonal variation models for each of the pavement layers; a temperature-based model for asphalt concrete, a freeze-thaw seasonal model, or a wet-dry seasonal model. Schematic diagrams of the freeze-thaw model and the wet-dry model are given in figures 1 and 2. Ramps in the layer moduli are modeled as a series of steps (dashed lines in the figures), with each step corresponding to a different season. Since the user defines the magnitude of the seasonal variation as well as the duration of each season, it is thought that these models are sufficiently versatile to model the present state of knowledge of seasonal variation for most circumstances.
- Miner's hypothesis of cumulative fatigue damage (*8*) is applied to sum the damage over the different seasons, and over the life of the pavement.

APPROACHES TO DATA EVALUATION

Having deflection data for roughly one hundred test points in a mile of pavement presents the engineer with an interesting problem—how the data can be used to derive a design overlay thickness (or thicknesses, if it is deemed appropriate to subdivide the section) or an overall remaining life estimate for the section. Traditional deflection based overlay design methods have used a single representative deflection measurement (e.g. mean Benkelman beam deflection plus two standard

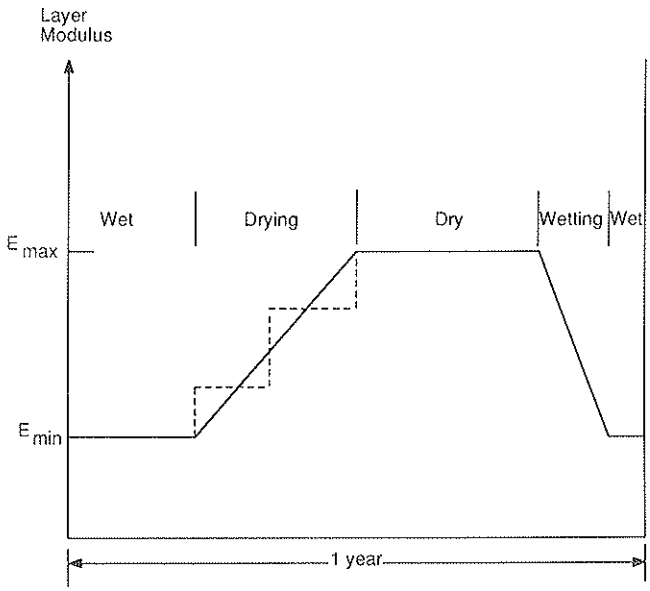

FIGURE 2 Wet-dry seasonal variation model.

deviations, 85th percentile deflection, etc.). At the other extreme, one could determine the required overlay thickness for each individual test point and then decide how to translate the individual overlay thicknesses into a design value.

In deciding between these two approaches to data evaluation, there are some definite tradeoffs. On the one hand, using a representative deflection basin is relatively simple and fast. However, it is not clear that the resulting design overlay thickness will be representative of what the pavement really needs. On the other hand, analyzing the data for each test point individually has the potential to provide much more information about the pavement, but is considerably more time consuming.

Both approaches to the data analysis were used in this case study so that the merits of each could be evaluated more thoroughly. The representative deflection basins used were determined by estimating the 85th percentile deflection (in other words, the deflection that was greater than or equal to 85 percent of the observed deflections) for each sensor in the data set. Separate 85th percentile deflection basins were derived for the test points at 50-ft intervals and those at 250-ft intervals, in the northbound outer wheel path. For both analysis approaches, the remaining life and overlay design analyses were based primarily on the December 1985 deflection data because it was the more extensive data set. Layer moduli derived from the May 1986 deflection data were used to define the magnitude of seasonal variation for the seasonal variation model.

RESULTS

General

Mechanistic Overlay Design

Moduli for the four unknown upper layers (surface, base, subbase, and subgrade) were derived from the deflection basin data using the MODCOMP 2 computer program. The results were evaluated and spurious data were rejected. (It sometimes happens that while MODCOMP 2 will give a good fit of the deflection data, within the specified tolerance, the results are unreasonable and, therefore, must be regarded as spurious.) After the screening process, a set of layer moduli were selected for each test point for use in the overlay calculations. The results were highly variable. A complete summary of the back-calculated moduli is given elsewhere (*3*). Some typical results are given in table 4.

TABLE 4 'TYPICAL' BACK-CALCULATED LAYER MODULI

Layer Depth (Inches)	Modulus (ksi)	Layer Depth (Inches)	Modulus (ksi)	Layer Depth (Inches)	Modulus (ksi)
0-9	380	0-9	668	0-9	588
9-36	6	9-36	28	9-24	94
36-66	30	36-66	7	24-48	5
66-336	250	66-336	250	48-360	250
336-∞	1,250	336- ∞	1,250	360-∞	1,250
0-9	218	0-9	100	0-9	270
9-24	6	9-24	10	9-24	19
24-72	14	24-72	7	24-72	13
72-300	250	72-291	250	72-204	250
300-∞	1,250	291-∞	1,250	204-∞	1,250

Required overlay thickness analyses were conducted for a 15-yr design life using the PAVMAN computer program. The results of the analyses for the individual test points were highly variable, ranging from zero (no overlay needed) to seven inches.

It is believed that this variability is primarily due to variations in the moisture content of the upper subgrade soil. A histogram of the required overlay thickness results is given in figure 3. The test points requiring the greater overlay thicknesses were predominantly in the outer wheel path of the northbound lane but were scattered over the full length of the test section. Many of the larger overlay thicknesses occurred for test points between the two 500-ft sections that were tested at 50-ft intervals (in other words, at points that would not have been tested if only the two 500-ft subsections of the pavement had been tested).

In order to determine the overlay thickness required for a given design life (in this case, fifteen years), PAVMAN calculates (and reports) the remaining life of the pavement for five different trial overlay thicknesses, ranging from zero to

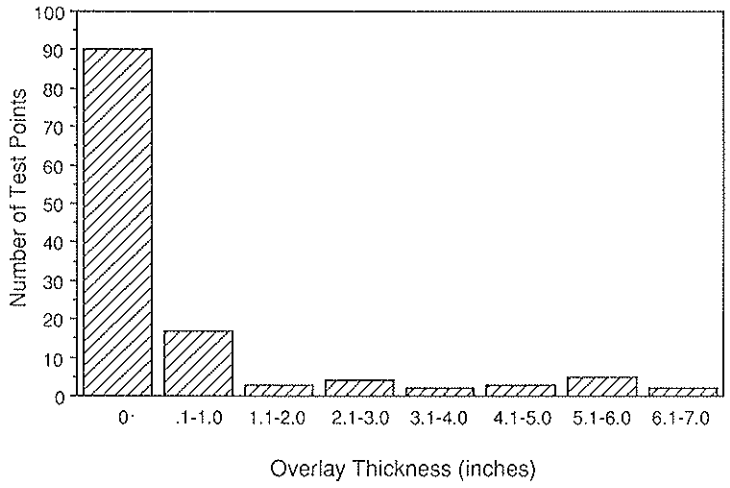

FIGURE 3 Required overlay thickness frequency.

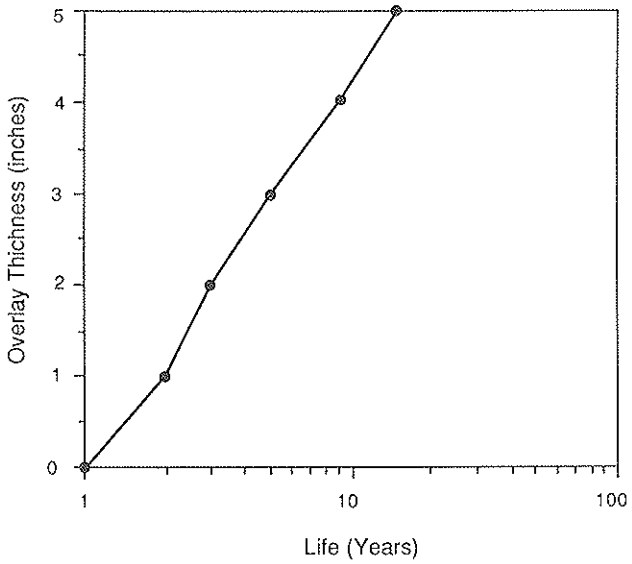

FIGURE 4 Pavement life versus overlay thickness.

a user specified maximum. A typical plot of overlay thickness versus pavement life is given in figure 4. The degree to which such plots are linear in semi-log space appears to depend, to some extent, on the layer that controls the design and whether the controlling layer is the same for all overlay thicknesses.

Eighty-fifth percentile overlay thicknesses were estimated from the individual overlay thickness results for the test points at 50-ft and 250-ft intervals in the northbound outer wheel path, as well as for all of the test points, with results of 2.6, 5.9, and 1.1 inches, respectively. The disparity between the results for the different sets of test points indicates that the number and location of test points selected may significantly affect the results. This indication is further supported by the variability in the individual overlay thickness results.

The required overlay thickness results for the 85th percentile deflection basins, 1.8 inches for the test points at 50-ft intervals, and 6.1 inches for those at 250-ft intervals, compare favorably with the 85th percentile overlay thicknesses derived from the individual test point results for this particular pavement. However, it should not be assumed that this would be true for all pavements. Furthermore, while the degree of variability in the pavement is clearly evident from the individual test point results, it is not at all evident when the representative deflection basin approach is used.

Overlay Design Using the Asphalt Institute Method

The required overlay thickness for the project site was also determined using the Asphalt Institute's deflection based overlay design procedure for comparison (*9*). For these comparisons, the overlay thickness requirement was first determined using the FWD data, so that the comparison would be between different analysis methods based on the same device. Since the Asphalt Institute procedure was developed for use with the Benkelman beam, the Benkelman beam data were used in a subsequent analysis to check the results.

The Asphalt Institute recommends that pavement testing for overlay design be conducted in the outer wheel paths. Therefore, only the data from the outer wheel paths were used in the overlay designs. It was assumed that the deflections measured in the spring of the year were 20 percent lower than the maximum spring values. This assumption was consistent with an assumption made in defining the seasonal variation in layer moduli for the mechanistic analysis. Both the FWD data and the Benkelman beam data were normalized to the 18-kip axle load prescribed in the Asphalt Institute overlay design method.

Although both FWD and Benkelman beam data were available for the project site, it was assumed that the maximum FWD deflection was equal to 50 percent of the Benkelman beam deflection under a similar load. This assumption was somewhat arbitrary, but is in reasonable agreement with the test results for the pavement in question. The assumed correlation was used instead of an exact correlation, so a typical assumption that might be made when only FWD data was available might be tested. Accordingly, the FWD deflections were doubled to approximate Benkelman beam deflections. The traffic volumes and design life used in the Asphalt Institute method were the same as those used for the mechanistically based analysis.

The overlay thicknesses derived from the doubled FWD deflections and the Benkelman beam deflections, for a 15-yr design life, were both approximately 3.8 inches. Thus, for the given pavement and assumptions, it does not matter which device is used, as long as the Benkelman beam deflections are twice the FWD deflections. This will not always be the case.

Interpretation and Application

If it is accepted that it is better to analyze the deflection data on a point by point basis, the question that arises is how does one apply the individual overlay thicknesses once they have been calculated? The strict 85th percentile overlay thickness approach used in the preceding comparisons is one approach, but it has several flaws. First, it does not really make use of the information on the variability in the pavement, and second, a design overlay thickness so derived can be unduly influenced by a few excessively weak test points. To make full use of the information available, the engineer must determine what the required overlay thickness results tell about the pavement.

One interpretation is that individual required overlay thicknesses that are substantially higher than some norm (the mean, median, eighty-fifth percentile value, an arbitrarily selected value, etc.) are indicative of areas that need spot improvements over and above the overlay to be place on the entire pavement. For the purposes of this case study, the following procedure for deriving a design overlay thickness was proposed and used:

1. Calculate the required overlay thickness for each test point.
2. Determine what proportion of the test results yield a negligible required overlay thickness.
3. If the proportion of test points requiring negligible overlay thicknesses is large, consider spot improvements (such as drainage improvements, cut-out and replacement of small sections of pavement, patching, etc.) for the locations that need

work, and use remaining life analyses to determine when the pavement needs to be considered for an overlay. Alternatively, one could determine the overlay thickness required in some given future year.

4. If the number of test points requiring negligible overlay thickness is small, proceed as follows:
   (a) Consider the spacing and magnitude of the non-zero required overlay thickness results to determine which points should be considered for spot improvements in addition to the overlay placed on the entire pavement. Spot improvements might include additional overlay thickness, drainage improvements, cut-out and replacement of small sections of pavement, etc..
   (b) Since the overlay is being designed to improve those areas that need an overlay, as opposed to those that do not, neglect all zero required overlay thicknesses in subsequent determinations.
   (c) Determine the 85th (or other design level) percentile overlay thickness from the set of non-zero overlay thicknesses for test points which have not been selected for spot improvements. This becomes the design overlay thickness. The presumption here is that spot improvements will reduce the required overlay thickness at the spot improvement locations to the level required by the remainder of the pavement.

Table 5 summarizes design overlay thicknesses derived from the data for the inner and outer wheel paths of both lanes, using the procedure outlined above, for the following improvement options:

- No spot improvements are to be made.
- Spot improvements will be made at locations requiring overlay thicknesses of 6 inches or more.
- Spot improvements will be made at locations requiring overlay thicknesses of 5 inches or more.
- Spot improvements will be made at locations requiring overlay thicknesses of 4 inches or more.
- Spot improvements will be made a locations requiring overlay thicknesses of 3 inches or more.

TABLE 5 DESIGN OVERLAY THICKNESSES FOR VARIOUS IMPROVEMENT OPTIONS

Improvement Options[a]	Design Overlay Thickness	Percentage of Pavement Requiring Spot Improvements
1	5.9	0.0
2	5.4	4.7
3	3.8	13.3
4	2.5	15.8
5	2.1	16.3

[a]Numbers refer to the list in the text.

For comparison, the 85th percentile value determined using all of the test points in the wheel paths (including those requiring no overlay) is 1.6 inches.

The data from the testing in the middle of the northbound lane were not included in the determination of the design overlay thickness for two reasons. First, unless some of the data for the northbound lane were omitted, the overlay design would be based more heavily on the northbound lane than the southbound lane because more testing was done in the northbound lane. With the mid-lane data omitted, the two lanes are equally represented in the data set. Second, the relevant portion of the pavement for overlay design purposes (in terms of structural requirements) is the portion of the pavement subjected to significant traffic. Since the portion of the pavement between the wheel paths is not subjected to significant traffic, it should not control or significantly affect the thickness of the overlay required for structural purposes and, therefore, should not be considered in the analysis of required overlay thickness.

In the discussions that follow, it is assumed that spot improvements will be made in the vicinity of all test points having required overlay thicknesses in excess of three inches (Improvement Option 5).

If it is assumed that the necessary spot improvements can be made by placing greater thicknesses of asphalt concrete or by installing underdrains, and that the incremental cost of a 1-in thickness of asphalt concrete is $4.25 per linear foot (based on a pavement width of 20 feet, as per pavement records, an asphalt concrete cost (in place) of $35 per ton, and an asphalt concrete density (in place) of 145 pounds per cubic foot), while underdrains cost $8.00 per linear foot (based on an average trench depth of two feet, a trench width of 18 inches, 6-in perforated steel pipe at $4.65 per linear foot, excavation at $12.00 per cubic yard, filter material (average total depth, 16 inches) at $25 per cubic yard, and backfill (8-in deep, on average) at $4.02 per cubic yard), the installation of underdrains is more economical than placing the required extra thickness of asphalt concrete whenever the underdrains replace more than 1.9 inches of asphalt concrete (whenever the required overlay thickness exceeds the design overlay thickness by more than 1.9 inches).

Under the assumption that spot improvements will be made at all locations requiring overlay thicknesses in excess of three inches, the design (85th percentile) overlay thickness is 2.1 inches. Therefore, the installation of underdrains is the more economical method of making the required spot improvements whenever the required overlay thickness is four inches or more (2.1 + 1.9), and the placement of a thicker overlay is more economical where the required overlay thickness is less than four inches. For the purpose of these comparisons, it assumed that the additional overlay thickness would be placed across the full width of the pavement. Under certain circumstances, it might be possible to taper the overlay so that only the portion of the pavement that needed the additional thickness got the full thickness.

Of the locations that need spot improvements, only one area has a required overlay thickness less than four inches. Therefore, under the given assumptions, with a design overlay thickness of 2.1 inches, the most economical method of rehabilitating the pavement is to place a total overlay thickness of 3.6 inches in that one area and to install underdrains at the other locations needing spot improvements.

Comparison With Other Methods

The thickness of the overlay placed at the project site in the summer of 1986 was determined by NYSDOT engineers using judgment and experience, without the benefit of the nondestructive testing or the subsequent analyses. That overlay consisted of up to 3½ inches of binder material placed to fill in pavement ruts, followed by a 1½-in binder course and a 1-in top course. Thus, the pavement was overlaid with a minimum of 2½ inches of asphalt concrete in areas with minimal rutting and a maximum of 6 inches in severely rutted areas. Spot drainage improvements were made only at the extreme northern end of the project site. Referring to table 5, the 2½-in minimum overlay thickness is comparable to the design overlay thickness determined for the instance where all points needing an overlay 4 or more inches in thickness were subject to spot improvements. If it is assumed that the test points for which high required overlay thicknesses were calculated were in the more severely rutted sections of the pavement, there is reasonable agreement between the required overlay thicknesses calculated for a 15-yr design life and the overlay actually placed.

The 3.8-inch design overlay thickness determined using the Asphalt Institute method is comparable to the design overlay thickness determined by using the PAVMAN program and assuming that spot improvements would be made at points requiring overlays in excess of 5 or 6 inches (see table 5). Thus, if the 3.8-in overlay were placed with no spot improvements, we would expect a higher premature failure rate than if the spot improvements were made, as is assumed in the mechanistically based design.

IMPLICATIONS AND UNANSWERED QUESTIONS

Why Bother?

The reader may well be wondering if mechanistically based pavement analysis and overlay design methods are really worth all the trouble. In the authors' opinion, the answer is absolutely yes, if they are used to their fullest potential. If the decision to place an overlay has already been made, and the year in which it is going to be placed has already been determined, so that the only reason for using the analysis procedure is to decide how thick the overlay should be, then a mechanistically based analysis procedure may not be worth the trouble. However, if the procedure is instead used to determine the optimal timing for a pavement rehabilitation project, and/or the most economical means of rehabilitating a pavement, preferably within the framework of a network-level pavement management system, then mechanistically based pavement analysis techniques have great potential.

With mechanistically based pavement analysis techniques, one can examine the consequences of putting off an overlay for a few more years or model the effects of base stabilization, surface recycling, or improved drainage. One can look at the tradeoffs involved in rehabilitating section A this year instead of section B, or in constructing a new pavement in stages, instead of placing the entire structure needed for the design life at once. In short, mechanistically based pavement analysis and design methods have the potential to be a tremendous tool for optimizing the use of funds in the highway industry.

What's Missing?

While mechanistically based pavement design and analysis methods have tremendous potential, there are several areas in which further research is needed to perfect the methodology. The following sections discuss some of these areas.

Testing Program

The optimal number and spacing of NDT test points for use with mechanistically based pavement evaluation and design methods has not been determined. This case study attempted to address the issue to a limited extent. From the work that was done, it appears that both closely spaced test points over short subsections of the pavement in question and uniformly spaced test points over the full length of the pavement have some advantages and disadvantages. Until further studies can be done to develop reliable criteria, a reasonable compromise would be to test the full length of the pavement in both the inner and outer wheel paths at 250-ft intervals, with the test points in the inner wheel path offset by 125 feet from those in the outer wheel path (in other words, if the first test point in the outer wheel path is at station 0+00, then the first test point in the inner wheel path should be at station 1+25).

Failure Criteria

It is generally held that the critical strains in a pavement structure are the maximum horizontal tensile strain in the surface material and the vertical compressive strain at the top of the subgrade. The criteria used to determine the allowable number of strain repetitions at each of these locations are, as a matter of necessity, empirically derived and, therefore, may not be entirely applicable to materials and circumstances that differ from those for which and under which they were developed. For example, The Shell revised subgrade strain criteria used in the PAVMAN program, as well as many other subgrade strain criteria, were derived from the AASHO Road Test data. Since the AASHO Road Test involved only one subgrade soil and one climate, the use of those criteria for pavements in other areas is an extrapolation that may or may not be valid. Further research is needed to develop more universally applicable strain criteria, for both subgrade and surface materials, and to establish limitations for those that currently exist.

The 18-kip Equivalent Axle Load Question

Frequently, pavement design is based on the 18-kip equivalent single-axle load (ESAL). That is, all vehicle loads are translated to an equivalent number of 18-kip single-axle loads. Like the subgrade strain criteria, most commonly used sets of 18-kip equivalency factors were derived from the AASHO Road Test data (separate factors exist for flexible and rigid pavements). The problem with this is that the number of loads of any given magnitude that is equivalent to an 18-kip ESAL is

different for every pavement, so that every time the AASHO equivalency factors are used, an error of unknown magnitude is made. In a mechanistically based analysis, this weakness could be eliminated by treating each vehicle category separately and summing the damage due to each. The cost of doing this would be an increase in computation time. Whether the accuracy gained would be worth the added cost is something that needs to be examined. Alternatively, as microcomputer technology improves, the added cost of considering the damage due to individual vehicle classes may become negligible and thus negate the advantage of using the 18-kip ESAL.

Staged Construction, Alternative Materials, and Rehabilitation Methods, and Network Level Pavement Management

While mechanistically based pavement analyses have the potential to consider staged construction, alternative pavement materials, and alternative rehabilitation methods (stabilized, recycled, or otherwise modified materials, improved drainage, etc.), such analysis alternatives have not necessarily been fully implemented at the project level, let alone at the network level.

The PAVMAN program developed for this case study is a starting point. However, more advanced computer programs with the capability to model staged construction, pavement networks instead of single projects, and rehabilitation methods other than simple overlays, are needed before mechanistically based pavement analysis methods can be used to their fullest potential.

SUMMARY

A case study, in which nondestructive test technology and mechanistically based analysis techniques were applied to the evaluation of required overlay thickness for an existing pavement has been described. A computer program, PAVMAN, developed to facilitate the mechanistic analysis of the pavement, is also described. The design overlay thickness determined using PAVMAN is in reasonable agreement with those derived for the same pavement using the Asphalt Institute's deflection-based overlay design procedure. Actual construction, based on design by experience, also closely matched the results from the mechanistic analysis. Recommendations regarding testing programs for similar activities are made, and areas in which the technology needs further development are discussed.

ACKNOWLEDGMENTS

The work discussed herein was supported by the New York State Department of Transportation and the Cornell Local Roads Program.

The views and opinions expressed herein are those of the authors, and do not represent official views or policies of the New York State Department of Transportation or Cornell University.

REFERENCES

1. D. T. Hartgen. Status of Highway Condition Scoring in New York State. In *Transportation Research Record 997*, TRB, National Research Council, Washington, D.C., 1984, pp. 85–90.
2. L. H. Irwin. *User's Guide to MODCOMP 2*. Cornell Local Roads Program Report No. 83-8, Cornell University, Ithaca, N.Y., November 1983.
3. C. A. Richter and L. H. Irwin. *Application of Nondestructive Testing to Pavement Evaluation and Overlay Design*. Cornell Local Roads Program Report No. 87-3, Cornell University, Ithaca, N.Y., June 1987.
4. L. H. Irwin and D. P. T. Speck. *NELAPAV User's Guide*. Cornell Local Roads Program Report No. 86-1, Cornell University, Ithaca, N.Y., January, 1986.
5. A. I. M. Claessen, J. M. Edwards, P. Sommer, and P. Uge. Asphalt Pavement Design—The Shell Method. *Proceedings, Fourth International Conference on the Structural Design of Asphalt Pavements*, Vol. I, 1977, pp. 39–74.
6. M. W. Witczak and K. R. Bell. Remaining Life Analysis of Flexible Pavements. *Proceedings, Association of Asphalt Paving Technologists*, Vol. 47, 1978, pp. 229–269.
7. W. Heukelom. *Observations on the Rheology and Fracture of Bitumens and Asphalt Mixes*. Shell Bitumen Report No. 19, Shell Laboratorium-Koniklijke, 1966.
8. M. A. Miner. Cumulative Damage in Fatigue. In *Journal of Applied Mechanics*, American Society of Mechanical Engineers, Vol. 12, No. 3, September 1945, pp. A-159–A-164.
9. The Asphalt Institute. *Asphalt Overlays and Pavement Rehabilitation*. Manual Series No. 17 (MS-17), College Park, Maryland, November 1977.

Publication of this paper sponsored by Committee on Pavement Rehabilitation.

Evaluation of the Performance of Bonded Concrete Overlay on Interstate Highway 610 North, Houston, Texas

KOESTOMO KOESNO AND F. FRANK MCCULLOUGH

The objective of the study was to evaluate the performance of the bonded concrete overlay project on IH 610 North in Houston and implement the findings in other studies on bonded concrete overlay. The performance of the bonded concrete overlay was monitored on ten experimental sections selected from the 3-½-mi project and ranging from 400 to 600 feet long. Periodic field measurements were conducted, and an assessment of overlay pavement life was made. The resulting conclusions and recommendations were to be used by the Texas State Department of Highways and Public Transportation to design overlays for rehabilitation programs on continuous reinforced concrete pavement (CRCP).

Since 1956 the United States has been involved in the largest public works project ever undertaken, the 42,500-mi system of interstate highways. Unfortunately, these highways have begun to wear out. Not only are we reaching the end of the design life of many sections of highways, but the amount of traffic is far exceeding the design estimates (*1*). In recent years, the general interest of the highway administration has shifted from construction to maintenance, rehabilitation, and resurfacing.

Portland cement concrete (PCC) overlays have been used to resurface pavements for more than 60 years. However, experience in the use of bonded concrete overlays is mostly with airport runways and bridge decks, although there are instances in which bonded concrete overlay has been used for improving skid resistance on highways (*2,3*).

The U.S. Air Force has more than 20 years of experience with thin bonded concrete overlay (*4*). Overlays ranging from 2- to 4-in thick have been constructed on runways subject to light as well as heavy traffic and used by small as well as large aircraft. The condition of the overlays over a period of 17 years has ranged from good to very good, but there have been a number of cases where problems were encountered. For example, severe reflection cracking and rapid deterioration following loss of interface bond was experienced in a taxiway at the Tulsa Airport.

During the past two to three years, several research studies were undertaken at the Center for Transportation Research to address questions concerning the use of thin bonded concrete overlays for highway pavement rehabilitation. Tests were made on laboratory specimens and cores from constructed slabs in the field in which a bonding agent was used. A major finding of this research (*5*) was that the interface between existing slab and overlay develops a shear strength three to four times the theoretically predicted shear stress due to wheel loads of the expected traffic. Also, a condition survey of the overlay section soon after overlaying and again in six months did not show any significant distress. This experience encourage the SDHPT to use a 4-in bonded concrete overlay on a length of about 3-½ mi to improve the pavement condition of Loop 610 North in Houston. It was suggested that several sections of this pavement be identified and monitored to father performance information periodically. It was planned that the analysis carried out using the resulting data would help answer questions about the relative merits of different types of overlay materials.

The overlay project is located on IH 610 North in Houston between East T.C. Jester Blvd. and IH 45 (see figure 1). At this location, the roadway is an eight-lane divided highway with four through lanes in each direction and a concrete median barrier. The main lanes are 12 feet wide and shoulders are 10 feet wide.

The 4-in bonded concrete overlay was placed on the existing 8-in continuous reinforced concrete pavement (CRCP). The existing concrete pavement rests on 6-in thick stabilized subbase. The typical cross section of the project is presented in figure 2.

OBJECTIVE OF THE STUDY

The primary objective of the study was to evaluate the performance of the bonded concrete overlay on IH 610 North in Houston and implement the findings of other studies on bonded concrete overlays.

The sub-objectives were—

1. To identify several sections to represent the variation in the original pavement condition and the material used for the overlay,
2. To observe and record the materials actually used for the overlay,
3. To make observations of the behavior parameters before and after-overlay, and
4. To perform statistical analyses to evaluate the field data.

Center for Transportation Research, The University of Texas at Austin, Austin, Tex. 78705.

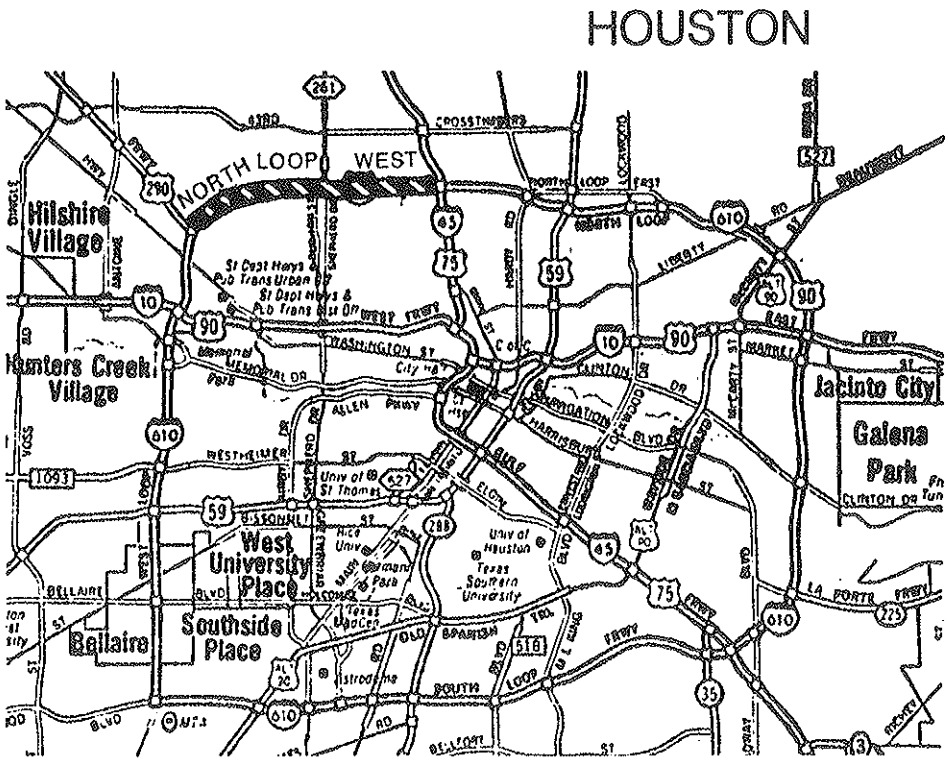

FIGURE 1 Location of the overlay project.

DESCRIPTION OF THE STUDY

The following variables were considered in the study:

1. Overlay reinforcement: CRCP and fiber reinforced concrete pavement,
2. Overlay aggregate: siliceous river gravel and limestone, and
3. Old pavement condition: no distress, moderate distress, and severe distress.

The use of the variables in 1 and 3 above is self-explanatory. The variables in 2 were used for two reasons: (1) the old pavement was constructed using siliceous river gravel, and (2) research done at the Center for Transportation Research at The University of Texas at Austin (*10*) showed that limestone is a better coarse aggregate than siliceous river gravel from a long-term performance standpoint. Therefore, siliceous river gravel was used in some sections and limestone was used in others.

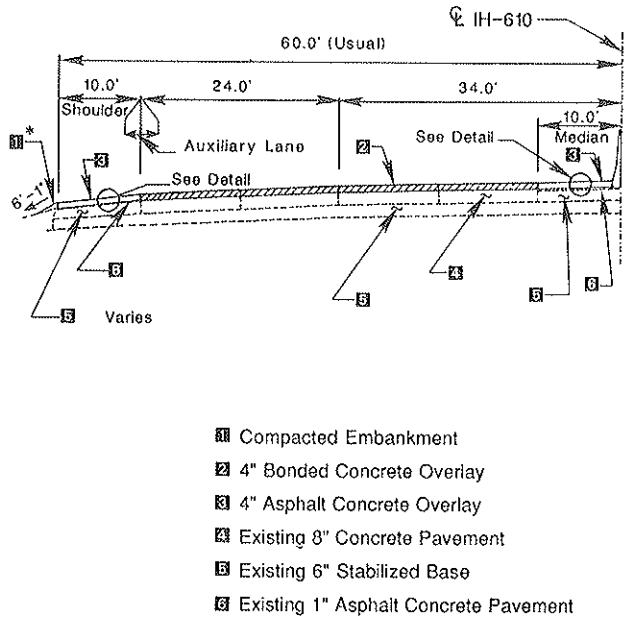

FIGURE 2 A typical cross section of the bonded concrete overlay pavement on IH 610 North, Houston.

From the 3-½-mi overlay project on eastbound IH 610 North ten test sections ranging from 400 to 600 feet long were identified, to maintain homogeneity within a section (similar overlay reinforcement, overlay aggregate, and distress) and also to have a length adequate for the desired observations. The ten sections were divided into two fiber-reinforced concrete overlay sections, two reinforced concrete overlays sections using limestone aggregate, and six reinforced concrete overlay sections using siliceous gravel aggregate. The reinforced concrete overlays were reinforced with a grade 70 wire fabric mesh with spacing and size of 6 × 12 – D16 × D10 throughout the sections. Across transverse construction joints, bars of the same grade and size as the mesh were used at 12-in intervals, in addition to the mesh. For the fiber reinforced concrete overlays, 85 pounds of fibers per cubic yard were used. The method of construction included the following steps:

1. Scarifying the old pavement to a ¼-in depth,
2. Placing reinforcing steel,
3. Grouting over reinforcing, using 11 gallons of water per sack of cement grout, and
4. Placing the concrete by slip forming.

TABLE 1 CONCRETE MIX DESIGNS

Material	Mix Using		
	Silicious River Gravel	Limestone	SRG with Fibers
Cement (lb)	658	658	752
Coarse Aggregate (lb)	1950	1770	1218
Fine Aggregate (lb)	1055	1235	1715
Retarder (POZZ.300R) (oz.)	30	30	38
Air Entrainer (AE-10) (oz.)	7	7	5
Water (lb)	233	233	250

Note: All weights are based on material in the SSD condition.

A summary of the concrete mix design data is shown in table 1. Summaries of tensile and flexural strengths are shown in tables 2 and 3, respectively. The average tensile strengths of fiber reinforced sections, welded wire fabric with limestone sections, and welded wire fabric with siliceous river gravel section are 698, 642, and 615 psi, respectively.

It was suggested that the ten experimental sections selected be monitored for at least three years so that it would be possible to identify any correlation between materials and performance based on the different environmental conditions.

Based on the results of the first condition survey, the distress indexes of each experimental section were determined using the following formula (*6*):

$$Z_c = 1.0 - 0.065\,FF - 0.015\,MS - 0.009SS$$

where

Z_c = distress index,
FF = number of failures per mile (sum of punchouts and patches),
MS = percent minor spalling, and
SS = percent severe spalling.

The distress values are subtracted from 1 and the value obtained in a maximum value. As the distress index decreases, the quality of the road deteriorates, with zero being the value where major rehabilitation is necessary.

Three levels of distress were used in this study:

- No significant distress, with distress index ranges from 0 to 1,
- Moderate distress, with distress index ranges from −2 to 0, and
- Severe distress, with distress index less than −2.

The factorial design of the study is shown in figure 3. It is important to note that the factorial experiment design does

TABLE 2 SUMMARY OF AVERAGE TENSILE STRENGTH (PSI) (OVERLAY PORTION), IH 610 NORTH, HOUSTON

Test Section Number	Dates Core Taken	
	February 1986	January 1987
1	676	615
2	582	544
3	422	575
4	671	625
5	650	950
6		718
7		638
8		652
9		868

TABLE 3 SUMMARY OF FLEXURAL STRENGTH VALUES OF CONCRETE SAMPLES FROM TEST SECTIONS

Test Section	Flexural Strength
1	870
2	- -
3	835
4	885
5	800
6	880
7	760
8	775
9	- -
10	- -

OVERLAY / PAVEMENT CONDITION / OVERLAY AGGREGATE		WELDED WIRE FABRIC			FIBER		
		ND	MD	SD	ND	MD	SD
SRG		2	1	6			4
		10	3	9			5
LST		8		7			

ND – No Distress
MD – Moderate Distress
SD – Severe Distress
SRG – Siliceous River Gravel
LST – Limestone

FIGURE 3 Factorial design of the eastbound IH 610 North, Houston, experimental project.

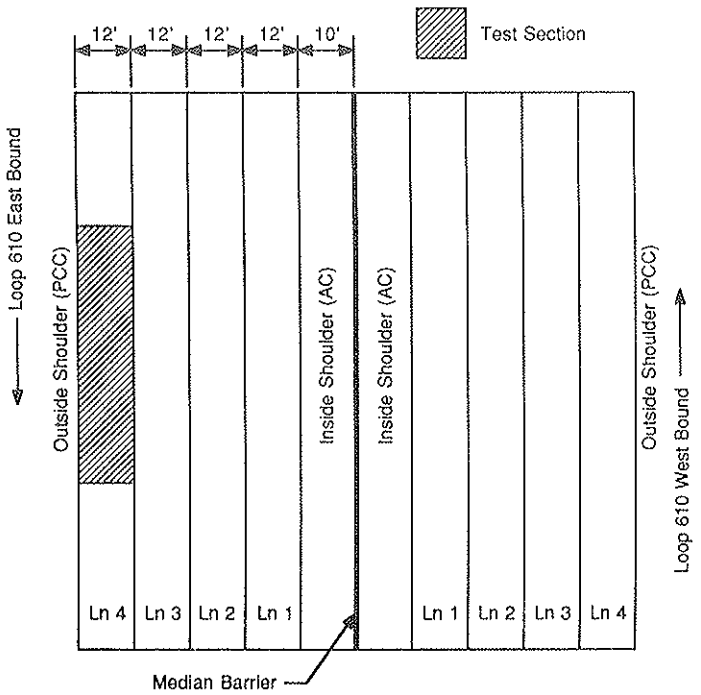

FIGURE 4 Plan view of a typical test section on IH 610 experimental project showing details of layout.

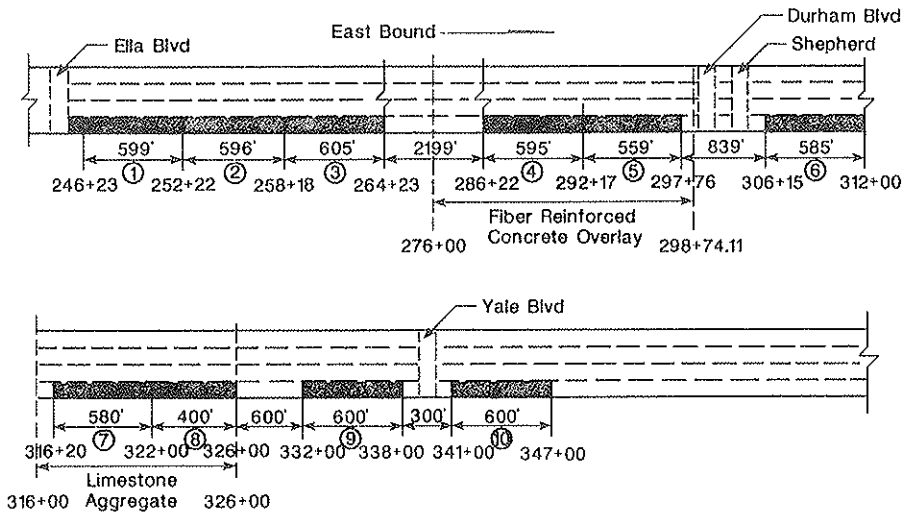

FIGURE 5 Plan view showing locations of the ten test sections, eastbound IH 610 North, Houston.

not include fiber reinforced concrete with limestone aggregate and is, therefore, a partial factorial.

DESCRIPTION OF TEST SECTION

The ten test sections are located on eastbound IH 610 North between Ella Boulevard and about 700 feet beyond Yale Boulevard. At this location, the roadway is a four-lane highway in each direction. All the test sections are in the outside lane (the lane furthest from the median barrier). A plan view of a typical test section is shown on figure 4. Figure 5 shows the locations and dimensions of each test section.

RESULTS

Various measurements were taken in order to gather data to use to evaluate the parameter behavior before and after overlay construction. The various data obtained pertain to deflection, condition survey, and roughness. In addition, data were gathered on a number of cores that were secured from various test sections.

Deflection Measurements

The Dynaflect was used to measure the pavement deflections before and after overlay. The deflection readings were taken at 50-ft intervals, approximately on the center line of the outside lane of each experimental section. In order to evaluate the performance of the pavement before and after overlay, measurements were taken at approximately the same test points before and after overlay construction. During the period of the study, Center for Transportation Research personnel took deflection measurements five different times.

Figures 6 and 7 show before and after overlay deflections of sensor 1 and sensor 5, respectively. As can be seen, the average deflection after overlay construction was significantly less for all test sections. The before-overlay data show that the deflections increased in the second set of readings. The increase may have been caused by a combination of factors. Weather conditions and pavement temperature may have influenced the pavement performance.

CRC sections, fiber reinforced concrete sections, and sections with limestone performed differently in deflection. CRC sections showed a better performance that the other sections did, with a 37.1 percent decrease in the average deflection of sensor 1. Limestone and fiber sections had 30.5 percent and 26.8 percent decreases in the average deflection of sensor 1.

Condition Survey

Condition surveys were conducted to monitor the development of distress and distress types found in the pavement before and after overlay construction. The method used in this study is called the Small Section Method. It is a detailed procedure and is conducted by a team of two people. The team walks along a lane; one person walks with a rolling meter, and the other maps all visible distress with reference to a highway milepost. The distress types that are mapped are transverse and longitudinal cracks, spallings, punchouts, and patches. This detailed procedure is appropriate for roadway that is experimental in nature (*6*).

The transverse cracking was presented as average crack spacing, which was obtained by dividing the total length of the test section by the number of transverse cracks on the section. The longitudinal cracking was measured in units of linear feet per 100-ft section.

Before overlay placements, the average crack spacings were fairly uniform for all test sections (figure 8). After overlay, the average crack spacings varied. Overlay materials can affect the crack spacing of the pavement. Section 8 (CRCP with limestone aggregate) had the greatest transverse crack spacing, with section 10 (CRCP with siliceous river gravel) and section 4 (Fiber reinforced concrete overlay), second and third, respectively. Overlay materials may not be the only cause of the large variations in after-overlay crack spacings. Concrete temperature during overlay placement, which is not considered in this study, may be another cause of variation.

The longitudinal cracks before the overlay was placed var-

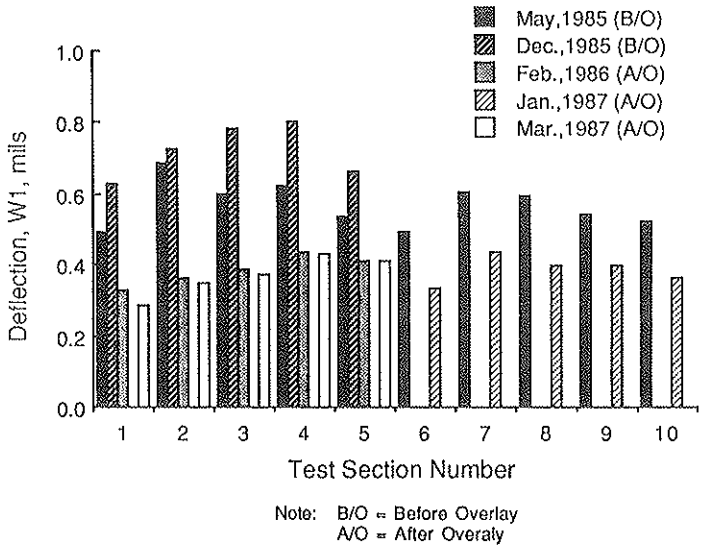

FIGURE 6 Comparison of before and after-overlay average deflection of sensor 1, IH 610 North, Houston.

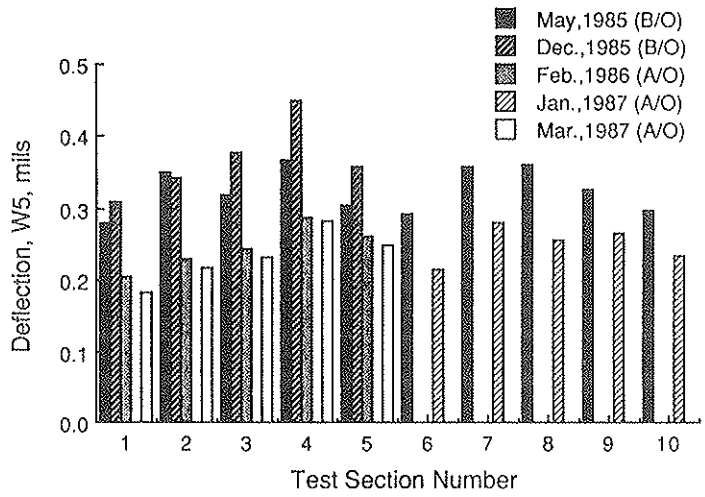

FIGURE 7 Comparison of before and after-overlay average deflection of sensor 5, IH 610 North, Houston.

ied for the ten test sections (figure 9). After overlay, the only longitudinal cracks were in section 4 (fiber reinforced) and section 10 (CRCP).

It is important to note that until the last condition survey was conducted, spalling and puchout did not exist in any of the test sections.

Roughness Data

The profilometer was used to evaluate the riding quality and changes in profile of the pavement. The profilometer readings were conducted before and after overlay. The after-overlay readings give an indication of improvement in the riding quality. It can be seen in figure 10 that, after overlay construction, a general increase in present serviceability index (PSI) occurred on all test sections except section 10.

ANALYSIS OF DATA

The existing pavement materials were characterized by using deflection measurements. The moduli of elasticity of the concrete layer (E_1), subbase (E_2), and subgrade (E_3) were determined by back-calculating from deflection data within each test section before and after overlay. The back-calculating was accomplished by using program RPEDD1 (*8*), which is available in the Center for Transportation Research.

Note that some test sections are on the embankment and some are on the flat area (natural grade). The moduli versus

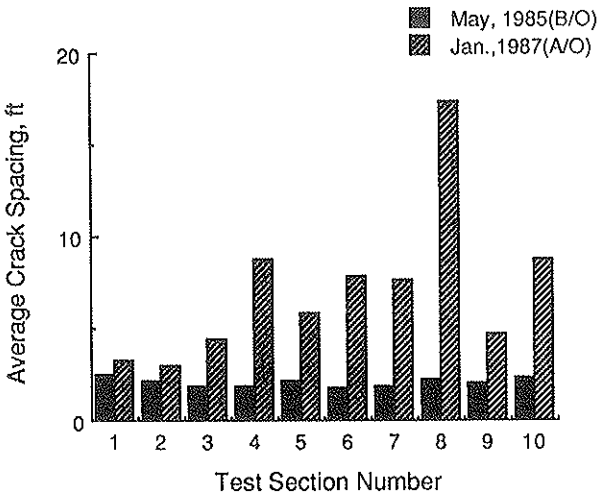

FIGURE 8 Comparison of before and after-overlay transverse crack spacing of the ten test sections, IH 610 North, Houston.

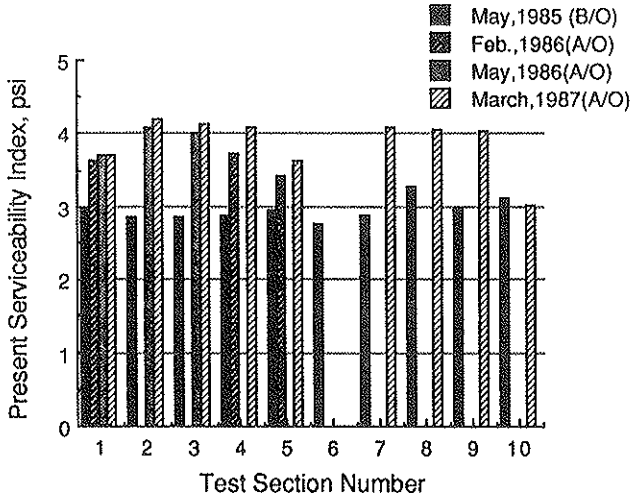

FIGURE 10 Comparison of before and after-overlay present serviceability indices of the ten test sections, IH 610 North, Houston.

the locations of test sections and various seasons are plotted on figures 11 through 13. Also note that the moduli vary with test section location and the environmental conditions when deflection readings are conducted.

CAUSES OF VARIATION IN LAYER STIFFNESS

CRC Layer

As can be seen in figure 11, modulus values of the CRC layer, E_1, for the first five sections were higher in May 1985 than those in December 1985, and the modulus values for sections 6 through 10 were higher in May 1985 than those in January 1987. This trend could be caused by the higher temperatures in May 1985. A high temperature condition results in a decrease in pavement deflection due to pavement expansion and narrowing of transverse cracks in CRC pavement. As the cracks narrow, the load transfer increases, which results in a stiffer CRC.

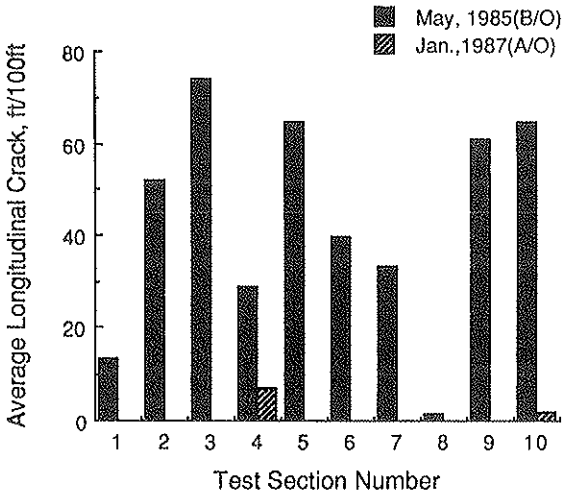

FIGURE 9 Comparison of before and after-overlay average longitudinal cracks per 100-ft section of the ten sections, IH 610 North, Houston.

Subbase Layer

Construction control may limit the variation in layer thickness and modulus. Some variation in subbase modulus, as shown in figure 12, may be caused by use of material from different sources in different areas of the project or use of different quantities of stabilizing agent. It also may be caused by different drainage conditions in different sections of the project. Sections with better drainage will have stiffer subbase layers. The subbase layer, which consists of sand and shell materials stabilized with cement, will be stiff with small amounts of moisture.

Subgrade Layer

Pavement in cut and fill areas may have different subgrade moduli of elasticity. In figure 13, most of the sections on the embankment have higher moduli. This may be the result of good drainage on the embankment sections; with good drainage, less water will remain in the subgrade layer. In contrast, low (flat) areas with higher water tables and poorer drainage will have a softer subgrade.

It also can be seen in figure 13 that the subgrade moduli vary with seasons. Periods of higher rainfall result in higher moisture content in the subgrade and a corresponding lower subgrade modulus.

COMPARISON OF PREDICTED AND MEASURED AFTER-OVERLAY DEFLECTION

Measured and predicted after-overlay deflections were compared for a partial verification of the design procedure; if these are similar then the life predictions are more reliable.

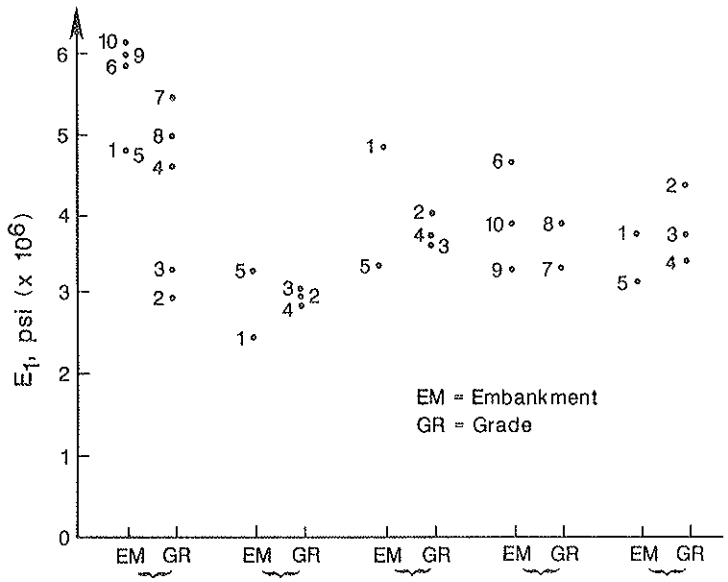

Note: Cumulative precipitation is total (cumulative) inches of rain from 10 days before deflection readings were taken.

NA = Data Not Available

FIGURE 11 Moduli of elasticity of concrete layer, E_1, versus test section locations and environmental conditions.

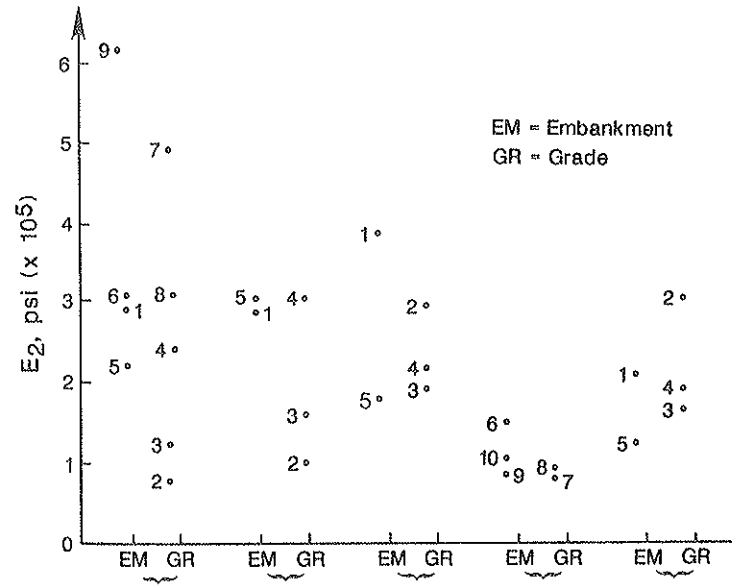

FIGURE 12 Modulus of elasticity of subbase layer, E_2, versus test section locations and environmental conditions.

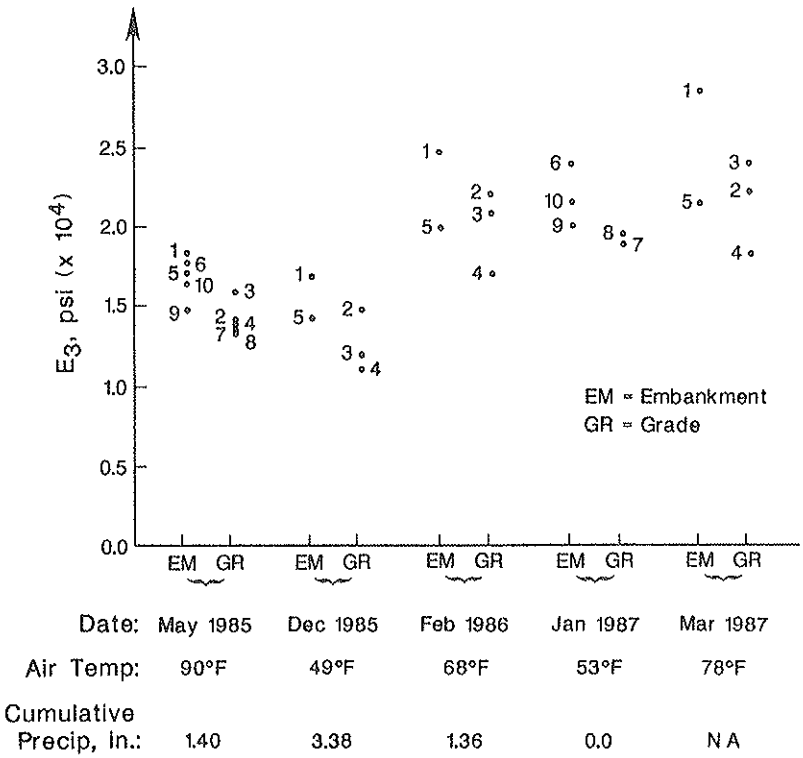

FIGURE 13 Modulus of elasticity of subgrade layer, E_3, versus test section locations and environmental conditions.

Layer characterization should be established before the predicted after-overlay deflection can be calculated. Calculating the after-overlay deflection involves the following steps:

1. Calculate the mean, $\bar{x}$, and standard deviation of before-overlay deflection for each experimental section.
2. Determine the moduli of the concrete layer (CRCP), subbase, and subgrade by back-calculating three deflection values ($\bar{x}$, $\bar{x} + s$, $\bar{x} - s$).
3. Assume the modulus value for the concrete overlay layer. Note that E_0 = 5,000,000 psi was used for the after-overlay deflection calculation in this study.
4. Measure the overlay thickness of the cores secured from the test sections. Use the average thickness for deflection calculation.
5. With the new four-layer system, the after-overlay deflections were calculated using program RPEDD1.

The accuracy of this method is reflected in the results presented in figure 14 (deflections of sensor 1) and figure 15 (deflections of sensor 5). In these figures, calculated deflections are a little above the equality line, which reflects conservatism in the predicted measurements.

There are a number of factors that may result in inaccurate prediction of after-overlay deflections:

- Seasonal effects,
- Concrete temperature effects, and
- Assumptions made for overlay layer modulus of elasticity.

As mentioned before, the first two factors lead to significant changes in the deflection measurements and, consequently, to the moduli predicted from these deflections.

ESTIMATION OF PAVEMENT FATIGUE LIFE AFTER OVERLAY PLACEMENT

Bonded concrete overlay is used not only to improve the riding quality and to correct grade problems but to add fatigue life to an existing pavement by utilizing the existing structural capacity. A pavement experiencing distress on the basis of condition surveys can be enhanced and its remaining life can be increased by using a bonded concrete overlay. Estimating the pavement fatigue life and pavement life in years after-overlay placement includes the following steps (*9*):

1. Calculate the mean after-overlay deflection, $\bar{x}$, of each experimental section.
2. Determine the moduli of pavement layers and predict the fatigue life of the pavement in 18-kip ESAL after the overlay was placed. Note that 12.5-in monolithic pavement was used in the calculation, which was performed by back-calculating the deflection obtained from step 1 using program RPEDD1.
3. Calculate the total 18-kip ESAL per lane for overlaid pavement for the first year opened to traffic.
4. Predict the pavement life after overlay using the following formula.

$$N_{18} = n_{18}\left[\frac{(1+g)^n - 1}{g}\right]$$

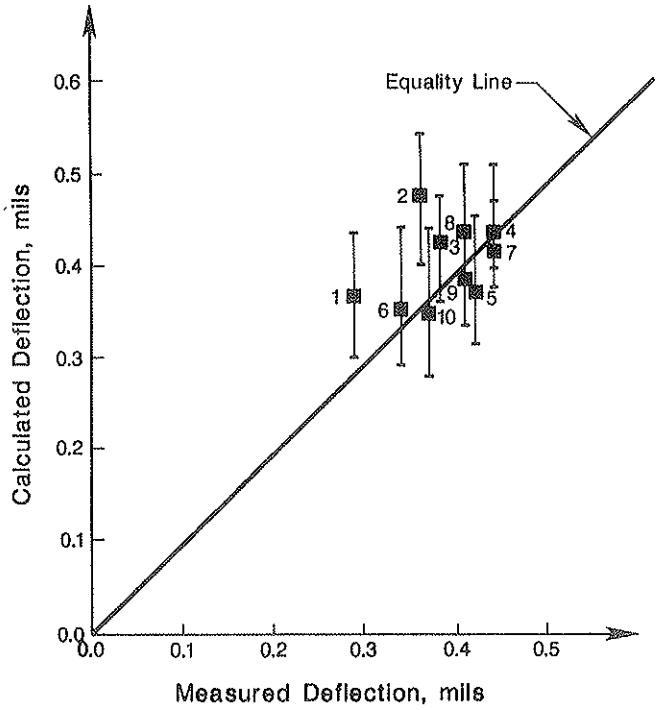

FIGURE 14 Comparison of calculated and measured after-overlay deflections of sensor 1.

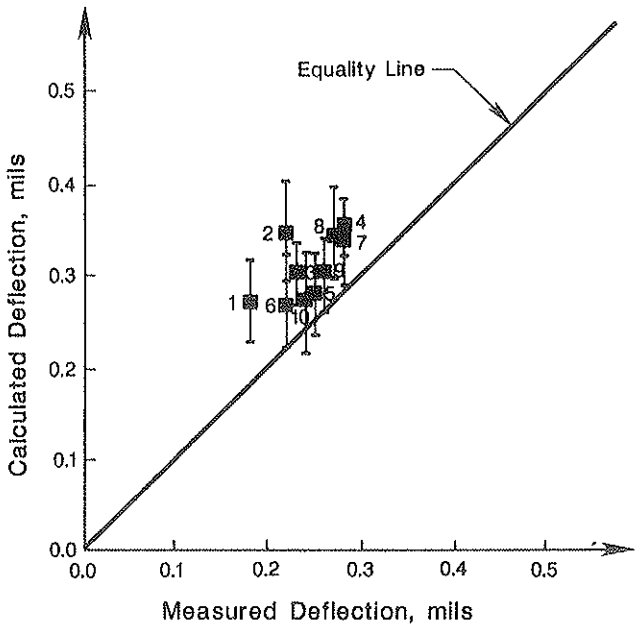

FIGURE 15 Comparison of calculated and measured after-overlay deflections of sensor 5.

where:

N_{18} = predicted fatigue life in 18-kip ESAL, as calculated by RPEDD1,
n_{18} = total 18-kip ESAL for the first year,
n = predicted pavement life in years, and
g = growth rate/100.

The predicted fatigue life of each of the ten test sections and the corresponding predicted pavement life are presented in table 4.

CONCLUSIONS

The conclusions from the field and laboratory measurements and the theoretical analysis are summarized as follows:

Deflections

1. A bonded concrete overlay reduces the pavement deflections by increasing the stiffness of pavement structure.
2. Siliceous river gravel sections show the greatest reduction in deflection.
3. High temperature conditions result in a decrease in pavement deflection, due to pavement expansion and reduction of transverse crack widths.

Material Properties

1. The limestone sections have the least number of transverse cracks.
2. The fiber and limestone sections showed a good bond strength at the layer interface.

Environmental Effects

1. The subbase layer is stiffer in sections with better surface drainage conditions.
2. The roadbed modulus varies with the season. Periods of higher rainfall result in higher roadbed moisture contents and a corresponding lower modulus.

Pavement Conditions

1. Bonded concrete overlay increases the load transfer across the CRCP cracks.

TABLE 4 PREDICTED FATIGUE LIFE

Test Section Number	Predicted Fatigue Life (18-kip ESAL)	Predicted Pavement Life (Years)
1	109,389,698	24.7
2	108,527,896	24.6
3	94,766,533	22.5
4	87,176,902	21.1
5	95,764,724	22.6
6	73,963,028	18.9
7	72,673,279	18.6
8	76,668,727	19.4
9	76,668,727	19.4
10	74,778,917	19.2

2. Bonded concrete overlay improves the riding quality.
3. Existing pavement conditions do not affect the overlay pavement performance as long as most of the existing distress is repaired before overlay placement.
4. Deflection measurements indicate that a bonded concrete overlay adds fatigue life to an existing rigid pavement.

RECOMMENDATIONS

The recommendations are presented in two parts: field implementation and future studies.

Field Implementation

1. A condition survey should be conducted shortly after a light rain, when the cracks on CRCP are most visible.
2. New cores should be taken close to the points where the old cores were secured, to monitor the progress of bond strength.
3. Steel rod sounding should be included in monitoring activities so that the progress of delamination can be monitored periodically.

Future Studies

1. The long term monitoring program should be continued in order to evaluate the long-term bonded concrete overlay performance.
2. Gathering of information on past and future traffic loading should continue. This information is very important for predicting the life of the overlay pavement.
3. The mode of failure of bonded concrete overlay pavement needs to be documented for future modeling.
4. The nature of interface bond failure should be modeled so that the delaminated sections may be formulated in terms of the distress producing mechanisms.
5. The effect of the temperature differential between the substrata and the overlay should be modeled.

REFERENCES

1. D. K. Ray. Repairing Concrete Pavements. *Concrete International*, June 1987, Vol. 9, No. 6.
2. M. M. Davis and J. A. Epps. *Engineering Economy and Energy Considerations Skid Resistant Surfaces*. Texas Transportation Institute, Texas A&M University, College Station, Texas, December 1975.
3. R. R. Forrestal. *Application and Field Evaluation of Very Thin Skid Resistant Pavement Surfaces*. Purdue University, Indiana State Highway Commission, August 1978.
4. R. E. Boyer. *Performance of Thin Bonded Portland Cement Concrete Overlays on Military Airfields*. Purdue University, West Lafayette, Indiana, April 1981.
5. K. Kailasanathan, B. F. McCullough, and D. W. Fowler. *A Study of the Effects of Interface Condition on Thin Bonded PCC Overlays*. Research Report 357-1, Center for Transportation Research, The University of Texas at Austin, December 1984.
6. M. Gutierrez de Velasco and B. F. McCullough. *Rigid Pavement Rehabilitation Scheduling Using Distress Quantities*. Research Report 249-5, Center for Transportation Research, The University of Texas at Austin, August 1983.
7. J. N. Anagnos and T. W. Kennedy. *Practical Method of Conducting the Indirect Tensile Test*. Research Report 98-10, Center for Highway Research, The University of Texas at Austin, August 1972.
8. W. Uddin, A. H. Meyer, and W. R. Hudson. *A User's Guide for Pavement Evaluation Programs RPEDD1 and FPEDD1*. Research Report 387-2, Center for Transportation Research, The University of Texas at Austin, July 1985.
9. A. Taute, B. F. McCullough, and W. R. Hudson. *Improvements to the Materials Characterization and Fatigue Life Prediction Methods of the Texas Rigid Pavement Overlay Design Procedure*. Research Report 249-1, Center for Transportation Research, The University of Texas at Austin, November 1981.
10. V. Torres-Verdin, B. F. McCullough, and G. B. Peck. *The Effect of Coarse-Aggregate Type on CRCP Thickness*. Research Report 249-7, Center for Transportation Research, The University of Texas at Austin, November 1983.

Publication of this paper sponsored by Committee on Pavement Rehabilitation.

Flexible Pavement Rehabilitation Using Asphalt-Rubber Combinations: Progress Report

ROBERT N. DOTY

Several flexible pavement rehabilitation strategies incorporating asphalt-rubber were used experimentally on a project in northeastern California in the fall of 1983. Included were rubberized dense-graded asphalt concrete (AC) overlays containing a binder then being marketed by the Arizona Refining Company, PlusRide dense-graded AC overlays, and four thicknesses of conventional dense-graded AC overlay for comparative evaluations. Some of the rubberized dense-graded AC overlays were placed on a stress-absorbing membrane interlayer. In addition, two sections of double stress absorbing membrane (SAM) and one section of conventional (single) SAM were placed. Distress began to develop in the conventional dense-graded AC within one year in the form of raveling, rutting, and cracking. This distress has become more extensive and more severe during subsequent years. Distress has also developed in the other overlays and surface treatments. To date, however, all the asphalt-rubber combinations are performing equal to or better than equivalent or greater thicknesses of conventional dense-graded asphalt concrete.

The California Department of Transportation (Caltrans) has been using a deflection-based flexible pavement rehabilitation design procedure for more than 30 years. This procedure is used to obtain 10 or more years of additional service life during which little or no pavement maintenance will be required. The rehabilitation strategy most frequently used is to overlay the existing asphalt concrete (AC) pavement with one or more layers of new AC. In May 1982 this procedure was used to develop an overlay design for a portion of Route 395 in northeastern California. To obtain the desired 10-yr service life, a 0.70-ft thick overlay of conventional Caltrans dense-graded AC (DGAC) would have been required. The cost of this overlay would have been significantly more than the funding available for the project. The results of limited Caltrans research and research by others had indicated that asphalt-rubber combinations might provide the desired service life at a lesser cost, due to the possibility of being able to use substantially thinner overlays or even surface treatments. Thus, it was decided to try several of these products in the fall of 1983 in lieu of the thick overlay required in the Caltrans standard procedure.

PROJECT FEATURES

The section of Route 395 involved was originally constructed in three segments. The first of these was built in 1948. This was followed by additional contracts in 1952 and 1954 that resulted in completion of the original pavement. Subsequently, at least two thin overlays had been placed.

The two-lane pavement is located in a somewhat remote portion of northeastern California about 100 miles north of Reno, Nevada. The highway at this location traverses a rocky valley between two mountain masses. The elevation of the highway is about 4,400 feet at the south end of the project and approximately 5,400 feet at the north end of the project. Most of the southernmost 2½ miles is on a low fill, whereas the remainder is on solid or nearly solid basalt. The average annual precipitation varies from 8 inches at the south end, to 12 inches in the middle, and 10 inches at the north end. This precipitation falls throughout the year. In addition, frost occurs throughout the year, with some snowfall during the period from November to March. During the summer, the ambient temperatures often exceed 90°F while winter temperatures occasionally drop to below zero°F. From May to November, the diurnal temperature range averages nearly 40°F. During the remainder of the year, it is generally about 20°F.

The traffic using the roadway varies from about 1,400 vehicles per day (VPD) in the summer to approximately 550 VPD in mid winter. The average annual daily traffic (AADT) is 1,100. This includes about 100 five-axle trucks per day.

The roadway structural section as of mid 1983 consisted of AC having an average thickness of 0.38 foot, supported by an aggregate base (AB) of 0.42-ft average thickness. Underlying the AB was aggregate subbase (ASB) that was 0.97-ft thick (average). There was some variation in these layer thicknesses, as shown on table 1.

In situ pavement deflections were measured using the Dynaflect (see figure 1). The measured values were converted to equivalent Deflectometer values per standard Caltrans procedures. The 80th percentile equivalent values ranged from 0.023 inch to 0.063 inch. The average value was 0.043 inch. The tolerable deflection for the existing pavement was 0.017 inch. The effects of this excessive deflection were obvious in that the pavement throughout the project was cracked extensively. The percent of pavement cracked, as determined using overhead photos of representative portions of each pavement segment, varied from 8 to 100 as indicated in table 1. For ten of the thirteen segments, the percent of pavement cracked was in excess of 50. The cracking included both wide transverse cracks of the type often associated with cold temperatures and extensive alligator cracking of the type associated with traffic loads. There was also substantial rutting noted

California Department of Transportation, Office of Transportation Laboratory, 5900 Folsom Boulevard, Sacramento, Calif. 95819.

TABLE 1 EXISTING PAVEMENT

Segment No.	ASB Thkn. (ft.)	AB Thkn. (ft.)	AC Thkn. (ft.)	Rutting (in.)	% of Pavmt Area Crkd.
1	0.85	0.50	0.45	0.40	33
2	0.95	0.30	0.55	0.32	76
3	0.93	0.40	0.47	0.40	15
4	1.16	0.26	0.28	0.40	8
5	0.82	0.48	0.30	1.15	83
6	0.82	0.48	0.38	0.40	52
7	1.10	0.37	0.33	1.25	100
8	1.13	0.34	0.33	0.50	74
9	0.96	0.46	0.38	0.40	83
10	1.05	0.52	0.33	0.50	100
11	0.77	0.57	0.36	0.25	57
12	1.08	0.40	0.42	0.50	74
13	1.00	0.40	0.30	0.75	100
Average	0.97	0.42	0.38		

Notes: "AC" = Asphalt Concrete
"AB" = Aggregate Base
"ASB" = Aggregate Subbase

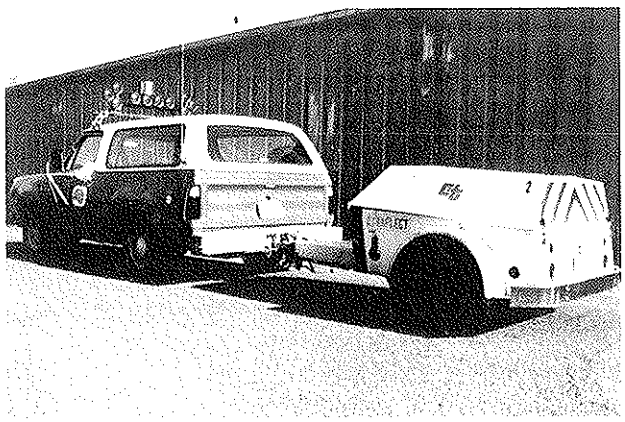

FIGURE 1 Dynaflect—used to measure pavement deflection.

throughout the project. This rutting varied from 0.25 inch to 1.25 inches in depth. The average rut depth was 0.60 inch.

TEST SECTIONS

The objective of this ongoing study is to evaluate several flexible pavement rehabilitation approaches involving the use of asphalt-rubber. The combinations being studied are:

1. Dense graded asphalt concrete (DGAC) containing an asphalt-rubber blend then (1983) being marketed by the Arizona Refining Company, both with and without a stress absorbing membrane interlayer (SAMI),
2. PlusRide DGAC, both with and without a SAMI,
3. Single- and double-stress absorbing membranes (SAMs) containing the binder referred to in 1 above, and,
4. A double stress absorbing membrane (SAM) containing the binder marketed by Sahuaro Petroleum in the early 1980s.

Conventional DGAC was used for four short segments involving different overlay thicknesses to serve as a basis for making determinations regarding the effectiveness of the asphalt-rubber combinations being studied. These products were used for the test sections depicted in figure 2 and table 2.

For the purpose of performance documentation, a representative 200-ft long, one-lane wide test section was selected in the northbound lane for each of the thirteen project segments. A second test section was selected within segments 2 and 5 because each of these segments is two miles long. The condition of the pavement within each of these test sections is being documented annually with overhead and oblique photographs as well as pavement deflection testing (Dynaflect) and pavement skid testing (towed trailer).

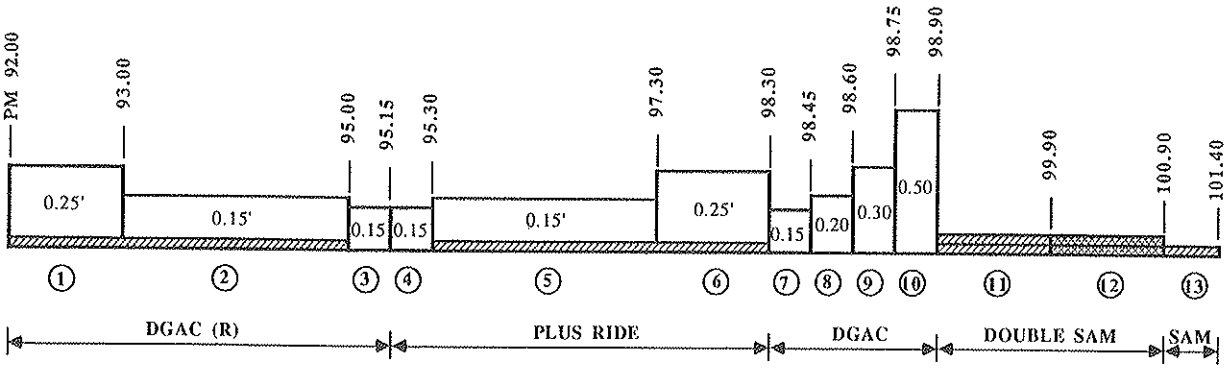

LEGEND

(R) = Rubberized
▨ = Ariz. Refining System
▩ = Sahuaro System

NOTES

1. Used type A 3/4" max. medium DGAC and AR 4000 asphalt.
2. Test sections placed in Sept, 1983.
3. Old pavement consists of 0.38' AC/0.41' AB/ 0.96' ASB.

FIGURE 2 Ravendale test section layout.

TABLE 2 PROJECT SEGMENTS

SEGMENT NUMBER	PM TO PM = MILES	DESIGN
1	92.00 - 93.00 = 1.00	0.25' of ARS DGAC over ARS SAMI
2	93.00 - 95.00 = 2.00	0.15' of ARS DGAC over ARS SAMI
3	95.00 - 95.15 = 0.15	0.15' of ARS DGAC
4	95.15 - 95.30 = 0.15	0.15' of PlusRide DGAC
5	95.30 - 97.30 = 2.00	0.15' of PlusRide DGAC over ARS SAMI
6	97.30 - 98.30 = 1.00	0.25' of PlusRide DGAC over ARS SAMI
7	98.30 - 98.45 = 0.15	0.15' of Conventional DGAC Control
8	98.45 - 98.60 = 0.15	0.20' of Conventional DGAC Control
9	98.60 - 98.75 = 0.15	0.30' of Conventional DGAC Control
10	98.75 - 98.90 = 0.15	0.50' of Conventional DGAC Control
11	98.90 - 99.90 = 1.00	ARS Double SAM
12	99.90 - 100.9 = 1.00	Sahuaro Double SAM
13	100.90 - 101.4 = 0.50	ARS Single SAM

PM = Post Mile

Binders

The paving asphalt selected for this project was Grade AR-4000. The vulcanized portion of the ground, reclaimed rubber used for several of the segments was supplied by Genstar and the devulcanized portion was supplied by U.S. Rubber Reclaiming.

The ARS binder (used for segments 1-3, 11, 13, and the SAMIs in segments 1, 2, 5, and 6) consisted of 78 percent AR-4000 grade paving asphalt, 18 percent ground reclaimed rubber, and 4 percent extender oil, all by weight of total binder. The reclaimed rubber consisted of 20 percent devulcanized rubber and 80 percent vulcanized rubber. The rubber and asphalt were combined at a temperature of approximately

350°F using a special mixing/blending unit. The blend to be used for the DGAC in segments 1 to 3 was then recirculated within a holding tank for approximately 45 minutes after which it was pumped into the contractor's asphalt storage tanks at the plant. This 45-min holding time requirement resulted in a discontinuous supply of binder to the plant that caused occasional interruptions in plant production of the DGAC for segments 1 to 3.

The asphalt-rubber binder used for segment 12 conformed to the specifications promulgated by the Sahuaro Petroleum Company. The primary differences between the ARS binder and the Sahuaro binder were that more reclaimed rubber was used (23 percent instead of 18 percent) and a diluent was used instead of an extender oil. The blending times and temperatures also differed somewhat.

The binder for the PlusRide segments (4 to 6) consisted of AR-4000 grade paving asphalt. This asphalt was also used for the conventional DGAC comprising segments 7 to 10.

Aggregate

AC aggregate conforming to the Caltrans' specifications for ¾-in maximum medium Type A DGAC was used for the conventional DGAC (see table 3). Aggregate conforming to Caltrans' specifications for ½-in maximum medium Type A DGAC was specified for the ARS mixes (segments 1 to 3). The gap grading shown in table 3 was specified for the PlusRide. This gap in the aggregate grading was required to accommodate the coarser portion of the reclaimed rubber that was included in the PlusRide mix. The need to provide this gap can and did result in the accumulation of some waste aggregate. The requirement of 8 to 12 percent passing the No. 200 also created a problem in that this resulted in the need to import and add 4.7 percent pozzolan to the mix.

The aggregate used for the SAMIs (segments 1, 2, 5, and 6) and for the single SAM (segment No. 13) conformed to Caltrans' specifications for ⅜ × No. 6 medium screenings (see table 3). The specifications for the screenings used in the double SAMs (segments 11 and 12) are also shown on table 3.

Construction

The project was constructed in August and September of 1983. A Standard 10,000-lb capacity batch plant was used to mix the DGAC in 8,000-lb batches. The design asphalt content (Hveem) for the conventional DGAC was 4.6 percent by dry weight of aggregate. The design binder content (asphalt-rubber blend) for the ARS DGAC, as provided by Arizona Refining Company personnel, was 8.0 percent by dry weight of aggregate. The design asphalt content for the PlusRide provided by All-Seasons personnel was initially 9.65 percent by dry weight of aggregate. In addition, 3.0 percent rubber by total weight of mix was added to PlusRide aggregate and pre-mixed for 20 seconds before the AR-4000 asphalt was added.

The mixes were transported to the street using bottom dumps and placed using a Ko-Cal pickup machine and a Blaw Knox PF-180 paver. A 20-ft ski was used for grade control.

No pre-leveling or milling was done to eliminate the pre-

TABLE 3 AGGREGATE GRADING SPECIFICATIONS (PERCENT PASSING)

Sieve Size	ARS DGAC	PlusRide DGAC	Conv. DGAC	Double SAM		SAM and SAMI
				1st Lift	2nd Lift	
1"			100			
3/4	100		95-100	100		
5/8		100				
1/2	95-100			90-100		100
3/8	80-85	60-80	65-80	50-80	100	90-100
1/4		30-50				
#4	55-65		46-56	0-15	60-85	5-30
#8	38-48		33-43	0-5	0-25	0-10
#10		19-32				
#16					0-5	0-5
#30	18-28	13-25	14-24		0-3	
#200	3-8	8-12	3-8	0-2	0-2	0-2

construction rutting prior to constructing the overlays. A leveling course was placed prior to placing the SAMs, however. The segments with design thicknesses of 0.15-foot and 0.20-foot were placed in one lift. Segments 1 and 7 (design thickness of 0.25 foot) were placed in lifts of 0.13-ft, then 0.12-ft. The 0.30-ft thick segment (No. 9) was placed in two lifts of 0.15-ft each. Segment 10 (0.50-ft total design thickness) was placed in lifts of 0.20-ft, then 0.15-ft, and 0.15-ft.

A Dynapac CC50A vibratory steel-wheel roller was used for breakdown compaction. This roller was operated at high amplitude and 2,400 VPM in accordance with prior Caltrans qualification testing of this roller for conventional DGAC paving. A Hyster C350 steel-wheel roller was used for finish rolling. No pneumatic rolling was required.

No problems were encountered when placing the ARS DGAC or the conventional DGAC. The PlusRide mix, however, had a consistency resembling bubble gum when placed and was noticeably springy even after compaction. This appeared to contribute to the initial difficulties in obtaining at least the specified 96 percent (minimum) of theoretical maximum density. A reduction in the design binder content (from 9.65 percent to 9.41 percent) and an adjustment in the amount of supplemental fines (pozzolan) being added to the mix resulted in compliance with the density specification but no change in the stickiness or resilience of the mix was noted. The tendency to stick to the rollers was subsequently alleviated somewhat when the breakdown compaction was delayed until the mix temperature had dropped to 285°F or less in lieu of the originally specified 300°F minimum.

The construction of the SAMIs (segments 1, 2, 5, and 6) and the SAMs (segments 11 to 13) involved placement of the ARS and Sahuaro binders using a distributor truck followed by application of the pre-heated pre-coated (0.33 percent asphalt) screenings. These surfaces were then rolled with a minimum of three coverages using pneumatic rollers. For segments 11 and 12, the design binder application rate was 0.50 gal/sy. For the SAMIs and segment 13, the design application rate was 0.60 gal/sy. The design application rates for the screenings were 34 lbs/sy for the first lift of segments 11 and 12, 26 lbs/sy for the second lift of segments 11 and 12, and 35 lbs/sy for the SAMIs and segment 13. Prior to the placement of the SAMs, a levelling course of minimal thickness was placed consisting of ½-in maximum conventional DGAC. This was needed to adjust the cross slope of the pavement and to eliminate the rutting at these locations. The only problem that occurred during the placement of the SAMs and SAMIs was caused by smoke generated by the distributor truck operation. This obscured the spray bar, which resulted in a somewhat streaked appearance, due to undetected intermittent partial or complete plugging of some of the spray-bar nozzles.

Cost Estimate

An estimate of the in-place cost of each of the segments is shown in table 4. This provides an indication of the extent to which the various asphalt-rubber products must out-perform the conventional DGAC to be cost effective.

As-built Properties

The data in Table 5 indicate that conformance to the aggregate gradation specifications was obtained. Table 6 contains data indicating that the as-built thickness of the various segments differed from the design thicknesses to some extent. The permeability data indicates that the PlusRide DGAC was virtually impermeable, whereas the permeability of the ARS DGAC was very low, and the permeability of the conventional DGAC was somewhat greater than the 150 ml/min considered typical of Caltrans mixes. This suggests the need for a SAMI

TABLE 4 ESTIMATED COST OF EACH STRATEGY

SEGMENT NUMBER		COST (Square Yard)
1	0.25' of ARS DGAC over ARS-SAMI	$10.41
2	0.15' of ARS DGAC over ARS-SAMI	6.88
3	0.15' of ARS DGAC	5.37
4	0.15' of PlusRide DGAC	6.32
5	0.15' of PlusRide DGAC over ARS-SAMI	7.83
6	0.25' of PlusRide DGAC over ARS-SAMI	12.00
7	0.15' of Conventional DGAC Control	3.04
8	0.20' of Conventional DGAC Control	4.03
9	0.30' of Conventional DGAC Control	6.02
10	0.50' of Conventional DGAC Control	9.99
11	Double SAM, ARS Binder	2.60
12	Double SAM, Sahuaro Binder	2.62
13	Single SAM, ARS Binder	1.56

TABLE 5 AGGREGATE GRADATION SPECIFICATION COMPLIANCE

SIEVE SIZE	PERECENT PASSING								
	ARS (Segment No. 1)		PLUSRIDE (Segment No. 5)		CONVENTIONAL DGAC				
					SEGMENT NUMBER				
	EXTRACTED	SPEC.	EXTRACTED	SPEC.	7	8	9	10	SPEC.
1"								100	100
3/4	100	100			100	100	98	100	95-100
5/8			100	100					
1/2	97	95-100	89		79	86	82	84	
3/8	80	80-85	63	60-80	70	72	69	75	65-80
1/4			47	30-50					
#4	57	55-65	36		48	51	46	53	46-56
#8	44	38-48	25		35	38	35	40	33-43
#10			23	19-32					
#30	25	18-28	17	13-25	21	23	21	23	14-24
#100	10		11		10	11	9	11	
#200	7	3-8	9	8-12	7	8	6	8	3-8

of some sort to provide a more impermeable pavement and thereby protect the underlying pavement from surface water (rainfall) intrusion.

Caltrans experience has revealed that surface abrasion losses greater than 35 grams (per Calif. Test 360, Method B) generally are associated with DGAC exhibiting marginal or unsatisfactory resistance to moisture. The surface abrasion test results in table 6 indicate that the ARS DGAC (with an average value of 17 g) and the PlusRide (average value of 13 g) are substantially more resistant to surface abrasion than is the conventional DGAC used on this job (average loss of 41 g).

The results of the towed-trailer skid testing indicated tnat the PlusRide pavement is adequate and the other surfaces (ARS DGAC, conventional DGAC, and the SAMs) are very good.

In situ pavement deflection measurements were made in May of 1984. Comparison of these values with those measure in May of 1983 provides an indication of the structural section stiffening provided by the various strategies. These values illustrate that substantial reductions in deflection were achieved in most cases. These values are discussed in more detail in the next section of this paper.

LONG-TERM PERFORMANCE

Four months after construction, the first report of pavement distress was received. A field condition survey revealed that a considerable loss of surface fines had occurred, especially in the wheel tracks in the two thinner segments of conventional DGAC (segments 7 and 8—see figure 3). In addition, transverse cracks about 2 feet apart had developed over a distance of approximately 400 feet and longitudinal cracking had developed in the southbound lane outer wheel track, both in segment 8. The other segments containing conventional DGAC (9 and 10) had experienced the loss of a minor amount of surface fines but no cracking.

FIGURE 3 Loss of fines in wheel tracks, 0.15 ft DGAC—segment 7 (age 4 months).

TABLE 6 AS-BUILT PROPERTIES

Material	Segment Number	Overlay Thkn[1] (ft) As-Built	Overlay Thkn[1] (ft) Design	% Comp.	Permea-bility[2] (ml/min)	Surface Abrasion[3] (gms loss)	Skid[4] No. (SN_{40})	Deflection[5] (0.001") 5/83	Deflection[5] (0.001") 5/84
ARS	1	0.27	0.28	93.3	36.3	17.1	55	54	26
DGAC	2	0.17	0.18	91.7	22.3	17.6	57	43	25
	3	0.12	0.15	92.8	-	18.7	54	25	16
PlusRide	4	0.19	0.15	97.1	-	9.7	39	55	27
DGAC	5	0.21	0.18	98.4	11.0	14.8	39	30	26
	6	0.28	0.28	96.1	6.8	11.4	44	27	16
Conv.	7	0.20	0.15	91.7	177.0	47.8	66	23	18
DGAC	8	0.18	0.20	91.2	-	48.2	68	60	44
	9	0.32	0.30	91.4	-	32.5	65	63	28
	10	0.52	0.50	92.1	-	35.1	67	46	13
Double	11	0.10	0.04	-	-	-	62	44	42
SAM	12	0.13	0.04	-	-	-	59	51	35
SAM	13	0.14	0.03	-	-	-	57	54	52

Notes: 1. Includes SAMI, segments 1, 2, 5, and 6
2. Per Calif. Test 341
3. Per Calif. Test 360, Method B
4. Per ASTM E274; Meas 10/83
5. 80th percentile deflections per Calif. Test 356 (Dynaflect Method)

The following June (nine months after construction), it was noted that a glaze observed on the PlusRide surface immediately after construction was no longer evident. In addition, the crack pattern in the underlying old AC pavement was beginning to become visible in segment 11 (double SAM using ARS binder). Also, some hairline cracking was observed in the SAM (segment 13). No other additional distress was observed at the time of the June 1984 review.

Because of some warm weather in July of 1984 (11 days with maximum temperatures of 90°F or more), the project was reviewed again on July 26, 1984. Some additional distress had become evident. There was some localized bleeding at some of the transverse construction joints in segment 4 (Plus Ride) and some flushing beginning to develop in the double SAMs (segments 11 and 12). In addition, rutting 0.25-in deep was noted in the thickest of the control sections (segment 10). No other significant rutting was noted.

Subsequent to the July 1984 survey, additional field condition surveys have been completed in the late spring or early summer of 1985, 1986, and 1987. In addition, pavement skid numbers and deflections have been measured each year. The results of these tests are summarized in table 7. Examination of this data reveals some anomalies for which no explanation is apparent. For example, the reason for the significant reduction in deflection between June of 1986 and May of 1987 for segments 1 to 4 is unknown. The remainder of the deflection data is plausible in most cases, in that it indicates that a measurable initial stiffening of the structural sections was achieved via placement of each of the asphalt-rubber and conventional overlays. The percent reduction in deflection was directly related to the thickness of the overlay placed in most cases. The surprisingly large percentage decreases in deflection as a result of the thinnest PlusRide overlay (segment 4) and the Sahuaro double SAM (segment 12) are difficult to explain. Based on inspection of the data, the May 1984 deflection reported for segment 12 may be erroneous. The subsequent deflections indicate that most or all this stiffening effect has dissipated with the exception of segments 1, 6, 9, and 10. These segments comprise the thickest of the rubber-modified DGAC (segments 1 and 6, each of which were 0.25-ft+ thick) and the conventional DGAC (segments 9 and 10, with nominal overlay thicknesses of 0.30 and 0.50

TABLE 7 PAVEMENT STIFFNESS AND SURFACE TEXTURE

Material	Segment	Deflections (80th percentile, 0.001") Date Tested					Skid No. (SN_{40})	
		5/83*	5/84**	6/85	6/86	5/87	10/83	5/87
ARS	1	54	26(52)	35	43	28	55	64
DGAC	2	43	25(42)	37	44	36	57	64
	3	25	16(36)	28	37	29	54	62
Plus	4	55	27(51)	42	56	45	39	60
Ride	5	30	26(13)	34	41	41	39	62
DGAC	6	27	16(41)	21	22	21	44	59
	7	23	18(22)	22	22	26	66	64
Conv.	8	60	44(27)	52	51	59	68	56
DGAC	9	63	28(56)	42	36	32	65	65
	10	46	13(72)	21	20	19	67	62
Double	11	44	42(5)	52	52	59	62	34
SAM	12	51	35(31)	53	54	51	59	26
SAM	13	54	52(4)	55	56	66	57	63

*Prior to construction of the segments in 9/83

**Percent reduction in deflection shown in parenthesis

foot, respectively). These also were the overlays that provided some of the largest initial stiffening as indicated by percent reduction in deflection.

As expected, the deflections measured for the SAMs suggest that the stiffening effect of these surface treatments was minimal. The significance of the pavement deflections, as related to the asphalt-rubber products, is one of the experimental features of this study.

All of the segments are now exhibiting some distress in the form of cracking (longitudinal, transverse, block, and/or alligator—see figures 4 to 13). There is a small amount of rutting present (conventional DGAC - segment 10) and some pot holes (in the PlusRide). The amount of cracking, however, is probably the best indication of the remaining service life for each of the segments. Table 8 contains an estimate of the amount of cracking that has developed. Because of the flushing and bleeding that has developed in segments 11 and 12, much of the cracking therein is sealed, due to the kneading action of traffic during warm weather. The deflections measured in the badly cracked segment 7 and, in some cases, segment 8 (both conventional DGAC) have been comparable to or less than those measured for segments 1 to 6; yet the amount of cracking in segments 1 to 6 is relatively insignificant. This suggests that the tolerable deflection for these asphalt-rubber dense graded AC pavements may be considerably greater than that for comparable thicknesses of conventional DGAC. It should be remembered that the conventional DGAC overlays were substantially under-designed in that 0.70-ft was the design thickness determined for this roadway using the conventional Caltrans design procedure.

FIGURE 4 Typical Cracking—longitudinal, test segment 2, 0.15 ft ARS DGAC on SAMI (age 48 months).

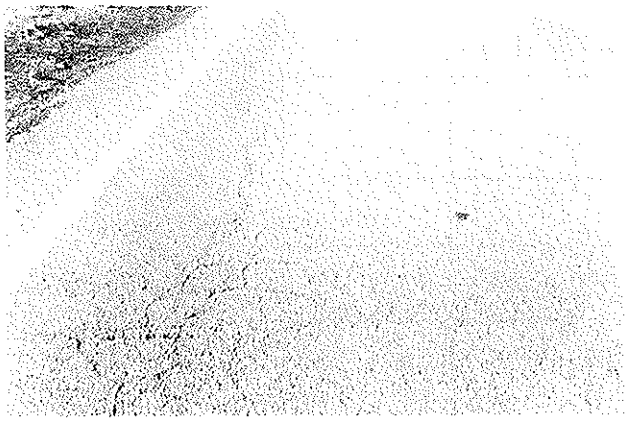

FIGURE 5 Typical cracking—alligator, test segment 3, 0.15 ft ARS DGAC (age 48 months).

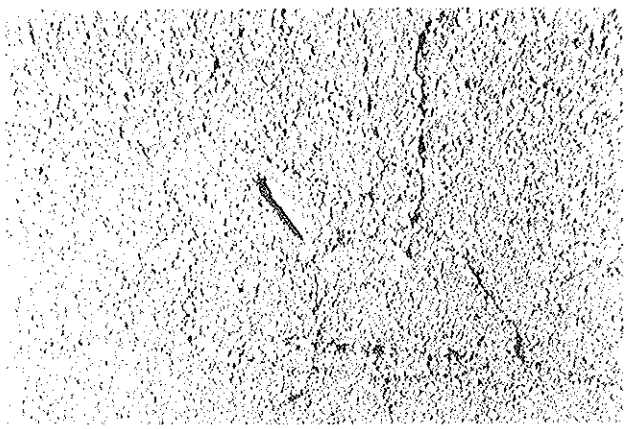

FIGURE 6 Typical cracking—alligator, test segment 3, 0.15 ft ARS DGAC (age 48 months).

FIGURE 7 Typical cracking, test segments 7 and 8, 0.15 and 0.20 ft conventional DGAC (age 48 months).

FIGURE 8 Typical raveling, test segments 7 and 8, 0.15 and 0.20 ft conventional DGAC (age 48 months).

FIGURE 9 Typical cracking—transverse, test segments 9 and 10, 0.30 and 0.50 ft conventional DGAC (age 48 months).

FIGURE 10 Typical wheel track bleeding, test segments 11 and 12, double SAM (age 48 months).

FIGURE 11 Typical wheel track bleeding, test segments 11 and 12, double SAM (age 48 months).

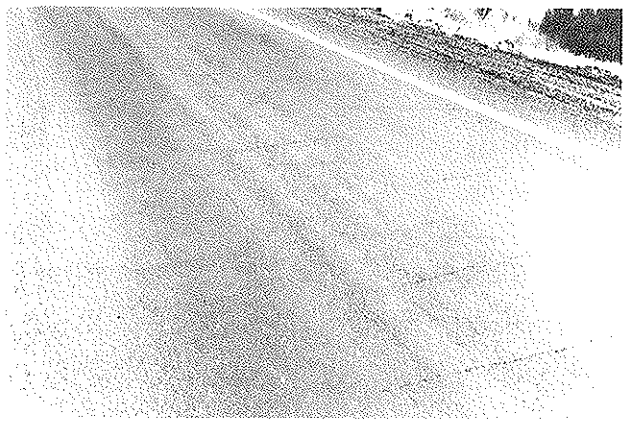

FIGURE 12 Typical cracking—transverse, test segments 11 and 12, double SAM (age 48 months).

FIGURE 13 Typical cracking, test segment no. 13, SAM (age 48 months).

The results of the skid testing (table 7) coincide with the loss of the glaze on the surface of the PlusRide after approximately 6 months of service. Thus, this glaze may have been the reason for the substantially lower skid numbers measured initially for the PlusRide as compared to the other segments. As of May 1987, the PlusRide values were comparable with all the other values measured except those for the Double SAMs. These substantially lower values indicate a marginal pavement and are no doubt associated with the flushing and bleeding that has been observed in segments 11 and 12 since the 1985 survey.

CONCLUSIONS

The findings and observations to date indicate that for the conditions present at the test site location, the initial stiffening effect of the asphalt-rubber overlays studied is equal to or greater than that of equivalent thicknesses of conventional DGAC and that the tolerable deflection of these asphalt-rubber overlays is greater than that of equivalent thicknesses of DGAC. This would suggest that the service life of the asphalt-rubber DAGC overlays under study may be considerably greater than those of equivalent thicknesses of conventional DGAC, at least with some combinations of traffic and climate. In addition, both of the thin conventional DGAC overlays have failed (figures 7 and 8) whereas the asphalt-rubber overlays of comparable thickness (segments 2 to 5—figures 14 to 17) have not yet failed. However, the cost-effectiveness of these more expensive overlays cannot yet be determined, as most of the segments being studied have not yet failed. In addition, although a substantial amount of cracking is visible in the SAM segments (11 to 13), these pavements have not yet required the amount of maintenance effort required in segments 7 and 8. This suggests that even the SAMs may be superior to conventional overlays 0.20-ft thick. Based on a comparison of the single SAM versus double SAMs, there is no apparent advantage provided by the double SAM.

Final conclusions for the conditions present at the test site location will be contingent on the performance of the various segments during the next few years. In addition, some additional similar experiments at locations having both similar and different traffic and/or climatic conditions are needed before overall conclusions regarding these asphalt-rubber combinations can be determined.

ACKNOWLEDGMENTS

The research described herein has been supported by the Federal Highway Administration. The contents of this paper, however, do not necessarily reflect the official views or policies of either the Federal Highway Administration or the State of California. They reflect the views of the author, who is responsible for the facts and accuracy of the data presented herein. Also, neither the State of California nor the United States Government endorse products or manufacturers. Trade and manufacturers' names are presented herein because they are considered essential to the objective of this document.

The Principal Investigators for the research project are Bobby G. Page of the Caltrans Office of Transportation Laboratory

TABLE 8 ESTIMATE OF PAVEMENT CRACKING

Material	Segment Number	Estimated Percent Cracked (May 1987)
ARS DGAC	1	<5%
	2	<5%
	3	5-10%
PlusRide DGAC	4	<5%
	5	5-10%
	6	5-10%
Conv. DGAC	7	70-75%*
	8	75-80%*
	9	10-15%
	10	<5%
Double SAM	11	60-65%
	12	65-70%
SAM	13	85-90%

*Failed

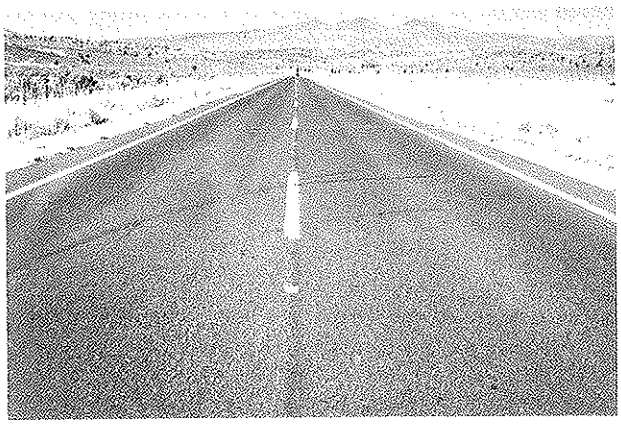

FIGURE 14 Typical "overall" view, ARS DGAC (age 48 months).

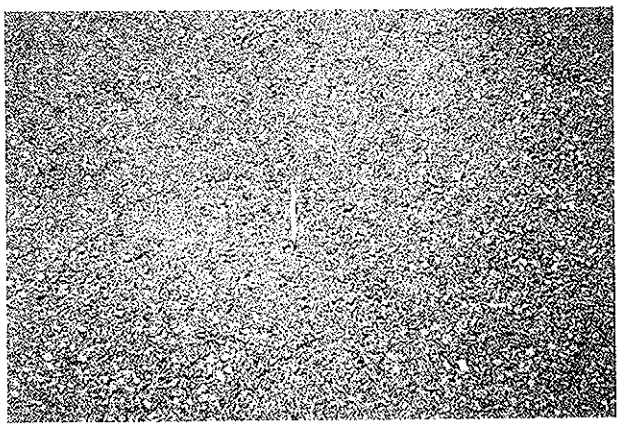

FIGURE 15 Typical texture, ARS DGAC (age 48 months).

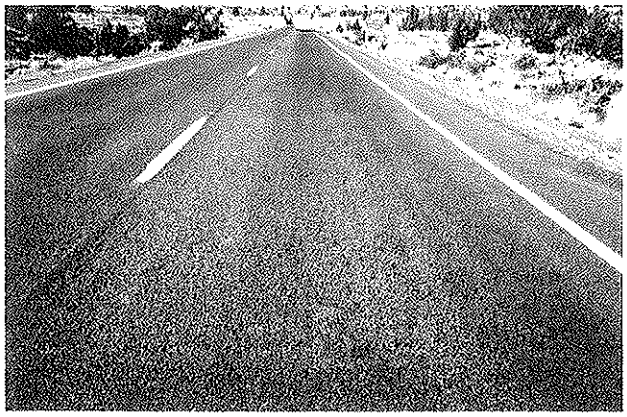

FIGURE 16 Typical "overall" view, PlusRide DGAC (age 48 months).

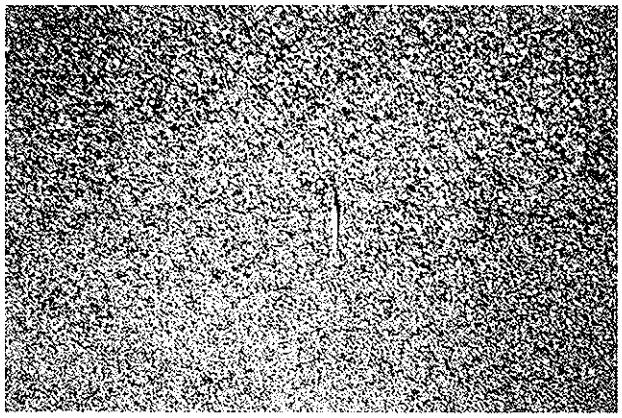

FIGURE 17 Typical texture, PlusRide DGAC (age 48 months).

and Larry deLaubenfels of Caltrans District 2. The previous Principal Investigator was Roger D. Smith, a former member of the Transportation Laboratory staff. Jack Van Kirk and other members of the Transportation Laboratory staff and Caltrans District 2 staff have also been involved with the study. In addition, the typing of this text by Lydia Burgin of the Transportation Laboratory staff is gratefully acknowledged.

Publication of this paper sponsored by Committee on Pavement Rehabilitation.

Network Level Optimization/Prioritization of Pavement Rehabilitation

ALI KHATAMI AND K. P. GEORGE

A procedure has been developed to optimize pavement rehabilitation strategies for the highway network in Mississippi. The methodology is developed in two stages: project level and network level. First, at the project level, a set of feasible double-action strategies and the corresponding times of implementation of each alternative of every strategy are determined. The optimum rehabilitative strategies are selected by maximizing pavement performance for a 12-yr analysis period. A univariant search technique is employed to solve for the nonlinear optimization problem. The second part of the analysis deals with network level optimization. Selection of the set of projects is done by maximizing pavements performance weighted with respect to traffic. The projects for rehabilitation for the next 12 years are selected using a 0-1 integer linear program, which, for computational convenience, is transformed into a dynamic program. The final results of the two-stage analysis are the selection and timing of major rehabilitative activities. An example problem involving 39 sections (250 two-lane miles) of Interstate highways in north Mississippi is solved, and salient results are presented in the report.

A major objective of a pavement management system (PMS) is to assist highway engineers in making consistent and cost-effective decisions related to the maintenance and rehabilitation of pavements. Realizing the importance of PMS, the Mississippi State Highway Department (MSHD) initiated a research project to develop a pavement management information system (PMIS) in April 1986. An integral part of a PMIS is a decision model that can be used to determine the optimum type and timing of preservation actions for different pavement segments. An optimization model, with provision to prioritize rehabilitation actions for maximum benefit, is described in this paper.

The PMIS, as envisioned, comprises four distinct but interrelated components: data base, pavement rating system, prediction model, and ranking method for the selection of annual maintenance and rehabilitation (M and R) program. A brief description of these items is included in the following sections.

The pavement data compiled for the PMIS include both historical data (geometric information, original construction data, overlay information, junction details, and traffic data) and inventory or condition data (road roughness and distress information). The dBase III Plus in conjunction with a second package, Symphony, compose the data base.

The inventory data, collected annually for the time being, need standardization, for which a rating scale, zero to 100, is adopted. The pavement rating, designated pavement condition rating (PCR), includes two component elements: road roughness (RR), measured in terms of present serviceability rating (PSR) on a zero to five scale, and the distress data determined by a subjective field survey but reduced to distress rating (DR) employing deduct values and weighting factors. A complete description of the data reduction and subsequent PCR calculation procedure by combining RR and DR can be seen elsewhere (*1*). The condition data is collected by RDM-5000 equipment supplied by Dynatest. The major components of RDM include HP-85 microcomputer, RDM-5000 electronic processor, ultra precision accelerometer, digital distance encoder, and an eight-push-button control box. The roughness measurement by RDM is fully automatic, whereas distress survey is subjective. A description of the equipment as well as the data collection procedure is given in the manufacturer's literature (*2*).

Not only the present condition of the network, but also the future condition of each pavement section is required for forecasting future needs. Site-specific prediction models are being investigated, and the details of these investigations can be found elsewhere (*3*). For the purpose of this paper, the deterioration of a road surface may be described by two basic relations: one equation that describes the evolution of road roughness and a second that describes the surface distress. Both equations are assumed to be linear, with a scale from zero to 100. A prediction model, designated as the performance curve, is depicted in figure 1. As the curve indicates, during the early life of the pavement, the roughness rating is generally lower than the distress rating, in which case the roughness rating governs the performance curve.

The fourth component of a PMS involves some form of ranking methodology or an optimization and/or prioritization system. The ranking methodology generally encompasses a ranking of the pavement sections for scheduling the annual rehabilitation program. Programming at the network level for a predetermined period in the future, designated as the analysis/programming period, would require complex optimization methodology that has the additional capability for shifting projects back and forth to result in maximum benefit to public road users. This paper presents the development of an optimization/prioritization model followed by an example problem that illustrates the salient features and typical results of the model.

OPTIMIZATION AND PRIORITIZATION

A comprehensive process of priority programming should enable one to answer the following three questions:

Department of Civil Engineering, Carrier Hall, University of Mississippi, University, Miss. 38677.

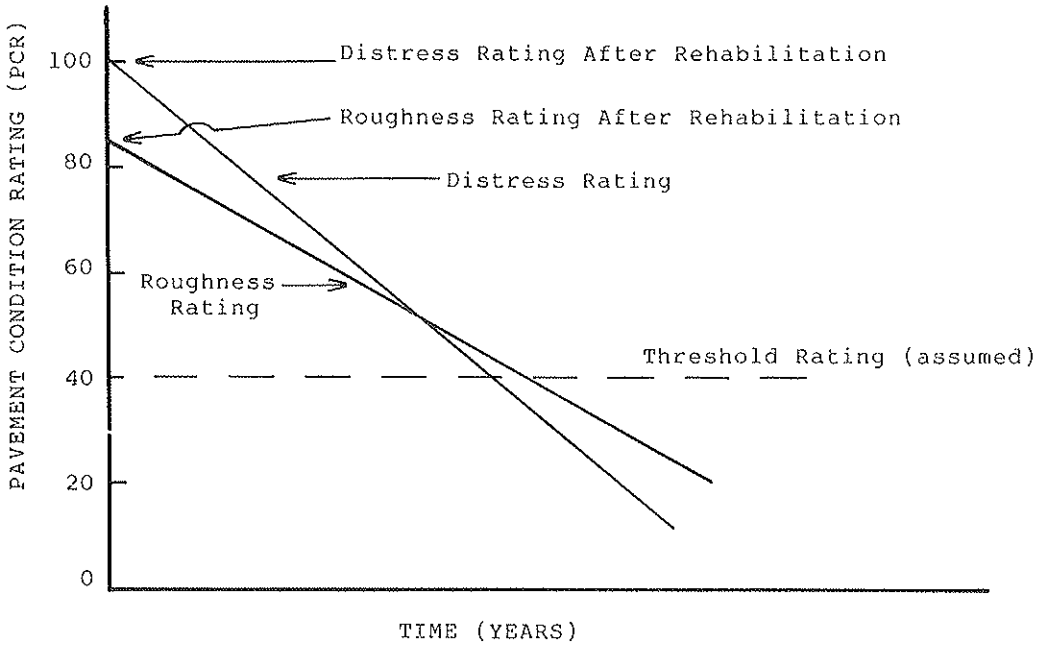

FIGURE 1 Performance trend lines.

- What projects (or sections) should be built? (selection of projects)
- How should they be built? (selection of alternative strategies within projects)
- When should they be built? (selection of project timings)

Models, however, that simultaneously deal with these three questions are complex. Consequently, most of the models used by highway agencies deal only with the first or first two questions. If the available funds are to be optimized, however, all three questions need to be considered; the present study addresses all three questions.

Because of their interdependence the three questions cannot be answered independently; the two main programs developed in this paper, however, address them collectively. Each program covers the two phases of an optimization methodology: project level and network level. The project-level optimization, employing the performance equations in conjunction with cost-benefit ratio and maximizing user benefit, solves for project timings and economically feasible strategies for each project. For a given set of annual budgets, the network-level analysis produces an optimum (again, maximizing user benefit) priority program of pavement improvements for a programming period of up to 12 years at the network level.

Project Level Optimization

The subsystem theoretically allows the engineer to analyze as many different types of alternatives as he desires for each road section analyzed. It is not unusual, however, for the engineer to select subjectively a few (three to five) alternatives from the list of all possible alternatives (see table 1). The selection of alternatives for a network depends primarily on the severity and extent of distresses on the road surface.

The selection of a single alternative or a combination of alternatives, hereafter referred to as a strategy, depends on the minimum life constraint. In other words, performance equations must be defined for each alternative in order to establish the most cost-effective rehabilitation strategy for each project. Analytical or empirical methods have been employed in the past for predicting pavement condition as a function of age and traffic (*4*). Judging from the previous studies, several years' inventory data would be required to derive reliable performance relationships. The lack of adequate data has mandated that linear performance models, based primarily on projected life of rehabilitation, be adopted in this study. That is, the course of deterioration is dictated by the expected life of each alternative, as listed in table 1.

The distress rating increase to 100 after a rehabilitation treatment; whereas the roughness rating, dictated by the treatment and also by the condition rating before the treatment, increases to a value not more than 84. A roughness rating of 84 corresponds to a PSR value of 4.2, the maximum attainable in a new or overlaid pavement (*5*). Following rehabilitation treatment, the condition rating continues to decrease linearly with time.

A word of caution concerning the linearity assumed in the above two models is appropriate. It is generally believed that the performance curves show an increasing rate of deterioration with time (*5*). Some recent studies (*6*), however, show the relationship to be neither linear nor exponential as generally assumed, it assumes a sigmoidal shape. For lack of a better relationship, and because the (prediction) model description is not crucial for purposes of this study, the researchers decided to employ linear relationships as shown in figure 1. Note that the linearity assumption does not alter the basic problem; its use, however, may affect t_1 and t_2—times at which the first and second rehabilitation actions are to be undertaken.

Using the performance prediction models described in figure 1, one must define a threshold region within which a rehabilitation alternative should be considered. As a pavement ages, its condition gradually deteriorates to a point where

TABLE 1 FIVE REHABILITATION ALTERNATIVES SELECTED FOR INTERSTATE HIGHWAYS

No	Description of Rehabilitation	Expected Life, years	Cost of Rehabilitation, $/sq. yd.
1.	1 1/2 inch HMAC overlay	3.75	4.65
2.	1 1/2 inch HMAC overlay with stress relieving layer	4.25	5.45
3.	3 inch HMAC overlay	6.00	7.20
4.	1 1/2 inch Milling and 3 inch HMAC overlay	7.50	9.00
5.	4 1/2 inch HMAC with stress relieving layer	10.00	11.00

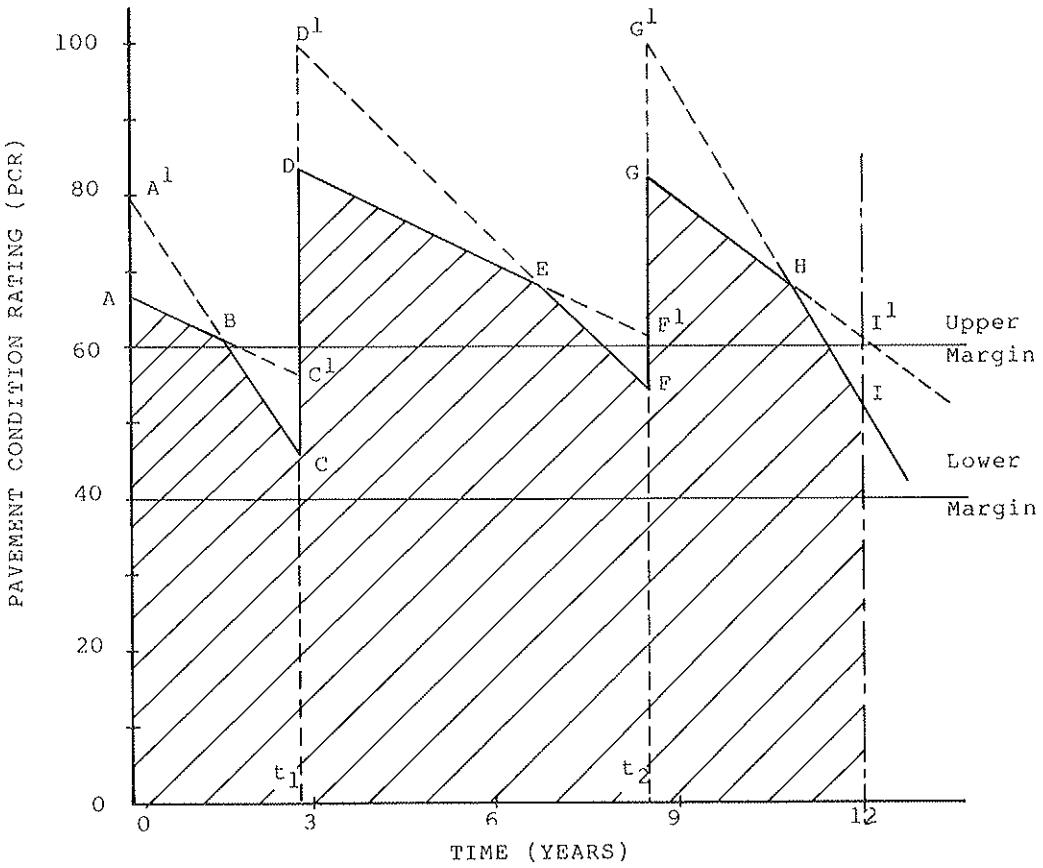

FIGURE 2 Performance trend when rehabilitated. Moment of the shaded area (bounded by line segments ABCDEFGHI) about the zero PCR level provides benefit.

some type of rehabilitation should be applied. At this state of deterioration distress is showing but might not yet be severe enough to call for immediate remedial action. Unfortunately, this point is all too often passed and the pavement continues to deteriorate until something must be done to rehabilitate it. These two points on the performance curve, aptly named the upper and lower margins (figure 2), define a probable rehabilitation period. This concept is slightly different from a single trigger rating, as shown in figure 1.

When rehabilitation treatment is eventually applied, the pavement rating increases abruptly, marking the beginning of a new cycle (see figure 2). Throughout the life of a pavement,

many restorative actions occur, demonstrating a new performance cycle each time rehabilitation is applied. Obviously, many different remedies are possible, and each one generates its own performance curve following application. Not only are many remedies possible, but a large number of different combinations are possible when the timing, sequence, or type of action are changed over an extended period. In this report, a rehabilitation strategy is defined as a combination of rehabilitation alternatives designated by type, sequence, and application time. Figure 2 illustrates pavement condition variation when two rehabilitation actions are applied at times t_1 and t_2, respectively.

Economic and Benefit Analysis

Each rehabilitation strategy that meets the minimum life constraints is subject to an economic analysis, which involves calculation of the capital cost of all the strategies for a 12-yr period from the start of the priority programming period. The present worth of the total costs is calculated (accounting for interest rate and inflation) in determining the cost-effectiveness of the strategy.

The benefit or effectiveness as used in this study is nonmonetary and is a measure of the reliability with which a pavement segment will serve its expected life. The area under the performance curve (ABCDEFGHI in figure 2), weighted with respect to user comfort, is judged to be an adequate measure to quantify the benefit accrued to the road user. Because a road section of higher condition level provides an improved ride and enhances user comfort, area elements closer to the performance curve (or farther away from the zero PCR level, figure 2) should be given a higher weighting factor than area elements closer to the zero PCR level. The weighting factor in benefit calculation is included by taking the first moment of the area about the zero PCR level (or time axis). The total benefit of each pavement section may be computed as the product of the above quantity with its length and with some function of the total traffic that it serves (AADT).

Project Level Optimization Program (PLOP)

Figure 3 is a flowchart demonstrating the operations and work flow in the optimizing program. The project level optimization is a systematic procedure to select all the optimal double-action strategies and the corresponding times of implementation for each project. (A double-action strategy comprises two alternatives.) Not 1 but 25 optimal double-action strategies are possible for each section. Five alternatives may result in more than 25 strategies (several hundreds) depending on the implementation times (t_1 and t_2) selected from 0- to 12-yr analysis period. Out of all possible strategies, the search technique selects 25 optimal double-action strategies. The selection procedure is based on maximizing the user benefit. First, the time of implementing all strategies is determined, followed by a benefit-cost analysis eliminating any unfeasible strategies for each project. The resulting ten to fifteen double-action strategies subsequently are subjected to incremental benefit-cost ratio (IBCR) analysis, as described later.

The decision variables of the first stage optimization include t_1 and t_2, the times of implementation of the double-action strategy, respectively. The objective function was to maximize the total benefit of each section, including the salvage value, for the analysis period of 12 years. Besides being lengthy, the objective function turned out to be nonlinear in t_1 and t_2, thus adding to the complexity of the solution procedure. Because conventional solution procedures (for example, Lagrangian multipliers, constraint variation, and penalty function, etc.) are time consuming for large problems such as that encountered in a PMS, a direct-search method (univariant search technique) is employed in this study. The univariant search is one-dimensional, with only one variable altered over its range at one time. Other details of the search technique and the software developed for this purpose can be seen elsewhere (*7*).

Selecting Feasible Strategies

The ten to fifteen double-action (optimal) strategies selected for each section are theoretically feasible for implementation because they satisfy the constraints of the Network Optimization/Prioritization System (NOPS).

The NOPS subsystem forms the priority or financial-planning analysis part of the PMS. Priority planning leads to a decision regarding which combination (based on highest benefit to the user), out of all the feasible combinations available in the PLOP program, will be used. The nonlinear optimization alluded to above results in five to eight alternatives that are technically and economically feasible. Which solution is selected depends on the condition of the rest of the network and the budget available. In order to select one alternative per section, one uses 0-1 integer programming to optimize the benefits accrued to the network system. The optimization provides the best solution that can be accommodated within budget limitations (figure 4).

The problem is formulated as follows:

$$\text{Maximize} \sum_{i=1}^{l} \sum_{j=1}^{m} X_{ij} R_{ij} \tag{1}$$

subject to:

$$\sum_{i=1}^{l} \sum_{j=1}^{m} X_{ij} C_{ij} \leq B_{XH} \tag{2}$$

$$\sum_{i=1}^{l} \sum_{j=1}^{m} X_{ij} C_{ijt} \leq B_t \qquad \text{for } t = 1, \ldots, 12; \tag{3}$$

$$\sum_{j=1}^{m} X_{ij} = 1 \qquad \text{for } i = 1,2, \ldots, l; \tag{4}$$

and

$$X_{ij} = 0 \text{ or } 1 \qquad \text{for } i = 1,2, \ldots, l, \quad j = 1,2, \ldots, m \tag{5}$$

where:

X_{ij} = jth double-action combination of the ith project (the decision variables),
= 1 if selected or 0 if not selected,
R_{ij} = benefit of ith project if the jth double-action combination is implemented,

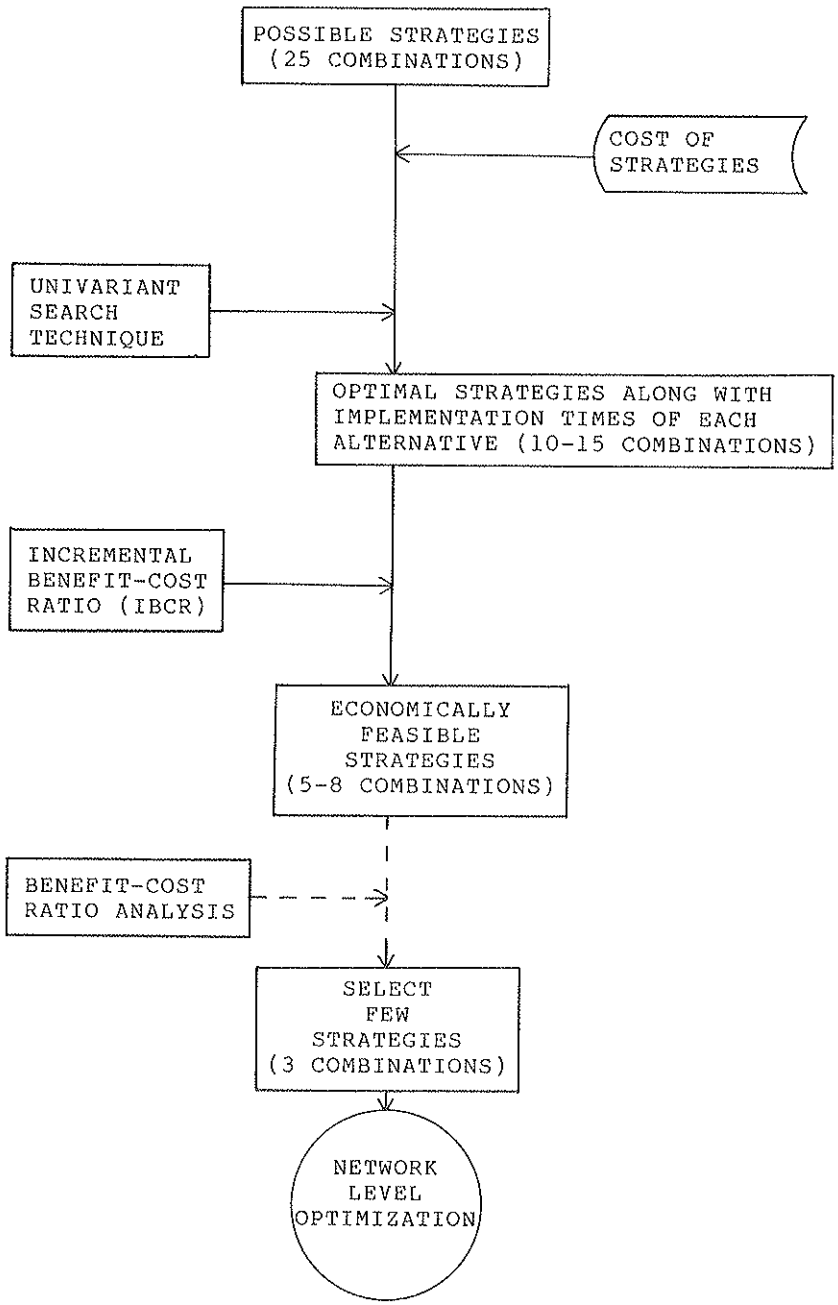

FIGURE 3 Various steps in the Project Level Optimization Program (PLOP). (Broken lines indicate optional operations.)

C_{ij} = cost of the jth double-action combination of ith project,
C_{ijt} = cost of implementation of first or second action of the double-action combination j on ith project in year t,
B_{XH} = overall analysis period budget, and
B_t = agency budget in year t.

A detailed description of integer optimization formulation is given in references (*7*) and (*8*). The integer programming model is found to be appropriate for problems with comparatively few variables. With an increase in the number of variables the computation time becomes prohibitively excessive, and the probability of convergence to an optimum solution is questionable. Taking advantage of the sequential structure of the integer programming model transforms the problem into a dynamic programming model.

The sequential structure of the integer programming model, from the first road section to the last one in the network, constitutes an N-decision problem, where N represents the number of road sections in the network. Using the dynamic programming model transforms the N-decision problem into N one-decision problems. For example, if the decision process included three feasible strategies (ascertained from PLOP) and 10 sections the number of possible combinations of decisions would be 3^{10}. Figure 5a depicts the complexity of the decision tree over just three decision levels.

When properly applied, dynamic programming reduces the

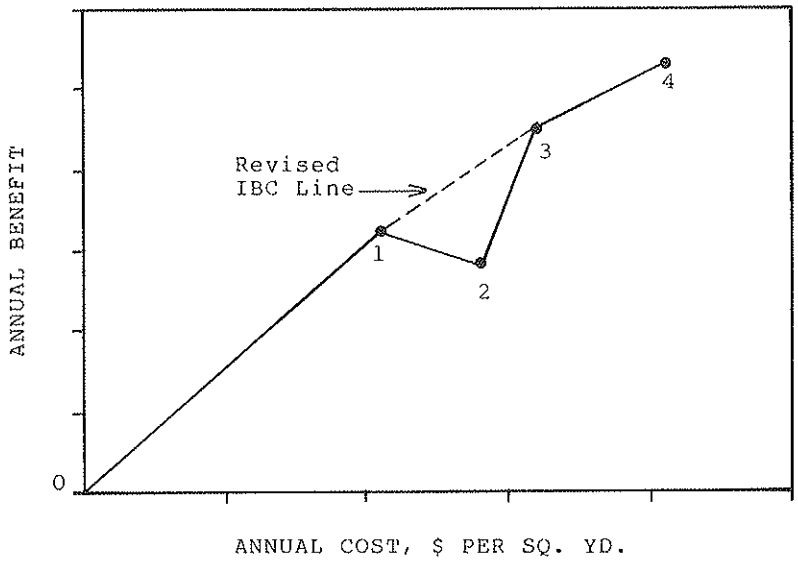

FIGURE 4 Incremental benefit-cost approach for selecting feasible strategies.

problem size and still guarantees an optimal or best solution within the bounds of the model used. In the cited example, the 3^{10} possible combinations or decisions reduce to $3 \times 3 \times 9$ decisions for the same period.

The decision process of pavement rehabilitation at the project level is modeled as a series of staged decisions. At each decision level or stage, all the feasible strategies (only three in this study, signified by the three branches a, b, and c of the decision tree) are applied to each section. Only the strategy that gives each of the entering sections its maximum benefit or performance is retained and passed on to the next stage. The property of the dynamic programming algorithm permits reduction of the decision tree to a feasible size for computer solution. This is illustrated in figure 5b.

The overall budget for the 12-yr analysis period is satisfied in the dynamic problem algorithm, but the yearly (annual) budget may or may not have been satisfied. Should the funds required in any of the 12 years exceed the annual budget for the corresponding year, a benefit-cost ratio analysis is performed on all the rehabilitation strategies included in the optimum solutions, and the strategy with the lowest benefit-cost ratio is eliminated from the set of economically feasible (three in this study) strategies. The dynamic programming procedure is repeated with the revised set (one less than in the previous set) of feasible combinations to arrive at a possibly different optimum combination. This procedure is repeated until all the yearly budgets are satisfied.

Alternatively, a nearly optimum solution may be obtained by judiciously revising the yearly budgets, as dictated by the network condition. In the event that the road network is in uniform condition, the annual rehabilitation costs may fluctuate significantly from year to year. An indication of the yearly budget requirements is initially compiled from the first run of the dynamic optimization problem, this time employing a uniformly increasing yearly budget or any other appropriate combination. Based on the first stage, or exploratory, solution, the engineer may want to revise the yearly budgets reflecting the trend of the exploratory solution and simultaneously satisfying the financial constraints of the department. A second or third application of the dynamic program with those revised budgets would guarantee a nearly optimum solution for most problems.

In the unlikely event that the yearly budgets remain uniform, and when the trial procedure is repeated to the extent that only one feasible combination remains for every road section, there is no optimum solution for the problem subject to the proposed budget level and the specified upper and lower margins. One or more of these parameters must be altered toward a constraint relaxation condition. The dynamic optimization problem should then be repeated following changes in the parameter(s).

Example Network Analysis

To illustrate the use of the programs developed, the researchers analyzed the interstate system (250 miles of two-lane highway) of District No. 2 of the Mississippi Highway Department. The system includes thirty-nine sections with both flexible and rigid pavements. The input included the features of the sections, the distress ratings and roughness ratings, and corresponding performance prediction models. The five pavement rehabilitation alternatives listed in table 1 were also input into the program. The output from the dynamic programming model is a listing of selected project plans giving the maximum objective function within the network funding limit.

The nonlinear optimization programming algorithm uses 20 processing seconds to solve for the feasible combinations for a network with 39 projects on an AMDHAL 470-V8 computer (for 39 projects, 5 alternatives or 25 double-action strategies for each project for a 12-yr analysis period). One run of the dynamic programming algorithm consumes 6 minutes to solve for the optimal double action combination for each project satisfying the overall 12-yr budget.

A partial output of the feasible alternatives for five typical sections is included in table 2. The rehabilitation strategy selected (along with the two actions) by employing the dynamic programming algorithm again for the five typical sections, can

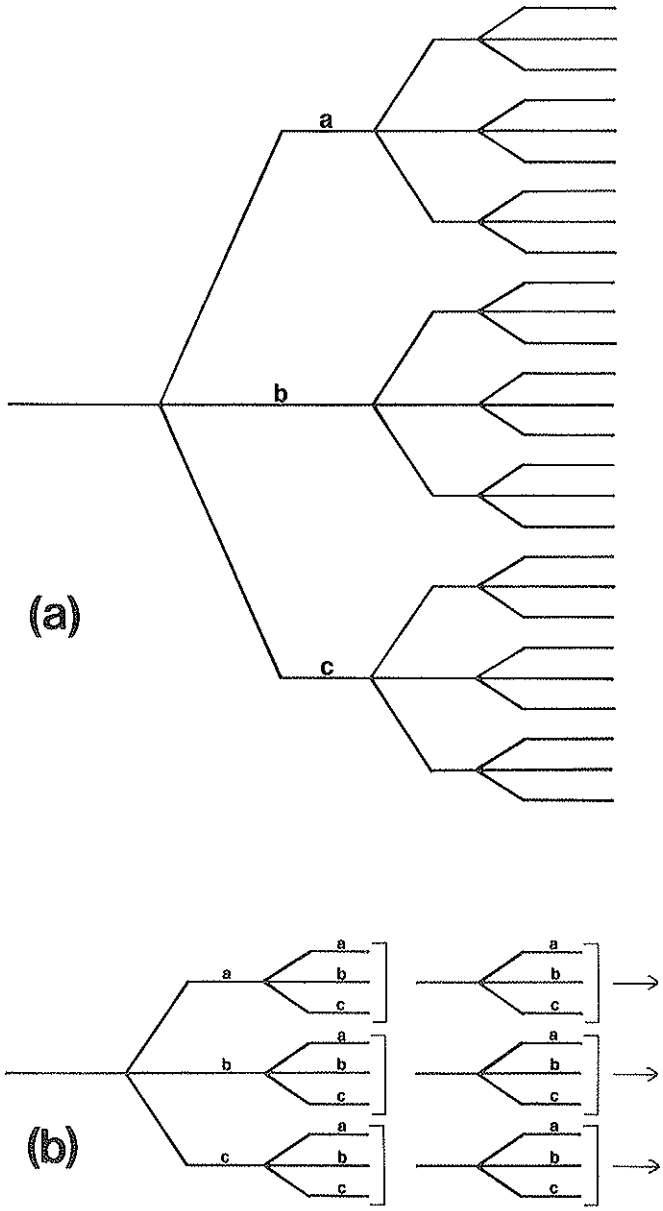

FIGURE 5 (a) Decision tree for network level decision process. (b) Dynamic programming equivalent of decision tree in (a).

be seen in the table. Note that for section 5, despite that alternative 3 (3-in. HMAS overlay) would have lasted for six years, the dynamic programming solution stipulated that alternative 5 be implemented at the end of five years. Simply stated, it is beneficial to place alternative 5 (4½-in. HMAC with stress relieving layer) over alternative 3 (3-in. HMAS) sooner than six years—the expected life of the latter. The first stage analysis (dynamic program) started with a uniform annual budget of \$4.5 × 106; subsequently it was revised, however, as listed in column 2 of table 3. The funds that may be spent according to the optimization model are listed in column 3 of the table. Undertaking a plan of rehabilitation, as shown in column 4 of the table, would maintain the weighted average (weighted with respect to length) PCR of the 250-mi interstate system at approximately 72. Figure 6 depicts the general condition level of the system graphically during the 12-yr analysis period. The top graph (figure 6a) signifies how the average PCR of the system evolves with time. The writers are encouraged that the rehabilitation plan in accordance with the optimization program maintains the average PCR at approximately 72. The estimated percentage of projects with PCR less than 50 is represented by the graph labeled (b) in figure 6. The fact that the optimum plan costing \$45.3 × 106 dollars cannot preserve the entire system at the minimum level of PCR = 50 suggests that the rehabilitation budget should be increased in the future.

For comparison purposes, rehabilitation alternatives for the same 39-section network are selected on the worst-first strategy in conjunction with benefit-cost ratio analysis. The network condition signified by the average PCR, in accordance

TABLE 2 SUMMARY OF SAMPLE OUTPUT

Section No.	Three Feasible Strategies Selected at Project Level	Strategy Chosen at Network Level	Implementation Time	
			First Alternative	Second Alternative
1	S (1,1)[a]; S(1,2); S (2,2)	S (1, 1)	7.4	11.1
2	S (3,5), S (4,5) S (5,5)	S (3,5)	0.7	5.7
3	S (3,5), S (4,5) S (5,5)	S (3,5)	0.2	5.2
4	S (1,3), S (3,2) S (4,2)	S (1,3)	4.6	8.3
5	S (3,5), S (4,5) S (5,5)	S (3,5)	2.2	7.2

[a]S(1,1): Strategy with alternative 1 (implemented at 7.4 years) followed by the same alternative (implemented at 11.1 years)

TABLE 3 ANNUAL REHABILITATION PROGRAM FOR 12-YEAR ANALYSIS PERIOD

Year	Yearly Budget, $ x 10^3	Funds for Optimal Rehabilitation Plan, $ x 10^3	Projects Selected for Rehabilitation
1988	2600	2590	2,3,21,27,28
1989	5300	5274	7,8,16,17,18,22,24,25,26,36,38
1990	3100	3110	5,6,9,10,33,37,39
1991	4000	3857	13,15,29,34,35
1992	1850	1838	4,11,14
1993	6650	6797	19,23,2,3,9,18,21,27,28,39
1994	6650	6644	7,8,16,22,24,25,26,36,38
1995	7400	7587	1,12,20,30,31,32,5,6,11,14, 29,34
1996	2100	2125	4,35
1997	2000	2020	13,15,17
1998	650	652	10,23,37
1999	3000	2870	1,12,19,20,30,31,32,33

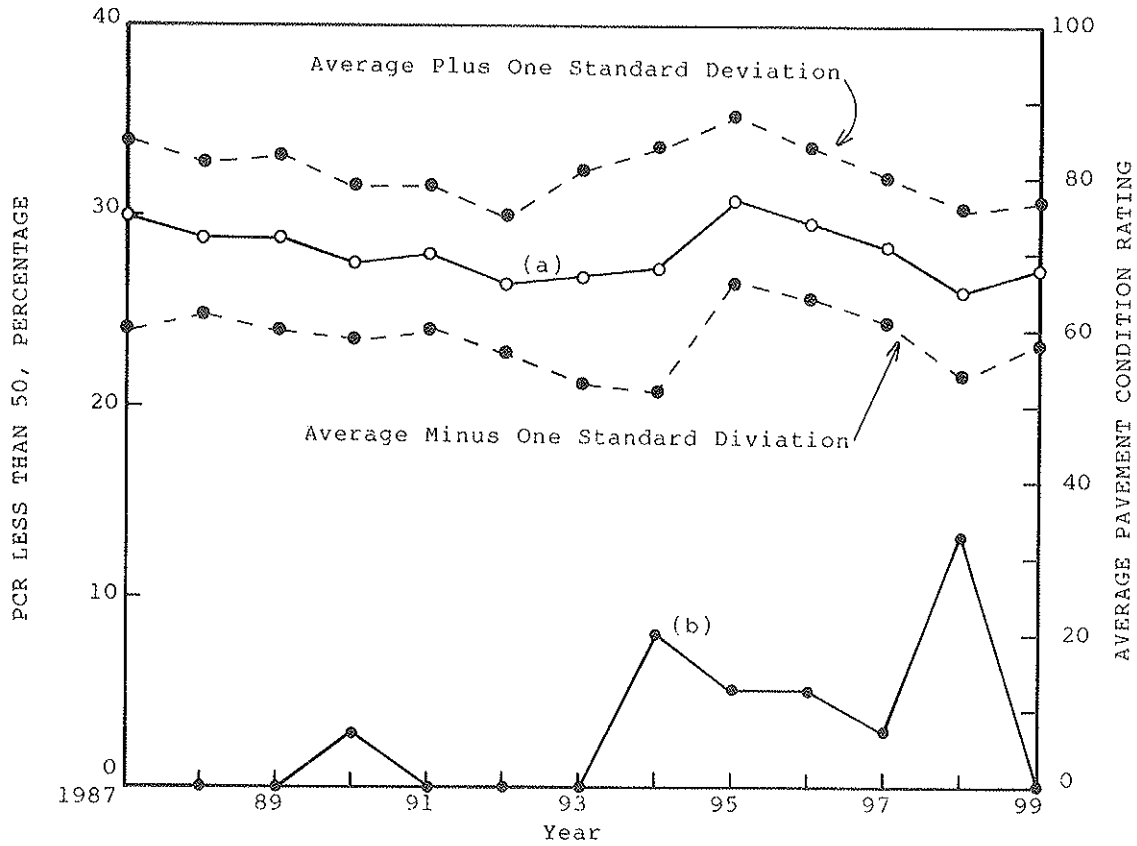

FIGURE 6 Optimization prioritization results. (a) Weighted average PCR (end of year) during the analysis period (b) percentage of projects with PCR less than 50.

with the ranking/benefit-cost ratio, is graphed in figure 7a. The effectiveness of optimal solution is substantial indeed, because with the same overall expenditure for a 12-yr period, the network remains at a higher average PCR level (≈72) as opposed to a widely fluctuating PCR level, notably a PCR of below 72. The percentage of projects with PCR less than 50, employing ranking/benefit-cost ratio, is graphed in figure 7b and compared to figure 6b. The fact that fewer sections in figure 6b have their ratings fall below 50 attests to the premise that the optimization-prioritization procedure indeed strives to provide maximum benefit (effectiveness) at a specific funding level.

Although not discussed in this paper, if one employs the algorithms, it is a simple matter to justify for adjustments to annual budgets in order to maintain the system at a higher condition level. By repeating the calculation, one can arrive at an approximate optimum level of network funding for the analysis period. In summary, the plan represents the best group of long-range rehabilitation plans at selected yearly budget levels, and also strives to serve the user and pavement structure in the best way possible.

SUMMARY AND CONCLUSIONS

The programs and procedures developed in this study focus on the long-range planning of only major rehabilitative measures of a highway network. The approach provides pavement engineers with a tool with which to consider many different alternative plans and rationally select the series of major rehabilitations that maximize the user benefit. The benefit is measured in terms of the first moment of the area under the performance curve. Employing the optimization methodology, one can comprehensively consider the available options and can identify the unique plan that is best for each pavement project at a specific funding level. Reports generated by this procedure describe work to be done and when to schedule it for all the projects in the network. The report listings summarize the results of the long-range plan with respect to total network composite parameters of condition, cost, and performance. Furthermore, if desired, all this information is generated at each of the funding levels considered.

The practical utility of the optimization methodology is illustrated by devising a 12-yr rehabilitation strategy for the Interstate system of the second district of the Mississippi Highway Department. A comparison of the optimal selection procedure with the conventional ranking/benefit-cost ratio approach reveals that the optimal approach strives to provide maximum benefit (effectiveness) at a specific funding level.

ACKNOWLEDGMENT

This report is a part of the study titled "Pavement Management Information System" conducted by the Department of Civil Engineering of The University of Mississippi, in cooperation with the Mississippi State Highway Department and the U.S. Department of Transportation, Federal Highway

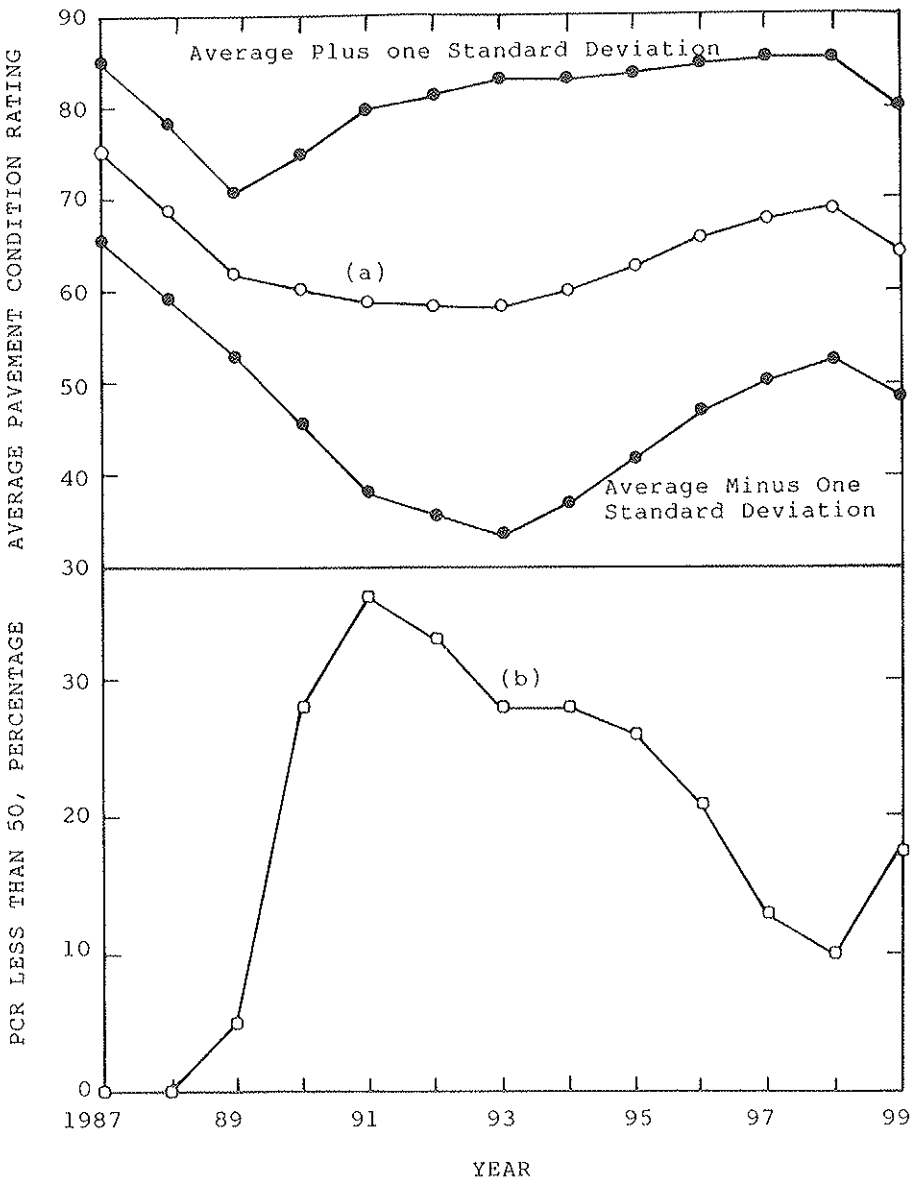

FIGURE 7 Ranking/benefit-cost method (a) weighted average PCR (end of year) during the analysis period (b) Percentage of projects with PCR less than 50.

Administration. The authors wish to acknowledge the excellent cooperation and assistance received from the Department personnel.

The opinions, findings and conclusions expressed in this report are those of the authors and not necessarily those of the Mississippi State Highway Department or the Federal Highway administration. This report does not constitute a standard, specification, or regulation.

REFERENCES

1. *Pavement Distress Manual—Pavement Management Information System*. Report No. 1, Department of Civil Engineering, The University of Mississippi, University, Miss., 1986.
2. *Dynatest 5000 PDM Test System, Owner's Manual*. Dynatest Consulting, Inc., Ojai, Calif., 1986.
3. *Pavement Management Information System*. Interim Report, Department of Civil Engineering, The University of Mississippi, University, Miss., 1987.
4. W. D. Cook, and R. Deighton. *Program Analysis of Rehabilitation Strategies—PARS*. Report No. 9, Ministry of Transportation and Communications, Toronto, Ontario, 1983.
5. *The AASHO Road Test—Special Report 61E*, HRB, National Research Council, Washington, D.C., 1961.
6. R. L. Lytton, F. L. Roberts, and Z. Hazeer. *The Development of New Load Equivalency Factors for Flexible Pavement Design in Texas*. Research Report 476-1, Texas Transportation Institute, Texas A&M University, College Station, Tex., 1986.
7. A. Khatami. *Network Level Optimization/Prioritization Methodology for Pavement Rehabilitation*. Ph.D. Dissertation, The University of Mississippi, University, Miss., 1987.
8. N. V. Ahmed. *A Code for 0-1 Integer Linear Programming Problems with Multiple Choice Constraints*. Ph.D. Dissertation, Texas A&M University, College Station, Tex., 1978.

Publication of this paper sponsored by Committee on Pavement Rehabilitation.

Cold, In-Place Recycling on Indiana State Road 38

REBECCA S. MCDANIEL

A narrow, two-lane road in Indiana was widened in 1986 by cold recycling the existing bituminous pavement in place. Bituminous binder and surface were placed over this base. A five-year research project was planned to compare the cost, strength and performance of the pavement with recycled base to a control section with conventional widening and resurfacing. The continuing evaluation of this recycled pavement includes measuring roughness and deflections annually. Visual inspections monitor development of cracking and other distress. Cores are analyzed for density, voids, asphalt content, and Hveem stability. After one year in service, the recycled pavement is performing better than the conventional pavement. Transverse reflection and longitudinal widening cracks are beginning to develop on the resurfaced section. No cracks have appeared in the recycled section. There is no significant difference between deflections on the two types of pavement. The recycled section cost nearly twice as much as the conventional pavement, but initial costs are expected to drop somewhat as the technique becomes more common. Maintenance costs will likely be lower on the recycled pavement and may result in lower life-cycle costs. This technique will likely be used again in Indiana for roads with low to moderate traffic volumes (under 2,500 directional ADT). Evaluation will continue to assess the performance, service life, and life-cycle costs for this method. Cold, in-place recycling seems to be a viable way to rehabilitate old pavements and seems especially well suited to widening pavements on fairly low-volume roads.

A substantial portion of the Indiana state highway network still has inadequate lane widths, by present standards. During rehabilitation, these roads are frequently widened. The standard technique used in Indiana is to cut a trench along the edge of the pavement. Typically 6 to 10 inches of bituminous base are placed and compacted in the trench. The entire pavement is then resurfaced with 3 to 6 inches of bituminous surface or binder and surface.

This widening technique has been used for years with fairly good results. Problems often develop, however, that shorten the life of the pavement. The major problem is the development of a so-called widening crack running the length of the pavement where the new material separates slightly from the original pavement. The potential for this cracking can be lessened by cleaning and tacking the edge of the original pavement. All too often, however, the crack develops within two to three years of widening. Reflection cracking through the overlay is another common problem.

Last year a cold, in-place recycling process was used for the first time in Indiana. The technique had been used previously in Pennsylvania and a few other states. It allows widening the pavement without creating an interface between the old and new sections where cracks can occur. Recycling obliterates other longitudinal and transverse cracks, so reflection cracking does not occur. After one year in service, the recycled pavement is performing well. Indications are that the technique will completely obviate the widening crack and reflection cracks as well.

The pavement recycled here was built up of several layers of hot mix with both asphalt cements and emulsions.

Indiana Department of Highways, Division of Research, P.O. Box 2279, West Lafayette, Ind. 47906

RESEARCH OBJECTIVES

A five-year research project was planned by the Indiana Department of Highways to study the cold, in-place recycling technique used on this project. Specifically, the research was designed to evaluate the efficiency of the recycling and the structural strength of the resulting pavement.

TECHNICAL APPROACH

This research compares the composite pavement with recycled base, binder and surface to the composite pavement with conventional widening and resurfacing. It was necessary to compare the composite pavements because different types and amounts of bituminous binder and surface were placed over the bases. The comparison focuses on cost and structural strength. Other factors are evaluated to ensure the quality of construction and to supplement the strength data. The tasks involved are as follows:

A. Before Construction
   1. Initial Dynaflect readings were recorded.
   2. The general condition of the existing pavement was documented.

B. During Construction
   1. In-place density was measured by nuclear gauge. A test strip was rolled to establish the target density, according to Indiana Standard Specifications.
   2. Random samples of the recycled material were taken to assess the particle size, asphalt content, and moisture content.
   3. Observations were made of the recycling process to assist in evaluating the efficiency of the operation.

C. After Construction
   1. Dynaflect testing was conducted shortly after construction and will continue periodically for five years.

2. Roughness is evaluated annually in conjunction with the state roughness inventory.
3. Visual inspections are conducted at least annually, and focus on rutting, cracking, and other distresses.
4. Cores of the recycled pavement are taken and analyzed for density, voids, asphalt content, and Hveem stabilities.

SITE OF TESTING

State Road 38 is a rural, two-lane highway in west central Indiana. The site is shown in figure 1. This area of Indiana, like most of the state, is subject to wet, freezing conditions in the winter, with lows around −10°F. Several cycles of freezing and thawing occur during a typical Indiana winter. Hot, humid conditions prevail in the summer, with highs in the upper 90s. The roadway has already weathered one mild winter and one very hot summer.

The original roadway was composed of 7 inches of bituminous hot mix over a gravel base. The road had received surface seals, crack seals and patching, leading to some concern that the material could be quite variable. The existing pavement had an asphalt content of about 5.6 percent. Other asphalt and mix properties are shown in table 1.

The two-lane pavement was 20-ft wide. The earthen shoulders were, and still are, very narrow. The total project length was 9.76 miles. Of this length, the western half (4.88 miles) received the standard widening treatment. The eastern half was cold recycled in-place. The cross sections of the resurfaced and recycled pavements are shown in figure 2.

Traffic volumes varied slightly over the length of the contract. The western end, which was resurfaced, had a directional average daily traffic (ADT) count of 1,150 vehicles per day (vpd) over most of its length, when last counted in 1981. In the small town of Mulberry, the traffic volume increased to about 1,600 vehicles per day. The eastern, or recycled, portion had an ADT of 1,430 vpd. The traffic on the entire road is expected to increase significantly in the next few years due to construction of a large automobile manufacturing plant near Lafayette, 4 miles west of the project.

RECYCLING PROCESS

The eastern half of the project was cold recycled in-place, by a company from Philadelphia, Pennsylvania. This company has used cold, in-place recycling on about 4 million square yards of pavement in Pennsylvania, New York, and West Virginia. A Lafayette-based asphalt paving contractor was the

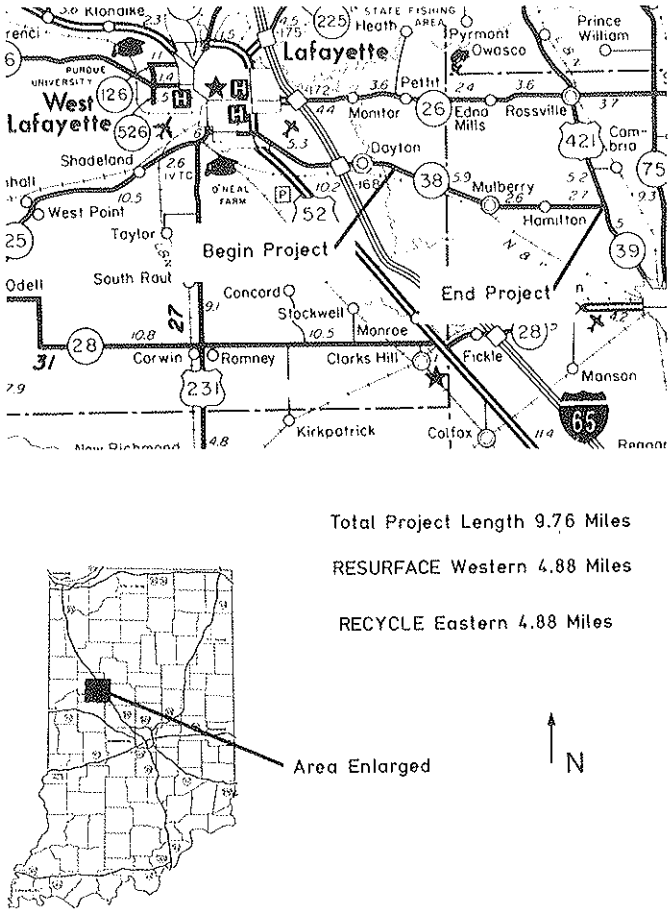

FIGURE 1 Location of test site.

TABLE 1 PROPERTIES OF RECOVERED ASPHALT

Asphalt Content	5.6%
Absolute Viscosity, 140°, 300mm Hg	11,670 poise
Asphalt Penetration, 77°, 5 sec.	36

RECOVERED AGGREGATE GRADATION

Sieve Size	Percent Passing
1"	100.0
3/4"	98.2
1/2"	85.4
3/8"	71.7
No. 4	39.1
No. 8	24.9
No. 16	18.1
No. 30	12.5
No. 50	7.8
No. 100	5.6
No. 200	4.3

prime contractor. The two companies worked together on the recycling, with the Pennsylvania company running the recycling machine and the Indiana contractor operating the grader, paver, rollers, and supply trucks.

The technique used required a minimum of equipment and material handling. The recycling train included the recycling machine, a water supply truck, an asphalt truck, and a conventional asphalt paver. Two rollers, one rubber tired and one vibratory, were used. A motor grader cut the widening trench ahead of the recycling and closed the shoulders after recycling. Two water trucks and two asphalt trucks were used to supply the recycling machine.

The primary piece of equipment was a downcutting recycling machine. This type of machine allowed the size of the milled material to be controlled by the forward speed. The milled material was mixed with water and asphalt emulsion at the cutter head. The water is used to facilitate coating. It also helped to control dust and to cool the cutter head.

A conveyor belt, attached to the recycling machine, discharged the recycled material into the hopper of a conventional paver. No windrowing was necessary. The paver was connected to the milling machine by a stiff leg to keep the two machines moving together.

The original 10-ft wide lanes were milled to a depth of 6 inches. A 1-in "cushion" was left to avoid milling into the subbase and to allow for some variation in the depth of material. The recycled material was relaid at a depth of about 5 inches to allow a finished lane width of 12 feet.

The rubber tired roller achieved most of the compaction. The vibratory roller followed to iron out the surface.

CONSTRUCTION OBSERVATIONS

This construction technique was totally new to the local paving crew, but they were able to adjust to it quickly. By the second day of recycling, they had learned to work with the recycling machine and the material it produced. The processed material was very sticky and hard to work by hand. There were no problems with rolling the recycled mix.

Recycling progressed at about 17 or 18 feet per minute after the start-up problems were solved. This is equivalent to placing about 375 to 400 tons per hour. Most downtime experienced during recycling was due to paver malfunctions. Efficiency varied from 68 to 93 percent.

The technique proved to be simple and efficient. The few problems experienced during this first attempt could be easily corrected. Better planning and more local experience should result in higher efficiency and production.

The recycled pavement was left exposed for seven weeks after recycling was completed, due to a series of delays. It is generally recommended to let this cold-recycled material cure for about two weeks before surfacing. A few soft spots showed up on this project before the binder was placed. The weak areas were believed to be caused by traffic action over localized areas of poor subgrade. All the soft spots were in the outer wheelpath near the shoulder, in the widened portion. This area had never been under traffic, and the trench had not been rolled when it was cut. The subgrade material, then, had never received much compaction. Traffic action plus heavy rains had brought the poor subgrade conditions to light.

The soft areas were cut out and patched with hot mix.

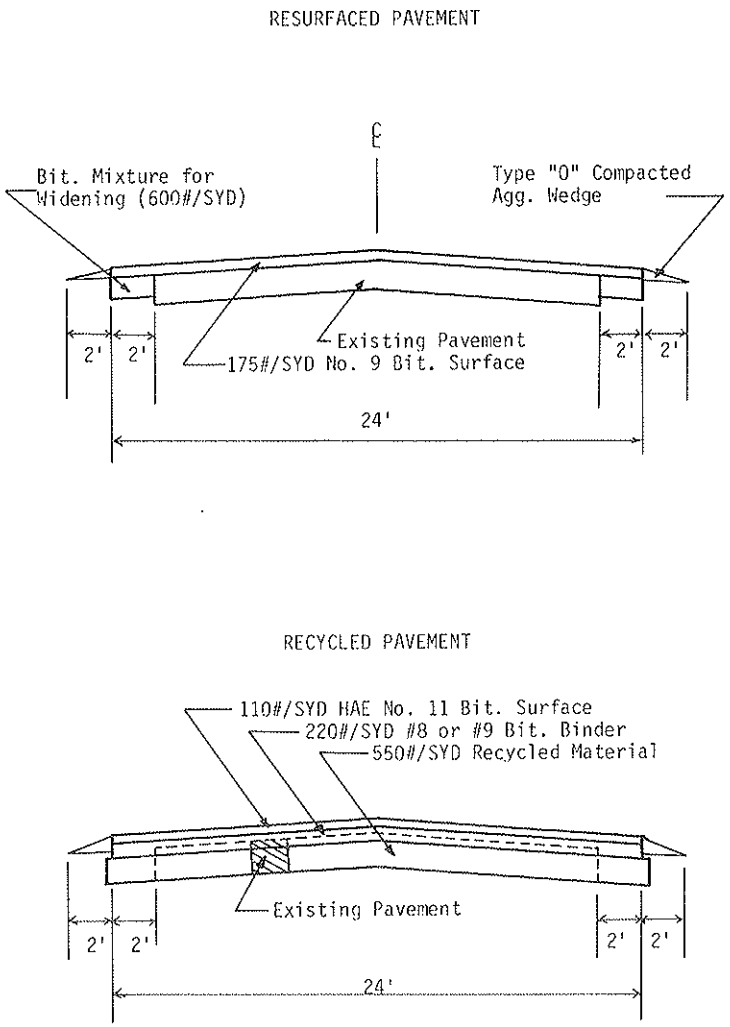

FIGURE 2 Typical cross sections.

Altogether, less than 1 ton of patching material was used. The patching evidently served its purpose; no further problems have developed to date.

RESULTS OF MATERIALS AND PERFORMANCE TESTING

Routine Construction Tests

Samples of the recycled material were taken randomly during construction and analyzed for asphalt content, moisture content, and aggregate gradation. Results of these tests are summarized in table 2. The gradation of the recycled material was finer than Indiana's dense-graded No. 5D Base. Specification limits for No. 5D Base are shown in table 2 for comparison. The recycled material was less variable than expected.

Approximately 2.5 percent asphalt emulsion was added during recycling. The emulsion used was AE-150, a medium-setting emulsion with about 69 percent residual asphalt and 4 to 4.5 percent kerosene. The specifications used in Indiana for AE-150 are listed in table 3. The amount of emulsion added was essentially determined and adjusted based on field experience. Very limited laboratory work was done before construction. The final asphalt content averaged 7.4 percent.

Density was monitored during construction with a nuclear gauge. A control strip was run at the beginning of recycling to establish a target density. Indiana's test strip method involves monitoring the increase in density with successive passes of a standard roller train until the density peaks. The target density is then set at the mean density of the test strip. The density of the recycled material had not peaked after 24 passes during the test strip rolling. Tiny cracks began to develop, which indicated the material was being over-compacted so rolling was terminated. The ambient temperature increased by 20° during the test strip rolling, which may help explain why the density did not peak.

The densities achieved during construction averaged 124.4 pounds per cubic foot ($s = 3.71$). A total of 220 tests were taken on the recycled material. No rutting or other distress, with the exception of those areas with a soft subgrade, occurred before the binder was placed, indicating the compaction was adequate.

After one year in service the recycled base is performing well. The results of various evaluations are as follows.

TABLE 2 RESULTS OF ROUTINE CONSTRUCTION TESTING

	Average	Standard Deviation
Asphalt Content	7.4%	0.45
Moisture Content	4.4%	0.88

Aggregate Gradation		
Sieve Size	RAP	No. 5D Base
1 1/2"	100.0%	100%
1"	100.0%	80-99%
3/4"	98.3%	68-90%
1/2"	87.5%	54-76%
3/8"	75.8%	45-67%
No. 4	48.1%	35-45%
No. 8	32.0%	20-45%
No. 16	22.3%	12-36%
No. 30	15.0%	7-28%
No. 50	8.8%	3-18%
No. 100	5.7%	1-12%
No. 200	4.2%	0-6%

TABLE 3 SPECIFICATIONS FOR AE-150 ASPHALT EMULSION

Furol Viscosity, 77°F, Min.	50 seconds
Residue from Residue by Distillation	68%
Oil Portion, from Residue by Distillation, ml. oil per 100 g. emulsion, Max.	7.0 ml.
Sieve Test, Max.	0.10%
Tests on Residue from Residue by Distillation	
Float Test at 140°F, Min.	1,200 seconds
Penetration, 77°F, 50 g, 5 sec.	100-300
Solubility in Organic Solvents, %, Min.	97.5%

Visual Inspections

After one unusually mild winter, a visual inspection of the conventionally resurfaced section revealed a few transverse reflection cracks and some faint, hairline cracking along the widening. This cracking will undoubtedly increase after a more typical Indiana winter. Within two or three years, it is expected that the widening cracks will be significant.

The recycled section, however, is virtually crack-free. There is no reflection cracking because all the existing cracks were obliterated during the recycling process. There is no widening crack because there is no interface between old and new mate-

TABLE 4 ROUGHNESS SUMMARY

	1986	1987
Conventional Pavement		
Eastbound	940	836
Westbound	846	869
Average	893	852
Recycled Pavement		
Eastbound	777	751
Westbound	652	688
Average	714	720

rial. An extremely hot summer has passed and no rutting is apparent in the recycled section. In short, there are no problems to date.

Roughness Data

The initial roughness was evaluated with the Cox Roadmeter in December 1986. Roughness measurements were performed again in July 1987. These results are summarized in table 4. Roughness measurements are included in this study mainly to monitor deterioration of the two pavements over time. The smoothness cannot be directly compared because the pavements include different surface materials and numbers of courses.

The readings indicate that the pavement with recycled base was initially smoother than the resurfaced pavement. One layer of hot asphaltic mixture was placed over the resurfaced pavement and two were placed over the recycled pavement, which helped level out the recycled section.

The follow-up testing in 1987 again showed the recycled pavement to be somewhat smoother than the resurfaced pavement. Neither pavement showed an increase in roughness. The roughness numbers measured in 1987 are not significantly different from those measured in 1986.

Dynaflect Deflections

Results of Dynaflect testing are shown in figures 3 and 4 and are summarized in table 5. Deflections measured before construction were essentially the same on the two portions of the project. The amount of variation in deflections, as indicated by the standard deviations and coefficients of variation, is also essentially the same.

After construction, the deflections were reduced by approximately half. The deflections measured on the recycled pavement were slightly lower than on the conventional resurface. The coefficients of variation show that the amount of variability is roughly the same as before construction.

Dynaflect measurements were made again in June of 1987. These results are not directly comparable to the previous tests because of the seasonal variation in deflection measurements on bituminous pavements. Nevertheless, the readings indicate that, even in the heat of summer, the pavement is now stronger than before construction. Again, there is no significant difference between the two pavement types.

Analysis of Cores

Cores of the recycled pavement were taken in July 1987 after the pavement had been in place for about one year. These cores were analyzed for density, voids, and Hveem R and S values. Cores will be taken annually to evaluate any further densification under traffic. The results of the 1987 analysis of cores are shown in table 6.

Intact cores of the recycled material were very difficult to take. The cores obtained were fragmented. An unsuccessful attempt was made to core without water to allow determination of the in situ moisture content of the recycled base.

PROJECT COSTS

Past experience has shown that a new technique or material is usually more expensive the first few times it is used than when it is more widely used. This is due, in part, to contractors becoming accustomed to the process and the problems they may encounter. Also, competition increases as more contractors obtain the necessary equipment and develop the expertise.

In the case of this new recycling technique, the cost for the recycled pavement was almost double the cost of the conventional pavement. The cost breakdown was as shown in table 7. If this recycling method is used more often in Indiana, the costs are expected to drop somewhat.

Since indications are that the recycled pavement will have significantly less cracking than the conventional pavement, at least initially, the maintenance costs will be reduced. Life-cycle costs for the recycled pavement may then be lower than for the conventional pavement, depending on the relative service lives of the two pavements. The continued evaluation of this project should help estimate the service lives of the pavements.

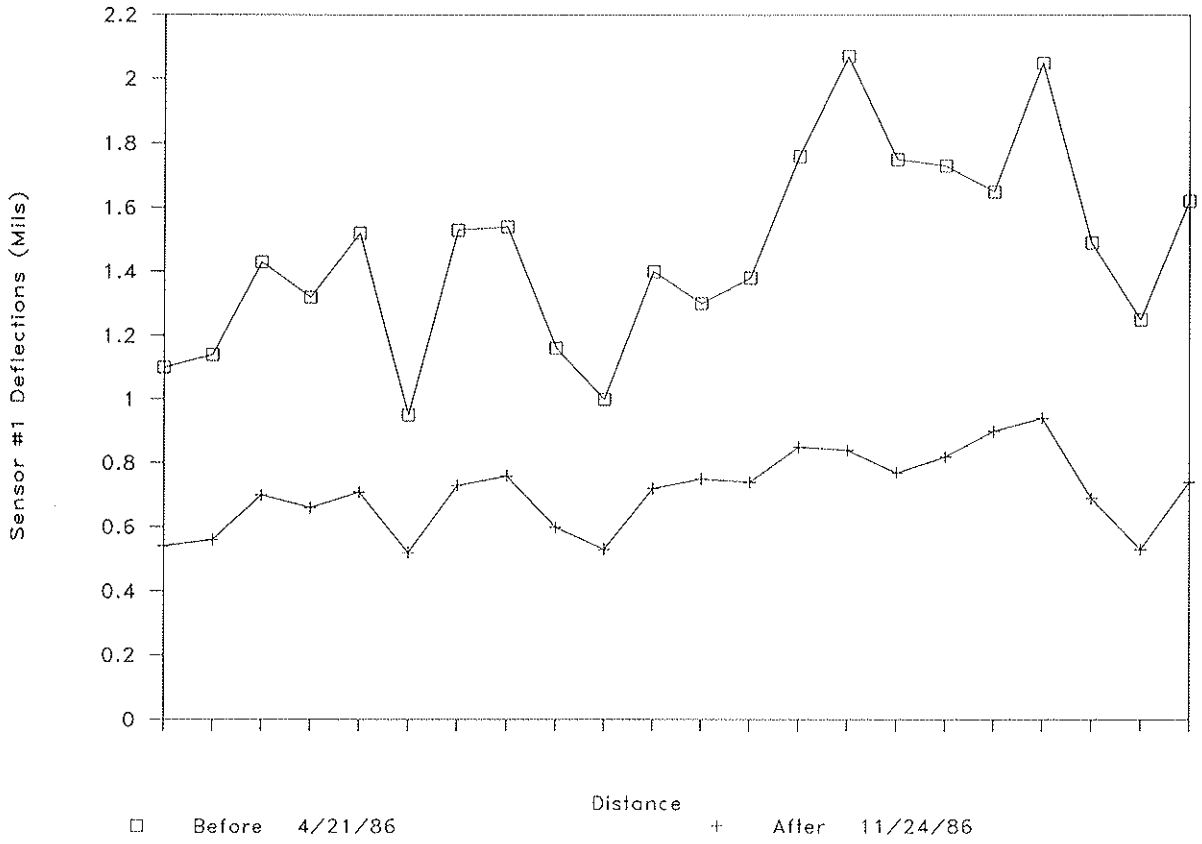

FIGURE 3 Dynaflect deflections, recycled section.

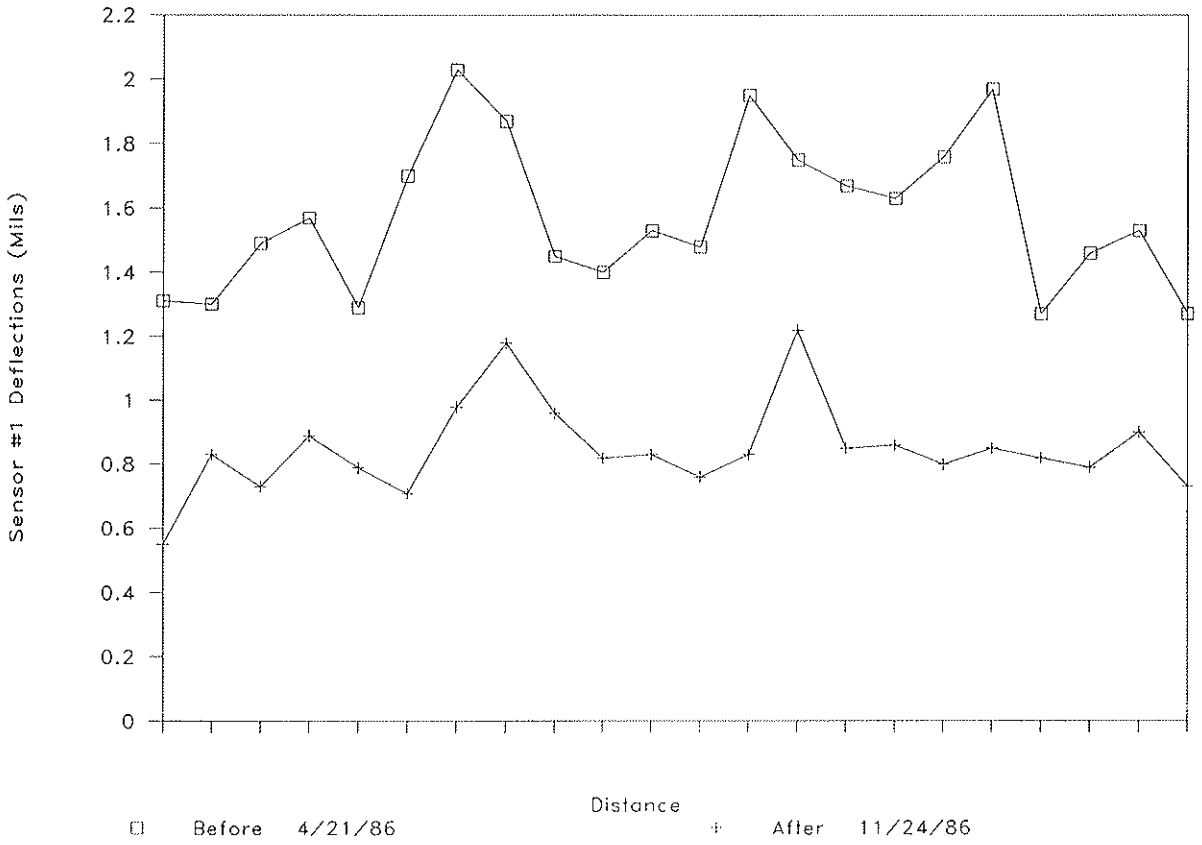

FIGURE 4 Dynaflect deflections, resurfaced section.

TABLE 5 DYNAFLECT DEFLECTIONS SUMMARY

	Before Construction	After Construction	
	4-86	11-86	6-87
Resurfaced Eastbound			
Average Sensor No. 1 (mils)	1.44	0.79	1.10
Standard Deviation (mils)	0.37	0.18	0.25
Coefficient of Variation (%)	25.7	22.8	22.7
Resurfaced Westbound			
Average Sensor No. 1 (mils)	1.52	0.84	1.24
Standard Deviation (mils)	0.42	0.20	0.34
Coefficient of Variation (%)	27.6	23.8	27.4
Recycled Eastbound			
Average Sensor No. 1 (mils)	1.50	0.73	1.24
Standard Deviation (mils)	0.38	0.18	0.36
Coefficient of Variation (%)	25.3	24.6	29.0
Recycled Westbound			
Average Sensor No. 1 (mils)	1.46	0.71	1.20
Standard Deviation (mils)	0.40	0.16	0.30
Coefficient of Variation (%)	27.4	22.5	25.0

TABLE 6 RESULTS OF ANALYSIS OF CORES

	Average	Standard Deviation
Density, pcf	141.5 pcf	3.1
Air Voids, %	5.0%	2.1
Hveem Stabilities		
S-value (140°)	25	--[1]
R-value (70°)	91[2]	--[1]

[1]Based on small sample size due to difficulties in getting samples of sufficient thickness for Hveem testing.

[2]Uncorrected for height of specimen.

CONCLUSIONS

After one year in service, the pavement with recycled base seems to be performing at least as well as the conventional pavement.

- The pavement with recycled base has less cracking than the conventional pavement. The deflections are essentially the same for the two types of pavements.
- Steps can be taken to improve the performance of the recycled pavement. When a widening trench is cut, as in this application, the trench should be rolled as specified for other widening. The length of time the recycled base is left without a surface should be limited to two weeks. This allows time for the base to cure, but limits the length of time the pavement is left open to traffic and weather.
- The efficiency of the recycling could be increased. The capacity of the water trucks should be similar to avoid delays.

TABLE 7 PROJECT COSTS

	Quantity	Unit Price	Total Cost
Resurfaced Section			
Widening(and Trenching)	3663 Tons	$23.00	$84,249.00
HAE No. 9 Surface	6118 Tons	$23.25	$142,243.50
Patching	52 Tons	$70.00	$3,640.00
Wedge and Level	796 Tons	$23.00	$18,308.00
Total			$248,440.50
	Cost per Lane Mile	$25,454.97	
Recycled Section			
Patching	1 Tons	$70.00	$70.00
Milling	57,300 SYD	$2.20	$126,060.00
Trenching	51,533 LFT	$0.20	$10,306.60
AE-150	460 Tons	$150.00	$69,000.00
Bit. Binder	7,560 Tons	$21.00	$158,760.00
HAE #11 Surface	3,780 Tons	$24.00	$90,720.00
Total			$454,916.60
	Cost per Lane Mile	$46,610.31	

Obviously, keeping the paver and other equipment in good repair would reduce down time.

- Further evaluation is necessary to determine the long-term performance and to estimate the service life of the recycled base, but at this point the recycled material is performing well.
- The recycled pavement cost nearly twice as much as the conventional pavement, but costs would likely drop if the process were used more. In this case, one more course of bituminous mix was placed over the recycled base, significantly increasing the cost over that of the resurfaced section. Life cycle costs for the recycled pavement may be lower than for the conventional pavement if the service life is comparable, due to reduced maintenance costs.

RECOMMENDATIONS

The experience with this recycling technique in Indiana has been very favorable so far. There is great interest in using the technique on more projects. Future uses may include the following:

- The use of more exotic binders, such as foamed asphalt, rejuvenators, polymer modifiers, etc.
- Improving granular bases or gravel roads; this may be especially attractive for county highway departments.
- Adding virgin aggregate, if needed, by spreading it on the roadway ahead of the recycling machine.
- Surfacing the recycled base with a double chip seal instead of a hot mix surface; again this may be especially useful on low-volume roads, such as county roads.

Further evaluation may show that this type of base can be used on roadways with higher traffic volumes. The increase in traffic volume due to the auto plant will be monitored on State Road 38. Until further evaluation shows that this type of base can withstand higher traffic volumes, it will only be used in low or moderate traffic volume situations in Indiana (under 2,500 directional ADT).

This cold, in-place recycling technique appears to be a viable way to rehabilitate old bituminous pavements and to prevent reflective cracking. Its use for widening bituminous pavements, as in this case, seems especially appropriate.

Publication of this paper sponsored by Committee on Pavement Rehabilitation.

Data Acquisition for Mechanistic-Empirical Overlay Design Equations for Reflection Cracking in Flexible Overlays

P. W. JAYAWICKRAMA, R. E. SMITH, R. L. LYTTON, AND M. R. TIRADO

This paper describes a mechanistic-empirical design procedure developed to assist pavement engineers in determining when flexible overlays of flexible pavements will develop reflection cracking. A mechanistic equation based on fracture mechanics was developed to predict when reflection cracking was expected to occur. Data on in-service pavements were collected for six environmental regions. The equations were used to predict the occurrence of reflection cracking. The performance data were then used to calibrate the mechanistic equations to three different damage levels. The final design equations were placed in a user-friendly microcomputer design program. This paper tries to demonstrate the data collection requirements and problems associated with developing mechanistic-empirical design equations. This approach to developing design equations has great promise; however, the data must be complete and accurate for the approach to be used fully. Some of the problems encountered are described, along with the approaches used to solve these problems.

Asphalt concrete overlays are one of the most common rehabilitation treatments applied to asphalt concrete pavements. Design procedures for these overlays have traditionally been empirical (*1*). In recent years, several mechanistic design approaches have been developed that use the strain at the lower surface of the asphalt layer as a fatigue related design criterion (*1*). This approach relies on the relationships developed between the calculated strain in new pavements and fatigue damage due to traffic loadings.

Reflection cracking is a common form of asphalt concrete deterioration in overlaid pavements, caused by cracks in the original pavement propagating through the new asphalt layer. These cracks in the overlay deteriorate over time, leading to failure of the overlay (*2*). The need for design procedures to address the problem of reflection cracking of asphalt concrete has long been recognized. Such a design methodology, using principles of fracture mechanics to predict overlay life against reflection cracking, was presented by Jayawickrama and Lytton (*3*). This work demonstrated how the mechanistic model could be calibrated using in-service overlay performance data to obtain design equations. The data used in that study were collected from the state of Texas and, therefore, represent the environmental conditions prevailing only in that part of the United States. This paper describes a recently completed project that expanded this effort by collecting data from 11 different states so that all six of the climatic regions shown in figure 1 and described in table 1 are represented.

The boundary between the wet and dry zones is the Thornthwaite Index contour 0, which indicates the moisture balance between annual rainfall (+) and the potential evapotranspiration (−). The boundary between the no-freeze and the freeze-thaw cycling zones represents the contour along which freezing temperatures will penetrate the pavement to a depth no greater than 5 inches (130 mm) (*4*). The boundary separating the freeze-thaw cycling and the hard freeze-spring thaw zones represents the contour along which freezing temperatures persist in the ground for more than 60 days continuously each year (*5*).

Environmental data adequate to define these boundaries were collected from participating state highway agencies, county soil maps, and the National Atmospheric Bureau. Data describing the properties and condition of the pavements over time were collected for use in developing mechanistic-empirical design equations for asphalt concrete overlays on flexible pavements for each climatic region. These results were then integrated into a microcomputer-based design program described elsewhere (*6*).

To develop a mechanistic-empirical design equation, a mechanistic equation is selected or developed that accurately models known forms of failure in the pavement; however, it is generally impossible to model all factors influencing the pavement failure mode. The mechanistic model is calibrated using performance data collected on pavements to reflect the influence of these factors. Data used in the mechanistic model must be available on the pavement sections used for the calibration process.

This paper briefly describes the process of selecting an appropriate mechanistic equation and the empirical calibration process. The model defined the data required for the calibration process. The problems encountered in collecting and using data from in-service pavements is described. A complete and detailed description of the design method is presented elsewhere (*3, 6*).

REVIEW OF MECHANISTIC MODEL DEVELOPMENT

The mechanisms generally thought to lead to reflection cracking are the vertical and horizontal movement of the underlying layers. These damaging movements may be caused by traffic

P. W. Jayawickrama, R. E. Smith, and R. L. Lytton, Texas Transportation Institute, College Station, Tex. 77843. M. R. Tirado, ERES Consultants, Inc., P.O. Box 1003, Champaign, Ill. 61820.

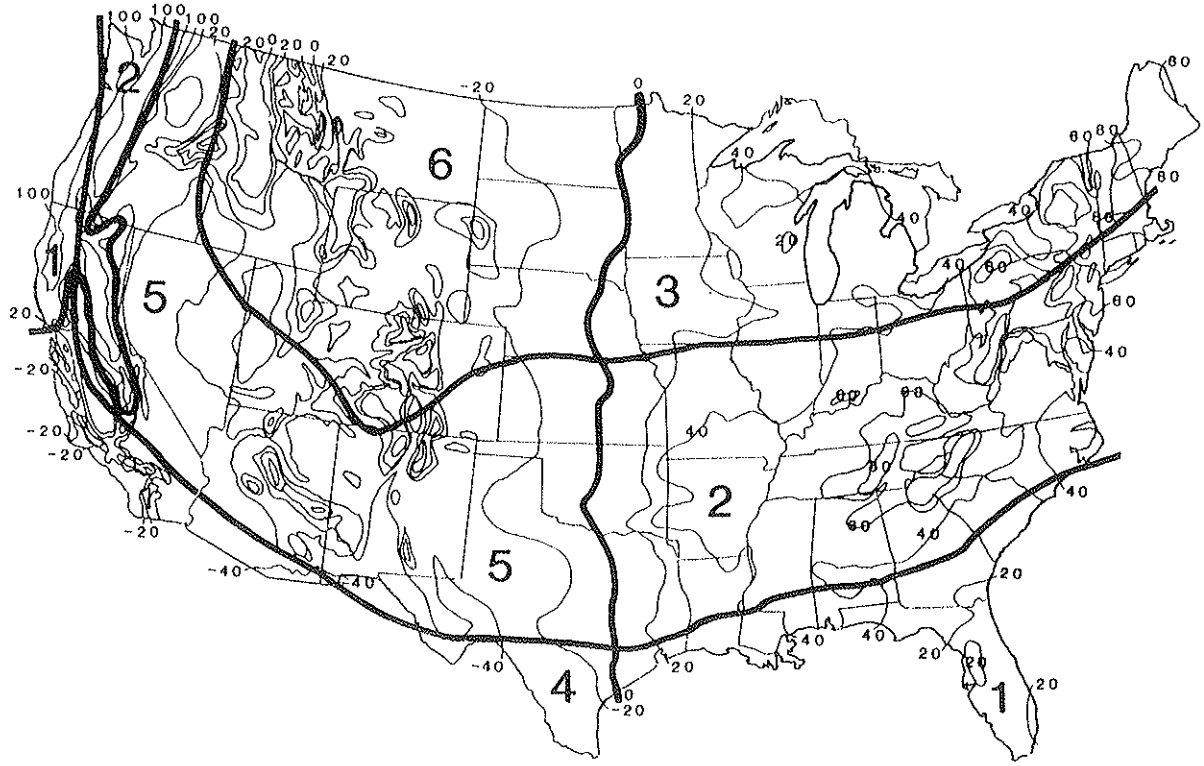

FIGURE 1 The six climatic regions in the United States (*1*).

loading, thermally induced contractions and expansions, or a combination of these mechanisms.

Figure 2 illustrates the changes in bending and shear stresses that occur within an overlay as a wheel load passes over a crack in the original pavement. These stress conditions cause the crack to propagate into the overlay, due to shearing movement in one direction followed by a bending movement and again by shearing movement in the opposite direction. In addition to the influence of the traffic loads, contraction and expansion of the pavement and the underlying layers with changes in temperature also contributes toward the growth of reflection cracks. In these three mechanisms of crack growth, the stresses generated cause a crack to form in the overlay and grow with repeated application. The principles of fracture mechanics are used to determine the rate of crack growth due to these mechanisms. In this process each crack growth mechanism is treated independently, and their influence is combined in a final design equation.

The recent developments in linear elastic and viscoelastic fracture mechanics concepts have enabled a rational design approach to the problem of reflection cracking of overlays. Experimental investigations carried out at Ohio State University (*7–9*) and Texas A&M University (*10–12*) have verified the applicability of fracture mechanics principles in predicting fatigue life of asphalt concrete mixes. The results indicate that the rate of crack propagation in asphalt concrete can be predicted by using the empirical power law relation developed by Paris (*13*).

$$\frac{dc}{dN} = A(\Delta K)^n \tag{1}$$

where

ΔK = stress intensity factor amplitude,
A,n = fracture parameters of the material,
c = crack length, and
N = number of load applications.

Integrating Equation 1 we obtain,

$$N_f = \int_0^h \frac{dc}{A(\Delta K)^n} \tag{2}$$

where

N_f = number of load applications to failure
h = thickness of the overlay

The use of Paris' crack growth law to determine the overlay life requires a knowledge of the stress intensity factor, K, and the material constants, A and n, within the in-service overlay. The stress intensity factor, K, in the overlay due to each of the crack growth mechanisms was determined by using a formulation that combines beam-on-elastic foundation theory and the finite element method. In the beam-on-elastic foundation analysis the original surface layer and the overlay are modeled as a beam. The base course and the subgrade are

TABLE 1 DESCRIPTION OF CLIMATIC REGIONS

Region	Character of the Region
1	Wet, No-Freeze
2	Wet, Freeze-Thaw Cycling
3	Wet, Hard Freeze, Spring Thaw
4	Dry, No-Freeze
5	Dry, Freeze-Thaw Cycling
6	Dry, Hard Freeze, Spring Thaw

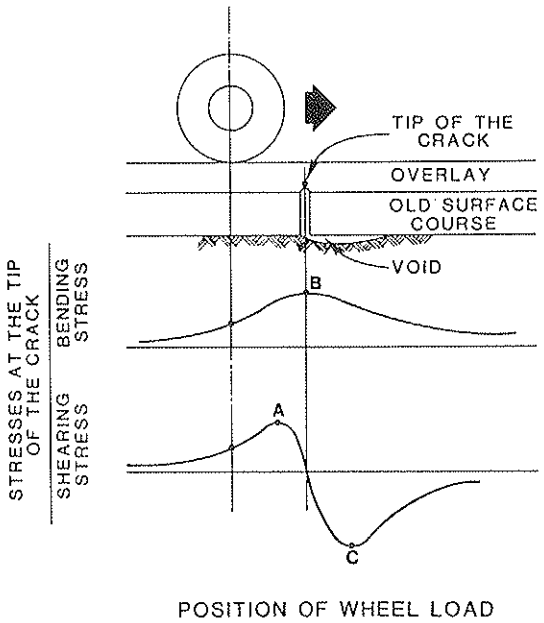

FIGURE 2 Stresses induced at a cracked section due to a moving wheel load.

represented as a homogenous elastic medium supporting the beam. In order to calculate the stress intensity factors accurately and determine their variation with the crack length, a finite element method was used (*6*).

The use of the mechanistic model for the analysis of crack propagation through an overlay requires a knowledge of overlay stiffness as well as fracture parameters, A and n. The mix stiffness is determined using the nomograph procedure outlined by Van der Poel (*14*) and Mcleod (*15*). In this study, computerized versions of the nomographs were used. In addition, the computer programs profile the slope, m, of the log of the mix stiffness versus log of the loading time curve which is used to determine the exponent, n, in Paris' equation as shown below:

$$n = 2/m \tag{3}$$

Theoretical justification for equation 3 can be found elsewhere (*16*). This relationship has been verified for asphalt concrete mixes by Germann and Lytton (*10*) and Molenaar (*17*).

The following empirical relationships, developed based on the crack growth tests of asphalt concrete mixes, were used to determine the parameter, A:

For traffic associated cracking:

$$n = -2.2 - 0.5 \log A \tag{4}$$

For thermal cracking:

$$n = -0.92 - 0.42 \log A \tag{5}$$

The propagation of reflection cracks is the result of all three failure mechanisms (bending, shearing, and thermal) acting simultaneously. However, in the integration of the Paris' equation the three failure mechanisms are treated independently.

It is recognized that this idealized model may not provide accurate estimates of the stress intensity factors induced by the different loading mechanisms in the various mixes. However, the model can be used to establish the form of the equation that reflects the correct influence trends of the variables. The form of the regression model in the empirical calibration was selected to incorporate the influence of the combined action of the three mechanisms into the final design equation. The in-service performance data is then used in the regression analysis, which compares the mechanistically calculated time-to-crack formation with recorded crack development to develop equations that reflect the expected performance in each of the six climatic regions.

DATA NEEDS

The data required by the mechanistic equation to calculate the time until the pavement develops a reflective crack must be available for the in-service pavement sections used in this process. This same data will be required for use in the design program. The following information is required for calculating the overlay life using the mechanistic equations in this project:

- Laboratory data on the bitumen and the mix—to characterize the asphalt material used in the overlay,
- Deflection test data—to characterize the existing pavement structure,
- Environmental data pertaining to the location, and
- Traffic data.

In order to combine the influence of the three different mechanisms, the mechanistically computed overlay responses are regressed against crack development rates in the overlays. Therefore it is also necessary to collect data on overlay performance.

DATA ACQUISITION

Previous studies indicated that sufficient data were not available to develop one overlay design equation for the whole United States, primarily because of the excessive amount of data required to account for climatic and regional differences. However, they did indicate that sufficient data were available to develop regional equations (*18*). Considerable effort is required to collect data adequate for use in calibrating mechanistic empirical design equations. Many state highway agencies have some of the data needed to develop mechanistic-empirical equations; however, very few have all of the data needed.

DATA SOURCE LOCATION

The information on available data (*18, 19*), along with other sources, were used to begin the search for in-service data. Many of the agencies stated that they did not have all such data for their pavements. Others were reluctant to participate in the project because the data required were not readily available or retrievable. Those agencies that did have the needed data generally did not have all required data in one file set.

In many instances during the data collection effort, it was found that the required data on a desirable in-service pavement section was missing from the files. So an agency would often start with 30 to 40 candidate in-service pavement sections on which the researchers expected to collect data only to end with 5 to 15 sections with adequate data for use in the project. As a result, the researchers never knew the number of sections on which data could be collected until they were on site at the agency. In some instances, it was not possible to be sure that the data were usable until after the data was collected and reduced into common-analysis units. When the data were normally stored in several different files, each file would often have a different referencing or cataloguing scheme, making it difficult to cross reference the data elements. So even when data could be found, it was not always possible to identify corresponding data sets, such as which asphalt properties corresponded to a given section of pavement.

DATA REDUCTION

Raw data were collected from several different agencies, as shown in table 2. In many instances the data gathered by the research team were not measured or collected in the same form by the various highway agencies from which it was gathered. When data in different forms are used, they must be reduced to similar forms of material and response characteristics before they can be used in developing the desired mechanistic-empirical design equations.

Asphalt Material Characterization for the Overlay

The stiffness of the asphalt-concrete overlay must be known in order to determine the fracture properties and was calculated using the Van der Poel or Mcleod method (*14, 15*). To use the Van der Poel method, the following properties of the bitumen and the mix must be known:

- Penetration at 77°F,
- Ring and ball softening point,
- Asphalt percentage in the mix or volume concentration of aggregate,
- Time of loading, and
- Age of mix or time in service.

Many of the pavement sections did not have ring and ball softening point data. In those cases, the McLeod procedure was used which requires the following data.

- Penetration at 77°F,
- Viscosity at 275°F or viscosity at 140°F,
- Service Temperature,
- Time of Loading,
- Asphalt percentage in the mix or volume concentration of aggregate, and
- Percent of air voids.

Any set of data that could be used in either of these two procedures was accepted. These data were generally determined from laboratory test results found in construction records. In some cases they were the result of many specific tests made for the project, which was the original intent; however, in other cases, asphalt properties were from asphalt sources tested over the period of time during which the project was constructed.

Mix design properties were taken from quality control records in the construction records in most cases. When these were not available, the mix design parameters were taken from standard mix design requirements in effect at the time of the overlay construction; however, this may add error to the results. Time of loading was selected to represent a moving wheel load of a truck; service temperature was selected based on environmental information for the areas; and age of mix was based on construction date. Availability, or locating, the asphalt cement and mix design properties for the overlay were major problems of this data collection effort.

Characterization of the Existing Pavement Structure

The mechanistic model represents the existing pavement prior to the overlay as a beam on elastic foundation. The stiffness characterizing the surface and foundation support can be determined from deflection testing data on the existing pavement prior to the time of the overlay, in conjunction with layer thickness. A record of construction history was obtained for each section used in this analysis to determine the thickness of each layer and its date of construction; in some cases this was supplemented with coring reports. It would have been beneficial to have had deflection data across a series of cracks in the pavement prior to the overlay to determine the load transfer level; however, those data were not available. Many projects with otherwise usable data were discarded from this project when deflection data could not be located for them.

Climatic Data

The temperature and moisture information defining the climatic zone in which the pavement section is located were described earlier. The 24-hour temperature drop and average monthly temperature were the other two climatic data elements required. They were found in the same sources.

Traffic

Traffic data regarding the average number of 18,000-lb equivalent single-axle loads (ESALs) per day over the life of the overlay were collected from the highway agencies. Where they had some other measure of traffic such as average daily traffic (ADT), their conversion system of converting ADT to ESAL was used. It was then converted to average ESAL per day. Several of the agencies expressed reluctance at providing traffic data because they were not sure of its accuracy.

Performance (Distress)

The mechanistically computed development of cracking is compared to the observed crack development in the regression process. To determine the amount of reflection cracking that developed over time, distress data regarding reflection

TABLE 2 DISTRIBUTION OF PAVEMENT SECTIONS ON WHICH DATA WERE COLLECTED AND USED

STATE	CLIMATIC ZONE 1		2		3		4		5		6		Total	
	AC	PCC	AC	PCC	AC	PCC	AC	PCC	AC	PCC	AC	PCC	AC	PCC
Arizona							03		34				37	
							---		---				---	
							06		43				49	
Arkansas			---	03									---	03
			---	---									---	---
			03	03									03	03
California	02		06				10		02				20	
	---		---				---		---				---	
	02		07				14		04				27	
Florida	---	---											---	---
	---	---											---	---
	09	03											09	03
Georgia			---	03									---	03
			---	---									---	---
			01	03									01	03
Idaho											11		11	
											---		---	
											14		14	
Illinois				20				14						34
				---				---						---
				24				15						39
Minnesota					10	06					03		13	06
					---	---					---	---	---	---
					10	08					03	01	13	09
Texas	01		08				03		24				36	
	---		---				---		---				---	
	01		08				03		24				36	
Utah									03		10		13	
									---		---		---	
									03		11		14	
Washington	07		35	05									42	05
	---		---	---									---	---
	07		36	05									43	05
TOTAL	10		49	31	10	20	16		63		24		172	51
	---	---	---	---	---	---	---		---		---	---	---	---
	19	03	55	35	10	23	23		74		28	01	209	62

Note $\frac{\#\#}{\#\#} = \frac{\text{No. Pavement Sections Used}}{\text{No. Pavement Sections Collected}}$

cracking after the application of the overlay is required. Since the performance used in the mechanistic approach considered damage that varied from zero to one, the distress data had to be transformed into equivalent levels of damage (*18*). Even had this not been required, the data would still have had to be transformed into a common set. Each agency collects distress data in its own form, and virtually no two agencies used the same distress identification system. The distress identification system from each agency was used to develop a conversion similar to that used in the initial program (*3*). The transformations used to convert the distress from each data set into a common damage function are presented elsewhere (*6*).

DEVELOPMENT OF PERFORMANCE CURVE

The observed damage levels over time and traffic were used to develop a mathematical equation to describe the growth of damage, or overlay reflection cracking, with increasing time and increasing number of load passes for each pavement section included in the project. By comparing the mechanistic crack development time with observed time to reach various levels of damage, design equations could be developed for different amounts of allowable reflection cracking.

Two forms of reflection cracking were considered: transverse and longitudinal. It was hoped to use both distress area and severity; however, only distress area was available for many of the in-service pavements. As a result, only area was used for the final equations.

Different forms of equation have been used to fit the observed pavement distress data over increasing time or axle load applications. The following equation was selected for use in the present analysis since it is in accordance with the physical boundary conditions (*18*):

$$g = e^{-(\rho/N)^{\beta}} \tag{6}$$

where

g = the damage rating of the pavement
N = the number of load applications in 18-kip ESALs
ρ,β = characteristic parameters

An equation that relates the damage level of the distressed pavement to the number of load applications is commonly referred to as a structural performance curve. The damage rating of the pavement is a variable that ranges between 0, representing a smooth riding or undistressed surface, to 1, representing a severely damaged pavement structure. Therefore, the performance curve of a pavement will be bounded by 0 and 1. Pavement distress observations show that the performance curve starts out horizontally, bounded from below by a rating of 0. As the number of load applications increases, the curve will asymptotically reach the damage rating of 1. These boundary conditions imply that the functional performance curve should be sigmoidal, or *S*-shaped.

Nonlinear regression analysis techniques were used to develop the performance cures to define a relationship between damage and the number of load applications, N_{18}. This allows the number of applications to be determined at any desired level of damage. Several problems were encountered in using these programs. The nonlinear regression procedures are not always straightforward, especially if the data are not well defined through the entire area defining all parameters in a curve. Thus, there is not always one unique curve that will fit the data points and meet the convergence criteria. Since many of the data sets contained data with damage levels only to levels of 0.1 or less, several sets of regression parameters could be fit through those points and still meet the convergence criteria. Luckily, the major differences in predicted values are above damage levels of 0.5 and have little impact on the results used in this project.

Because some of the distress identification procedures report distress in condition categories, for example, 5 to 15 percent equals distress rating of 2, some of the distress data had plateaus, as illustrated in figure 3. When regression was conducted, parameters could be calculated to define the curve shown as A in figure 4, or another set could be calculated to define the curve shown as B in figure 4. The performance curves for this type of data were forced to follow the shape identified as Curve B in figure 4 because it was believed that the observed data was in the earliest stages of distress development. Allowed to develop further, it is expected that they would develop the *S*-shape defined by Curve B in figure 4.

In some of the in-service pavement sections, no distress had developed at the time of data collection resulting in all zero damage levels. These sections could be ignored; however, ignoring pavements that were performing well would bias the data. To use these data, average ρ and β values for the non-

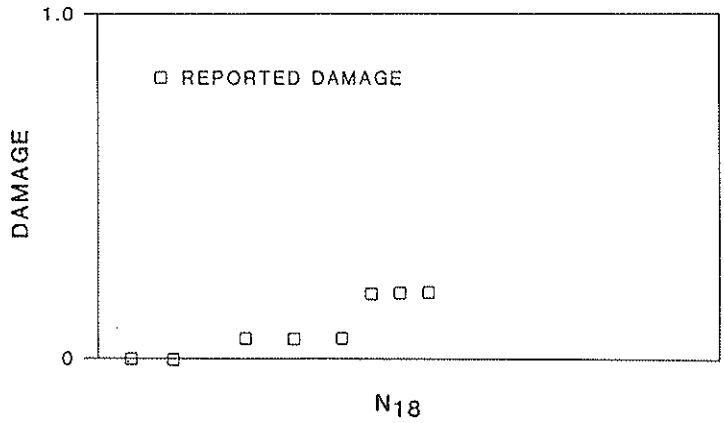

FIGURE 3 Distress data with plateaus.

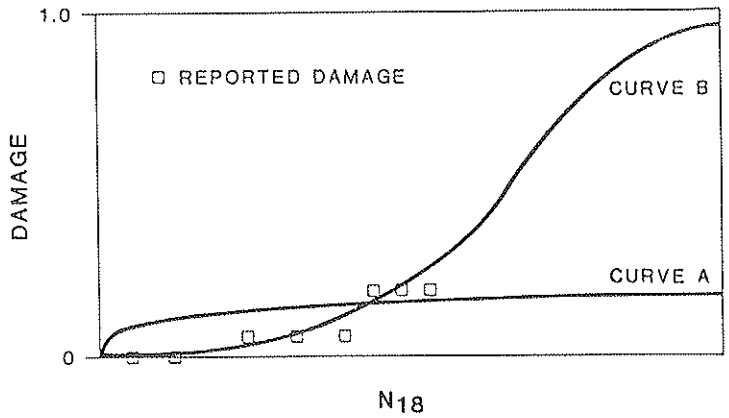

FIGURE 4 Curves fitting data with plateaus.

zero data sets within each climatic/pavement type group were determined. Those values were used to define the curve through the all zero data points, as illustrated in figure 5. If the all-zero points extended to the right of the curve from the average values, the ρ values were increased until the curve extended through all of the reported zero points as shown in figure 5. This allowed the influence of the all-zero points to be included in the analysis.

RESULTS

A final set of design equations to address reflection cracking were developed that allow the designer to select a damage level of 0.33 for a moderate amount of reflection cracking, 0.50 for a high amount, and 0.44 for an intermediate amount. They have been placed in a user-friendly microcomputer program that can be used by highway engineers to determine when reflection cracking is expected to develop in an overlay of desired thickness for different asphalt cement and mix properties. This research has extended the work that began in NCHRP Project ZO-7, Task 17, Phase II, and includes design equations for six climatic regions for asphalt overlays.

This is a major step forward in developing design equations that address the performance problems of asphalt concrete overlays. The best available data was used to calibrate the mechanistic equations; however, they would be more reliable if the data used to calibrate the mechanistic equations were more complete and comprehensive. They can be improved by using more accurate in-service data when it becomes available.

The data used to calibrate the mechanistic equations were collected from agencies with data on pavements of the type needed in the desired climatic zones. The data did not come from a designed experiment, and all the problems inherent in using this type of data are incorporated into these design equations. One of the biggest problems with this type of data is that unknown biases exist, making it impossible to determine the true reliability of the resulting data. In addition, the variability and reliability of the data collected were generally unknown. This does not mean that the equations are unreliable, but it does mean that the reliability of the design equations developed using this type of data cannot be accurately defined.

The mechanistic empirical approach to overlay design has been shown to be feasible and practical. It has also shown the need for collecting accurate data with variability and reliability information included for use in developing mechanistic-empirical equations. The mechanistic empirical approach provides an excellent means to develop design equations that are soundly based on mechanistically correct concepts with a limited number of parameters. However, they will only be as

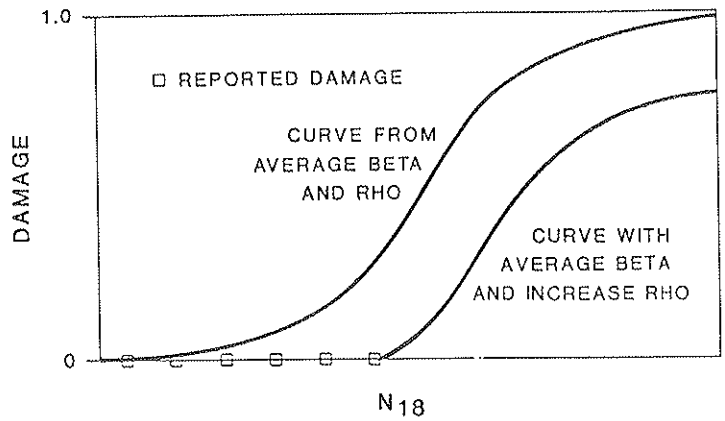

FIGURE 5 Using all zero data points.

good as the data used to calibrate them. Until accuracy of available data is known, accuracy of the resulting design equations will be unknown.

RECOMMENDATIONS

The data collection problems in this and other projects demonstrate the need for a comprehensive centralized data collection effort if mechanistic-empirical procedures are to be used in the pavement engineering field. The data required to calibrate these and other mechanistic empirical design equations should be collected in the Strategic Highway Research Program (SHRP). These data should be collected in a manner to avoid the problems of possible bias and uncertainties that occur in using available data to calibrate mechanistic equations. These data can then be used to update this first set of design equations.

ACKNOWLEDGMENTS

This paper is based on work completed by ERES Consultants, Inc., and the Texas Transportation Institute. The work was sponsored by the Office of Research and Development, Federal Highway Administration. The contracting officer's technical representative was Peter Kopac. The assistance of the several state highway department personnel is gratefully acknowledged.

REFERENCES

1. R. E. Smith, R. P. Palmieri, M. I. Darter, and R. L. Lytton. *Pavement Overlay Design Procedures and Assumptions, Volume I, Analysis of Existing Procedures*. FHWA/RD 85/006, FHWA, McLean, Va., 1986.
2. R. E. Smith, M. I. Darter, and S. M. Herrin. *Highway Distress Identification Manual*. FHWA-RD-79-66, FHWA, Washington, D.C., 1979.
3. P. W. Jayawickrama and R. L. Lytton. Methodology for Predicting Asphalt Concrete Overlay Life Against Reflection Cracking. *Proceedings, Vol 1, Sixth International Conference on Structural Design of Asphalt Pavements*, Ann Arbor, Mich., July 1987, pp. 912–924.
4. *Frost Action in Roads and Airfields. Special Report No. 1*, HRB, National Research Council, Washington, D.C., 1951, p. 123.
5. *Report on Frost: Investigation, 1944–45*. New England Division, U.S. Army Corps of Engineers, U.S. War Department, Boston, Mass., April 1947.
6. P. W. Jayawickrama, R. E. Smith, R. L. Lytton, and M. R. Tirado. *Development of Asphalt Concrete Overlay Design Equations, Vol. 1, Development of Design Procedures*. FHWA, Washington, D.C., 1987.
7. K. Majidzadeh, C. Buranarom, and M. Karakouzian. *Application of Fracture Mechanics for Improved Design of Bituminous Concrete*. Report No. FHWA-RD-76-91, Vol. I, June 1976.
8. K. Majidzadeh, D. V. Ramsamooj, and T. A. Fletcher. Analysis of Fatigue of Sand Asphalt Mixtures. *Proceedings, Association of Asphalt Paving Technologists*, Vol. 30, 1969.
9. K. Majidzadeh and D. V. Ramsamooj. *Development of Testing Procedures and a Method to Predict Fatigue Failures of Asphalt Concrete Pavement Systems*. The Ohio State University Research Foundation, Project RF 2873, March 1971.
10. F. P. Germann and R. L. Lytton. *Methodology for Predicting Reflection Cracking Life of Asphalt Concrete Overlays*. Report No. FHWA/TX 79/09/207-5, March 1979.
11. R. L. Lytton and U. Shanmugham. *Fabric Reinforced Overlays to Retard Reflection Cracking*. Report RF-3424-5, Texas A&M Research Foundation, February 1983.
12. R. L. Lytton and K. H. Tseng. *Laboratory Evaluation of Overlays Reinforced with Fabrics*. Texas Transportation Institute, Texas A&M University, College Station, Tex., May 1983.
13. P. C. Paris and F. Erdogan. A Critical Analysis of Crack Propagation Laws. Transactions of the ASME, *Journal of Basic Engineering*, Series D, S5, No. 3, 1963.
14. C. Van der Poel. A General System of Describing the Viscoelastic Properties of Bitumens and Its Relation to Routine Test Data. *Journal of Applied Chemistry*, Vol. 4, May, 1954.
15. N. W. Mcleod. Asphalt Cements:aPen-Vis Number and Its Application to Moduli Stiffness. *Journal of Testing and Evaluation*, Vol. 4, No. 4, 1976.
16. R. A. Schapery. *A Theory of Crack Growth in Viscoelastic Media*. Report MM-2764-73-1, Mechanics and Materials Center, Texas A&M University, College Station, Tex., 1973.
17. A. A. A. Molenaar. *Structural Performance and Design of Flexible Load Constructions and Asphalt Concrete Overlays*. Ph.D. thesis, Delft University of Technology, The Netherlands, May 1983.
18. R. L. Lytton and A. Garcia-Diaz. *Evaluation of AASHO Road Test Satellite and Environmental Studies*. NCHRP Project 20-7, Task 17, Texas Transportation Institute, Texas A&M University, College Station, Tex., 1983.
19. R. L. Lytton, and G. L. Kohutek. *Evaluation of AASHO Load Test Satellite and Environmental Studies*. Phase II Final Report, NCHRP Project 20-7, Task 17, Texas Transportation Institute, Texas A&M University, College Station, Tex., 1983.

Publication of this paper sponsored by Committee on Pavement Rehabilitation.

Serviceability Index Base for Acceptance of Jointed Concrete Pavements

WILLIAM H. TEMPLE AND STEVEN L. CUMBAA

This paper describes the techniques and relationships developed to design a Serviceability Index (SI)–based measurement system for acceptance of jointed concrete pavement construction in Louisiana. Pavement roughness statistics obtained from Mays Ride Meter equipment, a Surface Dynamics Profilometer, and a Chloe Profilometer were regressed to establish an AASHO Road Test–based SI measurement system for concrete pavements with 20-foot joint spacings (SI JCP 20). A 1986 panel rating of 25 concrete pavements confirmed the validity of the model. Field testing of 50 newly constructed concrete pavement test sections provided a relationship between the SI JCP 20 model and profile statistics from rolling profilograph equipment and a 10-ft rolling straightedge. The research resulted in the development of a rational method of providing specification limits for profilograph equipment that relate to pavement rideability. Specification limits in terms of profile statistics are provided to indicate the quality of paving necessary to construct a jointed concrete pavement with a Serviceability Index of 4.5.

The constructed ride quality of jointed concrete pavements has been the subject of considerable research in Louisiana, generally resulting in the conclusion that roughness that is built into new pavements has increased as transverse joint spacings were reduced. In an attempt to reverse this trend, efforts have been made to establish a level of rideability that is considered acceptable and that is also reasonably constructable. A specification index that can be related to ride quality has been incorporated into a system for determining contractor compliance to the specification limits.

The research contained herein describes techniques and relationships used to accomplish:

- The selection of a specific level of AASHO Road Test based Serviceability Index (SI), which was set as a bench mark for ride acceptability on new jointed concrete pavements and
- The development of mathematical relationships to implement a specification procedure that is manageable under field conditions and utilizes relatively inexpensive but repeatable test equipment. Conversion relationships among a variety of roughness measuring devices were developed to facilitate field determination of the selected SI level for jointed concrete pavements with 20-ft transverse joint spacing. The devices include two different types of rolling profilograph, a Chloe profilometer, a Surface Dynamics Profilometer (General Motors), a Mays Ride Meter trailer system, and a 10-ft rolling straightedge.

Louisiana Transportation Research Center, 4101 Gourrier Avenue, Baton Rouge, La. 70808.

SERVICEABILITY INDEX REQUIREMENTS

Paving specifications for jointed concrete in Louisiana have traditionally been expressed in terms of the percent of project length that exceeds a ⅛-in deviation in 10 feet as measured with a rolling straightedge. Surface tolerance specifications which have allowed up to 6 percent of the length of a project to be out of tolerance have typically resulted in "as constructed" Serviceability Index (SI) levels of between 3.0 and 4.0 for jointed concrete pavements. In an effort to increase the as-constructed SI level the surface tolerance specifications were amended and reduced from 6 percent to 0 percent, as measured with the rolling straightedge. At the same time, a decision was made to set a minimum acceptable SI level and to conduct research necessary to provide a limiting specification index that would produce this target SI.

At the request of the Federal Highway Administration, Louisiana DOTD adopted a target SI of 4.5 for construction of jointed concrete pavements. The basis for selecting this particular serviceability level was that it is an integral part of the assumptions in the current AASHTO design for rigid pavements. Jointed concrete pavements at the AASHO Road Test were constructed to a mean SI of 4.5, which, using equation 1, translates to a slope variance (SV) of approximately 2.2 (*1*).

$$SI = 5.41 - 1.80 \log (1 + \overline{SV}) \quad (1)$$

Flexible (non-jointed) pavement sections from the Road Test were constructed to a mean SI of 4.2, which, by equation 2, translates into an SV of approximately 1.7.

$$SI = 5.03 - 1.91 \log (1 + \overline{SV}) \quad (2)$$

A comparison of jointed concrete and flexible pavement smoothness using slope variance measurements indicates that the non-jointed sections at the Road Test contained less built-in roughness, since lower values of slope variance indicate a smoother pavement. A comparison by SI, however, seems to contradict the slope variance trend, since the jointed pavement was rated higher on a scale of 0 to 5, with 5 being perfectly smooth. This apparent contradiction is attributable to the panel service ratings (PSR) from which equations 1 and 2 were derived. The panel ratings confirm that at equal levels of serviceability rating, jointed-concrete pavements typically contain a greater measure of roughness. A dual method of relating roughness measurements obtained from jointed and non-jointed pavements is, therefore, indicated. This fact is graphically illustrated in figure 1.

Recognition of these trends is necessary for a contracting agency to correctly use AASHO-based SI to establish con-

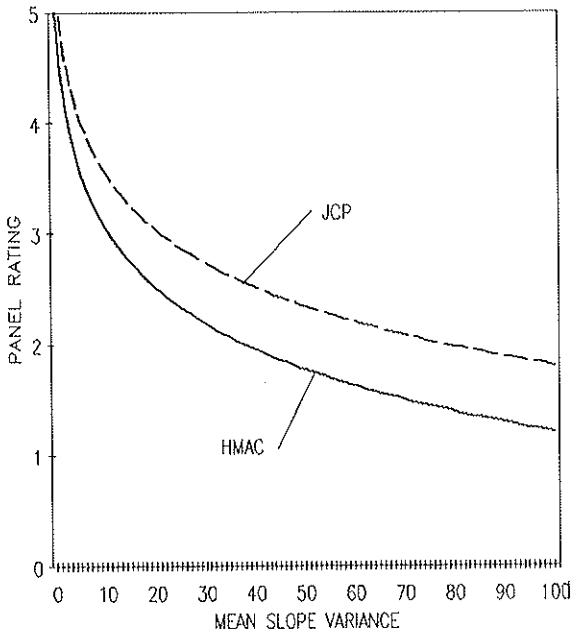

FIGURE 1 Panel rating versus slope variance for rigid and flexible pavements—AASHO Road Test.

struction limits for both jointed and non-jointed pavements to control ride quality.

SERVICEABILITY INDEX FROM FIELD MEASUREMENTS

Research studies since the early 1970s in Louisiana have involved a variety of rolling devices, each designed to provide an index of pavement roughness. The flow chart shown in figure 2 contains an overview of the procedures followed and the relationships between test equipment that lead to an AASHO-based SI measurement system for control of jointed-concrete paving.

A Mays Ride Meter (MRM) trailer system (with a suspension system modified according to Georgia DOT specifications to increase repeatability) provides a convenient means of estimating the SI of a pavement. Since 1975 MRM response measurements have been closely correlated to data from a Surface Dynamics Profilometer (SDP) at the Texas SDHPT using a procedure that relates SI to the inches-per-mile response measurement of the MRM (2). The SI equation indicated in figure 2 is a function of the vehicle ride characteristics of an individual vehicle (expressed as a and b) in conjunction with the MRM response index, inches-per-mile.

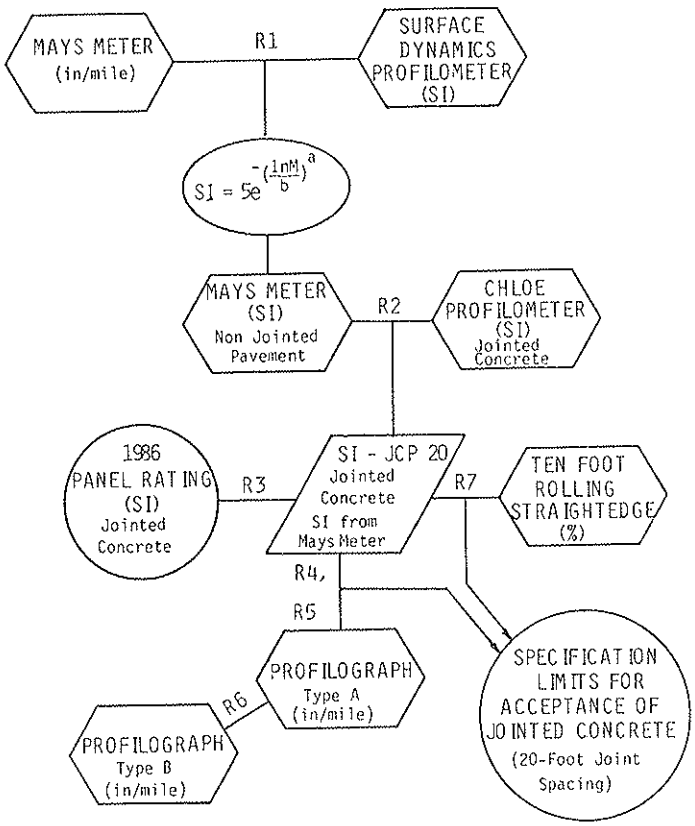

FIGURE 2 Regression relationships (R1–R7) for SI-based acceptance procedure using profilograph equipment.

The test sections used in the MRM-SDP correlation procedure have primarily been flexible, non-jointed pavements. The resulting relationships between the SI and inches-per-mile produced reasonable results when applied to flexible pavements in Louisiana; however, when applied to jointed concrete pavements, the SI predictions seem low. A review of pertinent literature confirmed the need for a dual rating system as previously indicated (*1*).

The Chloe Profilometer provided a mechanism for establishing a relationship between MRM-SDP SI for non-jointed pavements and a MRM-SI for concrete pavements with a 20-ft joint spacing, hereafter referred to as "SI JCP 20." In 1975, a field study of jointed-pavement roughness was initiated to develop the correlation. The results of the testing are presented in equation 3 and in figure 3.

$$[\text{MRM, SDP(SI)}] = 1.54\ (\text{Chloe, SI JCP 20}) - 2.82 \quad (3)$$

The regression analysis was performed in terms of SI values instead of using slope variance (SV) since the SVs of the two pavement types are not equal at a given SI level. Using this relationship, Louisiana DOT was able to implement a dual-rating system with correctly based SI relationships for field testing with MRM equipment, as depicted in figure 4.

PANEL RATING VERIFICATION

In 1986, as a result of the Louisiana Transportation Research Center's (LTRC) participation in NCHRP 1-23(2), a panel rating of 25 jointed-concrete pavements was conducted using 36 raters. MRM tests were also conducted on the rating sections to provide LTRC with an opportunity to verify their SDP-Chloe based SI relationship.

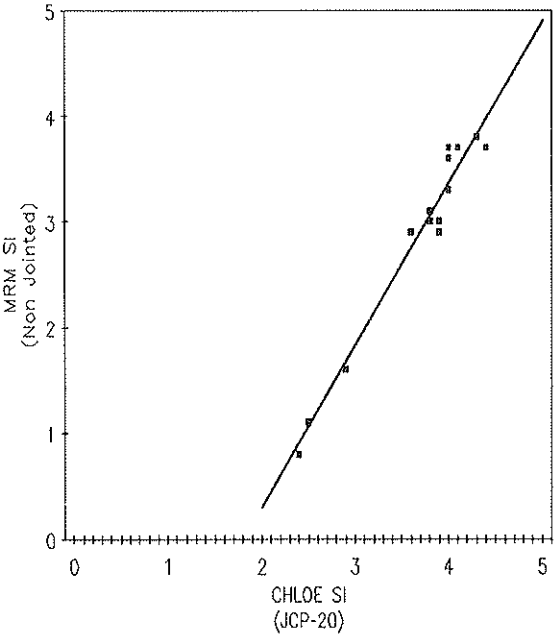

FIGURE 3 Mays ride meter/surface dynamics profilometer SI versus Chloe profilometer SI.

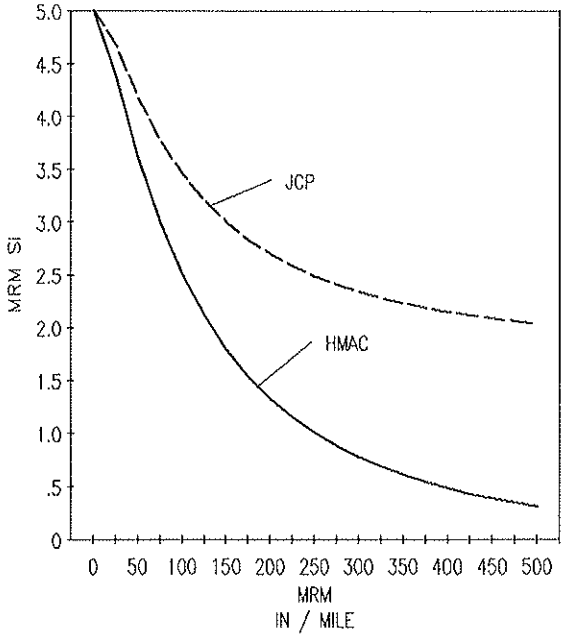

FIGURE 4 Mays ride meter (in/mile) versus SI for rigid and flexible pavements—Louisiana.

The results of the comparison, equation 4, provided a nearly 1:1 relationship between the 1986 panel rating and the "SI JCP 20" measurement as depicted in figure 5.

$$\text{SI JCP 20} = 0.94(\text{Rating}) + 0.19 \quad (4)$$

The SDP-SI (non-jointed) when applied to jointed pavement does not correspond to the 1986 panel rating data without the benefit of a correctly based panel relationship (Chloe) for jointed pavement as expressed in equation 3. This again illustrates the fact that panel raters respond differently to jointed-concrete and non-jointed pavements.

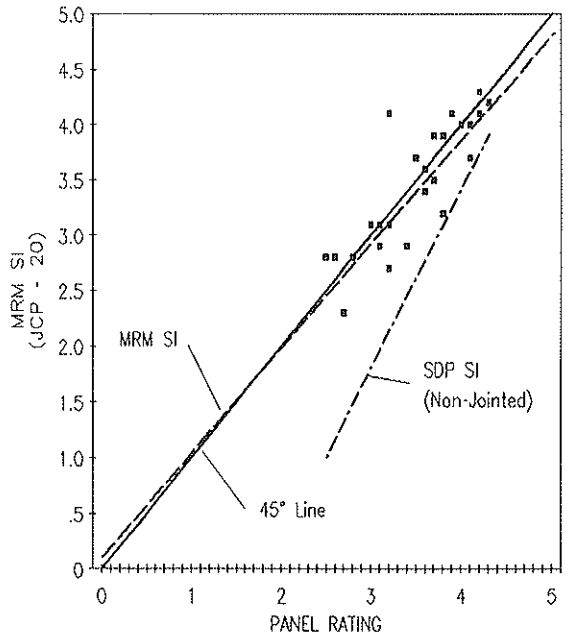

FIGURE 5 SI JCP 20 versus panel rating.

SPECIFICATION COMPLIANCE

Hand-operated rolling equipment can be used to provide construction personnel with verification of specification compliance in a timely manner. Vehicle response type measurement systems cannot be used as effectively to control a paving operation on a day-to-day basis, due to the physical limitations of heavy equipment being placed on concrete pavements that are gaining strength. The hand-operated devices must also provide reproducible results to instill in the users the level of confidence necessary for a successful testing program. Louisiana DOT has traditionally used only the 10-ft rolling straightedge for acceptance testing; however, because of calibration and reproducibility problems, the agency is now phasing in a rolling profilograph for concrete pavement acceptance.

10-FOOT ROLLING STRAIGHTEDGE

The rolling straightedge is a relatively inexpensive test device that can be used to control roughness during the paving process. Research testing with a carefully calibrated straightedge has resulted in a general correlation between "SI JCP 20" and the percentage of a test section that exceeds a ⅛-in deviation in 10 feet, expressed as equation 5 and depicted in figure 6.

$$\text{SI JCP 20} = 2.0 + 2.5\, e^{(-0.10(\%))} \quad (5)$$

Results of the testing indicate that in general a paving level of SI JCP 20 equivalent to 4.5 is possible only where there are zero deviations beyond ⅛-in in 10 feet. Surface tolerance specifications were amended in 1986 to require a "zero percent" specification in an attempt to implement this level of paving quality. Under the new specification, the consequence of non-compliance is surface grinding instead of a provision for contract payment reduction. The success of this approach

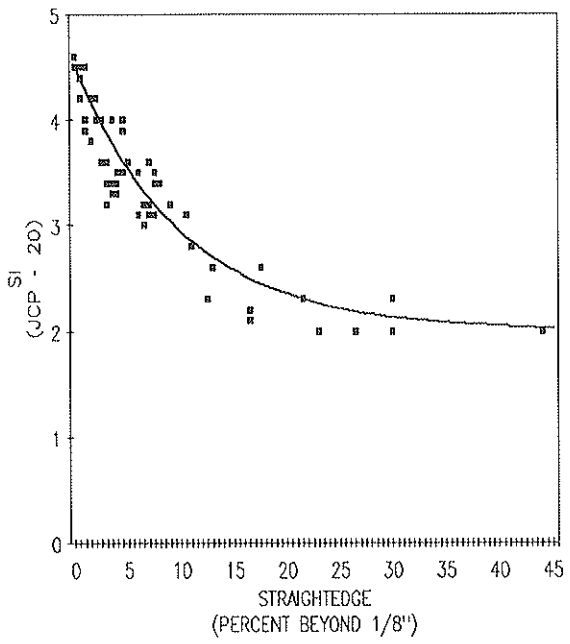

FIGURE 6 SI JCP 20 versus 10-foot rolling straightedge (percent out of tolerance).

in achieving the desired level of serviceability is currently being evaluated. In addition to calibration difficulties, it was observed that two rolling straightedge devices that were pulled together in the same wheelpath occasionally did not identify the same locations as needing grinding. Observations such as these quickly undermine confidence in a specification system that, at times, results in substantial quantities of ride correction on the part of the contractor.

ROLLING PROFILOGRAPH

Research underway using a 25-ft rolling profilograph (Ames model, designated Type A in figure 2) is producing improvements in terms of measurement repeatability and in the interpretation of exactly where ride correction is necessary. The profilograph is styled after the California profilograph in that the axes of the reference platform wheels are not uniformly spaced along the length of the device. Support is instead provided on each end by a group of wheels. Internal equipment calibration prior to testing is apparently not necessary for measurement reproducibility for this device. The pavement profile, which is graphically recorded, can be referenced to determine exactly where grinding is needed. Follow-up testing after grinding can be used to determine the need for additional reduction in the inches-per-mile statistic required for specification compliance.

Profile statistics (inches/mile) were calculated from the profile graphs on 50 test sections (0.2 miles in length) using both a 0.1-in and a 0.2-in blanking band for comparison. The profilograph roughness statistic accounts for only the magnitude of each bump or dip, whereas the rolling straightedge statistic accounts for the length of each deviation beyond a selected tolerance. For this reason profilograph testing on projects that contain many deviations of a small magnitude (such as 0.05 in) will result in a significantly lower summary statistic when using the 0.2-in band. Smoothness specification limits must, therefore, reflect the size of blanking band used to summarize the profile data.

A correlation between profilograph statistics and the SI JCP 20 reference data is depicted in figures 7 and 8 for the 0.1-in and 0.2-in bands, respectively. The equations for the two relationships are expressed as equations 6 and 7.

0.1-in band:

$$\text{in/mile} = 124.5 - 26.4 \quad (6)$$

0.2-in band:

$$\text{in/mile} = -1.9 + 8997.4\, e^{(-1.76(\text{SI}))} \quad (7)$$

The results indicate that to achieve an SI of 4.5, approximate specification limits should be 6 in/mi using a 0.1-in band and 1 in/mi using a 0.2-in band. The 12-in/mi specification limit currently used by several contracting agencies is likely to produce a SI level less than 4.0 using the 0.2-in blanking band relationship.

Another style of profilograph (Rainhart, designated Type B in figure 2) was used to test 18 sections. The device contains 12 reference platform wheels with axes evenly spaced along its length. The two different types of profilograph consistently agreed on the location of bumps and dips, although not to the same magnitude of surface deviation, as indicated by the relationship in equation 8 and figure 9. Specification limits

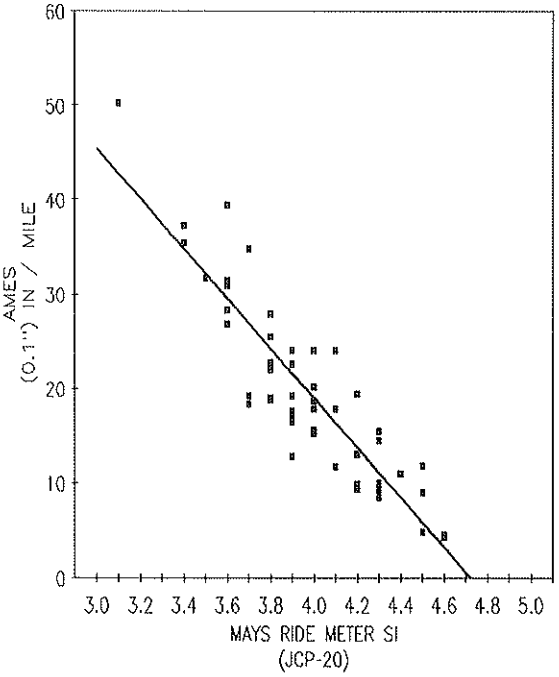

FIGURE 7 Ames Profilograph (in/mile) with 0.1-inch blanking band versus SI JCP 20.

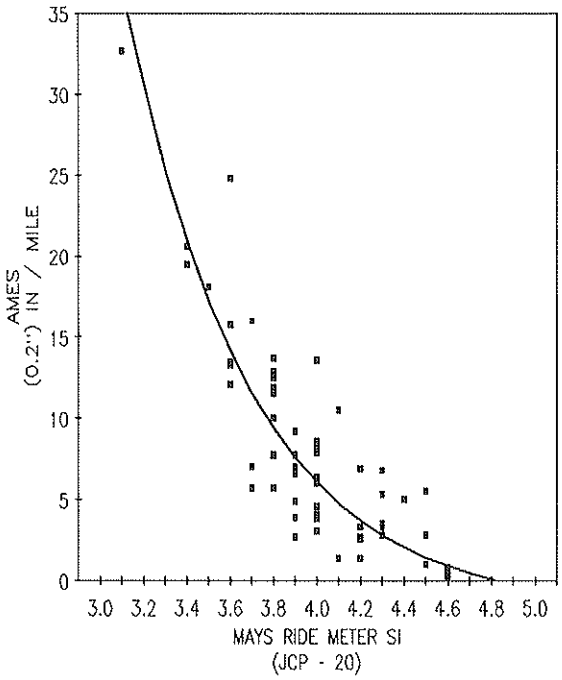

FIGURE 8 Ames Profilograph (in/mile) with 0.2-inch blanking band versus SI JCP 20.

expressed in inches-per-mile must recognize the proper SI equivalency associated with a particular style of profilograph used to conduct field tests.

$$\text{in/mi, Type B} = \frac{\text{(in/mile, Type A)} - 4.18}{1.04}$$

SIGNIFICANCE OF REGRESSION EQUATIONS

Statistical tables indicate that the six regression relationships developed in the study each contain correlation coefficients that are significant at all levels. Variance in test data is expressed as R^2 (coefficient of determination) and s^2 (residual mean square) in table 1.

ADDITIONAL RESEARCH

LTRC is using the rolling profilograph to evaluate roughness in newly constructed jointed concrete pavements to determine among other things:

- The magnitude and frequency of surface deviations typically occurring in paving projects,
- The location of surface deviations with respect to transverse joints created by sawing or by using inserts, and
- The success of grinding as a ride correction technique.

Early indications are that using the 10-ft rolling straightedge as an identifier for grinding does not result in significant improvements in SI measured after ride correction. Additionally, it appears that profilograph and rolling straightedge equipment often do not identify the same locations as needing ride correction.

CONCLUSIONS

1. Rating panels react differently to jointed concrete and non-jointed flexible pavements at equivalent levels of measured roughness; therefore, models used to predict the pave-

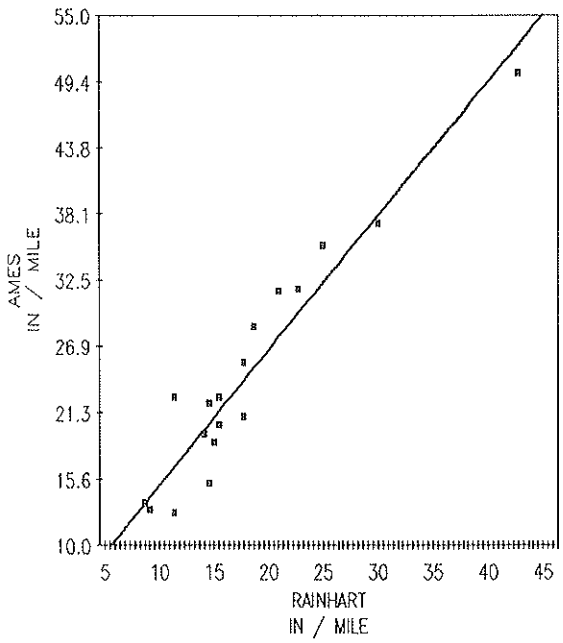

FIGURE 9 Rainhart Profilograph (in/mile) versus Ames Profilograph (in/mile).

TABLE 1 REGRESSION RELATIONSHIPS

REGRESSION MODELS	VARIABLES				STATISTICS	
Referenced in Figure 2	DEPENDENT		INDEPENDENT		R^2	s^2
R1	SI	Surface Dynamics Profilometer (Non Jointed)	In/Mile	Mays Meter (Non Jointed)	0.99	0.32
R2	SI	Mays Meter (Non Jointed)	SI	Chloe Profilometer (JCP 20*)	0.96	0.04
R3	SI	Mays Meter (JCP 20)	SI	Panel Rating (JCP 20)	0.73	0.10
R4	In/Mile	Profilograph - Type A 0.1" blanking band	SI	Mays Meter (JCP 20)	0.79	17.95
R5	In/Mile	Profilograph - Type A 0.2" blanking band	SI	Mays Meter (JCP 20)	0.75	3.03
R6	In/Mile	Profilograph - Type B 0.1" blanking	In/Mile	Profilograph - Type A 0.1" blanking band	0.91	9.43
R7	SI	Mays Meter (JCP 20)	Percent Out	10-Foot Rolling Straight Edge	0.89	0.05

Profilograph
Type A - California Style (Ames)
Type B - Multi-Wheel/Multi-Axle (Rainhart)

*Jointed Concrete with 20-foot Spacing

ment Serviceability Index using the output from response type roughness devices and profilographs need to reflect this fact.

2. Profile statistics from hand-operated profilograph equipment can be related to a selected level of SI for development of specification limits. A contracting agency can use this approach to develop a rational method of specifying a level of ride quality measured with profilograph equipment.

3. Roadway profile measurements obtained from two different styles of profilograph indicate that the devices agree on the location of surface deviations but do not agree on the magnitude of the deviations. The 10-ft rolling straightedge often did not agree with the two profilographs on either the location or the magnitude of surface deviations.

4. A Serviceability Index measurement procedure for jointed-concrete pavements developed from field tests using the Mays Ride Meter, the Surface Dynamics Profilometer, and the Chloe Profilometer was verified in 1986 by a 36-member panel rating.

REFERENCES

1. *The AASHO Road Test—Report 5 Pavement Research*, Special Report 61E, HRB, National Research Council, Washington, D.C., 1962.
2. R. S. Walker and W. R. Hudson. *Correlation Study of the Mays Road Meter with the Surface Dynamics Profilometer*. Center for Highway Research, University of Texas at Austin, February 1973.

Publication of this paper sponsored by Committee on Surface Properties—Vehicle Interaction.

Profilograph Correlation Study with Present Serviceability Index

ROGER S. WALKER AND HONG-TSUNG LIN

Several states are beginning to use roughness measurements from the Rainhart and California profilographs for construction control of rigid pavements. Texas is also considering using the profilograph for such purposes. However, the relationship between the roughness measurements provided by these devices and Present Serviceability Index (PSI), as obtained from the Surface Dynamics Profilometer (SDP), is unknown. Since the initial PSI of pavements is currently used in estimating the life of a pavement, the relationship between roughness measurements from the profilograph and PSI is needed. The other two roughness measuring devices used by the state, the Walker Self-Calibrating Roughness Device (WRD) and the Mays Ride Meter (MRM), have been correlated to PSI. A common measure of roughness, the PSI, is needed for all roughness measuring units to maintain consistent measurements. The paper provides correlations between Present Serviceability Index (PSI), as obtained from the Surface Dynamics Profilometer (SDP), and Profile Index (PI) from the California and Rainhart Profilographs. In addition to the correlations with PSI, correlations are also provided between each profilograph with one another and between roughness data from the WRD. A mathematical model of the two profilographs is provided, and the measuring capabilities of the two profilographs to various road profile frequencies or wavelength components is illustrated.

Several states are using roughness measurements from the Rainhart and California profilographs for construction control of rigid pavements. However, the relationship between the roughness measurements provided by these devices and Present Serviceability Index (PSI), computed from profile data obtained with the Surface Dynamics Profilometer (SDP), is unknown. Since the initial PSI of pavements is currently used in estimating the life of a pavement, the relationship between roughness measurements from the profilograph and PSI is needed.

Texas is considering the use of the profilograph for new construction specifications. The SDP has been used by the Texas State Department of Highways and Public Transportation (TSDHPT) for a number of years for obtaining road profile measurements. These measurements are then used for obtaining PSI. The PSI obtained has been found to provide consistent, objective, and reliable results and is currently used in the state as the standard for roughness measurements. Because of the high use and maintenance costs of the SDP, the less expensive Mays Ride Meter (MRM) and, more recently, the Walker Self Calibrating Roughness Measuring Device (WRD) are currently used in the state for large scale roughness measurements. These two devices are correlated to PSI from the SDP to provide a standard roughness measurement statistic. Since the profilographs may become the standard roughness measuring device for accepting or rejecting new or rehabilitated pavements, a study of its measuring capability was needed.

Department of Computer Science and Engineering, The University of Texas at Arlington, Arlington, Tex. 76019.

STUDY PLAN

The initial study plan of the project was to select 20 to 25 rigid pavement sections 0.2 mi long and to measure these devices with the California and Rainhart Profilographs, the SDP, and the WRD. The profile index of the two devices would then be computed using both a 0.1- and 0.2-in blanking band. The PSI of the sections would also be computed for both the SDP and WRD.

Details on the measuring equipment used and the data sections selected are presented. The equipment used is owned by the State Department of Highways and Public Transportation. Forty-one rigid sections were obtained as opposed to the originally planned 20 to 25. These sections were selected from newly constructed and older rigid pavements in the Beaumont, Angleton, and Dallas areas.

Mathematical models of the two profilographs are developed, and the accuracy of the model is determined by comparing the actual profilograph output and the output predicted. The models could be used to investigate the effects of different roughness wavelengths and amplitudes. Also included are the power spectral estimates of the road profile data of these sections, grouped according to PSI.

The Data Analysis section discusses the correlations performed. These correlations include correlations between the two profilographs for the two blanking bands, correlations between the profilographs and PSI, correlations between the profilographs and the WRD, and correlations between the SDP and the WRD.

MEASUREMENT EQUIPMENT AND DATA COLLECTION

Four different roughness measuring devices were used in this research study: the Surface Dynamics Profilometer, the California and Rainhart Profilographs, and the Walker Self-Calibrating Roughness Device (also known as the SIometer). Forty-one rigid pavement sections, each 0.2 mi long, were selected in three different areas of the state. Each device was used on each section to get roughness measurements.

A brief description of the roughness measuring devices is provided in the next four sections. The pavement sections,

data collection procedures used, and corresponding roughness measurements are given in the last section.

Surface Dynamics Profilometer

The Surface Dynamics Profilometer was originally designed by General Motors and built by K. J. Law Engineers in 1967. The device has, as primary sensors, two accelerometers and two linear potentiometers. The potentiometers are connected to road-following wheels. The accelerometers determine the amount and direction of vertical acceleration undergone by the vehicle while the potentiometers and wheels measure the distance from the vehicle body to the road surface. A profile measurement is calculated by summing the double integral of the accelerometer signal and the displacement signal from the potentiometer (*3*). Recently, two non-contact, or Selcom laser, probes were installed on the SDP, replacing the potentiometer/road-following wheel combination (*7*).

California Profilograph

The California style profilograph used is a 32-½-foot-long mechanical pavement roughness measuring device with 12 wheels, purchased from McCracken Co. The profilograph can be quickly assembled or diassembled so that it can be easily transported from location to location. When used to collect roughness information, it is pushed by an operator at walking speeds. It records roughness traces through a recording wheel at the center of the device. As the profilograph travels, a tracing pen connected to the recording wheel picks up the upward and downward motions of the wheel. The recorded trace (profilogram) usually has a 1-inch = 25-foot ratio in the horizontal direction and actual variation in the vertical direction.

Rainhart Profilograph

The Rainhart Profilograph operates on a similar principle as the California Profilograph. The major difference between these two devices is in the reference plane on which the recording device is supported. The Rainhart Profilograph also has 12 wheels; however, each wheel travels on a different profile path, whereas the California profilograph travels only on three profile paths (the left right wheels on one path, the right four wheels on another, and the third under the recording wheel). The Rainhart Profilograph, with a length of 26 feet 10 inches, is composed of a major body frame and four rigid tripods, each being a rigid frame and wheels at each apex. These four tripods are then connected to the major body of the profilograph through a ball joint support located on the geometric center of the tripods. The recording wheel travels on the center path of the profilograph and records the vertical movement of the recording wheels relative to the body frame.

The profilogram recorded by Rainhart profilograph is processed in the same manner as the California profilogram in order to obtain the Profile Index (*1*). However, a blanking band of 0.1 inch is typically used for Rainhart profilogram in calculation of PI. A similar ruler with a 0.1-in blanking band can be used to count the scallops and to compute the index.

Although a 0.1-in blanking band is typically used when comparing with the California profilograph, for the research effort both a 0.1- and 0.2-in blanking band were used and compared.

Walker Roughness Device

Even though the profilometer produces accurate measurements, it is rather expensive to obtain and operate. Because of this the Mays Ride Meter and, more recently, the WRD are currently being used in Texas for roughness measurements. The WRD provides an estimate of the road profile. From these measurements various statistics can then be obtained. The WRD currently uses slope variance of the predicted profile, which has been correlated to PSI, to determine the serviceability index (SI) of the road. Consideration is also being given to providing other statistics such as RMSVA or the International Roughness Index Statistic.

The WRD consists of three components: a sensor unit, main control module and, optionally, a computer for storing the results. The device uses an accelerometer as its primary sensor. Before using the device for measurements it is driven over a short road section, which is used by the WRD to perform a statistical model of the vehicle's response. The model parameters determined in this dynamic calibration procedure are later used during the measuring process for removing the vehicle's characteristics. Identifying and modeling the current or dynamic vehicle characteristics are referred to as the self-calibrating process.

The WRD, in general, is a compact device that can be installed and operated in virtually any vehicle. It is simple to use and can be operated by one person. It is inexpensive compared to the SDP and is not much more than the cost of the MRM with trailer.

Data Collection Procedures

Forty-one rigid pavements sections 0.2 mile long were selected for the research. These sections were selected from roads in the Angleton, Beaumont, and Dallas areas of Texas. Each section was run by all four roughness measuring devices. The general geographical section location and name given to each section can be found in Walker and Lin (*7*).

The time and effort required to assemble and dismantle each profilograph, as well as to operate them (such as traffic control, etc.), played a major role in selecting the sections. Additionally, attempts were made to select sections that had various levels of roughness, although more sections were selected for the newer and smoother sections. The larger number of smoother sections were selected, as one of the major interests in the study was to determine the relationship between PSI and profile index for control of newly constructed pavements. Some older and rougher sections were selected, however, so that a broader comparison could be made in correlating the devices with one another and to provide boundary points for the models.

Table 1 provides a matrix of the processed measurement values. The table provides the profile index of each profilo-

TABLE 1 VALUES OF PROCESSED MEASUREMENTS

SECTION NAME	SDP PSI	PROFILOGRAPHS				WRD	
		CALIFORNIA		RAINHART		SV	SI
		BB=0.1	BB=0.2	BB=0.1	BB=0.2		
A1A	2.11	111	93.3	81.07	77.14	2835	2.12
A1B	1.84	70.75	60.75	47.25	26.5		
A2A	4.44	7	3	2.5		176	4.33
A2B	4.22	5	2.25	1.75	0.75	232	4.11
A2C	4.21	10.5	4.25	2.75	0.25	249	4.05
A2D	4.28	10.75	3.75	3.25		245	4.06
A2E	4.32	4.75	2	2.75	0.5	205	4.27
A3A	4.17	10.25	2.25	3.5	0.5	205	4.27
A3B	3.99	12.25	7	5.56	1.4	81	3.89
A3C	4.1	13	4.5	4.25	0.5	192	4.26
A3D	4.22	14.75	9.5	7	1.5	148	4.46
A3E	4.16	11.5	2.75	3.75	0.25	169	4.36
A4A	3.88	15.5	6	6.25	0.5	254	4.04
A4B	4	11.25	5.25	3.25	0.25	227	4.12
B1	2.68	51.5	42.25	45.25	27.75	811	3.11
B2A	2.71	78.5	61.5	53.25	37.8	1601	2.57
B2B	3.11	73	55.5	50.5	34.8		
B2C	2.63	78	63.75	56	40	2433	2.24
B3A	2.9	38.5	26.25	32.5	12.5	934	3
B3B	2.87	44.25	29.75	34.5	9.75	764	3.16
B3C	2.73	39.75	26.5	27.5	13.25	612	3.34
B4	2.16	90.5	72.25	60.25	39.5		
B5	3.49	34.5	23.5	17.75	8	555	3.41
B6A	3.6	31.5	21.25	17	7.75	539	3.44
B6B	3.84	35	24	27	8.25	554	3.42
B7A	3.01	42.25	24.5	17.75	7.5	1006	2.94
B7B	3.03	42.75	28.25	26.25	13.75	757	3.17
B7C	3.16	46.75	30.5	22	7.5	724	3.2
B8A	3.21	30	19.5	15.75	9.5	688	3.24
B8B	3.14	28	17.5	13.25	10.5	453	3.58
B8C	3.22	26	18.75	13.6	5.5	631	3.31
D1A	3.79	19.5	11.5	9.75	2.75	524	3.68
D1B	3.7	22.5	12.25	10.25	2.25	1521	3.6
D1C	3.85	18.75	12	10.5	3.5	1120	3.85
D1D	3.9	21	16	9.75	1.25	651	3.92
D1E	4.02	18.75	9.75	8.75	2	302	4.02
D2A	4.51	10.75	5	3.25	2.5	295	4.37
D2B	4.58	9.25	3.75	1.5	1.25	204	4.5
D2C	4.54	6.25	1.75	1	0.25	180	4.3
D2D	4.15	18.5	9.75	7	3.25	317	3.93
D2E	3.97	17.25	9	6	1.75		3.64

graph for the 0.1- and 0.2-in blanking bands. The profilographs were run only once on each section. The PSI readings from the SDP are the average of two and three readings. The average of three runs was used for the WRD except for the Beaumont sections. For these sections, only one run was made. The slope variance readings from the WRD are unscaled (the WRD provides these values along with SI). Measurements from the WRD were made at 50 mph. Since three of the sections could not be used at this speed only 38 sections were used for the WRD data.

PROFILOGRAPH MODEL DEVELOPMENT

The Rainhart and California profilographs operate mechanically in a very similar fashion to measure pavement roughness. In order to understand better the mechanical behaviors of the profilographs, two mathematical models were built to simulate the operation of the measurements. With the flexibility of these two models, the responses of the models with respect to various profiles can be investigated.

Mathematical Modeling of Profilographs

With the information supplied by manufacturers and physical inspections of the profilographs, two mathematical models have been implemented such that, given an exact road profile, they will produce profilograms as in real measurement from the profilograph device. The following assumptions were adopted during the development of both California and Rainhart profilograph computer models:

- All structural connections are perfect rigid connections. This is true since all connections on the profilograph are reinforced.
- Since hinge joints are designed with bearing on the profilograph, all hinges and pivot joints are assumed to be perfect pin connection structures such that no friction occurs. All wheels are also assumed to have frictionless bearings.
- The profilograph is made of linear elastic material.
- The profilograph starts from a self-equilibrium state in the vertical direction, and it remains in this condition throughout the operation stage.
- The profilograph moves at a slow speed (usually less than 2 mph) such that dynamic effects can be neglected; in other words, the mass (inertia) effect of the profilograph structure is ignored.
- All wheels of the profilograph makes continuous contact with the road. In addition, a point (knife-edge) contact assumption for all wheels is adopted in the computer models. Each wheel can travel on a different profile.

With the above assumptions, the profilograph can be modeled as a skeletal-frame system. Detailed discussions of the

development of the profilograph models are given in Walker and Lin (*7*).

Verification of the Mathematical Models

Two mathematical models for the California and Rainhart profilographs were developed in accordance with the assumptions in the preceding section. They are later investigated by comparing their response to profile data measured with the SDP. The actual profilograph traces taken from the same sections are compared to the model's predicted traces. Several recordings have been made using both profilographs. Since it is difficult to get all profiles under each wheel of the profilograph for the model, the same profile measured and computed from the SDP will be used as the real profile for all wheel paths. This assumption can be justified when the sections measured have smooth lateral profiles. Furthermore, the path of the profile recorded by the SDP is carefully aligned with that of the recording wheel of the profilograph, since the profile under this wheel has a direct influence on the results produced by the model.

Figure 1 shows a recording from the California profilograph, SDP measured profile, and the result generated from the mathematical model. The profiles computed from the SDP are also shown in the corresponding figures (the SDP computes two profiles in one run. The right wheel profile from the SDP is the one coinciding with the path of the recording wheel of the profilograph). It should be noted that the profile recorded by the SDP is in digital discrete form such that there are some minor discrepancies compared with the analog recording from the actual profilographs. The results presented are computed using profile from the SDP for sample rates of 2 samples per foot. The Profile Index is also computed for each result using a 0.2-inch blanking band for the California device and 0.1-in for the Rainhart profilograph. The calculation procedures for PI follows specification as described by Georgia Highway Department and by State of California Department of Public Works (*1, 4*).

Inspection of the results reveals that the mathematical model produces a trace similar to the profilograph recording. The accuracy of the discrete profile fed into the model is the major factor influencing the results. That is, the greater the sample-per-foot resolution of the profile data used, the better the comparison. The better results were found as the sample rate of the profile data was changed from 2 to 10 and 20 samples per foot. Another factor influencing the accuracy is the fact that the models assume a point-contact wheel as compared to rubber wheels used in the actual device. The latter acts as a filter that smooths out some of the micro behavior of what the models predict. The models were used to compute the profile index for all 41 sections and compared to the actual measurements. In general, the results from the computer model are comparable to the real profilograph recordings.

Frequency Response Study Using the Model

In order to understand the behavior of these two models, a profile of unit-amplitude sine function for all wheel paths is fed into the models, and the simulated recordings are generated. That is, the function $P(x) = \sin(2\pi x/\lambda)$ is used for each wheel, where λ is the wave length or period of the sine function.

Figure 2 shows the simulated recordings from two profilograph models for unit amplitude sine function profiles with a wave period equal to 390 inches. Figure 3 shows the same results but with a sine function of shorter wave period, or 195 inches. It is noted that the maximum amplitude produced depends on the period of the input sine function. In Figure 2, the California model produces a higher peak amplitude than the Rainhart profilograph model. However, the situation

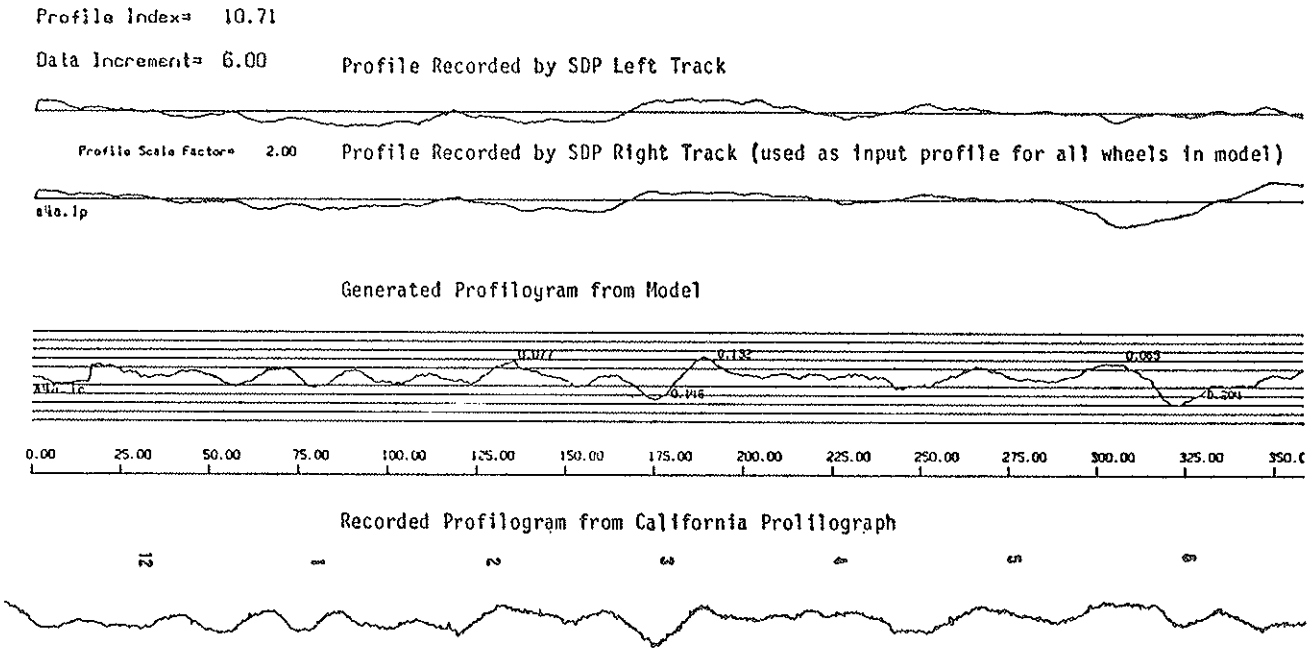

FIGURE 1 Computed and recorded profilograms for California profilograph.

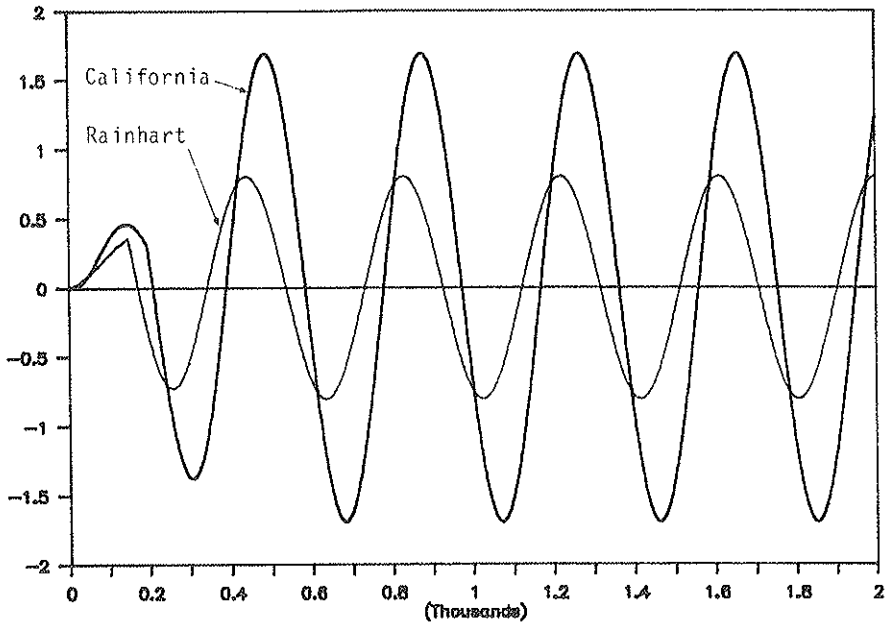

FIGURE 2 Responses of unit sinusoidal profile (period = 390 inches).

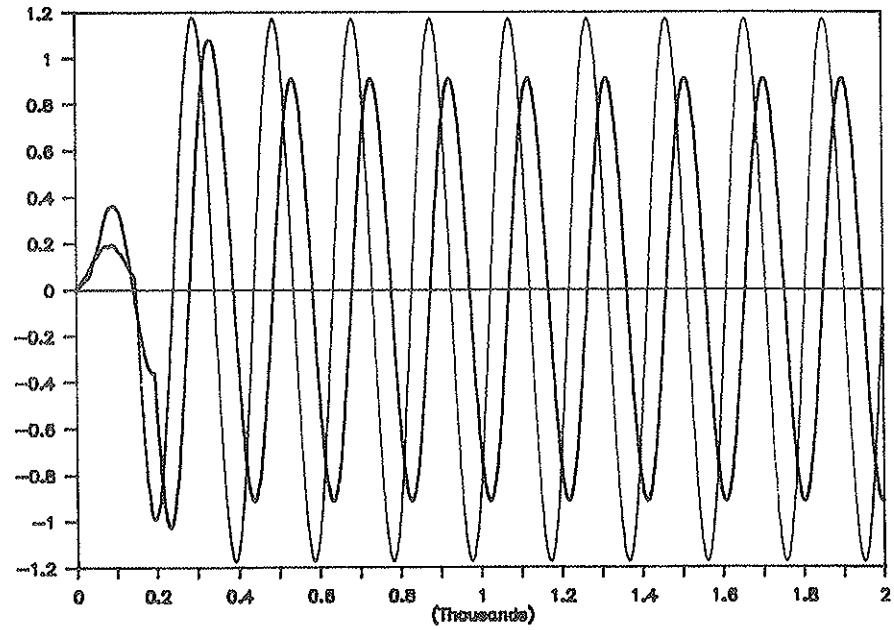

FIGURE 3 Responses of unit sinusoidal profile (period = 195 inches).

is reversed in the shorter wave period case, as shown in Figure 3.

The models can be used to investigate the response of the profilographs under various profile wavelengths. Figures 4 and 5 depict the maximum amplitude recorded from both models under sinusoidal style profiles of unit amplitude but with different wave periods. It is interesting to note that the models, and thus the actual profilographs, show amplification and attenuation with respect to different wave lengths. Since the model uses a point contact wheel assumption, it generates a profilogram even for very small wavelengths. In the actual profilograph device, wavelengths shorter than the wheel-pavement contact length cannot be measured. It is difficult to estimate the exact wavelength for this cut-off region. However, results of wavelengths greater than, say, about 0.2 feet should closely resemble the actual profilograph output.

Also note that the maximum amplitude recorded can reach as high as twice (approximately 1.9) the input sine wave amplitudes for the two models. However, the position of these peaks occurs at different sine wave periods for different profilographs. Since the Rainhart profilograph has equal wheel adjacent distance in the longitudinal direction, the maximum amplitude predicted could reach as high as twice the input amplitude when the wave period matches the wheel patterns.

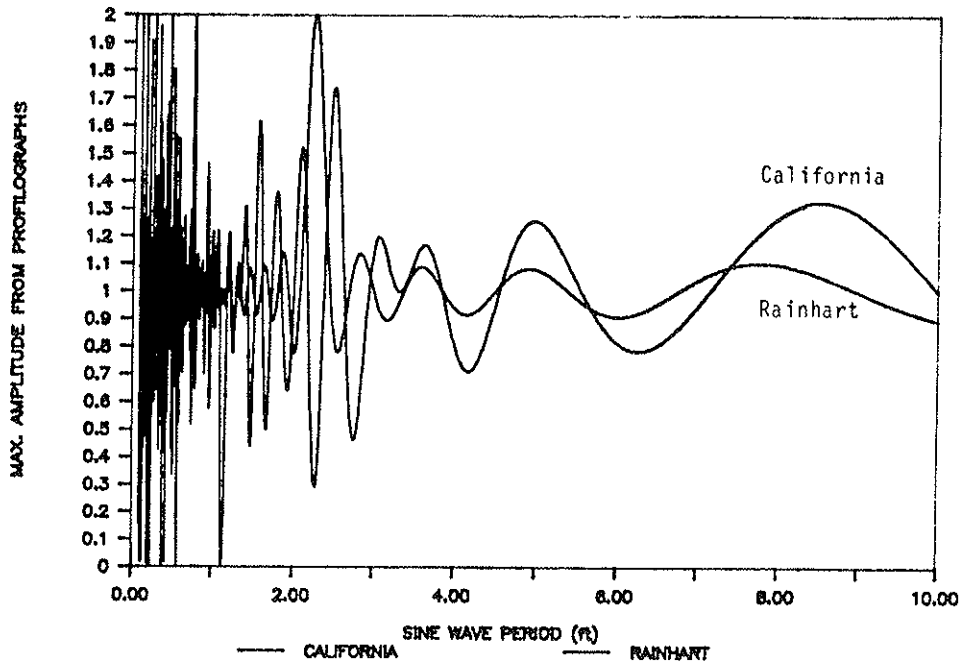

FIGURE 4 Frequency responses of profilographs.

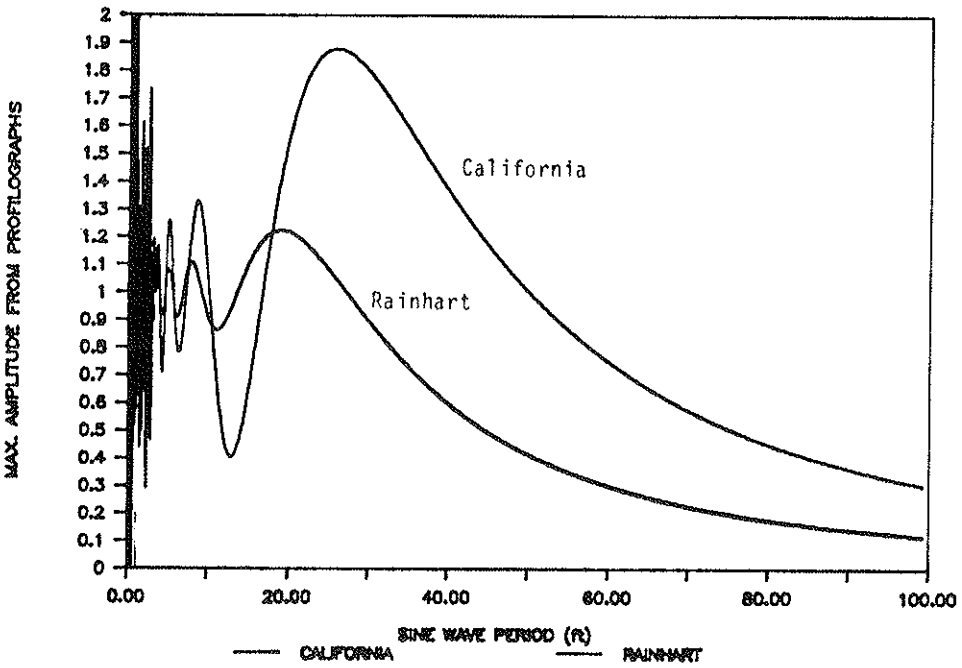

FIGURE 5 Frequency responses of profilographs.

As the wavelength increases beyond 25 feet (20 feet for Rainhart device), both models predict smaller maximum amplitude. It is also observed that the maximum amplitude recorded decreases smoothly for waves with lengths greater than the profilograph. At a wavelength of 100 feet, it records about 35 percent of the input wave amplitude for the California profilograph and about 15 percent for the Rainhart profilograph. One other observation is of interest. For wavelengths above about 18 feet, the California device response is greater than the Rainhart device. This might account for the different blanking band requirements in order to get similar amplitude results.

Spectral Analysis of Pavement Profiles

The power spectral estimates of the road profiles, in conjunction with the frequency response of the profilographs,

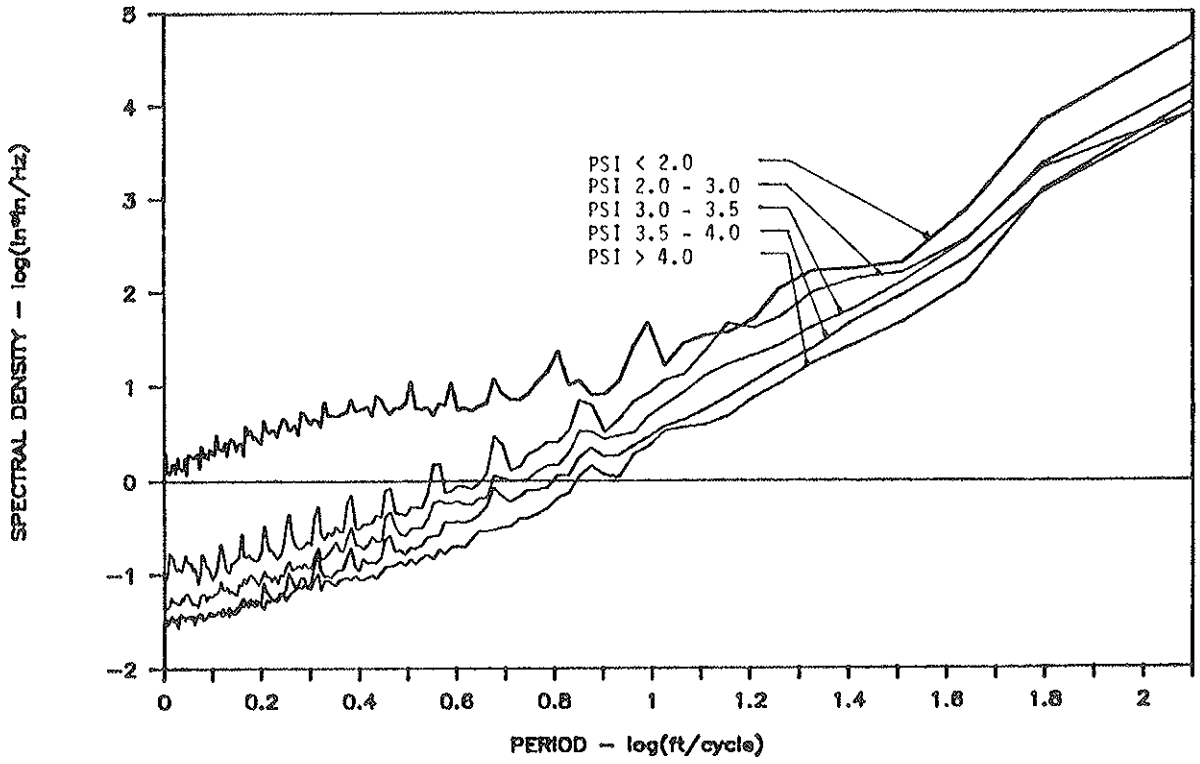

FIGURE 6 Pavement spectral density.

could be useful in investigating the measurement capabilities of the profilographs. For example, it is noted that the profilographs will underestimate some frequencies and overestimate or exaggerate others. If the sections investigated in this or other studies represent the population of rigid pavements and the profilograph measurement effects are well correlated to ride, then the devices would be useful for construction control. On the other hand, if a new construction method adds frequencies in the range that is over- or underestimated, then undesirable results could be obtained.

The power spectral estimates were run on all 41 sections and the average power presented in plots for various roughness classes in Figure 6. These estimates could be useful in comparing the road frequencies with the way the profilographs measure the various profile wavelengths. Also, the response of the statistics used in determining the PSI values from the SDP, RMSVA, and slope variance values from the WRD could be investigated. These results are included to indicate a future research area.

DATA ANALYSIS

In this section the data collected will be correlated and presented. First, a comparison between the Rainhart and California profilographs will be shown. This comparison will include the Rainhart versus California units for 0.1- and 0.2-in. blanking bands. Also each profilograph will be compared with the other for each of these two bands. The two profilographs will then be compared with PSI from the SDP. This comparison will include all sections, then only those with a profile index less than 20, since this is in the range where most new pavement construction would likely fall. A comparison between the WRD and the two profilographs is given. Finally, a comparison between the WRD and SDP is presented. Table 2 provides the equations for the linear regressions used.

California versus Rainhart Profilographs

As indicated earlier, profile indexes from the 41 sections were computed for both profilographs and for both the 0.1- and 0.2-in blanking bands. A simple linear regression was computed for each combination (the regression coefficients are given in Table 2). The correlation coefficient and standard error of regression are indicated. The independent variable used for each case is the variable along the x-axis, although no reason was used in selecting one particular variable over the other as the independent or dependent variable.

Figure 7 illustrates the relationships between the California profilograph using the 0.1-in blanking to the 0.2-in blanking. As previously discussed, the currently accepted practice has been to use the 0.2-in blanking band when computing the profile index for the California profilograph. As one would expect, there is a high correlation between these two plots: an R^2 of 0.99. The 2.38 standard deviation reflects both the differences in the measurement process and the human errors in computing the profile index. The measurement error in the reading of the profile index from the charts was typically about one profile index value.

Figure 8 depicts the relationship between the 0.1- and 0.2-in blanking bands for the Rainhart profilographs. As can be noted, the correlation and standard error of regression is not as good, 0.91 and 4.78 respectively. This difference could

TABLE 2 COEFFICIENTS OF REGRESSION MODELS

Dependent Variable	Independent Variable	Regression Constant	Coeff. Linear	Standard Err.	R Squared
CPI_0.2"	CPI_0.1"	-5.275	0.8577	2.379	0.989
RPI_0.2"	RPI_0.1"	-4.052	0.7642	4.783	0.911
RPI_0.1"	CPI_0.1"	-4.710	0.7537	3.670	0.966
RPI_0.2"	CPI_0.2"	-4.352	0.6829	4.517	0.921
RPI_0.2"	CPI_0.1"	-7.789	0.5804	5.220	0.894
RPI_0.1"	CPI_0.2"	-0.024	0.8764	3.344	0.972
PSI	CPI_0.1"	4.629	-0.03881	0.2230	0.742
PSI	CPI_0.2"	4.443	-0.04762	0.2335	0.705
PSI	RPI_0.1"	4.477	-0.06946	0.1907	0.824
PSI	RPI_0.2"	4.255	-0.1111	0.2632	0.628
PSI	SCPI_0.1"	5.199	-0.3147	0.2789	0.856
PSI	SCPI_0.2"	4.819	-0.3049	0.2799	0.855
PSI	SRPI_0.1"	4.771	-0.3161	0.2835	0.852
PSI	SRPI_0.2"	4.344	-0.3118	0.3403	0.786
WRD_SI	sqrt(CPI_0.2")	4.765	-0.2897	0.1933	0.901
WRD_SI	sqrt(RPI_0.1")	4.696	-0.2920	0.2119	0.882
PSI	log(WRD_SV)	8.432	-1.8281	0.2246	0.882

Note:

CPI: California Profile Index SCPI: Square root of CPI
RPI: Rainhart Profile Index SRPI: Square root of RPI
PSI: SDP Profile Service Index
WRD_SI: WRD Serviceability Index
WRD_SV: WRD Slope Variance (unscaled)

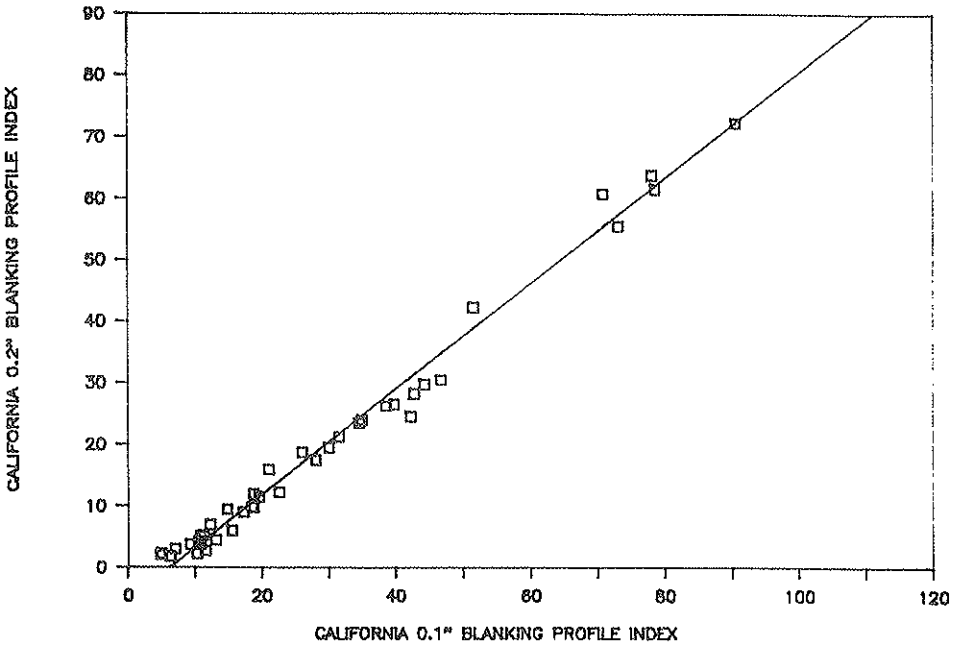

FIGURE 7 California 0.2-in versus 0.1-in blanking band profile index.

likely be explained by recalling the frequency response characteristics illustrated in Figure 4. Recall from this figure that the California device gave a much greater response to many of the frequencies than the Rainhart device, almost twice as much in some cases. This greater sensitivity to roughness values could account for the correlation differences. For example, one would expect a similar, or even poorer, correlation if 0.2- and 0.3-in blanking bands had been used for the California device. The 0.2-in blanking band does not measure as much roughness.

Figures 9 through 12 show the correlations between the two devices for each blanking band. Figure 9 illustrates the differences between the California and Rainhart devices for a 0.1-in blanking band and Figure 10 for the 0.2-in blanking band. Figure 11 illustrates the 0.1-in blanking band for the California vs. the 0.2-in blanking band for the Rainhart, and figure 12 illustrates the reverse. Notice that the California 0.2-in blanking band versus the Rainhart 0.1-in blanking band provides the best correlation and standard error of 0.97 and 3.34. The 0.1-in vs. 0.1-in blanking bands in figure 9 also has a 0.97 correlation but a slightly higher standard error, 3.67. However, when the 0.2-in blanking band is used for the Rainhart device the correlation and standard error get worse.

From these results, the standard practice of using a 0.1-in blanking band for the Rainhart device and a 0.2-in blanking band for the California device appears to be the best com-

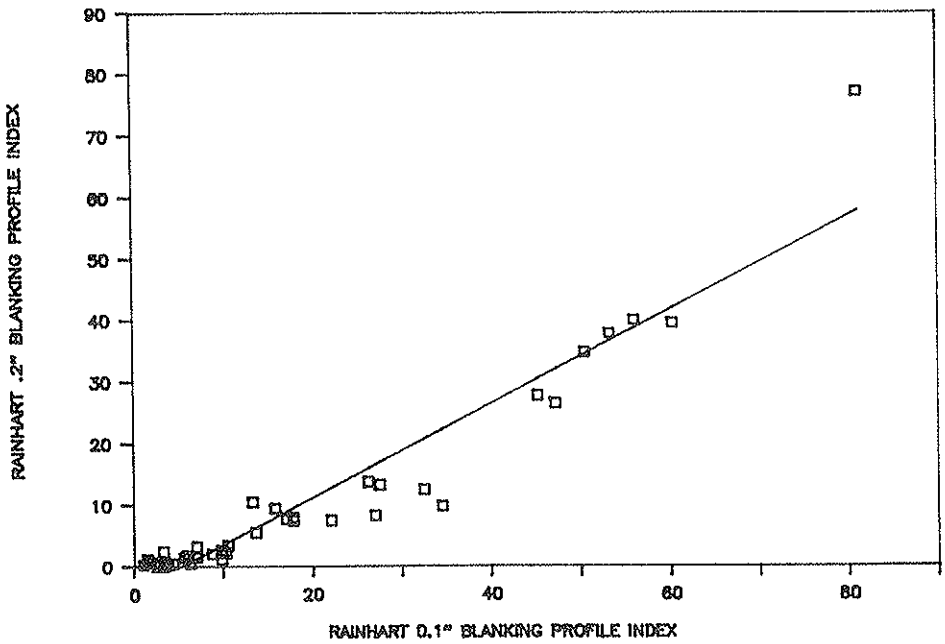

FIGURE 8 Rainhart 0.2-in versus 0.1-in blanking band profile index.

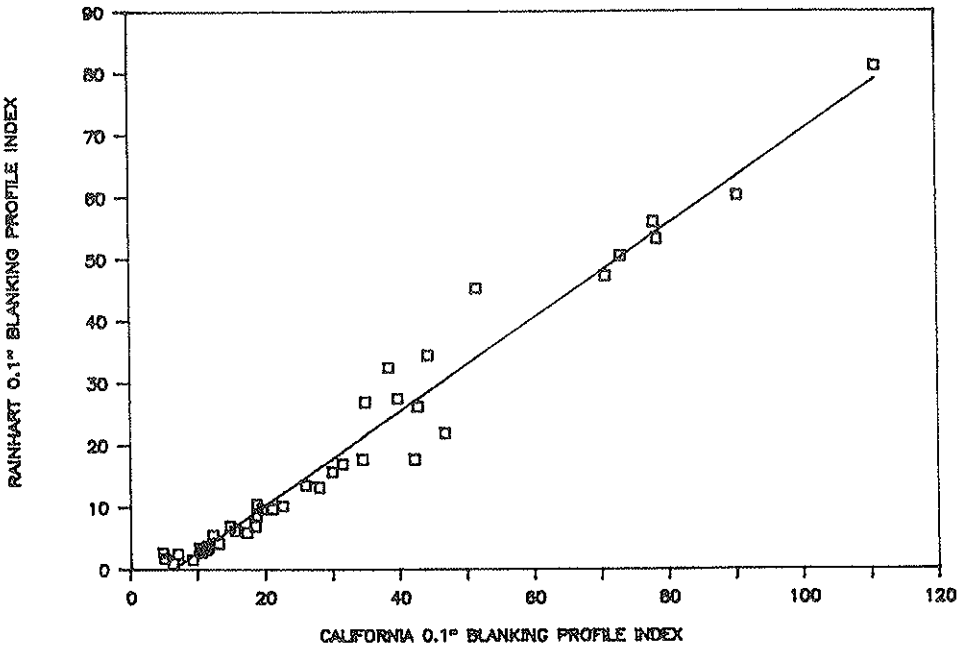

FIGURE 9 Rainhart 0.1-in versus California 0.1-in blanking band profile index.

bination. The 0.1-in blanking band used for the California unit gives close to the same results as the 0.2-in blanking band; however, the 0.2-in blanking band used for the Rainhart profilograph appears to lose too much roughness information.

California and Rainhart Profilograph versus PSI

Figures 13 through 16 provide relationships between PSI from the SDP and profile index for all sections used and for both profilographs and blanking bands. Figures 17 through 20 provide similar information, except that a square root transformation has been applied to the PI values and a regression performed with PSI. From these figures it is noted that the California 0.1-in and 0.2-in blankings give the same results (RSQ = 0.86 and STD = 0.28). The Rainhart 0.1-in blanking, once again, appears superior to the 0.2-in blanking as the R^2 drops from 0.85 to 0.79. The variation between PSI and profile index is greater for the rougher sections, as one would expect. Figures 21 through 24 provide relationships of

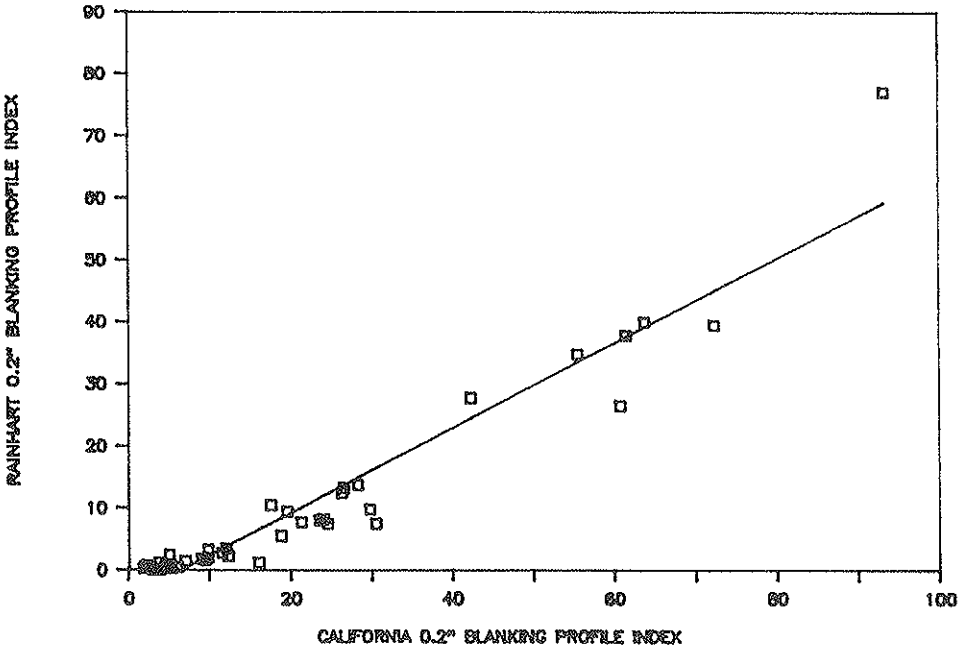

FIGURE 10 Rainhart 0.2-in vs. California 0.2-in blanking band profile index.

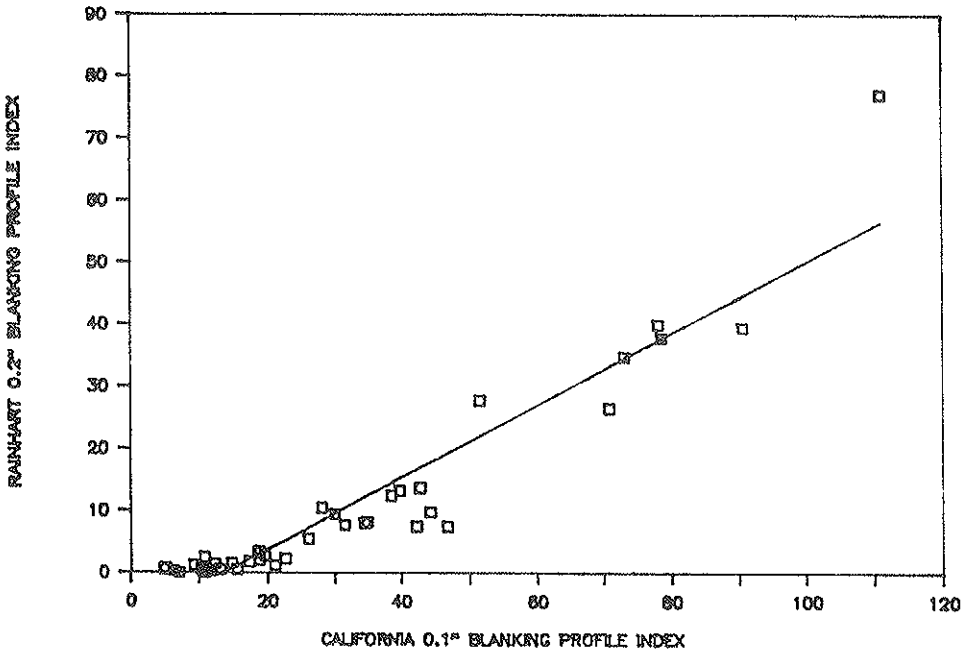

FIGURE 11 Rainhart 0.2-in vs. California 0.1-in blanking band profile index.

the smoother sections, or those with a profile index of 20 or less, as measured using the 0.2-in blanking band on the California profilograph. This range was selected, as the greater use of the profilograph has been in construction control for new pavements where pavements with a profile index of 12 or less are usually considered acceptable. The 0.2-in blanking band data of the Rainhart device once again gave the poorest results. However, the 0.1-in blanking band for the California unit gave somewhat better results than the 0.2-in blanking band. As previously indicated, the same set of sections was used in all cases. The Rainhart 0.1-in blanking gave the better results.

In these figures, a linear regression was performed between PSI and profile index. The regression line is shown along with the 90 percent confidence bands. It should be noted that, in regression, the independent variable is the one considered with the least error. If the PSI is the standard, then one might want to regress the other way or use an inverse regression. Since we wanted to examine the standard error of the PSI values, and were really not sure which had the least error,

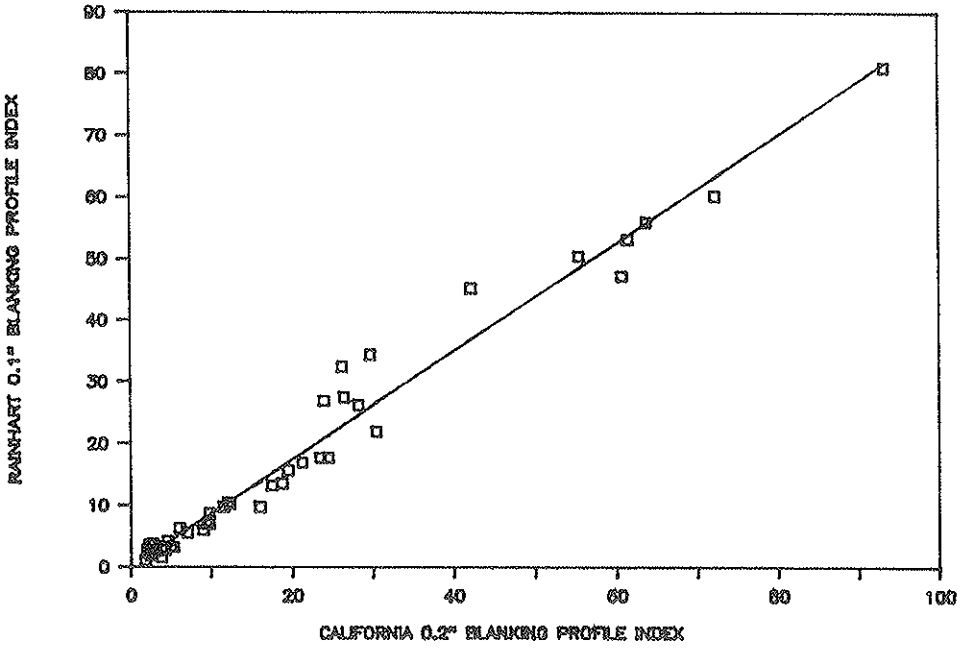

FIGURE 12 Rainhart 0.1-in vs. California 0.2-in blanking band profile index.

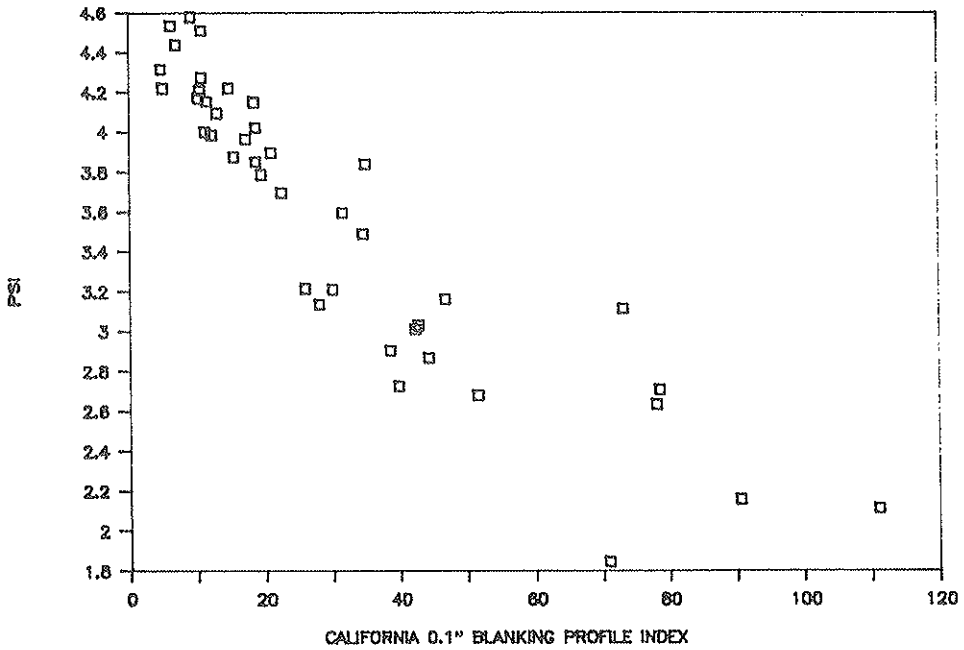

FIGURE 13 PSI vs. California 0.1-in blanking band profile index.

the regression was performed as indicated. From the figures, the range of profile index values for various PSI values can be investigated.

California and Rainhart Profilographs vs. WRD

Figures 25 and 26 provide the correlations found between SI predicted by the WRD and profile index. Only the profile index values using the 0.1-in and 0.2-in blanking bands are given. The others were slightly less correlated as found above. As also noted in Chapter 2, not all the sections were included. The SI values shown are obtained from the regression performed in the next section, relating the WRD slope variance statistic to PSI. As noted, a slightly higher correlation was obtained between SI from the WRD than PSI with the SDP (0.88 vs. 0.86 for the California). An R^2 of 0.91 was obtained when the slope variance statistic was correlated directly to the profile index from the California profilograph. The SI values currently used with the WRD are those modeled from flexible pavements. Since the PSI model for the SDP is different for flexible and rigid pavements, these SI values were not used.

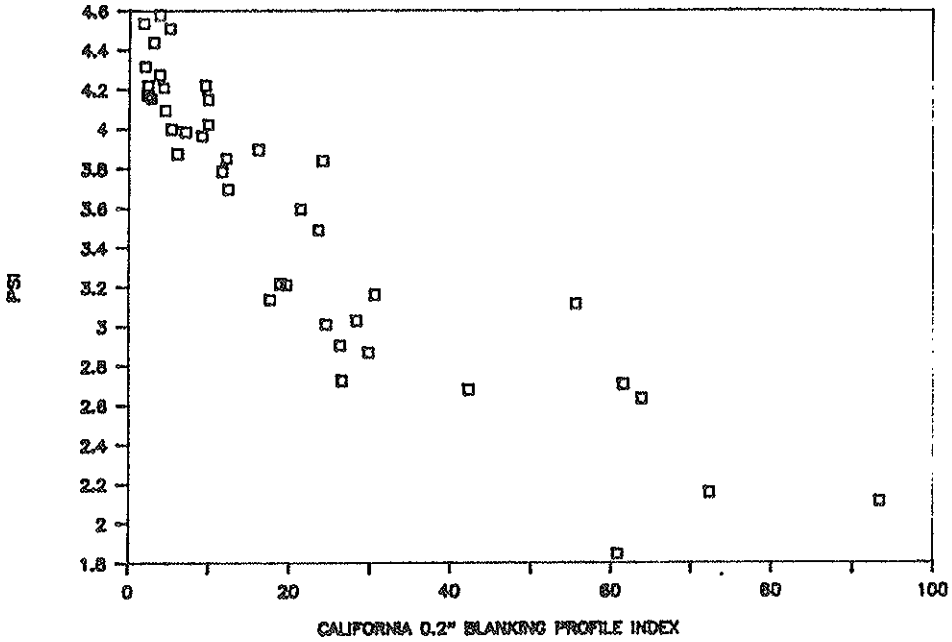

FIGURE 14 PSI vs. California 0.2-in blanking band profile index.

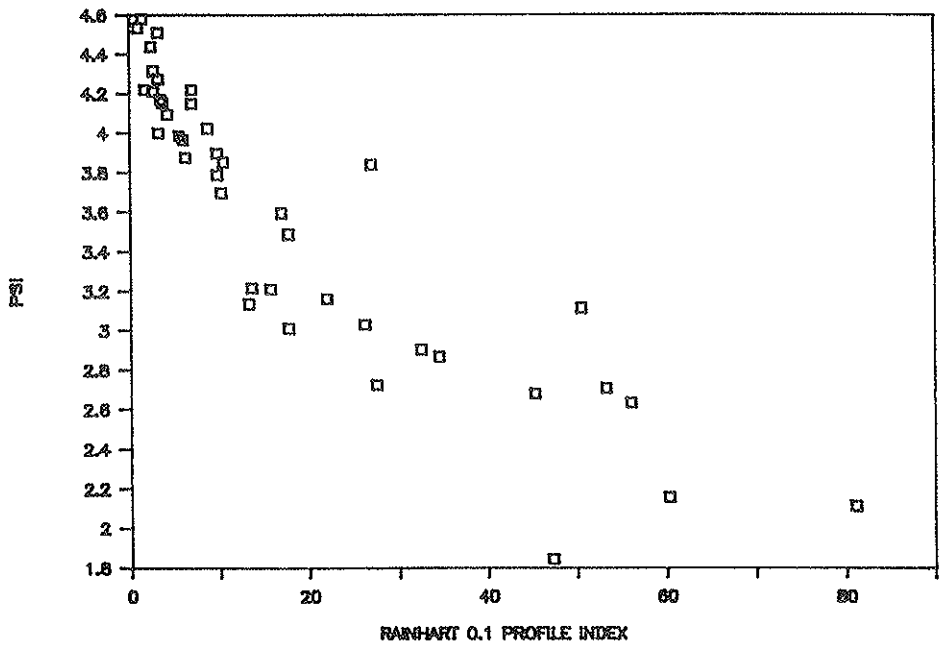

FIGURE 15 PSI vs. Rainhart 0.1-in blanking band profile index.

CONCLUSIONS

This research effort was initiated to determine relationships between roughness measurements from the California and Rainhart profilographs and PSI.

The research indicated that there exists a high correlation between the Rainhart and California profilographs. The best correlation found between the two devices from the sections tested was when a 0.1-in blanking band was used for the Rainhart device and a 0.2-in blanking band was used for the California device. The most common practice has been to use this combination. Using a 0.1-in blanking band for the California device gave good results. It gave better results for the correlation done with PSI on the smoother pavements. However, using a 0.1-in blanking band for the Rainhart profilograph gave significantly better results than the 0.2-in blanking band. The California profilograph was easier to operate.

A good correlation was found between PSI from the SDP and the profile index from the two profilographs. For all sections investigated, the California profilograph correlated

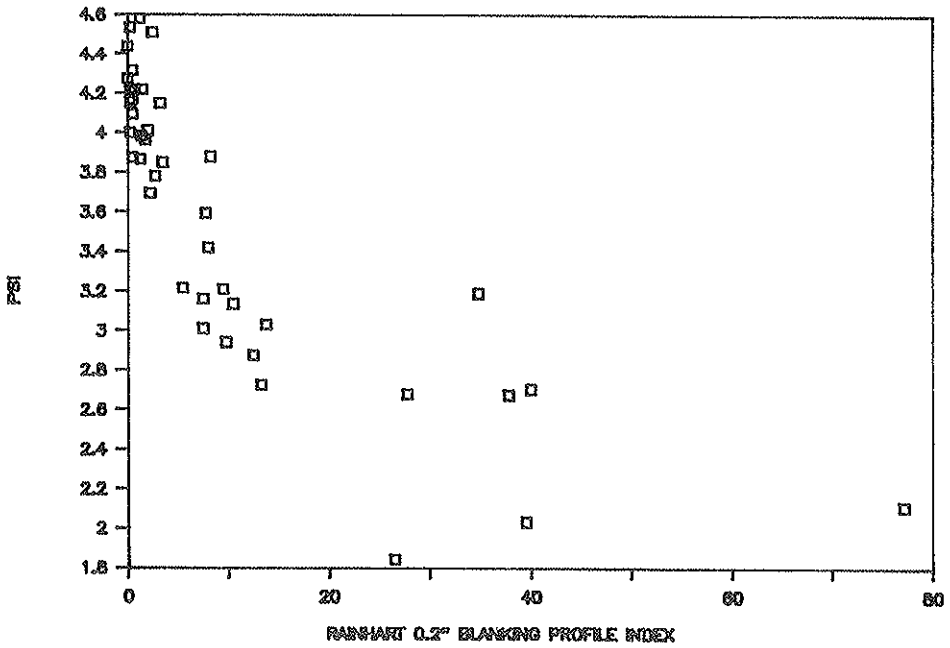

FIGURE 16 PSI vs. Rainhart 0.2-in blanking band profile index.

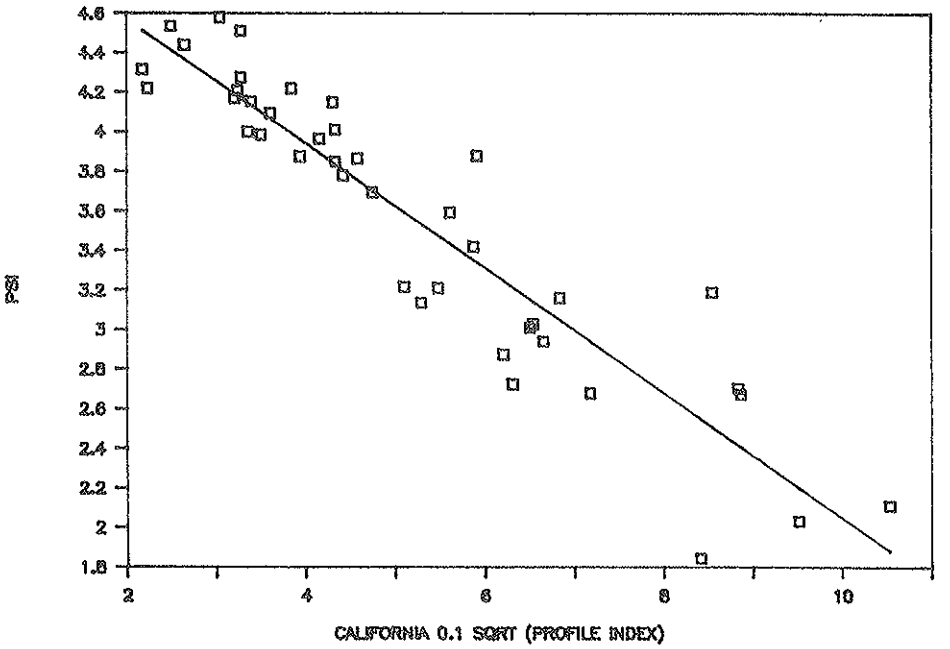

FIGURE 17 PSI vs. square root of California 0.1-in blanking band profile index.

slightly higher to PSI than the Rainhart. The current model used for computing PSI from the SDP does not appear to give many sections with PSI values much greater than 4.5. This made it difficult to get many sections above 4.5, which is needed to establish points in this upper range. The Rainhart profilograph using the 0.1-in blanking band gave the best results for the smoother pavements.

A good correlation was also found between SI and the slope variance statistic provided by the WRD and the profilographs. The California profilograph also was found to be slightly better correlated.

This study is useful for investigating PSI relations with profile index and in comparing data from the two profilograph types. As noted, the Rainhart and California Profilographs are currently being used by several states for construction control measurements and may be the best devices for such measurements. The profilograph is less expensive than most currently used roughness measuring devices, is easy to under-

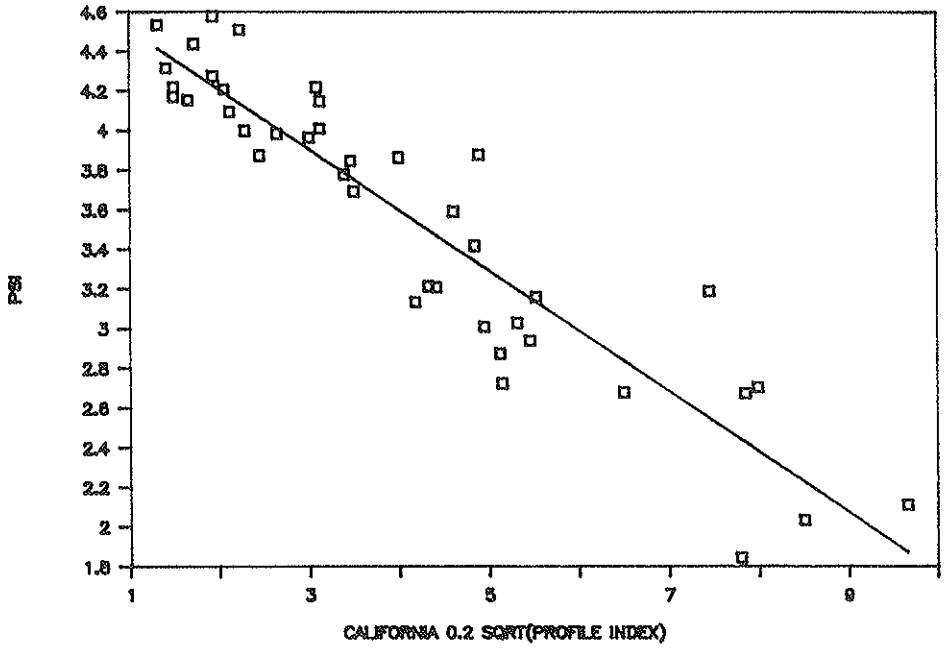

FIGURE 18 PSI vs. square root of California 0.2-in blanking band profile index.

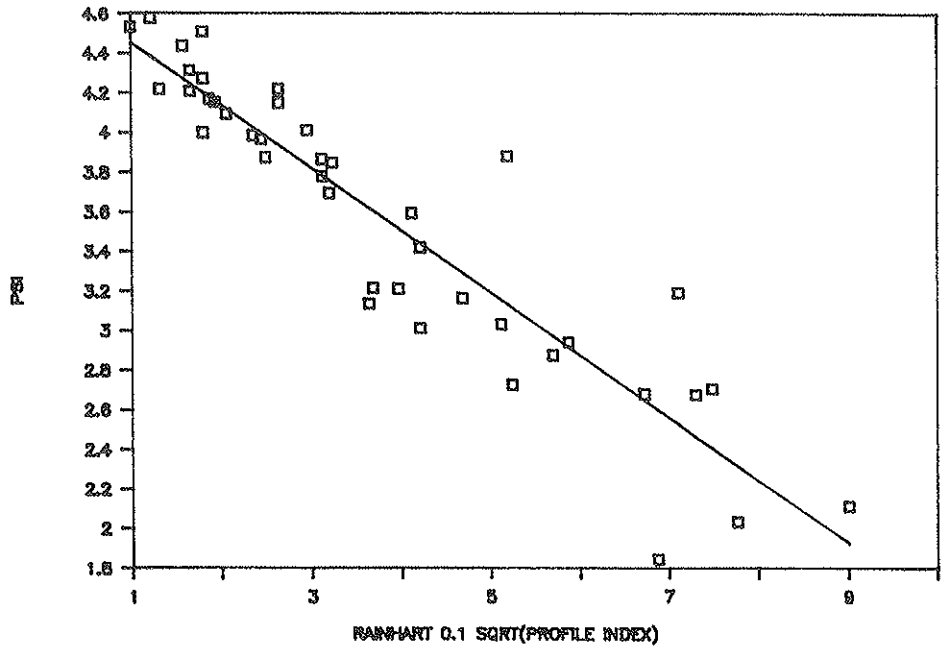

FIGURE 19 PSI vs. square root of Rainhart 0.1-in blanking band profile index.

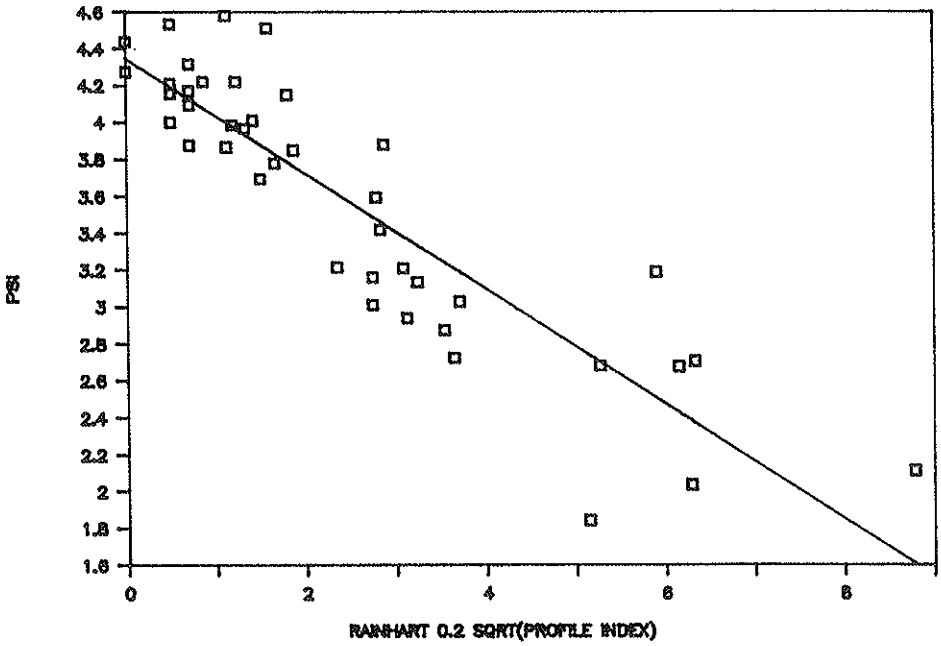

FIGURE 20 PSI vs. square root of Rainhart 0.2-in blanking band profile index.

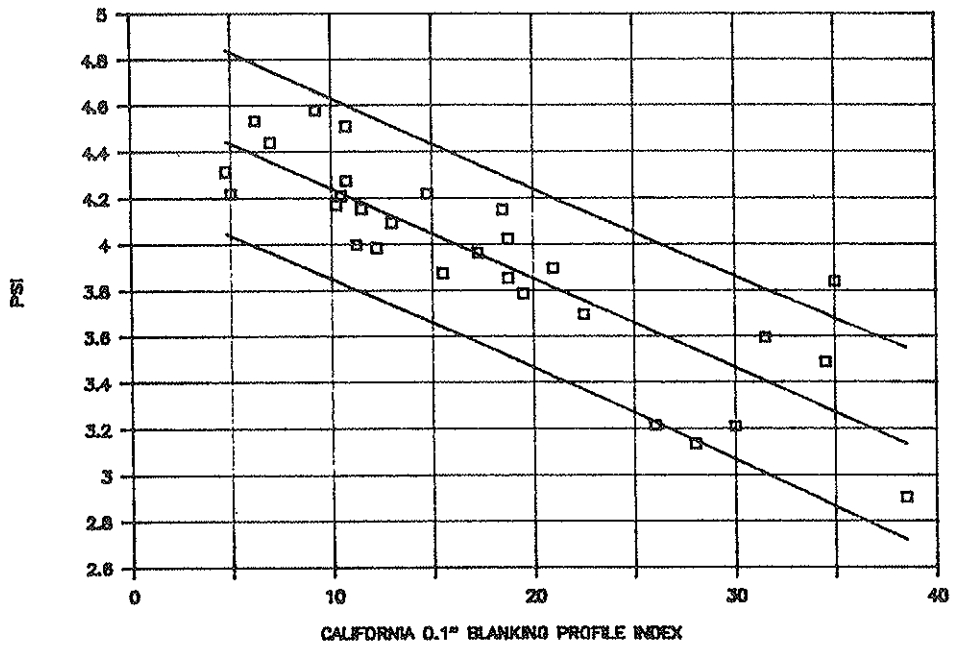

FIGURE 21 PSI vs. California 0.1-in blanking band profile index with 90 percent confidence band.

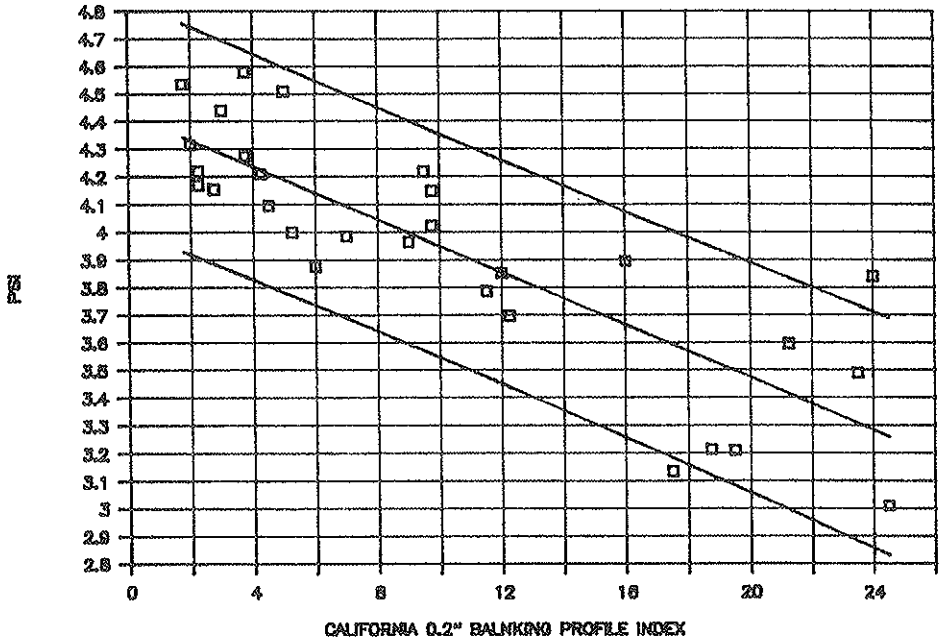

FIGURE 22 PSI vs. California 0.2-in blanking band profile index with 90 percent confidence band.

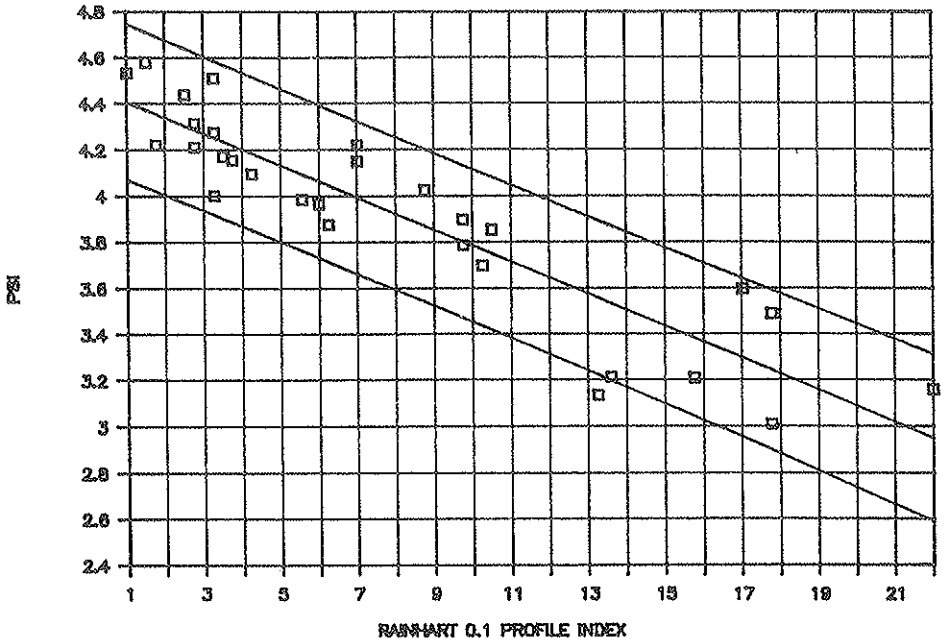

FIGURE 23 PSI vs. Rainhart 0.1-in blanking band profile index with 90 percent confidence band.

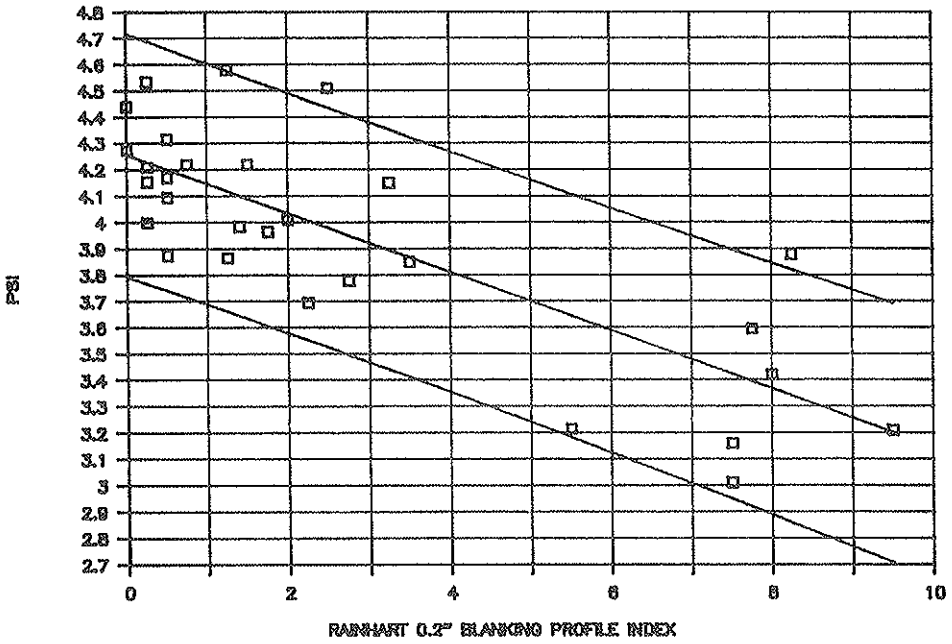

FIGURE 24 PSI vs. Rainhart 0.2-in blanking band profile index with 90 percent confidence band.

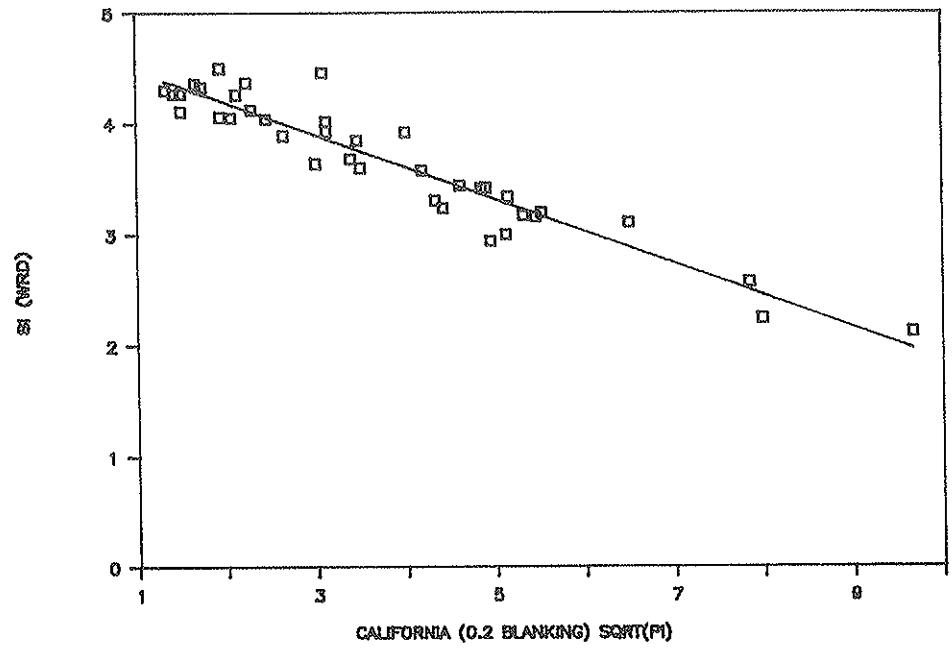

FIGURE 25 California 0.2-in blanking band profile index vs. WRD serviceability index.

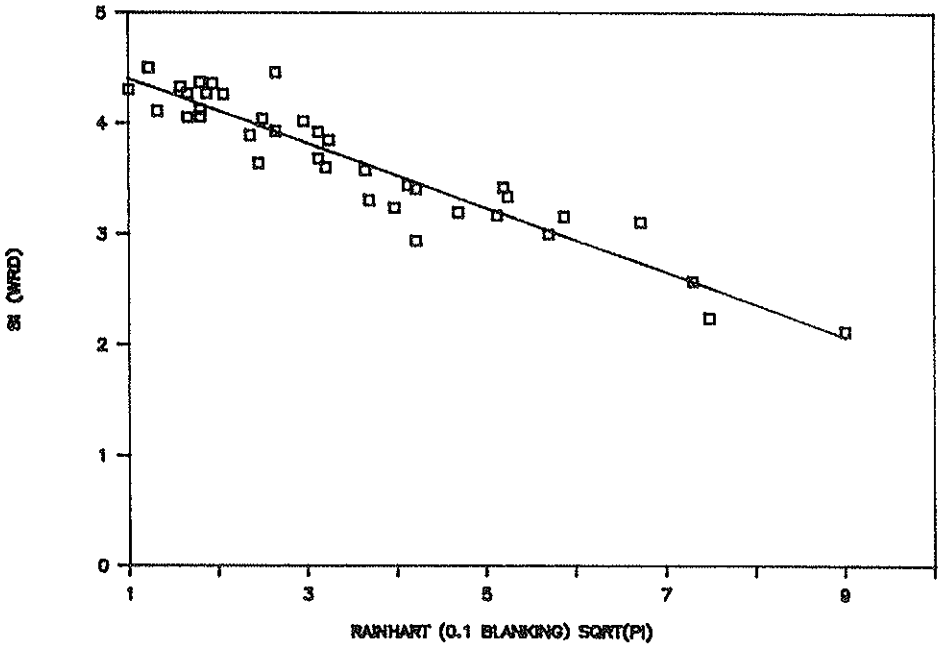

FIGURE 26 Rainhart 0.1-in blanking band profile index vs. WRD serviceability index.

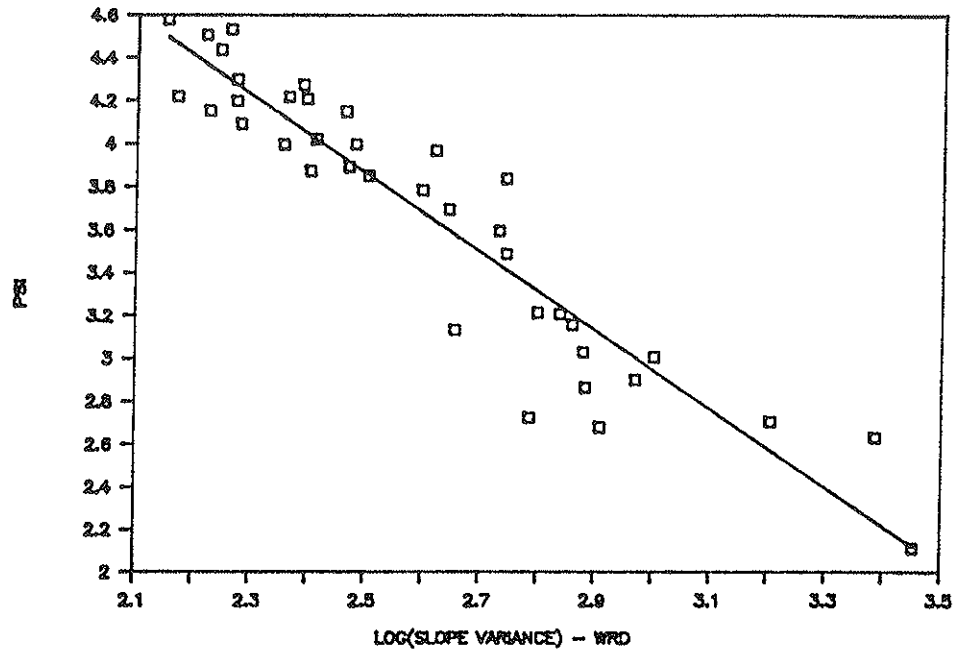

FIGURE 27 PSI vs. WRD log (slope variance).

stand, has a low operations cost, and requires no special skills from the operator. However, the frequency response of these two devices to road profile are such that the effects of some roughness frequencies can be underestimated and others overestimated. Thus, although such devices may be best, particularly for new construction, based on the models developed, they do appear to have certain limitations.

ACKNOWLEDGMENTS

This study was sponsored by the Texas State Department of Highways and Public Transportation and the Federal Highway Administration.

REFERENCES

1. *Method of Test for Determining Profile Index Value*. Georgia Highway Department, October 1980.
2. F. L. Roberts and W. R. Hudson. *Pavement Serviceability Equations Using the Surface Dynamics Profilometer*. Research Report 73-3, Center for Highway Research, University of Texas at Austin, April, 1970.
3. E. B. Spangler and W. J. Kelly. *GMR Road Profilometer—A Method for Measuring Road Profiles*. Research Publication GMR-452, General Motors Corporation, December 1964.
4. *Operation of California Profilograph and Evaluation Profiles*. State of California Department of Public Works. Test Method No. Calif. 526-E, October 1972.
5. R. S. Walker. *A Self-Calibrating Roughness Measuring Process*. Research Report 279-1, Texas Department of Highways and Public Transportation, August 1982
6. R. S. Walker and J. S. Schuchman. *Upgrade of 690D Surface Dynamics Profilometer for Non-Contact Measurements*. Research Report 494-1F, Texas Department of Highways and Public Transportation, January 1987.
7. R. S. Walker and H.-T. Lin. *Profilograph Correlation Study with Present Serviceability Index*. Report submitted for publication by DOT, Contract DTFH 71-86-72-TX-22.

Publication of this paper sponsored by the Committee on Surface Properties—Vehicle Interaction.

Establishing Relationships Between Pavement Roughness and Perceptions of Acceptability

ARUN GARG, ALAN HOROWITZ, AND FRED ROSS

A psychological scaling experiment was conducted in Wisconsin to establish relationships between pavement roughness and users' perceived need to improve the road. A total of 32 road segments were selected for user evaluation. Except for their surface, they had very similar characteristics (speed limit, length, terrain, traffic volumes, scenery, etc.). Physical roughness was measured with both a response-type instrument (roadmeter) and a profilometer. Fifty paid subjects were selected randomly from the general population. They were asked to rate ride quality on both the traditional Weaver/AASHO categorical scale and on a newly designed magnitude estimation scale. In addition, subjects were asked, using a Likert scale, about their willingness to resurface and were asked to estimate the amount of extra time they would be willing to spend to avoid a particular segment, considering its roughness. The experiment yielded several useful mathematical relations between physical roughness and users' willingness to resurface. It was found that the magnitude estimation scale was preferable to the Weaver/AASHO scale for measuring subjective roughness. Surprisingly, the roadmeter was better than the profilometer for measuring physical roughness.

For the most part state DOTs assign dollars for pavement resurfacing on the basis of the statistical distribution of roughness across the highway system, political considerations, and budgetary limitations, rather than on rigorous consideration of highway users' satisfaction. There is a consensus of previous studies that the definition of a roughness standard should reasonably be guided by the degree of user satisfaction or dissatisfaction that can be expected at any particular level of roughness (*1–5*). Indeed, several studies have established a relationship between mechanical measures of roughness and the percentage of users saying that the road should be resurfaced (*1–3, 6, 7*). From the public's viewpoint pavement roughness, more than structural adequacy, drives the desire for pavement improvement.

In Wisconsin, the present serviceability index (PSI) is used to establish a standard for pavement roughness, called a "terminal" roughness level. The terminal roughness level is defined as the roughness level (expressed in PSI) at which a pavement is considered to be deficient and hence in need of improvement. The terminal levels in Wisconsin are 2.5 for the Interstate system, 2.25 on principal arteries, and 2.0 on other roads. PSI, in Wisconsin, is determined by converting the output of a roadmeter (a response-type instrument that yields inches per mile) to a 0 to 5 scale.

The objectives of this study were to establish more precise relationships between pavement roughness, user satisfaction with ride quality, and the perceived need to improve the road (willingness to incur costs to make the pavement smoother). In order to meet these objectives, a psychological scaling experiment was conducted. Fifty Wisconsin drivers, selected randomly, were asked to rate 32 road segments. Rather than being representative of all Wisconsin roads, most test segments were selected to have PSIs of 1.0 to 4.0. The segments were chosen to be similar in length, speed limit, terrain, traffic volume, and scenery. Subjects rated several different aspects of ride quality on both traditional scales (such as the Weaver/AASHO scale) and on scales specifically designed to achieve a better understanding of terminal roughness.

PSYCHOLOGICAL SCALING ISSUES

Of most interest here are automobile users' perceptions of pavement roughness. Although the manner in which human beings rate pavement roughness is necessarily an empirical problem, the known facts of psychophysics set certain valuable guidelines. An observer is sensitive not only to the physical stimuli he or she is trying to measure, but also to a large number of other factors that can distort judgment to varying degrees (*5*). This makes the task of subjectively measuring ride quality more difficult, although it is still quantifiable. Since human observers are susceptible to external influences in communicating their psychological impressions, most psychophysical studies use a scale to measure psychological experience and relate this to physical measurement. Then, psychological measurements can be estimated from measurements of the physical correlate. The original PSI (*7*) was developed within this type of framework. However, it appears that this subjective measurement procedure was developed without full cognizance of the basic principles of subjective rating scale construction (*5*).

Although some attempts have been made to correlate ride quality (a subjective measure) with pavement roughness (an objective measure), little information exists to define this relationship. Nearly all studies (*2, 3, 6, 7*) have used a category rating scale, usually the Weaver/AASHO scale, which was the original basis for PSI. Most of these scales suffer from

A. Garg and A. Horowitz, College of Engineering and Applied Science, University of Wisconsin—Milwaukee, P.O. Box 784, Milwaukee, Wis. 53201. F. Ross, Division of Highways and Transportation Services, Wisconsin Department of Transportation, 718 Clairemont Avenue, Eau Claire, Wis.

the error of leniency, the halo effect, and the error of central tendency (5). The Weaver/AASHO scale uses five categories, and there is additional concern that the scale does not effectively use a subject's power of discrimination. Hutchinson (5) suggests that cues of a very general character such as "excellent," "poor," etc., should be avoided. Further, if the scale is to be manipulated mathematically (as in ride quality studies), one must be able to measure psychological ratios (ratio scale) or at least differences (interval scale). In other words, a linear relationship should exist between the different sets of scale values. Hutchinson (5) suggests that such a relationship is not possible with the Weaver/AASHO scale. Based on a study of different scales, Holbrook (1) suggested that for predicting ride quality from physical measures of pavement roughness, magnitude estimation scales are preferred over categorical scales. This suggestion has not, as yet, been rigorously tested.

In a classical magnitude estimation experiment subjects rate a series of comparative stimuli as a fraction or multiple of a given rating for a single, standard stimulus (8). For example, a subject may be asked to rate the brightness of lights. The subject is first presented a standard amount of light and is told that this amount of light has a rating of 10. The subject is then presented a comparative stimulus. If the subject thinks that the light is one-half as bright, it would be rated "5." Conversely, if the subject thinks that the light is twice as bright, the rating should be "20." Thus, a magnitude estimation scale has a minimum value of zero and a maximum value of infinity. Extensive tests of magnitude estimation scales have demonstrated that they possess the ratio property.

Magnitude estimation is best implemented in a laboratory where both standard and comparative stimuli can be alternately presented to subjects in rapid succession. This procedure cannot be implemented on a road course because it is not possible to find a sufficient number of identical road segments to serve as standard stimuli. An alternative procedure, adapted for this study, is to first train the subjects about characteristics of the standard stimulus by repeated exposure. Then, subjects are presented several comparative stimuli, again presented the standard stimulus, again presented several more comparative stimuli, etc.

In order to implement this procedure, the comparative segments (stimuli) were organized into loops with all loops originating and terminating at the standard segment. Figure 1 shows the three loops used in this study. Since it is important that the standard segment remain distinct in the subjects' minds, one of the rougher segments (PSI = 1.6) was chosen. The standard segment was given an arbitrary value of 10.

EXPERIMENTAL DESIGN

The unusual requirements of this experiment necessitated the adoption of different procedures than have been used in previous studies. These procedures are briefly reviewed here.

Road Segment Selection

The study was conducted in rural Sheboygan County near Plymouth, Wisconsin. As shown in Figure 1, the course for the study was divided into three loops (A, B, and C). The loops A, B, and C included, respectively, 9, 12, and 11 comparative segments. In addition, a "standard segment" was located near the center of the course; thus, there were a total of 33 segments. All segments were 0.5 mi long. Of the 32 comparative segments, 11 were portland cement and 21 were bituminous concrete. Only six comparative segments had four lanes; the remaining twenty-six had two lanes. The standard segment was portland cement and had two lanes.

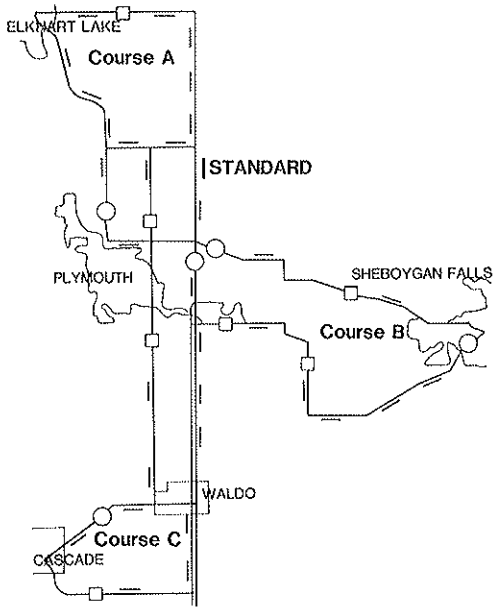

FIGURE 1 Geographical location of road segments.

The comparative segments were selected to represent different levels of pavement roughness, with PSIs ranging from 1.1 to 3.9. Successive segments were close to each other so as to minimize driving time and associated physical and mental fatigue to the subjects. All segments had a posted speed limit of 55 miles per hour. None of the segments was on freeways.

Vehicle Selection and Operation

A single, mid-sized car was selected because it is most representative of a typical car driven on Wisconsin highways. The car speed was maintained at 50 mph on test segments using cruise control. Windows were always rolled up to minimize road noise and wind effect on the subjects. Air conditioning was used as needed. Subjects were passengers and were required to wear seat belts. No smoking was allowed in the car.

Subject Selection

It was deemed critical to this study that the panel be representative of Wisconsin road users. Potential subjects were recruited at a nearby driver's license office and were asked several background questions. This background information was later used to select fifty subjects, twenty-five males and twenty-five females. The subjects represented a variety of age groups, family income groups, occupations, and places of res-

idence (rural versus urban). Subjects were paid to participate in the study.

Data Collection Forms

Three different forms were filled out by the subjects. Information about each subject was collected on the Background Information Form. A Road Segment Evaluation Form was used to rate subjective ride quality and related issues for each comparative segment. A Course Evaluation Form was used to rate passenger comfort, personal well-being, weather conditions, and driver skill. Thus, for each subject the Background Information Form was completed once, the Road Segment Evaluation Form was completed 32 times, and the Course Evaluation Form was completed three times, once for each loop. All three forms and instructions were assembled in loose-leaf notebooks.

The Background Information Form was used to obtain information on subjects' backgrounds (age, sex, formal education, household income, etc.), driving habits (type of car, years of driving, miles driven/week, etc.), overall impression of Wisconsin highways, and relative importance of a number of variables related to subjects' satisfaction with an automobile ride. A total of 25 different pieces of information were collected on subjects' backgrounds.

Two different psychophysical scales were used to rate pavement ride quality. One was the traditional five-point Weaver/AASHO scale, the other a newly designed magnitude estimation scale where the standard segment was arbitrarily assigned a ride quality rating of 10.

The acceptability of pavement ride quality was determined using two different scales. The first question asked subjects to agree or disagree with this statement: "State and/or county money should be allocated within the next year to resurface or reconstruct this road in order to improve its ride quality." The second question determined how much extra time subjects would be willing to spend to avoid this type of pavement over a 50-min trip.

Previous studies had used a two-point (yes, no) scale for determining the acceptability of pavements, whereas this study has adopted a five-point Likert scale ("strongly agree" to "strongly disagree"). A five-point scale allows subjects to avoid definitive statements when the ride quality is neither very smooth nor very rough. Furthermore, a Likert scale can better provide a statistical relation between acceptability rating and pavement roughness.

In addition to ride quality and acceptability, the subjects were asked to rate other aspects of the ride (amount of traffic, appearance of the road surface, scenery, safety of the road and importance of the road) on five-point semantic differential scales. It was believed that some of these factors, along with subjects' background, could have some effect on ride quality and acceptability ratings, in spite of efforts to minimize such effects.

The purpose of the Course Evaluation Form was to determine if the subjects felt well, if the seats were comfortable, if the seating room was sufficient, and if they were satisfied with the driver. These ratings were collected in order to determine if adverse conditions influenced subjects' ratings of ride quality.

Data Collection Procedures

Each subject was randomly assigned a passenger seating position in the car. A research assistant drove over the standard segment six times, so that subjects were fully aware of the ride quality offered by that segment. Then the research assistant started evaluation of one of the three loops (A, B, or C). The order of the loops was randomly preselected. After each segment, the research assistant made a safe stop so that subjects could fill out the Road Segment Evaluation Form. The research assistant drove the car to a nearby rest area for a short break; then the procedure was repeated for the remaining loops.

Course Evaluation

In general, seating room, comfort of seats, interaction with other passengers, skill of the driver, personal well-being and weather conditions received very favorable responses from the subjects. Mean ratings for the six variables and the three courses ranged from 1.5 to 1.9, where "1" was most desirable and "5" was most undesirable. Thus, it would seem that none of these six variables had an adverse effect on ride quality and acceptability ratings.

Physical Road Roughness Measurement

Physical roughness of each segment was measured three times with the Wisconsin DOT response-type instrument—a roadmeter. The roadmeter yielded inches per mile, which was transformed into PSI. In addition each segment was measured by Michigan DOT with its profilometer. The profile was converted into a 0 to 100 scale of roughness called the Ride Quality Index (RQI). Michigan actually uses two versions of RQI; this study used the newer, more sophisticated version, so it is referred to here as "new RQI." No attempt was made to find an optimal transfer function between road profile and subjective evaluation of roughness.

MAJOR FINDINGS

Physical and Subjective Measures of Road Roughness

In the past, studies on road roughness have used averages (or mean values) for each segment to determine correlation coefficients and to perform regression analysis. However, statistics based on raw data are more desirable and powerful. All the statistics reported in this study are based on raw data unless otherwise stated. Correlations based on average values from the subjects will, in general, be substantially higher than those based on raw data. For example, Table 1 compares correlation coefficients based on raw data with those based on mean values.

Throughout this discussion, "ride quality rating" refers to the results of the magnitude estimation experiment.

Besides those correlations found in Table 1, extensive correlation analysis was performed on all variables from the Road Segment Evaluation Form. Most interestingly, road surface appearance was found to be highly correlated with all mea-

TABLE 1 COMPARISON OF CORRELATIONS BASED ON RAW DATA WITH THOSE BASED ON MEANS FROM THE FIFTY SUBJECTS

Variable No.	Variable	Correlation on Raw Data Variable No.					Correlation on Means Variable No.				
		1	2	3	4	5	1	2	3	4	5
1	Ride Quality Rating	1	-0.71	-0.58	0.48	0.51	1	-0.96	-0.85	0.70	-0.93
2	Weaver/AASHO Rating		1	0.53	-0.46	0.68		1	0.80	-0.68	0.93
3	PSI			1	0.85*	0.49			1	0.85*	0.92
4	New RQI				1	-0.42				1	-0.77
5	Money Allocated					1					1

*Independent of subject variability

sures of road roughness (subjective, physical, and acceptability). The measure of road roughness with the highest correlation with road surface appearance was the Weaver/AASHO scale (0.72). A lower correlation (0.59) was found between the ride quality rating and road surface appearance. It is understandable that the Weaver/AASHO scale would be highly correlated with the road surface appearance because of the general nature of the cues; the scale tends to capture other aspects of the road in addition to physical roughness. However, the ride quality rating does not have general cues, so it is less sensitive to other aspects of the road, such as road surface appearance, safety features, etc.

A typical objective of a ride quality study is to determine a quantitative relationship between subjective perceptions and physical measures of pavement roughness in order to make routine psychological estimates from measurement of the physical correlate. Least-squares regression analysis resulted in the following equations:

$$\text{Ride Quality Rating} = 13.76 - 2.33\ \text{PSI} \quad (r = 0.58\ SE = 2.56) \quad (1)$$

$$\text{Ride Quality Rating} = -4.31 + 0.187\ \text{New RQI} \quad (r = 0.48\ SE = 2.78) \quad (2)$$

$$\text{Weaver/AASHO Rating} = 1.48 + 0.637\ \text{PSI} \quad (r = 0.503\ SE = 0.78) \quad (3)$$

$$\text{Weaver/AASHO Rating} = 6.44 - 0.051\ \text{New RQI} \quad (r = 0.46\ SE = 0.82) \quad (4)$$

These relationships are illustrated in Figures 2–5. Note that

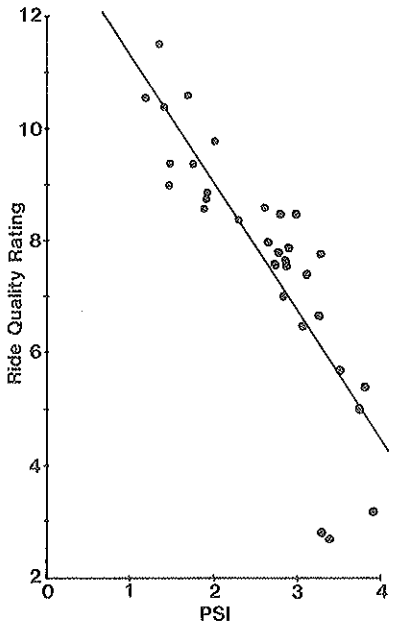

FIGURE 2 Relationship between mean subjective ride quality rating and PSI. (The regression shown is on the mean ride quality rating from the 50 subjects; $r = 0.85$.)

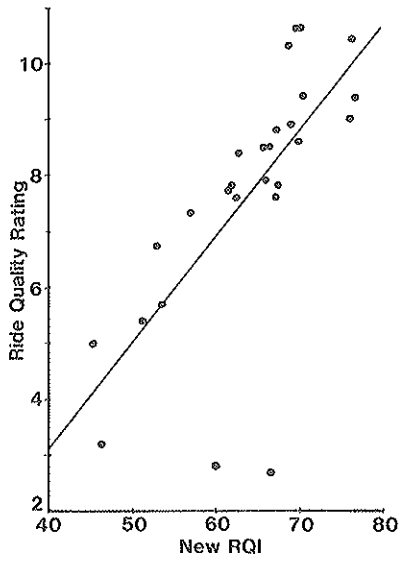

FIGURE 3 Relationship between mean subjective ride quality rating and new RQI. (The regression shown is on the mean ride quality rating from the 50 subjects; $r = 0.70$.)

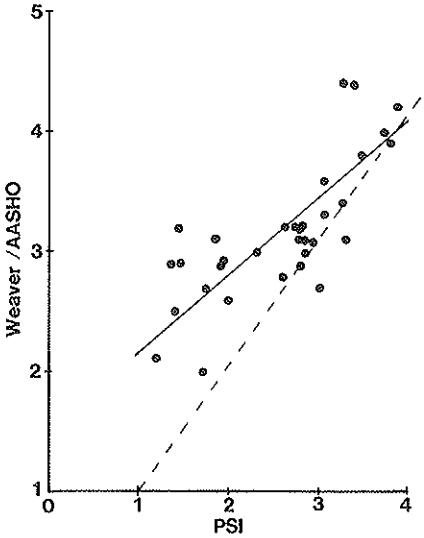

FIGURE 4 Relationship between mean Weaver/AASHO scale and PSI. (The regression shown is on the mean Weaver/AASHO rating from the 50 subjects; r = 0.80.)

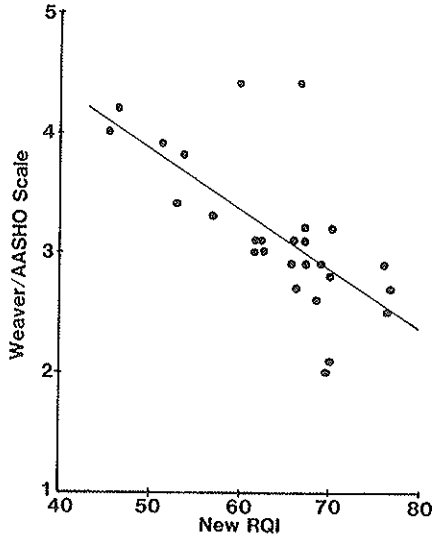

FIGURE 5 Relationship between mean ride quality rating on Weaver/AASHO scale and PSI. (The regression is shown on the mean Weaver/AASHO rating from the 50 subjects; r = 0.68.)

TABLE 2 RESULTS FOR STEPWISE FORWARD REGRESSIONS OF SUBJECTIVE MEASURE OF RIDE QUALITY AGAINST PSI AND OTHER ASPECTS OF THE RIDE

Dependent Variable	Independent Variables						
	Constant	Road Surface Appearance	PSI	Safety	Amount of Traffic	Correlation Coefficient (r)	Standard Error
Ride Quality Rating	2.44	1.92	-	-	-	0.59	2.54
	8.08	1.29	-1.52	-	-	0.67	2.33
	7.81	0.96	-1.69	0.62	-	0.69	2.27
	8.55	0.99	-1.72	0.59	-0.35	0.70	2.25
Weaver/AASHO Scale Rating	5.05	-0.70	-	-	-	0.72	0.64
	4.06	-0.59	0.27	-	-	0.75	0.61
	4.14	-0.49	0.32	-0.19	-	0.77	0.59
	4.04	-0.49	0.32	-0.18	0.05	0.77	0.59

only the mean values from the fifty subjects for the ride quality and Weaver/AASHO ratings are plotted in Figures 2–5; the regression lines in these figures were found from mean values and differ slightly from Equations 1–4.

Based on the above linear regressions, it appears that road roughness is best estimated by using the magnitude estimation type of scale for the psychophysical measure (ride quality rating) and PSI for the physical measure. The above relationship resulted in a correlation coefficient of 0.58 on raw data and 0.85 on mean values from the fifty subjects. The linear relationships between the subjective measures (ride quality and Weaver/AASHO ratings) and new RQI was found to be good, but not as strong as between the subjective measures and PSI.

Several other regressions were attempted to improve the relationship between ride quality rating and PSI. These included log transformation, polynomial equations, and others. However, none of those equations resulted in a significant improvement.

It is particularly interesting to note that PSI does not correspond closely to the Weaver/AASHO scale, as it should. Given the origins and interpretation of PSI, the y-intercept of equation 3 should have been about 0.0, and the slope should have been about 1.0 (dotted line on Figure 4). Either Wisconsin's method of measuring PSI no longer replicates PSI from the AASHO Road Test or the type of panel used in this study (a random sample of road users) differs substantially from the type of panel selected for the AASHO Road Test.

On balance, subjects were far less willing than the Wisconsin roadmeter to rate a road as "poor."

Since appearance of the road surface, scenery, amount of traffic, safety of the road, and importance of the road had significant correlations with the subjective road roughness ratings, forward stepwise linear regressions were performed between the subjective measures, these variables, and PSI. A level of significance of 0.01 was used for inclusion of an independent variable. The resulting regression equations are given in Table 2. It is clear from Table 2 that appearance of the road surface has a strong effect on the ride quality rating and an even stronger effect on the Weaver/AASHO scale rating. Road surface appearance and PSI explain 45 percent and 56 percent of the variation in ride quality rating and Weaver/AASHO rating, respectively. Thus, while PSI is important in determining subjective measures of ride quality, appearance of the road surface plays an equally important role.

The effect of road surface appearance on ride quality ratings is readily seen in Figure 2. There are three comparative segments that received particularly favorable ride quality ratings (about 3.0) but had PSI values of less than 4. These segments deviate substantially from the regression line. All three segments had new surfaces (two portland cement and one bituminous concrete) at the time of the experiment. There were no cracks, patches, discoloration, or any other evidence of deterioration. Objectively, however, there was some roughness to the surface.

The ride quality ratings show that subjects were significantly influenced by the excellent appearance of the road. The effect of appearance is even more pronounced when the ride quality rating is compared with new RQI (Figure 3).

Acceptability Measures

A series of linear regressions was performed to relate physical measures of road roughness to acceptability measures (for example, "money should be allocated"). Those regressions included a number of subject background variables such as seating comfort, use of seat belts, helpful road signs, percentage of miles driven on highways, privacy in vehicle, years of formal education, sex, weather, lack of construction, etc. However, the contribution of a single background variable was very small, and the number of variables was very large. By and large, little was learned from these regressions beyond the information contained in Table 1. That is, both PSI and new RQI are strongly related to the acceptability measures, with PSI providing a somewhat better fit. The fit could not be substantially improved by inclusion of information about the subjects' backgrounds. This result is important because it means that the results of this study (and similar studies) are likely to be insensitive to the location from which the sample is drawn.

Terminal Roughness

The major objective of this study was the determination of a terminal roughness, in other words, a value of PSI, that causes a predictable percentage of drivers to become dissatisfied with the road surface. In the past, this dissatisfaction has been measured by asking the subjects to answer yes or no to a question about spending tax dollars to improve the ride quality of a given road. Some studies have used a third category of undecided. In this study, however, a Likert scale ranging from 1 (strongly agree) to 5 (strongly disagree) was used.

It is first necessary to establish a single criterion for dissatisfaction; in other words, which value on the Likert scale should be used to represent the "money-should-be-allocated" level of dissatisfaction with road roughness. For example, the value can range from 1 (strong agreement with the statement that "money should be allocated") to 3 (neutral point). Ideally, the cutoff value for "money should be allocated" should depend upon several factors, such as percentage of drivers dissatisfied, class of road (freeway versus local road), volume of traffic served, importance of the road to the travelling public, resources available, and so on. For the following discussion the criterion for dissatisfaction is set at 2.5. A value of 3.0 must be interpreted as ambivalent, and a value of 2.0 is too strict, considering the likelihood of central tendency in the scale. A value of 2.5 can be interpreted as being in slight to moderate agreement with the idea of spending money to resurface the road.

The percentage of subjects with a rating of 2.5 or less for "money should be allocated" is plotted against PSI in Figure 6. The linear correlation coefficient between the percentage of subjects and PSI was 0.89. In addition to a linear regression, curvilinear regressions were also tried. The linear regression resulted in a slightly better fit. The following equations can be used to estimate percent dissatisfied (PD) from PSI for a value of 2.5 for "money should be allocated."

$$PD = 72.49 - 19.74\ \text{PSI} \qquad (r = 0.89,\ SE = 8.2) \qquad (5)$$

$$PD = -19.81 + 95.48/\text{PSI} \qquad (r = 0.87,\ SE = 8.7) \qquad (6)$$

Equation 6 is recommended for determining the relationship between PSI and the percent of dissatisfied subjects. Equation 6 is recommended over equation 5 only because

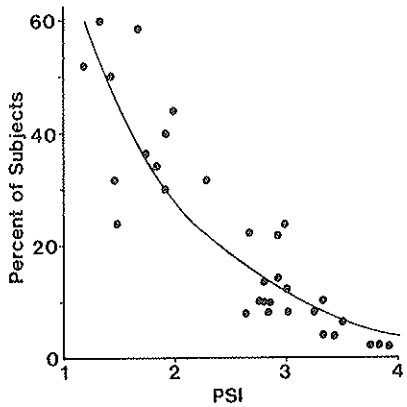

FIGURE 6 Relationship between percentage of subjects dissatisfied with ride quality based on a rating of 2.5 or less for "money should be allocated" and PSI.

TABLE 3 PSIs AS A FUNCTION OF PERCENTAGE OF RATERS DISSATISFIED AND LEVEL OF DISSATISFACTION

Percent of Raters Dissatisfied	PSI for "money should be allocated" rating of ≤ 2.5
50	1.36
45	1.47
40	1.60
35	1.74
30	1.91
25	2.13
20	2.39

it appears to fit better at lower values of PSI (between 1 and 2).

If desired, terminal roughness can easily be determined for any percentage of subjects dissatisfied from the graph, from Equations 5 and 6, or from Table 3. For example, the terminal roughness is 1.36 (PSI) for 50 percent of the Wisconsin drivers to be dissatisfied (as estimated by a value of 2.5 or less on the scale used for "money should be allocated"). This terminal roughness is considerably lower than those currently used by the Wisconsin DOT (2.0 to 2.5).

Willingness To Spend Extra Time

Subjects were asked to estimate the amount of time they would be willing to spend to avoid each segment, assuming they were to make a 50-min trip. The results are summarized in Figure 7. In addition, extra time may be computed from the following:

$$\text{Extra time} = 8.68 - 2.13\ \text{PSI} \qquad (r = 0.32,\ SE = 4.85) \qquad (7)$$

It is seen that the amount of extra time is small, but significant. For example, Equation 7 shows that subjects were willing to spend 5.5 minutes (or 11 percent) more time to avoid a road with a PSI of 1.5.

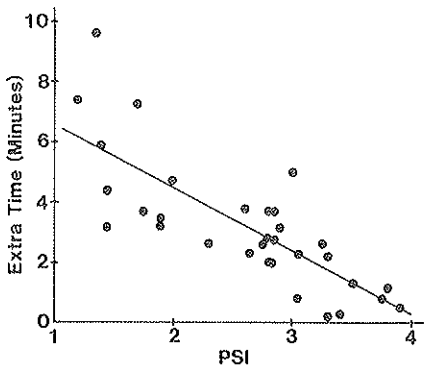

FIGURE 7 Relationship between extra time, in minutes, for a 50 min road trip and PSI.

These extra-time evaluations are analogous to time savings benefits. They can be converted to monetary units by using accepted values of time. Knowing the traffic volumes and speeds on a road, and the rate of pavement deterioration, it would be possible to compute total benefits of a new surface and to compare them with project costs.

CONCLUSIONS

Analysis of subjects' evaluations of ride quality leads to the following conclusions.

A number of subjects' personal and background variables had statistically significant effects on both the subjective measures of road roughness and the acceptability measures. However, these variables were found not to be of practical significance as they explained very little variation in either road roughness or acceptability measures. This suggests that the results of this study are generalizable; that is, they are not dependent on the location from which the sample is drawn.

Even though magnitude estimation is most easily accomplished in a laboratory, it is possible to successfully use this technique for measuring ride quality.

PSI has a higher correlation with the magnitude estimation scale (ride quality rating) than with the Weaver/AASHO scale. The magnitude estimation scale appears to have a greater power of discrimination between various roads, and it is less influenced by road surface appearance. Magnitude estimation is the preferred method of measuring subjective ride quality.

The best physical measure of road roughness appears to be PSI. PSI has the highest correlations with both the ride quality rating and the Weaver/AASHO scale. In a completely hands-off comparison, the less expensive roadmeter was found to be superior to the profilometer in predicting both subjective road roughness and the acceptability of the road. However, both instruments failed to relate with subjective measures of ride quality for those segments judged to be very good by the subjects.

Appearance of the road surface is extremely important to subjects rating ride quality.

People are willing to spend approximately 11 percent (5.5 minutes on a 50-min road trip) more time to take a better ride quality road and avoid a road with PSI of 1.5. This represents a significant resource expenditure. It is recommended that such time savings benefits be incorporated into evaluations of road resurfacing plans.

PSI, as measured in Wisconsin, does not closely approximate the Weaver/AASHO scale. There can be two explanations:

1. The measurement of PSI has somehow changed since it was first established, or
2. The subjects in this experiment differ considerably from the subjects in the AASHO Road Test.

If the latter explanation is true, then it is likely that PSI, regardless of where it is currently being measured, is not properly reflective of the opinions of road users.

A panel can provide detailed information about the need for road resurfacing. In order to properly use this information, it is necessary to establish both a criterion level of dissatisfaction and a percentage of road users who would be so dissatisfied.

ACKNOWLEDGMENTS

A number of people contributed both time and effort to bring this study to completion. The authors are grateful to Karl Dunn and his staff at WisDOT for their encouragement, suggestions, cooperation, and assistance. A special note of thanks is extended to the subjects without whose enthusiasm and cooperation this project would never have been completed.

Professor Edward Beimborn provided advice and encouragement. Professor Umesh Saxena made valuable suggestions in the statistical design and analysis of the experimental data.

We are also appreciative of the efforts of the staffs of the Human Performance Laboratory and the Center for Urban Transportation Studies of the University of Wisconsin at Milwaukee, among them: David Sincere and Richard Clark who collected, coded, and stored the data in the computer; Randal Zakowski who provided graphical illustrations; and Tarun Gupta who performed all statistical analyses.

REFERENCES

1. L. F. Holbrook. Prediction of Subjective Response to Road Roughness by Use of the Rapid Travel Profilometer. In *Highway Research Record 69*, HRB, National Research Council, Washington, D.C., 1969, pp. 212–226.
2. S. Mohan. *Development of a System for the Evaluation of Pavements in Indiana*. Joint Highway Research Project No. C-36-63-G, Purdue University, Ind., 1978.
3. S. K. Nair and W. R. Hudson. Serviceability Prediction from User-Based Evaluations of Pavement Ride Quality. Presented at the 65th Annual Meeting of the Transportation Research Board, Washington, D.C., 1986.
4. W. R. Hudson. Road Roughness: Its Elements and Measurements. In *Transportation Research Record 836*, TRB, National Research Council, Washington, D.C., 1981, pp. 1–7.
5. B. G. Hutchinson. Principles of Subjective Rating Scale Construction. In *Highway Research Record 46*, HRB, National Research Council, Washington, D.C., 1964, pp. 60–70.
6. M. S. Janoff and J. B. Nick. *Evaluation and Quantifying User Perception of Pavement Serviceability*. Report for Pennsylvania Department of Transportation, Pennsylvania, 1983.
7. W. N. Carey and P. E. Irick. The Pavement Serviceability Performance Concept. *Bulletin 250*, HRB, National Research Council, Washington, D.C., 1960, pp 40–50.
8. S. S. Stevens. On the Operation Known as Judgement. *American Scientist*. Vol. 54, 1966, pp. 385–401.

DISCUSSION

MICHAEL S. JANOFF
JMJ Research, P.O. Box 144, Newtown, Pa. 18940.

This is a well written paper that presents potentially valuable information. However, because of some omissions, misinterpretations, and possible mistakes, the results are not readily applicable. The authors have not considered the results of recent work by NCHRP and by Ohio DOT and have incorrectly interpreted a number of their references.

1. The authors state that little information is available to define the relationship between ride quality and roughness. This is false. Studies conducted in Texas, Ohio, Louisiana, New Mexico, Michigan, New Jersey, and Pennsylvania define such relationships quite well (*1–5*). The data from Ohio, New Jersey, Michigan, New Mexico, and Louisiana also reveal that the relationship between roughness measured with a profilometer and subjective ratings of ride quality are nearly identical for each of the five different states.

2. Perhaps the greatest problem in this paper is the relatively poor correlations that the authors have found between physical measures of pavement roughness and subjective ride quality ratings. For profile-derived roughness measures the authors have found correlations of at most .7 with (mean) ride quality ratings, which are far lower than the correlations found between profile measures of roughness and ride quality ratings in Ohio, New Jersey, Michigan, New Mexico, Louisiana, and Texas. For four different models of profile-derived roughness used in these other states, correlations between the roughness and ride quality ratings were always in excess of .9, and for the data from five states combined they were better than .93. A number of explanations for the authors' low correlations can be suggested.

First, the instrument used to collect profiles was the older one-wheelpath unit of Michigan DOT, which is not as accurate in measuring profiles as the more common two-wheelpath versions used in the states mentioned above. Although the profile from one wheelpath can be accurately used to predict rideability (*3*) the instrument used to collect this one-wheelpath profile must provide accurate data; it is suspected that the instrument used by Wisconsin DOT was not. In tests conducted as part of the NCHRP research (*3, 6*) the older one-wheelpath profilometer yielded correlations between RQI and ride quality of .85, while for the two-wheelpath profilometer these correlations between RQI and ride quality rose to .93.

Second, the magnitude estimation scale, which the authors believe is preferred to the similar interval scale, may not be yielding accurate and consistent rating data. As the authors point out, magnitude estimation is best suited to laboratory

research where the "standard" level can be presented to the test subjects along with each test condition. Was this scale pretested in any way to determine if it was suitable for such ratings of ride quality? (It appears that the raw rating data obtained with the magnitude estimation scale, as illustrated in their final report, appeared to have rather high rater variability, indicating a lack of consistency in the rating procedure.)

Both Holbrook (*7*) and Janoff and Nick (*5*) have shown that the choice of rating scale has no effect on the quality of the subjective ratings. The analysis by Hutchinson that the authors use to support their selection of the magnitude estimation scale as the preferred one was shown to be unimportant in panel ratings of ride quality (*5*). Although I believe that Hutchinson is correct in theory, in application drivers can use almost any scale to accurately and consistently rate ride quality, as demonstrated by Holbrook and by Janoff and Nick.

The instructions to the raters could also have had a significant effect on the quality of the ride quality ratings. In the past research for Pennsylvania DOT (*5*) three different rating scales were tested, and it was disclosed that with proper instructions to the raters either one could be used to derive accurate and consistent ratings of ride quality. This same result was also found by Holbrook. Did the authors test their instructions in any way?

The authors' finding that surface appearance is affecting the ratings of ride quality may also be a result of the instructions; Holbrook showed that the use of blindfolds had no effect on such subjective ratings, hence with proper instructions appearance should have no effect on ride quality (*7*).

3. PSI is not a physical measure of roughness but a value derived from a regression equation that relates a physical measure of roughness (typically an RTRRMS index) with a subjective rating of ride quality (such as mean panel ratings or PSR). That the authors found a correlation of .35 between their magnitude estimation scale and PSI and a correlation coefficient of .9 between PSI and the Weaver/AASHO rating is not unexpected. When RTRRMS data from New Jersey, Ohio, and Louisiana were compared to ride quality ratings a correlation of .79 was found for the Weaver/AASHO scale, almost identical to the authors' results. Unless the surfaces are separately analyzed for each type (BC, PCC, composite) no better results can be expected.

The problem is that RTRRMS instruments do not provide roughness data that are highly correlated with ride quality ratings except for BC surfaces (actually such instruments fail to respond to all of the roughness frequencies present in PCC or composite surfaces). On surfaces other than BC, and when the range of ride quality is great, the correlations fall to very low values. The authors should have analyzed the surface types individually to disclose the effect of surface type on the correlations.

The authors' conclusion that PSI, therefore, no longer approximates the Weaver/AASHO scale is conjecture only. A better explanation is that when RTRRMS are used, correlations of .8 to .85 are typical; to increase the correlation it is necessary to use profiles to measure roughness.

4. The Weaver/AASHO scale used by the authors (and illustrated in their final report) is not the same scale that was used by either Carey and Irick (*8*), Weaver (*9*), Janoff and Nick (*5*), or NCHRP (*2*, *3*); it is a completely different type of scale. The Weaver/AASHO scale is a vertical line, typically 5-in long, with major subdivisions at 1-in intervals (labelled 0, 1, 2, 3, 4, and 5) and minor subdivisions at ½-in points labelled "very poor" (at ½-in) "poor" (at 1½-in), "fair" (at 2½-in), "good" (at 3½-in), "very good" (at 4½-in), "perfect" (at the top) and "impassable" (at the bottom). The authors' scale includes the word and number cues but not the vertical line. In addition, the instructions to the raters used by the authors do not explain how to even mark this scale. In past uses of the Weaver/AASHO scale the raters were told to place a horizontal mark across the scale (in other words, across the vertical line) at the point that they feel best describes the ride quality of the test section. It appears that on the authors' scale the subject is instead placing a mark into one of the categories defined by the ½-in divisions. This is completely different from past applications and hence the data (that the authors refer to as Weaver/AASHO ratings) may be incomparable to past applications of this scale.

5. The authors use a five-point Likert scale instead of a two-point yes versus no rating to indicate need for improvement, claiming that such a scale is better for the intended use. Again no pretest or pilot results are shown, and it is suspected that the results may suffer the same problems as those related to the magnitude estimation scale.

6. In summary, the authors conclude that magnitude estimation is the preferred rating procedure and that PSI (or actually RTRRMS indexes) are preferred to profile-derived roughness for predicting ride quality. The opinion of this writer is that these conclusions are unsupported. The correlations between the roughness and rating data are too low in comparison to other recent ride quality research to draw such conclusions and the authors' lack of attention to and misinterpretation of past research sheds serious doubts on the validity of their results.

REFERENCES

1. K. N. Sukumar and W. R. Hudson. Serviceability Prediction from User-Based Evaluations of Pavement Ride Quality. In *Transportation Research Record 1084*, TRB, National Research Council, Washington, D.C., 1986.
2. M. S. Janoff et al. *Pavement Roughness and Rideability*. NCHRP Report 275, 1985.
3. M. S. Janoff. *Pavement Roughness and Rideability Field Experiment*. NCHRP Project 1-23(2), Final Report, Dec. 1987.
4. J. McQuirk and E. Spangler. *Use of the Inertial Profilometer in the Ohio DOT Pavement Management System*. ASTM Committee E-17 Symposium, Columbus, Ohio, June 1985.
5. M. S. Janoff and J. B. Nick. *Evaluating and Quantifying User Perception of Pavement Serviceability*. Penn-DOT, 1983.
6. M. S. Janoff. *Quarterly Report on NCHRP Project 1-23(2)*. Dec. 1986.
7. L. F. Holbrook. Prediction of Subjective Response to Road Roughness by Use of the Rapid Travel Profilometer. In *Highway Research Record 69*, HRB, National Research Council, Washington, D.C., 1963.
8. W. N. Carey and P. E. Irick. The Pavement Serviceability Performance Concept. In *Highway Research Record 250*, HRB, National Research Council, Washington, D.C., 1968.
9. R. J. Weaver. *Quantifying Pavement Serviceability as It Is Judged by Highway Users*. NYSDOT, 1978.

AUTHORS' CLOSURE

The basis of Mr. Janoff's criticism is that our results are in disagreement with his own work. Such criticism is a two-edged sword; it can raise doubts about the validity of Mr. Janoff's earlier efforts in measuring ride quality. Indeed, the principal reason for our conducting a ride quality experiment was disappointment with the experimental design of the NCHRP study to which Mr. Janoff refers. We chose not to make an issue of Mr. Janoff's work in our paper. However, we were particularly disturbed by the subject selection procedures, instructions to subjects, the way stimuli were presented, and the rating scales in the NCHRP study. That the results of the two studies are different is unremarkable; we attempted to correct problems in the NCHRP study design that we believe could have skewed the results.

We believe the low correlations between subjective measures of ride quality and physical measures of ride quality stem from the "hands-off" nature of our study design. We chose to take physical measures from other sources so that their transferability could be evaluated. The physical measure from the response-type instrument (PSI in our case) behaved as expected. The performance of the profilometer (new RQI) was much poorer than expected. Based on many earlier studies (including Mr. Janoff's) we do not feel that the problem stemmed from the quality of either equipment or data analysis. One-wheelpath profilometers have served quite nicely in the past. Instead, it appears that complex transformations of profilometer data are not applicable when there are significant variations in study design (for example, location, subject selection, or stimuli presentation). A major lesson of these comparisons is that engineers cannot take any physical measure of ride quality at face value; they must fully understand the conditions under which panel data were assembled.

Magnitude estimation is one of the most respected psychophysical measurement techniques. Its use in ride quality measurement has been suggested by many authors, and an abbreviated version was tried by Holbrook with very encouraging results. Mr. Janoff has seriously misrepresented Holbrook's conclusions. Holbrook states, "The equations predicting ride from physical input by means of magnitude estimation are to be preferred" (Janoff's reference 7, page 255). A magnitude estimation scale is quite different from any of the three categorical scales tested by Janoff and Nick. Their conclusions are not relevant.

Our experience indicates Hutchinson's criticism of the Weaver/AASHO scale is correct in practice as well as in theory. It is unfortunate that Mr. Janoff decided to disregard Hutchinson's advice.

We found intersubject variability to be about the same for magnitude estimation and for the Weaver/AASHO scales. We did not address this issue in our paper because it is uninteresting. Mr. Janoff's erred during his casual inspection of summary data from our full report.

PSI is a physical measure of ride quality; its peculiar historical origins cannot alter the fact that only mechanical data are used to compute it.

Our conclusion that Wisconsin's PSI no longer approximates the Weaver/AASHO scale is based on Figure 4 in our paper. Regardless of surface type, the regression line is plainly at the wrong angle.

Mr. Janoff has apparently received incorrect information about our depiction of the Weaver/AASHO scale. It was purposefully identical to the one used in his NCHRP study. In regard to another scaling issue, we are perplexed why Mr. Janoff believes an ad hoc 2-point scale of acceptability is inherently superior to a Likert scale—a standard tool of psychometrics.

We appreciate Mr. Janoff's interest in our research. However, we do not feel that his discussion is helpful for either understanding or extending our work.

Publication of this paper sponsored by Committee on Surface Properties—Vehicle Interaction.

Use of the Inertial Profilometer To Calibrate Kentucky Department of Highways Mays Ride Meter Systems

ELSON B. SPANGLER, ROLANDS L. RIZENBERGS, JAMES L. BURCHETT, AND DONALD C. ROBINSON

The National Bureau of Standards (NBS), the Commonwealth of Kentucky Department of Highways (DOH), and Surface Dynamics, Inc. joined in a project in the Commonwealth of Kentucky to calibrate five Kentucky DOH vehicle-mounted Mays Ride Meter (MRM) systems. In this project, an NBS-operated inertial profilometer system was used to measure the elevation profiles of selected pavement test sections. The measured elevation profiles were used to compute the Standard Mays Ride Meter Index (SMRMI) values for each pavement test section. The computed SMRMI values were then used as reference values for the calibration of the actual Kentucky DOH MRM systems. The profilometer was used to identify suitable pavement sections from test sites selected by the Kentucky DOH using an MRM system. The site selection process included sufficient repeat runs to establish a mean SMRMI value for each pavement and a standard deviation from that mean for the repeat runs. Six pavement test sites with the desired SMRMI values and low standard deviations were selected. The five Kentucky DOH MRM systems were then driven over the selected test sites a number of times to determine a mean measured value and a standard deviation about that measured mean value for each system on each pavement test site. The test data from the profilometer and the five Kentucky DOH MRM systems were used to develop a calibration equation and expected standard deviation for each of the MRM systems. The resulting calibration equations will be used by the Kentucky DOH to compute SMRMI values for each system. Included in the project was a correlation of the Ohio Department of Transportation inertial profilometer with the NBS-operated inertial profilometer to establish the validity of using another identically constructed inertial profilometer for the same calibration procedure.

The inertial profilometer was developed in the early 1960s by Elson Spangler and William Kelly at the General Motors Research Laboratory in Warren, Michigan. The profilometer was designed to be a research tool that would allow pavement profiles to be brought into the laboratory for use as computer input data for vehicle suspension studies. The first presentation of the inertial profilometer was made by Spangler and Kelly (*1*) at the Transportation Research Board Annual Meeting in Washington, D.C., in 1965. Through the efforts of the General Motors Corporation, the technology associated with the inertial profilometer has been made available for use in the highway testing community. Early inertial profilometer implementations were used by Michigan (*2*), Pennsylvania, Kentucky (*3*), and Texas (*4*) and by Brazil as part of a World Bank project. More recent implementations are in use in five states including Texas, West Virginia, Minnesota, Michigan, and Ohio and in Chile, as part of a World Bank project.

E. B. Spangler, Surface Dynamics, Inc., 800 West Long Lake Road, Suite 145, Bloomfield Hills, Mich., 48013. R. L. Rizenbergs and J. L. Burchett, Kentucky Department of Highways, Room 701, Clinton and High Streets, Frankfort, Ky. 40622. D. C. Robinson, National Bureau of Standards, Acoustics Measuring Group, Gaithersburg, Md. 20899.

INTRODUCTION

The most recent implementation is an inertial profilometer purchased by the Federal Highway Administration (FHWA) from K. J. Law Engineers, Inc., and was being evaluated by the National Bureau of Standards (NBS) for the FHWA during the work reported in this paper. In May 1987, the NBS, the Commonwealth of Kentucky Department of Highways (DOH), the Ohio Department of Transportation (DOT) and Surface Dynamics, Inc. joined in a project in the Commonwealth of Kentucky to calibrate five Kentucky DOH vehicle-mounted MRM systems using an NBS-operated inertial profilometer to perform this calibration. Fourteen pavement test sections in the vicinity of Frankfort, Kentucky, were selected as candidate sites for the calibration of Kentucky DOH MRM systems. Seven of the pavement test sections were portland cement concrete and seven were bituminous concrete.

PROFILOMETER MEASUREMENTS AND ANALYSIS

The elevation profiles of all the pavement test sections were measured with an NBS-operated inertial profilometer multiple times to evaluate the precision of the measuring method. After the multiple measurements of the elevation profiles of the fourteen pavement test sections, a SMRMI value was computed for each test section.

The SMRMI value is a computed output of a computer simulation of an MRM system including the vehicle and the MRM measuring instrument. The MRM vehicle parameters ("Golden Car") used in the computer simulation are those proposed in NCHRP Project 1-18 (*5*), which are being defined further in a new proposed ASTM standard. The inputs to the computer simulation are the elevation profile measurements

TABLE 1 INERTIAL PROFILOMETER MEASUREMENTS

Kentucky DOH Test Site No.	Number of Repeat Measurements	Standard Mean MRM Index Value (in/mi)	Standard Deviation (in/mi)
PCC			
101*	9	75.0	0.34
102	5	82.4	2.52
103	6	100.5	0.82
104*	5	103.0	0.57
105*	9	144.1	1.38
106	5	151.4	1.57
107	5	160.7	2.71
BC			
201	20	47.1	0.56
202*	5	49.4	0.45
203	5	63.3	0.42
204	6	57.5	1.04
205	5	83.5	0.93
216*	10	111.4	1.03
207*	6	133.9	1.38

made with the inertial profilometer. Using this computer simulation, the SMRMI value was computed for each of the multiple profile measurements. The computed mean SMRMI value and standard deviation for the multiple measurements for each of the fourteen Kentucky DOH test sites are shown in Table 1.

Although readings were taken every 0.1 mile, it was found that averaging readings over a longer test section improved the precision of SMRMI values computed from the profilometer measurements. It was determined that the precision of the measurements improved significantly as the length of the test section was increased from 0.1 mile to 0.5 mile and continued to improve as the test section length was increased to one mile. Where possible, all measurements were made over a test section length of one mile.

The asterisks beside the test site numbers in Table 1 indicate the final six test pavements selected for the calibration study. Three of those sites were constructed with portland cement and the other three with bituminous concrete pavement. These six pavement test sites were chosen because they represented a range of desired SMRMI values and because they exhibited low standard deviations. Although there is a wide range of standard deviations for each test site, it is important to note that the six calibration test pavements selected exhibited about a 1 percent maximum standard deviation.

Test site 201, a smooth bituminous concrete pavement, was the site where the precision or repeatability of the NBS-operated profilometer was evaluated in detail. Twenty test runs were conducted on this particular site. The results of twenty tests runs are shown in Figure 1 as a plot of the computed SMRMI value (inches/mile) for each of the twenty runs. The variation in the computed SMRMI values can be attributed to three factors:

- Variation in the profilometer's elevation profile measuring performance,
- Variation in the path driven by the profilometer driver, and
- Transverse variations in the elevation profile of the test site pavement.

It is suggested that a test site with little variation in computed SMRMI values (low standard deviation) would be a test site with little transverse variation in the elevation profile, and the computed SMRMI values would be less affected by the path driven by the profilometer driver.

The computed cumulative mean SMRMI value (inches/mile) is shown in Figure 2 as a function of the number of test runs included in the computation. As would be expected, the computed mean becomes more stable as the number of included tests runs increases. The computed standard deviation of the computed SMRMI values (inches/mile) as a function of the number of test runs is shown in Figure 3. Again, as would be expected, the standard deviation is reduced as the number of runs increases. Although some improvement is still occurring at test run twenty, the majority of the improvement has occurred by run ten and on the less variable sites, measuring stability appears possible with five test runs with the profilometer.

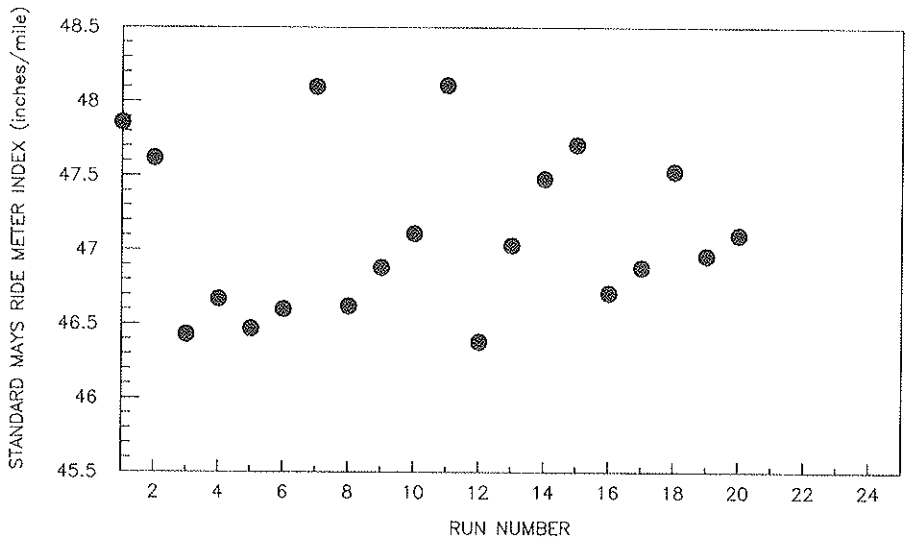

FIGURE 1 Computed standard MRM index value by run number.

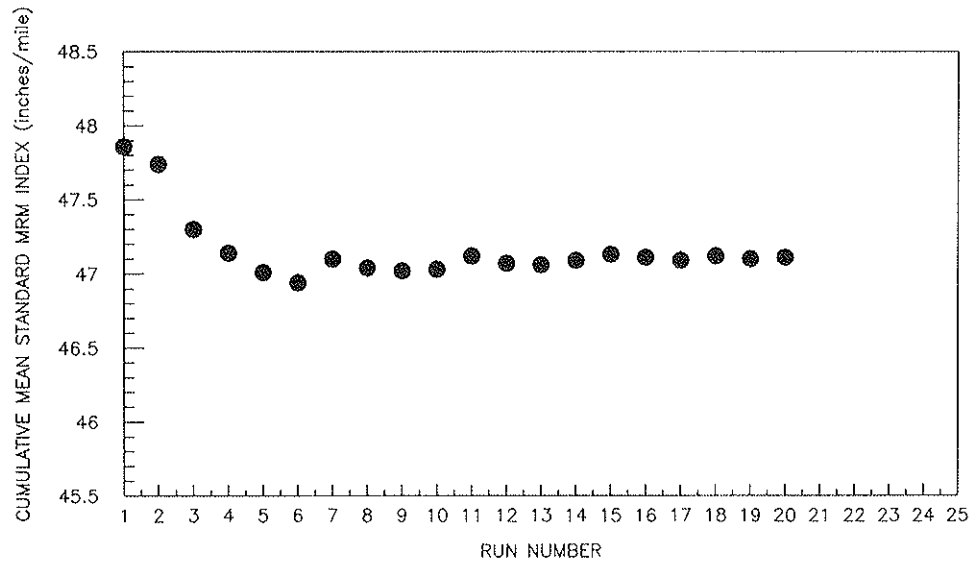

FIGURE 2 Computed mean standard MRM index value by run number.

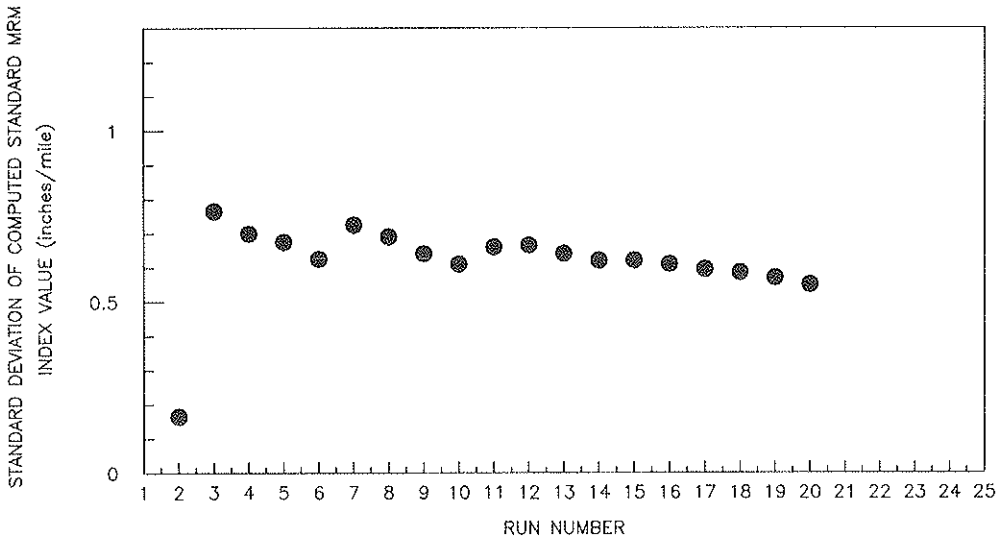

FIGURE 3 Standard deviation of the mean standard MRM index value by run number.

Simultaneous to measuring the Kentucky DOH test sites with the inertial profilometer, the five Kentucky DOH MRM vehicles were used to obtain MRM index values for each of the six test sites. Each of the test sites was measured at least ten times by each Kentucky DOH MRM system. The repeat measurements were made to compute a mean MRM index value and standard deviation about the mean for each MRM system for each test site. The computed mean MRM index value ($\bar{x}$) and standard deviation (σ) in inches/mile for each Kentucky DOH MRM system for each of the six Kentucky DOH test sites are shown in Table 2. Also shown in Table 2 are the computed SMRMI values (from Table 1) computed from elevation profile measured with the inertial profilometer.

The MRM index values in Table 2 show a wide range values for the different MRM vehicles. For example, Kentucky DOH vehicle 2678 had a mean MRM index value of 136.2 inches/mile on test site No. 105 while vehicle 3664 had a mean MRM index value of 184.8 inches/mile for the same site. Since the SMRMI value as established by the NBS inertial profilometer was 144.1 inches/mile, vehicle 2678 was measuring 5 percent too low, and vehicle 3664 was measuring 28 percent too high. The measurements shown in Table 2 clearly show the problem associated with using uncalibrated MRM measurements and emphasizes the need for good MRM calibration procedures.

The computed SMRMI values from the inertial profilometer were then used with the computed mean MRM index value for each Kentucky DOH MRM system to compute the least-squares best fit straight line relationship between the two data sets. This relationship is shown graphically in Figure 4 for Kentucky DOH MRM vehicle No. 2678. For the data set shown in Figure 4, we can compute the slope and *y*-

TABLE 2 MEAN MAYS RIDE METER INDEX VALUES FOR KENTUCKY DOH MRM SYSTEMS

Kentucky DOH Test Site No.	Standard* Mean MRM Index Value (in/mi)	Mean MRM Index Value ($\bar{x}$) and Standard Deviation (σ) by Kentucky DOH Vehicle No.									
		2678		3664		3665		4323		4325	
		$\bar{x}$	σ	$\bar{x}$	σ	$\bar{x}$	σ	$\bar{x}$	σ	$\bar{x}$	σ
PCC											
101	75.0	70.3	3.98	98.3	2.83	72.9	1.47	76.2	0.85	77.7	2.78
104	103.0	98.1	4.22	139.3	1.44	108.9	2.45	107.8	1.64	104.1	3.19
105	144.1	136.2	4.25	184.8	2.59	154.1	2.42	150.3	1.73	142.4	3.75
BC											
202	49.4	40.6	3.14	69.2	4.51	41.0	2.18	43.7	0.83	47.0	3.26
216	111.4	108.4	4.95	143.0	6.61	115.5	3.36	101.1	1.90	109.9	4.61
207	133.9	128.0	2.84	163.0	3.53	139.6	3.77	127.4	2.34	127.8	2.34
Average Std. Dev.			3.90		3.58		2.61		1.55		3.32

* Computed from Profilometer Measurements

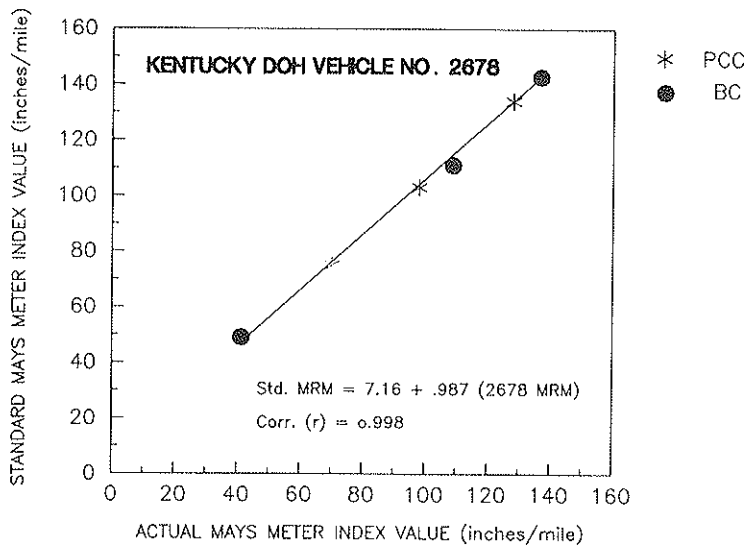

FIGURE 4 Calibration curve for Kentucky Mays Meter Vehicle No. 2678.

intercept for the least-squares best fit line through the data points. The computed line slope and *y*-intercept can then be used to develop a transform or calibration equation between the MRM Index values obtained with the Kentucky DOH MRM system and the SMRMI values computed from the inertial profilometer elevation profile measurements. The calibration equation and the data set correlation coefficient (r) for Kentucky DOH MRM vehicle No. 2678 are shown in Figure 4.

Calibration equations and correlation coefficients for Kentucky DOH MRM vehicles Number 3664, 3665, 4323, and 4325 were developed using the same procedure shown in Figure 4. The results for these four MRM systems are shown in Figures 5 through 8. The high correlation coefficients for the five Kentucky DOH MRM systems is an indication that the "Golden Car" computer model used to compute the SMRMI values is an accurate representation of the actual MRM systems. It is also an indication that the Kentucky DOH MRM systems are in good condition and are functioning as expected.

The calibration equations for each of the five Kentucky DOH MRM systems are summarized in Table 3. Also shown in Table 3 are the average standard deviation for each of the

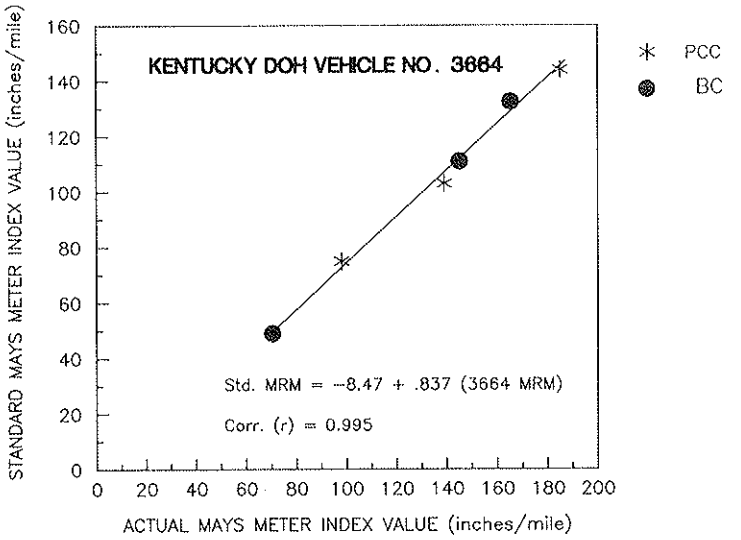

FIGURE 5 Calibration curve for Kentucky Mays Meter Vehicle No. 3664.

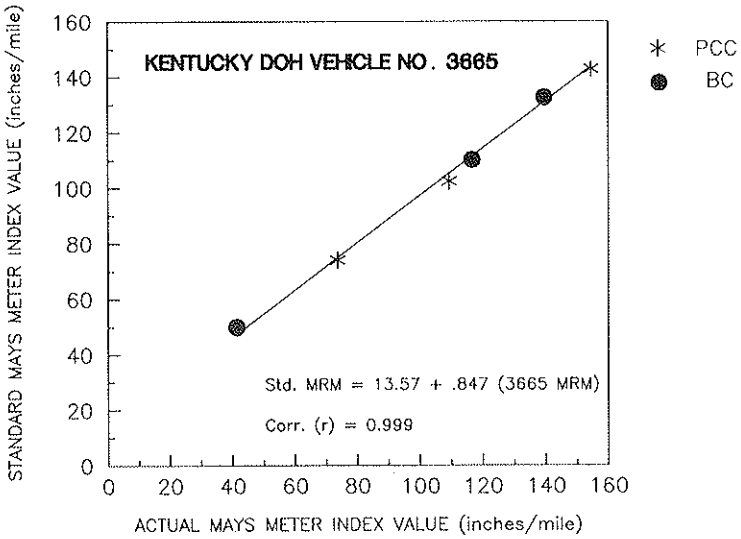

FIGURE 6 Calibration curve for Kentucky Mays Meter Vehicle No. 3665.

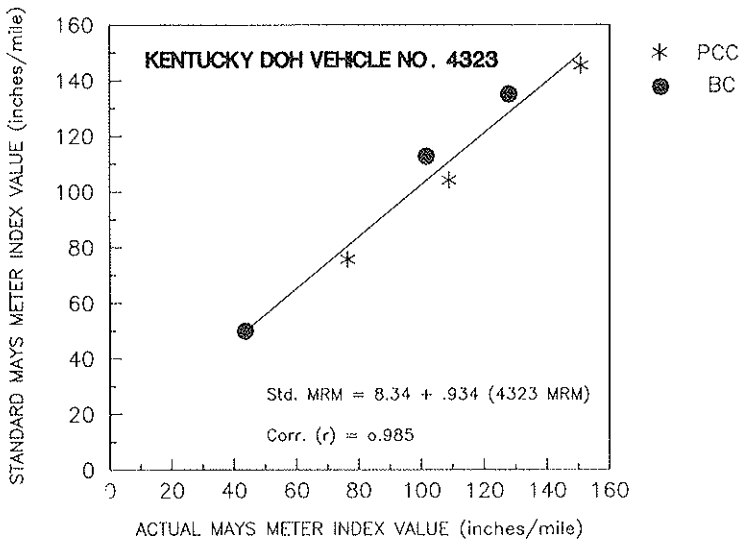

FIGURE 7 Calibration curve for Kentucky Mays Meter Vehicle No. 4323.

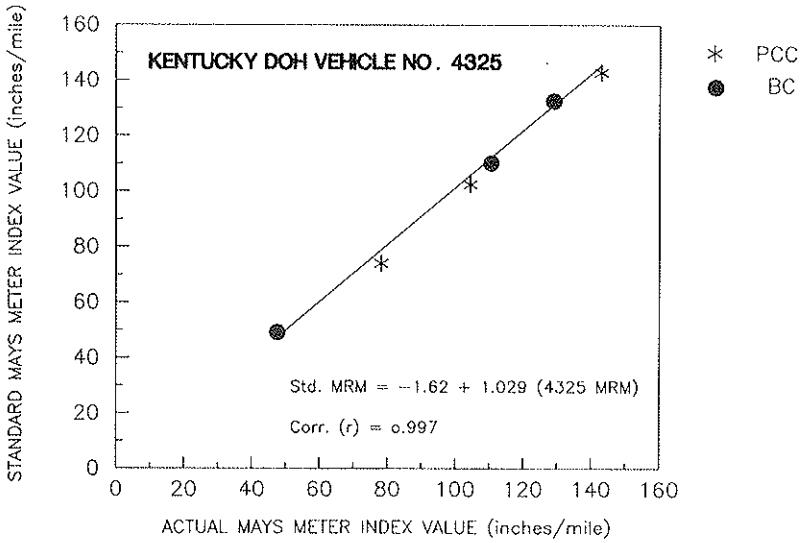

FIGURE 8 Calibration curve for Kentucky Mays Meter Vehicle No. 4325.

TABLE 3 CALIBRATION EQUATIONS FOR KENTUCKY DOH MAYS RIDE METER VEHICLES

Kentucky DOH MRM Vehicle No.	Calibration Equations
2678	Standard MRM = 7.16 + .987 (vehicle MRM)
	Average Std. Dev. = 3.90
3664	Standard MRM = −8.47 + .837 (vehicle MRM)
	Average Std. Dev. = 3.58
3665	Standard MRM = 13.57 + .847 (vehicle MRM)
	Average Std. Dev. = 2.61
4323	Standard MRM = 8.34 + .934 (vehicle MRM)
	Average Std. Dev. = 1.55
4325	Standard MRM = −1.62 + 1.029 (vehicle MRM)
	Average Std. Dev. = 3.32

five Kentucky DOH MRM systems (from Table 2). This average standard deviation is probably the best that might be expected for each system, since these values were computed for pavement test sites that were initially selected for their low standard deviations when measured with the inertial profilometer.

PROFILOMETER CORRELATION

Although the NBS-operated inertial profilometer was used to establish the SMRMI values for the Kentucky DOH calibration test sites, a second K. J. Law Engineers, Inc., inertial profilometer, owned and operated by the Ohio Department of Transportation, was used to measure and compute the SMRMI values for seven of the Kentucky DOH test sites used in the calibration project. This simultaneous measurement of seven test sites provided an excellent opportunity to compare the measuring performance of the two inertial profilometers manufactured by K. J. Law Engineers, Inc., and to determine if equivalent MRM calibrations can be obtained from two identical inertial profilometers.

The measuring results for the NBS and Ohio DOT profilometers are shown in Table 4 for the seven Kentucky DOH test sites. The SMRMI values for each profilometer are plotted in Figure 9 for each of the seven sites. Also shown in Figure 9 is the best fit straight line for the data point pairs, and the y-intercept, slope, and the correlation coefficient (r) for the best fit straight line. The high correlation coefficient of 0.99934 would support the interchangeable use of identical inertial profilometers for the calibration of MRM systems.

DISCUSSION

The calibration procedure developed in this project provides a method that can be used to convert MRM measurements

TABLE 4 COMPUTED STANDARD MAYS RIDE METER DATA

Kentucky DOH Test Site No.	NBS Profilometer			Ohio DOT Profilometer		
	Number of Runs	$\bar{x}$ in/mi	σ in/mi	Number of Runs	$\bar{x}$ in/mi	σ in/mi
PCC						
101	7	75.1	0.15	4	75.1	0.35
102	5	85.7	0.49	5	82.8	0.78
105	9	143.1	0.26	4	141.1	0.78
BC						
201	20	47.1	0.79	20	46.8	0.60
202	5	48.6	0.39	4	49.4	0.44
203	5	63.7	0.23	4	64.7	0.60
205	5	84.7	1.32	4	83.5	0.92

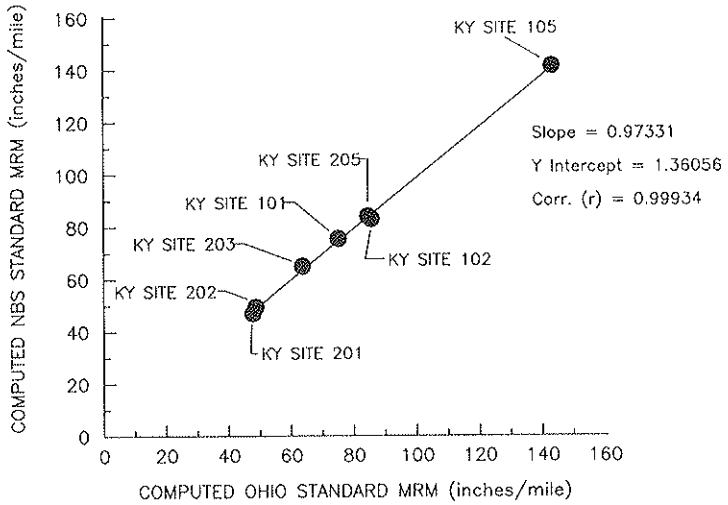

FIGURE 9 Correlation of identical inertial profilometers.

made with individual MRM systems into SMRMI values. The experiences gained in developing calibration procedure suggest the following recommendations related to the calibration and use of MRM systems, in particular, and to response-type ride meters, in general:

- Due to the higher standard deviation values for MRM systems compared to the profilometer, measurements should be made by averaging multiple repeat measurements for each test site. Ten repeat measurements would be desirable.
- One calibration site for each pavement type should be used periodically to confirm the calibration of individual MRM systems. The confirmation would consist of computing the standard mean MRM index value for ten repeat measurements at each site. A deviation from the expected SMRMI value would indicate a change in the system and the need for recalibration.
- A change in the measuring characteristics of an individual MRM system would indicate the need for a full calibration on all calibration sites. As in the original calibration, the mean of ten repeat measurements would be used with the SMRMI value to compute a new calibration equation and correlation coefficient.
- A reduction in the correlation coefficient computed in the recalibration process might be an indication that the SMRMI value for one or more of the established calibration test sites has changed. A significant reduction in the computed correlation coefficient would be an indication that the SMRMI values for the calibration test sites should be reestablished using an inertial profilometer.

Although it would be a significant task, it would be desirable to monitor the time stability of calibration sites with an inertial profilometer to develop a short-term (24-hour) and long-term (daily, monthly and annually) time history for each site. A research project in this area may be highly desirable.

CONCLUSION

- MRM systems can be effectively calibrated using an inertial profilometer.
- The observed variability between MRM systems supports the need for an accurate system calibration.
- Additional research is required to investigate the time stability of both the MRM systems and the pavement sections used in calibration.

REFERENCES

1. E. B. Spangler and W. J. Kelly. GMC Road Profilometer—A Method for Measuring Road Profile. In *Highway Research Record 121*, HRB, National Research Council, Washington, D.C., 1966.
2. J. R. Darlington and P. Milliman. A Progress Report on the Evaluation and Application Study of the General Motors Rapid Travel Road Profilometer. In *Highway Research Record 214*, HRB, National Research Council, Washington, D.C., 1968, pp. 50–67.
3. J. L. Burchett, R. L. Rizenbergs and T. A. Moore. *Surface Dynamics Profilometer and Quarter-Car Simulator: Description, Evaluation, and Adaptation*. Research Report 465, Kentucky Department of Transportation, Lexington, 1977.
4. W. R. Hudson. High-Speed Road Profile Equipment Evaluation. In *Highway Research Record 189*, HRB, National Research Council, Washington, D.C., 1967, pp. 150–163.
5. T. D. Gillespie, M. W. Sayers and L. Segel. *NCHRP Report 228: Calibration of Response-Type Road Roughness Measuring Systems*. TRB, National Research Council, Washington, D.C., 1980.

Publication of this paper sponsored by the Committee on Surface Properties—Vehicle Interaction.

Road Characteristics and Skid Testing

JAMES C. WAMBOLD

This paper reports the results of many years of skid tests and macrotexture and microtexture measurements as well as newer sets of data obtained during a mini-test conducted in connection with a Federal Highway Administration (FHWA) study to develop a normalization procedure for seasonal effects. The mini-test was concerned mainly with the variation of skid number as a function of placement on the pavement; both lateral and longitudinal placement were examined. It was found that longitudinal placement was not significant if the entire test section was uniform; however, lateral placement is very important, as it can result in the skid numbers differing by more than 10. All of the data available from this mini-test and previous tests were used to correlate macrotexture (*MTD*), microtexture (*BPN*), speed gradient data (SN_0 and *PNG*), and ribbed- and blank-tire skid numbers (SN^R and SN^B). Linear correlations between texture measurements and skid numbers and between speed gradient data and skid numbers were found to be adequate in the normal range of measured skid numbers. Further work is needed before limiting values can be established.

Early in the project, a test plan was developed to study the variation of skid number in both the lateral and longitudinal placement on a test section. The data showed very little variation in the longitudinal direction as long as the entire test section was of the same construction and had no patching.

In the lateral direction, on the other hand, there was considerable variation. Figure 1 shows the variation in *SN* with lateral placement at four sites. Site 2 showed much wear (such as rutting) compared with the others, which is reflected by the *SN*. Site 4 was a fairly new road, while site 1 was a much older road than the rest of the sites. Site 3 is located in a curved section.

Figure 2 shows the variation of microtexture and macrotexture (*BPN* and *MTD*) with lateral placement. The results are similar to those determined from tests conducted in Switzerland (Figure 3) and presented by S. Huschek at a Permanent International Association of Road Congresses meeting (*1*).

It can be concluded that lateral placement is critical and that care must be taken in an ASTM E 274 test to position the test wheel at the lateral location desired (for example, in the center of the left wheel track).

CORRELATIONS

An initial experiment (called a minitest) was conducted to compare the correlation of the skid number (*SN*) from a blank tire (SN^B) with that from a ribbed tire (SN^R) with texture and SN_V (skid number at speed *V*). SN_V is obtained from the following equation:

$$SN_V = SN_0 \, e^{-PNG/100 \cdot V}$$

where SN_0 and *PNG* are the regression coefficients given below.

Similarly, texture was also correlated to SN_0 and *PNG* and, thus, indirectly, to SN_V. Five sets of data were collected by the Pennsylvania Transportation Institute (PTI) at the test track and at several sites around State College. Two sets were collected by the Texas Transportation Institute (TTI) at its calibration site. Table 1 lists the sites, their locations, and the testing dates. Figure 4 shows ribbed- and blank-tire *SN*s for the test track. The database included test data taken during a previous project at Penn State in the fall of 1978 and spring of 1979, as reported by J. J. Henry (*2*). Mean texture depth (*MTD*) was measured for macrotexture (in milli-inches), and British pendulum number (*BPN*) was the measure for microtexture. All data given for skid number as a function of speed (SN_V) are for the ribbed (ASTM E 501) tire.

SN^B AND SN^R VERSUS TEXTURE

The first correlation was performed for SN^B and SN^R with *MTD* and *BPN*. Linear and nonlinear regressions were performed; in all, thirteen different forms were tried. The three models with the highest correlations and smallest standard deviations are as follows:

Model	R^2	*S*
$BPN = A1 + B1\ SN^R + C1\ (SN^R)^2$	.90	8.3
$BPN = A2 + B2\ SN^B + C2\ SN^R$	.86	9.6
$BPN = A3 + B3\ SN^R$	.87	9.3
$MTD = D1 + E1\ (SN^B/SN^R) + F1\ (SN^B/SN^R)^2$	.88	10.2
$MTD = D2 + E2\ (SN^B - SN^R) + F2\ (SN^B - SN^R)^2$	.84	11.8
$MTD = D3 + E3\ SN^B + F3\ SN^R$	.83	12.4

There were very few differences among these models for either measurement. The following two equations are plotted in Figure 5.

$$BPN = 11.0 - 0.472\ SN^B + 1.59\ SN^R \quad (2)$$

$$MTD = 40.9 + 1.77\ SN^B - 1.20\ SN^R \quad (3)$$

SN^B, SN^R VERSUS SN_V

SN_0 and *PNG* were also correlated with SN^B and SN^R. The results of these regressions suggest the following models:

Model	R^2	*S*
$SN_0 = 5.6 + 1.8\ SN^R - 0.72\ SN^B$	.96	4.7
$PNG = 1.1 + 0.02\ SN^R - 0.03\ SN^B$	.79	0.3

Pennsylvania Transportation Institute, The Pennsylvania State University, University Park, Pa. 16802.

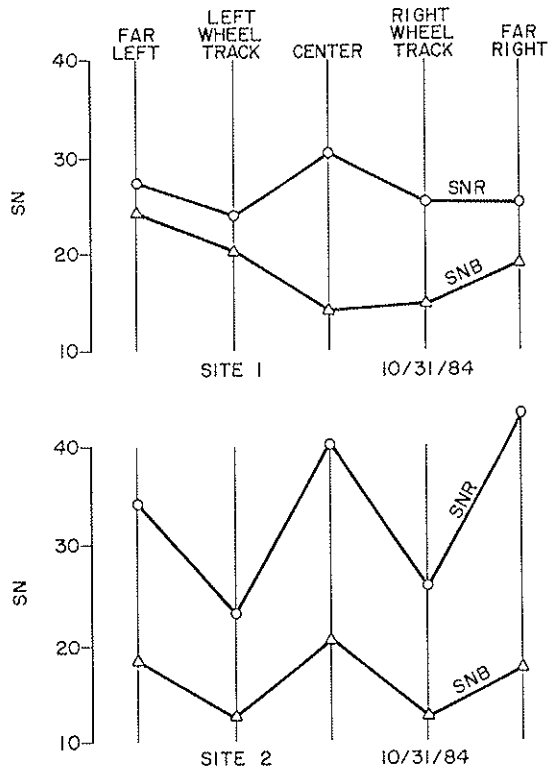

FIGURE 1 Variation in skid number with lateral placement.

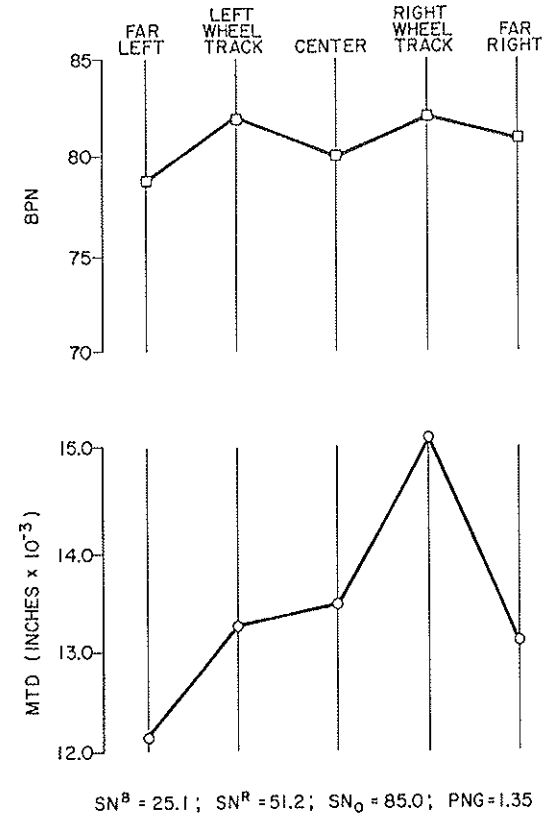

FIGURE 2 Variation in *BPN* and *MTD* with lateral placement.

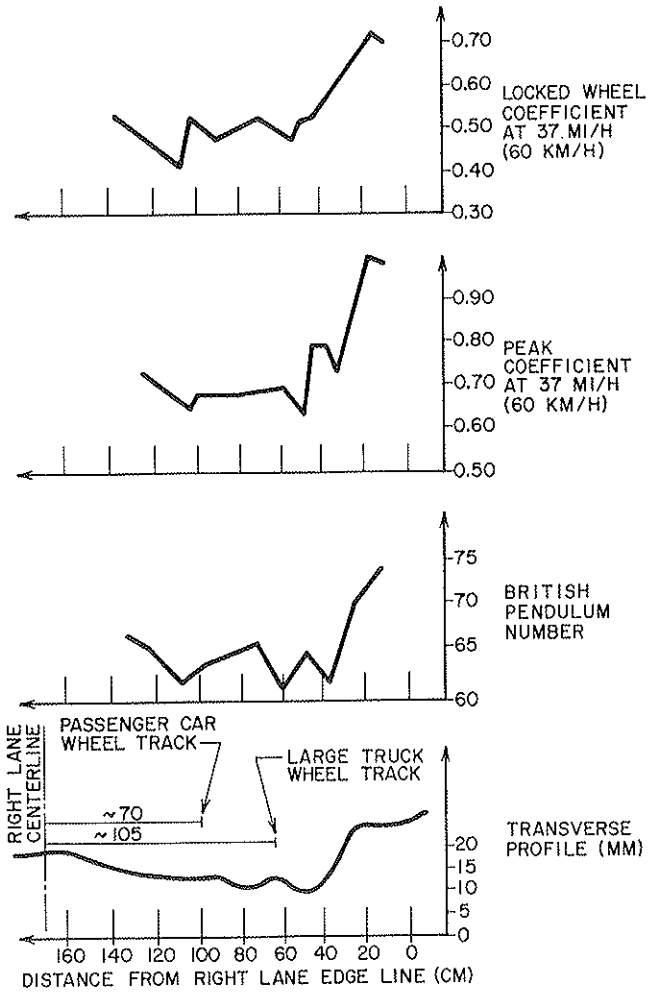

FIGURE 3 Transverse measurements in the right half of the right lane of an 8-yr-old heavily traveled asphalt pavement, PIARC tire, 0.002-in (0.5-mm) water depth (*1*).

These equations are plotted and presented graphically in figure 6. Although the model for *PNG* can be improved to $R^2 = .82$ if $(SN^R)^{1/2}$ and $1/(SN^B)^{1/2}$ are added, there are not enough data points to ensure an improvement. In addition, this change makes the relationship nonlinear.

TEXTURE VERSUS SN_V

A similar set of correlations was performed to establish the relations between SN_0 and *PNG* with *MTD* and *BPN*. The regressions for *PNG* were good, indicating that *MTD* and *PNG* are highly correlated. SN_0 and *BPN* showed high correlations within a given time period and region but not when different times and regions were used. The best regression model for *PNG* follows:

$$PNG = -0.26 = 0.19/\sqrt{MTD} \qquad R^2 = 0.92,\ S = 0.14 \qquad (4)$$

The regression model for SN_0 gives the following:

$$SN_0 = 9.1 + 0.95\ BPN \qquad R^2 = 0.32,\ S = 17.3 \qquad (5)$$

TABLE 1 SITES FOR MINITEST

Site Number	Date	Location
PS1	8/15/85	Test Track, Section 2
PS2	6/4/86	PA Rt. 45E, between 3/70 and 3/75
PS3	6/4/86	PA Rt. 45W, between 3/75 and 3/70
PS4	5/7/86	Test Track, between 3 and 3.1
PS5	5/12/86	Test Track, between 4.1 and 5.2
TX6	3/27/86	SRS No. 5
TX7	3/31/86	SRS No. 7

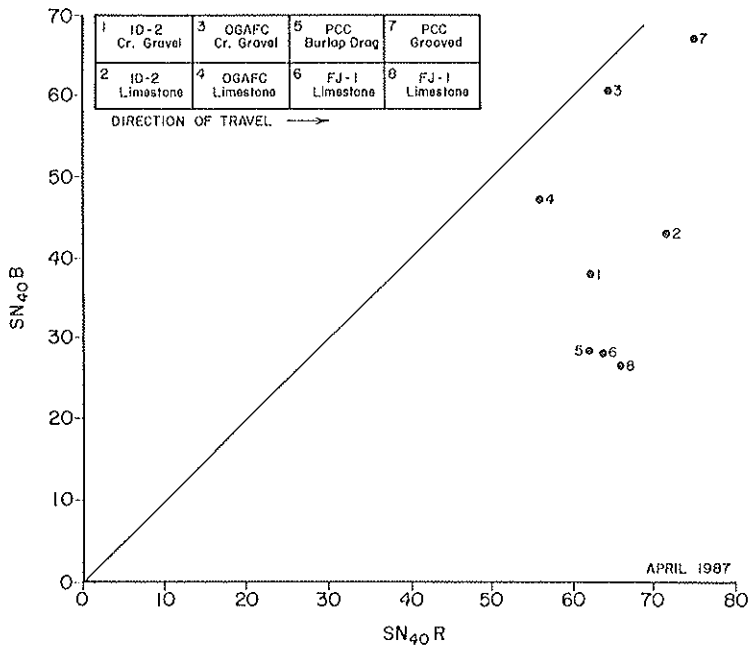

FIGURE 4 PTI skid test facility results.

when all the sites are used. If site PS1 (earlier test) and sites TX6 and TX7 (another region) are removed so that all the data are for the same region and time frame, the regression model becomes:

$$SN_0 = -68.4 + 2.41\ BPN \qquad R^2 = 0.98,\ S = 2.8 \qquad (6)$$

These results lead to the conclusion that, at a given time and place, the two texture parameters (*BPN* and *MTD*) are highly correlated to SN_0 and *PNG*. However, the tire responds to factors other than *BPN* and *MTD*; and, thus, the prediction of *SN* from texture cannot be used for different times and locations. The ribbed- and blank-tire *SN* measurement method does not have this limitation.

SN_0 AND *PNG* MEASUREMENTS

SN_0 and *PNG* are defined by a skid number/speed model referred to as the Penn State Model (*3*). SN_0 is related mainly to microtexture, and *PNG* is related mainly to macrotexture. The model is used to calculate SN_V, the skid number at velocity *V*:

$$SN_V = SN_0\, e^{-PNG/100 \cdot V} \qquad (7)$$

If the logarithm of each side is taken, this relation becomes:

$$\ln SN_V = \ln SN_0 - \frac{PNG}{100} V \qquad (8)$$

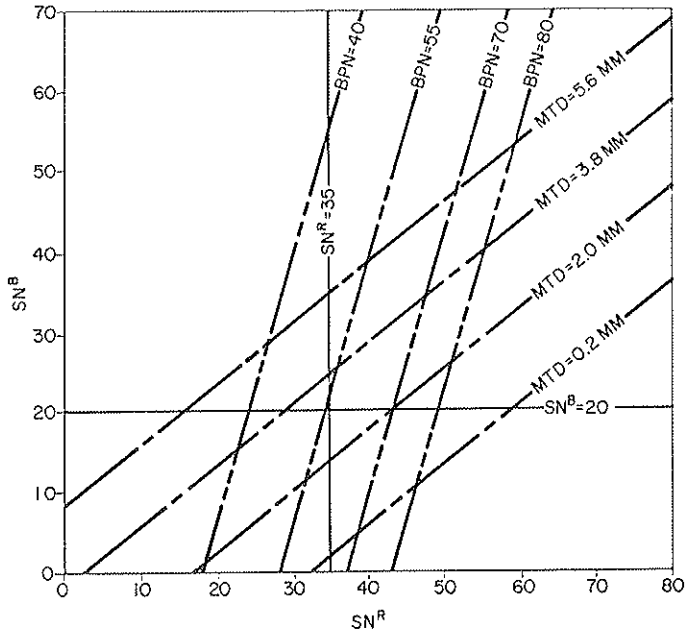

FIGURE 5 Constant SN_0 and PNG versus SN^B and SN^R.

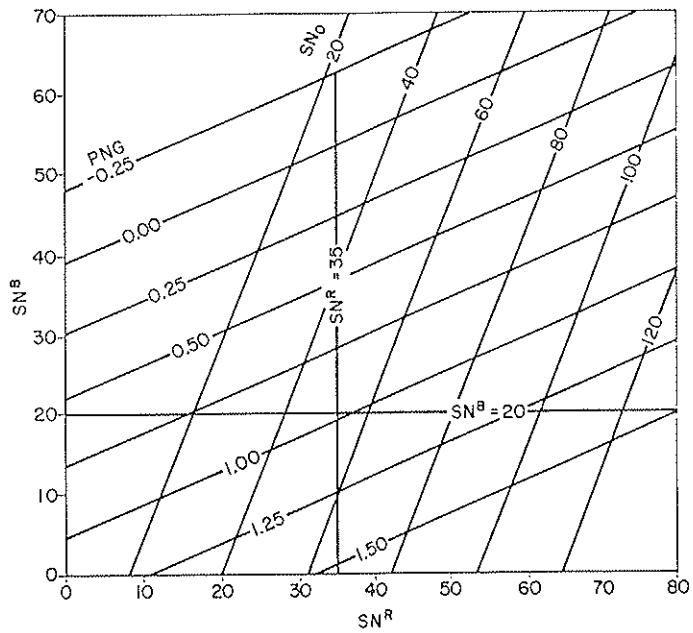

FIGURE 6 Constant SN_0 and PNG versus SN^B and SN^R.

If

$$\ln SN_0 = y,\ \ln SN_0 = A,\ -\frac{PNG}{100} = B, \text{ and } V = \chi$$

then equation 8 can be written as a linear regression:

$$y = A + B\chi \tag{9}$$

Thus, it is possible to run a skid test at several speeds, perform a linear regression of the ln SN with V, and obtain the constants, A and B, of the regression.

Then

$$SN_0 = \ln^{-1} A \tag{10}$$

$$PNG = -B \times 10^2 \tag{11}$$

Good results can be obtained by performing five skid tests at 30, 40, and 50 mph. If a transient test is run, then the same procedure is used except that SNT20, SNT30, SNT40, and SNT50 for a 50-mph test or SNT20, SNT30, and SNT40 for a 40-mph test are used in place of SN_{20}, SN_{30}, and SN_{40}, where

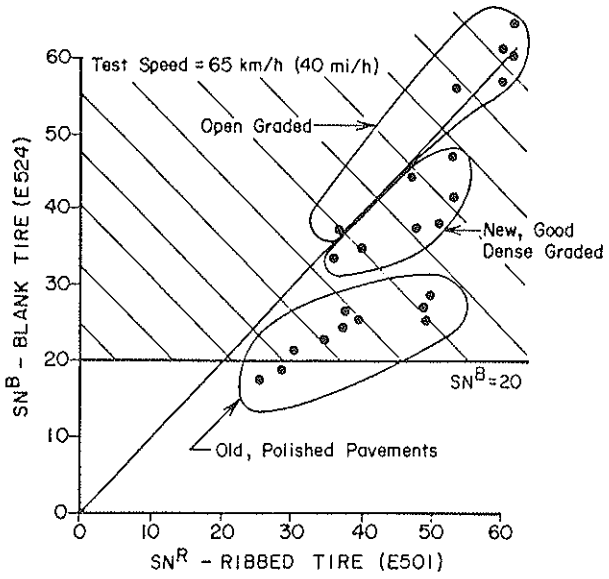

FIGURE 7 Acceptance criteria (shaded area) using blank-tire skid numbers (SN^B_{40}).

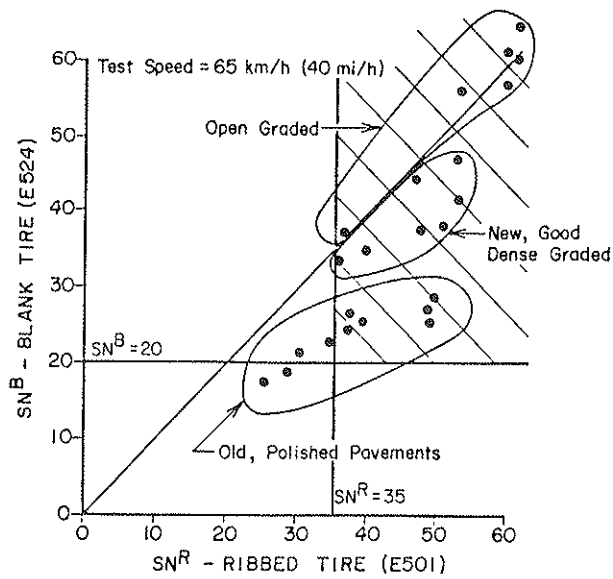

FIGURE 9 Acceptance criteria using both blank- and ribbed-tire skid numbers (SN^B_{40} and SN^R_{40}).

SNTV is the skid number at speed V obtained from a transient test.

SUMMARY

A summary of the relationships developed is given in Figures 7 through 11, which show lines of constant SN_0 and PNG on graphs of SN^B versus SN^R. Also included is a line of constant BPN equal to 55 and a line of constant MTD equal to 0.03 inch. These two values were suggested by Huschek and represent the limits on microtexture and macrotexture (for 55 mph) in Switzerland (*1*). Figures 7 through 11 illustrate various criteria for acceptable pavements. The limits of the acceptable regions, which are superimposed on data from a 1978 study (*2*), are shown only as an example. For instance, if only blank-tire skid numbers (SN^B_{40}) are available and the level of 20 is chosen, the acceptable region will be above the line at $SN^B_{40} = 20$ in figure 7. On the other hand, if only ribbed-tire skid numbers (SN^R_{40}) are available and the limit of 35 is chosen, only the pavements to the right of the line $SN^R_{40} = 35$ in Figure 8 will be acceptable. If data from both tires are available and the same limits are chosen, the upper right quadrant of Figure 9 will contain acceptable pavements. If mean texture depth (MTD) and British pendulum numbers (BPN) are available, the acceptable region will be to the right

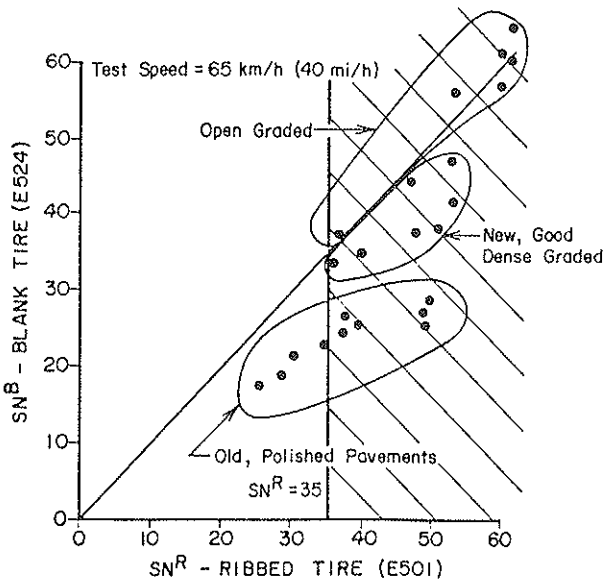

FIGURE 8 Acceptance criteria using ribbed-tire skid numbers (SN^R_{40}).

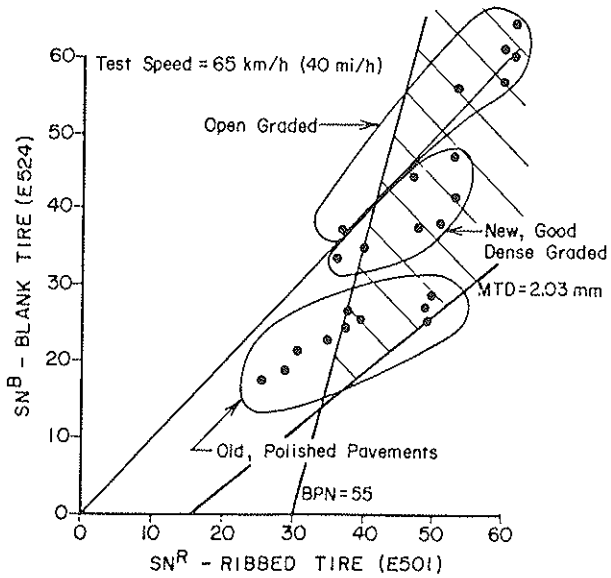

FIGURE 10 Acceptance criteria using sand-patch MTD and BPN.

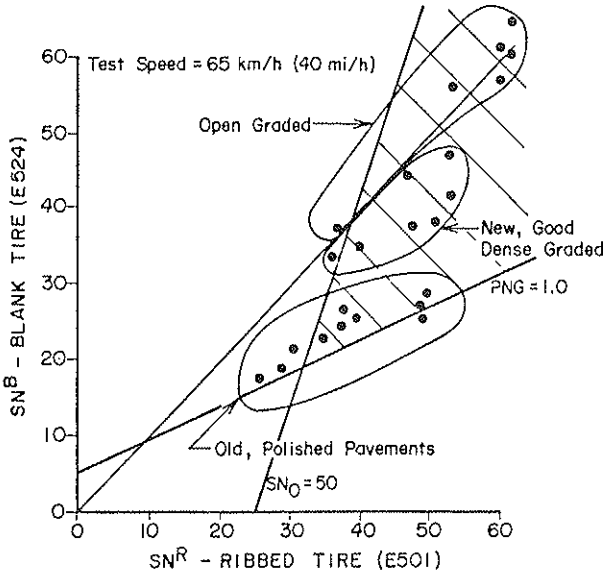

FIGURE 11 Acceptance criteria using skid number/speed intercept (SN_0) and percent normalized gradient (*PNG*).

of the *BPN* = 55 line and above the *MTD* = .030 line in Figure 10. Finally, if SN_0 and *PNG* data are used, the acceptable region will be to the right of the SN_0 = 50 line and above the *PNG* = 1.0 line in Figure 11. The levels of acceptability shown in the figures are not intended to be conclusive. Further research should be conducted to determine levels of acceptability from accident data. However, it is clear that the use of any one or two of these parameters would delimit different areas of acceptance, and, thus, some roads that are acceptable on the basis of one criterion are unacceptable on the basis of other criteria.

ACKNOWLEDGMENTS

Many of the statistical data calculations were performed by Jacov Norman, a visiting scientist from Israel. Test data from Texas were supplied by A. J. Stocker of the Texas Transportation Institute. The work was done as part of Federal Highway Administration Contract No. DTFH61-84-C-00078, "Pavement Friction Measurements Normalized for Operational, Seasonal, and Weather Effects."

REFERENCES

1. S. Huschek. Recent Progress in the Measurement of Skid Resistance and Improvement Procedures. *Surface Characteristics*. Technical Committee Report No. 1, 18th World Road Congress, Permanent International Association of Road Congresses, Paris, France, 1987, pp. 49–60.
2. J. J. Henry. The Use of Blank and Ribbed Test Tires for Evaluating Wet Pavement Friction. In *Transportation Research Record 788*, TRB, National Research Council, Washington, DC, 1981, pp. 23–28.
3. J. J. Henry, K. Saito, and R. Blackburn. *Predictor Model for Seasonal Variations in Skid Resistance*, Report No. FHWA/RD-83/005, Federal Highway Administration, Washington, D.C., 1983.

Publication of this paper sponsored by the Committee on Surface Properties—Vehicle Interaction.

Obtaining Skid Number at Any Speed from Test at Single Speed

JAMES C. WAMBOLD

This paper reports the results of a set of tests from New York, Pennsylvania, Texas, and Florida that were used to correlate skid number measurements made with ASTM ribbed and blank tires with skid number (*SN*) data recorded at any speed [in other words, the calculation of *SN* at any speed from the determination of the skid number/zero speed intercept (SN_0) and percent normalized gradient (*PNG*)]. Correlations were made with actual data at three or four speeds. Similarly, SN_0 and *PNG* were determined from transient tests of a ribbed-tire run at a single speed, and these results were correlated with the actual speed data. It was found that a transient skid test made with a ribbed tire at 40 or 50 mph, or a locked-wheel test with both the ribbed and blank tire at 40 mph, produced excellent results. *SN* could be calculated over a range of 20 to 60 mph with a correlation (R^2) better than 0.96 and as high as 0.99.

Two methods stand out as lending themselves to a new skid tester design: the method employing a ribbed and a blank tire in combination, and the spinup method. A series of tests was undertaken to determine the feasibility of these methods. With one minor exception no special equipment or instrumentation was constructed or obtained. The available friction testers were used, and a large number of the tests were conducted as part of the overall testing program of this project.

The objective of the experiments was to determine if the results of ribbed/blank tire tests and of spinup/spindown tests can be used to compute SN_0 and *PNG*, hence the *SN*/speed relationship. The reference was the SN_0 and *PNG* obtained from lockup tests with the ribbed ASTM E 501 tire at several speeds. Tests the results of which were to be compared were made at the same locations and wheel tracks of public highways, or of the Pennsylvania Transportation Institute Skid Resistance Research Facility, and as close together in time as practical in order to eliminate as many extraneous variables as possible from the comparisons.

The ribbed/blank tire comparisons were made in only one (left) wheel track, thus eliminating the effect of the possible differences between wheel tracks. This required changing the tires, or rather the wheels to which either a ribbed E 501 or a blank E 524 tire had been mounted. This procedure eliminated errors that could be caused by differences in water application and instrumentation of the two wheels of the two-wheel tester. Thus the results of the tests were kept free of influences that might obscure the validity of the comparisons.

Department of Mechanical Engineering and Vehicle/Surface Interaction and Safety Program, Pennsylvania Transportation Institute, The Pennsylvania State University, University Park, Pa. 16802.

For the spinup/spindown investigations, the standard locked-wheel tests were used except that oscillograph chart speed was set at the maximum to get optimum resolution. The test wheel speed trace was quite free of noise, and the force trace was smoothed visually. This permitted wheel speed and force to be related, thereby obtaining the transient skid numbers TSN_VSD (spindown) and TSN_VSU (spinup). Examples of such charts are reproduced as Figure 1.

The following data sets were used:

SN_{30}, SN_{40}, SN_{50}, and SN_{40}^B, or SN_{20}, SN_{30}, SN_{40}, and SN_{40}^B, and TSN_VSU, TSN_VSD

to calculate from either one of the first two sets of *PNG* and SN_0 by performing a least squares fit of the three points to

$$SN_V = SN_0\, e^{-PNG/100 \cdot V} \tag{1}$$

This equation is referred to as the Penn State Model (*1*).

Taking the log of each side:

$$\ln SN_V = \ln SN_0 - \frac{PNG}{100} V$$

If $\ln SN_v = y$, $\ln SN_0 = A$, and $PNG/100 = B$ then

$$y = A - BV \tag{2}$$

A linear least-squares fit can then be used to calculate A and B, from which SN_0 and *PNG* result. These are considered the actual or standard SN_0 and *PNG* to which everything else is to be correlated.

In a similar manner, *PNGSU*, *PNGSD*, SN_0SU, and SN_0SD (*SU* and *SD*, referring to spinup and spindown, respectively) can be calculated from the transient skid numbers TSN_VSU and TSN_VSD. In addition, the following regressions were performed:

$$\begin{aligned} PNG &= A_1 + B_1\, SN_{40}^R + C_1\, SN_{40}^B \\ &= A^2 + B_2\, SN_{40}^R + C_2\, SN_{40}^B \\ &\quad + D_2\sqrt{SN_{40}^R} + E_2\, 1\sqrt{SN_{40}^B} \\ SN_0 &= A_5 + B_5\, SN_{40}^R + C_5\, SN_{40}^B \\ &= A_6 + B_6\, SN_{40}^R + C_6\, SN_{40}^B \\ &\quad + D_6\sqrt{SN_{40}^R} + E_6\, 1\sqrt{SN_{40}^B} \end{aligned}$$

For each pair of SN_0 and *PNG* calculated (test at three speeds, spinup, spindown, and SN^B and SN^R), CSN_{30}, CSN_{40}, and CSN_{50} could then be calculated (*C* indicating the calculated skid numbers).

Next, the correlations were obtained. The following com-

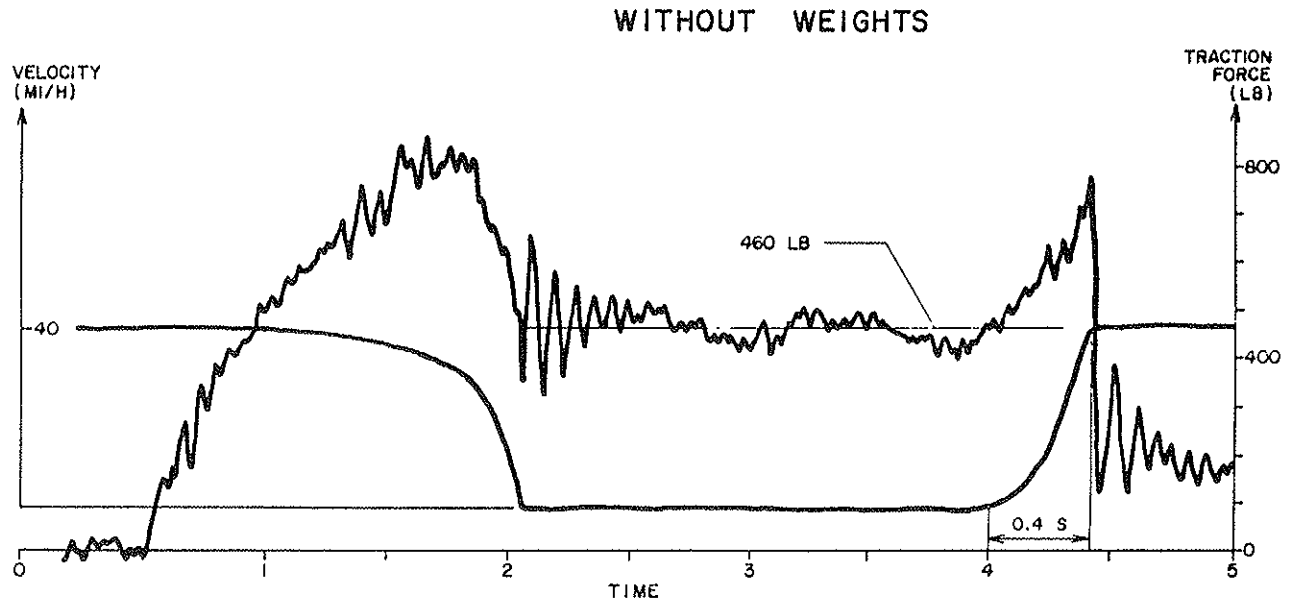

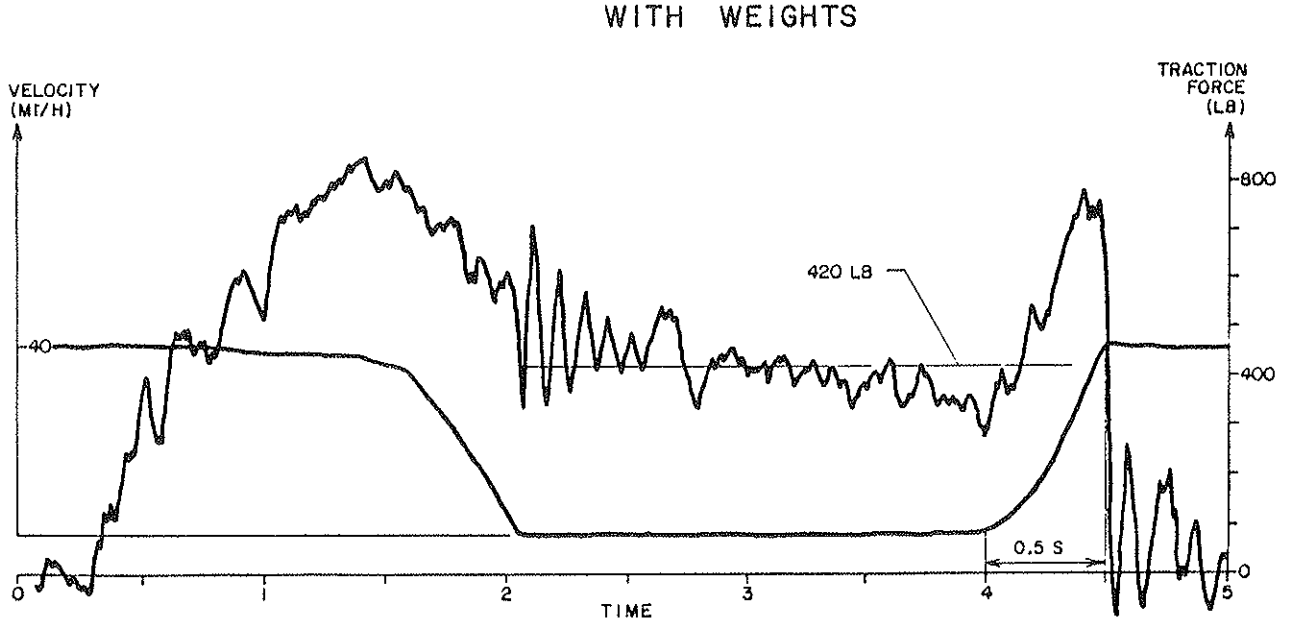

FIGURE 1 Oscillograph charts illustrating spindown and spinup tests.

TABLE 1 CORRELATIONS OF SN_0 AND *PNG* FROM RIBBED/BLANK TIRE TEST

COEFFICIENTS

Equation		NY (ALL)	NY (S)	NY(C)	FL	TX	NY(S) + FL	NY(S) + FL + TX
	A	-0.582	-0.704	-0.495	-0.851	-0.365	-0.8172	-0.801
1	B	1.59	1.77	1.48	2.03	1.32	1.9292	1.784
	C	9.97	6.19	11.9	0.3	12.8	2.901	8.571
	α	-0.0272	-0.0303	-0.0254	-0.0419	-0.0173	-0.0336	-0.0317
2	β	0.0102	0.0158	0.00626	0.0159	0.0032	0.0188	0.0175
	γ	1.23	1.10	1.33	1.44	1.057	1.06	1.0372
	A	-0.858	-1.53	-0.801	-0.73		-0.876	-0.682
	B	-7.66	17.2	-8.7	24.6		2.778	2.894
3	C	124.0	188.0	137.0	-293	*	-11.29	-12.75
	D	-79	-315	-52	-227		-19.0	24.7
	E	-382	-537	-424	981		45.5	35.4
	a	-0.0204	-0.0417	-0.0202	-0.102		-0.0198	-0.01996
	β	-0.286	-0.46	-0.307	0.43		0.069	0.0106
4	γ	3.99	6.41	4.21	-5.33	*	-0.680	0.113
	δ	2.75	-4.86	3.12	-24.2		4.708	3.844
	ε	-12.8	-19.1	-13.14	24.8		2.504	-0.49

R^2

Equation	NY (ALL)	NY (S)	NY(C)	FL	TX	NY(S) + FL	NY(S) + FL + TX
1	0.92	0.90	0.96	0.95	0.99	0.99	0.94
2	0.77	0.70	0.90	0.89	0.99	0.85	0.78
3	0.96	0.96	0.99	0.99	*	0.95	0.96
4	0.90	0.87	0.99	0.90	*	0.85	0.79

*Too few data points to give five coefficients

Equations:

1. $SN_O = A \cdot SN^B + B \cdot SN^R + C$
2. $PNG = \alpha \cdot SN^B + \beta \cdot SN^R + \gamma$
3. $SN_O = A \cdot SN^B + B \cdot SN^R + C \sqrt{SN^R} + D/\sqrt{SN^B} + E$
4. $PNG = \alpha \cdot SN^B + \beta \cdot SN^R + \gamma \sqrt{SN^R} + \delta/\sqrt{SN^B} + \varepsilon$

TABLE 2 R^2 VALUES OF SN_0 AND *PNG* WITH SN_{40}^B AND SN_{40}^R

	SN_{40}^B	SN_{40}^R
SN_0	.059	.869
PNG	-.832	-.151

parisons were made to determine the correlation factor R^2 (or R, if so noted):

SN_0 with SN_0SU

SN_0SD

SN_0 from SN^R and SN^B

SN_0 from SN^R, SN^B, SN^R, and $1/(SN^B)^{1/2}$

PNG with *PNGSU*

PNGSD

PNG from SN^R & SN^B

PNG from SN^R, SN^B, SN^R, and $1/(SN^B)^{1/2}$

What follows are the comparisons of CSN_V with the measured SN_V for each of the four methods.

RESULTS OF RIBBED/BLANK TIRE METHOD

The results of the correlation of SN_0 and *PNG* are given in Table 1. In the case of the New York sites, straight and curved sections were first combined [NY (all)] and then separated [NY(S) and NY(C)]. When the New York sites were combined with the Texas and Florida sites, only the straight, or tangent, sites were used since the non-tangent sites produce a poor correlation in calculating *PNG*.

The correlation coefficients (R^2) of SN_0 and *PNG* for the four equations are given in Table 1. The R^2 values N(S), FL, TX, and combined are excellent for SN_0 (R^2 = 0.94 for all sites combined to R^2 = .99 for the Texas sites). The correlations of *PNG* are also very good but less than for SN_0. The R^2 values range from .778 for all sites combined to .99 for the Texas sites, and can be improved slightly by using $(SN^R)^{1/2}$ and $1/(SN^B)^{1/2}$. However, the improvement is not worth the added complexity of the calculation.

Table 2 shows the correlation, using all of the New York sites, between SN_0 and *PNG*, with SN_{40}^B and SN_{40}^R. This correlation shows that the ribbed tire is mostly sensitive to SN_0 and only mildly sensitive to *PNG*. The blank tire is sensitive mainly to *PNG* and has very little sensitivity to SN_0.

TABLE 3 SN_0 AND *PNG* CORRELATIONS (R^2 VALUES) USING SPINUP AND SPINDOWN METHOD, NEW YORK SITES

	SN_0	SN_0T40SD	SN_0T40SU	SN_0T50SD	SN_0T50SU
SN_0	1	.902	.890	.898	.901
SN_0T40SD		1	.932	.919	.959
SN_0T40SU			1	.933	.955
SN_0T50SD				1	.959
SN_0T50SU					1

	PNG	PNGT40SD	PNGT40SU	PNGT50SD	PNGT50SU
PNG	1	*.208/.810	*.200/.611	*.814/.90	*.683/.810
PNGT40SD		1	.616	.538	.730
PNGT40SU			1	.495	.531
PNGT50SD				1	.909
PNGT50SU					1

Note: *All sites/tangent only sites
Numbers without an asterisk represent results for all sites.

TABLE 4 CORRELATIONS (R^2 VALUES) OF CALCULATED CSN_V FOR SPINDOWN AND SPINUP TESTS WITH MEASURED SN_V

SN (Measured)	Calculated					
	*SN_0 & PNG	T5OSD	T4OSD	T5OSU	T4OSU	Site
SN_{30}	.992	.974	.987	.978	.980	NY
SN_{40}	.994	.971	.987	.981	.985	NY
SN_{50}	.987	.964	.984	.979	.986	NY
SN_{30}	.995	--	.989	--	.989	TX
SN_{40}	.996	--	.991	--	.989	TX
SN_{50}	.994	--	.993	--	.985	TX

*Values calculated from actual speed data.

$$CSN_V = SN_0 \, e^{-\frac{PNG}{100} V}$$

RESULTS OF SPINUP/SPINDOWN METHOD

Two separate sets of spinup and spindown tests were performed. One set included all of the New York sites, the calibration site at the Texas Transportation Institute, and the Bryan, Texas, sites. Table 3 shows the correlations of SN_0 and *PNG* with the spinup and spindown tests run at both 40 mph and 50 mph on the New York sites. SN_0 correlates with all the tests with an R^2 of about .9, showing very good correlation.

Table 3 also shows the values of R^2 when *PNG* is compared with the values of *PNG* computed from spinup and spindown tests. These tests showed lower correlations than those for SN_0. However, the results at 50 mph were considerably better than those at 40 mph. When the curved sections are removed, all the R^2 values improve—the 40 mph tests more than the 50 mph tests. Once the curved sections were removed, the correlations were very good: R^2 values ranged from .611 to .90.

In summary, it may be said that good *PNG* correlations are fairly easy to obtain, but very good SN_0 correlations can also be obtained easily. This indicates that macrotexture is less homogeneous than microtexture.

The next set of correlations was performed by using the SN_0 and *PNG* values calculated from the various tests to calculate CSN_{30}, CSN_{40}, and CNS_{50}. These were then correlated with the SN_{30}, SN_{40}, SN_{50} values actually measured. Table 4 gives the correlation values (R^2) for each speed for all the New York sites and for the Bryan and TTI sites. While the SN_0 and *PNG* correlations were good, these results show that when the SN_0 and *PNG* values were used to calculate CSN_V the calculated values were excellent. For all the speeds and methods, the lowest R^2 value was .964. In fact, the spindown and spinup tests produced results almost as good as the values calculated directly for the curve fit to the actual speed data.

Because these results were so good, calculated CSN_{20} and CSN_{60} were also compared with those values calculated from the original speed data. Again, the same correlations were found. The tests were then run at the PTI Skid Resistance Research Facility at speeds up to 60 mph, and again no significant degradation of results was found.

SUMMARY

The results of these tests show that the spinup or spindown transient tests can be used to obtain skid number versus speed data from 20 mph up to at least 60 mph from a single test at one speed. Similarly, a ribbed and blank tire can be used and similar results obtained.

It is recommended that where a standard *SN* cannot be obtained at 40 mph a transient test be made. From those data an *SN* can be calculated for 40 mph so that all test data would be reported at the same speed. If this method were always used, then on the basis of the reported SN_0 and *PNG* one would know whether the microtexture, or the macrotexture, or both, needed corrective action.

ACKNOWLEDGMENT

This paper is based on research sponsored by the Federal Highway Administration, Contract No. DTFH61-84-C-00078, "Pavement Friction Measurements Normalized for Operational, Seasonal, and Weather Effects." Many of the statistical calculations were performed by Xioaying Ma, a visiting scientist from China. The test data from Texas were supplied by A. J. Stocker of the Texas Transportation Institute, who made the arrangements for obtaining the Florida data, which

were supplied by Larry Hewett of the Florida Department of Transportation.

REFERENCE

1. J. J. Henry, K. Saito, and R. Blackburn. *Predictor Model for Seasonal Variations in Skid Resistance.* Report No. FHWA/RD-83/005, Federal Highway Administration, U.S. Department of Transportation, Washington, D.C., 1983.

Publication of this paper sponsored by the Committee on Surface Properties—Vehicle Interaction.

Concrete Pavement Rehabilitation for the Texas State Department of Highways and Public Transportation

JAMES L. BROWN

In order to formulate recommendations for rehabilitation strategies that should be considered for concrete pavements the author has: (a) Reviewed the performance of different solutions used in Texas, (b) Reviewed the performance of other methodologies in other states, and (c) Examined costs of several recent projects in Texas and Kentucky. This paper summarizes the findings and recommendations.

Historically, rehabilitation of concrete pavements has consisted of (1) attempts to stabilize pumping with asphalt undersealing, joint sealing, and grouting; (2) repairs varying from spall repairs to joint replacement to full slab replacement; (3) leveling attempts include grinding, mudjacking, and thin asphalt overlays; and (4) strengthening with thick asphalt overlays, bonded and unbonded concrete overlays, and retrofitted tied portland cement concrete (PCC) shoulders.

Recent work by the concrete paving industry has lumped many of these items into a program called concrete pavement restoration (CPR). The author feels this program, properly applied, is a viable approach to contracting for deferred maintenance, and that CPR should often be used to restore the pavement to an acceptable operating condition. It is also believed that the reason such maintenance is often deferred in Texas is the difficulty of performing such maintenance under heavy traffic. It is further believed that soon after completion of CPR there will again arise the need for maintenance and it will be again deferred. In other words, there comes a time in the life of all heavily trafficked concrete pavements when either strengthening or replacement is needed. This paper deals with those situations.

The following types of PCC pavements have been built in Texas and are discussed hereafter. They are plain concrete pavements (CPCD) with a variety of load transfer devices and active joints from twenty to fifty feet; jointed reinforced concrete pavements (JRCP), with 50- to 60½-ft joint spacing; and continuously reinforced concrete pavements (CRCP).

The following rehabilitation solutions have been considered:

1. Simple asphalt overlays,
2. Asphalt overlays with crack relief layers,
3. Asphalt overlays after cracking and seating the PCC,
4. Bonded concrete overlays, and
5. Unbonded concrete overlays.

Within certain limits it is believed all of the above solutions can provide a viable extension of life of the existing pavement. It is also believed that a sixth solution, complete reconstruction, will ultimately be necessary. The expected performance of each type of rehabilitation for each type of pavement is discussed briefly below.

Reflected joints through simple asphalt overlays have usually been the scourge of this solution for jointed PCC pavements. Water enters the broken asphalt at the reflection crack, and potholing, crack spalling, and stripping often follow.

Simple asphalt overlays should, therefore, be limited to pavements with less traffic and good load transfer across the joints. The only reasons that justify the need for such overlays, then, are slickness and roughness. In summary, a slick or rough, but sound, jointed PCC might be successfully overlaid with asphalt concrete pavement (ACP). (Sawing of the ACP over the old joints is being researched in some states. This may be an improvement on this technique.)

Texas' experience has indicated that simple asphalt overlays have been very successful when placed over repaired CRCP. Based on the performance of more than 20 such projects ranging in age from one to eighteen years, it appears conservative to expect a ten-year life for such solutions (results of unpublished condition surveys conducted on asphalt overlays of 8-in CRCP in Texas in 1986). Thickness of the asphalt overlays has varied from 1 inch to 6½ inches. Current recommendations are to carefully repair the CRCP with full-depth, fully reinforced patches and place a 3½-in to 4½-in ACP overlay.

One asphalt overlay with a crack relief layer has been tried in Texas. Several projects in Arkansas and other states have also been built (*1*). Mixed success has been reported. One factor that has not been completely resolved with this technique is how much joint movement—both horizontally and vertically—can be accommodated by what size aggregate in the crack relief layer. Additionally, the crack relief layer acts as a drainage layer with all the attendant problems associated with outlets. In summary, enough success has been reported with this technique to not rule it out, but specific recommendations on optimizing the design are not possible.

Many projects using the "crack and seat" or "break and seat" technique followed by an asphalt overlay have been built in recent years. California and Kentucky (*2*) have been leading states using this method. Existing PCCs in California

Pavement Design Section, Highway Design Division, Texas State Department of Highways and Public Transportation, 11th and Brazos, Austin, Tex. 78701.

are plain pavements without reinforcement and only aggregate interlock for load transfer. Stabilized subbases are usually present. Kentucky, on the other hand, uses mesh reinforcement and dowels. The California overlays are approximately 3½-in, plus a fabric reinforcement. The Kentucky overlays are approximately 6½-in thick. Other states are also trying this technique.

Questions related to factors that should be optimized include:

1. How close should one be to crack the pavement?
2. How thick should the ACP overlay be?
3. How much difference does reinforcement make?
4. How should breaking or cracking and the seating operation be inspected?
5. Is the fabric needed or beneficial?
6. Is drainage necessary?
7. What will the ultimate wearout and, thus, future rehabilitation be like?

Even with these uncertainties, it appears the technique used in Kentucky is a viable one for rehabilitating CPCD and JRCP pavements.

Bonded concrete overlays are being tried more and more on highway pavements. This technique, developed to strengthen sound airfield pavements to handle heavier aircraft, was first used in the highway field for bridge deck repair. Many projects have been placed in the Midwest on jointed concrete pavements (*3*). Two critical elements must be present, however, for bonded concrete overlays to be successful. Most engineers believe that bonding to an existing pavement is a process that requires a sound existing pavement. Unfortunately, these same engineers will likely differ widely in what they determine to be a sound pavement. Second, bonded is the critical word in bonded concrete overlay. Very careful construction is necessary to achieve bonding.

Two full-scale bonded PCC overlays of CRCP were built in the late 1970s in Minnesota and Iowa, another in 1983–84 in Wisconsin, and one in 1986–1987 in Houston, Texas. Some debonding is being experienced on the Houston project at this time. As will be shown later, this technique has an economic advantage over unbonded PCC overlays in urban freeway construction if it performs well.

Unbonded PCC overlays (*4*) have been used many times throughout the United States. Provided the designer recognizes that the existing pavement provides only an excellent base upon which to build a new PCC and, therefore, does not try to make the overlay too thin, unbonded PCC overlays should last as long as a new PCC pavement.

COST PERFORMANCE

In order to determine the cost-effectiveness of some of the previously mentioned techniques, fifteen full-scale Texas freeway rehabilitation projects were studied. Additionally Drake (*2*) provided data on 12 projects using the break and seat technique. Table 1 summarizes the 27 projects. The projects from Texas include two simple-asphalt overlays, one ACP overlay plus extensive repairs, one bonded PCC over CRCP, six unbonded overlays, and five reconstruction projects. Twelve crack and seat projects from Kentucky are shown. Five of the Texas projects are capacity improvement projects: two change from a six-lane freeway to an eight-lane freeway plus an authorized vehicle lane (AVL); two change from a four-lane freeway to an eight-lane freeway; and one changes from a four- to a six-lane freeway. In Texas, three of the old pavements were plain, eight were jointed reinforced, and five were CRCP. All the old Kentucky pavements were 25-ft, jointed, mesh-doweled pavements. Data on six "Texas Comparison Projects" are also supplied. These were not PCC-rehabilitation projects and are not discussed. The data are provided so the reader can make comparisons, if desired.

Table 2 summarizes bid prices for these projects. The column labeled "Unit Bid" shows the bid per square yard for all paving items used on the main lanes and shoulders. The column labeled "Total Cost of Paving" attempts to isolate all costs associated with pavement rehabilitation. This column includes repairs, mobilization, traffic handling, and pavement markings for the Texas projects. It excludes drainage structures, grading, and frontage roads except where upgrading the frontage road was explicitly required for traffic handling. Figure 1 shows that the total cost of paving exceeds the unit bid by significant amounts.

In order to develop a better estimate for optimal solutions, estimates of pavement life were made as shown in Table 3. Thirty-year, life-cycle cost calculations were made using these estimates and a discount rate of 5 percent. The column labeled "Net Present Worth" shows these results.

Note that the expected life estimates are the author's and are based only on very limited evidence for most of the techniques. Unfortunately, it is necessary to make decisions on enormous construction outlays based on limited data.

These calculations indicate tremendous advantages for solutions that incorporate significant portions of the existing pavement into the new pavement, in other words the ACP overlays, the ACP plus crack and seat, and the bonded PCC overlay. Many engineers, including the author, believe another factor, reliability, or the probability that the design will perform as expected, should be considered (*5*). Reliability should be high whenever the consequences of failure are critical. This factor, as well as the cost of delay for rehabilitation construction, has not been quantified but has subjectively influenced the recommendations that follow.

Annual cost per-vehicle-mile, per-lane using present ADT for the thirty-year cycle were computed and are also shown in Table 3. Texas State Department of Highways and Public Transportation rehabilitation funds are currently allocated on a basis that is closely related to this number. The basis for allocation is 50 percent for lane-miles and 50 percent for vehicle-miles. Highways (or districts) with heavier traffic receive more rehabilitation funds.

The recommendations that conclude this paper are based on the following assumptions:

1. The previously stated assumptions about pavement life, interest rate, etc., are accurate enough to be useful.
2. There is not enough rehabilitation money available to select the longer life/higher life-cycle cost solutions for rural freeway projects.
3. The potential cost savings for the bonded PCC overlay outweighs the uncertainty associated with it.
4. The urban freeway capacity improvement projects are not wholly funded with rehabilitation funds. Their excessive costs must be balanced by the opportunity to effect user delay

TABLE 1 SUMMARY OF CONCRETE REHABILITATION PROJECTS—TEXAS PROJECTS

JOB #	EXISTING PAVEMENT	DESCRIPTION	SHOULDERS	TYPE	(E) # LANES	ADT	LENGTH (MILES)	(C) TOTAL BID (10^6)	DATE LET
1	CRCP	3" ACP O.L.	4" ACP O/L	RURAL	4/4	15,000	14.1	$6.2	SEP 85
2	CRCP&JRCP	4" ACP O.L.	4" ACP	URBAN	8/8	80,000	3.3	$6.3	OCT 83
3	JRCP	3" ACP O.L. & REPAIRS (3.1)*	3" ACP O/L	RURAL	4/6	26,000	3.9	$20.5	SEP 86
4	CRCP	4" BONDED CRCP O.L.	4" ACP	URBAN	8/8	165,000	3.4	$10.8	APR 85
5	JRCP	10" CRCP O.L.	10" CRCP	RURAL	4/4	17,000	14.9	$21.2	APR 85
6	CPCD	10" CRCP O.L. (6.1)	10" CRCP	RURAL	4/4	15,000	9.5	$18.6	OCT 85
7	CPCD	10" CPCD O.L. (7.1)	8"&10" CPCD	RURAL	4/4	21,000	10.7	$28.4	AUG 86
8	CRCP	10" CPCD O.L. (8.1)	10" ACP	RURAL	4/4	16,000	6.3	$12.2	AUG 85
9	CPCD	13" CPCD RECONSTR (9.1)	1" ACP	URBAN	4/4	20,000	6.5	$16.4	OCT 85
10	JRCP	13" CRCP RECONSTR	13" CRCP	URBAN	4/8	135,000	2.7	$50.0	OCT 85
11	JRCP	10" CRCP O.L. (11.1)	10" CRCP	URBAN	6/8+AVL	127,000	4.7	$34.1	APR 85
12	JRCP	11" CRCP O.L. (12.1)	11" CRCP	URBAN	6/8+AVL	175,000	4.1	$70.0	JAN 86
13	JRCP	14" CRCP RECONSTR (13.1)	14" CRCP	RURAL	4/6	26,000	1.5	$20.5	SEP 86
14	CRCP	12" CRCP RECONSTR (14.1)	12" CRCP	URBAN	4/8	73,000	3.4	$45.8	JAN 86
15	JRCP	13" CRCP RECONSTR (15.1)	13" CRCP	URBAN	8/8	73,000	2.5	$68.9	MAR 87
		TEXAS COMPARISON PROJECTS							
16	ACP	3" ACP O.L.	3" ACP	RURAL	4/4	14,000	4.2	$3.4	MAR 87
17	ACP	4" ACP O.L. & 15" WIDEN (17.1)	1.5"&4" ACP	URBAN	4/6	90,000	5.6	$15.4	SEP 86
18	ACP	COMPLETE ACP RECONSTR (18.1)	2" ACP	RURAL	4/4	11,000	8.3	$ 8.6	MAR 85
19	ACP	10" CRCP RECONSTR (19.1)	10" CRCP	RURAL	4/6	7,000	8.8	$11.2	SEP 86
20	NEW	12" CPCD	12" CPCD	RURAL	4/4	35,000	4.3	$18.5	NOV 85
21	CRCP	8" CRCP WIDENING (21.1)	8" CRCP	URBAN	6/8	90,000	1.9	$16.6	AUG 86
		KENTUCKY PROJECTS							
1	JRCP	6.5" ACP W/ CRACK & SEAT	6.5" ACP	RURAL	4/4	11,000	13.2	$8.0	FEB 82
2	JRCP	6.5" ACP W/ CRACK & SEAT	6.5" ACP	RURAL	4/4	21,000	19.1	$9.3	JUL 82
3	JRCP	6.5" ACP W/ CRACK & SEAT	6.5" ACP	URBAN	4/4	38,000	2.4	$1.5	MAY 83
4	JRCP	6.5" ACP W/ CRACK & SEAT	6.5" ACP	RURAL	4/4	12,000	7.5	$4.9	JUN 83
5	JRCP	6.5" ACP W/ CRACK & SEAT	6.5" ACP	RURAL	4/4	12,000	12.5	$7.1	JUN 83
6	JRCP	6.5" ACP W/ CRACK & SEAT	6.5" ACP	URBAN	4/4	45,000	7.9	$6.2	JUL 83
7	JRCP	6.5" ACP W/ CRACK & SEAT	6.5" ACP	RURAL	4/4	22,000	11.3	$6.9	JUL 83
8	JRCP	6.5" ACP W/ CRACK & SEAT	6.5" ACP	RURAL	4/4	13,000	15.4	$8.3	AUG 83
9	JRCP	6.5" ACP W/ CRACK & SEAT	6.5" ACP	RURAL	4/4	19,000	14.5	$8.8	SEP 83
10	JRCP	6.5" ACP W/ CRACK & SEAT	6.5" ACP	URBAN	4/4	30,000	16.3	$8.6	SEP 83
11	JRCP	6.5" ACP W/ CRACK & SEAT	6.5" ACP	RURAL	4/4	21,000	5.1	$4.0	NOV 83
12	JRCP	6.5" ACP W/ CRACK & SEAT	6.5" ACP	RURAL	4/4	21,000	11.1	$6.8	JUN 84
	AVERAGE:	6.5" ACP W/ CRACK & SEAT			4/4	22,000	11.4	$6.677,937.80	

*See "Notes for Tables" for additional project specific information.

TABLE 2 SUMMARY COSTS FOR CONCRETE REHABILITATION PROJECTS— TEXAS PROJECTS

JOB #	EXISTING PAVEMENT	DESCRIPTION	TYPE	(A) UNIT BID ($/SY)	(B) UNIT COST OF PAVING ($/SY)	UNIT BID UNIT COST	(D) COST/MILE (4 LANES)
1	CRCP	3" ACP O.L.	RURAL	5.56	8	0.70	357,000
2	CRCP&JRCP	4" ACP O.L.	URBAN	9.85	13	0.76	580,000
3	JRCP	3" ACP O.L. & REPAIRS	RURAL	6.03	20	0.30	892,000
4	CRCP	4" BONDED CRCP O.L.	URBAN	17.79	25	0.71	1,115,000
5	JRCP	10" CRCP O.L.	RURAL	19.13	25	0.77	1,115,000
6	CPCD	10" CRCP O.L.	RURAL	15.96	34	0.47	1,516,000
7	CPCD	10" CPCD O.L.	RURAL	20.44	36	0.57	1,605,000
8	CRCP	10" CPCD O.L.	RURAL	23.94	38	0.63	1,694,000
9	CPCD	13" CPCD RECONSTR	URBAN	33.13	41	0.81	1,828,000
10	JRCP	13" CRCP RECONSTR	URBAN	35.28	55	0.64	2,452,000
11	JRCP	10" CRCP O.L.	URBAN	35.80	56	0.64	2,497,000
12	JRCP	11" CRCP O.L.	URBAN	39.32	57	0.69	2,541,000
13	JRCP	14" CRCP RECONSTR	RURAL	41.77	57	0.73	2,541,000
14	CRCP	12" CRCP RECONSTR	URBAN	38.81	61 (14.2)	0.64	2,720,000
15	JRCP	13" CRCP RECONSTR	URBAN	28.68	65	0.44	2,898,000
		TEXAS COMPARISON PROJECTS					
16	ACP	3" ACP O.L.	RURAL	4.06	7	0.58	312,000
17	ACP	4" ACP O.L. & 15" WIDEN	URBAN	11.45	14	0.82	624,000
18	ACP	COMPLETE ACP RECSTR	RURAL	13.21	18	0.73	803,000
19	ACP	10" CRCP RECONSTR	RURAL	18.55	24	0.77	1,070,000
20	NEW	12" CPCD	RURAL	24.10	48	0.50	2,140,000
21	CRCP	8" CRCP WIDENING	URBAN	38.05	58	0.66	2,586,000
		KENTUCKY PROJECTS					
1	JRCP	6.5" ACP W/ CRACK & SEAT	RURAL	6.22	14	0.44	601,000
2	JRCP	6.5" ACP W/ CRACK & SEAT	RURAL	7.79	11	0.71	488,000
3	JRCP	6.5" ACP W/ CRACK & SEAT	URBAN	9.61	15	0.64	639,000
4	JRCP	6.5" ACP W/ CRACK & SEAT	RURAL	8.33	13	0.64	646,000
5	JRCP	6.5" ACP W/ CRACK & SEAT	RURAL	7.74	13	0.60	567,000
6	JRCP	6.5" ACP W/ CRACK & SEAT	URBAN	6.29	15	0.42	777,000
7	JRCP	6.5" ACP W/ CRACK & SEAT	RURAL	6.36	12	0.53	610,000
8	JRCP	6.5" ACP W/ CRACK & SEAT	RURAL	6.67	12	0.56	538,000
9	JRCP	6.5" ACP W/ CRACK & SEAT	RURAL	9.88	17	0.58	605,000
10	JRCP	6.5" ACP W/ CRACK & SEAT	URBAN	6.41	11	0.58	526,000
11	JRCP	6.5" ACP W/ CRACK & SEAT	RURAL	6.87	16	0.43	763,000
12	JRCP	6.5" ACP W/ CRACK & SEAT	RURAL	6.93	13	0.53	614,000
	AVERAGE:	6.5" ACP W/ CRACK & SEAT		7.42	14	0.55	614,500

TABLE 3 COST ANALYSES—TEXAS PROJECTS

JOB #	EXISTING PAVEMENT	TYPE	DESCRIPTION	EXPECTED LIFE	UNIT BID	TOTAL COST OF PAVING ($/SY)	NET PRESENT WORTH $/SY)*	ANNUAL COST /LN MI /VEHICLE (1986 $)	ADT	ADT /LANE
1	CRCP	RURAL	3" ACP O.L.	10	5.56	8	16	1.00	15,000	3,750
2	CRCP&JRCP	URBAN	4" ACP O.L.	10	9.85	13	26	0.61	80,000	10,000
3	JRCP	RURAL	3" ACP O.L. & REPAIRS	10	6.03	20	40	2.16	26,000	4,330
4	CRCP	URBAN	4" BONDED CRCP O.L.	15	17.79	25	37	0.42	165,000	20,630
5	JRCP	RURAL	10" CRCP O.L.	30	19.13	25	25	1.38	17,000	4,250
6	CPCD	RURAL	10" CRCP O.L.	30	15.96	34	34	2.13	15,000	3,750
7	CPCD	RURAL	10" CPCD O.L.	30	20.44	36	36	1.61	21,000	5,250
8	CRCP	RURAL	10" CPCD O.L.	30	23.94	38	38	2.23	16,000	4,000
9	CPCD	URBAN	13" CPCD RECONSTR	30	33.13	41	41	1.92	20,000	5,000
10	JRCP	URBAN	13" CRCP RECONSTR	30	35.28	55	55	0.76	135,000	16,880
11	JRCP	URBAN	10" CRCP O.L.	30	35.80	56	56	0.93	127,000	14,110
12	JRCP	URBAN	11" CRCP O.L.	30	39.32	57	57	0.69	175,000	19,440
13	JRCP	RURAL	14" CRCP RECONSTR	30	41.77	57	57	3.09	26,000	4,330
14	CRCP	URBAN	12" CRCP RECONSTR	30	38.81	61	61	1.57	73,000	9,130
15	JRCP	URBAN	13" CRCP RECONSTR	30	28.68	65	65	1.67	73,000	9,130
			TEXAS COMPARISON PROJECTS							
16	ACP	RURAL	3" ACP O.L.	10	4.06	7	14	0.93	14,000	3,500
17	ACP	URBAN	4" ACP O.L.&15" WIDEN	10	11.45	14	28	0.44	90,000	15,000
18	ACP	RURAL	COMPLETE ACP RECOSTR	20	13.21	18	27	2.33	11,000	2,750
19	ACP	RURAL	10" CRCP RECONSTR	30	18.55	24	24	4.81	7,000	1,170
20	NEW	RURAL	12" CPCD	30	24.10	48	48	1.29	35,000	8,750
21	CRCP	URBAN	8" CRCP WIDENING	30	38.05	58	58	1.21	90,000	11,250
			KENTUCKY PROJECTS							
1	JRCP	RURAL	6.5" ACP W/ CR & SEAT	15	6	14	21	1.77	11,000	2,750
2	JRCP	RURAL	6.5" ACP W/ CR & SEAT	15	8	11	16	0.73	21,000	5,250
3	JRCP	URBAN	6.5" ACP W/ CR & SEAT	15	10	15	22	0.55	38,000	9,500
4	JRCP	RURAL	6.5" ACP W/ CR & SEAT	15	8	13	19	1.51	12,000	3,000
5	JRCP	RURAL	6.5" ACP W/ CR & SEAT	15	8	13	19	1.51	12,000	3,000
6	JRCP	URBAN	6.5" ACP W/ CR & SEAT	15	6	15	22	0.46	45,000	11,250
7	JRCP	RURAL	6.5" ACP W/ CR & SEAT	15	6	12	18	0.76	22,000	5,500
8	JRCP	RURAL	6.5" ACP W/ CR & SEAT	15	7	12	18	1.28	13,000	3,250
9	JRCP	RURAL	6.5" ACP W/ CR & SEAT	15	10	17	25	1.24	19,000	4,750
10	JRCP	URBAN	6.5" ACP W/ CR & SEAT	15	6	11	16	0.51	30,000	7,500
11	JRCP	RURAL	6.5" ACP W/ CR & SEAT	15	7	16	24	1.06	21,000	5,250
12	JRCP	RURAL	6.5" ACP W/ CR & SEAT	15	7	13	19	0.86	21,000	5,250
	AVERAGE:		6.5" ACP W/ CR & SEAT		7	14	20	1.02	22,000	5,520

savings by "fixing it right the first time" and by the need for greater reliability in the design solution.

RECOMMENDATIONS

Various concrete rehabilitation strengthening solutions have been discussed and costs compared. For Texas, the following recommendations are made.

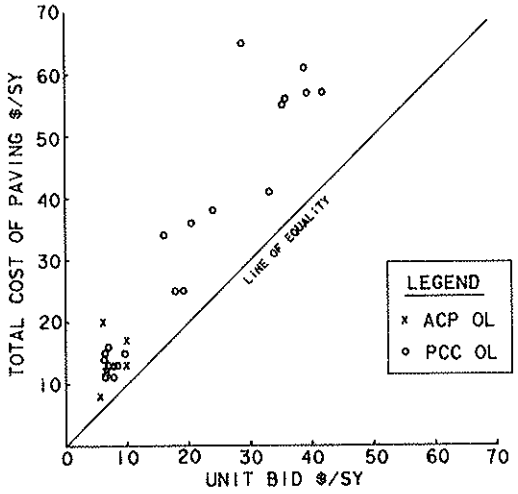

FIGURE 1 Total cost versus unit bid.

1. For non-freeway jointed pavements that must be overlaid due only to slickness or roughness, use 1½- to 3½-in ACP.
2. For all rural CRCP pavements experiencing punchouts or spalling, repair the punchouts, full depth, fully reinforced, and immediately overlay with 3½- to 4½-in ACP.
3. For urban CRCP pavements, fully repair all structural distress and then overlay with 3½- to 4½-in ACP or bonded CRCP.
4. For rural JRCP or CPCD, either use the crack and seat or combine the crack and seat with the Arkansas crack relief layer.
5. For urban freeway capacity-improvement projects, consider widening unbonded overlays now and in the future, as well as unbonded overlays now.

Applying these recommendations to the projects reviewed, in retrospect, one sees in Table 4 that six of the Texas selected solutions were acceptable, four were marginal, and five would not have been recommended.

NOTES FOR TABLES

Tables 1 and 4

(3.1) The ACP O/L and CRCP work for this job have been separated into two separate projects for this analysis. Also, the cost for the ACP O/L included $1,330,425.00 for repairing the existing concrete pavement.

TABLE 4 COST ANALYSES

JOB #	EXISTING PAVEMENT	TYPE	DESCRIPTION	UNIT COST OF PAVING ($/SY)	NET PRESENT WORTH ($/SY)	ANNUAL COST/LN MI /VEHICLE (1986 $)	ADT	
4	CRCP	URBAN	4" BONDED CRCP O.L.	25	37	0.42	165,000	OK for use
2	CRCP	URBAN	4" ACP O.L.	13	26	0.61	80,000	OK for use
12	JRCP	URBAN	11" CRCP O.L. (12.1)	57	57	0.69	175,000	OK for use
10	JRCP	URBAN	13" CRCP RECONSTR	55	55	0.76	135,000	OK for use
*	JRCP/CPCD	R OR U	6.5" ACP W/ CRACK & SEAT*	14	20	0.85	22,000	OK for use
11	JRCP	URBAN	10" CRCP O.L. (11.1)	56	56	0.93	127,000	OK for use
1	CRCP	RURAL	3" ACP O.L.	8	16	1.00	15,000	OK for use
5	JRCP	RURAL	10" CRCP O.L.	25	25	1.38	17,000	marginal
14	CRCP	URBAN	12" CRCP RECONSTR (14.1)	61	61	1.57	73,000	marginal
7	CPCD	RURAL	10" CPCD O.L. (7.1)	36	36	1.61	21,000	marginal
15	JRCP	URBAN	13" CRCP RECONSTR (15.1)	65	65	1.67	73,000	marginal
9	CPCD	URBAN	13" CPCD RECONSTR (9.1)	41	41	1.92	20,000	not recommended
6	CPCD	RURAL	10" CRCP O.L. (6.1)	34	34	2.13	15,000	not recommended
3	JRCP	RURAL	3" ACP O.L.& REPAIRS (3.1)	20	40	2.16	26,000	not recommended
8	CRCP	RURAL	10" CPCD O.L. (8.1)	38	38	2.23	16,000	not recommended
13	JRCP	RURAL	14" CRCP RECONSTR (13.1)	57	57	3.09	26,000	not recommended

* AVERAGE VALUES FOR KENTUCKY PROJECTS

(6.1) 5 percent of job is 13-inch CRCP Reconstruction (22,173 sy).

(7.1) The project includes 8-inch CONC PAV for shoulders and 13-inch CONC PAV RECONSTRUCTION.

21 percent of job is CRCP Reconstruction (57,674 sy). Primary Bid Item quantity does not include 81,312 sy of AC shoulders.

(9.1) 10 feet of the old 10-inch PCC was left in place for outside shoulder base.

(11.1) Added 10-inch CRCP AVL.

(12.1) Added 11-inch CRCP AVL, only 25 percent of bond breaker/level up was included when calculating the costs for rehabilitating the roadway since only 4.451 MI was overlaid of the 16.012 miles leveled up. The bond breaker/level up was let in DEC 83 as a separate O/L contract to Williams Bros. Constr. Co. The table combines both projects together for cost analysis.

(13.1) Same as Note (3.1). The job included a weigh station and frontage road work, which was not included when totaling the costs for rehabilitating the roadway, the 10- and 12-inch concrete paving were substantial amounts of concrete used in the frontage roads.

(14.1) The ramps for the highway are constructed with 8-inch CRCP.

(15.1) All 13-inch CRCP work was included while all 8-inch CRCP work was excluded. The project included a major interchange at IH 20 and IH 35.

(17.1) The project includes some inlays and variable thickness overlays.

(18.1) The description of COMPLETE ACP RECONSTRUCTION includes: 2-inch ACP surf (new), a fabric underseal, 8-inch hot recycled ACP, 6-inch lime treated base, and 6-inch existing base. The project had a substantial amount of salvaging and treating of existing base and subgrade.

(19.1) The project included an immigration station, which was not included in the rehabilitation costs for the roadway.

(21.1) The project is an addition of new lanes (from 4 to 6 lanes) to the highway without overlaying the existing lanes.

Table 2

(6.2) The ratio is low due to substantial costs for shoulder and fr. road work, which increased the UNIT COST FOR PAVING, but was not included in the UNIT BID.

(14.2) The 8-inch CRCP cost is included in the UNIT COST OF PAVING but is not included in the UNIT BID.

REFERENCES

1. M. J. Hensley. Open Graded Asphalt Concrete Base for the Control of Reflective Cracking. *Proceedings, Association of Asphalt Paving Technologists*, February 1980.
2. E. B. Drake. Breaking and Seating of Existing Portland Cement Concrete Pavement Prior to Bituminous Concrete Overlays in Kentucky. Presentation to the Design Committee, Region II, Kentucky, 1986.
3. M. J. Knutson. A Ten Year Performance Summary of PC Concrete and Concrete Overlay Research in Green County Iowa. *Proceedings of the Third International Conference in Concrete Pavement Design and Rehabilitation*, Purdue University, 1985.
4. R. L. Hutchinson. Resurfacing with Portland Cement Concrete. *National Cooperative Highway Research Program Synthesis of Highway Practice 99*, TRB, National Research Council, Washington, D.C., 1982.
5. *Guide for the Design of Pavement Structures*. AASHTO, Washington, D.C., 1986.

Publication of this paper sponsored by Committee on Pavement Rehabilitation.

Relative Influence of Accelerometer and Displacement Transducer Signals in Road Roughness Measurements

BOHDAN T. KULAKOWSKI, JOHN J. HENRY, AND JAMES C. WAMBOLD

Highway agencies conduct regular testing programs to monitor road roughness characteristics. Measurement of road roughness does not present an extremely challenging problem conceptually. On the other hand, the cost of the measuring equipment is significant. In this paper, the possibility of evaluating road roughness without an accelerometer is considered. The analysis of the frequency characteristics of displacement transducer and accelerometer signals indicates that the latter signal carries very little additional profile-related information within the frequency range of interest in the measurement of road roughness. The analytical conclusions are confirmed by statistical analysis of actual road roughness data.

Roughness is a property of pavement surface that affects not only ride comfort but also highway safety and vehicle energy consumption. Highway agencies conduct regular testing programs to monitor road roughness characteristics. From a conceptual standpoint, measurement of road roughness does not present an extremely challenging problem. On the other hand, the cost of the measuring equipment is a significant factor in the evaluation of road roughness. The cost of commercially available profilometers ranges from $35,000 to over $250,000. The cost of response-type road roughness meters is significantly lower, but these devices require periodic calibration using profilometers.

The technique most widely employed in the United States for obtaining road profile data is measurement of acceleration and displacement between the test vehicle and the road surface with an inertial profilometer (*1*). High-pass filtering of the accelerometer signal followed by double integration gives a record of the absolute vertical position of the vehicle body. The displacement signal is then subtracted from the integrated accelerometer signal to produce the road profile record, which can be further processed to obtain road roughness measures.

An alternative approach to determining road roughness was proposed by Watugala (*2*). In this method the calculation of the elevation profile is eliminated, and road roughness index values are generated by the quarter-car model using the accelerometer and displacement transducer signals as the inputs. This simplifies somewhat the data processing involved, but the procedure is still relatively complex and costly.

In this paper, the possibility of evaluating road roughness without an accelerometer is considered. The analysis of the frequency characteristics of displacement transducer and accelerometer signals indicates that the latter signal carries very little additional profile-related information within the frequency range of interest in the measurement of road roughness. The analytical conclusions are confirmed by statistical analysis of actual road roughness data.

Pennsylvania Transportation Institute, The Pennsylvania State University, University Park, Pa. 16802.

FREQUENCY ANALYSIS OF THE QUARTER-CAR MODEL

An objective measure of road roughness is based on the dynamic response of the standard quarter-car model, which is shown in Figure 1 (*3*, *4*). The quarter-car dynamics is described by the following equations:

$$M_s\ddot{z}_s + C_s(\dot{z}_s - \dot{z}_u) + K_s(z_s - z_u) = 0 \quad (1)$$

$$M_u\ddot{z}_u - C_s(\dot{z}_s - \dot{z}_u) - K_s(z_s - z_u) = K_t(w - z_u) \quad (2)$$

The road roughness index is expressed as

$$R_{QC} = 1/L \int_0^L (\dot{z}_s - \dot{z}_u)dl \quad (3)$$

The road profile, w, is calculated using the equation

$$w(t) = \int_0^t a(\tau)\, d\tau d\tau - x(t) \quad (4)$$

where both the displacement transducer signal, $x(t)$, and the accelerometer signal, $a(t)$, are recorded by an inertial profilometer.

A transfer function block diagram of the quarter-car model employed in road roughness analysis is shown in Figure 2. Road profile, $W(s)$, is the input signal to the system. The displacement transducer and accelerometer responses to the input are generated through the transfer functions $G_{WH}(s)$ and $G_{WA}(s)$, relating vehicle body displacement to road profile, and body acceleration to road profile, respectively:

$$G_{WH}(s) = \frac{H(s)}{W(s)} \quad (5)$$

and

$$G_{WA}(s) = \frac{A(s)}{W(s)} \quad (6)$$

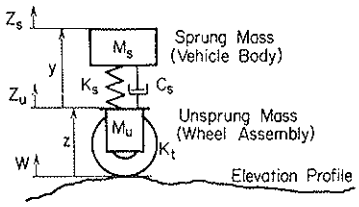

FIGURE 1 Standard quarter-car model.

The relative displacement of the two masses $y(t) = z_s(t) - z_u(t)$ represents the system output. It is related to the displacement transducer and the accelerometer signals through transfer functions $G_{HY}(s)$ and $G_{AY}(s)$ so that

$$Y(s) = G_{HY}(s) \cdot H(s) + G_{AY}(s) + A(s) \tag{7}$$

Using Equations 1 and 2, and noting that

$$H(s) = Z_s(s) - W(s) \tag{8}$$

the detailed expression for $G_{WH}(s)$ in terms of the quarter-car model parameters can be obtained as shown in the Appendix, Equation A1.

Also, taking the Laplace transform of equation 4 we have

$$W(s) = \frac{1}{s^2} A(s) - H(s) \tag{9}$$

and hence the profile-acceleration transfer function can be found as

$$G_{WA}(s) = s^2 [1 + G_{WH}(s)] \tag{10}$$

A detailed expression for $G_{WA}(s)$ is also given in the Appendix, Equation A2.

The other two transfer functions, $G_{HY}(s)$ and $G_{AY}(s)$, can also be expressed in terms of the quarter-car model parameters as shown in the Appendix, Equations A4 and A5. In order to compare the relative effects of the displacement transducer and accelerometer signals on the output signal $Y(s)$, the power spectral densities of the two signals will be considered. First, the power spectral densities of $H(j\omega)$ and $A(j\omega)$ are related to the power spectral density of the input profile signal, $W(j\omega)$, as follows:

$$S_H(j\omega) = S_W(j\omega) \cdot |G_{WH}(j\omega)|^2 \tag{11}$$

and

$$S_A(j\omega) = S_W(j\omega) \cdot |G_{WA}(j\omega)|^2 \tag{12}$$

Next, the power spectral densities of the two components of $Y(j\omega)$, one due to $H(j\omega)$ and the other due to $A(j\omega)$, are expressed as

$$S_{HY}(j\omega) = S_H(j\omega) \cdot |G_{HY}(j\omega)|^2 \tag{13}$$

$$S_{AY}(j\omega) = S_A(j\omega) \cdot |G_{AY}(j\omega)|^2 \tag{14}$$

Combining Equation 11 with Equation 13, and Equation 12 with Equation 14, the expressions for the power spectral densities of the relative body-suspension displacement components caused by the displacement transducer and accelerometer signals, $S_{HY}(j\omega)$ and $S_{AY}(j\omega)$, are found:

$$S_{HY}(j\omega) = S_W(j\omega) |G_{WH}(j\omega)|^2 |G_{HY}(j\omega)|^2 \tag{15}$$

$$S_{AY}(j\omega) = S_W(j\omega) |G_{WA}(j\omega)|^2 |G_{AY}(j\omega)|^2 \tag{16}$$

In order to evaluate the relative effects of the displacement transducer and accelerometer signals on the relative axle-body displacement the function $G(\omega)$ is introduced defined as

$$\sigma(\omega) = \frac{S_{AY}(j\omega)}{S_{HY}(j\omega)} \tag{17}$$

Using equations 15 and 16, $\sigma(\omega)$ can be represented by

$$\sigma(\omega) = \frac{|G_{WA}(j\omega)|^2 |G_{AY}(j\omega)|^2}{|G_{WH}(j\omega)|^2 |G_{HY}(j\omega)|^2} \tag{18}$$

Employing previously derived equations for the transfer functions on the right hand side of Equation 18, $\sigma(\omega)$ can be expressed in terms of the quarter-car parameters, (see Equation A6 in the Appendix).

The plot of $\sigma(\omega)$ is shown in Figure 3. Function $\sigma(\omega)$, introduced above, represents a measure of the relative effect of accelerometer and displacement transducer signals on the axle-body displacement, which, in turn, is used to determine road roughness, Equation 3. It can be observed from Figure 3 that $\sigma(\omega)$ decreases rapidly with the increasing wave number of the road profile. For profile wave number equal to approximately 0.05 cycle/ft the power spectral density of the axle-body displacement related to the accelerometer signal constitutes only about 10 percent of the axle-body displacement component related to the displacement transducer signal. It can therefore be concluded that for wave numbers equal to or greater than approximately 0.05 cycle/ft the dynamics of the axle-body displacement can be accurately represented by the displacement transducer signal only. In a recent study (5) it was found that a subjective measure of road roughness correlates best with the objective measure, represented by the roughness index given by Equation 3, in the range of frequency from 0.125 to 0.63 cycles/ft. It can be seen in Figure 3 that the contribution of the accelerometer signal to the road roughness measure within this frequency range is negligible in comparison with the displacement transducer signal. This analytical conclusion will be verified by statistical analysis of

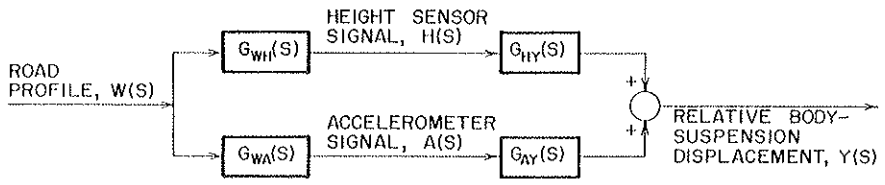

FIGURE 2 Block diagram of the system generating relative axle-body displacement.

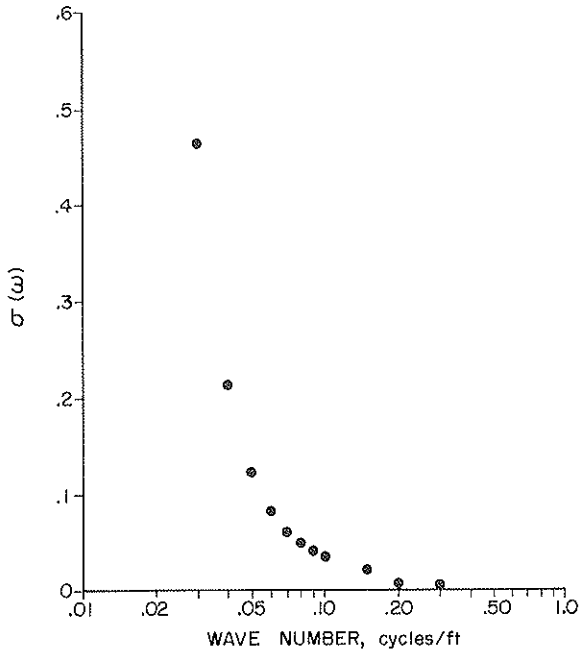

FIGURE 3 Function σ(α) representing relative effect of acceleration and displacement signals on axle-body displacement.

actual road roughness data, which is presented in the next section.

STATISTICAL ANALYSIS

In order to validate the results of the analytical considerations presented in the previous section, a statistical analysis of actual data collected on 15 road sites in Central Pennsylvania was performed. The data were used to calibrate the Pennsylvania DOT's Mays meters (*6*).

First, the roughness index values were calculated for a full quarter-car model using Equation 3. Both the displacement transducer and the accelerometer signals were used as inputs. Next, the accelerometer signal was rejected and only the displacement transducer signal was used as the input to the quarter-car model. This model, with a displacement transducer signal only, will be referred to as the reduced model. The roughness index values were averaged over 0.25-mi intervals. Each road site was 0.5 mi long, and the total number of data points was 30. A regression analysis was performed to yield the following two equations for 25 mph and 40 mph:

$$\hat{R}_{QC} = 3.68 + 1.58R^*_{QC} \text{ at 25 mph} \quad (19)$$

and

$$\hat{R}_{QC} = 5.66 + 1.58R^*_{QC} \text{ at 40 mph} \quad (20)$$

where carets and asterisks are used to denote road roughness index values obtained with the full and reduced models, respectively.

The standard deviation between the road roughness index values obtained from the quarter-car model, R_{QC}, and the values predicted by equations 19 and 20, R_{QC} was found to be 8.51 in/mile and 8.53 in/mile, respectively. The correlation

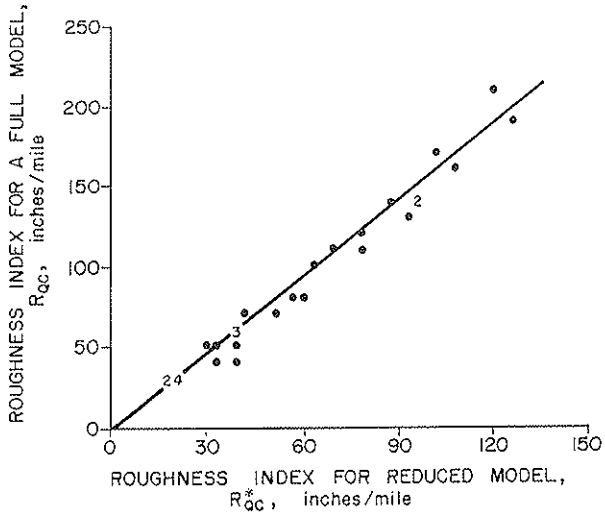

FIGURE 4 Correlation between roughness index values obtained with standard and reduced quarter-car models at 25 mph.

coefficients characterizing the relationship between the complete and the reduced model were 0.99 and 0.98, at 25 mph and 40 mph, respectively. Therefore, it can be concluded that the regression Equations 19 and 20 are statistically meaningful at both speeds. These results are shown in Figures 4 and 5.

In order to further evaluate the usefulness of the reduced model, calibration of the Pennsylvania DOT's Mays meter was performed using the reduced model, and the results were compared with those obtained using a complete quarter-car model (*6*).

The following formulas were obtained with the quarter-car model as the calibration standard:

$$\hat{R}_{QC} = 9.62 + 0.7272R_{MM} \text{ at 25 mph} \quad (21)$$

and

$$\hat{R}_{QC} = 13.1 + 0.664R_{MM} \text{ at 40 mph} \quad (22)$$

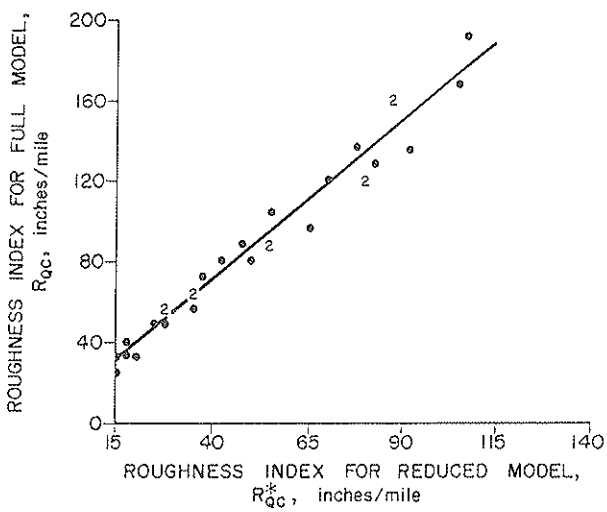

FIGURE 5 Correlation between roughness index values obtained with standard and reduced quarter-car models at 40 mph.

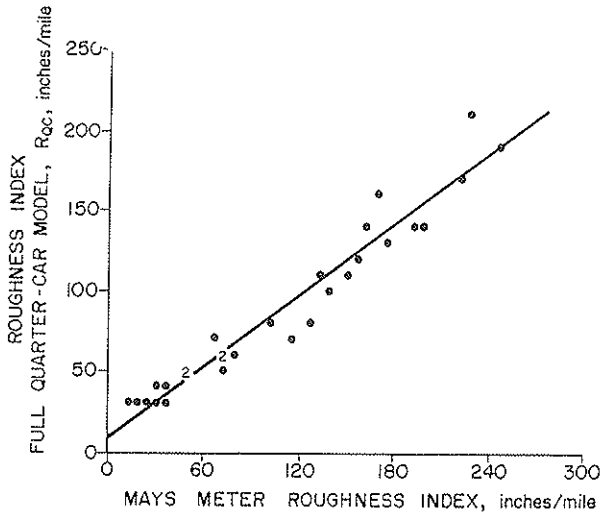

FIGURE 6 Mays meter calibration data using standard quarter-car model at 25 mph.

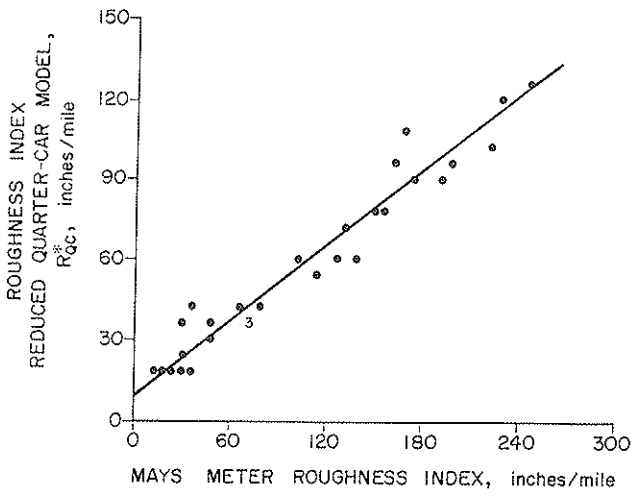

FIGURE 8 Mays meter calibration data using reduced quarter-car model at 25 mph.

The distribution of the experimental data is shown in Figures 6 and 7. Using the reduced quarter-car model as the calibration standard, the following equations were obtained:

$$R^*_{QC} = 9.03 + 0.456R_{MM} \text{ at 25 mph} \quad (23)$$

$$R^*_{QC} = 6.97 + 0.401R_{MM} \text{ at 40 mph} \quad (24)$$

The distribution of the calibration data is shown in Figures 8 and 9. The standard deviations of the measured data from the corresponding regression models were found to be significantly smaller for the reduced model at both speeds: 7.85 versus 12.68 at 25 mph and 9.84 versus 11.53 at 40 mph.

An important aspect of the Mays meter calibration procedure is its sensitivity to speed. In order to investigate the speed effect, the road roughness index values obtained with the reduced model at 25 mph, 35 mph, and 55 mph were correlated, with the quarter-car model at 40 mph used as the reference. The following relations were obtained:

$$\hat{R}_{QC} = 14.0 + 1.29R^*_{QC} \text{ at 25 mph} \quad (25)$$

$$\hat{R}_{QC} = 4.06 + 1.53R^*_{QC} \text{ at 35 mph} \quad (26)$$

$$\hat{R}_{QC} = 11.6 + 1.60R^*_{QC} \text{ at 55 mph} \quad (27)$$

The regression lines described by the above equations, together with the line given by Equation 20 obtained for 40 mph, are shown in Figure 10. It can be seen that the effect of speed is very slight between 35 to 55 mph and that only the results obtained for 25 mph differ significantly.

CONCLUSIONS

The results obtained from both the theoretical and the experimental data analysis indicate that the amount of relevant information carried by the accelerometer signal within the frequency range related to the profile wavelengths that affect road roughness is marginal. The determination of standard

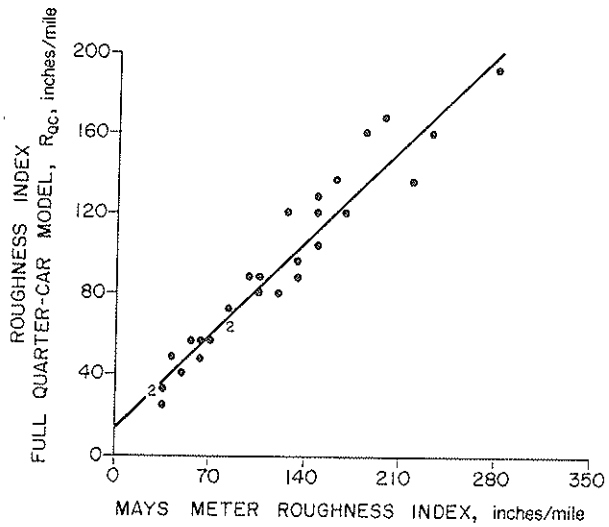

FIGURE 7 Mays meter calibration data using standard quarter-car model at 40 mph.

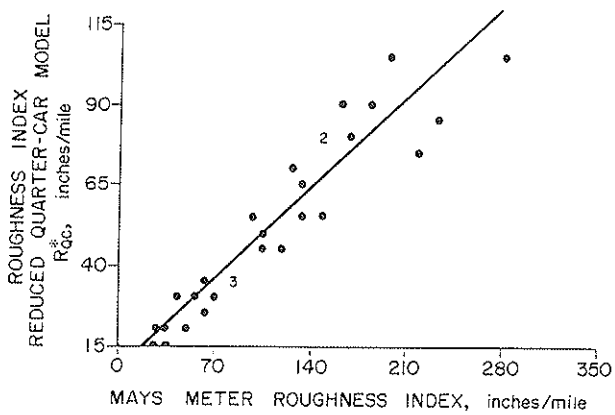

FIGURE 9 Mays meter calibration data using reduced quarter-car model at 40 mph.

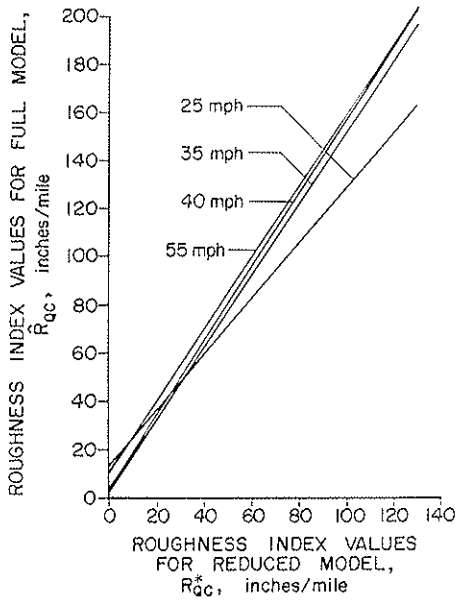

FIGURE 10 Effect of speed on Mays meter calibration lines using reduced quarter-car model.

road roughness measures can, therefore, be accomplished using the body displacement data only. Elimination of the accelerometer will certainly simplify the hardware of the road roughness measurement system; but, more important, it will also allow the software necessary to generate the roughness index to be limited to the processing of the displacement transducer signal. The computational process of calculating the road roughness index without double integrating the accelerometer signal will thus become considerably less expensive.

The results of the analysis presented in this paper, which were obtained with actual displacement and acceleration data, confirm the feasibility of the proposed reduced quarter-car model when used solely for the purpose of roughness index determination.

REFERENCES

1. J. C. Wambold et al. The State of the Art of Measurement and Analysis of Highway Roughness. In *Transportation Research Record 836*, TRB, National Research Council, Washington, D.C., 1981, pp. 21–29.
2. G. K. Watugala. *Determination of Road Roughness from Inertial Profilometer Data*. Ph.D. dissertation, The Pennsylvania State University, 1984.
3. New Standard Practice for Simulating Vehicular Response to Longitudinal Profiles of a Vehicular Traveled Surface. *ASTM Ballot*, September 1985.
4. T. D. Gillespie, M. W. Sayers, and L. Segel. *NCHRP Report 228: Calibration and Correlation of Response-Type Road Roughness Measuring Systems*. TRB, National Research Council, Washington, D.C., 1980.
5. M. S. Janoff et al. *NCHRP Report 1-23: Pavement Roughness and Ride Quality*. TRB, National Research Council, Washington, D.C., 1984.
6. B. T. Kulakowski. *Correlation of Road Roughness Measurements Obtained with the 1962 Chevrolet Impala and with the Standard Quarter-Car Model*. Final Report, Pennsylvania Department of Transportation, July 1985.

APPENDIX

Combining Equations 1 and 2 and taking a Laplace transformation, the transfer function $G_{WH}(s)$ relating the displacement transducer signal to the road profile is obtained:

$$G_{WH}(s) = \frac{s^4 + C_s/M_s + C_s/M_u\, s^3 + K_s/M_s + K_s/M_u + K_t/M_u s^2}{B(s)} \tag{A1}$$

where the polynomial $B(s)$ is

$$B(s) = s^4 + \frac{C_s}{M_s} + \frac{C_s}{M_u} s^3 + \frac{K_s}{M_s} + \frac{K_s}{M_u} + \frac{K_t}{M_u} s^2 + \frac{C_s K_t}{M_s M_u} s + \frac{K_s K_t}{M_s M_u} \tag{A2}$$

Substituting this form into Equation 1 yields the following expression for the transfer function $G_{WA}(s)$:

$$G_{WA}(s) = \frac{C_s K_t/M_s M_u\, s^3 + K_s K_t/M_s M_u\, s^2}{B(s)} \tag{A3}$$

The transfer functions $G_{HY}(s)$ and $G_{AY}(s)$ can also be obtained from the model equations 1 and 2:

$$G_{HY}(s) = \frac{K_t/M_u\, s^2}{B(s)} \tag{A4}$$

$$G_{AY}(s) = -\frac{K_t/M_u}{B(s)} \tag{A5}$$

Letting $s = j\omega$ in Equations A1, A3, A4 and A5 and substituting into Equation 18, the expression for $\sigma(\omega)$ is found as follows:

$$\sigma(\omega) = \frac{(K_s K_t/M_s M_u)^2 + \omega^2 (C_s K_t/M_s M_u)^2}{\omega^4 \left[\left(-\omega^2 + \frac{K_s}{M_s} + \frac{K_s}{M_u} + \frac{K_t}{M_u}\right)^2 + \omega^2 \left(\frac{C_s}{M_s} + \frac{C_s}{M_u}\right)^2\right]} \tag{A6}$$

Publication of this paper sponsored by the Committee on Surface Properties—Vehicle Interaction.